University of Sheffield

NEK1-mediated regulation of ER/Mitochondria tethering, and its role in ALS

Natalie Alison Pye

A thesis submitted in partial fulfilment of the requirements for the degree of Doctor of Philosophy

The University of Sheffield

School of Medicine and Population Health

Division of Neuroscience

Sheffield Institute of Translational Neuroscience

August 2024

Abstract

The endoplasmic reticulum (ER) and mitochondria are connected at specialised contact sites. At these contact sites tethering proteins such as VAPB on the ER membrane and PTPIP51 on the outer mitochondrial membrane maintain the apposition of the organelles. Reduced ER-mitochondria coupling has been reported in models of amyotrophic lateral sclerosis (ALS), a progressive neurodegenerative disease. Since ER-mitochondria tethering mediates several processes that are dysregulated in ALS including autophagy, calcium homeostasis, and synaptic function, loss of contacts may be an early, upstream event in ALS aetiology.

Heterozygous loss-of-function mutations in NEK1 are a cause of familial and sporadic ALS. NEK1 is involved in DNA damage repair pathways, but how loss of NEK1 causes ALS remains unclear. It has been reported that in response to DNA damage NEK1 is recruited to mitochondria where it regulates the protein VDAC1 to prevent cell death. Additionally, NEK1 may interact with the tethering protein VAPB, suggesting a direct link between ER-mitochondria contacts and DNA damage repair.

In this study, NEK1 was found to interact with the VAPB/PTPIP51 tether by direct binding to PTPIP51. In response to activation by DNA damage VAPB/PTPIP51 interaction significantly increased, which is NEK1-dependent. This suggests NEK1 may mediate ER-mitochondria contacts in response to DNA damage. Conversely, loss of NEK1 caused a significant reduction in VAPB/PTPIP51 interactions. Consistent with the loosening of ER-mitochondria contacts, reduced VAPB/PTPIP51 interactions correlated with dysregulation of calcium signalling between the ER and mitochondria. Both VAPB/PTPIP51 tethering, and calcium handling defects were rescued by reintroducing NEK1 protein, confirming specificity.

We have identified a novel signalling complex involving NEK1 and the VAPB/PTPIP51 tether that regulates ER-mitochondria interactions. This complex may provide a direct link between defective DNA damage repair and ER-mitochondria contacts in ALS and suggests a new axis for therapeutic intervention of ALS.

Declaration

I, the author, confirm that the thesis is my own work. I am aware of the University's Guidance on the Use of Unfair Means (*www.sheffield.ac.uk/ssid/unfair-means*). This work has not previously been presented for an award at this, or any other, university.

Acknowledgement of collaborative work within the thesis

I, the author, confirm that the work submitted is my own, except where work that has formed part of jointly authored publications has been included. The contribution of the other authors to this work has been explicitly indicated below. I confirm that appropriate credit has been given within the thesis where reference has been made to the work of others.

The following PhD thesis contains published material from the book chapter 'Evidence of mitochondrial dysfunction in ALS and methods for measuring in model systems'. This was published in the International Review of Neurobiology, Academic Press, volume 176, 2024, pages 269-325, (DOI:10.1016/bs.irn.2024.04.006). Permission for reuse of this work in this thesis was granted by Elsevier, licence number: 5854230106652.

Permission has been given by the co-authors Dr J. Lee, Miss L. Ellis, Professor K. J. De Vos, and Professor H. Mortiboys. Dr J. Lee and L. Ellis wrote sections of the manuscript and prepared tables/figures discussing evidence of mitochondrial dysfunction and morphology in ALS which are not reused in this thesis. I wrote sections of manuscript discussing mitochondria associated membranes and evidence of their dysfunction in ALS. I prepared the tables associated to these sections, which are reused in this thesis. Professors K. J. De Vos and H. Mortiboys provided feedback and edited the manuscript.

I planned the experiments for the LC3 autophagy flux assays (Figure 4-11) and the co-immunoprecipitation experiments in chapter 5. The immunoprecipitation and immunoblots were performed by Miss Eloise Brown under my supervision and I analysed the results.

The samples for electron microscopy experiments (Figure 4-7, Figure 4-8) were prepared and imaged by Dr Chris Hill. I prepared the samples for mass spectrometry (Figure 4-17, Figure 4-22), whilst the mass spectrometry was performed and analysed by Dr Rachel George and Dr Mark Collins. Professor Guillaume Hautbergue and Dr Ya-Hui Lin provided training for the radioactive *in vitro* assays.

Acknowledgements

First and foremost, I would like to thank my primary supervisor Professor Kurt De Vos for his constant support, expertise, and encouragement, which have been invaluable throughout this entire process. My thanks also to my secondary supervisor Dr Andrew Grierson for his ongoing support throughout this project. I'm particularly grateful for all the advice I received in our Friday lab meetings which were invaluable to my project, and the many pizza celebrations we shared together as lab groups.

In addition to my supervisors, I am extremely thankful for my amazing lab mates, both past and present, whose support has been a continuous source of motivation. A special thanks to Claudia and Emma for always being willing to share your expertise with me, and for making the lab a fun and enjoyable place to work. Thank you also thesis mentor Bridget, who provided me with invaluable advice and encouragement throughout the writing process.

SITraN has become more than just a workplace for me, and I'm truly thankful for all the friends I've made here during my PhD. A particular thanks to the PhD gals, for welcoming me into your circle and for the ongoing support, friendship, and great nights out you've provided. Thank you also to the SITraN ladies football team, the volleyballers, and the book club for helping me keep my sanity with a social life, after spending long hours in the lab.

A special thank you to the Motor Neurone Disease Association (MNDA) for funding my PhD, as this research would not be possible without your generosity.

Lastly, I want to express my deepest gratitude to my family, who have always believed in me and supported my ambitions. Thank you to mum, dad, Char and nan for always encouraging me to be my best, and always answering the phone when I'm in need of some words of wisdom. Finally, I dedicate this thesis to Jools and Merlin, for being there for me every day throughout the highs and lows of this academic journey.

Table of contents

Abstract ..... **i**

Declaration ..... **ii**

Acknowledgement of collaborative work within the thesis ..... **ii**

Acknowledgements ..... **iii**

Table of contents ..... **iv**

List of tables ..... **x**

List of figures ..... **xii**

Abbreviations ..... **xv**

Chapter 1 Introduction **1**

1.1 Amyotrophic lateral sclerosis 1

1.1.1 Clinical features of ALS 1

1.1.2 Neuropathological features of ALS 2

1.1.3 Genetics of ALS 3

1.1.4 Mechanisms of disease 9

1.1.4.1 Aberrant RNA processing 9

1.1.4.2 Dysregulated proteostasis 11

1.1.4.2.1 Ubiquitin-proteasome system (UPS) 11

1.1.4.2.2 Autophagy 13

1.1.4.3 Excitotoxicity 16

1.1.4.4 Mitochondrial dysfunction 16

1.1.4.4.1 Disrupted mitochondrial function and morphology 17

1.1.4.4.2 Oxidative stress 17

1.1.4.5 DNA damage accumulation 18

1.1.4.6 Axonal transport 19

1.2 ER-mitochondria contact sites are disrupted in ALS 21

1.2.1 Structural and functional ER-mitochondria tethers 21

1.2.1.1 IP3R-Grp75-VDAC1 23

1.2.1.2 ATAD3A-WASF3-Bip 23

1.2.1.3 BAP31-Fis1-PACS2 24

1.2.1.4 MFN1-MFN2/MFN2-MFN2 24

1.2.1.5 PDZD8-FKBP8 24

1.2.2 The VAPB/PTPIP51 ER-mitochondria tether 25

1.2.2.1 Structure and function of VAPB 25
1.2.2.2 Structure and function of PTPIP51 29
1.2.2.3 VAPB/PTPIP51 ER-mitochondria tethering 30
1.2.3 The physiological role of ER-mitochondria contacts in neurons 31
1.2.3.1 Calcium homeostasis 31
1.2.3.2 Autophagy 35
1.2.3.3 Lipid metabolism 35
1.2.4 ER-mitochondria tethering is disrupted in ALS 38
1.2.4.1 TDP-43 and FUS 38
1.2.4.2 SigmaR1 and SOD1 38
1.2.4.3 C9orf72 39
1.2.4.4 VCP 39
1.3 The NEK1/C21orf2 protein complex in health and disease 44
1.3.1 NEK1 and C21orf2 mediate ciliogenesis 46
1.3.2 The role of NEK1 and C21orf2 in the DNA damage response 47
1.3.2.1 The DNA damage response 47
1.3.2.2 NEK1 is involved in multiple DDR pathways 48
1.3.2.3 Nucleus to mitochondria signalling in the DDR 51
1.3.2.3.1 PARP1-SIRT1 signalling 51
1.3.2.3.2 Mitophagy-apoptosis crosstalk 53
1.3.2.4 NEK1 may link ER-mitochondria contacts to the DDR 55
1.3.3 Mutations in *NEK1* and *C21orf2* are linked to ALS 57
1.3.3.1 NEK1 missense and loss of function mutations cause ALS 57
1.3.3.2 C21orf2 variants confer susceptibility to developing ALS 57
1.4 Summary, hypotheses, and aims 58
Chapter 2 Materials and methods 61
2.1 Cell culture techniques 61
2.1.1 Cell lines 61
2.1.2 Subculture of cell lines 61
2.1.3 Thawing cell lines 62
2.1.4 Freezing cell lines 62
2.1.5 CRISPR/Cas9 gene editing 63
2.1.6 Plasmid DNA transfection 65
2.1.7 siRNA transfection 68
2.1.8 Induction of DNA damage 70

2.1.9 Induction of autophagy 70
2.2 Molecular DNA techniques 70
2.2.1 Site-directed mutagenesis 70
2.2.2 Restriction digest of plasmid DNA 73
2.2.3 Agarose gel electrophoresis 74
2.2.4 Gel extraction and purification of DNA 74
2.2.5 DNA ligation 75
2.2.6 Phusion PCR 76
2.2.7 Gibson assembly 78
2.2.8 Transformation of XL10-Gold ultracompetent cells 79
2.2.9 Preparation of bacterial glycerol stocks 79
2.2.10 Preparation of plasmid DNA from bacterial cultures 80
2.2.11 Quantification of DNA concentration 80
2.3 Protein biochemistry 81
2.3.1 Cell lysis and protein extraction 81
2.3.1.1 Cell lysis for Immunoblot 81
2.3.1.2 Cell lysis for immunoprecipitation 81
2.3.2 Bradford assay for protein quantification 81
2.3.3 Immunoprecipitation 82
2.3.4 Cell fractionation 82
2.3.5 SDS-PAGE 83
2.3.6 Transfer to membrane 84
2.3.7 Immunoblotting 84
2.3.8 Quantification of band intensities 86
2.4 Fluorescence microscopy 87
2.4.1 Immunofluorescence 87
2.4.2 Proximity ligation assay (PLA) 90
2.4.3 Image acquisition 90
2.4.4 Image analysis 91
2.4.4.1 Quantification of PLA 91
2.4.4.2 Quantification of nuclear phosho-H2AX intensity 92
2.5 Live cell Ca^{2+} imaging 93
2.5.1 Live cell Ca^{2+} imaging with Fura2-AM dye 93
2.5.2 Analysis of live cell calcium imaging 93
2.6 RT-qPCR 94
2.6.1 RNA extraction 94
2.6.2 Reverse transcription for cDNA synthesis 95

2.6.3 Real time quantitative PCR 96
2.6.4 Relative fold change analysis 98
2.6.5 Melt curve analysis 98
2.7 *In vitro* protein assays 99
2.7.1 Production of GST-tagged proteins in bacteria 99
2.7.2 Extraction and purification of GST-tagged proteins 100
2.7.3 *In vitro* binding assay 100
2.7.3.1 In vitro translation 100
2.7.3.2 Binding assay 100
2.7.4 *In vitro* phosphorylation assay 101
2.7.5 Coomassie staining 101
2.7.6 Drying acrylamide gels onto filter paper 101
2.7.7 Imaging *in vitro* assays 102
2.8 Mass spectrometry 102
2.8.1 S-trap digest of GST-tagged proteins 102
2.8.2 Trypsin digest of eGFP-VAPB 103
2.8.3 Mass spectrometry 104
2.8.4 Analysis of mass spectrometry 104
2.9 Electron microscopy 104
2.10 Bioinformatics tools 105
2.10.1 Kinase prediction 105
2.10.2 Protein sequence alignment 105
2.10.3 *In silico* protein modelling 105
2.11 Statistical analysis 106
2.12 Figure creation 106
Chapter 3 Characterising the interaction between NEK1, C21orf2 and the VAPB/PTPIP51 ER-mitochondria tether 107
3.1 Introduction 107
3.2 Development of a toolbox to investigate the NEK1/C21orf2 protein complex 108
3.2.1 Creation and validation of C21orf2 knock out HeLa cells 108
3.2.2 Validation of NEK1 and C21orf2 endogenous antibodies 109
3.2.3 Production of wild type and kinase dead V5-tagged NEK1 constructs 112
3.2.4 Production of HA-tagged C21orf2 constructs 112
3.3 Characterisation of the NEK1/C21orf2 protein complex 115
3.3.1 NEK1 and C21orf2 do not localise to mitochondria 115
3.3.2 Disruption of the C21orf2 N-terminal domain disrupts NEK1/C21orf2 interaction 115

3.3.3 C21orf2 localises to microtubules 120
3.4 NEK1 and C21orf2 interact with the VAPB/PTPIP51 tether 124
3.4.1 NEK1 interacts with PTPIP51 124
3.4.2 C21orf2 interacts with PTPIP51 128
3.4.3 C21orf2 may require NEK1 to bind to PTPIP51 128
3.4.4 NEK1 but not C21orf2 partially localises to MAM 131
3.4.5 NEK1 binds directly to PTPIP51 *in vitro* 131
3.5 Discussion 137
3.5.1 Characterisation of the NEK1/C21orf2 protein complex 137
3.5.2 NEK1 and C21orf2 interact with the VAPB/PTPIP51 tether. 137
3.5.3 Conclusion. 139
Chapter 4 NEK1 regulates the VAPB/PTPIP51 tether 140
4.1 Introduction 140
4.2 Loss of NEK1 or C21orf2 function disrupts VAPB/PTPIP51 tethering 141
4.3 Loss of NEK1 or C21orf2 decreases ER-mitochondria apposition 149
4.4 Loss of NEK1 or C21orf2 disrupts the induction of autophagy 155
4.5 NEK1 kinase activity regulates VAPB/PTPIP51 tethering 157
4.5.1 NEK1 activation by DNA damage promotes NEK1/PTPIP51 interaction 157
4.5.2 NEK1 activation by DNA damage promotes VAPB/PTPIP51 tethering 157
4.5.3 NEK1 phosphorylates VAPB *in vitro* 160
4.5.4 Mutation of VAPB T201 may disrupt VAPB/PTPIP51 tethering 164
4.5.5 Mutation of VAPB T201 may disrupt VAPB/VAPA dimerisation 167
4.5.6 Activation of NEK1 promotes VAPB and PTPIP51 phosphorylation in HeLa cells 170
4.6 Discussion 175
4.6.1 Loss of NEK1 or C21orf2 disrupts VAPB/PTPIP51 tethering. 175
Chapter 5 Characterisation of the VAPB/PTPIP51 tether 179
5.1 Introduction 179
5.2 *In silico* modelling of PTPIP51 binding to VAPA/VAPB using AlphaFold3 181
5.2.1 Modelling binding of the PTPIP51 phospho-FFAT motif with MSP domains 181
5.2.2 Modelling binding of the PTPIP51 FFAT-like motif with MSP domains 185
5.2.3 Modelling binding of the PTPIP51 FFAT-like motif Y176 with MSP domains 188

5.3 Modelling PTPIP51 binding to VAPA/VAPB using co-immunoprecipitation 191
5.4 The PTPIP51 phospho-FFAT motif does not regulate binding to VAPA/VAPB 191
5.5 The PTPIP51 conventional FFAT-like motif does not regulate binding to VAPB/VAPA. 195
5.6 The PTPIP51 tyrosine 176 is not necessary for binding to VAPB or VAPA. 197
5.7 Disruption of the MSP domain disrupts VAPB and VAPA binding to PTPIP51 199
5.8 Discussion 203
Chapter 6 Discussion 208
6.1 NEK1 may regulate nucleus to mitochondria signalling in the DDR 208
6.1.1 DNA damage repair 208
6.1.2 Apoptosis 210
6.1.3 Cell cycle regulation 217
6.2 NEK1/AMPK signalling may regulate VAPB/PTPIP51 tethering 218
6.3 Disruption of MAM disruption in NEK1/C21orf2 related ALS 221
6.3.1 NEK1 and C21orf2-deficiency disrupts VAPB/PTPIP51 tethering 221
6.3.2 *NEK1* mutations as a 'second hit' in ALS aetiology 224
6.4 Future directions 227
6.4.1 How does NEK1-mediated phosphorylation regulate VAPB/PTPIP51 tethering? 227
6.4.2 How does loss of NEK1 regulation of VAPB/PTPIP51 tethering lead to ALS? 228
6.5 Conclusions 229

List of tables

Table 1-1 Summary of causative and risk ALS-associated genes. 5

Table 1-2 Structural and functional ER-mitochondria tethering proteins and their functions in cell homeostasis. 22

Table 1-3 Summary of VAPB interactors at ER-contact sites. 28

Table 1-4 Summary of ER-mitochondria tethering dysfunction in *in vitro* and *in vivo* models of ALS. 41

Table 2-1 Volume of trypsin and media used for subculturing of cell lines. 61

Table 2-2 Volume of media used for experimental cell culture plates and their applications. 62

Table 2-3 Reagent mixture for Cas9 transfection of 1 well of a 12 well plate. 64

Table 2-4 CRISPR Cas9 crRNA target sequences. 64

Table 2-5 Plasmid DNA constructs. 66

Table 2-6 Reagents and conditions for plasmid DNA transfection. 68

Table 2-7 siRNA sequences. 69

Table 2-8 siRNA transfection conditions with Lipofectamine RNAiMax. 69

Table 2-9 Primer sequences for site directed mutagenesis. 71

Table 2-10 Composition of QuikChange Lightning mutagenesis reaction. 72

Table 2-11 Parameters for PCR cycle of QuikChange Lightning mutagenesis reaction. 72

Table 2-12 Composition of plasmid DNA restriction digests. 73

Table 2-13 Composition of DNA ligation reaction. 75

Table 2-14 Composition of Phusion PCR reaction. 76

Table 2-15 Parameters for PCR cycle of Phusion PCR. 77

Table 2-16 Sequences of primers used for Phusion PCR. 77

Table 2-17 Composition of Gibson assembly reaction. 79

Table 2-18 Composition of acrylamide gels. 83

Table 2-19 Antibodies used for immunoblot. 85

Table 2-20 Primary antibodies for immunofluorescence. 88

Table 2-21 Volume of TRIzol and RNAse-free water used RNA extraction. 94

Table 2-22 Parameters for PCR cycle of qScript reverse transcription PCR. 95

Table 2-23 Primer sequences used in RT-qPCR. 96

Table 2-24 Composition of master mix for RT-qPCR. 96

Table 2-25 Parameters for PCR cycle of RT-qPCR. 97

Table 4-1 Phosphorylation sites in VAPB interactors identified with mass spectrometry. 173

Table 5-1 Confidence values for predictions of protein interactions with AlphaFold3. 207

List of figures

Figure 1-1 Summary of pathophysiological mechanisms in ALS. 10
Figure 1-2 The ubiquitin-proteasome system (UPS). 12
Figure 1-3 The macroautophagy pathway is disrupted in ALS. 14
Figure 1-4 Schematic of VAPA and VAPB protein domains. 27
Figure 1-5 Schematic of the PTPIP51 protein domains. 29
Figure 1-6 Summary of ER-mitochondria tethers involved in Ca^{2+} homeostasis. 34
Figure 1-7 Summary of ER-mitochondria tethers involved in lipid homeostasis. 37
Figure 1-8 Summary of ER-mitochondria tethering dysfunction in ALS. 40
Figure 1-9 Schematic of the NEK1 and C21orf2 proteins and disease-associated mutations. 45
Figure 1-10 Summary of the key pathways of NEK1 and C21orf2 in the DNA damage response. 50
Figure 1-11 PARP1-SIRT1 signalling in response to DNA damage. 52
Figure 1-12 Mitophagy-apoptosis crosstalk in response to DNA damage. 54
Figure 1-13 Hypotheses of the project. 60
Figure 2-1 Process of cloning with Gibson Assembly. 78
Figure 2-2 Quantification of proximity ligation assay (PLA) signal per cell. 91
Figure 2-3 Quantification of nuclear phospho-H2AX intensity. 92
Figure 3-1 Validation of a C21orf2 knock out (KO) HeLa cell line by immunoblot and qPCR. 110
Figure 3-2 Validation of endogenous NEK1 and C21orf2 antibodies for immunoprecipitation. 111
Figure 3-3 Characterisation of V5-tagged active and kinase dead NEK1. 113
Figure 3-4 Characterisation of HA-tagged C21orf2 constructs. 114
Figure 3-5 NEK1 and C21orf2 do not localise to mitochondria. 117
Figure 3-6 Disruption of the C21orf2 N-terminal domain prevents binding to NEK1. 118
Figure 3-7 Disruption of the C21orf2 N-terminal domain prevents co-occurrence with NEK1. 119
Figure 3-8 Overexpression of C21orf2 leads to two distinct phenotypes. 121
Figure 3-9 C21orf2 partially localises to endosomal compartments. 122
Figure 3-10 Overexpressed C21orf2 localises to microtubules. 123
Figure 3-11 NEK1 interacts with exogenous PTPIP51. 125
Figure 3-12 NEK1 interacts with endogenous PTPIP51. 126
Figure 3-13 NEK1 is not recruited to mitochondria by PTPIP51. 127
Figure 3-14 C21orf2 binds to PTPIP51. 129
Figure 3-15 Disruption of the C21orf2 N-terminal domain prevents interaction with PTPIP51. 130
Figure 3-16 NEK1 but not C21orf2 partially localises to MAM. 132
Figure 3-17 Purification of GST-tagged PTPIP51 and VAPB. 133
Figure 3-18 NEK1 binds directly to PTPIP51 *in vitro*. 135

Figure 3-19 NEK1 protein fragments bind to PTPIP51 *in vitro*. 136
Figure 3-20 Summary of NEK1/C21orf2 interaction with the VAPB/PTPIP51 tether. 139
Figure 4-1 Loss of NEK1 or C21orf2 disrupts VAPB/PTPIP51 tethering. 142
Figure 4-2 Validation of endogenous VAPB and PTPIP51 antibodies for PLA. 143
Figure 4-3 Reintroduction of NEK1 protein rescues disrupted VAPB/PTPIP51 tethering. 144
Figure 4-4 NEK1 kinase activity is necessary to regulate VAPB/PTPIP51 tethering. 146
Figure 4-5 C21orf2 is unable to rescue NEK1-deficiency mediated VAPB/PTPIP51 tethering defects. 147
Figure 4-6 C21orf2 requires NEK1 to rescue VAPB/PTPIP51 tethering defects. 148
Figure 4-7 Loss of NEK1 leads to disrupted ER-mitochondria contact and mitochondrial size. 150
Figure 4-8 Loss of C21orf2 leads to disrupted ER-mitochondria contact. 151
Figure 4-9 Summary of Oxotremorine-M stimulated Ca^{2+} release from ER stores. 153
Figure 4-10 Loss of NEK1 disrupts transfer of calcium from ER stores to mitochondria. 154
Figure 4-11 Loss of NEK1 or C21orf2 causes loss of induction of autophagy. 156
Figure 4-12 Induction of DNA damage promotes NEK1/PTPIP51 interaction. 158
Figure 4-13 NEK1 regulates VAPB/PTPIP51 tethering in response to DNA damage. 159
Figure 4-14 Induction of DNA damage promotes ER-mitochondria Ca^{2+} transfer. 161
Figure 4-15 VAPB and PTPIP51 contain NEK1 consensus phosphorylation motifs. 162
Figure 4-16 NEK1 phosphorylates VAPB *in vitro*. 163
Figure 4-17 NEK1 phosphorylates VAPB *in vitro* at Threonine 201. 165
Figure 4-18 Production and validation of phospho-deficient and phospho-mimetic Myc-VAPB T201 166
Figure 4-19 Mutation of VAPB T201 ablates NEK1 regulation of VAPB/PTPIP51 tethering. 168
Figure 4-20 Mutation of VAPB T201 disrupts VAPB-VAPA interaction. 169
Figure 4-21 Confirmation of successful co-transfection of V5-NEK1 and eGFP-VAPB for mass spectrometry. 171
Figure 4-22 Identification of NEK1-induced VAPB phosphorylation sites in HeLa cells. 172
Figure 4-23 Summary of NEK1 regulation of VAPB/PTPIP51 tethering. 178
Figure 5-1 Summary of PTPIP51 mutations investigated within this study. 180
Figure 5-2 AlphaFold3 modelling of the PTPIP51 phospho-FFAT binding to the VAPB MSP domain. 182
Figure 5-3 AlphaFold3 modelling of the PTPIP51 phospho-FFAT binding to the VAPA MSP domain. 184
Figure 5-4 AlphaFold3 modelling of the PTPIP51 FFAT-like motif binding to the VAPB MSP domain. 186
Figure 5-5 AlphaFold3 modelling of the PTPIP51 FFAT-like motif binding to the VAPA MSP domain. 187
Figure 5-6 AlphaFold3 modelling of PTPIP51 Y176 binding to the VAPB MSP domains. 189
Figure 5-7 AlphaFold3 modelling of PTPIP51 Y176 binding to the VAPA MSP domains. 190

Figure 5-8 Phosphorylation of the PTPIP51 phospho-FFAT motif acidic tract is not necessary for VAPB binding. 193
Figure 5-9 Disruption of the PTPIP51 phospho-FFAT motif does not disrupt binding to VAPA/VAPB. 194
Figure 5-10 The PTPIP51 FFAT-like motif does not mediate binding to VAPA or VAPB. 196
Figure 5-11 PTPIP51 tyrosine 176 is not necessary for binding to VAPA and VAPB. 198
Figure 5-12 Summary of VAPB and VAPB MSP mutations investigated within this study. 200
Figure 5-13 Mutation of key MSP domain residues disrupts VAPB binding to PTPIP51. 201
Figure 5-14 Mutation of key MSP domain residues disrupts VAPA binding to PTPIP51. 202
Figure 5-15 RMDN2 contains a conserved tyrosine residue that may regulate VAPB binding. 205
Figure 5-16 AlphaFold3 modelling does not predict PTPIP51 coiled coil binding to the VAPB MSP domain. 206
Figure 6-1 NEK1/C21orf2 regulation of VAPB/PTPIP51 tethering in response to DNA damage. 211
Figure 6-2 NEK1-induced VAPB phosphorylated sites cluster in disordered linker regions. 213
Figure 6-3 NEK1-induced phosphorylation of VAPB may regulate apoptosis. 214
Figure 6-4 NEK1-induced phosphorylation of PTPIP51 may regulate apoptosis. 216
Figure 6-5 Potential NEK1/AMPK/GSK3β regulation of VAPB/PTPIP51 tethering. 220
Figure 6-6 C21orf2-mediated disruption of NEK1 in ALS. 223
Figure 6-7 Potential mechanisms of MAM disruption in NEK1-related ALS. 226
Figure 6-8 Conclusions of the thesis. 229

Abbreviations

53BP1	p53-binding protein 1
ACBD4/5	Acyl-CoA-binding domain-containing protein 4/5
ACN	Acetonitrile
ALS	Amyotrophic lateral sclerosis
AMBRA1	Activating molecule in BECN1-regulated autophagy protein 1
AMPA	α-amino-3-hydroxy-5-methyl-4-isoxazolepropionic acid
AMPK	5’ Adenosine monophosphate-activated protein kinase
APS	Ammonium persulfate
ATAD3A	ATPase family AAA domain-containing protein 3A
ATM	Ataxia-telangiectasia mutated
ATR	Ataxia telangiectasia and Rad3-related protein
ATRIP	ATR-interacting protein
BAP31	B cell receptor-associated protein 31
BER	Base excision repair
Bid	BH3-interacting domain death agonist
BSA	Bovine serum albumin
CaMKK2	Calcium/calmodulin-dependent protein kinase kinase 2
CDC25A	M-phase inducer phosphatase 1
CDK1	Cyclin-dependent kinase 1
Cep104	Centrosomal protein of 104 kDa
Cep110	Centriolar coiled-coil protein of 110 kDa
CERT	Ceramide transfer protein
CFAP410/C21orf2	Cilia- and flagella-associated protein 410
Chk1	Checkpoint serine/threonine-protein kinase 1
Chk2	Checkpoint serine/threonine-protein kinase 2
CL	Cardiolipin
CNS	Central nervous system
COP	Coat protein complex
CPT	Camptothecin
CUL1	Cullin1
DAG	Diacylglycerol

DDR	DNA damage response
DMEM	Dulbecco's modified Eagle's medium
DNA-PK	DNA-dependent protein kinase
DPRs	Dipeptide repeat proteins
DRAM1	DNA damage-regulated autophagy modulator protein 1
Drp1	Dynamin-related protein 1
DSB	Double-strand break
EAAT2	Excitatory amino acid transporter 2
EDTA	Ethylene-diamine-tetraacetic acid
EF1A1	Elongation factor 1-α-1
EGTA	Ethylene-glycol-tetraacetic acid
EPG5	Ectopic P granules protein 5 homolog
EPP	Epoxypropane
ER	Endoplasmic reticulum
ERLIN1	Endoplasmic reticulum lipid raft-associated protein 1
ESCRT	Endosomal sorting complex required for transport
FADD	FAS-associated death domain protein
fALS	Familial ALS
FBS	Foetal bovine serum
FBXO3	F-box only protein 3
FFAT	Two phenylalanines in an acidic tract
Fis1	Mitochondrial fission protein 1
FKBP8	Peptidyl-prolyl cis-trans isomerase 8
FOXO3A	Forkhead box protein O3
FTD	Frontotemporal dementia
FUNDC1	FUN14 domain containing protein 1
FUS	Fused in sarcoma
GABA	γ-aminobutyric acid
GABARAP	γ-aminobutyric acid receptor-associated protein
GLUT1	Glucose transporter type 1
Grp75	Glucose-related protein 75
GSK3β	Glycogen synthase kinase-3β

GWAS	Genome wide association studies
HDAC6	Histone deacetylase 6
HNRNPA1	Heterogeneous nuclear ribonucleoprotein A1
HR	Homologous recombination
HRP	Horseradish peroxidase
IAM	2-Iodoacetamide
IDH	Isocitrate dehydrogenase
IMM	Inner mitochondrial membrane
Indels	Insertions/deletions
INF2	Inverted formin 2
IP3	Inositol-1,4,5-trisphosphate
IP3R	Inositol 1,4,5-triphosphate receptor
iPSC	Induced pluripotent stem cell
ipTM	Interface predicted template modelling
IR	Ionising radiation
JNK	Jun N-terminal kinase
KIF5A	Kinesin-1 heavy chain isoform 5A
KO	Knock out
LATS2	Large tumour suppressor kinase 2
LDH	Lactate dehydrogenase
LFQ	Label-free quantification
LOF	Loss of function
M3R	Muscarinic acetylcholine receptor M3
MAP1B	Microtubule-associated protein 1B
MAP1LC3/LC3	Microtubule-associated protein 1A/1B light chain 3B
MAPK	p38 Mitogen-activated protein kinase
MCU	Mitochondrial calcium uniporter
MFN1/2	Mitofusin 1/2
MGMT	O6-methylguanine-DNA methyltransferase
MIGA2	Mitoguardin 2
MMP	Mitochondrial membrane potential
MMR	Mismatch repair

MOSPD	MSP domain-containing protein
mPTP	Mitochondrial permeability transition pore
MSP	Major sperm protein
mTORC1	Mechanistic target of rapamycin complex 1
NEK1	Never in mitosis A-related kinase 1
NEMO	NF-κB essential modulator
NER	Nucleotide excision repair
NHEJ	Non-homologous end-joining
NMDA	N-methyl-D-aspartate
NPM	Nucleophosmin
NRBF2	Nuclear receptor-binding factor 2
ODGC	Oxoglutarate dehydrogenase complex
OMM	Outer mitochondrial membrane
OPA1	Optic atrophy protein 1
OPTN	Optineurin
ORP	OSBP-related protein
OSBP	Oxysterol-binding protein
OXPHOS	Oxidative phosphorylation
PA	Phosphatidic acid
PACS2	Phosphofurin acidic cluster sorting 2
PAE	Predicted aligned error
PARP1	Poly ADP-ribose polymerase 1
PBS	Phosphate-buffered saline
PC	Parental cell
PCR	Polymerase chain reaction
PDH	Pyruvate dehydrogenase
PDZD8	PDZ domain-containing protein 8
PE	Phosphatidylethanolamine
PEI	Polyethylenimine
PERK	RNA-dependent protein kinase (PKR)-like ER kinase
PI3KC3-C1	Class III phosphatidylinositol 3-kinase complex I
PI3P	Phosphatidylinositol 3-phosphate

PITPNM1	Phosphatidylinositol transfer protein 1
PKM	Pyruvate kinase M
PLA	Proximity ligation assay
pLDDT	Predicted local distance difference test
PLEKHM1	Pleckstrin homology domain-containing family M member 1
PS	Phosphatidylserine
PS1/2	Presenilin 1/2
pTM	Predicted template modelling score
PTP1B	Protein tyrosine phosphatase 1B
Rab	Ras-related protein
RIPA	Radioimmunoprecipitation assay buffer
RIPK1/3	Receptor-interacting protein kinase 1/3
RMDN2	Regulator of microtubule dynamics protein 2
RMDN3/PTPIP51	Regulator of microtubule dynamics protein 3
ROI	Region of interest
ROS	Reactive oxygen species
RRBP1	Ribosome-binding protein 1
sALS	Sporadic ALS
SCF	SKP1-CUL1-F-box protein
SDS	Sodium dodecyl sulfate
siRNA	Small interfering RNA
SIRT1	Sirtuin1
SKP1	S phase kinase associated protein 1
SMD	Spondylometaphyseal dysplasia
SNARE	Soluble N-ethylmaleimide-sensitive factor attachment protein receptor
SNX	Sorting nexin
SOD1	Superoxide dismutase 1
SPIRE1C	Spire homolog 1C
SSB	Single-strand break
STARD3	StAR related lipid transfer domain-3
SYNJ2BP	Synaptojanin-2-binding protein
TAE	Tris-acetate-EDTA buffer

TBK1	TANK-binding kinase 1
TBS	Tris-buffered saline
TCA	Tricarboxylic acid
TCEP	Tris (2-carboxyethyl) phosphine
TDP-43	TAR DNA-binding protein 43
TEAB	Triethylammonium bicarbonate
TEMED	Tetramethylethylenediamine
TFA	Trifluoroacetic
TLK1	Tousled-like kinase 1
TM	Transmembrane
TMEM41B	Transmembrane protein 41B
TPR	Tetratricopeptide-repeat-like
TPX2	Targeting protein for Xklp2
UBQLN2	Ubiquilin-2
ULK1	Unc-51 like autophagy activating kinase 1
UPR	Unfolded protein response
UPS	Ubiquitin-proteasome system
VAPA/B	Vesicle-associated membrane protein-associated protein A/B
VCP	Valosin-containing protein
VDAC1	Voltage-dependent anion channel 1
VMP1	Vacuole membrane protein 1
VPS	Vacuolar protein sorting-associated protein
Wee1	Wee1-like protein kinase
WIPI	WD repeat domain phosphoinositide-interacting protein
WT	Wild type

Chapter 1 Introduction

1.1 Amyotrophic lateral sclerosis

1.1.1 Clinical features of ALS

Amyotrophic lateral sclerosis (ALS) is a fatal neurodegenerative disorder characterised by the selective and progressive degeneration of both the upper and lower motor neurons, with onset of disease typically occurring between the 40 – 63 years of age (Logroscino *et al.*, 2010). This most commonly leads to heterogeneous clinical presentations and death within 3 – 5 years of disease onset, due to paralysis of respiratory muscles (Chio *et al.*, 2009; Niedermeyer *et al.*, 2019; Traxinger *et al.*, 2013).

Onset of ALS presents with unilateral muscle weakness, cramping and atrophy in the distal upper or lower limb muscles, such as dropping of one foot or weakness and muscle wasting of one hand (Verma, 2021). As the disease progresses, this spreads along the affected limb and across to the opposite side of the body, reaching the trunk, chest, and head. In roughly 30% of cases, the disease first begins in the lower brainstem, known as bulbar onset, presenting with difficulties speaking and swallowing due to atrophy of the tongue (Green *et al.*, 2013). Bulbar onset has been associated with faster disease progression (Chio *et al.*, 2009).

In addition to motor symptoms, up to 50% of ALS patients present with signs of mild cognitive impairment, with approximately 15% reaching the threshold for diagnosis of frontotemporal dementia (FTD) (Lomen-Hoerth *et al.*, 2002; Lomen-Hoerth *et al.*, 2003; Portet *et al.*, 2001; Ringholz *et al.*, 2005; Strong *et al.*, 1999). FTD is the second most common form of early-onset dementia, which is characterised by degeneration of the frontal and temporal lobes (Bang *et al.*, 2015). FTD and ALS are considered to be on a clinical, genetic, and pathophysiological spectrum, with approximately 10 – 15 % of FTD patients also developing ALS (Neary *et al.*, 2000; Parobkova and Matej, 2021).

There is currently no cure for ALS. To date there is only one drug approved for use within the EU and UK, Riluzole. Riluzole was approved for use as a treatment for ALS in 1996, however it only slows the progression of disease and is not a cure (Lacomblez *et al.*, 1996). Since the approval of Riluzole only two more drugs have been approved for treatment within the United States; Edaravone in 2017 (Takei *et al.*, 2017) and Qalsody (Toferson) in 2023 (Blair, 2023). Treatment with Toferson is only available for patients with SOD1-ALS. However, similarly to Riluzole these drugs only delay disease progression and do not repair neurodegeneration.

Currently, development of an effective cure is limited by the lack of understanding of the cellular mechanisms leading to disease manifestation. Thus, by elucidating the pathological mechanisms leading to development of ALS, we may discover new targets for therapeutic intervention.

1.1.2 Neuropathological features of ALS

ALS is characterised by the degeneration of motor neurons in the anterior horn of the spinal cord, lower cranial motor nuclei of the brainstem and Betz cells in the motor cortex (Hammer *et al.*, 1979; Nihei *et al.*, 1993). In addition to motor neuron degeneration, intracellular protein aggregates are a hallmark neuropathology observed in the disease, including ubiquitin-positive inclusions, neurofilament accumulations and Bunina bodies (Julien *et al.*, 1995; Mackenzie *et al.*, 2007; Okamoto *et al.*, 1993).

Ubiquitin-positive inclusions are found in patients and can be formed as skein-like filamentous inclusions or Lewy body-like hyaline inclusions (Hasegawa *et al.*, 2008; Lin and Dickson, 2008). Both are typically positive for the ubiquitin binding protein p62/Sequestosome-1 (Gal *et al.*, 2007). In approximately 97% of cases these inclusions are positive for misfolded wild type TAR DNA-binding protein 43 (TDP-43), except for cases harbouring *SOD1* and *FUS* mutations (Arai *et al.*, 2006; Mackenzie *et al.*, 2007; Tan *et al.*, 2007). Along with TDP-43, several of the proteins encoded by genes mutated in ALS are components of these ubiquitinated inclusions, such as superoxide dismutase 1 (SOD1) (Bosco *et al.*, 2010; Cheroni *et al.*, 2005), fused in sarcoma (FUS) (Vance *et al.*, 2009), optineurin (OPTN) (Hortobágyi *et al.*, 2011), and ubiquilin-2 (UBQLN2) (Williams *et al.*, 2012).

Hyperphosphorylated neurofilament accumulations have been reported in the axonal hillock of motor neurons in both human postmortem tissue and mouse models of ALS (Julien *et al.*, 1995; Rouleau *et al.*, 1996). These accumulations form pre-symptomatically in the soma and proximal axonal regions in a $SOD1^{G93A}$ mouse model and cause impaired axonal integrity in stem cell-derived motor neuron models of *SOD1* and *C9orf72* related ALS (Lefebvre-Omar *et al.*, 2023; Rouleau *et al.*, 1996). Currently, the levels of neurofilament light chain and phosphorylated neurofilament heavy chain are being considered as promising biomarkers for diagnosis and prognosis of ALS (Behzadi *et al.*, 2021; Verde *et al.*, 2019).

Bunina bodies are small (1 – 5 μm) intra-neuronal inclusions observed in surviving lower motor neurons in patient postmortem tissue of sporadic ALS cases (Okamoto *et al.*, 1993). They are observed in approximately 85% of ALS patients, including sporadic ALS (sALS) and TDP-43 related familial ALS (fALS), and are suggested to be ALS-specific (Mori *et al.*, 2019; Piao *et al.*, 2003). Postmortem brain and spinal tissue of two fALS SOD1-ALS cases did not exhibit Bunina bodies, suggesting Bunina body formation is not a pathological feature of SOD1-ALS, although more research is needed to confirm this result (Tan *et al.*, 2007). Bunina bodies are composed of cystatin C and transferrin proteins, although whether other proteins may contribute to formation of these inclusions has not been intensively studied (Mizuno *et al.*, 2006; Okamoto *et al.*, 1993). The mechanisms by which Bunina bodies

contribute to ALS development is currently unclear. However, they have been shown to be related to TDP-43-positive inclusions, with Bunina bodies occurring more commonly in motor neurons with TDP-43 mislocalisation and inclusions (Mori *et al.*, 2014; Mori *et al.*, 2010). Both protein inclusions were found to contain autophagosomes and lysosomes, suggesting they may act through disruption of autophagic pathways (Mori *et al.*, 2019). Together, the presence of characteristic protein aggregations in ALS suggests imbalance and dysfunction of protein homeostasis, which may be a pathological mechanism of the disease.

1.1.3 Genetics of ALS

Approximately 10% of patients with ALS have a family history of the disease, known as familial ALS (fALS), whilst the remaining patients are considered sporadic ALS (sALS) (Barberio *et al.*, 2023). Whilst sALS cases have no hereditary link to the disease, both sALS and fALS are connected by the prevalence of genetic mutations that increase the risk of developing ALS, with approximately 76% of fALS and 25% of sALS patients harbouring an ALS-linked genetic mutation (Renton *et al.*, 2014; Shepheard *et al.*, 2021). Currently, mutations in over 40 genes have been identified as genetic mutations that cause or increase the risk of developing ALS (Abel *et al.*, 2012), which is summarised in Table 1-1. The proteins encoded by these genes are involved in multiple cellular processes that are disrupted in ALS, such as protein homeostasis, deoxyribonucleic acid (DNA) damage repair, mitochondrial function and axonal transport, suggesting that ALS is a multifaceted disease.

Interestingly, evidence suggests that approximately 3 – 6% of cases harbour more than one ALS-linked genetic mutation, and that this is linked to an earlier onset of and faster progression of disease, suggesting ALS may be an oligogenic disease (Cady *et al.*, 2015; Iacoangeli *et al.*, 2024; Van Daele *et al.*, 2023). Whilst there is convergence of genetic mutations related to processes dysregulated in ALS, how disruption of these processes leads to disease manifestation, or which processes are upstream in disease aetiology, is not yet understood. Genetic mutations in the four most common ALS-associated genes *C9orf72, SOD1, TARDBP* and *FUS* are found to cause ALS in 60% of fALS and 11% of sALS cases (Akçimen *et al.*, 2023). Loss-of-function (LOF) and missense mutations in the *NEK1* gene are linked to development of sporadic and familial ALS (Brenner *et al.*, 2016; Kenna *et al.*, 2016). Non-synonymous mutations in the *C21orf2* gene confer susceptibility to developing ALS (van Rheenen *et al.*, 2016). As this project focusses on investigating a novel role for NEK1 and C21orf2 in ALS neuropathology, evidence of their contribution to ALS is described in detail in section 1.3.3.

A hexanucleotide (GGGGCC) repeat expansion in the *C9orf72* gene is the most common genetic cause of both ALS and FTD, accounting for 40% of fALS and 7% of sALS cases (Majounie *et al.*, 2012). Currently, there are three proposed mechanisms of C9orf72 pathology in ALS. Firstly, the formation of sense and antisense ribonucleic acid (RNA) foci cause disruption of RNA metabolism by sequestering

RNA binding proteins in the nucleus (Lee *et al.*, 2013; Xu *et al.*, 2013). The second theory suggests a loss of function mechanism due to *C9orf72* haploinsufficiency, leading to impairment of processes that the C9orf72 protein regulates, such as autophagy and the immune response (O'Rourke *et al.*, 2016; Shi *et al.*, 2018; Webster *et al.*, 2016). The final mechanism is a toxic gain of function due to the non-canonical non-AUG-initiated translation of toxic dipeptide repeat proteins (DPRs) (Mackenzie *et al.*, 2015; Schludi *et al.*, 2015). Translation in all six reading frames in either the sense or antisense direction leads to the expression of five distinct dipeptide repeat species: glycine–alanine (GA), glycine–arginine (GR), proline–alanine (PA), proline–arginine (PR) and glycine–proline (GP). Studies suggest that GA, GP, and GR positive inclusions are the most prevalent, although the expression and aggregation patterns for each species varies (Ash *et al.*, 2013; Mackenzie *et al.*, 2015; Schludi *et al.*, 2015). Whilst these protein inclusions are negative for TDP-43, like other ALS-related protein inclusions they are positive for p62 and ubiquitin, suggesting these inclusions may contribute to impaired autophagy and protein homeostasis in ALS (Troakes *et al.*, 2012). DPRs have been shown to impede RNA biogenesis, promote the formation of pathogenic stress granules, and impede axonal transport (Fumagalli *et al.*, 2021; Kwon *et al.*, 2014; Tao *et al.*, 2015). It is currently not clear which of these mechanisms lead to development of ALS. Although considering that neither the C9orf72 RNA foci, DPRs or loss of C9orf72 protein alone lead to an ALS phenotype in mice, a combination of all three mechanism may be involved in disease manifestation (Sudria-Lopez *et al.*, 2016).

Mutations in the *SOD1* gene were the first to be identified as ALS-causative and are known to account for 12% of fALS and 2% of sALS cases (Rosen *et al.*, 1993). The pathological mechanism underlying *SOD1*-ALS is suggested to be due to a toxic gain of function, whereby mutant SOD1 protein misfolds to form pathological aggregates (Wang *et al.*, 2008). These aggregates have been suggested to disrupt multiple mechanisms implicated in ALS pathology, such as excitotoxicity, oxidative stress, and mitochondrial dysfunction (Wang *et al.*, 2024a). In line with this theory of toxic protein aggregation, wild type misfolded SOD1 protein was suggested to be pathogenic in sALS, although whether the disease mechanisms of wild type and mutant SOD1 are the same, is not yet clear (Bosco *et al.*, 2010).

Table 1-1 Summary of causative and risk ALS-associated genes.

Adapted from (Mead *et al.*, 2023).

Gene symbol	Protein name	Risk/ causative?	ALS/FTD?	Suggested pathophysiology	References
ANXA11	Annexin A11	Causative	ALS-FTD	Intracellular trafficking, calcium dyshomeostasis, and stress granule function	(Smith *et al.*, 2017; Sung *et al.*, 2022; Wang *et al.*, 2022)
ATXN1	Ataxin-1	Risk	ALS	RNA processing	(Conforti *et al.*, 2012; Tazelaar *et al.*, 2020)
ATXN2	Ataxin-2	Risk	ALS	RNA processing	(Daoud *et al.*, 2011; Elden *et al.*, 2010)
C9orf72	Guanine nucleotide exchange factor C9orf72	Causative	ALS-FTD	RNA processing, nucleocytoplasmic transport defects, proteasome impairment, autophagy, inflammation, and protein aggregation (DPRs)	(DeJesus-Hernandez *et al.*, 2011; Renton *et al.*, 2011; Troakes *et al.*, 2012; Xu *et al.*, 2013)
CCNF	Cyclin-F	Causative	ALS-FTD	Autophagy, axonal defects, and protein aggregation	(Farrawell *et al.*, 2023; Williams *et al.*, 2016)
C21orf2 (CFAP410)	Cilia- and flagella-associated protein 410	Risk	ALS	Microtubule assembly, DNA damage response and repair, neurite outgrowth, and interacts with NEK1	(Gregorczyk *et al.*, 2023; van Rheenen *et al.*, 2016; Watanabe *et al.*, 2020)
CHCHD10	Coiled-coil-helix-coiled-coil-helix domain-containing protein 10	Causative	ALS-FTD	Mitochondrial function and synaptic dysfunction	(Bannwarth *et al.*, 2014; Johnson *et al.*, 2014; Woo *et al.*, 2017)
FUS	Fused in sarcoma	Causative	ALS-FTD	RNA processing, DNA damage repair defects, nucleocytoplasmic transport defects, stress granule function, and protein aggregation	(Kwiatkowski *et al.*, 2009; Vance *et al.*, 2009)
HNRNPA1	Heterogenous nuclear ribonucleoprotein A1	Causative	ALS	RNA processing	(Kim *et al.*, 2013; Liu *et al.*, 2016)

Gene symbol	Protein name	Risk/ causative?	ALS/FTD?	Suggested pathophysiology	References
KIF5A	Kinesin-1 heavy chain isoform 5A	Causative	ALS	Axonal defects and intracellular trafficking	(Baron *et al.*, 2022; Nicolas *et al.*, 2018)
NEK1	Serine/threonine-protein kinase NEK1	Causative	ALS	Intracellular trafficking, DNA-damage response, and microtubule stability	(Brenner *et al.*, 2016; Higelin *et al.*, 2018; Kenna *et al.*, 2016; Mann *et al.*, 2023)
NIPA1	NIPA magnesium transporter 1	Risk	ALS	Intracellular trafficking	(Blauw *et al.*, 2012; Van Daele *et al.*, 2023)
OPTN	Optineurin	Causative	ALS-FTD	Autophagy, protein aggregation, inflammation, membrane trafficking, exocytosis, vesicle transport, reorganization of actin and microtubules, and cell cycle control	(Maruyama *et al.*, 2010; Mou *et al.*, 2022; Zhao *et al.*, 2023)
PFN1	Profilin-1	Causative	ALS-FTD	Axonal defects and cytoskeletal disorganisation	(Wu *et al.*, 2012)
SOD1	Superoxide dismutase 1	Causative	ALS	Oxidative stress, protein aggregation, mitochondrial dysfunction, axonal transport defects, proteasome impairment, and glial dysfunction	(Bunton-Stasyshyn *et al.*, 2015; Cheroni *et al.*, 2005; Rosen *et al.*, 1993; Rouleau *et al.*, 1996; Urushitani *et al.*, 2002)
TARDBP	TAR DNA-binding protein 43 (TDP-43)	Causative	ALS-FTD	RNA processing, nucleocytoplasmic transport defects, stress granule function, DNA damage accumulation and protein aggregation	(Arai *et al.*, 2006; Hasegawa *et al.*, 2008; Rutherford *et al.*, 2008; Sreedharan *et al.*, 2008; White *et al.*, 2018)
TBK1	Serine/threonine-protein kinase TBK1	Causative	ALS-FTD	Autophagy, mitophagy, inflammation, and mitochondrial dysfunction	(Freischmidt *et al.*, 2015; Harding *et al.*, 2021; Oakes *et al.*, 2017)

Gene symbol	Protein name	Risk/ causative?	ALS/FTD?	Suggested pathophysiology	References
TUBA4A	α-Tubulin 4A isoform	Risk	ALS	Axonal defects and cytoskeletal disorganisation	(Perrone *et al.*, 2017; Smith *et al.*, 2014)
UBQLN2	Ubiquilin-2	Causative	ALS-FTD	Proteasome impairment, autophagy, protein aggregation, oxidative stress, and axonal defects	(Chang and Monteiro, 2015; Deng *et al.*, 2011; Williams *et al.*, 2012)
UNC13A	Unc-13 homolog A	Risk	ALS-FTD	Impaired neurotransmission	(van Es *et al.*, 2009; van Rheenen *et al.*, 2021; Willemse *et al.*, 2023)
VAPB	Vesicle-associated membrane protein-associated protein B	Causative	ALS	Proteasome impairment and intracellular trafficking	(Aliaga *et al.*, 2013; Chen *et al.*, 2010a; Nishimura *et al.*, 2005; Nishimura *et al.*, 2004; Tripathi *et al.*, 2021)
VCP	Transitional endoplasmic reticulum ATPase	Causative	ALS-FTD	Autophagy, proteasome impairment, stress granules, protein aggregation, mitochondrial dysfunction, and endoplasmic reticulum dysfunction	(Johnson *et al.*, 2010; Scarian *et al.*, 2022; Tang and Xia, 2016)

Mutations in the gene *TARDBP* account for 4% of fALS and 1% of sALS cases (Renton *et al.*, 2014). The toxic formation of TDP-43 positive inclusions in motor neurons are found in 97% of all ALS cases (Mackenzie *et al.*, 2007), which is described in more detail in section 1.1.2. The nuclear depletion of TDP-43 and the formation of pathological inclusions are suggested to contribute to ALS by disrupting RNA processing (Suk and Rousseaux, 2020). Mutations in the *FUS* gene are also suggested to disrupt RNA processing due to the nuclear mis-localisation and pathogenic inclusion formation, similar to mutations in *TARDBP* (Kwiatkowski *et al.*, 2009; Vance *et al.*, 2009). These *FUS* mutations account for 4% of fALS and 1% of sALS cases and have been associated with an earlier age of disease onset (Hübers *et al.*, 2015; Renton *et al.*, 2014; Suzuki *et al.*, 2010).

Missense mutations in the gene *VAPB* have been identified in both fALS and sALS patients (Nishimura *et al.*, 2004). The *VAPB*^{P56S} mutation is associated with the autosomal dominant inherited atypical form of ALS known as ALS8, which is characterised by selective degeneration of the lower motor neurons and slower disease progression (Nishimura *et al.*, 2005). A similar phenotype to ALS8 is also presented by patients with the *VAPB*^{P56H} mutation (Sun *et al.*, 2017). Other *VAPB* missense mutations (V234I, T46I and A145V) have been reported in ALS patients (Chen *et al.*, 2010a; Kabashi *et al.*, 2013; van Blitterswijk *et al.*, 2012). Although, the potential pathological mechanisms of these mutations have not been investigated. Wild type vesicle-associated membrane protein-associated protein B (VAPB) is essential for regulation of endoplasmic reticulum (ER)-mitochondria apposition and the unfolded protein response (UPR) in response to ER stress (De Vos *et al.*, 2012; Kabashi *et al.*, 2013). In addition to *VAPB*^{P56S}, the VAPB^{T46I} mutation causes an ALS8 phenotype (Chen *et al.*, 2010a). Mutant VAPB^{T46I} and VAPB^{P56S} proteins are prone to aggregation and form into intracellular inclusions in cell and mouse models of ALS (Nishimura *et al.*, 2004; Papiani *et al.*, 2012; Tudor *et al.*, 2010). However, VAPB^{P56S} is readily degraded by the proteosome *in vitro*, suggesting there may be a loss of function effect, due to haploinsufficiency (Mitne-Neto *et al.*, 2011; Papiani *et al.*, 2012). In agreement with this theory, it has been shown that VAPB expression levels are reduced in the spinal cord of sALS cases and individuals with ALS associated with the VAPB^{P56S} mutation (Anagnostou *et al.*, 2010; Hartopp *et al.*, 2022; Mitne-Neto *et al.*, 2011). In support of a wider role for VAPB in ALS, recent evidence proposes disruption of ER-mitochondria contact sites (MAM) where VAPB localises, as a common pathomechanism in ALS (Hartopp *et al.*, 2022; Lee *et al.*, 2024). As this project focuses on elucidating mechanisms of VAPB/PTPIP51 ER-mitochondria tethering regulation by NEK1, evidence of MAM disruption in ALS is described in detail in section 1.2.4.

1.1.4 Mechanisms of disease

ALS presents with heterogenous clinical manifestations, suggesting that multiple pathological mechanisms may contribute to the disease (Beghi *et al.*, 2007). Proteins encoded by ALS-associated genes are linked to several cellular processes that are thought to be disrupted in ALS, such as DNA damage repair, mitochondrial function, and axonal transport (Mead *et al.*, 2023). Several proteins such as TDP-43 are involved in several disrupted process involved in ALS pathology, including aberrant RNA metabolism, oxidative stress, and mitochondria dysfunction, which suggests that ALS is a multifaceted disease (Nilaver and Urbanski, 2023). The most commonly reported pathological mechanisms are described below and summarised in Figure 1-1.

1.1.4.1 Aberrant RNA processing

Following the discovery of *TARDBP* and *FUS* as ALS-causative genes, mRNA transcription, transport, localisation, and alternative splicing, have been implicated as dysfunctional in ALS (Butti and Patten, 2018). The ALS-associated RNA-binding proteins TDP-43 and FUS are involved in sequestration of mRNA for translation regulation (Bhardwaj *et al.*, 2013; Masuda *et al.*, 2015). Both TDP-43 and FUS are mislocalised from the nucleus to cytosol in ALS, leading to improper chromatin remodelling (Tibshirani *et al.*, 2017), microRNA (miRNA) biogenesis (Emde *et al.*, 2015) and inclusion of cryptic exons (Gittings *et al.*, 2023). Recent evidence has implicated stress granules, which control RNA translation during stress conditions, as a pathological feature of ALS that promotes protein aggregation (Sama *et al.*, 2013). Many proteins implicated in ALS are involved in the physiological assembly of stress granules in normal conditions, such as FUS (Sama *et al.*, 2013), TDP-43 (Khalfallah *et al.*, 2018) and heterogeneous nuclear ribonucleoprotein A1 (HNRNPA1) (Gui *et al.*, 2019). Aberrant stress granule formation is prominent in multiple cell models of ALS, including *UBQLN2* (Peng *et al.*, 2022), *ATXN2* (Zeballos *et al.*, 2023) and *C9orf72*-related ALS (Zhang *et al.*, 2018b), further implicating aberrant RNA translation as a contributor to protein dyshomeostasis in ALS.

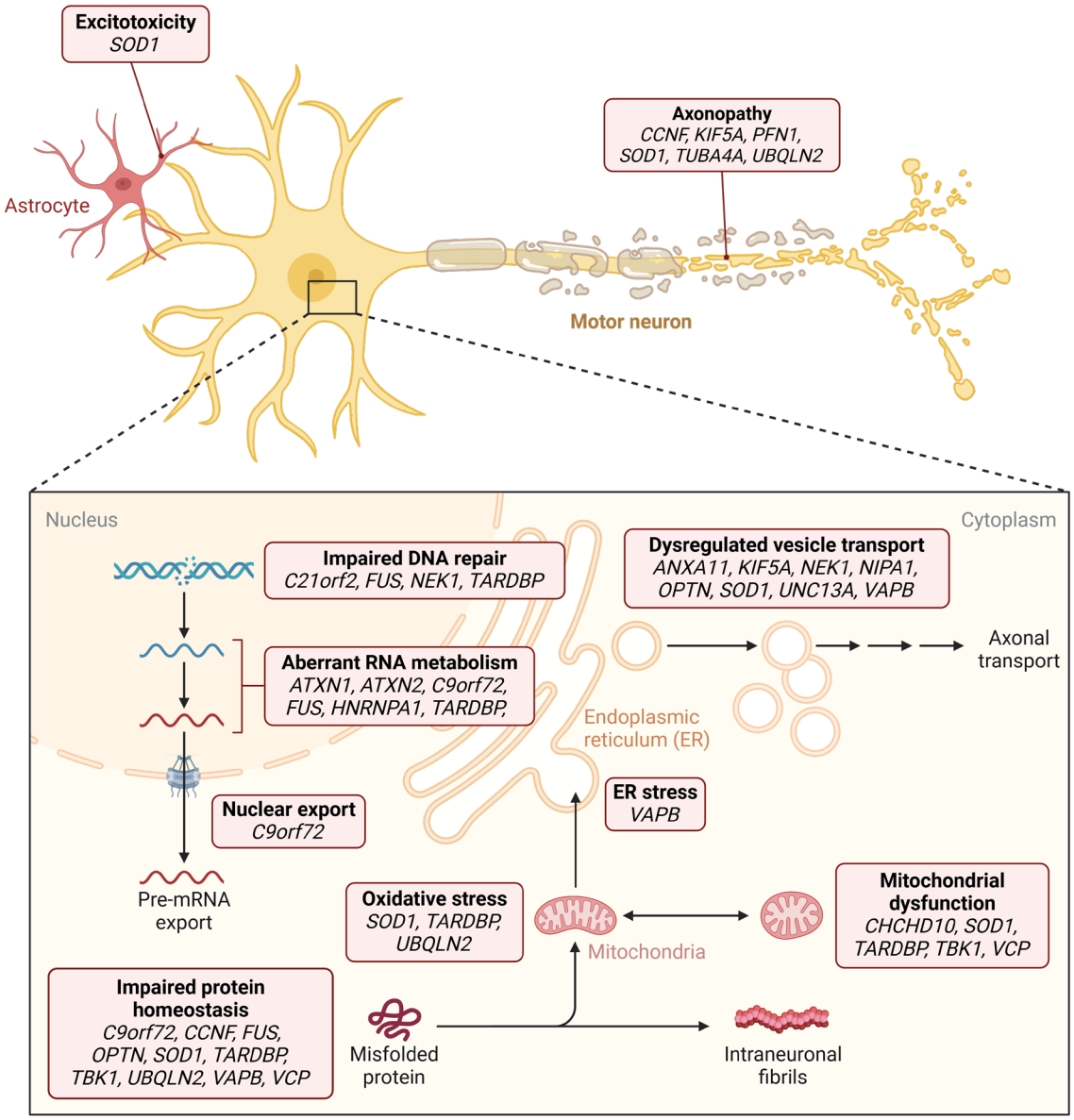

Figure 1-1 Summary of pathophysiological mechanisms in ALS.

Modified from (Hardiman *et al.*, 2017). Genetic mutations in over 40 genes have been associated with ALS. The proteins encoded by ALS-associated genes are involved in multiple cellular processes disrupted in the disease. This figure depicts the best characterised pathological mechanisms that contribute to ALS, and the genetic mutations involved in each process, which is discussed in detail in section 1.1.4.

1.1.4.2 Dysregulated proteostasis

The prevalence of pathological protein aggregates suggests that there is dysregulation of protein clearance in ALS. Protein degradation is controlled by two main pathways: the ubiquitin-proteasome system (UPS) and the autophagy-lysosome system. There is evidence to suggests that both clearance pathways are disrupted in ALS (Chua *et al.*, 2022; Quinet *et al.*, 2020), which is discussed in more detail below.

1.1.4.2.1 Ubiquitin-proteasome system (UPS)

The UPS typically degrades short-lived and misfolded proteins by ubiquitinating and delivering them to the proteasome for degradation (Gong *et al.*, 2016), summarised in Figure 1-2. Dysfunction of the UPS has been shown to lead to protein accumulation and dysregulation of apoptosis (Bennett *et al.*, 2005; Li *et al.*, 2022; Melino, 2005). Inhibition of the proteome in healthy motor neurons leads to ALS-like pathologies such as TDP-43 aggregation, suggesting it may be a contributing mechanism in the disease (van Eersel *et al.*, 2011). ALS mutant SOD1 protein interacts with regulatory subunits of the proteasome, which may lead to proteasomal inhibition seen in various ALS models (Cheroni *et al.*, 2005; Urushitani *et al.*, 2002). Reduced expression of UPS components in the spinal cords of $SOD1^{G93A}$ transgenic mice and poly-ubiquitination and clearance of mutant SOD1 by the proteasome have also been observed (Basso *et al.*, 2009; Marino *et al.*, 2015). ALS-associated mutations in *UBQLN2*, encoding the ubiquilin-2 protein, result in ubiquitinated protein aggregates (Deng *et al.*, 2011). These mutant proteins fail to bind properly to the proteasome, impairing substrate delivery and increasing sensitivity to protein stress (Chang and Monteiro, 2015). Mutant VAPB protein, associated with ER stress and defective UPR, may also impair the UPS. The mutant $VAPB^{P56S}$ protein forms cytoplasmic aggregates and promotes the accumulation of ubiquitinated aggregates and other proteasomal substrates (Chen *et al.*, 2010a). Wild type and mutant VAPB interact with the 20S subunit of the proteasome, which accumulates in aggregates (Moumen *et al.*, 2011). Together, this implicates defective UPS as a pathomechanism contributing to reduced protein clearance and subsequent pathogenic aggregations in ALS.

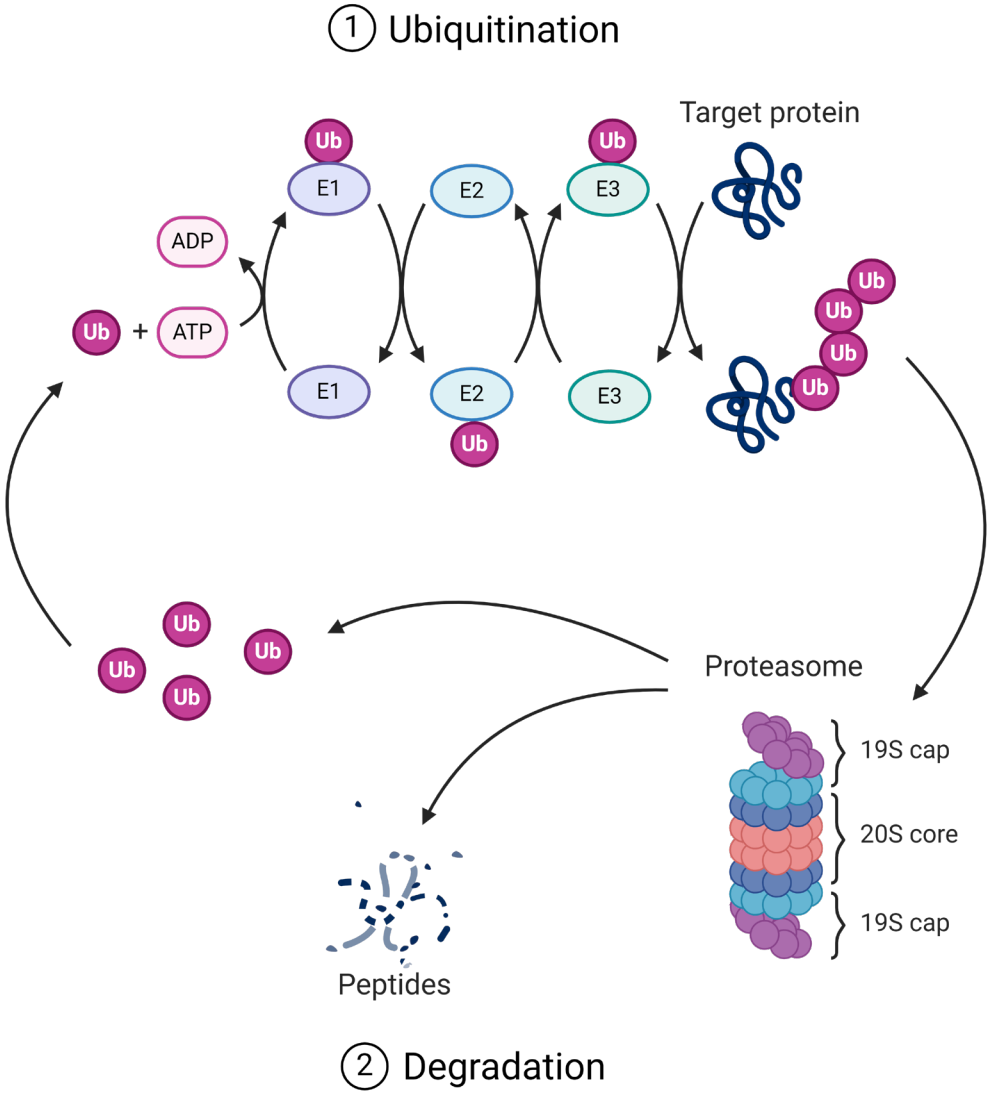

Figure 1-2 The ubiquitin-proteasome system (UPS).

The UPS targets proteins for degradation by the proteosome via ubiquitination.

1) To adhere ubiquitin to the target protein, there is a three-step enzymatic pathway. The E1 ubiquitin activating enzyme binds ATP and ubiquitin at the E1 cystine active site. The activated ubiquitin is then passed to the conjugation enzyme E2, which conjugates the ubiquitin to the E3 ligase. The E3 ligase binds to the target protein and transfers the ubiquitin, which determines the specificity of the target protein for degradation. This cycle is repeated to poly-ubiquitinate the protein.

2) The poly-ubiquitin chain is recognised by the proteasome 19S regulatory cap. This triggers protein unfolding and passage into the 20S core where proteases degrade the protein into peptides.

1.1.4.2.2 Autophagy

Macro-autophagy (known commonly as autophagy) selectively degrades bulk protein aggregates and damaged organelles, which is crucial for neuronal health (Ramesh and Pandey, 2017). Autophagy is characterised by four key stages (initiation, formation, closure, and lysosome fusion), each of which has been implicated as defective in ALS (Parzych and Klionsky, 2014) (summarised in Figure 1-3). The initiation of autophagy occurs at the endoplasmic reticulum membrane by the ULK1 complex, consisting of the unc-51 like autophagy activating kinase 1 (ULK1), the scaffolding protein FIP200 and the autophagy related proteins 13 and 101 (ATG13) and (ATG101) (Ganley *et al.*, 2009). In response to starvation, this complex is activated by disinhibition by the mechanistic target of rapamycin complex 1 (mTORC1) (Hosokawa *et al.*, 2009; Jung *et al.*, 2009). Activation is also promoted by the dual action of the 5' adenosine monophosphate-activated protein kinase (AMPK), which recruits autophagy-related protein 9 (ATG9) to the ULK1 complex by phosphorylation of ULK1 and inhibition of mTORC1 (Kim *et al.*, 2011; Park *et al.*, 2016). Alternatively, initiation of autophagy can be driven by selective autophagy cargos. For example, p62 targets ubiquitinated proteins and interacts with FIP200 (Turco *et al.*, 2019), whilst OPTN targets ubiquitinated mitochondria and binds to ATG9 vesicles (Yamano *et al.*, 2020). In either case, recruitment of ATG9 vesicles to the ULK1 complex is thought to be the key step for initiation of membrane formation (Sawa-Makarska *et al.*, 2020).

Upon activation at the ER membrane, the ULK1 complex recruits the class III phosphatidylinositol 3-kinase complex I (PI3KC3–C1), consisting of Beclin1, vacuolar protein sorting-associated proteins (VPS) VPS15, VPS34, autophagy-related protein 14 (ATG14) and nuclear receptor-binding factor 2 (NRBF2), by phosphorylation of Beclin1 (Burman and Ktistakis, 2010; Russell *et al.*, 2013). The PI3KC3-C1 complex binds to the membrane via ATG14, Beclin1 and VPS34, where activated VPS34 generates the effector phosphatidylinositol 3-phosphate (PI_3P) (Russell *et al.*, 2013). PI_3P recruits effector proteins WD repeat domain phosphoinositide-interacting proteins -2 and -4 (WIPI2/WIPI4) to the phagophore membrane (Dooley *et al.*, 2014). WIPI4 recruits autophagy-related protein 2 (ATG2), which promotes the transfer of phospholipids from the ER, with assistance from ATG9, vacuole membrane protein 1 (VMP1) and transmembrane protein 41B (TMEM41B), leading to expansion of the phagophore membrane (Ghanbarpour *et al.*, 2021; Maeda *et al.*, 2019; Osawa *et al.*, 2019; Ren *et al.*, 2020). WIPI2 recruits the autophagy-related protein complex ATG12-ATG5-ATG16 to promote lipidation and insertion of microtubule-associated protein 1A/1B light chain 3B (MAP1LC3/LC3) into the phagophore membrane, which further recruits ATG2 to promote elongation (Bozic *et al.*, 2020; Dooley *et al.*, 2014).

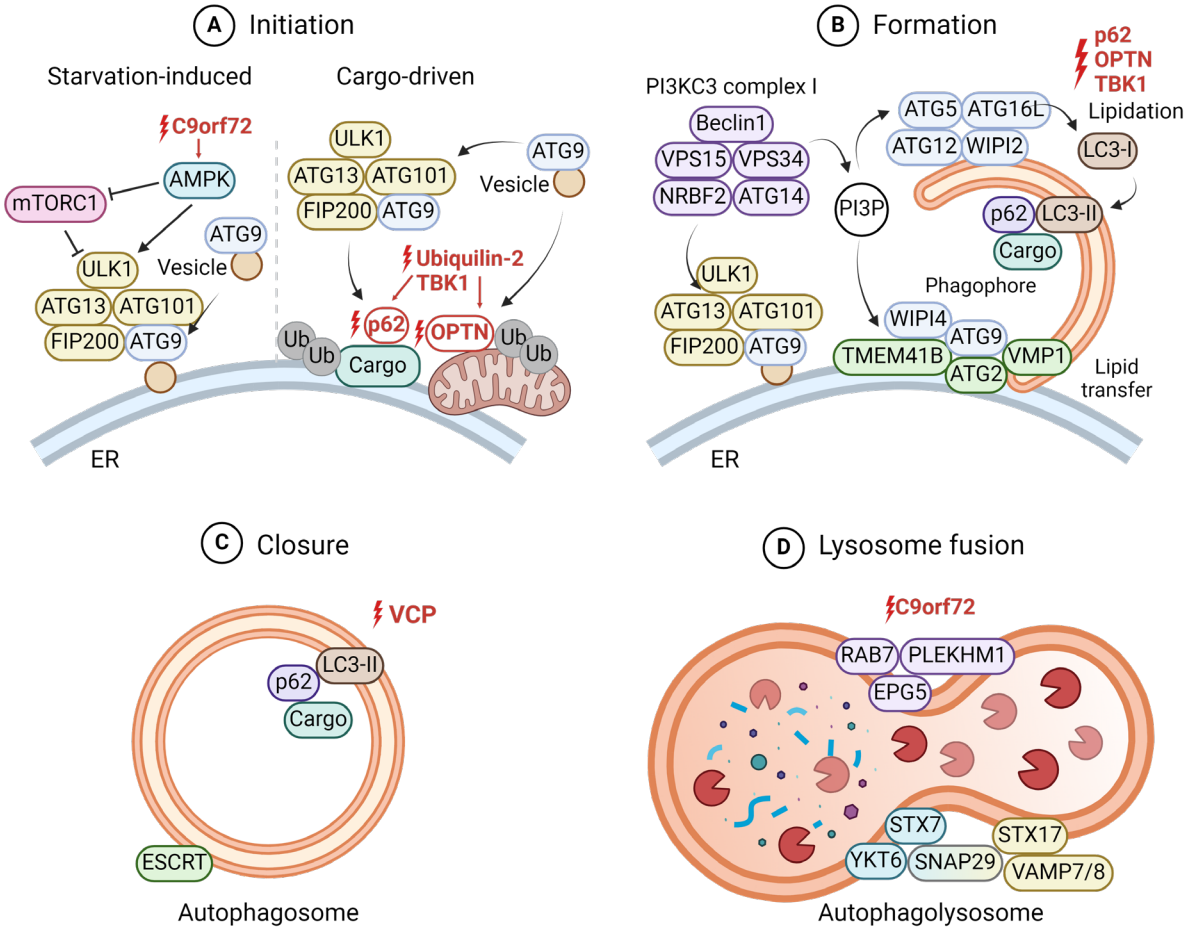

Figure 1-3 The macroautophagy pathway is disrupted in ALS.

The autophagy pathway selectively degrades proteins to maintain proteostasis. Multiple proteins encoded by ALS-associated genes are involved in autophagy, which are highlighted in red and denoted by a lightning bolt.

A) In response to starvation the ULK1 complex (ULK1, ATG13, ATG101 and FIP200) recruits ATG9 vesicles to the ER membrane by interaction with ATG101. Alternatively, initiation can be cargo-driven by adaptors such as p62 which promotes ULK1 complex assembly via interaction with FIP200, whilst mitophagy-related OPTN recruits ATG9 vesicles.

B) To form the phagosome, the ULK1 complex recruits the class III phosphatidylinositol 3–kinase complex I (PI3KC3–C1). This produces PI3P, which recruits its effector proteins WIPI2 and WIPI4. WIPI2 recruits the ATG12–ATG5–ATG16 complex to promote LC3 lipidation and insertion into the phagophore membrane. WIPI4 directs ATG2 to the phagophore membrane, to transfer phospholipids from the ER with ATG9, VMP1 and TMEM41B.

C) Autophagosomes are closed by the ESCRT complex.

D) Lysosomes are fused by tethering to autophagosomes by PLEKHM1, EPG5. Fusion is initiated by two SNARE complexes, STX17–SNAP29–VAMP7/8 and YKT6–SNAP29–STX7.

Closure of the autophagosome is mediated by the endosomal sorting complex required for transport (ESCRT), although this is not well characterised in mammals (Zhen *et al.*, 2020; Zhou *et al.*, 2019). After closure, pleckstrin homology domain-containing family M member 1 (PLEKHM1), ectopic P granules protein 5 homolog (EPG5) and Ras-related protein 7 (Rab7) tether autophagosomes to lysosomes (McEwan *et al.*, 2015; Wang *et al.*, 2016b). The two souble N-ethylmaleimide-sensitive factor attachment protein receptor (SNARE) complexes, STX17–SNAP29–VAMP7/8 and YKT6–SNAP29–STX7, trigger fusion of the autophagolysosomes (Bas *et al.*, 2018; Itakura *et al.*, 2012). This leads to degradation of their contents by acidic hydrolases, releasing the components back into the cytosol for recycling (Zhao and Zhang, 2019).

The C9orf72 protein is involved in the initiation of autophagy by aiding ULK1 translocation to the phagophore, and ALS-associated haploinsufficiency is thought to impair this process (Webster *et al.*, 2016). Ubiquilin-2 co-localises with optineurin, p62 and ULK1 to promote induction of autophagy, however ALS-mutant ubiquilin-2 no longer colocalises, suggesting a loss of function mechanism (Osaka *et al.*, 2015). Mutations in *OPTN* and *SQSTM1* (p62) are suggested to impair substrate delivery to the autophagosome (Rea *et al.*, 2014; Wong and Holzbaur, 2014). The *OPTN*^{E478G} mutation prevents binding to ubiquitin on the cargo, whilst *SQSTM1*^{L341V} mutation disrupts interaction with lipidated LC3-II on the phagosome (Goode *et al.*, 2016; Maruyama *et al.*, 2010). Both p62 and OPTN are partially regulated by TANK-binding kinase 1 (TBK1) phosphorylation, which promotes their interaction with LC3-II (Matsumoto *et al.*, 2015; Richter *et al.*, 2016). *TBK1* loss of function mutations cause ALS, further implicating dysregulation of autophagy as a pathogenic mechanism (Freischmidt *et al.*, 2015). Valosin-containing protein (VCP) is involved in proteasome-mediated protein degradation and affects autophagosome maturation (Ju *et al.*, 2009; Meyer and Weihl, 2014; Tresse *et al.*, 2010). ALS-linked mutations in *VCP* reduce its activity and thus decrease autophagosome maturation, further implicating autophagy defects in ALS pathology (Tang and Xia, 2016). Finally, the C9orf72 protein is recruited to lysosomes upon induction of starvation-induced autophagy (Amick *et al.*, 2020). In line with lysosomal dysfunction, it is well established that functional knock out of C9orf72 causes accumulation of enlarged lysosomes in mice (O'Rourke *et al.*, 2016; Shao *et al.*, 2020). This further implicates defective autophagy as a pathomechanism in ALS, due to lysosomal dysfunction.

1.1.4.3 Excitotoxicity

Secretion of glutamate by presynaptic terminals is the principal excitatory neurotransmission mechanism of the central nervous system (CNS) (Zhou and Danbolt, 2014). This elicits action potentials in postsynaptic neurons through the activation of N-methyl-D-aspartate (NMDA) and α-amino-3-hydroxy-5-methyl-4-isoxazolepropionic acid (AMPA) receptors, leading to the influx of sodium (Na^{2+}) and calcium (Ca^{2+}) ions and subsequent depolarisation of the neuron (Zhou and Danbolt, 2014). Neurotransmission is tightly regulated by both glutamatergic excitation and conversely by inhibition by the main inhibitory neurotransmitter γ-aminobutyric acid (GABA). GABA binds to two main postsynaptic receptors (GABA-A and GABA-B), to modulate chloride (Cl^-) and potassium (K^+) ion conductance respectively (Bowery *et al.*, 2002). This leads to hyperpolarisation and inhibition of action potential transmission. Imbalance of excitatory and inhibitory neurotransmission can lead to persistent Ca^{2+} influx into the postsynaptic neuron which can induce neuronal death (termed excitotoxicity) (Shaw and Ince, 1997).

There is increasing evidence that excitotoxity is involved in ALS development. Diminished GABA levels and depletion of GABAergic interneurons is reported in the cortex and spinal cord of ALS patients, leading to disinhibition of the motor neurons (Foerster *et al.*, 2012). Moreover, cell models of ALS and $SOD1^{G93A}$ transgenic mice exhibit reduced expression of excitatory amino acid transporter 2 (EAAT2) in astrocytes (Fray *et al.*, 1998; Howland *et al.*, 2002; Rothstein *et al.*, 1995). This results in reduced clearance of glutamate from synaptic clefts and thus increases vulnerability to restimulation (Boston-Howes *et al.*, 2006). Overactivation of excitatory receptors leads to prolonged and increased influx of Na^{2+} and Ca^{2+}, activating Ca^{2+} dependent enzymatic pathways and generating free radicals, which promote neurodegeneration (Carriedo *et al.*, 1998; Van Den Bosch *et al.*, 2006).

Finally, the drug Riluzole has been shown to extend survival in ALS patients by inhibiting glutamate release from presynaptic terminals and enhancing the function of postsynaptic GABA-A receptors (Vucic *et al.*, 2013). This suggests Riluzole acts by modulating the GABAergic system and reducing cortical hyperexcitability, although its effectiveness diminishes in later stages of ALS.

1.1.4.4 Mitochondrial dysfunction

There is increasing evidence from both *in vitro* and *in vivo* ALS models, that disruption of mitochondrial function is a common disease mechanism (Lee *et al.*, 2024). Mitochondria are closely associated to the endoplasmic reticulum at specialised contact sites known as MAM. These sites are essential for regulation of multiple physiological mechanisms, such as Ca^{2+} homeostasis, autophagy, and mitochondrial quality control, which are all processes disrupted in ALS (Basso *et al.*, 2018; De Vos *et al.*, 2012; Gomez-Suaga *et al.*, 2017). Increasing evidence suggests that disruption of ER-mitochondria

contacts may be a key early event in the development of ALS, and this is discussed in detail in section 1.2.

1.1.4.4.1 Disrupted mitochondrial function and morphology

In response to dynamic changes in cellular energy demands, mitochondria regulate the levels of oxidative phosphorylation (OXPHOS) to produce ATP. During OXPHOS, the mitochondrial electron transport chain creates an electrochemical gradient through a series of redox reactions (Chance and Williams, 1956). This electrochemical gradient generates the mitochondrial membrane potential (MMP), which can be measured as a proxy of mitochondrial function (Chen, 1988). In sporadic and familial models of *C9orf72, SOD1*, and TDP-43 related ALS, there is a decline in MMP (Dafinca *et al.*, 2016; Rajpurohit *et al.*, 2020; Walczak *et al.*, 2019; Wang *et al.*, 2019). This coincides with a reduction in the expression and activity of OXPHOS complexes, particularly complex I (Mehta *et al.*, 2021; Scaricamazza *et al.*, 2020; Wang *et al.*, 2021b). In line with reduced OXPHOS, in studies of *SOD1, FUS,* TDP-43 and sporadic ALS, there is consistent reduction in oxygen consumption and ATP production (Ghiasi *et al.*, 2012; Scaricamazza *et al.*, 2020; Wang *et al.*, 2019). Neurons rely on OXPHOS to meet energy demands and synaptic transmission (Hall *et al.*, 2012). Thus, loss of the mitochondrial capacity to produce ATP will prevent neuronal energy homeostasis and neuronal function, which precedes neurodegeneration (Lee *et al.*, 2024).

In addition to decreased mitochondrial function, defective mitochondrial morphology has been well documented in models of ALS. Increased mitochondrial fragmentation, indicated by decreased mitochondrial area or length and increased roundness has been reported in models of *C9orf72* (Onesto *et al.*, 2016), *SOD1* (De Vos *et al.*, 2007), TDP-43 (Choi *et al.*, 2020), and *FUS*-related ALS (Cha *et al.*, 2020). However, the expression of fusion/fission-regulating proteins such as mitofusin (MFN) -1 and -2, optic atrophy protein 1 (OPA1), and dynamin-related protein 1 (Drp1) varies between cell models, so what influences these pathological changes in morphology is not yet clear (Choi *et al.*, 2020; Khalil *et al.*, 2017; Onesto *et al.*, 2016).

1.1.4.4.2 Oxidative stress

Reactive oxygen species (ROS) are a group of molecules derived from molecular oxygen, which are formed by reduction–oxidation (redox) reactions (Sies and Jones, 2020). Imbalance between ROS production and the levels of antioxidants can lead to an excessive level of cellular ROS and a condition called oxidative stress (Gandhi and Abramov, 2012). Oxidative stress contributes to damage to DNA, proteins and lipids, and induces many pathophysiological mechanisms such as protein aggregation, ER stress and cell death (Cao and Kaufman, 2014; Kannan and Jain, 2000; Levy *et al.*, 2019). There is increasing evidence that oxidative damage occurs in ALS, as increased levels of ROS and levels of

biomarkers of oxidative stress have been reported in sALS patient cerebrospinal fluid and urine (Mitsumoto *et al.*, 2008) and in postmortem tissue from sALS and *SOD1*-associated ALS (Chang *et al.*, 2008; Shibata *et al.*, 2001). In addition to *SOD1*-ALS, other ALS-associated proteins have been linked to oxidative stress. In cell models of ALS, oxidative stress induced the mis-localisation and aggregation of TDP-43 and FUS protein inclusions, which is increased with ALS-associated *UBQLN2* mutations (Cohen *et al.*, 2015; Finelli *et al.*, 2015; Peng *et al.*, 2022). Overexpression of C9orf72 GR DPRs causes increased oxidative damage in an age-dependent manner (Lopez-Gonzalez *et al.*, 2016), suggesting that oxidative damage may be a common pathomechanism in ALS.

1.1.4.5 DNA damage accumulation

Persistent genotoxic stress leads to activation of signalling pathways that act to protect and repair DNA known as the DNA damage response (DDR) (Jackson and Bartek, 2009). There are multiple pathways that can be activated dependent on the type of DNA injury, which is discussed in more detail in section 1.3.2. Failure to complete DNA repair results in cellular senescence or apoptosis, therefore this response is vital for post-mitotic cells such as motor neurons (Iyama and Wilson, 2013). There is accumulating evidence that DNA damage accumulates during aging and in neurodegenerative diseases, and DNA damage is observed in multiple cell models of ALS (Schumacher *et al.*, 2021).

TDP-43 is the most researched ALS-associated protein with respect to defective DDR. Overexpression of pathological mutant TDP-43 protein in SHSY-5Y cells perturbs DNA repair (Guerrero *et al.*, 2019). Whilst postmortem spinal tissue from TDP-43-related ALS cases display accumulation of DNA damage markers such as γH2AX (Guerrero *et al.*, 2019). Furthermore, induction of DNA damage promotes the mislocalisation of wild type and mutant TDP-43, and the formation of stress granules (Konopka *et al.*, 2020). Considering TDP-43 aggregates are observed in 97% of ALS cases, DNA damaged induced TDP-43 pathology could underlie neurodegeneration in most ALS cases. Accumulation of DNA damage has also been observed in induced pluripotent stem cell (iPSC)-derived motor neurons harbouring *FUS* mutations in response to genotoxic treatments (Naumann *et al.*, 2018). In line with DNA damage accumulation, spinal postmortem tissue from *FUS*-ALS patients show significant nuclear markers of DNA damage (Wang *et al.*, 2018). Interestingly, mutation of the FUS nuclear localisation signal leads to impaired DDR signalling and formation of FUS aggregates, suggesting that FUS mislocalisation and DNA damage defects may be an early event in FUS-associated ALS (Naumann *et al.*, 2018).

DPRs produced by mutant C9orf72 cause the formation of foci that sequester proteins involved in DDR such as ataxia telangiectasia mutated (ATM), TDP-43, FUS, nucleophosmin (NPM) and DNA repair nuclease/redox regulator (APEX1), which could lead to loss of the repair pathways they mediate (Lee *et al.*, 2013; Nihei *et al.*, 2020). Overexpression of these toxic DPRs in iPSC-derived motor neurons lead to induction of DNA damage and oxidative stress (Lopez-Gonzalez *et al.*, 2016), whilst postmortem

tissue from C9orf72-ALS patients exhibit increased DNA damage accumulation (Nihei *et al.*, 2020). The never in mitosis A-related kinase 1 (NEK1) protein is essential for the proper function of the DDR, which is discussed in more detail in section 1.3.2.2 (Liu *et al.*, 2013). Briefly, human iPSC-derived motor neurons harbouring an ALS-associated *NEK1*^{R784*} mutation show increased basal levels of DNA damage, impaired DDR after induction of DNA damage and increased cell death (Higelin *et al.*, 2018). In line with the suggestion that NEK1 haploinsufficiency leads to defective DDR in ALS, iPSC-derived motor neurons from a patient harbouring both a *C9orf72* hexanucleotide repeat expansion and *NEK1* LOF mutation, showed increased levels of basal and induced DNA damage compared to cells with only a *C9orf72* mutation (Santangelo *et al.*, 2024). Together this implicates defective DNA damage response and repair as a key pathological mechanism in ALS.

1.1.4.6 Axonal transport

Neurons are morphologically complex cells that require efficient transport of proteins and organelles synthesised in the cell body to the distal axons (De Vos *et al.*, 2008). This is completed by a microtubule-based mechanism called axonal transport. Axonal transport can transport cargo to the synaptic terminals in an anterograde manner mediated by kinesins, or back to the cell body in a retrograde manner mediated by dynein (Hirokawa *et al.*, 2010). Evidence of disrupted mitochondrial transport has been reported in multiple models of ALS, including SOD1^{G93A} transgenic mice models (Bilsland *et al.*, 2010; De Vos *et al.*, 2007; Magrané *et al.*, 2012), overexpression of mutant VAPB^{P56S} (Mórotz *et al.*, 2012) and overexpression of mutant TDP-43 (Wang *et al.*, 2013; Xu *et al.*, 2010).

Axonal transport defects in ALS were first observed in SOD1^{G93A} mouse models (Zhang *et al.*, 1997). SOD1^{G93A} mice exhibit significantly reduced retrograde transport, with the level of transport correlating with disease progression (Bilsland *et al.*, 2010). Expression of SOD1 protein harbouring G93A, A4V, G85R or G37R ALS-linked mutations in cortical neurons disrupts transport in both directions (De Vos *et al.*, 2007). This suggests that mutant SOD1 may disrupt retrograde and anterograde transport. The kinase p38 mitogen-activated protein kinase (MAPK) is involved in regulation of microtubule dynamics (Komis *et al.*, 2011). Hyperactivated MAPK has been reported in SOD1^{G93A} transgenic mice and cells derived from ALS patients, leading to inhibition of anterograde and retrograde axonal transport (Ackerley *et al.*, 2003; Gibbs *et al.*, 2018; Morfini *et al.*, 2013). This suggests the transport defects in *SOD1*-ALS may be partly due to dysregulation of microtubule stability.

Defective mitochondrial transport is prominent in SOD1-ALS models, leading to depletion of, or abnormal clustering of mitochondria in the axon (De Vos *et al.*, 2007; Magrané *et al.*, 2012). In addition to SOD1, overexpression of ALS mutant VAPB^{P56S} leads to disrupted anterograde mitochondrial

transport (Mórotz *et al.*, 2012). *In vitro* and *in vivo* models of TDP-43 Q331K and M337V mutants exhibit reduced mitochondrial transport and prominent mitochondrial aggregation in neuron axons (Magrane *et al.*, 2014; Wang *et al.*, 2013). Additionally, overexpression of mutant human FUS^{P52L} in drosophila causes reduced mitochondrial motility (Chen *et al.*, 2016). Lastly, C9orf72 patient iPSC-derived motor neurons exhibit impaired mitochondrial transport (Fumagalli *et al.*, 2021). As mitochondrial dysfunction is widely reported in ALS (see section 1.1.4.4.1), reduced mitochondrial transport to the axons may exacerbate neurodegeneration due to the inability to meet cellular energy demands.

Mutations in proteins involved in axonal transport machinery, such as dynactin subunit 1 (*DCTN1*) and kinesin-1 heavy chain isoform 5A (*KIF5A*) and α-tubulin 4A isoform (*TUBA4A*) are suggested to contribute to ALS pathology, possibly by disrupting mitochondrial transport and microtubule stability (Nicolas *et al.*, 2018; Puls *et al.*, 2003; Smith *et al.*, 2014). As part of the dynactin complex, dynactin subunit 1 binds to dynein for retrograde transport (Hirokawa *et al.*, 2010). ALS-associated G59S mutation in *DCTN1* reduces the proteins microtubule binding affinity (Puls *et al.*, 2003). $DCTN1^{G59S}$ transgenic mice develop ALS-like phenotype including motor neuron loss and pathogenic protein aggregation (Lai *et al.*, 2007). Dynactin subunit 1 has been shown to bind to TDP-43 and loss of function mutations in *DCTN1* lead to TDP-43 accumulation (Deshimaru *et al.*, 2021). As TDP-43 aggregation disrupts axonal transport of mitochondria, this may be due to disruption of dynein.

Functional knock out of KIF5A impairs neurofilament transport leading to neurodegeneration (Xia *et al.*, 2003). ALS risk mutations in *KIF5A* change the proteins cargo-binding domain and lead to abnormal mitochondrial transport (Baron *et al.*, 2022; Xia *et al.*, 2003). The gene *TUBA4A* encoding the microtubule component α-tubulin 4A isoform is also implicated in ALS. *In silico* modelling suggests ALS-related *TUBA4A* mutations change the α-tubulin tertiary structure and affect protein dimerisation, which may prevent microtubule stabilisation, leading to protein aggregation (Ganne *et al.*, 2023).

Microtubule stability, regulated by proteins such as microtubule-associated protein 1B (MAP1B), is crucial for transport (Jimenez-Mateos *et al.*, 2006). MAP1B was found to be abnormally aggregated in the spinal cord of ALS patients, whilst in drosophila restoration of MAP1B was found to be protective in a model of ALS (Coyne *et al.*, 2014). Modifications such as acetylation of α-tubulin and phosphorylation of motor proteins also impact transport efficiency (Hammond *et al.*, 2010). Mutant TDP-43 has been shown to promote the deacetylation of tubulin tracks by dysregulating the levels of histone deacetylase 6 (HDAC6), which in turn disrupts mitochondrial transport (Fazal *et al.*, 2021; Kim *et al.*, 2010b). Mutant C9orf72 DPRs may obstruct translocation of kinesin and dynein to microtubules,

further hindering axonal transport (Fumagalli *et al.*, 2021). Overall, while axonal transport impairment is a key aspect of ALS, its precise role in disease progression requires further investigation.

1.2 ER-mitochondria contact sites are disrupted in ALS

1.2.1 Structural and functional ER-mitochondria tethers

Up to 20% of the mitochondrial surface area is closely opposed to the endoplasmic reticulum membrane, physically interacting at specialised regions of the ER (Rowland and Voeltz, 2012). It is well established that MAM are responsible for communication between the mitochondria and ER, which allows regulation of many physiological processes including Ca^{2+} homeostasis, synaptic activity and autophagy (Gomez-Suaga *et al.*, 2017; Gómez-Suaga *et al.*, 2019; Szabadkai *et al.*, 2006). Currently, over 10 protein complexes have been identified as structural (complexes that physically scaffold the organelles) and functional (complexes that regulate functional coupling of the organelles) ER-mitochondria tethering complexes (Lee *et al.*, 2024). These tethering complexes form stable contact sites, which in turn allows the organelles to respond dynamically to cellular changes. The identified tethering complexes and their known functions are discussed below and summarised in Table 1-2. As this project focusses on regulation of the VAPB/PTPIP51 tether, the structure and function of this is discussed in greater detail in section 1.2.2.

There are multiple newly established ER-mitochondria tethering proteins that have not yet been well characterised. The activating molecule in BECN1-regulated autophagy protein 1 (AMBRA1) protein has been shown to localise to Beclin1 at MAM to promote autophagosome formation (Garofalo *et al.*, 2016). This complex is also composed of endoplasmic reticulum lipid raft-associated protein 1 (ERLIN1), which is necessary for autophagosome formation in response to starvation (Manganelli *et al.*, 2021). FUN14 domain containing protein 1 (FUNDC1) has been suggested to be involved in maintenance of contact site formation, mitophagy and Ca^{2+} homeostasis (Li *et al.*, 2021). Mitochondrial FUNDC1 interacts with the ER-membrane inositol 1,4,5-triphosphate receptor 2 (IP3R2) to facilitate Ca^{2+} transfer between the organelles (Salin Raj *et al.*, 2023; Wu *et al.*, 2017). Loss of FUNDC1 impairs this Ca^{2+} signalling, whilst in response to high glucose levels the FUNDC1-IP3R2 interaction is augmented, leading to mitochondrial fragmentation (Salin Raj *et al.*, 2023).

Table 1-2 Structural and functional ER-mitochondria tethering proteins and their functions in cell homeostasis.
Adapted from (Lee *et al.*, 2024).

Tethering proteins	Functions	Reference
ATAD3A-WASF3-BiP	Physical tethering[1] and apoptosis[2]	Teng *et al.,* 2016[1], Chiang *et al.,* 2012[2]
BAP31-Fis1-PACS2	Physical tethering[1], lipid synthesis[1], apoptosis[1,2] and mitophagy[3]	Simmen *et al.,* 2005[1], Zhao *et al*., 2017[2], Moulis *et al.,* 2019[3]
Beclin1-AMBRA1-ERLIN1	Autophagy	Manganelli *et al.,* 2021
FUNDC1-IP3R2	Physical tethering and Ca^{2+} transfer	Wu *et al.,* 2017
INF2-SPIRE1C	Physical tethering and mitochondrial fission	Manor *et al.,* 2015
IP3R-Grp75-VDAC1	Ca^{2+} transfer	Szabadkai *et al.,* 2006, Atakpa-Adaji and Ivanova 2023
MFN1-MFN2/ MFN2-MFN2	Physical tethering[1,2], ER morphology[1] and Ca^{2+} transfer[1,2]	de Brito and Scorrano, 2008[1], Naon *et al.,* 2016[2]
MIGA2-VAPB	Phospholipid transfer	Kim *et al.,* 2022
MOSPD2-PTPIP51	Physical tethering	Di Mattia *et al.,* 2018
PDZD8-FKBP8	Phospholipid transfer[1], mitochondrial quality control[2,3,5], mitochondrial function[3] and Ca^{2+} transfer[4], physical tethering[5]	Shirane *et al*., 2020[1], Hewitt *et al.,* 2022[2], Liu *et al.,* 2023[3], Hirabayashi *et al.,* 2017[4], Nakamura *et al.,* 2024[5]
PS1-PS2	Ca^{2+} transfer and ATP production	Contino *et al.,* 2017
RRBP1–SYNJ2BP	Physical tethering and protein translation	Hung *et al.,* 2017
VAPB-PTPIP51	Physical tethering, Ca^{2+} transfer[1], autophagy[2], ATP production[3,] synaptic activity[4] and phospholipid transfer [5]	De Vos *et al.,* 2012[1], Gomez-Suaga *et al.,* 2017[2], Paillusson *et al.,* 2017[3], Gomez-Suaga *et al*., 2019[4], Yeo *et al.,* 2021[5]

To mediate mitochondrial division at MAM, the protein spire homolog 1C (SPIRE1C) localises to mitochondria where it links the actin cytoskeleton to the ER-anchored isoform of the protein inverted formin 2 (INF2) (Manor *et al.*, 2015). INF2 further stimulates mitochondrial division by recruitment of Drp1 to promote mitochondrial Ca^{2+} uptake through the mitochondrial Ca^{2+} uniporter (MCU) and Drp1-mediated membrane construction (Chakrabarti *et al.*, 2018). The presenilin proteins (PS1/PS2) are enriched at MAM and regulate Ca^{2+} shuttling between the ER and mitochondria (Contino *et al.*, 2017). This is suggested to be essential for ATP production, as loss of PS1 or PS2 leads to reduced mitochondrial respiration and disrupted mitochondrial morphology (Contino *et al.*, 2017). Finally, the tail-anchored, PDZ-domain-containing outer mitochondrial membrane (OMM) protein synaptojanin-2-binding protein (SYNJ2BP) has been reported to bind to the ER via ribosome-binding protein 1 (RRBP1) (Hung *et al.*, 2017). This is suggested to be a physical ER-mitochondria tether, as overexpression of SYNJ2BP increases ER-mitochondrial contact (Hung *et al.*, 2017). Whilst the function of this tether is not yet clear, it is suggested to be involved in protein translation, as the translation inhibitor cycloheximide reduces their interaction (Hung *et al.*, 2017).

1.2.1.1 IP3R-Grp75-VDAC1

The first ER-mitochondria tethering complex described was between IP3R, localised on the ER, and the OMM protein voltage-dependent anion channel 1 (VDAC1), acting through the chaperone glucose-related protein 75 (Grp75) (Rapizzi *et al.*, 2002; Szabadkai *et al.*, 2006). Knockdown or inhibition of Grp75 leads to loss of IP3R-VDAC1 interaction, although it is unclear whether this alters ER-mitochondria contact (Honrath *et al.*, 2017). Whilst this trimeric complex is essential for the propagation of ER-derived Ca^{2+} signals to mitochondria, it is not involved in physical tethering at MAM, as it has been shown that the loss of IP3R does not affect ER-mitochondria tethering (Csordás *et al.*, 2006). Modulation of the IP3R-Grp75-VDAC1 complex by DJ-1 has been reported, as loss of DJ-1 impairs the binding of this complex and causes IP3R accumulation at MAM (Liu *et al.*, 2019). Furthermore, modulation of this functional tether has been reported by Sigma-R1, which accumulates at MAM to stabilise IP3R in monomeric form and prolongs Ca^{2+} signalling into the mitochondria (Hayashi and Su, 2007).

1.2.1.2 ATAD3A-WASF3-Bip

ATPase family AAA domain-containing protein 3A (ATAD3A) is an inner mitochondrial membrane (IMM) protein that has been shown to physically tether the ER and mitochondria by interaction with the ER chaperone BiP via the cytosolic protein actin-binding protein WASF3 (Gilquin *et al.*, 2010; Teng *et al.*, 2016). It was reported that this tether is promoted in response to ER stress, due to increased localisation of WASF3 to the mitochondria, which can lead to mitochondrial dysfunction (Chiang *et al.*, 2012; Wang *et al.*, 2023). Further implicating this tether in regulation of ER stress, knockdown of

ATAD3A leads to dysregulation of protein processing that is necessary for inducing ER stress (Huang *et al.*, 2021). Sigma-R1 has been shown to stabilise ER-mitochondria contacts by interaction with ATAD3A, in order to prevent mitochondrial fragmentation (Watanabe *et al.*, 2023).

1.2.1.3 BAP31-Fis1-PACS2

The ER-associated B cell receptor-associated protein 31 (BAP31) can physically interact with the mitochondrial fission protein-1 (Fis1), which is regulated by the phosphofurin acidic cluster sorting 2 (PACS2) (Simmen *et al.*, 2005). PACS2 has been shown to regulate ER-mitochondria apposition by regulation of this tether, as depletion of PACS2 causes BAP31-dependent mitochondrial fragmentation and uncoupling from the ER (Simmen *et al.*, 2005). This protein complex is involved in induction of apoptosis, as procaspase-8 is recruited to Fis1/BAP31 during the early stages of apoptosis, leading to increased transfer of Ca^{2+} from ER to mitochondria to promote cell death (Iwasawa *et al.*, 2011; Zhao *et al.*, 2017). PACS2 is further implicated in the control of apoptosis, as it recruits BH3-interacting domain death agonist (Bid) to mitochondria to promote the release of cytochrome c and caspase-3 to initiate cell death (Moulis *et al.*, 2019; Simmen *et al.*, 2005). BAP31 has also been shown to form a bridging complex with the mitochondria-localised protein TOM40, mediating the regulation of autophagy and mitochondrial functions such as oxygen consumption (Namba, 2019).

1.2.1.4 MFN1-MFN2/MFN2-MFN2

MFN2 is one of the most studied tethers involved in ER-mitochondria juxtaposition. The protein is found in both organelles, as MFN2 localised on the ER generates homo- and heterotypic interactions with MFN1 or MFN2 on the OMM (de Brito and Scorrano, 2008; Filadi *et al.*, 2015). This interaction regulates Ca^{2+} transfer between the two organelles (de Brito and Scorrano, 2008). It was previously controversial as to whether MFN2 alone was sufficient to bind ER to mitochondria. However, recent studies have verified that loss of MFN2 reduces ER-mitochondria apposition and Ca^{2+} dynamics, confirming it is a true functional and structural ER-mitochondria tether (Filadi *et al.*, 2015; Naon *et al.*, 2016).

1.2.1.5 PDZD8-FKBP8

PDZ domain-containing protein 8 (PDZD8) is known to be present at MAM, where it is necessary for contact site formation and Ca^{2+} dynamics in synapses (Hewitt *et al.*, 2022; Hirabayashi *et al.*, 2017). Regulation of ER-mitochondria contacts was shown to be essential in regulating mitochondrial functions in neurons, such as mitochondrial morphology, mitochondrial membrane potential and respiratory metabolism (Liu *et al.*, 2023; Shirane *et al.*, 2020). It is currently elusive as to how PDZD8 regulates ER-mitochondria apposition, as no interacting partner had been identified. A recent preprint study suggests that the OMM protein peptidyl-prolyl cis-trans isomerase (FKBP8) is responsible for tethering PDZD8 to MAM, as overexpression of FKBP8 promotes ER-mitochondrial apposition

(Nakamura *et al.*, 2024). However, more research and peer view are necessary to determine if this a true physical tether, and whether loss of FKBP8 leads to the same effect as loss of PDZD8.

1.2.2 The VAPB/PTPIP51 ER-mitochondria tether

One of the best characterised structural and functional ER-mitochondria tethers is that of the ER resident protein VAPB and its mitochondrial tethering partner PTPIP51 (De Vos *et al.*, 2012). This protein tether is essential for the regulation of Ca^{2+} homeostasis, autophagy, and synaptic function (De Vos *et al.*, 2012; Gomez-Suaga *et al.*, 2017; Gómez-Suaga *et al.*, 2019; Paillusson *et al.*, 2017). The independent interactions and functions of VAPB and PTPIP51, and their role as an ER-mitochondria tether is discussed below.

1.2.2.1 Structure and function of VAPB

Vesicle-associated membrane protein (VAMP)-associated proteins (VAPs) are ubiquitously expressed transmembrane proteins located predominantly in the ER membrane (James and Kehlenbach, 2021). In humans there are two well characterised VAP proteins: VAPA and VAPB. VAPA and VAPB are structurally similar, both containing an N-terminal major sperm protein (MSP) domain, a putative coiled-coil domain, a C-terminal transmembrane (TM) domain, and two intrinsically disordered regions (Subra *et al.*, 2023) (Figure 1-4). Both proteins exist as dimeric proteins and can form homo- and heterodimers, which is suggested to be mediated by the coiled-coil domain (Kim *et al.*, 2010a; Nishimura *et al.*, 1999). Although both proteins contain GXXXG dimerisation motifs within their TM domains, this alone is insufficient to mediate dimerisation (Kim *et al.*, 2010a). Recent evidence suggests that the disordered regions act as flexible linkers between the conserved domains to mediate protein interactions (Subra *et al.*, 2023). Considering these linker regions are not well conserved between the VAP proteins, it is suggested they can specify protein binding to either VAPA or VAPB (James and Kehlenbach, 2021).

The MSP domain is considered to be the main binding domain of VAP proteins, mediating interactions with proteins containing an FFAT (two phenylalanines [FF] in an acidic tract) motif, which has a consensus sequence of $E_1F_2F_3D_4A_5X_6E_7$, (Kaiser *et al.*, 2005; Loewen *et al.*, 2003). When in complex, the aromatic ring of the phenylalanine in position four and the side chain of the alanine in position 5 of the FFAT motif bind to a hydrophobic pocket at the surface of the MSP domain (Di Mattia *et al.*, 2020; Kaiser *et al.*, 2005). This hydrophobic pocket is formed by aliphatic portions of side chains of key 'KFM' residues within the domain, which are K87/F88/M89 in VAPB and K94/F95/M96 in VAPA (Cabukusta *et al.*, 2020; Di Mattia *et al.*, 2020). Indeed, mutation of these key binding residues reduces interaction between VAPB and FFAT-containing proteins (Cabukusta *et al.*, 2020; Kors *et al.*, 2022a).

Contrary to this, only approximately 50% of VAP interactors contain an FFAT motif, suggesting that binding may not be limited to MSP-FFAT interactions (Murphy and Levine, 2016).

VAPB has been shown to mediate tethering of the ER to multiple other organelles, including peroxisomes, autophagosomes and the plasma membrane. The reported VAPB mediated ER-organelle contacts are summarised in Table 1-3. Peroxisomes are small enzyme-filled organelles that involved in metabolic pathways. ER-peroxisome interactions are suggested to be mediated by the VAPB MSP domain binding to the FFAT motifs of Acyl-CoA-binding domain-containing (ACBD) proteins -4 and -5 (Costello *et al.*, 2017a; Costello *et al.*, 2017b). This is suggested to regulate peroxisomal growth and motility.

The interaction between VAPB and endolysomal proteins StAR related lipid transfer domain-3 (STARD3), OSBP-related protein 1L (ORP1L) and sorting nexin 2 (SNX2) regulates cholesterol sensing and endolysomal dynamics (Alpy *et al.*, 2013; Dong *et al.*, 2016; Weber-Boyvat *et al.*, 2015). ER-golgi contacts mediated by VAPB/YIF1A binding are required for intracellular membrane trafficking in dendrites, regulating their morphology (Kuijpers *et al.*, 2013). VAPB has also been shown to interact multiple oxysterol-binding protein (OSBP) family proteins at ER-golgi contacts. These interactions regulate lipid homeostasis, alongside interactions with ceramide transfer protein (CERT) and membrane-associated phosphatidylinositol transfer protein 1 (PITPNM1) (Kawano *et al.*, 2006; Peretti *et al.*, 2008; Venditti *et al.*, 2019). To mediate OSBP cholesterol exchange, VAPB binds to the ER resident protein phosphatidylinositol-3-phosphatase SAC1 (Wakana *et al.*, 2015).

VAPB interactions with the plasma membrane are necessary for calcium dynamics, by interaction and clustering of Kv2.1 potassium channels and interaction with OSBP-related protein 3 (ORP3) (Darbyson and Ngsee, 2016; Johnson *et al.*, 2018). VAPB has also been implicated in ER interactions with the nuclear membrane, although this is not well characterised. VAPB is necessary for correct localisation of Emerin to the nucleus and is suggested to interact with the nucleoporin ELYS to regulate mitosis (James *et al.*, 2024; James *et al.*, 2019). VAPB is also involved in the regulation of autophagy, as VAPB interacts with FIP200, ULK1 and WIPI2 which are proteins necessary for autophagosome biogenesis (Zhao *et al.*, 2018).

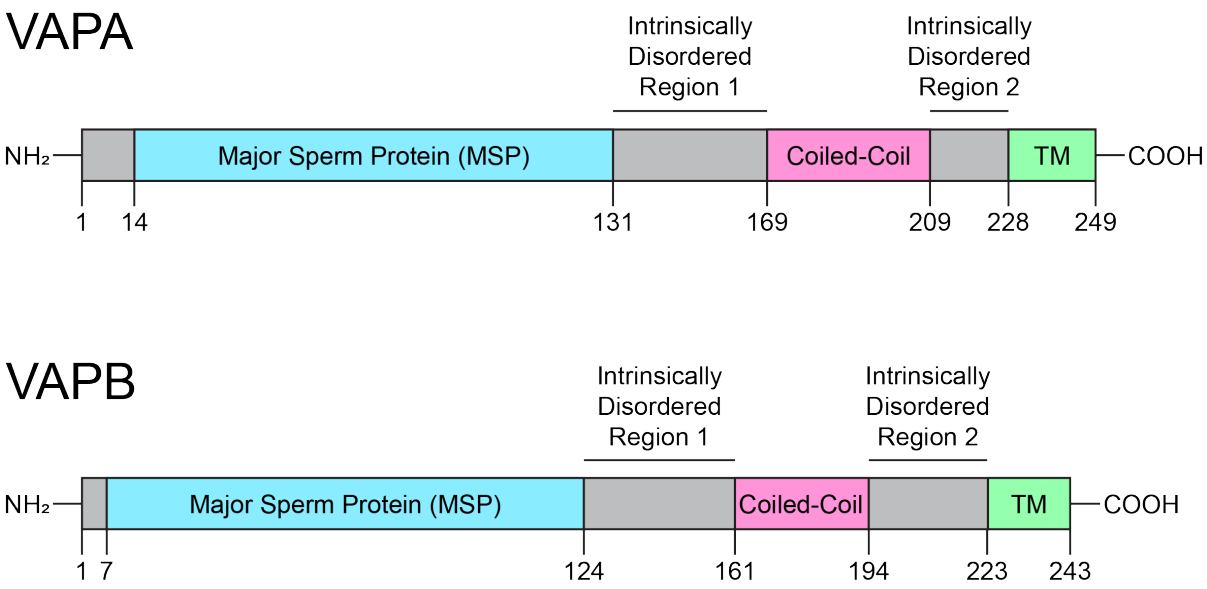

Figure 1-4 Schematic of VAPA and VAPB protein domains.

VAPA and VAPB are structurally similar proteins containing an N-terminal major sperm protein (MSP) domain (blue), a predicted coiled-coil domain (pink), and a C-terminal transmembrane (TM) domain (green). Both proteins also contain two intrinsically disordered regions.

Table 1-3 Summary of VAPB interactors at ER-contact sites.

Contact site	Interacting protein(s)	Function	Reference
ER-Golgi	OSBP family proteins	Lipid and cholesterol transfer	(Venditti *et al.*, 2019)
	CERT	Lipid transport	(Kawano *et al.*, 2006)
	PITPNM1	Phosphatidylinositol transport	(Peretti *et al.*, 2008)
	YIF1A	Axon and dendrite extension	(Kuijpers *et al.*, 2013)
ER-Plasma membrane	Kv2.1 potassium channels	Clustering of potassium channels at PM	(Johnson *et al.*, 2018)
	ORP3	Calcium dynamics, cell adhesion and migration, cytoskeletal regulation	(Darbyson and Ngsee, 2016; Gulyas *et al.*, 2020)
ER-Endosomes	STARD3	Endosomal dynamics and morphology, cholesterol sensing	(Alpy *et al.*, 2013)
	ORP1L	Cholesterol sensing, endo-lysosomal regulation	(Rocha *et al.*, 2009)
	SNX2	Physical tethering to endosomes	(Dong *et al.*, 2016)
ER-Mitochondria	PTPIP51	Calcium homeostasis, ATP production, autophagy, lipid transfer, synaptic function	(De Vos *et al.*, 2012; Gomez-Suaga *et al.*, 2017; Gómez-Suaga *et al.*, 2019)
	MIGA2	Mitochondrial metabolism, lipid storage in lipid droplets, neuronal homeostasis	(Freyre *et al.*, 2019; Xu *et al.*, 2020)
ER-Peroxisomes	ACBD4/5	Peroxisomal growth and motility	(Costello *et al.*, 2017a; Costello *et al.*, 2017b; Kors *et al.*, 2022a)
ER-Phagophore	FIP200, ULK1, WIPI2	Autophagosome biogenesis	(Zhao *et al.*, 2018)
ER-ER	SAC1	OSBP-mediated cholesterol exchange	(Wakana *et al.*, 2015)
ER-Nuclear membrane	Emerin	Emerin nuclear localisation	(James *et al.*, 2019)
	ELYS	Nuclear pore assembly and mitosis	(James *et al.*, 2024; James *et al.*, 2019)

1.2.2.2 Structure and function of PTPIP51

Regulator of microtubule dynamics protein 3 (RMDN3), more commonly known as PTPIP51, is a mitochondrial protein localised on the OMM. In humans there are three RMDN proteins (1-3), although they are not functionally or structurally similar. The functions of RMDN-1 and -2 have not been well characterised, but both are suggested to localise to the cytoskeleton to regulate microtubule growth and mitosis (Oishi *et al.*, 2007). RMDN2 has been suggested to bind to PTPIP51 in high throughput studies, however the pathways regulated by this interaction have not been investigated (Huttlin *et al.*, 2017). PTPIP51 is the best characterised RMDN protein and is known to contain an N-terminal TM domain, a putative coiled-coil domain, a tetratricopeptide-repeat-like (TPR) domain and two tandem FFAT-like motifs (Figure 1-5). The TM domain is essential for the localisation of PTPIP51 to mitochondria, which is suggested to regulate the induction of apoptosis (Lv *et al.*, 2006). The role of PTPIP51 in apoptosis is suggested to be mediated through its interaction with regulatory 14-3-3 proteins, as PTPIP51 contains two conserved 14-3-3 binding domains (AA 43 – 48 and 146 – 154) and reduction of PTPIP51 binding to 14-3-3 inhibits induction of apoptosis (Yu *et al.*, 2008). PTPIP51 was also shown to bind to protein tyrosine phosphatase 1B (PTP1B), a protein involved in the UPR and apoptosis (Brobeil *et al.*, 2010; Stenzinger *et al.*, 2009). This interaction has been confirmed in multiple human cell types and in mice, but the function of this interaction is not yet clear (Bobrich *et al.*, 2011; Brobeil *et al.*, 2011; Brobeil *et al.*, 2010).

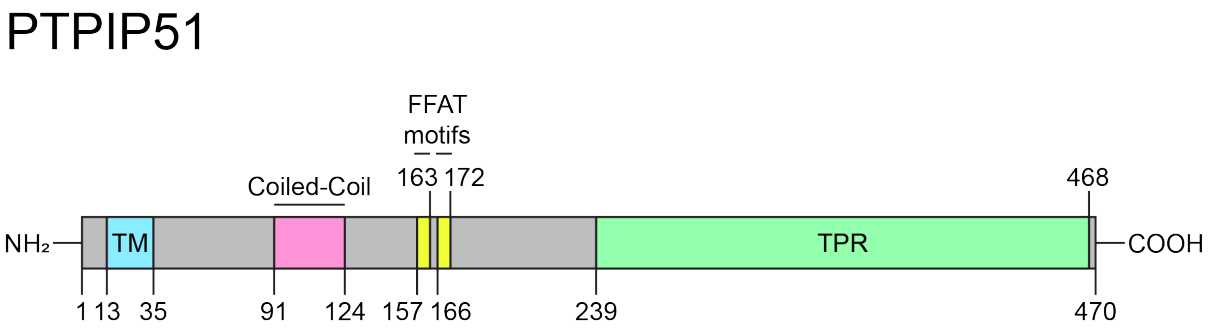

Figure 1-5 Schematic of the PTPIP51 protein domains.

The PTPIP51 protein contains a mitochondrial targeting N-terminal transmembrane (TM) domain (blue), a predicted coiled-coil domain (pink), and a C-terminal tetratricopeptide-repeat-like (TPR) domain (green). The protein also contains two tandem FFAT (two phenylalanines [FF] in an acidic tract) motifs (yellow).

1.2.2.3 VAPB/PTPIP51 ER-mitochondria tethering

It is well established that PTPIP51 forms a functional and structural ER-mitochondria tether with VAPB. Loss of either protein disrupts ER-mitochondria contact, whilst overexpression increases apposition between the organelles (De Vos *et al.*, 2012). PTPIP51 contains two FFAT-like motifs, one conventional FFAT-like motif ($_{166}$TFTDAES$_{172}$) and one phospho-FFAT motif ($_{157}$VYF**T**ASS$_{163}$) (Di Mattia *et al.*, 2020; Neefjes and Cabukusta, 2021). Multiple lines of evidence suggest that VAPB/PTPIP51 tethering is mediated by binding between the VAPB MSP domain and the PTPIP51 phospho-FFAT motif (Di Mattia *et al.*, 2018; Yeo *et al.*, 2021). Phosphorylation of the threonine in position four of the PTPIP51 phospho-FFAT motif has been suggested to act as a switch mechanism that regulates binding to the MSP domain of VAPB, however this has not yet be proven (Di Mattia *et al.*, 2020). A recent study suggests that phosphorylation of the acidic tract flanking the phospho-FFAT motif is necessary to promote binding to the MSP domain (Kors *et al.*, 2022a). This is suggested to be due to the addition of negatively charged phosphate groups which bind to the basic electropositive surface of the MSP domain. Indeed, the PTPIP51 phospho-FFAT motif is preceded by a series of serine and threonine residues which may be phosphorylated (S149, S151, T152, S154). Although, whether phosphorylation of these residues is necessary for binding is not yet clear. The model of MSP-FFAT binding is currently under contention, as a recent study found that removal of the PTPIP51 coiled-coil domain but not the phospho-FFAT motif led to reduced VAPB/PTPIP51 interaction (Mórotz *et al.*, 2022). Thus, more research is needed to elucidate this binding mechanism between VAPB and PTPIP51.

The interaction between VAPB and PTPIP51 is essential for regulation of multiple physiological processes, which is discussed in more detail in section 1.2.3. Alterations in expression of either protein results in changes to the extent of Ca^{2+} exchange between the two organelles (De Vos *et al.*, 2012). Through the regulation of mitochondrial Ca^{2+} uptake, the complex can control the autophagic process. Loss of VAPB/PTPIP51 tethering promotes the induction of autophagy, whilst tightening their contact inhibits the process (Gomez-Suaga *et al.*, 2017). The VAPB/PTPIP51 tether has been reported to form within synapses (Gómez-Suaga *et al.*, 2019). Here, stimulation of neuronal activity promotes ER-mitochondria contact, which may be necessary for formation of proper dendritic spine morphology (Gómez-Suaga *et al.*, 2019).

In addition to VAPB, PTPIP51 has been shown to bind to VAPA in multiple proteomic studies (Hein *et al.*, 2015; Vinayagam *et al.*, 2011). A recent study suggested that VAPB and VAPA may dimerise to interact with PTPIP51, but this needs further investigation to confirm (Cabukusta *et al.*, 2020). This study also confirmed the interaction between PTPIP51 and the MSP domain-containing proteins (MOSPD) -1, -2 and -3. MOSPD2 colocalises at the ER with VAPA and VAPB, although loss of MOSPD2 does not disrupt ER-mitochondria tethering, suggesting the PTPIP51/MOPSD2 interaction is not a true

structural tether (Di Mattia *et al.*, 2018). However, MOSPD -1 and -3 are suggested to form a protein complex that is sufficient to recruit PTPIP51 to the ER, although if loss of either protein disrupts ER-mitochondria apposition has not been investigated (Cabukusta *et al.*, 2020).

VAPB is also implicated in ER-mitochondria tethering independent of PTPIP51. Interactions between VAPB and the protein mitoguardin 2 (MIGA2) are necessary for regulation of mitochondrial dynamics and neuronal homeostasis (Freyre *et al.*, 2019; Xu *et al.*, 2020). Recent evidence suggests that contact between the ER and mitochondria in axons is regulated by coat protein complex I (COPI), as loss of COPI disrupts these contact sites and localisation of VAPB (Maddison *et al.*, 2023). Whilst VAPB is known to bind to multiple COP subunits, it is not yet clear whether these proteins form a protein tether at MAM (Yamanaka *et al.*, 2020).

1.2.3 The physiological role of ER-mitochondria contacts in neurons

ER-mitochondria communication regulates multiple cellular functions, including Ca^{2+} homeostasis, autophagy, and synaptic functions, which are critical for maintaining neuronal health (Gómez-Suaga *et al.*, 2019; Hirabayashi *et al.*, 2017). These functions are tightly regulated by ER-mitochondria contacts and are considered common features of neurodegenerative diseases (Krols *et al.*, 2016; Lee *et al.*, 2024). This leads to the hypothesis that apparently disparate pathological conditions could all be linked by common cellular pathways (Paillusson *et al.*, 2016).

1.2.3.1 Calcium homeostasis

The ER is the major site of Ca^{2+} storage within the cell. Whereas mitochondria protect the cytosol from high Ca^{2+} levels by playing the role of temporary Ca^{2+} buffer (Carreras-Sureda *et al.*, 2018). The transfer of Ca^{2+} from the ER to mitochondria is facilitated by the close proximity between the organelles. Release of Ca^{2+} from ER stores is mediated by the IP3R localised on the ER (Ahumada-Castro *et al.*, 2021). Upon release into the cytosol, mitochondria Ca^{2+} uptake is controlled by the OMM protein VDAC1, acting through the chaperone Grp75 (Rapizzi *et al.*, 2002; Szabadkai *et al.*, 2006). Import of Ca^{2+} into the mitochondria is then facilitated by transport through the inner mitochondrial membrane by the MCU (Marchi and Pinton, 2014). This ER-mitochondria Ca^{2+} exchange is pivotal for regulation of ER and mitochondrial dynamics (Figure 1-6). Influx of Ca^{2+} into the mitochondria promotes the synthesis of NAD+ and ATP by OXPHOS, as Ca^{2+} stimulates dehydrogenase enzymes with the TCA cycle to catalyse NADH and $FADH_2$ for the electron transport chain (Denton, 2009; Denton *et al.*, 1972). This ensures sufficient ATP is produced in response to dynamic changes in cellular energy demands (Bravo *et al.*, 2011; Denton *et al.*, 1972; Paillusson *et al.*, 2017; Turkan *et al.*, 2004).

In low levels of ATP and/or elevated cytosolic Ca^{2+}, a reduction in mitochondrial motility promotes the recruitment of mitochondria. This enhances local Ca^{2+} buffering and ATP synthesis to respond to the

change in the energy needs (Saotome *et al.*, 2008). In these conditions, the Ca^{2+} sensitive mitochondrial Miro/Milton protein complex, interacts directly with the kinesin-1 motor domain (Wang and Schwarz, 2009). This induces a shift of kinesin-1 from an active state to inactive state, preventing its interaction with microtubules and arresting anterograde mitochondrial movement in a Ca^{2+} - dependent manner (Wang and Schwarz, 2009). Dynamics of mitochondria are tightly interconnected with the dynamics of the ER, and these associations can be maintained when both organelles are moving. Therefore, the alteration of mitochondrial dynamics will impair ER dynamics, and vice versa (Brough *et al.*, 2005).

Due to the high metabolic cost to neurons required for synaptic activity, mitochondrial function and dynamics are tightly regulated at synapses (Datta and Jaiswal, 2021). VAPB/PTPIP51 ER-mitochondria tethering has been observed within synapses and it is reported that this regulates synaptic function (Gómez-Suaga *et al.*, 2019). Loss of either VAPB or PTPIP51, which reduces ER-mitochondria contacts, inhibits synaptic activity, and perturbs dendritic spine morphology (Gómez-Suaga *et al.*, 2019). The precise mechanism by which VAPB/PTPIP51 tethering regulates synaptic activity is not completely elucidated, but it is speculated that efficient Ca^{2+} signalling is fundamental to synaptic transmission since the discovery that presynaptic Ca^{2+} levels regulate neurotransmission release and synaptic plasticity (Datta and Jaiswal, 2021; Devine and Kittler, 2018; Gómez-Suaga *et al.*, 2019).

In mammalian neurons the ER-membrane protein PDZD8 has been shown to be necessary for ER-mitochondria tethering, and it has been suggested that this is due to tethering with the OMM protein FKBP8 (Hirabayashi *et al.*, 2017; Nakamura *et al.*, 2024). Importantly, PDZD8 is essential for the regulation of dendritic Ca^{2+} dynamics, as knockdown of PDZD8 in cortical neurons reduces dendritic mitochondrial Ca^{2+} after presynaptic-induced release from ER-stores (Hirabayashi *et al.*, 2017). This suggests that regulation of ER-mitochondria tethering is involved in regulation of dendritic Ca^{2+} dynamics, potentially contributing to synaptic plasticity (Tsuboi and Hirabayashi, 2021). As loss of Ca^{2+} homeostasis and synaptic activity are both correlated with a deviation from the physiological interaction between ER and mitochondria (Gómez-Suaga *et al.*, 2019).

Whilst Ca^{2+} influx is essential for mitochondrial function, prolonged or excessive mitochondrial Ca^{2+} exposure can lead to the opening of the mitochondrial permeability transition pore (mPTP), inducing cytochrome c release which activates the apoptosis pathway (Boehning *et al.*, 2003; Kroemer *et al.*, 2007). Impairment of Ca^{2+} homeostasis and exchange between the ER and mitochondria causes malfunction of folding of ER-localised proteins and an accumulation of these unfolded proteins (Bahar *et al.*, 2016). This stress leads to the activation of the UPR, which blocks the synthesis of the proteins in order to re-establish ER homeostasis. ER stress induces a preliminary activation of UPR, whereas its persistence triggers the apoptotic process (Rutkowski and Kaufman, 2004; Simmen *et al.*, 2005). In

response to prolonged ER stress Bid promotes translocation of the protein PACS2 from the ER to mitochondria to promote initiation of apoptosis (Simmen *et al.*, 2005). At the mitochondria surface Bid is cleaved from PACS2 leading to interaction with Bax/Bak to promote OMM permeability and cytochrome C release, initiating apoptosis. Moreover, PACS2 regulates apoptosis by inhibiting the cleavage of its tethering partner BAP31, which when activated acts as a pro-apoptotic signal by facilitating transfer of Ca^{2+} from ER to mitochondria (Simmen *et al.*, 2005; Wang *et al.*, 2011). The tight regulation of Ca^{2+} transfer between the ER and mitochondria is therefore pivotal for determination of cell fate.

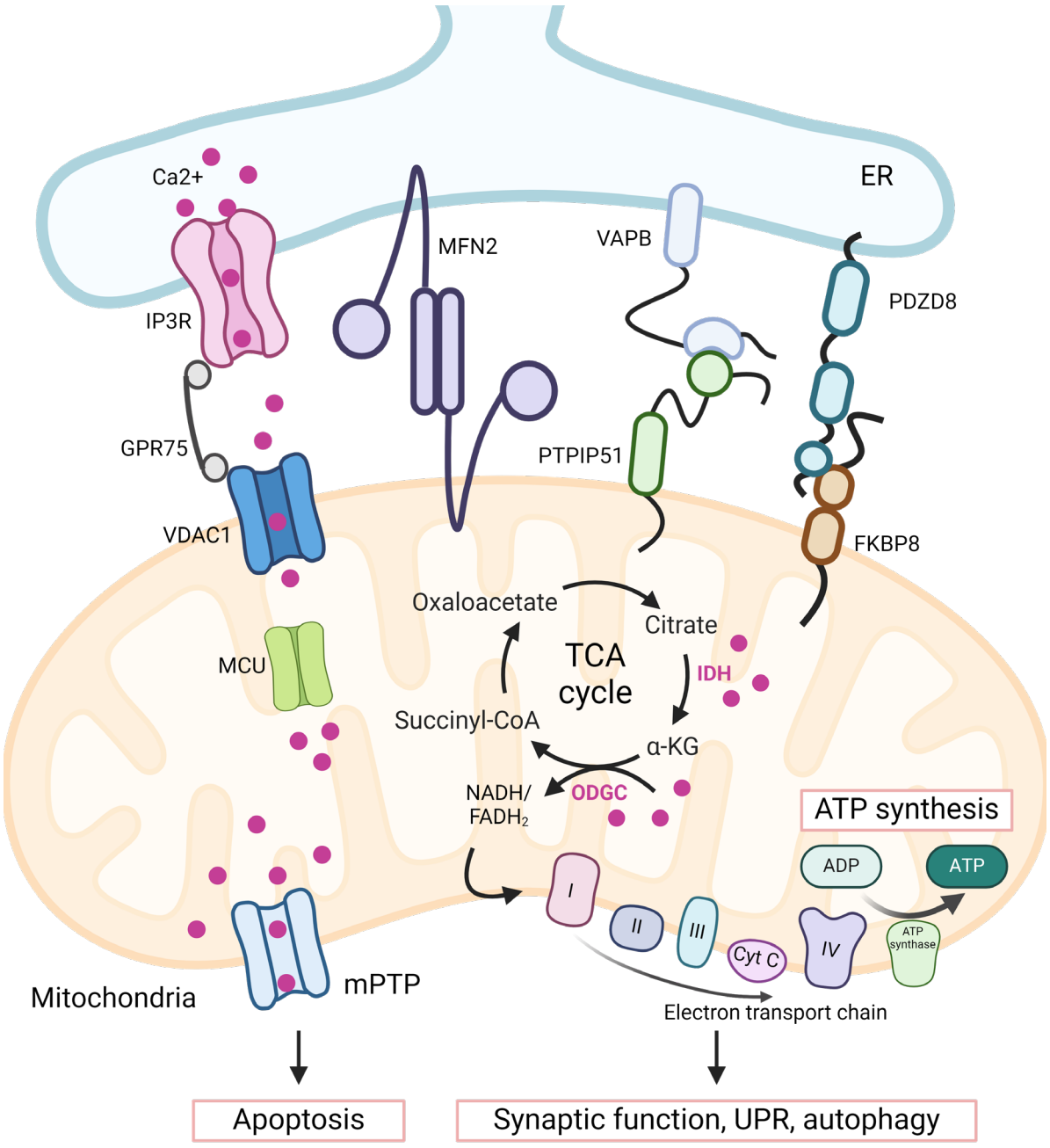

Figure 1-6 Summary of ER-mitochondria tethers involved in Ca^{2+} homeostasis.

The IP3R-Grp75-VDAC1 signalling complex mediates transfer of Ca^{2+} from ER stores to mitochondria. Upon mitochondrial uptake, the mitochondrial Ca^{2+} uniporter (MCU) mediates Ca^{2+} entry into the mitochondrial matrix. Ca^{2+} activates dehydrogenases isocitrate dehydrogenase (IDH) and oxoglutarate dehydrogenase complex (ODGC) in the tricarboxylic acid (TCA) cycle to produce NADH/$FADH_2$ which promote ATP synthesis. Maintenance of Ca^{2+} homeostasis is regulated by tethering between the two organelles. The complex formed by VAPB/PTPIP51 is essential for regulation of ER-mitochondria apposition and Ca^{2+} homeostasis. This leads to downstream regulation of autophagy and synaptic function. Mitofusin 2 (MFN2) homodimers regulate the ER-mitochondria apposition to control Ca^{2+} homeostasis. The PDZD8/FKBP8 tether is essential for the regulation of dendritic Ca^{2+} dynamics and synaptic function.

1.2.3.2 Autophagy

Neurons have stringent quality control pathways to ensure cellular homeostasis and functionality throughout their extended life cycle. Autophagy is critical for neuronal homeostasis through the removal of damaged or retired cellular components, and failure to properly regulate protein and organelle integrity is associated with the development of neurodegenerative diseases (Guo *et al.*, 2018; Kulkarni *et al.*, 2018). ER-mitochondria contacts have been implicated as the site of autophagosome formation, as in response to starvation the PI3K complex component ATG14 is recruited to these sites (Hamasaki *et al.*, 2013). Disruption of ER-mitochondria coupling inhibits ATG14 localisation and formation of the phagophore (Hamasaki *et al.*, 2013). Dysregulation of Ca^{2+} can also lead to disrupted autophagy. Disruption of Ca^{2+} transfer leads to translocation of AMPK to MAM, which activate autophagy via Beclin1, which is independent of mTORC1 (Ahumada-Castro *et al.*, 2019; Vicencio *et al.*, 2009). Contrary to the idea that ER-mitochondria contacts are the site of autophagosome formation, reduction of VAPB/PTPIP51 tethering causes a decrease in mitochondrial Ca^{2+} uptake, which triggers the activation of the autophagic process (Gomez-Suaga *et al.*, 2017). This discrepancy may be due to the differing methods of autophagy induction, suggesting the effect of ER-mitochondria contact domains in autophagy are dependent on the stimuli-specific signalling mechanisms of autophagy induction.

The selective degradation of impaired or excess mitochondria is known as mitophagy and emerging evidence suggests that multiple ER-mitochondria contact proteins are involved in this process. Prior to degradation, mitochondria are isolated from the mitochondrial network via fission which is regulated by Drp1 and Fis1 (Friedman *et al.*, 2011; Iwasawa *et al.*, 2011). The isolated mitochondria are engulfed by autophagosomes and degraded by fusion with the acidic lysosomes (Youle and Narendra, 2011). This process is regulated by the PINK1-Parkin pathway, whereby PINK1 localised to the OMM of depolarised mitochondria recruits Parkin from the cytoplasm (Narendra *et al.*, 2008). This leads to ubiquitination of OMM proteins present at MAM, including MFN2 (McLelland *et al.*, 2018) and VDAC1 (Ham *et al.*, 2020). Ubiquitination of these membrane proteins leads to identification by, and binding of LC3 and p62 on the autophagosome membrane, leading to mitochondrial degradation (Geisler *et al.*, 2010).

1.2.3.3 Lipid metabolism

ER-mitochondria contact sites are essential for the synthesis and transport of phospholipids (Yeo *et al.*, 2021) (Figure 1-7). These contact sites act as a hub for the synthesis of the phospholipid phosphatidylserine (PS) which is involved in apoptotic signalling (Glade and Smith, 2015). At the contact sites mitochondria uptake PS, which is converted into phosphatidylethanolamine (PE) (Petrungaro and Kornmann, 2019). PE is essential for promotion of mitochondrial biogenesis and

OXPHOS (Becker *et al.*, 2013; Bottinger *et al.*, 2012). As mitochondria cannot directly import PE, close association with the ER is necessary to maintain enrichment of PE in mitochondria (Vance and Tasseva, 2013). Disruption of mitochondrial PE levels impairs mitochondrial morphology, respiration, and dynamics, highlighting the importance of its regulation at MAM (Steenbergen *et al.*, 2005; Tasseva *et al.*, 2013). Cardiolipin (CL) regulates mitochondrial respiration, apoptosis and mitophagy (Belikova *et al.*, 2006; Chu *et al.*, 2013; McMillin and Dowhan, 2002). MAM regulate homeostasis of CL, as the CL precursor phosphatidic acid (PA) is derived from these sites (Osman *et al.*, 2011). Both PE and CL can bind to electron transport chain complexes to regulate OXPHOS and ATP production (Bottinger *et al.*, 2012; Tasseva *et al.*, 2013). Additionally, PE or CL deficiency results in mitochondrial dysfunction, exhibited by reduced MMP and ATP production (Bottinger *et al.*, 2012; Jiang *et al.*, 2000). Thus, MAM regulation of phospholipid transport is necessary for both energy metabolism and control of apoptosis.

Multiple ER-mitochondria tethering proteins are involved in the regulation of lipid homeostasis. The VAPB/PTPIP51 tether is necessary for transport of PA at MAM (Yeo *et al.*, 2021). Other VAPB and PTPIP51 tethering partners are also involved in this regulation. The PTPIP51 binding proteins ORP -5 and -8 interact with PTPIP51 at their lipid binding domain (Galmes *et al.*, 2016). This interaction is necessary to anchor ORP -5 and -8 at MAM (Galmes *et al.*, 2016). As ORP -5 and -8 promote transfer of PS at ER-plasma membrane contact sites, their interaction with PTPIP51 may involve this same lipid transfer function (Chung *et al.*, 2015).

The OMM protein MIGA2 forms a tether at MAM with VAPB (Freyre *et al.*, 2019; Kim *et al.*, 2022). At these contact sites MIGA2 has been shown to link the mitochondria to lipid droplets which are formed from the ER membrane (Freyre *et al.*, 2019). The MIGA2/VAPB interaction enhances the transport of PS and promotes the synthesis of triacylglycerols, which may facilitate lipid storage in lipid droplets (Freyre *et al.*, 2019; Kim *et al.*, 2022). RNA-dependent protein kinase (PKR)-like ER kinase (PERK), a protein with lipid kinase activity, interacts with VAPB (Sassano *et al.*, 2021). The function of this interaction is not yet clear, but PERK is also known to bind to the ER-mitochondria tethering protein MFN2 in response to cellular stress (Cao *et al.*, 2021; Munoz *et al.*, 2013). In homeostatic conditions MFN2 mediates the transfer of PS at MAM, although whether this involves PERK activity is not yet clear (Hernandez-Alvarez *et al.*, 2019).

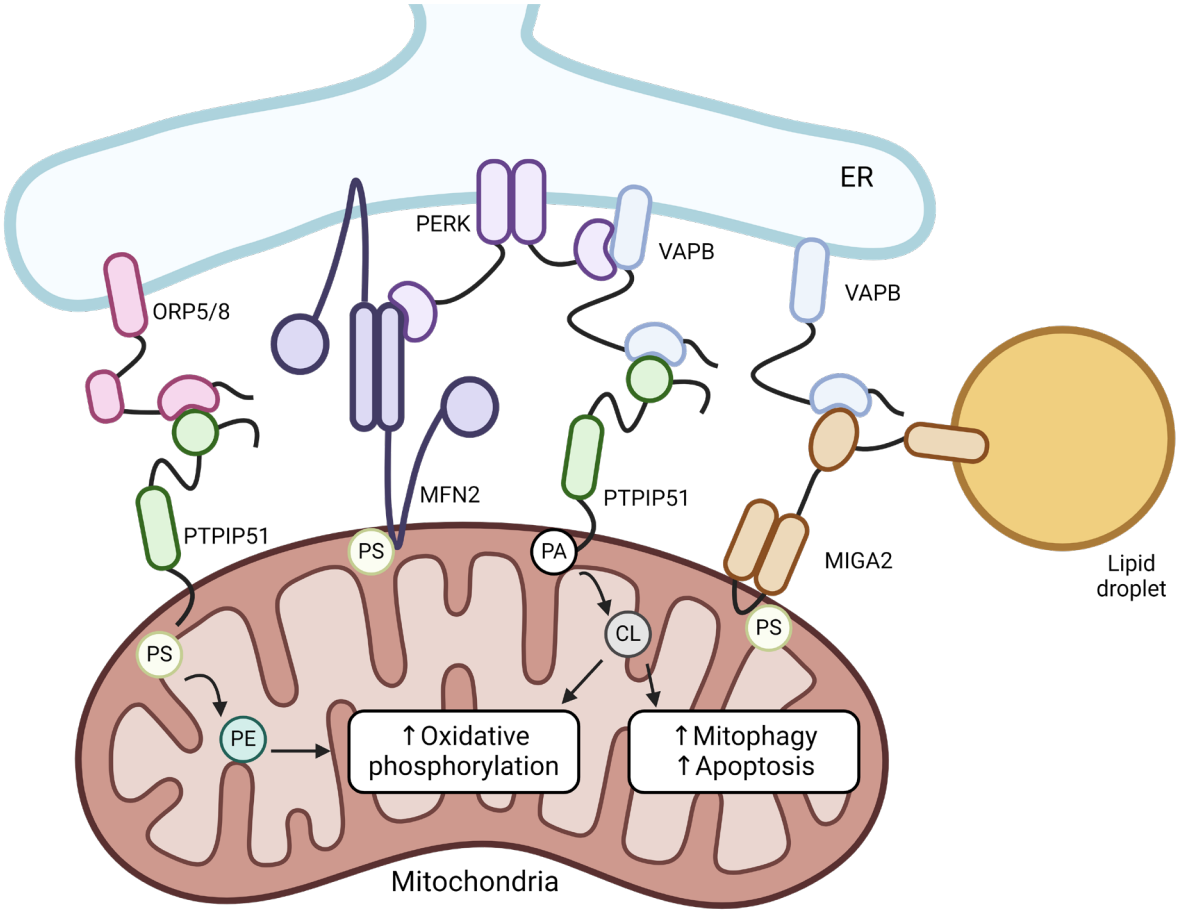

Figure 1-7 Summary of ER-mitochondria tethers involved in lipid homeostasis.

Modified from (Martín-Guerrero *et al.*, 2022). Multiple ER-mitochondria tethering proteins are involved in the regulation of lipid homeostasis. The VAPB-PTPIP51 tether is necessary for transport of phosphatidic acid (PA) which is a precursor of cardiolipin (CL) that regulates mitochondrial respiration, apoptosis and mitophagy. The PTPIP51-ORP5/8 interactions are suggested to promote transfer of phosphatidylserine (PS) which is converted into phosphatidylethanolamine (PE) in mitochondria. PE promotes mitochondrial biogenesis and oxidative phosphorylation. MIGA2/VAPB tethers link the mitochondria to lipid droplets and enhance the transport of PS. PERK, a protein with lipid kinase activity, interacts with VAPB and MFN2, but the role of these interactions is not yet clear. MFN2 homodimers mediate the transfer of PS at ER-mitochondria contact sites.

1.2.4 ER-mitochondria tethering is disrupted in ALS

Increasing evidence suggests that the disruption of ER-mitochondria contacts is a key pathological mechanism in ALS. In a recent high-throughput study of the effect ALS genes on ER-mitochondria contact, it was found that 76% (16/21) of the genes investigated caused disruption of contact site integrity (Sakai *et al.*, 2021). This suggests that dysregulation of ER-mitochondria contacts may be a common pathomechanism in ALS (Figure 1-8). Evidence of disrupted ER-mitochondria contact in models of ALS is described below, and a summary is described in Table 1-4.

1.2.4.1 TDP-43 and FUS

Expression of wild type or pathological TDP-43 or FUS fALS mutants leads to significant reductions in VAPB/PTPIP51 ER-mitochondria tethering and perturbed Ca^{2+} homeostasis (Stoica *et al.*, 2014; Stoica *et al.*, 2016). Neither TDP-43 nor FUS directly interact with PTPIP51 or VAPB but act through the activation of the glycogen synthase kinase-3β (GSK3β) by inhibiting its phosphorylation on Serine-9. Activated GSK3β results in reduced VAPB/PTPIP51 interaction, and disrupted Ca^{2+} signalling and ATP production (Stoica *et al.*, 2014; Stoica *et al.*, 2016). Inhibiting GSK3β corrected the TDP-43 or FUS damage to ER-mitochondria signalling (Stoica *et al.*, 2016). This suggests the VAPB/PTPIP51 tether complex may be targeted for damage by TDP-43 and FUS through GSK3β activation, thereby contributing to the pathological features of ALS.

In transgenic mice, overexpressing human TDP-43 caused abnormal juxtanuclear aggregation of mitochondria and dysfunctional mitochondrial dynamics, with enhanced levels of ER-mitochondria contact protein Fis1 and reduced levels of MFN1 (Xu *et al.*, 2010). On the other hand, TDP-43 down-regulation in HeLa cells leads to a loss of ER-mitochondria contact site density (Peggion *et al.*, 2021). This may explain why loss of functional TDP-43 in ALS leads to dysregulated ER-mitochondria contacts, thereby contributing to the pathological features of ALS.

1.2.4.2 SigmaR1 and SOD1

Under physiological conditions, SigmaR1 is found highly expressed at MAM of spinal motor neurons where it is involved in Ca^{2+} signalling by maintaining the stability of IP3R (Hayashi and Su, 2007; Mavlyutov *et al.*, 2010). The downregulation or loss of SigmaR1 function in motor neurons has been shown to stunt axon extension and results in disrupted ER-mitochondria contacts and Ca^{2+} dysfunction, thus generating ER stress and defects in mitochondrial dynamics and transport (Bernard-Marissal *et al.*, 2015). Additionally, SigmaR1 requires the mitochondria membrane AAA ATPase ATAD3A to remain at MAM. Here SigmaR1 inhibits mitochondrial fragmentation, with both SigmaR1-deficient or SOD1-linked ALS mice exhibiting fragmented mitochondria (Watanabe *et al.*, 2023). Moreover, disruption of SigmaR1 in mice causes an ALS-like motor disability phenotype (Luty *et al.*, 2010). Whereas the same SigmaR1 disruption in transgenic mice expressing ALS-associated mutant

SOD1 resulted in earlier disease onset and disturbed ER-mitochondria contact site integrity (Watanabe *et al.*, 2016).

Motor neurons from SOD1^{G93A}-mutant mice have disrupted Ca^{2+} homeostasis (Lautenschlager *et al.*, 2013). *In vitro* ALS-related mutant SOD1 aggregates and accumulates at MAM, impairing the integrity of this domain (Watanabe *et al.*, 2016). Interestingly, activation of SigmaR1 in SOD1-mutant mice protects ER-mitochondria contact site integrity and maintains ER-mitochondria contacts and Ca^{2+} homeostasis (Watanabe *et al.*, 2016). SOD1^{G93A} transgenic mice exhibit reduced levels of VAPB protein, which may result in reduced VAPB/PTPIP51 tethering (Teuling *et al.*, 2007). Neuronal overexpression of human VAPB in SOD1^{G93A} transgenic mice, caused prolonged lifespan and survival of spinal motor neurons in addition to slowed disease progression (Kim *et al.*, 2016). This suggests that rectification of ER-mitochondria contact site dysfunction could be a viable therapeutic strategy in SOD1-ALS.

1.2.4.3 C9orf72

Recent evidence has shown that in iPSC-derived cortical neurons from patients carrying a mutation in C9orf72, there is disruption of the VAPB/PTPIP51 tether and IP3R-VDAC1 interactions (Gomez-Suaga *et al.*, 2022). In hippocampal neurons isolated from C9orf72 transgenic mice containing 450 hexanucleotide GGGGCC repeats, a decrease in interaction between VAPB and PTPIP51 has also been observed prior to onset of disease (Gomez-Suaga *et al.*, 2022). Furthermore, expression of mutant C9orf72-associated pathogenic DPR proteins also disrupted VAPB/PTPIP51 and IP3R-VDAC1 interactions in rat cortical neurons and caused disruption of Ca^{2+} signalling in SH-SY5Y cells (Gomez-Suaga *et al.*, 2022). This has been suggested to be due to activation of GSK3β, in a manner similar to FUS and TDP-43. Together, this implicates a common pathological mechanism of dysregulated MAM caused by the three of the most common ALS-associated mutations.

1.2.4.4 VCP

Vacuolar protein sorting-associated protein 13D (VPS13D) is a ubiquitously expressed protein with known roles in mitochondrial morphology, dynamics and mitophagy (Anding *et al.*, 2018; Insolera *et al.*, 2021). VPS13D interacts with VCP in order to negatively regulate the level of VAPB at MAM, leading to a reduction in VAPB/PTPIP51 tethering (Du *et al.*, 2021). On the other hand, inhibition of VPS13D, leads to an increase in ER-mitochondria tethering which is only rescued by the suppression of PTPIP51 and VAPB. As VCP mutations cause familial ALS and VCP is known to regulate the stability of FUS granules, this negative regulation of ER-mitochondria contacts may be linked to mechanisms related to ALS development (Johnson *et al.*, 2010; Yasuda *et al.*, 2022).

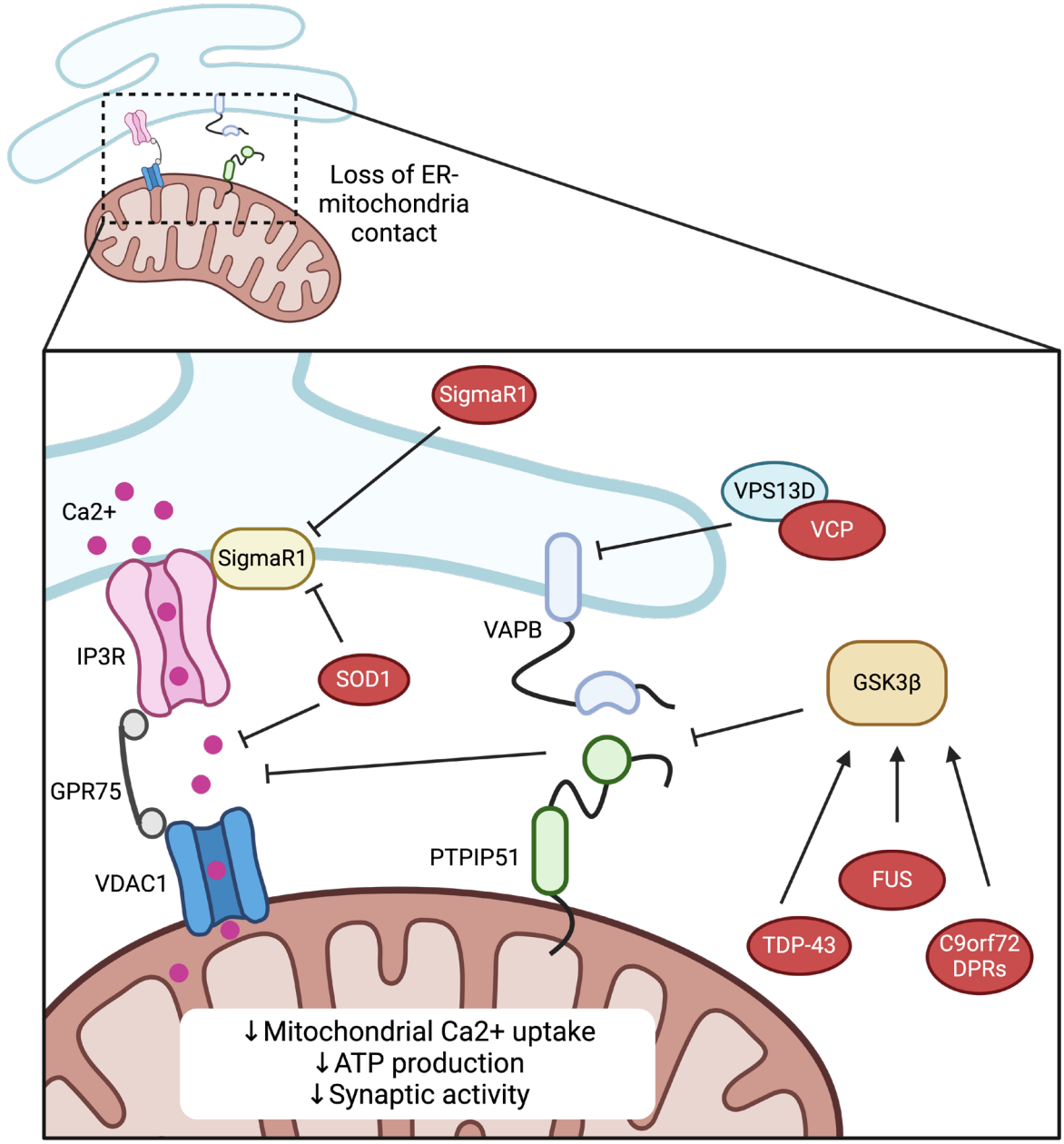

Figure 1-8 Summary of ER-mitochondria tethering dysfunction in ALS.

Modified from (Martin-Guerrero *et al.* 2022). ALS-associated genetic mutations disrupt IP3R-Grp75-VDAC1 and VAPB/PTPIP51 ER-mitochondria contacts. Mutant SigmaR1 and SOD1 disrupt the function of wild type SigmaR1 to maintain IP3R at the ER membrane. This leads to defective transport of Ca^{2+} from ER stores to the mitochondria and downstream effects on ATP production and synaptic activity. C9orf72-derived toxic DPRs, mutant TDP43 and FUS activate GSK3β kinase. GSK3β activation inhibits VAPB/PTPIP51 tethering. Wild type VCP in association with VPS13D negatively regulates VAPB protein. Mutant VCP leads to increased VAPB/PTPIP51 tethering which can lead to Ca^{2+} overload and mitochondrial dysfunction.

Table 1-4 Summary of ER-mitochondria tethering dysfunction in *in vitro* and *in vivo* models of ALS.
Modified from (Lee et al., 2024).

Model	ALS Mutation/Pathology	Observed ER-mitochondria tethering dysfunction	Reference
C9orf72			
iPSC-derived cortical neurons	C9orf72 GGGGCC repeat expansions	Loss of VAPB-PTPIP51 tethering and loss of IP3R-VDAC1 interaction	Gomez-Suaga *et al.* 2022
Mutant C9orf72 hippocampal neurons	Transgenic mice expressing 450 C9orf72 GGGGCC repeat expansions	Loss of VAPB-PTPIP51 tethering	Gomez-Suaga et al. 2022
Rat cortical neurons	Overexpression of poly-GA, poly-GR and poly-PR DPRs	Loss of VAPB-PTPIP51 tethering and loss of IP3R-VDAC1 interaction	Gomez-Suaga et al. 2022
SH-SY5Y cells	Overexpression of poly-GA, poly-GR and poly-PR DPRs	Disrupted Ca^{2+} transfer	Gomez-Suaga et al. 2022
FUS			
HEK293 cells	Overexpression of WT or fALS FUS mutations (R521C & R518K)	Disrupted Ca^{2+} transfer	Stoica *et al.*, 2016
NSC34 cells	Overexpression of WT or fALS FUS mutations (R521C & R518K)	Loss of VAPB-PTPIP51 tethering, decreased MAM density and reduced ATP production	Stoica *et al.,* 2016
Mouse spinal motor neurons	Transgenic mice expressing WT human FUS (hFUS)	Loss of VAPB-PTPIP51 tethering	Stoica *et al.* 2016
TDP-43			
HEK293 cells	Overexpression of WT or fALS TDP-43 mutations (M337V, Q331K, A382T, G348C)	Loss of VAPB-PTPIP51 tethering and disrupted Ca^{2+} transfer	Stoica *et al.,* 2014
NSC34 cells	Overexpression of WT fALS TDP-43 mutations (M337V, Q331K, A382T, G348C)	Loss of VAPB-PTPIP51 tethering and decreased MAM density	Stoica *et al.,* 2014

Model	ALS Mutation/Pathology	Observed MAM dysfunction	Reference
TDP-43			
$TDP\text{-}43_{PrP}$ mouse spinal motor neurons	Transgenic mice expressing WT human TDP-43 (hTDP-43)	Loss of VAPB-PTPIP51 tethering[1], mitochondrial aggregation[2] and dysregulated expression of MAM proteins Fis1 and MFN1[2]	Stoica *et al.,* 2014[1], Xu *et al.,* 2010[2]
HeLa cells	Knock down of TDP-43	Decreased MAM density and disrupted Ca^{2+} transfer	Peggion *et al.,* 2021
SigmaR1			
$SigmaR1^{-/-}$ mouse spinal motor neurons	Knock out of SigmaR1	Loss of IP3R-VDAC1 interaction[1], decreased MAM density[1,3], disrupted Ca^{2+} transfer[1], ER stress[1], disrupted mitochondrial morphology, dynamics and transport[1], mitochondrial fragmentation[2]	Bernard-Marissal *et al.* 2015[1], Watanabe *et al*. 2023[2], Watanabe *et al.* 2016[3]
N2A cells	Overexpression of SigmaR1 fALS mutations (E102Q & L95fs)	Disrupted Ca^{2+} transfer	Watanabe *et al.* 2016
HeLa cells	Knock down of SigmaR1	Mitochondrial fragmentation	Watanabe et al. 2023
SOD1			
$SOD1^{G85R}$ mouse spinal motor neurons	Transgenic mice expressing mutant human $SOD1^{G85R}$	Decreased MAM density and IP3R mis-localisation	Watanabe *et al.* 2016
$SOD1^{G93A}$ mouse spinal motor neurons	Transgenic mice expressing mutant human $SOD1^{G93A}$	Mitochondrial fragmentation[1] and disrupted Ca^{2+} transfer[2]	Watanabe *et al*. 2023[1], Lautenschlager et al. 2013[2]
VAPB			
COS-7, N2A and NSC-34 cells	Overexpression of mutant $VAPB^{T46I}$	Aggregation of VAPB into insoluble puncta	Chen *et al.* 2010

Model	ALS Mutation/Pathology	Observed MAM dysfunction	Reference
VAPB			
Rat cortical neurons	Overexpression of mutant VAPB^{P56S}	Disrupted mitochondrial transport and disrupted Ca^{2+} transfer	Morotz *et al.* 2012
VAPB^{P56S} mouse spinal motor neurons	Transgenic mice expressing mutant human VAPB^{P56S}	Aggregation of VAPB into insoluble puncta, increased ER stress, increased apoptosis and VAPB mis-localisation	Aliaga *et al.* 2013
Post-mortem spinal cord tissue	Various sALS and fALS patients	Decreased expression of VAPB[1,2] and loss of VAPB-PTPIP51 tethering[2]	Anagnostou *et al.* 2010[1] and Hartopp *et al.* 2022[2]
iPSC-derived motor neurons	Expression of mutant VAPB^{P56S}	Decreased expression of VAPB	Mitne-Neto *et al.* 2011
VCP			
U2OS cells	Inhibition of VCP with allosteric inhibitor NMS873 or knock down of VCP	Hyper increased MAM density	Du *et al.* 2021

1.3 The NEK1/C21orf2 protein complex in health and disease

Never in mitosis A-related kinase 1 (NEK1), encoded by the *NEK1* gene, is a member of the NEK family of serine/threonine kinases that mediate cell cycle regulation (Fry *et al.*, 2017; Fry *et al.*, 2012). The NEK1 protein consists of an N-terminal kinase domain, a basic domain, four sequential coiled-coil domains and two nuclear export sequences (Figure 1-9). It was recently reported that the C-terminal domain of NEK1 is necessary for binding to the N-terminal leucine-rich repeat domains of the protein C21orf2 (also known as cilia- and flagella-associated protein 410 (CFAP410)) (Gregorczyk *et al.*, 2023). NEK1 is both physically and functionally associated to C21orf2, and both proteins are essential for the regulation of ciliogenesis (Wheway *et al.*, 2015; White and Quarmby, 2008) and DNA damage repair (Chen *et al.*, 2011; Fang *et al.*, 2015). The C21orf2 protein has not been well characterised, but it is suggested to contain an N-terminal mitochondrial localisation sequence, three leucine rich repeats and a C-terminal leucine rich repeat (Figure 1-9). A recent study suggested that the C-terminus of C21orf2 forms a tetrameric helical bundle that regulates its localisation, although this is yet to be validated (Stadler *et al.*, 2022).

The C21orf2 protein is targeted for degradation by ubiquitination by the substrate recognition component of the SCF (SKP1-CUL1-F-box protein)-type E3 ubiquitin ligase complex; F-box only protein 3 (FBXO3) (Watanabe *et al.*, 2020). It is reported that NEK1-mediated phosphorylation stabilises the C21orf2 protein by inhibiting its interaction with FBXO3, which in turn stabilises the NEK1 protein (Watanabe *et al.*, 2020). It is suggested that in cells C21orf2 protein only exists when in complex with NEK1, but not vice versa, which would explain the C21orf2-independent roles of NEK1 such as mitosis regulation (Gregorczyk *et al.*, 2023).

Genetic mutations in *NEK1* and *C21orf2* are linked to several skeletal dysplasias such as Jeune syndrome, spondylometaphyseal dysplasia (SMD) and autosomal recessive Majewski type short-rib polydactyly syndrome (SRPS) (McInerney-Leo *et al.*, 2015; McInerney-Leo *et al.*, 2017; Thiel *et al.*, 2011; Wang *et al.*, 2017; Wang *et al.*, 2016a). Missense and loss of function mutations in *NEK1* and risk mutations in *C21orf2* are linked to ALS, which is described in more detail in section 1.3.3 (Brenner *et al.*, 2016; van Rheenen *et al.*, 2016). This suggests that close association of the two proteins may be necessary for their proper function. Therefore, further investigation into the pathways that NEK1 and C21orf2 regulate may highlight novel targets for therapeutic intervention of multiple diseases.

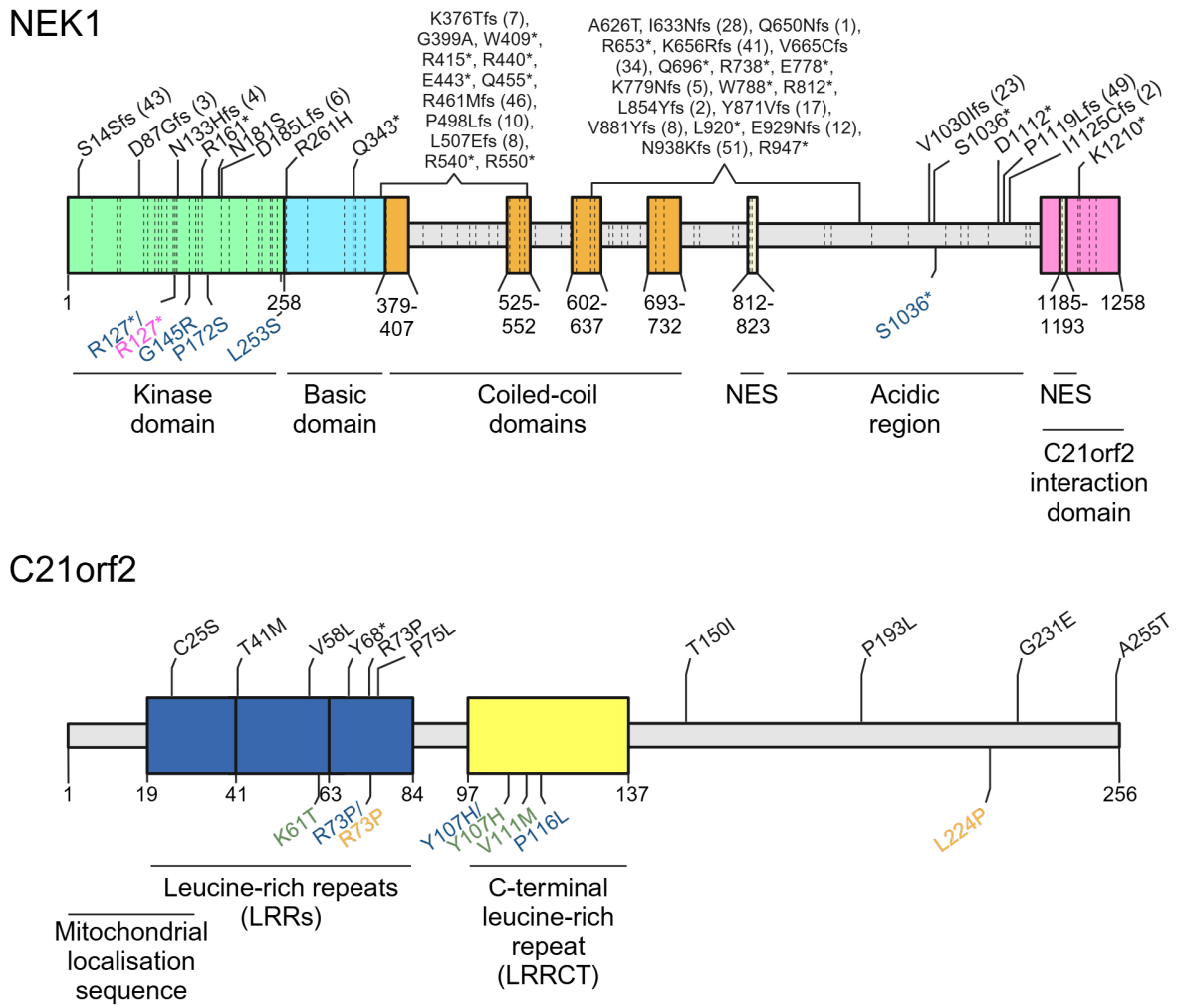

Figure 1-9 Schematic of the NEK1 and C21orf2 proteins and disease-associated mutations.

Asterisk denotes the mutation into a premature stop codon. For NEK1 fs denotes a frameshift mutation, followed by the number of amino acids until a premature stop codon in brackets. The amino acid substitutions encoded by missense mutations are colour-coded according to disease as indicated. Red labelled ALS-associated mutations for NEK1 are loss of function, whilst the location of identified missense mutations are indicated by a black dashed line. ALS = Amyotrophic lateral sclerosis, SMD = Spondylometaphyseal dysplasia, SRPS = Short-rib polydactyly syndrome, NES = Nuclear export sequence.

1.3.1 NEK1 and C21orf2 mediate ciliogenesis

Primary cilia are non-motile microtubule projections that protrude from the surface of mammalian cells. Cilia act as sensory organelles, to allow cells to respond to stimuli in the extracellular environment and are involved in multiple essential signalling pathways such as sonic hedgehog, Wnt and mTOR (Wheway *et al.*, 2018). The eukaryotic cell cycle is broadly divided into 4 phases; DNA replication (S), cell division (M), cell growth (G1) and preparation for division (G2), whilst cells can be arrested by checkpoint control proteins in G0. Cilia are a feature of post-mitotic cells, formed during phases G0 and G1 of the cell cycle, due to being rooted to the centrosome-derived basal body, which is essential for nucleation of the mitotic spindle during cell division (Sorokin, 1968). Thus, prior to mitosis the cilia are released and reabsorbed from the centrosome, to allow cell division and then ciliogenesis restarted after mitotic division (Basten and Giles, 2013).

NEK1 was first linked to the formation of cilia, known as ciliogenesis, as NEK1-deficient Kat2J mice present with classic symptoms of ciliopathy such dwarfism, reduced spermatogenesis, and progressive polycystic kidney disease (Mahjoub *et al.*, 2005; Shalom *et al.*, 2008; Upadhya *et al.*, 2000). *In vitro*, functional knock out of NEK1 causes defective ciliogenesis in mouse NIH3T3 fibroblasts and human ARPE-19 cells, further implicating the role of NEK1 in ciliogenesis (Evangelista *et al.*, 2008; Gregorczyk *et al.*, 2023). It is reported that NEK1 protein localises to the centrosome, which is the microtubule-organizing centre involved in ciliogenesis, and that this localisation is mediated by its coiled-coil domain (Mahjoub *et al.*, 2005; White and Quarmby, 2008). At the centrosome, NEK1 is suggested to be necessary for stabilisation of the microtubule axial filament of growing cilia, as depletion of NEK1 leads to abnormal cilia branching (Wang *et al.*, 2014). NEK1 binds to and phosphorylates key microtubule component tubulin α-1B chain, which is necessary for microtubule stabilisation which is an early stage of ciliogenesis (Mann *et al.*, 2023; Pitaval *et al.*, 2017). NEK1 may promote ciliogenesis at the centrosome by binding to the tubulin-interactor centrosomal protein of 104 kDa (Cep104), which localises at the ciliary tip during cilia assembly (Al-Jassar *et al.*, 2017; Satish Tammana *et al.*, 2013). This leads to disinhibition of Cep104 by outcompeting binding of Cep104 to the protein centriolar coiled-coil protein of 110 kDa (Cep110), which negatively regulates ciliogenesis by capping the mother centriole (Al-Jassar *et al.*, 2017; Li *et al.*, 2013; Spektor *et al.*, 2007).

Contrary to the role of NEK1 kinase activity in microtubule stabilisation, overexpression of NEK1 leads to inhibition of ciliogenesis, an effect that is ablated with expression of kinase dead NEK1 (Shalom *et al.*, 2008; White and Quarmby, 2008). One possible explanation of this, is that NEK1 has a dual kinase function in ciliogenesis, promoting cilia stability once the process is initiated, but halting initiation by its role in cell cycle regulation. Activation of NEK1 by DNA damage leads to activation of the checkpoint serine/threonine-protein kinase (Chk1), which is necessary for cell cycle arrest at G1 phase (Chen *et*

al., 2011). Considering ciliogenesis occurs during G1, overexpression of NEK1 may lead to inhibition of ciliogenesis by halting cell cycle progression, suggesting that NEK1 kinase activity may be tightly regulated to mediate ciliogenesis.

C21orf2 was first identified as a key ciliopathy-associated protein, and loss of functional C21orf2 has been reported to disrupt cilia growth and cilia-associated Shh signalling in multiple cell models (De Decker *et al.*, 2022; Gregorczyk *et al.*, 2023; Lai *et al.*, 2011). Currently the role of C21orf2 is not yet understood. However, ciliopathy associated R73P and L224P mutations in *C21orf2* lead to dissociation from NEK1, suggesting that the protein complex is necessary for regulation of cilia function (Wheway *et al.*, 2015). Knock out of either NEK1 or C21orf2 causes a significant decrease in localisation to cilia of the other protein (Gregorczyk *et al.*, 2023). However, this could be due to loss of protein stabilisation, as NEK1-mediated phosphorylation stabilises C21orf2, which in turn stabilises NEK1 protein (Watanabe *et al.*, 2020). Overexpression of C21orf2 does not lead to ciliary defects, suggesting that whilst C21orf2 may stabilise NEK1 protein, it does not regulate its kinase activity (De Decker *et al.*, 2022). Both NEK1 and C21orf2 play key roles in the regulation of ciliogenesis and cilia function, although further research is needed to conclude the specific mechanism this involves.

1.3.2 The role of NEK1 and C21orf2 in the DNA damage response

1.3.2.1 The DNA damage response

The genome is under constant threat of damage and mutation due to environmental factors such as ionising radiation (IR) or toxic chemicals. Damage to DNA can also occur dye to physiological processes, such as by excessive cellular ROS or defective transcription machinery (Hoeijmakers, 2001). Thus, cells have evolved a tightly regulated response mechanisms to detect and repair DNA lesions, known as the DNA damage response (DDR) (Harper and Elledge, 2007). Considering the variety of DNA-lesions that can occur, the DDR involves multiple mechanisms of DNA repair, specific to each DNA insult (Iyama and Wilson, 2013). Briefly, some of the main DNA repair pathways are O6-methylguanine-DNA methyltransferase (MGMT) (Yu *et al.*, 2019), nucleotide excision repair (NER) (Costa *et al.*, 2003), base excision repair (BER) (Mullins *et al.*, 2019), DNA single-strand break repair (SSBR) (Caldecott, 2022), and mismatch repair (MMR) (Jiricny, 2006). Double-strand breaks (DSBs) to DNA are one of the most deleterious forms of damage, which result in cell death if not repaired efficiently (Jackson and Bartek, 2009). Induction of DSB repair is regulated by three main kinases; ataxia telangiectasia and Rad3-related protein (ATR), ataxia-telangiectasia mutated (ATM) and DNA-dependent protein kinase (DNA-PK) (Stiff *et al.*, 2004). Induction of the DDR, the protein kinases phosphorylate the histone H2AX, resulting in the accumulation of γH2AX around the DNA lesion. This phosphorylation of H2AX at S139 is critical in DDR signalling and is a key marker of DNA damage induction (Mah *et al.*, 2010).

There are two main repair mechanisms to deal with DSBs; homologous recombination repair (HR) and non-homologous end-joining (NHEJ) (Giglia-Mari *et al.*, 2011). HR occurs during the S and G2 phases of the cell cycle, particularly in response to DSBs formed by collapse of the replication fork where DNA replication takes place (Prado, 2018). This process involves using an intact sister chromatid as a template to ensure accurate repair. DSBs are recognised by the MRN complex, composed of DSB repair protein MRE11, DNA repair protein RAD50, and Nibrin, leading to recruitment of the ATM kinase, which initiates the recombination process (Lee and Paull, 2007). On the other hand, NHEJ occurs mostly during G1 phase, when a template sister chromatid is not available (Delacote and Lopez, 2008), thus this pathway directly ligates broken DNA ends (Lieber, 2010). Induction of NHEJ is mediated by the Ku70/Ku80 heterodimer binding to the DSB ends, which recruits the DNA-dependent protein kinase catalytic subunit (DNAPKC) (Pannunzio *et al.*, 2018). Alternatively, NHEJ can be induced by poly ADP-ribose polymerase 1 (PARP1)-dependent DSB sensing, which completes DDR signalling by recruitment of ATM and the MRN complex (Haince *et al.*, 2008). As mature neurons are post-mitotic, they do not follow the replicative cell cycle during which most DDR pathways take place (Frade and Ovejero-Benito, 2015). Evidence suggests that NHEJ is the primary repair pathway for DSBs (Iyama and Wilson, 2013). It was recently suggested that neurons can undergo an RAD52-dependent HR mechanism for DSBs, that uses an RNA template (Welty *et al.*, 2018). Although this pathway is not yet well understood.

The DDR promotes cell cycle arrest, which is performed at regulated checkpoints, to allow for efficient DNA repair (Campos and Clemente-Blanco, 2020). Briefly, checkpoint at G1 is controlled by the signalling complex of ATM, checkpoint serine/threonine-protein kinase 2 (Chk2) and cellular tumour antigen p53 (Smith *et al.*, 2020). Whilst arrest at S and G2/M checkpoints are mediated by signalling between ATR-Chk1 and Wee1-like protein kinase (Wee1) (Vera *et al.*, 2015). Failure to arrest cell cycle at checkpoints can lead to DNA damage accumulation and apoptosis (Boice *et al.*, 2022). The p53 protein is critical in the DDR, as it regulates multiple processes to decide cell fate such as DNA damage repair, apoptosis, and cellular senescence (Hafner *et al.*, 2019). In a positive feedback mechanism, cell cycle arrest kinases Chk1, Chk2 and the cyclin-dependent kinase inhibitor 1 p21 activates p53 to promote cell cycle arrest, although prolonged activation due to DNA damage will lead to cell death initiation (Shen and White, 2001; Simabuco *et al.*, 2018).

1.3.2.2 NEK1 is involved in multiple DDR pathways

NEK1 protein is best characterised for its role in the DDR process (summarised in Figure 1-10), which was first reported in 2004. It was shown that DNA damage due IR leads to upregulation of NEK1 kinase activity (Polci *et al.*, 2004). In response to IR-induced DNA damage NEK1 colocalises to the key DDR protein γH2AX in the nucleus to promote DNA repair (Polci *et al.*, 2004). NEK1 is proposed to be

involved in three main signalling pathways within the DDR, responding to primarily to DNA DSBs. Prior to DNA damage, NEK1 associates with the major DDR regulator ATR kinase leading to ATR autophosphorylation at T1989 and stabilisation of the ATR-interacting protein (ATRIP) complex that is essential for priming before DDR signalling (Cortez *et al.*, 2001; Liu *et al.*, 2013). NEK1 can act independently of ATR or ATM protein kinases, as inhibition of ATR/ATM did not alter NEK1 upregulation or translocation of NEK1 in response to DNA damage (Chen *et al.*, 2011). On the other hand, silencing NEK1 does not disrupt ATM/ATR localisation or phosphorylation in response to DNA damage (Chen *et al.*, 2011). Loss of NEK1 does not lead to embryonic lethality in mice as seen with ATR-deficiency, confirming that NEK1 can act independently of master DDR regulators (Brown and Baltimore, 2000; Chen *et al.*, 2011).

In response to DSBs by IR or toxic agents, tousled-like kinase 1 (TLK1) phosphorylates NEK1 at T141 to promote cell cycle arrest via the TLK1 > NEK1 > ATR > Chk1 pathway, as inhibition of TLK1 leads to reduced NEK1 and Chk1 phosphorylation and increased apoptosis (Singh *et al.*, 2017; Singh *et al.*, 2019). Upon TLK1-phosphorylation of NEK1, Chk1 is activated by an unknown mechanism and in turn inhibits M-phase inducer phosphatase 1 (CDC25A) activity by phosphorylation at PS76 (Chen *et al.*, 2011; Knoblochova *et al.*, 2023). This results in CDC25A proteasomal degradation and the disinhibition of cyclin-dependent kinase 1 (CDK1)/Cyclin B, which arrests the cell cycle (Sakurikar *et al.*, 2012). Indeed, it is well reported that loss of NEK1 leads to failure of cells to initiate cell cycle arrest and accumulate DNA damage, due to lack of Chk1 and Chk2 activation (Chen *et al.*, 2008; Pelegrini *et al.*, 2010).

The NEK1-interacting protein C21orf2 has been suggested to be necessary for NEK1 to function effectively in HR, although this is controversial. Multiple papers have reported that silencing C21orf2 leads to defective proliferation and DNA damage repair by HR after IR, although this could be rescued by overexpressing NEK1, suggesting it is due to loss of NEK1 protein stabilisation (Fang *et al.*, 2015; Watanabe *et al.*, 2020). Contradictory to this, small interfering RNA (siRNA) knockdown of C21orf2 in SHSY-5Y did not disrupt the formation of γH2AX foci in response to DNA damage, suggesting no change in DNA damage response efficiency (De Decker *et al.*, 2022). Thus, further investigation is needed to conclude whether C21orf2 is necessary for NEK1-mediated regulation of HRR.

In response to IR, lack of NEK1-mediated phosphorylation of Rad54 S572 during G2 leads to replication fork instability and defective homologous recombination repair, although this is currently being disputed (Ghosh *et al.*, 2022; Spies *et al.*, 2016). Finally, in response to DNA damage, a portion of NEK1 is recruited to mitochondria where it phosphorylates VDAC1 in order to prevent apoptosis, which is discussed in more detail in section 1.3.2.4.

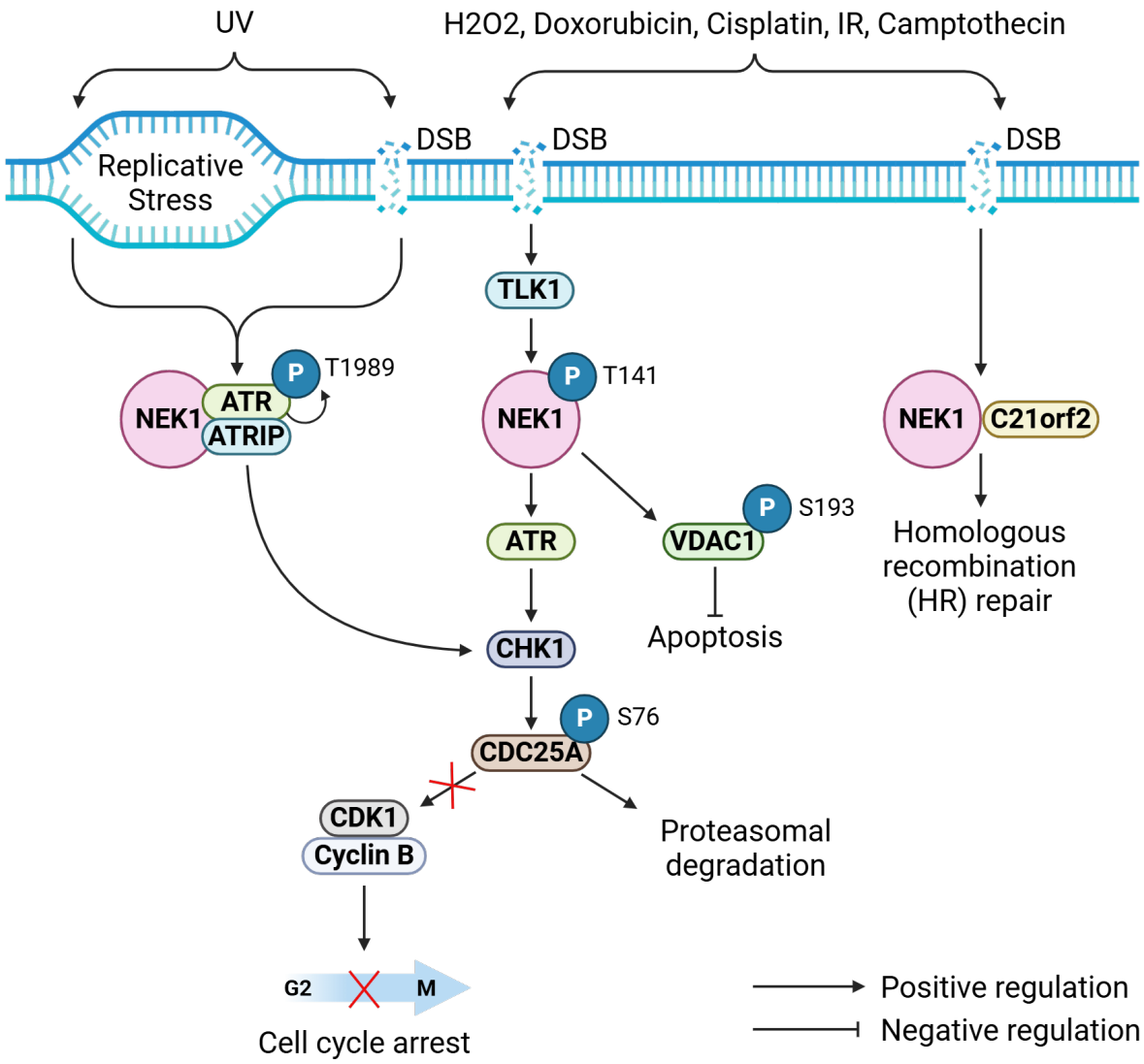

Figure 1-10 Summary of the key pathways of NEK1 and C21orf2 in the DNA damage response.

Modified from (Pavan *et al.*, 2021). In response to UV-induced replicative stress or double strand breaks (DSB), NEK1 interacts with ATR, leading to autophosphorylation on T1989 and stabilisation of the ATR-ATRIP complex. In response to DSBs, TLK1 phosphorylation NEK1 at T141 leads to NEK1-mediated phosphorylation of VDAC1 S193 to prevent apoptosis. This also leads to initiation of the TLK1 > NEK1 > ATR > Chk1 pathway that causes cycle arrest due to CDC25A-mediated CDK1 inhibition. NEK1 also interacts with C21orf2 in response to DSBs to regulate homologous recombination repair (HR).

1.3.2.3 Nucleus to mitochondria signalling in the DDR

1.3.2.3.1 PARP1-SIRT1 signalling

Mitochondrial dysfunction and DNA damage accumulation are both hallmarks of aging and have been reported in numerous neurodegenerative diseases (Maynard *et al.*, 2015; Reddy, 2009). Emerging evidence has implicated a role of mitochondria in the DDR, as it suggested that signalling between the nucleus and mitochondria in response to DNA damage is pivotal for DNA repair (Cucchi *et al.*, 2021). One key protein family involved in nucleus to mitochondria signalling are sirtuins (SIRTs). Sirtuins are NAD+ dependent deacetylases that are involved in cellular response to stresses, such as oxidative or genotoxic stress (Grabowska *et al.*, 2017). In response to DNA damage PARP1 consumes the coenzyme NAD+ and acetyl-CoA, to recruit PAR-binding DNA repair proteins (Murata *et al.*, 2019; Yang *et al.*, 2023). NAD+ is a rate-limiting metabolite for both PARP1 and sirtuin 1 (SIRT1), as SIRT1 requires NAD+ for the regulation of mitochondrial biogenesis and promotion of DNA damage repair (Cerutti *et al.*, 2014). Thus, upregulation of PARP1 or SIRT1 can lead to inhibition of the other due to competition for NAD+ (Fang *et al.*, 2014) (Figure 1-11).

SIRT1 inhibition leads to decreased activation of stress-activated proteins such as AMP-activated protein kinase (AMPK). AMPK is a crucial cellular energy sensor that helps maintain energy balance and supports cell survival (Herzig and Shaw, 2018). Upon changes in the ATP:ADP ratio during low energy availability or high energy demand, AMPK phosphorylates multiple proteins to promote catabolism, regulate mitophagy and mitochondrial dynamics (Gwinn *et al.*, 2008; Liang *et al.*, 2015). In addition to SIRT1 activation, AMPK can also be activated by DNA damage factors such as ROS, elevated calcium levels via calcium/calmodulin-dependent protein kinase kinase 2 (CaMKK2), ATM, and p53 (Budanov and Karin, 2008; Tripathi *et al.*, 2013). Once activated, AMPK enhances glucose and fatty acid oxidation via glucose transporters (GLUTs) (Muraleedharan and Dasgupta, 2022) and stimulates mitochondrial biogenesis via activation of forkhead box protein O3 (FOXO3A) (Urushihara *et al.*, 2023). When activated these proteins signal to the mitochondria in order to cope with oxidative stress, by activation of SOD proteins (Marino *et al.*, 2021). Thus, inhibition of SIRT1 due to out-competition by PARP1 in response to DNA damage, leads to decreased activation and increased mitochondrial ROS.

In a positive feedback manner, production of ROS signals back to the nucleus to promote activation of PARP1-mediated DNA repair, although prolonged or hyperactivation of PARP1 is linked to mitochondrial dysfunction (Fang *et al.*, 2014; Rodriguez-Vargas *et al.*, 2012). These actions contribute to mitochondrial function regulation and cellular stress responses, controlling both production of ROS and NAD+ as a feedback mechanism for PARP1 and SIRT1 function.

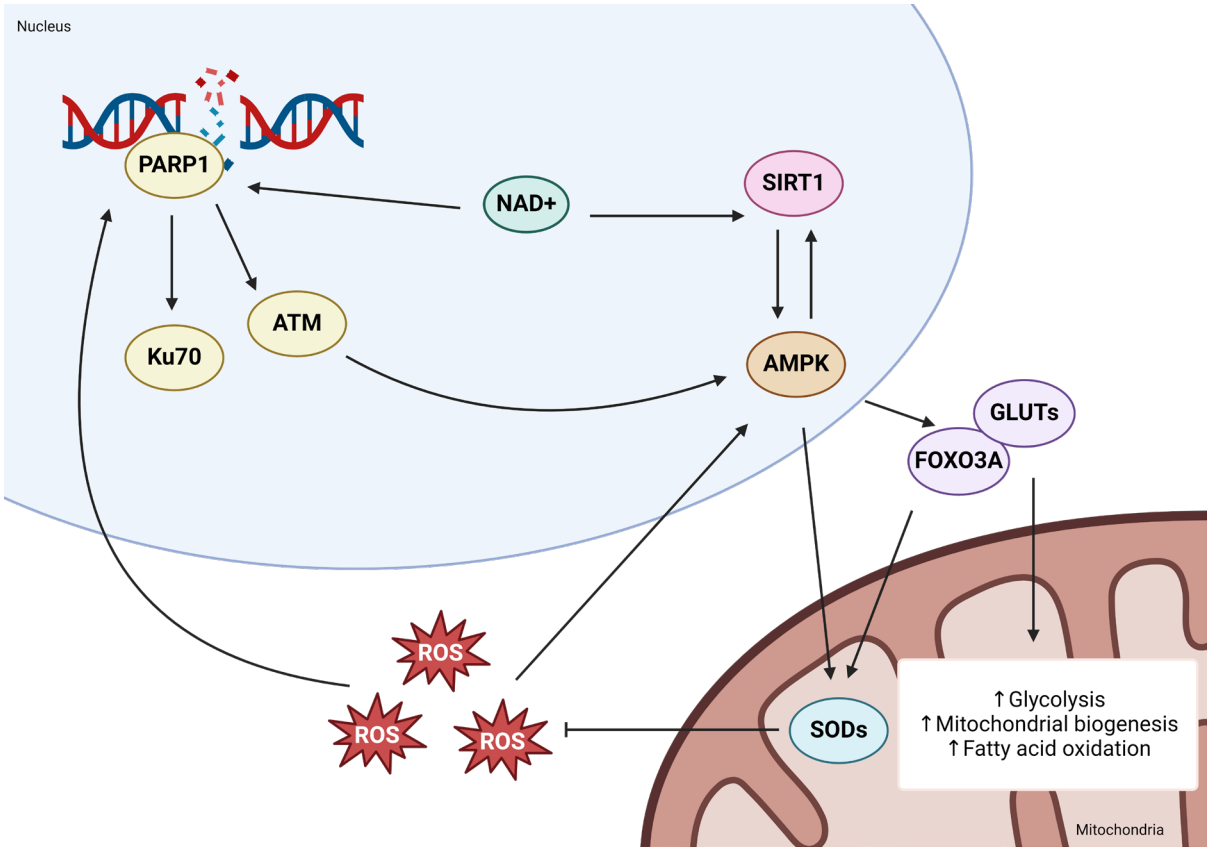

Figure 1-11 PARP1-SIRT1 signalling in response to DNA damage.

In response to DNA damage PARP1 and SIRT1 consume the coenzyme NAD+ to promote DNA damage repair by activation of DNA repair proteins Ku70 and ATM. Thus, upregulation of PARP1 or SIRT1 can lead to inhibition of the other due to competition for NAD+. SIRT1 activates AMPK which enhances glucose and fatty acid oxidation via glucose transporters (GLUTs) and Forkhead box protein O3 (FOXO3A). This activates SOD proteins to respond to oxidative stress. Inhibition of SIRT1 due to out-competition by PARP1 in response to DNA damage, leads to decreased activation and increased mitochondrial ROS. In a positive feedback manner, production of ROS signals back to the nucleus to promote activation of PARP1-mediated DNA repair.

1.3.2.3.2 Mitophagy-apoptosis crosstalk

Low levels of DNA damage stimulate mitophagy to promote cell survival by removal of damaged or abnormal mitochondria (Kim *et al.*, 2021). Whilst high levels of sustained genotoxic stress stimulate apoptosis, suggesting that this nucleus to mitochondria signalling may be critical for deciding cell fate (Biton and Ashkenazi, 2011; Shiloh and Ziv, 2013). This communication is mediated by three proteins ATM, p53 and SIRT1 (Figure 1-12). Upon DNA damage, ATM, along with the NF-κB essential modulator (NEMO), activates the Jun N-terminal kinase (JNK), which balances autophagy and apoptosis (Biton and Ashkenazi, 2011; Picco and Pages, 2013). In low levels of genotoxic damage JNK promotes Beclin-1 initiation of autophagy, whilst upon extensive DNA damage, JNK promotes apoptosis by deactivating Beclin-2 and activating the FAS-associated death domain protein (FADD)–caspase 8 pathway (Marino *et al.*, 2014). ATM also regulates mitochondrial function by preventing Bid translocation to mitochondria, thus reducing ROS production and apoptosis (Maryanovich *et al.*, 2012). Under mild stress, p53 can promote mitophagy by inducing pro-autophagy genes like DNA damage-regulated autophagy modulator protein 1 (DRAM1) (Crighton *et al.*, 2006). However, under severe genotoxic stress, p53 activates pro-apoptotic proteins, leading to apoptosis, senescence, or growth arrest (Oda *et al.*, 2000). p53 is suggested to inhibit autophagy and mitophagy via the ULK1 autophagy complex or suppressing the PINK1–Parkin mitophagy pathway (Gao *et al.*, 2011; Hoshino *et al.*, 2013). Finally, SIRT1 deacetylates and inactivates p53, thereby preventing apoptosis and promoting survival after genotoxic stress (Luo *et al.*, 2001; Vaziri *et al.*, 2001). SIRT1 also facilitates mitophagy via multiple pathways, including deacetylation of LC3 and stabilising PINK1 by regulation of MMP (Fang *et al.*, 2014; Huang *et al.*, 2015). Furthermore, SIRT1 facilitates AMPK to stimulate mitophagy and energy homeostasis, possibly creating a positive feedback loop, as AMPK can also activate SIRT1 (Egan *et al.*, 2011). Therefore, ATM, p53, and SIRT1 each play critical roles in mediating the balance between autophagy/mitophagy and apoptosis to determine cell fate in response to DNA damage.

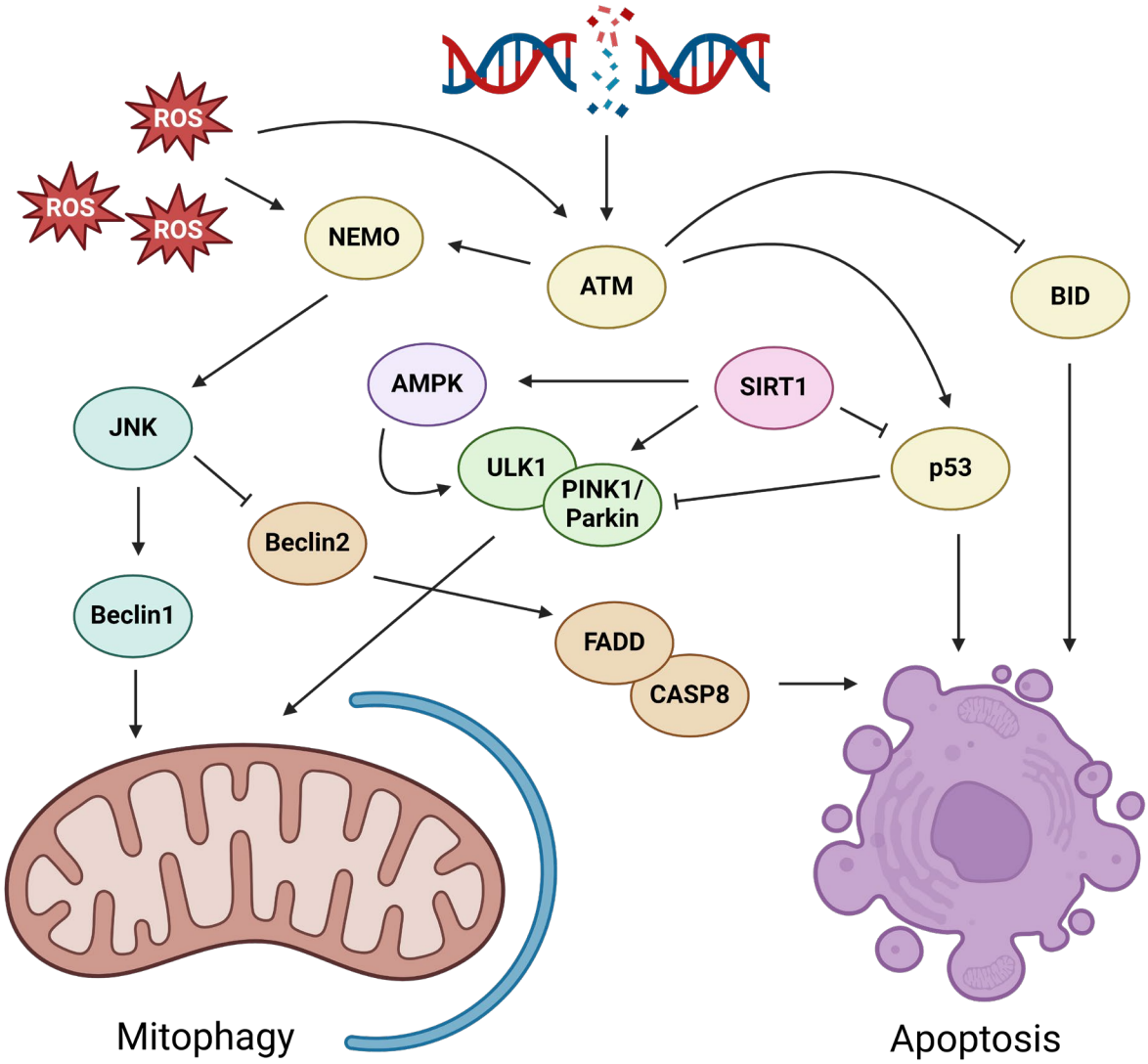

Figure 1-12 Mitophagy-apoptosis crosstalk in response to DNA damage.

Determination of cell fate is mediated by three proteins ATM, p53 and SIRT1. Upon DNA damage, ATM, along with the NF-κB essential modulator (NEMO), activates the Jun N-terminal kinase (JNK). In low levels of genotoxic damage JNK promotes Beclin-1 initiation of autophagy, whilst upon extensive DNA damage, JNK promotes apoptosis by deactivating Beclin-2 and activating the FAS-associated death domain protein (FADD)–caspase 8 pathway. ATM inhibits BID translocation to mitochondria, inhibiting ROS production and apoptosis. p53 promotes mitophagy by inducing the pro-autophagy gene DNA damage-regulated autophagy modulator protein 1 (DRAM1). Upon severe genotoxic stress, p53 activates pro-apoptotic proteins, leading to apoptosis. p53 is inhibits ULK1 autophagy complex and the PINK1–Parkin mitophagy to prevent mitophagy. SIRT1 deacetylates and inactivates p53, to inhibit apoptosis and promote survival after genotoxic stress. SIRT1 facilitates AMPK to stimulate mitophagy and energy homeostasis.

1.3.2.4 NEK1 may link ER-mitochondria contacts to the DDR

Several lines of evidence suggest that NEK1 may regulate ER-mitochondria contacts or the processes that they regulate. A proteomic analysis of HEK293 and mouse NSC-34 neuronal cell lines found that NEK1 protein interacts with the ER-mitochondrial tethering protein VAPB (Cirulli *et al.*, 2015). Considering it is well established that NEK1 is recruited to mitochondria upon DNA damage to prevent cell death via VDAC1-phosphorylation, it is probable that NEK1 is active at these ER-mitochondria sites where VDAC1 resides under these conditions (Chen *et al.*, 2009; Chen *et al.*, 2010b). Accumulating evidence shows that NEK1 is involved in regulation of many of the same pathways as MAM, such as apoptosis, autophagy, and mitochondrial dynamics, which is discussed in more detail below. Thus, NEK1 may be the key mediator of nucleus to mitochondria signalling in response to DNA damage, by interaction with key MAM tethering proteins VDAC1 and VAPB.

Mitochondrial homeostasis is tightly regulated by both MAM and the DDR pathway (discussed in sections 1.2.3.1 and 1.3.2.3 respectively). Accumulating evidence suggest that NEK1 is a key mediator of mitochondrial homeostasis. MEFs from NEK1-deficient kat2J mice have decreased levels of the glucose transporter type 1 (GLUT1), leading to reduced glucose uptake, oxygen consumption levels and ATP production (Wang *et al.*, 2021a). NEK1-deficient HAP1 cells additionally show decreased complex I activity with decreased expression of some key components of the complex and increased mitochondrial ROS, which may be linked to increased DNA damage (Martins *et al.*, 2021). The NEK1 interactome included many proteins essential for metabolism, such as pyruvate kinase M (PKM), the 2,4-dienoyl-CoA reductase and GSK3β (Melo-Hanchuk *et al.*, 2017). The kinase GSK3β is suggested to inhibit VAPB/PTPIP51 tethering, although whether this is due to direct phosphorylation is not yet clear (Stoica *et al.*, 2014; Stoica *et al.*, 2016). However, how NEK1 interacts with these proteins to regulate metabolism, possibly via ER-mitochondria contacts, needs further investigation.

In addition to dysregulated metabolism, mitochondrial fragmentation was reported in NEK1 kat2j MEFs, which was suggested to be due to loss of NEK1-mediated endosomal trafficking (Wang *et al.*, 2021a). NEK1 phosphorylation of vacuolar protein sorting-associated protein 26 (VPS26B) at residues S302/S304 to regulate the sorting nexin-27 (SNX27)-mediated trafficking from endosome to the plasma membrane, with phospho-deficient VPS26B leading to the same mitochondrial dysfunction in MEFs (Wang *et al.*, 2021a). Loss of functional NEK1 in embryonic stem cell-derived motor neurons leads to impaired retromer formation and decreased neurite outgrowth, implicating dysregulation of retromer trafficking as a potential pathway in ALS pathophysiology (Huang *et al.*, 2024). Although this effect could be due to disruption of microtubule homeostasis, as treatment with the microtubule stabilisation drugs paclitaxel or laulimalide rescued reduced neurite regrowth after photobleaching in iPSC-derived motor neurons with NEK1 siRNA-mediated knockdown (Mann *et al.*, 2023).

In response to DNA damage, it is reported that a portion of NEK1 localises to mitochondria, where it regulates the opening of the mitochondria permeability transition pore (mPTP) via phosphorylation of the VDAC1 on the OMM (Chen *et al.*, 2009; Chen *et al.*, 2010b). Loss of NEK1 or expression of kinase-dead NEK1 mutants results in loss of NEK1-dependent phosphorylation of VDAC1, leading to increased mitochondrial membrane permeability and accelerated cell death. This suggests that the interaction between NEK1 and VDAC1 is vital to regulate apoptosis. Indeed, loss of phosphorylation of NEK1 by TLK1 leads to increased apoptosis upon low doses of apoptotic stimulant doxorubicin, as shown release of cytochrome C into the cytoplasm (Singh *et al.*, 2020). In addition to regulation apoptosis via VDAC1, NEK1 is involved in TNFα-associated receptor-interacting protein kinase 1 (RIPK1)-dependent apoptosis (Amin *et al.*, 2018). Functional knockdown of NEK1 sensitises cells to RIPK1-dependent apoptosis and cell death in response to stimulation by TNFα/5Z-7 and increases levels of activated RIPK1 (Amin *et al.*, 2018). This is suggested to act by NEK1 binding to RIPK1 to inhibit formation of a pool of activated RIPK1. Contrary to this, NEK1 has been suggested to indirectly modulate RIPK1 by regulating the trafficking of the mammalian retromer complex upstream of RIPK1 inhibition by A20 (Wang *et al.*, 2021a). Considering both ER-mitochondria contacts and the DDR decide cell fate by regulating apoptosis (discussed in sections 1.2.3.1 and 1.3.2.3.2 respectively), NEK1 may link these two seemingly disparate processes.

The NEK1 interactome contains several proteins involved in autophagy and mitophagy, including LC3B, γ-aminobutyric acid receptor-associated protein (GABARAP), ATG5 and Beclin1 (Martins *et al.*, 2021). Furthermore, a recent CRISPR kinome-wide screen identified NEK1 as an inhibitor of both basal and starvation-induced autophagy (Losier *et al.*, 2024), and NEK1 KO HAP1 cells show decreased levels of basal mitophagy (Martins *et al.*, 2021). Multiple lines of evidence suggest that MAM are the site of autophagosome formation (Gomez-Suaga *et al.*, 2017; Hamasaki *et al.*, 2013). Considering the role of NEK1 in microtubule regulation and its interaction with proteins on the autophagosome membrane, NEK1 may be necessary for autophagosome formation at these contact sites. Together, this implicates a critical role for the regulation of ER-mitochondria contact sites in response to DNA damage.

1.3.3 Mutations in *NEK1* and *C21orf2* are linked to ALS

1.3.3.1 NEK1 missense and loss of function mutations cause ALS

Multiple studies investigating whole exome sequences of ALS patients have reported heterozygous LOF and missense mutations in *NEK1* to be a cause of both familial and sporadic ALS (Brenner *et al.*, 2016; Cirulli *et al.*, 2015; Lattante *et al.*, 2021). *NEK1* mutations are observed in 3 – 5% of ALS cases, with approximately 1% these being LOF mutations (Kenna *et al.*, 2016; Naruse *et al.*, 2021). Furthermore, approximately 1.8% of all cases and 30 – 50% of *NEK1* mutation carriers are oligogenic, therefore carrying an additional ALS risk mutation (Iacoangeli *et al.*, 2024; Lattante *et al.*, 2021; Nguyen *et al.*, 2018). Typically, patients with *NEK1* LOF mutations present with upper limb onset of disease, with shorter survival duration than missense mutation carriers, suggesting the LOF mutations to be more pathogenic (Jiang *et al.*, 2023; Tsai *et al.*, 2020).

Whilst there is a lack of knowledge of the pathological phenotype of *NEK1*-ALS, recent evidence shows that post-mortem tissue from both *NEK1* LOF and missense mutations contain pathological TDP-43 aggregates that are a hallmark of ALS (Rifai *et al.*, 2024). The motor cortex of a patient with *NEK1*^{R261H} missense mutation presented with NEK1-positive cytoplasmic aggregates, suggesting that missense mutations may lead to LOF due to protein aggregation (Rifai *et al.*, 2024). In line with this finding, fibroblasts derived from missense *NEK1* mutation harbouring ALS patients have decreased NEK1 protein expression, possibly due to protein aggregation (Lattante *et al.*, 2021). NEK1 is involved in regulation of primary cilia and human iPSC-derived motor neurons and brain organoids harbouring a *NEK1*^{A261*} LOF mutation had significantly fewer and shorter cilia (Nice *et al.*, 2024). Finally, iPSC-derived motor neurons harbouring a *NEK1*^{R540*} ALS-associated mutation exhibited defective microtubule homeostasis and nucleus-cytoplasmic transport, suggesting there may be multiple pathways of NEK1 pathology in ALS, dependent on the specific mutation (Mann *et al.*, 2023). NEK1 is well established as a protein involved in response to DNA damage, and NEK1 LOF mutations are suggested to lead to DNA damage accumulation, which is discussed in order detail in section 1.1.4.5.

1.3.3.2 C21orf2 variants confer susceptibility to developing ALS

A meta-analysis of genome wide association studies (GWAS) identified *C21orf2* as a risk variant in ALS (van Rheenen *et al.*, 2016). Whilst the mechanisms by which C21orf2 may confer disease susceptibility in unclear, mouse embryonic stem cell-derived motor neurons harbouring an ALS-associated V58L mutation in *C21orf2* leads to accumulation of NEK1 protein and impaired neurite outgrowth, suggesting it may be due to loss of NEK1 protein function (Watanabe *et al.*, 2020). Investigation into the effect of *C21orf2* ALS mutations on its interaction with NEK1 reported that R73P mutation within the LRR domain but not T150I mutation led to disassociation with the NEK1 protein (Gregorczyk *et al.*, 2023). This suggests that the location of the mutation within the protein may influence its pathology.

C21orf2 is best characterised as a cilia-related protein. Ciliary defects observed with siRNA-mediated C21orf2 knock down are rescued with overexpression of wild type but not ALS-associated V58L mutant C21orf2 constructs (De Decker *et al.*, 2022). Furthermore, patient iPSC-derived motor neurons harbouring a V58L or V58L/R60W compound mutation show significantly reduced ciliary frequency and length, suggesting that C21orf2 ALS-mutations may have a unique primary ciliary defect, although how this leads to disease is not clear (De Decker *et al.*, 2022).

1.4 Summary, hypotheses, and aims

Missense and heterozygous LOF mutations in the gene *NEK1* are a cause of familial and sporadic ALS (Brenner *et al.*, 2016; Cirulli *et al.*, 2015). NEK1 is a multi-functional kinase with roles in DNA damage repair (Pelegrini *et al.*, 2010) and primary cilium formation (Shalom *et al.*, 2008). C21orf2 is a known interactor of NEK1 and has been shown to be required for NEK1 to function (Fang *et al.*, 2015). C21orf2 also has functions in DNA damage repair and studies have found nonsynonymous and LOF mutations in C21orf2 to be associated with increased ALS risk (van Rheenen *et al.*, 2016). It is unclear how these mutations may contribute to ALS, however as DNA damage accumulates in neurons in ALS (Kim *et al.*, 2020) and a LOF mutation in *NEK1* leads to DNA damage accumulation in ALS patient-derived motor neurons (Higelin *et al.*, 2018), it is suspected that it may involve dysfunctional DNA damage repair.

Neurons are cells with high metabolic requirements, so the function of ATP producing mitochondria is vital for neuronal function and survival. Mitochondria are closely associated with the endoplasmic reticulum (ER), forming physical associations known as ER-mitochondria contact sites (MAM), that regulate several physiological processes that are dysregulated in ALS, such as calcium handling, autophagy, and synaptic function (De Vos *et al.*, 2012; Gomez-Suaga *et al.*, 2017; Gómez-Suaga *et al.*, 2019). In multiple forms of ALS there is reported reduced ER-mitochondria coupling and signalling (Bernard-Marissal *et al.*, 2015; Gomez-Suaga *et al.*, 2022; Stoica *et al.*, 2014; Stoica *et al.*, 2016). There is a specific reduction between the binding partners of vesicle-associated membrane protein associated protein B (VAPB) on the ER membrane and outer mitochondrial protein tyrosine phosphatase interacting protein 51 (PTPIP51) (Hartopp *et al.*, 2022; Stoica *et al.*, 2014; Stoica *et al.*, 2016). Although how and why this reduced ER-mitochondria apposition may lead to neurodegeneration is still elusive.

In response to DNA damage, NEK1 has been found to localise to mitochondria where it inhibits apoptosis by regulating opening of the mitochondria permeability transition pore (mPTP) via phosphorylation of the voltage dependent anion channel 1 (VDAC1) on the outer mitochondrial membrane (Chen *et al.*, 2009; Chen *et al.*, 2010b). Proteomic studies suggest that NEK1 interacts with the ER-mitochondria tethering protein VAPB. Thus, it is possible that NEK1 and VAPB form a signalling

complex that regulates ER-mitochondria interactions, calcium homeostasis and autophagy in response to DNA damage.

We hypothesised that NEK1 and its interactor-C21orf2 regulate ER-mitochondria apposition in response to DNA damage and that ALS-associated loss of NEK1 or C21orf2 function will disturb these processes to cause disease. This project aimed to elucidate the role of this novel complex and understand how it may directly link impaired DNA damage repair and ER-mitochondria contacts in neurodegeneration, furthering our knowledge towards the mechanisms underlying ALS (Figure 1-13).

In order to investigate the above hypotheses, my aims were:

- To characterise the interaction between NEK1, C21orf2 and the VAPB/PTPIP51 ER-mitochondria tether
- To determine if loss of NEK1 and C21orf2 may disrupt ER-mitochondria contacts
- To elucidate the mechanism of NEK1-mediated regulation of VAPB/PTPIP51 tethering

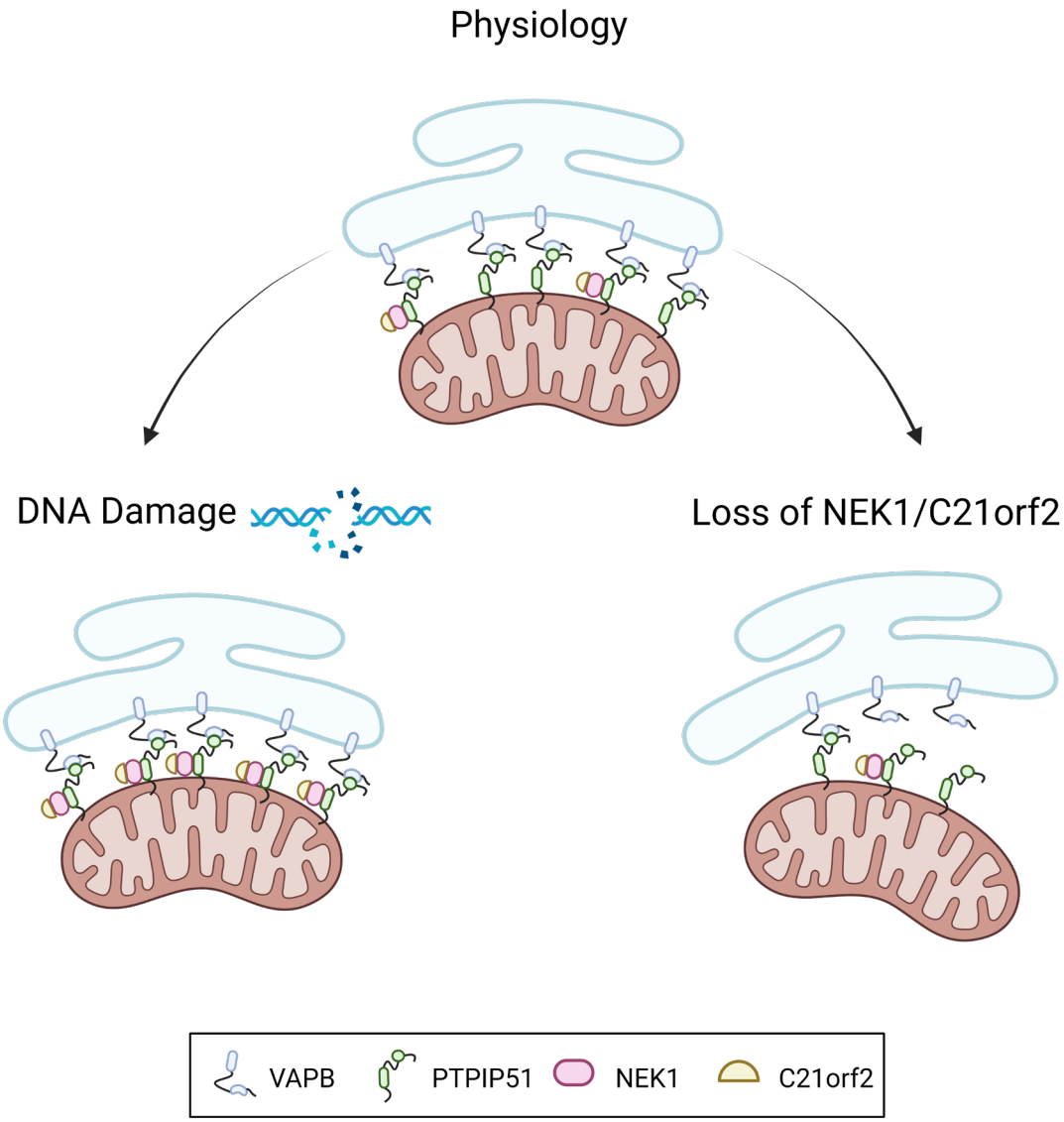

Figure 1-13 Hypotheses of the project.

We hypothesised that NEK1 and C21orf2 regulate ER-mitochondria apposition by mediating VAPB/PTPIP51 protein tethering in response to DNA damage (left) and that ALS-associated loss of NEK1 or C21orf2 function will disturb these processes (right).

Chapter 2 Materials and methods

Unless otherwise indicated, chemicals were purchased from Sigma Aldrich and stock solutions made using ultrapure water from a Milli-Q purification system (Merck Millipore).

2.1 Cell culture techniques

2.1.1 Cell lines

The cell lines used in this study include HEK293, wild type (WT) HeLa and C21orf2 knock out (KO) HeLa cells. Parental cell wild type (PC) HeLa and NEK1 KO HeLa cells were a gift from Dr Carl Laflamme (Montreal Neurological Institute).

2.1.2 Subculture of cell lines

All cell lines were grown to a confluency of 100% and sub-cultured twice weekly in 4500 mg/L glucose containing Dulbecco's modified Eagle's medium (DMEM, Sigma-Aldrich, D5796), supplemented with 10% foetal bovine serum (FBS) (Sigma-Aldrich, F7524), and 1mM sodium pyruvate (Sigma-Aldrich, S8636), at 37 °C in a 5% CO_2 incubator. All cell lines were subjected to monthly testing for mycoplasma contamination.

Briefly, media was removed, and cells washed once with phosphate-buffered saline (PBS, 137 mM NaCl, 2.7 mM KCl, 10 mM Na_2HPO_4, 1.8 mM KH_2PO_4). Cells were incubated for 3 min at 37 °C with trypsin-ethylene-diamine-tetraacetic acid (EDTA) (Gibco, 15400054), then neutralised by addition of fresh prewarmed media and triturated to create a single cell suspension.

An appropriate volume of cell suspension was diluted in fresh media in new flask for continuation of cell culture (Table 2-1), or into an appropriately sized plate for experimental purposes (Table 2-2). For immunofluorescence or live imaging experiments, cells were plated on Ø13 mm (Academy, NPS16/2424) or Ø18 mm glass coverslips (VWR, 631-1580) respectively, which were pre-sterilised by baking for 2 h at 180 °C.

Table 2-1 Volume of trypsin and media used for subculturing of cell lines.

Flask size	Trypsin volume (mL)	Total media volume (mL)
T25	1	5
T75	3	15
T175	5	30

Table 2-2 Volume of media used for experimental cell culture plates and their applications.

Plate size	Media volume per well (mL)	Application
96 wells	0.1	CRISPR/Cas9
24 wells	0.5	siRNA transfection & immunofluorescence
12 wells	1	siRNA transfection, live cell imaging & CRISPR/Cas9
6 wells	2	siRNA transfection & immunoblot
10 cm^2 dish	10	Immunoprecipitation & electron microscopy

2.1.3 Thawing cell lines

All cell lines were stored long term at -80 °C in cryovials. Vials were thawed quickly in hand and diluted in 9 mL fresh warmed media and gently mixed. The cell suspension was split 3 mL into a T25 flask for continuation of cell culture and 7 mL into a T75 flask, to be frozen down once confluent to allow expansion of the cell line stocks.

2.1.4 Freezing cell lines

To freeze the cell lines for long term storage, cells were grown until 100% confluent in a T75 flask, washed and trypsinised, as described in 2.1.2. The cell suspension was centrifuged for 4 min at 400 x g, the supernatant was removed, and the cell pellet resuspended in 3 mL of freezing media (FBS + 10% DMSO (dimethyl sulfoxide, Sigma-Aldrich, D2650)). The resuspended cells were transferred into cryovials (Thermo Scientific, 375353) and frozen for 24 h at -80 °C in a CoolCell® freezing container (Corning, 432010), prior to long term storage at -80 °C.

2.1.5 CRISPR/Cas9 gene editing

CRISPR/Cas9 technology was used to functionally knock out the C21orf2 protein. WT HeLa cells were seeded in a 12 well plate and grown in standard supplemented media to approximately 80% confluency on the day of transfection. The Cas9 transfection was completed using Dharmacon Edit-R reagents following the manufacturer's protocol. The Edit-R trans-activating CRISPR RNA (tracrRNA) (Dharmacon, U-00200) and Edit-R CRISPR RNA (crRNA) designed to target either exon 3 or 5 of the C21orf2 gene (Dharmacon, CM-019913-03-0002 and CM-019913-05-0002) were diluted to 10 µM stock in 10 mM Tris-HCl pH 7.5. The Edit-R Cas9 plasmid (Dharmacon, U-005300-120) was diluted to a 100 ng/µl stock in Tris-HCl pH 7.5.

A mixture of puromycin resistant Edit-R Cas9 plasmid, Edit-R tracrRNA, Edit-R crRNA and Tris-HCl pH 7.5 was diluted in Opti-MEM (Gibco, 11058021). Separately, the transfection reagent Lipofectamine 2000 (Invitrogen, 11668019) was diluted in Opti-MEM and incubated for 5 min. The Cas9 and Lipofectamine 2000 mixtures were combined, vortexed for 10 s and incubated for 20 min, before adding dropwise to the cells. The media was changed 5 hours post-transfection.

Twenty-four hours post-transfection, the cells were washed once in PBS and trypsinised to detach them from the plate surface. The cells were resuspended in media containing 3 µg/mL puromycin (Sigma-Aldrich, 540411) and plated into a fresh 12 well plate, to allow selection of successfully transfected puromycin resistant cells. Forty-eight hours after replating, the puromycin media was replaced for puromycin-free media to allow growth of selected Cas9 transfected cells.

Once 90% confluent, the cells were split in both a serial and limiting dilution across 96 well plates, and wells with single cells marked as single clones. The remaining cells were frozen down as an 'edited pool'. Single cell clones were expanded into 6 well plates and analysed by immunoblot and qPCR. Details of the Cas9 transfection mix for 1 well of a 12 well plate are described in Table 2-3 and the crRNA sequences are described in Table 2-4.

Table 2-3 Reagent mixture for Cas9 transfection of 1 well of a 12 well plate.

Reagent	Volume (µL)
Cas9 mixture	
Edit-R Cas 9 plasmid 100 ng/µl	20
Edit-R trans-activating CRISPR RNA (tracrRNA) 10 µM	2
Edit-R CRISPR RNA (crRNA) 10 µM	2
Tris pH 7.5 10 mM	6
Opti-MEM	70
Lipofectamine mixture	
Lipofectamine2000	4
Opti-MEM	96

Table 2-4 CRISPR Cas9 crRNA target sequences.

crRNA product number	Target exon	Target sequence 5' – 3'	Protospacer adjacent motif (PAM)
Dharmacon CM-019913-03-0002	5	CTGTCCCGTGCACTGAGTGA	GGG
Dharmacon CM-019913-05-0002	3	TTGCCAGGAGATGCCCAGCC	TGG

2.1.6 Plasmid DNA transfection

HeLa and HEK293 cells were transfected with plasmid DNA with either Lipofectamine 2000 according to the manufacturer's instructions, or with polyethylenimine (PEI).

Separately, Lipofectamine 2000 (2 µL/µg DNA) and plasmid DNA were diluted in Opti-MEM and incubated for 5 min. The mixtures were combined, vortexed for 10 s and then incubated for 20 min. After incubation the mixture was added dropwise directly to cells in culture medium and incubated at 37°C.

For transfection with PEI, plasmid DNA was diluted in Opti-MEM and incubated for 5 min. The PEI (3 µL/µg DNA) was added directly to the DNA/Opti-MEM mix and immediately vortexed for 15 s. The DNA/PEI mixes were incubated for 20 min and then added dropwise directly to cells in culture medium and incubated at 37°C.

All transfection reagents were incubated for at least 24 h prior to experimentation. The DNA plasmids used in transfections are listed in Table 2-5. The amount of DNA and transfection reagent used for transfections in different culture plates are listed in Table 2-6.

Table 2-5 Plasmid DNA constructs.

Plasmid DNA construct	Attribution
Empty vectors	
pCI-neo	Promega
pCI-neo-mCherry-N	In house (Dr Annekathrin Möller)
pGEX6p1	GE Healthcare
pEGFPc2	Clontech
C21orf2	
pCI-neo-Myc-C21orf2	In house (Dr Rebecca Cohen) from human C21orf2 cDNA (Dharmacon MHS6278-202832621)
pCI-neo-C21orf2-HA	In house (Miss Natalie Pye)
pCI-neo-C21orf2-HA Δ2 – 15	In house (Miss Natalie Pye)
pGEX6p1-C21orf2-HA	In house (Miss Natalie Pye)
NEK1	
pCI-neo-Myc-NEK1	In house (Dr Rebecca Cohen) from human NEK1 cDNA (Dharmacon MHS6278-211690479)
pCI-neo-V5-NEK1	In house (Miss Natalie Pye)
pCI-neo-V5-NEK1 K33R	In house (Miss Natalie Pye)
pCI-neo-mCherry-NEK1	In house (Miss Natalie Pye)
pCI-neo-V5-NEK1 (AA 1-258)	In house (Miss Natalie Pye)
pCI-neo-V5-NEK1 (AA 1-379)	In house (Miss Natalie Pye)
pCI-neo-V5-NEK1 (AA 1-732)	In house (Miss Natalie Pye)
PTPIP51	
pCI-neo-PTPIP51-HA	Prof Chris Miller (King's College London)
pGEX6p1-PTPIP51-ΔTM-HA	In house (Prof Kurt De Vos)
pCI-neo-PTPIP51-HA S149A	GenScript
pCI-neo-PTPIP51-HA S151A	GenScript
pCI-neo-PTPIP51-HA T152A	GenScript
pCI-neo-PTPIP51-HA S154A	GenScript

Plasmid DNA construct	Attribution
PTPIP51	
pCI-neo-PTPIP51-HA S149A/S151A/T152A/S154A	Genscript
pCI-neo-PTPIP51-HA Y158A/F159A/T160A	In house (Miss Lucy Jennings)
pCI-neo-PTPIP51-HA F167A/A170D	GenScript
pCI-neo-PTPIP51-HA F167A/T168A/D167A/A170D	GenScript
pCI-neo-PTPIP51-HA Y176A	GenScript
pCI-neo-PTPIP51-HA Y176F	GenScript
pCI-neo-PTPIP51-HA Y176E	GenScript
pCI-neo-PTPIP51-HA Y176A/A179F	GenScript
VAPB	
pCI-neo-Myc-VAPB	Prof Chris Miller (King's College London)
pCI-neo-Myc-VAPB T201A	In house (Miss Natalie Pye)
pCI-neo-Myc-VAPB T201E	In house (Miss Natalie Pye)
pCI-neo-Myc-VAPB K87D/M89D	GenScript
pGEX6p1-VAPB-ΔTM	In house (Prof Kurt De Vos)
pEGFPc2-VAPB	Prof Chris Miller (King's College London)
VAPA	
pcDNA3.1-FLAG-VAPA	Prof Chris Miller (King's College London)
pcDNA3.1-FLAG-VAPA K94D/M96D	GenScript

Table 2-6 Reagents and conditions for plasmid DNA transfection.

Transfection reagent	Plate size	DNA per well (µg)	Transfection reagent per well (µL)	Transfection mix per well (µL)
Lipofectamine2000	24 well	0.5	1	50
	12 well	1	2	100
	6 well	2	4	200
	10 cm^2 dish	10	20	500
PEI	24 well	0.5	1.5	50
	12 well	1	3	100
	6 well	2	6	200
	10 cm^2 dish	10	30	500

2.1.7 siRNA transfection

Small interfering RNA (siRNA) for knockdown of protein expression were obtained from Sigma-Aldrich, Integrated DNA Technologies (IDT) or Dharamacon and are described in Table 2-7. HeLa and HEK293 cells were transfected with siRNA using Lipofectamine RNAiMAX (Invitrogen, 13778150) according to the manufacturer's instructions.

Separately, Lipofectamine RNAiMAX (0.1 µL/pmol siRNA) and siRNA were diluted in RNA-se free Opti-MEM and incubated for 5 min. The Lipofectamine RNAiMAX mix was then added to the siRNA, vortexed for 10 s and incubated for 20 min. The mixture was then added dropwise to cells in culture medium and incubated at 37°C. Media was changed 5 h post-transfection.

Cells were used for experimentation 4 days post-siRNA transfection. When subsequent plasmid DNA transfection was required, this was performed on day 3, 24 h before cells were used in experimentation. The amount of siRNA and Lipofectamine RNAiMAX used for siRNA transfections in different sized culture plates are listed in Table 2-8.

Table 2-7 siRNA sequences.

siRNA	Sequence(s) 5' – 3'	Company	Product Code	Reference
NEK1 #1	GUGCUAAGUGCUGGUGGAA	Sigma-Aldrich	SASI_Hs01_00035386	
NTC	UGGUUUACAUGUCGACUAA UGGUUUACAUGUUGUGUGA UGGUUUACAUGUUUUCUGA UGGUUUACAUGUUUUCCUA	Dharmacon	D-00181-10-20	(Anderson *et al.*, 2008)
PTPIP51 #11	GAAGCUAGAUGGUGGAUGAUU	Sigma-Aldrich	N/A	(De Vos *et al.*, 2012)

Table 2-8 siRNA transfection conditions with Lipofectamine RNAiMax.

Plate Size	siRNA per well (pmol)	RNAiMax per well (µL)	Total volume per well (µL)
24 well	6	0.6	50
12 well	12	1.2	100
6 well	24	2.4	200

2.1.8 Induction of DNA damage

DNA damage in the form of double strand breaks was induced by DNA topoisomerase inhibitor camptothecin (CPT). CPT has been shown to cause increased expression of γH2AX and increased caspase 3 activity (Berniak *et al.*, 2013; Rodriguez-Hernandez *et al.*, 2006). DNA damage was induced by incubation with 10 µM CPT (Abcam, ab120115) for 1 hour at 37 °C. After incubation, cells were immediately lysed or fix to prevent the repair of DNA before analysis.

2.1.9 Induction of autophagy

Autophagy was induced by incubation with 250 nM Torin1 (Sigma-Aldrich, 475991) for 3 h. Fusion of autophagosomes with lysosomes was inhibited by treatment of 100 nM Bafilomycin A1 (LKT laboratories, B0025) for 6 h. Where cells were treated with Torin1 and Bafilomycin A1, the Torin1 was added 3 h after addition of Bafilomycin A1.

2.2 Molecular DNA techniques

2.2.1 Site-directed mutagenesis

Site-directed mutagenesis was utilised to cause the mutation of a single amino acid, such as to produce phospho-mutants or insertion of premature stop codons. Primers for mutagenesis were designed using the QuikChange primer design tool (Agilent), purchased from IDT, and are described in Table 2-9. Mutagenesis was performed according to the manufacturer's protocol using a QuikChange Lightning kit (Agilent, 210518).

Briefly, 50 ng of plasmid DNA was mixed with 125 ng of the designed mutagenesis primers supplemented with 10x QuikChange Lightning buffer, deoxynucleotide (dNTP) mix and QuikSolution reagent and nuclease free water. The QuikChange Lightning enzyme was then added immediately before running the mixture on a PCR cycle to cause amplification and mutation of the template DNA. The composition of the reaction is described in Table 2-10.

Amplification was performed in a thermocycler using the following parameters: 2 min at 95 ˚C, followed by 18 cycles of 95 °C for 20 s to melt double stranded DNA (dsDNA), 60 °C for 10 s to anneal primers and an elongation step at 68 °C for 30 s per kbp of plasmid to be amplified (Table 2-11). Parental DNA, lacking the mutation, was digested by incubation with 2 µL of *Dpn I* enzyme for 10 min at 37 °C. Plasmid DNA was transformed into XL-10 Gold ultracompetent cells (2.2.8). All constructs harbouring a mutation generated in house were verified by sequencing.

Table 2-9 Primer sequences for site directed mutagenesis.

Construct	Primer	Sequence (5'-3')
pCI-neo-V5-NEK1-K33R	Forward	CTTGAGATGTTAATTTCCCTGATAACATACTGTCTGCCATCTTCT
	Reverse	AGAAGATGGCAGACAGTATGTTATCAGGGAAATTAACATCTCAAG
pCI-neo-V5-NEK1 (AA 1-258)	Forward	GCTGAGGAGAGAGAAACTTTTAAATGCGTTTGGCTATAAAACC
	Reverse	GGTTTTATAGCCAAACGCATTTAAAAGTTTCTCTCTCCTCAGC
pCI-neo-V5-NEK1 (AA 1-379)	Forward	TCAGCCTTCATTAAACTAATAATCTAATCCTTTTGTTTCTTTTCTTTTTCAATAAATTC
	Reverse	GAATTTATTGAAAAAGAAAAGAAACAAAAGGATTAGATTATTAGTTTAATGAAGGCTGA
pCI-neo-V5-NEK1 (AA 1-732)	Forward	ATCTTCATGAACATTTATCTAAAAAGTATCAGAGAGATTCTGCTTTCC
	Reverse	GGAAAGCAGAATCTCTCTGATACTTTTTAGATAAATGTTCATGAAGAT
pCI-neo-Myc-VAPB-T201A	Forward	TGTTGCTCTGCACTGCCTTCCTCATCCGCAG
	Reverse	CTGCGGATGAGGAAGGCAGTGCAGAGCAACA
pCI-neo-Myc-VAPB-T201E	Forward	GGCTGTTGCTCTGCACTTCCTTCCTCATCCGCAGTC
	Reverse	GACTGCGGATGAGGAAGGAAGTGCAGAGCAACAGCC

Table 2-10 Composition of QuikChange Lightning mutagenesis reaction.

Reagent	Volume or Amount
10x QuikChange Lightning buffer	3 µL
Plasmid DNA	50 ng
dNTP mix	0.6 µL
QuikSolution reagent	0.9 µL
Forward primer 10 µM	1.25 µL
Reverse primer 10 µM	1.25 µL
Nuclease free water	13 µL
QuikChange Lightning enzyme	1 µL

Table 2-11 Parameters for PCR cycle of QuikChange Lightning mutagenesis reaction.

Cycles	Temperature (°C)	Time
1	95	2 minutes
18	95	20 seconds
	60	10 seconds
	68	(30 seconds/kbp)
1	68	5 minutes

2.2.2 Restriction digest of plasmid DNA

For sub-cloning of cDNA into a new plasmid vector with compatible restriction enzyme sites, a restriction digest was performed to cut the insert from the existing vector and to open the recipient destination vector. Three µg of insert plasmid DNA and 1 µg of vector plasmid DNA were digested in FastDigest green buffer (Thermo Fisher Scientific, B72), using the required FastDigest restriction enzymes (Thermo Fisher Scientific), by incubating at 37 °C for 15 min. For the vector plasmid, digests were supplemented with FastAP Thermosensitive Alkaline Phosphatase (Thermo Fisher Scientific, EF0651) to prevent re-ligation, by catalysing the release of 5'- and 3'-phosphate groups from DNA dephosphorylating the vector. The composition of restriction digests is described in Table 2-12. Digested DNA was run on an agarose gel for purification (2.2.3).

Table 2-12 Composition of plasmid DNA restriction digests.

	Volume or amount	
Reagent	DNA insert	DNA vector
Plasmid DNA	3 µg	1 µg
Fast Digest green 10x buffer	2 µL	2 µL
Restriction enzyme 1	1 µL	1 µL
Restriction enzyme 2	1 µL	1 µL
Fast AP	-	1 µL
Nuclease free water	Up to 20 µL	Up to 20 µL

2.2.3 Agarose gel electrophoresis

Separation of DNA products on an agarose gel was performed in order to extract and purify PCR DNA products for subsequent plasmid cloning or to confirm the successful insert of a DNA fragment into a vector, prior to sequencing. Prior to loading on the gel, 6x loading buffer dye (Thermo Fisher, R0611) was diluted to 1x in each of the samples.

DNA samples were run on one % agarose gels (1 % agarose (BioLine, BIO-41026), 0.002 % ethidium bromide in Tris-acetate-EDTA (TAE) buffer (40 mM Tris, 20 mM acetic acid, 1 mM EDTA pH 8)), for 45 min at 100 V in TAE buffer. Bands were visualised on a G:Box UV box (Syngene). The size of DNA products was estimated using Hyperladder 1 kbp (BioLine, BIO-33053) or Hyperladder 25 bp (Bioline, BIO-33057) as required.

2.2.4 Gel extraction and purification of DNA

Following the agarose gel electrophoresis of restriction digested plasmid DNA or Phusion PCR DNA products, bands corresponding to the insert and vector were excised from the gel using a scalpel under a UV light box.

Excised DNA was eluted from the gel using a GenElute kit (Sigma-Aldrich, NA1111-1KT) according to the manufacturer's protocol for spin procedure, with all centrifugation steps performed at 14,000 x g at room temperature. Briefly, excised bands were dissolved in gel solubilisation buffer at 55 ˚C for 10 min. During solubilisation, binding columns were prepared by a spin for 1 min with column preparation solution. 100% isopropanol was added to the dissolved gel and the sample passed through the prepared spin column for 1 min. The column was washed in wash buffer at for 1 min and dried by centrifugation at for 1 min. DNA was eluted from the column using GelElute elution solution by centrifugation for 1 min. The concentration of the eluted DNA was determined on a NanoPhotometer N60 (Implen).

2.2.5 DNA ligation

For the cloning of insert DNA into a new vector using restriction enzyme sites, ligation was performed by incubating linearised insert and vector at a 3:1 molar ratio using the Quick Ligation kit (NEB, M2200). For each reaction 50 ng vector DNA was used, with the amount of insert DNA used calculated by the following formula:

$$\frac{\left(ng(vector) * basepairs(insert)\right)}{\left(basepairs(vector)\right)} * 3 = ng(insert)$$

Briefly, DNA for vector and insert were diluted in nuclease free water (Qiagen, 129114) and 2 X Quick Ligase buffer to a final volume of 19 µL. One µL of Quick Ligase enzyme was added and the reaction and incubated for 15 min at room temperature (Table 2-13). The ligates were transformed into XL-10 Gold ultracompetent cells (2.2.8).

Table 2-13 Composition of DNA ligation reaction.

Reagent	Volume
DNA insert	Variable
DNA vector	Variable
2X Quick Ligate buffer	10 µL
Quick Ligase enzyme	1 µL
Nuclease free water	Up to 20 µL

2.2.6 Phusion PCR

For sub-cloning of plasmid DNA into a new vector without compatible restriction enzyme sites, Gibson Assembly was performed (2.2.7), which requires amplification of a PCR product with overlapping regions to the destination vector. Primers for Phusion PCR were designed using the NEBuilder assembly tool (NEB) and purchased from IDT.

Phusion High-Fidelity PCR kit (NEB, E0553L) was used according to manufacturer's protocol to amplify insert DNA fragments with complementary overlapping regions to the destination vector DNA. Briefly, 5 ng of template DNA was mixed with 100 ng of the designed primers, Phusion High-Fidelity buffer, and dNTP mix. Immediately prior to amplification by PCR, 1 µL of Phusion enzyme was added (Table 2-14).

Amplification (Table 2-15) was performed in a thermocycler using the following parameters: 1 min at 98 ˚C for initial denaturation, followed by 30 cycles of 98 °C for 10 s to denature dsDNA, 45-72 °C (depending on primers) for 20 s to anneal primers and an extension step at 72 °C for 30 s per kbp of plasmid to be amplified, followed by a final extension at 72 °C for 10 min. The primers used for Phusion PCR are described in Table 2-16.

Table 2-14 Composition of Phusion PCR reaction.

Reagent	Volume or amount
Plasmid DNA	5 ng
Phusion High-Fidelity buffer	4 µL
dNTP mix	1 µL
Forward primer 10 µM	1 µL
Reverse primer 10 µM	1 µL
Phusion enzyme	1 µL
Nuclease free water	Up to 20 µL

Table 2-15 Parameters for PCR cycle of Phusion PCR.

Step	Cycles	Temperature (°C)	Time
Initial Denaturation	1	98	1 min
Denaturation	30	98	10 s
Annealing		45 – 72 depending on primer	20 s
Extension		72	30 s per kbp
Final Extension	1	72	10 min

Table 2-16 Sequences of primers used for Phusion PCR.

Construct	Primer	Sequence (5'-3')
pCI-neo-C21orf2-HA	Forward	TTAATACGACTCACTATAGGCTAGCGCCACCATGAAGCTGACGCGGAAGATG
	Reverse	AACCCTCACTAAAGGGAAGCGGCCGCTCAAGCGTAATCTGGAACATCGTATGGGTAGTCGACCTCGGCGTGCTCCTGCAC
pCI-neo-C21orf2-HA Δ2-15	Forward	TTAATACGACTCACTATAGGCTAGCGCCACCATGGAGCTGCACAGCGTG
	Reverse	AACCCTCACTAAAGGGAAGCGGCCGCTCAAGCGTAATCTGGAACATCGTATGGGTAGTCGACCTCGGCGTGCTCCTGCAC
pGEX6p1-C21orf2-HA	Forward	GGGGCCCCTGGGATCCCCGGGAATTCGCGCCACCATGAAGCTGACGCGGAAG
	Reverse	TCGTCAGTCAGTCACGATGCGGCCGCTCAAGCGTAATCTGGAACATCG
pCI-neo-V5-NEK1	Forward	GCTGGGCCTGGATAGCACCCTCGTCGACGAGAAGTATGTTAGACTACAG
	Reverse	AACCCTCACTAAAGGGAAGCTTATTCATCATTATCTTCTTGGTAG
pCI-neo-mCherry-NEK1	Forward	GCGGGAGTGCTAGCCTCGAGTCTAGAGAGAAGTATGTTAGACTACAG
	Reverse	AACCCTCACTAAAGGGAAGCGTCGACTTATTCATCATTATCTTCTTGGTAG

2.2.7 Gibson assembly

Following Phusion PCR to create DNA inserts with overlapping ends to the destination vector, the DNA products were excised from agarose gels (2.2.3) and purified (2.2.4). Restriction digest to open the destination vector DNA was performed as described in 2.2.2. Gibson assembly was performed by incubating linearised insert and vector at a 2:1 molar ratio with Gibson Assembly Master Mix (NEB, E2611) (Figure 2-1), using the following equation.

$$\frac{\left(ng(vector) * basepairs(insert)\right)}{\left(basepairs(vectors)\right)} * 2 = ng(insert)$$

For each reaction, 50 ng vector DNA and calculated amount of insert were diluted in nuclease free water (Qiagen, 129114) and 2 X Gibson Assembly Master Mix to a final volume of 20 µL (Table 2-17) and the reaction incubated for 15 min at 50 °C in a thermocycler. Plasmid DNA was transformed into XL-10 Gold ultracompetent cells (2.2.8).

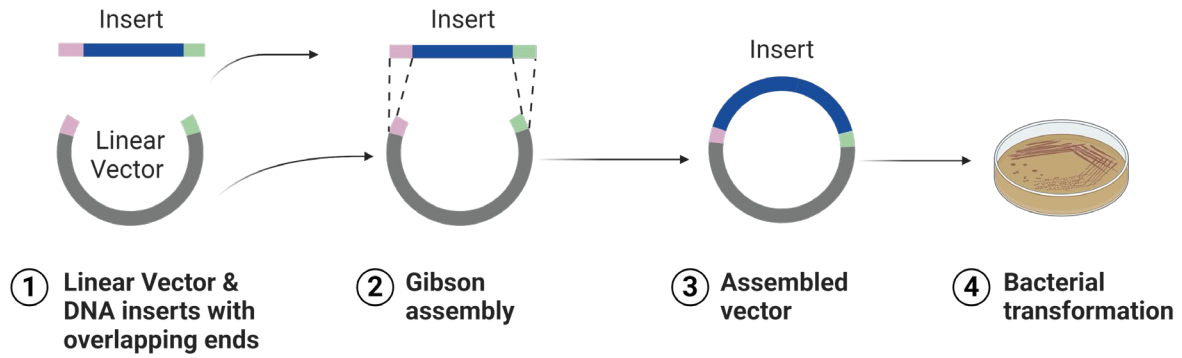

Figure 2-1 Process of cloning with Gibson Assembly.

1) PCR is used to produce DNA inserts with overlapping ends to the intended vector. The vector is de-linearised by restriction digestion.

2) Gibson Assembly is employed to ligate the insert and vector by use of three enzymes. The 5´ exonuclease exposes the complementary sequence for annealing the 5´ end sequences. The DNA polymerase fills in the gaps on the annealed regions. A DNA ligase covalently binds the DNA fragments together.

3) The assembled plasmid DNA is then transformed into bacteria for downstream applications **(4)**.

Table 2-17 Composition of Gibson assembly reaction.

Reagent	Volume
DNA insert	Variable
DNA vector	Variable
2x Gibson assembly master mix	10 µL
Nuclease free water	Up to 20 µL

2.2.8 Transformation of XL10-Gold ultracompetent cells

Plasmid DNA was transformed into XL-10 Gold ultracompetent cells (Agilent, 200315) according to the manufacturer's protocol. Briefly, bacteria were thawed gently on ice and 20 µL transferred to a pre-chilled tube, supplemented with 1 µL ß-mercaptoethanol to improve competency. Two µL of ligated plasmid was incubated with the bacteria for 30 min on ice, followed by a heat shock at 42 ˚C in a heat block for 30 s. Bacteria were returned to ice for 2 min, followed by addition of 250 µL Miller's LB broth (Thermo Fisher Scientific, 11372599) in sterile conditions, and subsequent incubation for 1 h at 37 ˚C in a shaker at 200 rpm. Transformed bacteria were then plated onto pre-warmed LB agar (Thermo Fisher Scientific) plates containing the appropriate antibiotic (ampicillin (100 µg/mL) or kanamycin (30 µg/mL)) and grown overnight at 37 ˚C.

2.2.9 Preparation of bacterial glycerol stocks

Once transformed into ultracompetent bacterial cells, bacterial colonies were picked using a sterilised loop in sterile conditions into 5 mL LB broth and cultured overnight at 37 ˚C with constant shaking at 200 rpm. In sterile conditions, 500 µL of overnight bacterial culture in LB broth was added to 500 µL of 50 % glycerol, to obtain a final concentration of 25 % glycerol (Thermo Fisher Scientific, BP2291) in cryovials. The cryovials were gently inverted to mix the bacterial cells with glycerol and immediately transferred to storage at -80 ˚C.

2.2.10 Preparation of plasmid DNA from bacterial cultures

Bacteria were streaked from glycerol stocks onto LB agar plates containing the appropriate antibiotic (ampicillin (100 µg/mL) or kanamycin (30 µg/mL)) and grown overnight at 37 ˚C in an incubator. The following morning, single colonies were picked in sterile conditions into 1 mL starter cultures of LB broth containing the appropriate antibiotic (ampicillin (100 µg/mL) or kanamycin (30 µg/mL)) and grown at 37 ˚C in an incubating shaker at 200 rpm. After 8 h cultures were expanded to 5 mL cultures which were grown overnight at 37 ˚C in in an incubating shaker at 200 rpm.

DNA was extracted from bacteria using a NucleoSpin plasmid kit (Macherey-Nagel, 740588.250), according to the manufacturer's instruction, all centrifugation steps were at 11,000 xg. Briefly, bacteria were pelleted by centrifugation at for 10 min at room temperature. Bacterial pellets were resuspended in A1 buffer and subjected to SDS/alkaline lysis by addition of A2 buffer for 5 min. The lysis was neutralized by addition of A3 buffer and bacterial debris pelleted by centrifugation for 5 min at room temperature. The supernatant was transferred to a spin column and centrifuged 1 min. DNA was washed once in AW buffer 1 min and once in A4 buffer containing ethanol for 1 min. The column was dried by centrifugation for 2 min. The DNA was then eluted from the column by the addition of elution buffer and incubation at room temperature for 1 min followed by centrifugation for 1 min. DNA concentration was determined on a NanoPhotometer N60 (2.2.11).

2.2.11 Quantification of DNA concentration

The concentration and quality of DNA samples were determined using a NanoPhotometer N60 (IMPLEN) which measured the absorption value of the samples at 260 nm and 280 nm. The concentration of the DNA in ng/µl is then calculated using the following equation (IMPLEN):

$$Concentration\ (ng/\mu g) = A_{260} * 50\ (ng * cm/\mu l)$$

The purity of DNA was assessed based on the A260/A280 ratio, with an acceptable ratio of ~1.8 being considered 'pure' (Lucena-Aguilar *et al.*, 2016). A significantly lower ratio (≤1.6) may be due to contamination of proteins, whilst a higher ratio (≥2.0) may be due to the presence of RNA and thus lead to overestimation of the DNA concentration (Hassan *et al.*, 2015).

2.3 Protein biochemistry

2.3.1 Cell lysis and protein extraction

2.3.1.1 Cell lysis for Immunoblot

Cells plated in 10 cm dishes or 6 well plates were washed once in ice cold PBS, then lysed in 500 or 200 µL respectively of ice cold radioimmunoprecipitation assay (RIPA) buffer (10 mM Tris HCl pH 8, 140 mM NaCl, 1 mM EDTA, 0.5 mM EGTA, 0.1 % SDS, 0.1 % deoxycholic acid, 1 % Triton X-100) supplemented with and 1 X Halt Protease Inhibitor Cocktail (Thermo Fisher Scientific, 78429). Cells were scraped into Eppendorfs and lysed for 1 h at 4 °C with constant rotation and clarified by centrifugation at 17,000 x g for 20 min at 4 °C.

The supernatant was collected, and the protein concentration of the whole cell lysate was determined by Bradford protein assay (2.3.2). Samples were diluted to a standard concentration in RIPA buffer and 5 X Laemmli buffer (1 X Laemmli buffer: 60 mM Tris-HCl pH 6.8, 2.5 % SDS, 5 % glycerol, 5 % β-mercaptoethanol, 0.002 % bromophenol blue) and stored at -20 °C.

Cells plated in a 24 or 12 well plate were directly lysed in 70 µL or 130 µL 2.5 X Laemmli buffer respectively. The cells were scraped using a pipette tip and transferred into an Eppendorf. All protein samples were boiled for 5 min at 95 °C to denature the proteins, prior to running on SDS-PAGE.

2.3.1.2 Cell lysis for immunoprecipitation

Cells were washed once in ice cold PBS and then lysed in 500 µL ice cold modified BRB80 buffer (80 mM K-PIPES pH 6.8, 1 mM EDTA, 1 mM $MgCl_2$, 1 % NP-40, 140 mM NaCl) supplemented with 1 X Halt Protease Inhibitor Cocktail, 1 X PhosStop phosphatase inhibitor tablet (Roche, 4906845001), 1 mM NaF, 1 mM Na_2VO_4, 1 mM $Na_4P_2O_7$ and 40 mM β-glycerophosphate. Cells were scraped into Eppendorfs and lysed for 1 h at 4 °C with constant rotation and clarified by centrifugation at 17,000 x g for 20 min at 4 °C.

Protein concentration was determined by Bradford protein assay (2.3.2). Input samples diluted to a standard concentration in BRB80 buffer and 5 X Laemmi buffer and stored at -20 °C.

2.3.2 Bradford assay for protein quantification

Protein samples, or the corresponding lysis buffer as a background control, were diluted 1:500 in Bradford reagent (Bio-Rad, 5000006). The samples were measured using a S1200 Diode Array Spectrophotometer (WPA) at optical density 595 nm (OD_{595}), as binding with protein results in a confirmational change of the Coomassie Brilliant Blue G-250 in the Bradford and a shift of absorbance from 465 nm to 595 nm. The protein concentration was determined assuming a line of best fit with a slope of 15.

2.3.3 Immunoprecipitation

Immunoprecipitation samples contained at least 1 mg of whole cell protein lysate diluted in BRB80 buffer and incubated overnight at 4 °C with 1 - 2 µg primary antibody with constant rotation. Fifteen µL per sample of magnetic Protein G Sepharose beads (GE Healthcare, 28-9670-70) were washed 3 times in BRB80 prior to incubation with the protein lysates for 2 h at 4 °C with constant rotation. For capture of FLAG-tagged proteins, samples were incubated for 10 µL anti-FLAG conjugated agarose magnetic beads O/N at 4°C (Sigma-Aldrich, M8823). Bead-antibody complexes were washed in BRB80 using an Extractman magnetic bead extraction platform (Gilson, 22100000). The beads were finally resuspended in 20 µL BRB80 and 5 µL 5 X Laemmli buffer. The proteins were eluted from the beads by boiling for 5 min at 95 °C.

2.3.4 Cell fractionation

For cell fractionation, HEK293 cells were grown to 100% confluency in a T75 growth flask. The cells were harvested by addition of 5 mL trypsin-EDTA (Gibco, 15400054) for 3 min at 37 °C and the trypsin quenched by addition of 10 mL DMEM. The cells were pelleted by centrifugation at 400 x g for 4 min and washed twice with PBS on ice. All subsequent centrifugation steps were performed at 4 °C.

Isolation of MAM by cell fractionation was performed as previously described (De Vos *et al.*, 2012; Vance, 1990). The cell pellet was washed once and then resuspended in 600 µL isolation buffer (250 mM mannitol, 5 mM HEPES pH 7.4, 0.5 mM EGTA, 0.1% BSA) (Vance, 1990) supplemented with x 1 Halt Protease Inhibitor Cocktail. For whole cell lysate, 100 µL of resuspended pellet was washed in PBS and lysed in RIPA buffer as previously described (2.3.1.1). The resuspended pellet was homogenised using a teflon/glass dounce homogenizer (100 strokes; Kontes Pestle 19; Kimble Chase). The homogenate was centrifuged twice at 600 x g for 5 min to remove nuclei and unbroken cells.

The MAM-enriched mitochondrial fraction was pelleted by centrifugation for 10 min at 10, 300 x g. To extract the cytosol and small vesicles, the supernatant was centrifuged for 30 min at 100,000 x g in a TLA55 ultracentrifuge (Beckman Coulter). The cytosol containing supernatant, and the small vesicle enriched pellet were separated and collected.

To separate MAM and mitochondria, the MAM-enriched mitochondrial pellet was resuspended in isolation buffer and layered on top of a self-forming 30% Percoll gradient (225 mM mannitol, 25 mM HEPES pH 7.4, 1 mM EGTA, 0.05% BSA, 30% Percoll). The samples were centrifuged for 35 min at 95,000 x g in a TLA55 ultracentrifuge (Beckman Coulter). After centrifugation, a dense band containing the mitochondria was recovered at the bottom of the gradient. The MAM-containing band was retrieved above the mitochondrial band. To remove residual Percoll, both the mitochondria and MAM-containing bands were diluted in isolation medium and washed thrice by centrifugation at 6,300

x g for 10 min. To remove residual mitochondria from the MAM fraction, the sample was centrifuged for 30 min at 100,000 x g in a TL100 ultracentrifuge (Beckman Coulter). The MAM-enriched pellet was recovered, diluted in isolation buffer and centrifuged again for 30 min at 100,000 x g.

All final organelle pellets were resuspended and lysed in RIPA buffer (2.3.1.1), the protein concentrations determined by Bradford assay (2.3.2) and the samples prepared to a standard concentration with Laemmli buffer (2.3.1.1).

2.3.5 SDS-PAGE

Protein lysates were separated by SDS-PAGE on single percentage (7.5%, 10 %, 12 % or 15%) polyacrylamide gels, with either a 6% stacking gel (for >10% acrylamide resolving gel) or 4% stack (≤10% acrylamide resolving gel) (Table 2-18).

Polyacrylamide gels were run in the 4-gel Mini-PROTEAN Vertical Tetra Cell system (BioRad, 1658004EDU), at 120 V for approximately 1.5 h whilst immersed in 1X SDS-PAGE running buffer (25 mM Tris, 192 mM glycine, 0.1 % SDS). The size of protein bands was estimated by running 3 µL of Precision Plus Protein All Blue Protein Standard (Bio-Rad, 1610373) ladder alongside the protein samples.

Table 2-18 Composition of acrylamide gels.

Reagent	Stacking gel	Resolving Gel
30% Acrylamide (Geneflow, A2-0074)	4 or 6%	7.5, 10, 12 or 15 %
0.5M Tris-HCl pH 6.8	125 mM	-
1.5M Tris-HCl pH 8.8	-	375 mM
10% Sodium dodecyl sulfate (SDS)	0.1 %	0.1 %
10% Ammonium persulfate (APS)	0.1 %	0.6 %
Tetramethylethylenediamine (TEMED) (Melford, T18000)	0.001 %	0.003 %

2.3.6 Transfer to membrane

For immunoblotting of proteins separated by SDS-PAGE, the proteins were transferred onto 0.45 µm nitrocellulose membrane (GE Healthcare, 10600002). The polyacrylamide gels were sandwiched, whilst immersed in buffer, into a cassette in direct contact with the membrane, between 2 sheets of filter paper and sponge. The membranes were transferred in the Criterion Blotter system (BioRad, 1704070) at 100 V for 30 min or at 30 V for 16 h, whilst immersed in 1X transfer buffer (25 mM Tris, 192 mM glycine, 20 % methanol).

After transferring, the membranes were subject to reversible Ponceau S (0.1 % Ponceau S, 5 % acetic acid) staining, to confirm successful transfer and ensure the protein samples were loaded equally. The membranes were washed in distilled water to remove the Ponceau S stain prior to blocking the membranes.

2.3.7 Immunoblotting

Prior to immunoblotting, the membranes were incubated for 1 h in either 5 % milk or 5% BSA (if using a phospho-specific antibody) diluted in 1X TBS-T (20 mM Tris HCl pH 7.5, 137 mM NaCl, 0.1 % Tween-20) at room temperature for 1 h to block aspecific binding of the primary antibodies.

After blocking, the membranes were incubated for 1 h at room temperature or overnight at 4 °C in primary antibodies diluted in 2 mL blocking buffer. After 3 X 10 min washes in TBS-T, the membranes were incubated for 1 h whilst protected from light in either horseradish peroxidase (HRP)-conjugated or fluorescent fluorophore-conjugated secondary antibodies diluted in 25 mL TBST-T.

A final 3 washes for 10 min in TBS-T were performed before imaging. If membranes were incubated with HRP-conjugated antibodies, they were incubated prior to imaging with SuperSignal West Pico PLUS Chemiluminescent substrate (Thermo Scientific, 34577) according to the manufacturer's instructions. An equal volume of the stable peroxide and luminol/enhancer was added to the membrane and incubated for 3 min at room temperature. The membranes were imaged on a Licor Odyssey FC, with the Image Studio software v5.2 (Licor), using the necessary channels (680 for protein ladder & rabbit fluorescent antibodies, 800 for mouse fluorescent antibodies or chemi for HRP-conjugated antibodies) for a standard 2 min exposure per channel. The antibodies used in for immunoblotting are described in Table 2-19.

Table 2-19 Antibodies used for immunoblot.

Antibody Target	Host Species	Dilution	Supplier	Product Code
Primary antibodies				
Alpha-tubulin (DM1A)	Mouse	1:5000	Sigma	T6199
ACSL4	Rabbit	1:1000	Thermo Fisher	PA5-27137
Actin (C4)	Mouse	1:5000	Sigma	MAB1501
C21orf2	Rabbit	1:2000	Proteintech	27609-1-AP
Chk1	Mouse	1:1000	ProteinTech	60277-1-Ig
Phospho Chk1 S345	Rabbit	1:1000	Cell Signalling	2348
FLAG	Mouse	1:1000	Sigma	F3165
GAPDH	Rabbit	1:2000	Cell Signaling	2118
GFP (JL-8)	Mouse	1:5000	TaKaRa Bio	632381
HA	Rabbit	1:1000	Sigma	H6908
HA (7)	Mouse	1:1000	Sigma	H9658
H2AX	Rabbit	1:1000	Proteintech	10856-1-AP
Phospho H2AX S139	Mouse	1:1000	Biolegend	613401
LC3B	Rabbit	1:1000	Novus Biologicals	NB100-2220
Myc (71D10)	Rabbit	1:500	Cell Signaling	2278
Myc (9B11)	Mouse	1:2000	Cell Signaling	2276
NEK1	Rabbit	1:1000	Bethyl Laboratories	A304-570A
NEK1	Rabbit	1:1000	Proteintech	27146-1-AP
PDI	Mouse	1:1000	Genetex	GTX25484
PTPIP51	Rabbit	1:1000	Proteintech	20641-1-AP
VAPB	Rabbit	1:2000	Genetex	GTX131631
VAPB	Mouse	1:2000	Proteintech	66191-1-Ig
VDAC1	Rabbit	1:1000	Abcam	Ab15895

Antibody Target	Host Species	Dilution	Supplier	Product Code
Secondary antibodies				
Alexa Fluor® 790 AffiniPure Anti-Mouse IgG (H+L)	Donkey	1:50,000	Jackson ImmunoResearch	715-655-150
Alexa Fluor® 790 AffiniPure Anti-Mouse IgG (L)	Goat	1:50,000	Jackson ImmunoResearch	115-655-174
Alexa Fluor® 680 AffiniPure Anti-Rabbit IgG (H+L)	Donkey	1:50,000	Jackson ImmunoResearch	711-625-152
Anti-Mouse Immunoglobulins/HRP	Goat	1:5000	Dako	P0447
HRP AffiniPure Anti-Rabbit IgG (H+L)	Donkey	1:25,000	Jackson ImmunoResearch	711-035-152

2.3.8 Quantification of band intensities

Quantification of band signal intensities was performed using the Image Studio Lite software v5.2 (Licor). A region of interest (ROI) was drawn around the band using the add rectangle feature. The ROI were set with a border width of 3 above and below, with the median signal intensities of these bordering spaces being subtracted as background. The signal intensities were normalised to the loading control, or the immunoprecipitated protein if quantifying protein interactions.

2.4 Fluorescence microscopy

2.4.1 Immunofluorescence

Coverslips were washed once with PBS and fixed for 20 min at room temperature in 3.7 % formaldehyde followed by 20 min at -20 °C in ice cold methanol if imaging ER-mitochondria contacts. The coverslips were then washed twice in PBS, followed by 1 wash in 50 mM ammonium chloride quenching solution (50 mM NH4Cl in PBS) and a subsequent incubation in quenching solution for 15 min at room temperature to quench the fixing agents and any autofluorescence. The cells were then permeabilised with 0.2 % Triton X-100 in PBS for 3 min at room temperature to allow entry of the antibodies through the plasma membrane. Following permeabilisation, the coverslips were incubated for 20 min in blocking buffer (0.2 % fish gelatine in PBS) at room temperature, to block aspecific binding of the primary antibodies.

The coverslips were then incubated with primary antibodies diluted in blocking buffer for 1 h at room temperature in a humidity chamber to prevent evaporation of the primary antibody. Following primary antibody incubation, the coverslips were washed 3 times with blocking buffer and then incubated for 1 h in secondary antibodies diluted in blocking buffer at room temperature in a humidity chamber, protected from light. Following secondary antibody incubation, the subsequent washes and incubations were performed in the dark to prevent quenching of the fluorescent antibodies.

The coverslips were washed 3 times in PBS prior to incubation with 1 µg/mL Hoechst 33342 (Invitrogen, H1399) in PBS for 10 min for nuclear staining. Coverslips were washed for a final 3 times with PBS and then mounted onto slides (Academy, N/A132) using fluorescence mounting media (Dako, S3023), which was allowed to dry overnight whilst protected from light prior to imaging. The antibodies used in for immunofluorescence are described in Table 2-20.

Table 2-20 Primary antibodies for immunofluorescence.

Antibody Target	Host Species	Dilution	Supplier	Product Code
Primary antibodies				
Alpha-tubulin (DM1A)	Mouse	1:500	Sigma	T6199
HA	Rabbit	1:1000	Sigma	H6908
HA	Chicken	1:1000	Abcam	ab9111
HA (7)	Mouse	1:1000	Sigma	H9658
Phospho H3A.X S139	Mouse	1:200	Biolegend	613401
LAMP2 (CD107B)	Mouse	1:250	Biolegend	345302
LC3B	Rabbit	1:100	Novus Biologicals	NB100-2220
Myc (71D10)	Rabbit	1:200	Cell Signaling	2278
Myc (9B11)	Mouse	1:2000	Cell Signaling	2276
PDI	Mouse	1:200	Genetex	GTX25484
PEX14	Rabbit	1:100	Invitrogen	PA5-78103
PTPIP51	Mouse	1:1000	Abcam	ab69337
Rab5	Rabbit	1:250	Abcam	218624
Rab7	Rabbit	1:100	Abcam	ab137029
TOM20	Mouse	1:200	BD Biosciences	612278
V5	Chicken	1:200	Bethyl Laboratories	A190-118A
V5 (D3H8Q)	Rabbit	1:500	Cell Signaling	13202
VAPB	Rabbit	1:100	Genetex	GTX131631
Vimentin	Chicken	1:5000	IMD Millipore	ab5733
Secondary antibodies				
Anti-Mouse IgG (H+L) Alexa Fluor™ Plus 488	Donkey	1:500	Invitrogen	A32766
Anti-Mouse IgG (H+L) Alexa Fluor™ Plus 568	Donkey	1:500	Invitrogen	A10037

Antibody Target	Host Species	Dilution	Supplier	Product Code
Secondary antibodies				
Anti-Rabbit IgG (H+L) Alexa Fluor™ Plus 488	Donkey	1:500	Invitrogen	A32790
Anti-Rabbit IgG (H+L) Alexa Fluor™ Plus 568	Donkey	1:500	Invitrogen	A10042
Anti-Chicken IgG (H+L) Alexa Fluor™ Plus 488	Goat	1:500	Invitrogen	A32931
Cy5-conjugated AffiniPure Anti-Chicken IgG (H+L)	Donkey	1:500	Jackson ImmunoResearch	703-175-155

2.4.2 Proximity ligation assay (PLA)

Proximity ligation assays were performed using Duolink PLA reagents (Sigma-Aldrich), according to the manufacturer's protocol. The coverslips were washed, fixed, and quenched as previously described for immunofluorescence (2.4.1). Following quenching, the cells were permeabilised with 0.2 % Triton X-100 for 15 min at room temperature, followed by blocking with the Duolink blocking solution for 30 min at 37 °C in a humidity chamber.

Coverslips were then incubated with primary antibodies diluted in Duolink antibody diluent for 1 h at room temperature in a humidity chamber. The primary antibodies were used at the same dilutions as for immunofluorescence (Table 2-20). After primary antibody incubation, the coverslips were washed 2 X 5 min in wash buffer A (Sigma-Aldrich, DUO82049). Coverslips were then incubated with the Duolink PLUS anti-rabbit (Sigma-Aldrich, DUO92002) and MINUS anti-mouse (Sigma-Aldrich, DUO92004) PLA probes for 1 h at 37 °C in a humidity chamber. If the addition of a fluorescent secondary antibody was needed, this was added to the PLA probe incubation at the same dilution as described for immunofluorescence (Table 2-20).

Following 2 X 5 min washes in wash buffer A, coverslips were incubated with ligase diluted in ligation buffer (Sigma-Aldrich, DUO92008) to anneal the PLA probes for 30 min at 37 °C in a humidity chamber. After 2 X 5 min washes in wash buffer A, the coverslips were incubated with polymerase diluted in amplification buffer (Sigma-Aldrich, DUO92008) for 100 min at 37 °C in a humidity chamber, to allow amplification of the PLA signal by rolling loop PCR. The amplification buffer is light sensitive, so from this step onwards, all steps were performed whilst protected from light.

The coverslips were washed 2 X 10 min in wash buffer B (Sigma-Aldrich, DUO82049), followed by incubation with 1 µg/mL Hoechst 33342 in 0.01 X wash buffer B for 10 min. After a final 3 X 10 min wash in 0.01 X wash buffer B, the coverslips were mounted onto glass slides with fluorescence mounting medium and allowed to dry overnight whilst protected from light prior to imaging.

2.4.3 Image acquisition

Images were acquired using the MicroManager 2.0 software (Edelstein *et al.*, 2014) on a BX61 microscope (Olympus) fitted with a Retiga R3 (QImaging) CCD camera or a Zyla4.4 (Andor) sCMOS camera, PE-4000 Ultra LED illumination (CoolLED), and either an UPlanFLN 40x/0.75na objective (Olympus), or a Plan-APOCHROMAT 63×/1.4na oil objective (Zeiss).

All samples were blinded prior to imaging and where possible, single cells were selected for analysis based on fluorescence in a second channel. Illumination intensities, exposure times, and camera settings were kept constant during experiments.

2.4.4 Image analysis

2.4.4.1 Quantification of PLA

For quantification of PLA signal, composite images (Figure 2-2A) were separated into their individual channels. ROI for analysis were created on the vimentin or protein of interest-stained channel using the polygon selection tool to manually outline individual cells (Figure 2-2B). Overlapping cells or cells not fully in frame were excluded from analysis. The respective PLA images (Figure 2-2C) were filtered using a Hat filter (17x17 kernel) to extract single PLA signals (Figure 2-2D). PLA signal was quantified using an in-house ImageJ macro that uses the 'Find maxima' function of ImageJ (Figure 2-2E). Prior to image analysis the prominence needed for image analysis was determined by testing a random image from each sample and adjusting the prominence on the 'Find maxima' function with the 'strict' and 'count' settings applied, until all PLA signal but no background is counted.

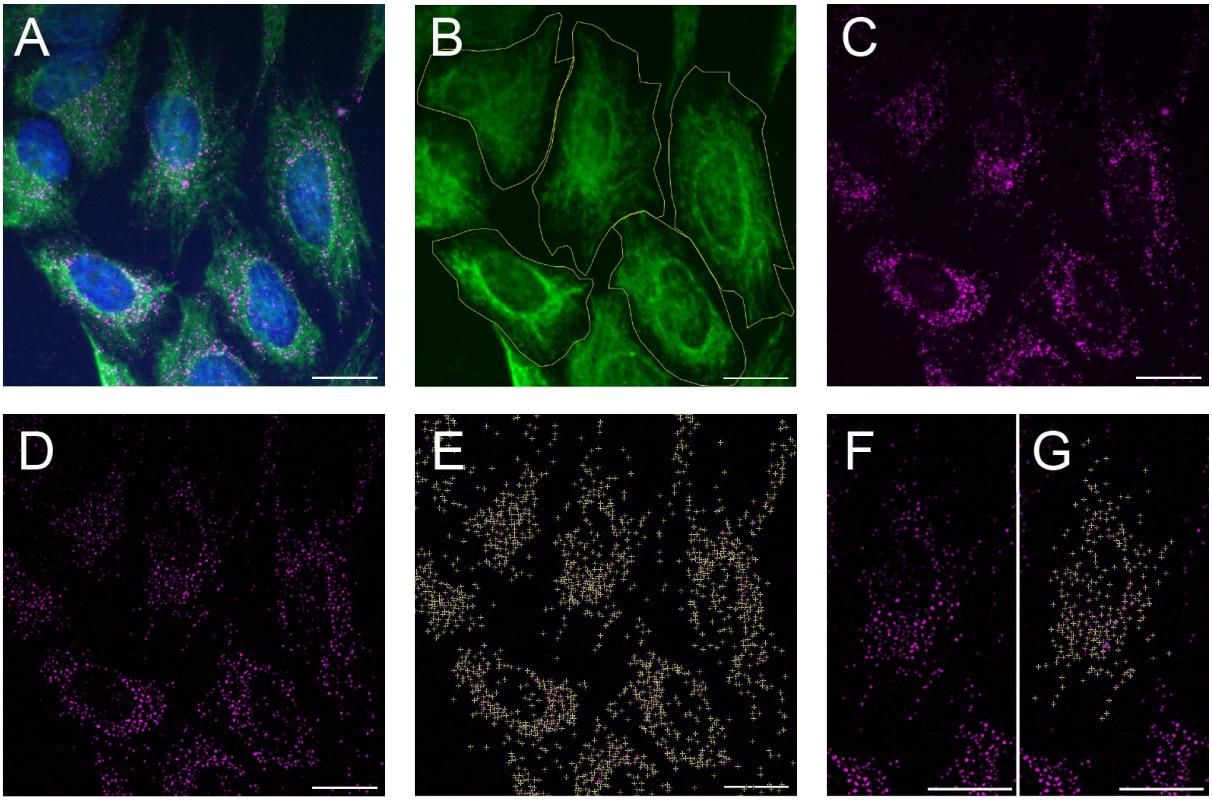

Figure 2-2 Quantification of proximity ligation assay (PLA) signal per cell

A) The composite image as acquired showing PLA signal (magenta), vimentin stain (green) and nuclear Hoechst stain (blue). **B)** The images were split into separate channels and regions of interest (ROI) drawn around cells to be analysed using the vimentin-stained channel. The PLA channel **(C)** was filtered with a Hat filter (17x17 kernel) to allow identification of single PLA signals **(D)**. **E)** The prominence needed for the 'Find maxima' function of ImageJ was determined by adjusting the parameter until all PLA signal and no background was counted. **F)** Example image of the Hat filtered PLA signal of a cell. **G)** The output count of PLA signal using the ROI of the same cell. Scale bars = 20 µm.

2.4.4.2 Quantification of nuclear phosho-H2AX intensity

For quantification of nuclear phospho-H2AX intensity, composite images (Figure 2-3A) were separated into their individual channels and the nuclei ROI for analysis were manually created on the Hoechst-stained channel using the polygon selection tool (Figure 2-3B). Overlapping nuclei or nuclei not fully in frame were excluded from analysis. The number of phospho-H2AX positive puncta (Figure 2-3C) was quantified using an in-house ImageJ macro that uses the 'Find maxima' function of ImageJ. Prior to image analysis the prominence needed for image analysis was determined by testing a random image from each sample and adjusting the prominence on the 'Find maxima' function with the 'strict' and 'count' settings applied, until all phospho-H2AX puncta but no background is counted.

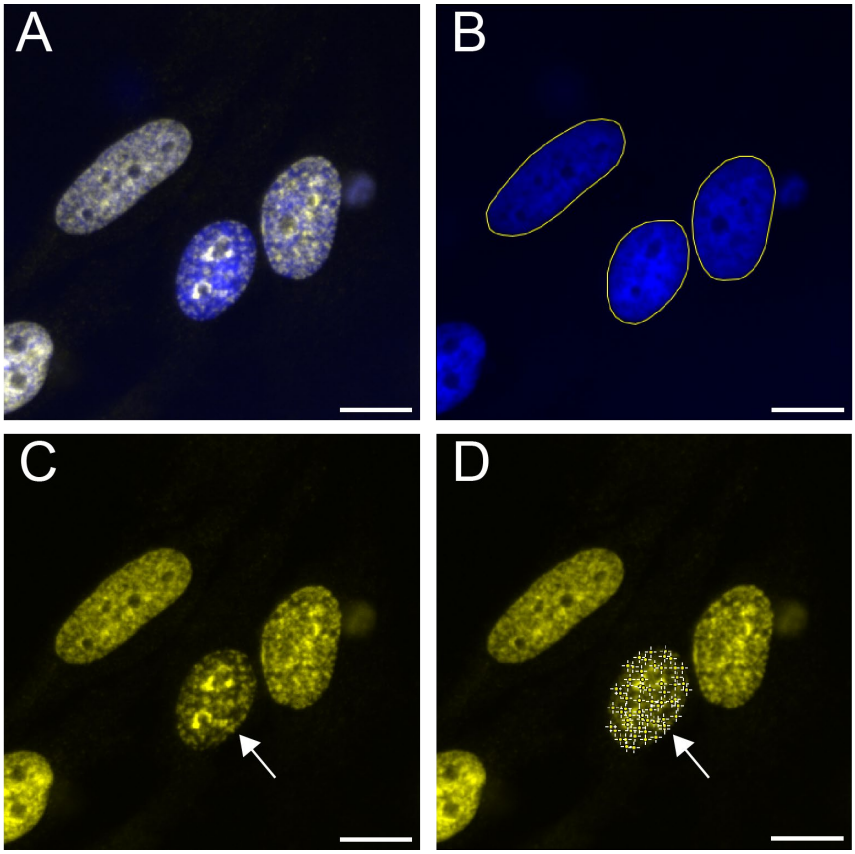

Figure 2-3 Quantification of nuclear phospho-H2AX intensity.

A) The composite image as acquired, opened in ImageJ showing phosphorylated H2AX (yellow) and Hoechst nuclear stain (blue).

B) The images were split into separate channels and regions of interest (ROI) drawn around nuclei to be analysed using the Hoechst-stained channel.

C) Example image of the phospho-H2AX signal of cell nuclei.

D) The output count of phospho-H2AX signal using the ROI of the indicated cell, analysed with the 'Find maxima' function. Scale bars = 10 µm.

2.5 Live cell Ca^{2+} imaging

2.5.1 Live cell Ca^{2+} imaging with Fura2-AM dye

To measure the cytoplasmic Ca^{2+} concentration in HEK293 cells, the cells were washed once in loading media (DMEM + 2 % FBS), then loaded with 2 µM Fura2-AM (Calbiochem, 344905) in loading media for 15 min at 37°C followed by washing in DMEM for 15 min at 37°C. Fura2-AM is a radiometric Ca^{2+} indicator dye, that in low Ca^{2+} concentrations has an excitation maximum at 362 nm, whilst at high conditions has an excitation maximum at 335 nm. Simultaneous measurement at 340 nm and 380 nm is used to create a Fura2 ratio (340/380) that is directly proportional to the level of cytosolic Ca^{2+} (Oakes et al., 1988).

During experiments, cells were perfused continuously with Tyrode's solution (2.5 mM $CaCl_2$, 1 mM $MgCl_2$, 129 mM NaCl, 5 mM KCl, 30 mM glucose, 25 mM HEPES, pH 7.4) using MINIPULS Evolution peristaltic pumps (Gilson), set to deliver 2 mL/min. To invoke Ca^{2+} release from ER stores, 200 µM Oxotremorine-M (Sigma-Aldrich, O100) was applied in Tryrode's solution for 30s. To image the Ca^{2+} sensitive-Fura2-AM dye sequential 340 nm and 380 nm excitation images were recorded in time-lapse mode (1 s interval) at 37°C using MetaFluor software (Molecular Dynamics) on an IX73 inverted microscope (Olympus) equipped with a Dual OptoLED light source (Cairn Research), Optospin filter wheel (Cairn Research), UApoN-340 40×/1.35na oil objective (Olympus), and a Prime BSI sCMOS camera (Photometrics). Cells were kept at 37°C on the microscope using an objective heater (Bioptechs) and stage heater (Warner Instruments).

2.5.2 Analysis of live cell calcium imaging

Using the MetaFluor software, the ratio of Fura2 fluorescence at 340 and 380 nm (Fura2 340/380) was calculated as a measure of cytoplasmic Ca2+ levels. To calculate the baseline cytoplasmic Ca^{2+} level, the average Fura2 340/380 ratio was calculate between the first 30 – 120 s of recording. To calculate the amplitude of response to Oxotremorine-M-stimulated Ca^{2+} release from the ER, the peak Fura2 ratio for each cell after stimulation was normalised by subtraction of the respective baseline ratio value.

2.6 RT-qPCR

2.6.1 RNA extraction

To extract RNA from cells, an appropriate amount of TRIzol reagent (Invitrogen, 15596026) was added to the cells and scraped into an Eppendorf, before incubating at room temperature for 5 min. Next, 200 µL chloroform (Fisher Scientific, 10572714) was added per 1 mL of TRIzol reagent, shaken for 15 s and incubated at room temperature for 3 min, before centrifugation for 15 min at 12,000 x g at 4°C. This causes separation of the samples into a lower red phenol-chloroform layer, an interphase layer and a colourless upper aqueous layer. The upper aqueous layer containing the RNA was transferred into a fresh Eppendorf, ensuring not to disturb the interphase layer beneath.

To isolate the RNA, 0.5 mL isopropanol (Fisher Scientific, 11917993) per 1 mL TRIzol reagent was added and incubated for 10 min at 4°C, followed by centrifugation at 12,000 x g for 10 min at 4°C to cause precipitation of the RNA into a pellet. The supernatant was then discarded, and the pellet dried at room temperature, before resuspending in 1 mL of 75% ethanol (Fisher Scientific, 10542382) per 1 mL TRIzol reagent used, to wash the pellet. The sample was then vortexed for 10 s and centrifuged at 7,500 x g for 5 min at 4°C. The supernatant was then discarded, and the pellet again dried at room temperature.

Finally, the RNA pellet was resuspended in an appropriate amount of RNase-free water (Qiagen, 129114) and incubated at 55°C for 15 min, and then frozen at -80°C until use. The concentration of RNA was determined using a NanoPhotometer N60 (Implen). The volume of TRIzol and RNase-free water used for different sized culture plates is described in Table 2-21.

Table 2-21 Volume of TRIzol and RNAse-free water used RNA extraction.

Plate Size	Volume of TRIzol per well	Volume of RNase-free water per well
6 well plate	1 mL	21 µL
12 well plate	500 µL	16 µL
24 well plate	200 µL	11 µL

2.6.2 Reverse transcription for cDNA synthesis

Reverse transcription was utilised to synthesise the extracted RNA into cDNA. On ice, 1 µg RNA was diluted in RNase free water, and incubated for 10 min at 37°C with 1 µl of DNase I reaction buffer and 1 µl of DNase I (New England BioLabs, M0303S) to degrade any potential contaminating genomic DNA from the RNA samples. The DNAse I was then inactivated to prevent further DNA degradation by heating at 75°C for 10 min with the addition of 1 µl of 25 mM EDTA.

A master mix of 5 X qScript cDNA SuperMix (QuantaBio, 95048-025) was then diluted in RNase free water and 9 µl added to each sample. The qScript cDNA SuperMix contains optimized concentrations of MgCl2, dNTPs, recombinant RNase inhibitor protein, qScript reverse transcriptase, oligo(dT) primer and stabilizers for efficient synthesis from RNA to cDNA. The samples were then subjected to the following PCR cycles: 5 min at 25°C for annealing and extension of the primers, 30 min at 42°C for DNA polymerization and a final 5 min at 85°C for deactivation of the reverse transcriptase enzyme (Table 2-22).

Assuming a 100 % conversion from RNA to cDNA, 1 µg cDNA was obtained from the reverse transcription PCR, and the resulting cDNA was stored at 4 °C.

Table 2-22 Parameters for PCR cycle of qScript reverse transcription PCR.

Step	Temperature (°C)	Time
Annealing & extending primers	25	5 minutes
DNA polymerisation	42	30 minutes
Enzyme denaturation	85	5 minutes

2.6.3 Real time quantitative PCR

For use in RT-qPCR, the amount of cDNA and the dilution of primer used was optimised for each experiment.The cDNA and 100 µM primer stock were diluted as required in nuclease free water (Qiagen, 129114), the primer sequences and dilutions used are described in Table 2-23. The RT-qPCR reactions were performed in triplicate, with a negative control that contains only nuclease free water and no cDNA. For each primer set a master mix was produced, comprised of 5 X HOT FIREPol EvaGreen qPCR Mix Plus (Solis Biodyne, 08-25-00001), complementary forward and reverse primers and nuclease free water (Table 2-24). Nine µL of master mix and 1 µL of cDNA or nuclease free water were loaded in white 96 well plates (Azenta, PCR0980) sealed with clear flat optical caps (Azenta, PCR1066).

Table 2-23 Primer sequences used in RT-qPCR.

Target	Primer	Sequence (5'-3')	Dilution	Reference
C21orf2	Forward	CCCAGGGTGAAGACAGTCAC	1:80	(Watanabe et al., 2020
	Reverse	TCCACCCTCTATGTCCCGAG		
GAPDH	Forward	GGGTGGGGCTCATTTGCAGGG	1:33	(Webster et al., 2016)
	Reverse	TGGGGGCATCAGCAGAGGGG		

Table 2-24 Composition of master mix for RT-qPCR.

Reagent	Volume per well
5 X HOT FIREPol EvaGreen qPCR Mix Plus	2 µL
Forward primer	0.5 µL
Reverse primer	0.5 µL
Nuclease free water	6 µL

RT-qPCR reactions were performed in a CFX96 Touch Real-Time PCR Detection System (BioRad). The thermocycling conditions for the RT-qPCR were as follows: 95 ˚C for 5 min for denaturation, followed by 39 cycles of 95 ˚C for 30 s for denaturation and 60 ˚C for 1 min for primer annealing and extension. RT-qPCR cycles were followed by a melt curve cycle to ensure specificity of the primers and ensure single dsDNA products were generated. Thermocycling conditions for the melt curve were 1 min at 95 ˚C, followed by 1 cycle at 65 ˚C, followed by 57 cycles increasing by 0.5 ˚C/cycle (Table 2-25).

Table 2-25 Parameters for PCR cycle of RT-qPCR.

Step	Cycles	Temperature (°C)	Time
Initial denaturation	1	95	1 min
Denaturation	39	95	30 s
Annealing and extension		60	1 min
Melt curve	1	95	1 min
	1	65	1 min
	57	65 + 0.5 per cycle	1 min

2.6.4 Relative fold change analysis

The CFX Manger software (BioRad) was used to analyse the RT-qPCR data. The relative mRNA levels of the gene of interest were determined by normalising to the GAPDH control via the $\Delta\Delta C_t$ method (Livak and Schmittgen, 2001)

Briefly, the cycle threshold (C_t) values from the triplicate cDNA samples for the gene of interest and GAPDH control gene were averaged. The normalised C_t value (ΔC_t) was calculated by subtracting the GAPDH C_t from the gene of interest C_t, to normalised for amount of cDNA used between samples.

$$\Delta\, Ct \;=\; Ct\,(Gene\ of\ interest) - Ct\,(GAPDH)$$

The ΔC_t for the experimental sample was then normalised to the ΔC_t of the control sample by subtracting control ΔC_t from the experimental ΔC_t.

$$\Delta\Delta\, Ct \;=\; \Delta\, Ct\,(experimental) - \Delta\, Ct\,(control)$$

To determine fold change of mRNA expression relative to the control samples, $2^{-\Delta\Delta Ct}$ is calculated. This produced a value relative to the control sample, such as 0.5 would be a 50% decrease in gene expression, compared to the control.

$$mRNA\ expression\ relative\ to\ control = \;2\ \hat{}(-\Delta\Delta\, Ct)$$

2.6.5 Melt curve analysis

To ensure a single product has been produced and there is no contaminating dsDNA, primer dimers or non-specific primer binding, the melt curve is analysed. For each primer pair used, the melt curve should have one peak, indicating a single product.

2.7 *In vitro* protein assays

2.7.1 Production of GST-tagged proteins in bacteria

Empty vector GST, GST-C21orf2, GST-VAPB and GST-PTPIP51 were expressed in a pGEX-6p1 plasmid vector. Bacteria were grown overnight from glycerol stocks in 100 mL of Terrific Broth (TB) (Fisher Scientific, 12801670) supplemented with 100 µg/mL ampicillin, at 37 ˚C with constant shaking.

The following morning, the bacterial growth of the pre-culture was determined by measuring the optical density at 600 nm (OD_{600}) using a S1200 Diode Array Spectrophotometer (WPA). To calculate the volume of bacterial pre-culture to add to the TB culture (supplemented with 100 µg/mL ampicillin), the following formula was used:

$$Volume\ of\ preculture\ (mL) = \frac{Desired\ culture\ starting\ OD600\ *\ volume\ of\ culture\ (mL)}{OD600\ of\ preculture}$$

For the main bacterial culture, a volume of 750 mL and a starting OD_{600} of 0.04 was chosen. The bacterial cultures were grown at 37 ˚C with constant shaking for 2 h, after which the OD_{600} was measured to assess growth. The OD_{600} was measured every 30 min until a reading of 0.7 was obtained, at which the production of GST-protein was induced by addition of 0.5 mM Isopropyl β-D-1-thiogalactopyranoside (IPTG, Fluorochem, M02726) for 3h for empty vector GST and GST-VAPB or overnight for GST-C21orf2 and GST-PTPIP51, at 37 ˚C with constant shaking.

After incubation with IPTG, the bacteria were pelleted by centrifugation at 6,000 rpm (6,371 x g MAX / 3,951 x g AVG) in an Avanti J26 centrifuge using a JA-10 rotor for 10 min at 4 °C. The supernatant was discarded, and the pellets frozen at -20 °C until use.

2.7.2 Extraction and purification of GST-tagged proteins

For the *in vitro* assays, the amount of bacterial pellet lysed per reaction was 0.1g of GST and GST-VAPB, and 0.2g GST-C21orf2 and GST-PTPIP51. The bacterial pellet for each GST-protein was weighed and lysed in 1 mL RB100 buffer (25 mM HEPES pH 7.5, 100 mM KOAc, 10 mM MgCl2, 1 mM DTT, 0.05 % Triton X-100, 10 % glycerol), supplemented with 1 X Halt Protease Inhibitor Cocktail (Thermo Fisher Scientific, 78429). If GST-proteins were produced for use in *in vitro* phosphorylation assays, the RB100 buffer was also supplemented with 1 X PhosStop phosphatase inhibitor tablet (Roche, 4906845001). The pellets were kept on ice and lysed by sonication at 100%, 3 X 10 s. The lysates were then clarified by centrifugation at 4 °C for 5 min at 17,000 X g, the supernatant taken and centrifuged again at 17,00 X g for 5 min, to ensure removal of any insoluble debris.

Per sample, 30 µL of Glutathione (GSH) Sepharose 4B beads (GE17-0756-01, Cytiva) were prewashed 3 X in RB100 buffer, with centrifugation at 4 °C for 1 min at 600 X g to pellet the beads between washes. The clarified lysates were then incubated with the washed GSH beads for 1 h at 4 °C, with constant rotation. The beads were then washed 3 X with RB100 buffer as previously described, to remove any unbound protein. The captured and washed GST-proteins were then used on-bead for both the binding (2.7.3) and phosphorylation assay (2.7.4).

2.7.3 *In vitro* binding assay

2.7.3.1 In vitro translation

In vitro translation was used to produce recombinant C21orf2 and NEK1 proteins with the incorporation of radioactively labelled ^{35}S-methionine. Briefly 0.5 µg plasmid DNA diluted in 1.5 µL nuclease free water was added to 8 µL of TnT® Quick Coupled T7 Transcription/Translation System Master Mix (Promega, L1171) and 0.5 µL ^{35}S-Methionine (PerkinElmer, NEG709A500UC). The master mix was incubated at 37 °C for 90 min.

2.7.3.2 Binding assay

After the GST-proteins captured on GSH beads were washed (2.7.2), they were resuspended in 400 µL RB100 buffer. Eight µL of radiolabelled *in vitro* translated protein was added to the resuspended GST-proteins and incubated on bead for 1h at 4 °C with constant rotation. The beads were then washed three times in RB100 buffer as previously described (2.7.2). The RB100 buffer was removed, and the beads eluted in 50 µL GSH elution buffer (50 mM Tris-HCl pH 7.5, 100 mM NaCl, 40 mM reduced glutathionine) by trituration and incubated for 10 min at room temperature.

The samples were prepared by diluting 1 µL of GST or GST-VAPB in 15 µL of GSH elution buffer and 4 µL 5 X Laemmli buffer. GST-PTPIP51 and GST-C21orf2 were prepared by adding 16 µL of GST-protein elution to 4 µL of 5 X Laemmli buffer. An input sample of in vitro translated protein was made by adding 0.5 µL of translated protein to 7.5 µL of GSH elution buffer and 2 µL of 5 X Laemmli. The samples were then boiled for 5 min at 95 °C and ran on SDS-PAGE (2.3.4), stained with Coomassie (2.7.5), dried onto filter paper (2.7.6) and imaged for radioactivity (2.7.7).

2.7.4 *In vitro* phosphorylation assay

After the GST-proteins captured on GSH beads were washed (2.6.2), they were resuspended in 100 µL RB100 buffer supplemented with 1 mM adenosine triphosphate (ATP) (Sigma-Aldrich, A2383). To each reaction, 100 ng of recombinant active NEK1 kinase (Abcam, ab268812) was added with 0.5 µL γ-^{32}P-ATP (PerkinElmer, NEG502Z250UC) and incubated for 1 h at 37 °C. The beads were then washed three times in RB100 buffer, eluted in 50 µL GSH elution buffer and the samples prepared as previously described (2.7.3.2). The samples were then boiled for 5 min at 95 °C and ran on SDS-PAGE (2.3.4), stained with Coomassie (2.7.5), dried onto filter paper (2.7.6) and imaged for radioactivity (2.7.7).

2.7.5 Coomassie staining

To confirm the expression of the GST-tagged constructs, the polyacrylamide gels were stained with Coomassie solution (0.1 % Coomassie Blue R-250, 50 % methanol, 10 % acetic acid). Briefly, the gels submerged in Coomassie solution were heated for 15 s in a microwave in a sealed container and incubated overnight at room temperature with constant movement. The following morning the Coomassie solution was removed, and the gels were destained by heating for 15 s in destain solution (30 % methanol, 10 % acetic acid) and incubated for 20 min. After 20 min the destain was removed and the gels heated and incubated in fresh destain until the gel was clear. The gel was washed twice in ddH2O, to remove any residual destaining solution and imaged with a phone camera or dried onto filter paper (2.7.6).

2.7.6 Drying acrylamide gels onto filter paper

To expose the polyacrylamide gel onto the phosphoscreen for imaging of radioactivity, the gels were dried onto filter paper. Briefly, the destained and washed gels were placed onto Whatman filter paper, ensuring no bubbles formed between the two surfaces. The gels were then placed in a Model 582 gel dryer (BioRad), preheated to 80 °C and dried for at least 40 min, until completely dried.

2.7.7 Imaging *in vitro* assays

Prior to use, the phosphor screens (Amersham, 28956475) were subjected to light exposure for 10 min to quench any residual signal. The dried polyacrylamide gel was then placed into the exposure cassette (Amersham, 29175523) and a reference photo taken to record the position of the gel in the cassette. The phosphor screen was then placed directly onto the dried gel, the cassette closed and incubated in the dark for at least 2 days before imaging.

After incubation, the phosphor screens were imaged on a Typhoon FLA 7000 Laser Scanner (GE Healthcare) using the phosphorimaging setting on the Typhoon FLA 7000 Control Software (GE Healthcare). The images were acquired with a standard pixel size of 50 µm. Following exposure, the phosphoscreens were exposed to light for 10 min to quench any signal.

To analyse the results, the image of the Coomassie stained gel and the phosphorimage were digitally overlayed, to confirm which GST-protein the radioactive band corresponded to.

2.8 Mass spectrometry

For mass spectrometry, GST-VAPB protein were produced (2.7.1), extracted and purified (2.7.2), and incubated with or without 100 ng recombinant active NEK1 kinase and eluted into GSH elution buffer (2.7.4) as previously described. The concentration of eluted GST-VAPB protein was then determined by Bradford assay (2.3.2). The proteins were diluted to 0.4 µg/µL using GSH elution buffer and frozen at -80 °C until digestion. For analysis by mass spectrometry, four technical replicates of each sample were prepared.

For mass spectrometry of HeLa cells transfected with eGFP-VAPB, the cells were lysed with BRB80 buffer as previously described in section 2.3.1.2. VAPB was captured by immunoprecipitation with eGFP-trap magnetic agarose beads (ChromoTek, 17323363) for 2h at 4°C and the samples washed with BRB80 using an Extractman (Gilson, 22100000). The samples were stored on ice prior to protein digestion.

2.8.1 S-trap digest of GST-tagged proteins

For digestion of the GST-proteins for mass spectrometry the S-Trap micro-MS sample prep kit (Protifi, K02-micro) was used. Five µg (12 µL) of eluted protein sample was diluted with an equal volume of 2 X S-trap lysis buffer (10% SDS (Sigma-Aldrich, 05030), 100 mM TEAB (Triethylammonium bicarbonate) pH 8.5 (Thermo Scientific, 90114)).

The proteins were reduced to break any disulphide bonds by incubation with 5 mM TCEP (tris (2-carboxyethyl) phosphine) (Supelco, 646547) at 70 °C for 20 min at 750 rpm in a shaking incubator then cooled down for 5 min at room temperature. The samples were alkylated to cap the disulphide bonds by incubation with 10 mM IAM (2-Iodoacetamide) (Sigma-Aldrich, I6125) for 30 min at room

temperature in the dark, followed by addition of 1.2% phosphoric acid to denature the proteins by acidification.

Two hundred and fifty µL of binding buffer (100 mM TEAB pH 7.1 in 90% methanol) was added to the samples and loaded to the S-Trap column by centrifuged at 4,000 X g for 1 min at room temperature. The S-Traps were washed four times with 150 µL binding buffer by centrifugation at 4,000 X g for 1 min and finally dried by centrifugation without any additional wash buffer for 1 min at 4,000 X g.

Following drying, the samples were digested by addition of 1 µg trypsin. Briefly, trypsin (Thermo Scientific, 13464189) was resuspended in 0.1 % TFA (trifluoroacetic acid) to a concentration of 0.1 µg/µL, then diluted to 40 ng/µL in 50 mM TEAB. Twenty-five µL of trypsin in TEAB was added to the S-Trap column and incubated for 1 ½ h at 47 °C without shaking. The peptides were eluted from the S-Trap column by sequential elution buffers, for each elution the buffer was added to the column and centrifuged at 4,000 X g for 1 min at room temperature. The first elution was with 40 µL 50 mM TEAB, followed by 40 µL 0.2 % formic acid (Fisher Scientific, A117-50), 40 µL 50% ACN (acetonitrile) containing 0.2 % formic acid and a final elution with 40 µL 80% ACN containing 0.2% formic acid.

The eluted samples were dried for 1 ½ h at 45 °C in a Concentrator plus (Eppendorf). The dried samples were finally resuspended in 50 µL 0.5% formic acid and 30 µL loaded into mass spectrometry vials, for loading into the mass spectrometer. Remaining elutions were stored at -20°C.

2.8.2 Trypsin digest of eGFP-VAPB

For digestion of eGFP-VAPB immunoprecipitated on GFP-trap magnetic agarose beads, the BRB80 buffer was removed, and cells washed twice with 200 µL 50 mM ammonium bicarbonate. The samples were digested in 25 µL of 2 M urea, 50 mM ammonium bicarbonate with 1 µg trypsin for 2 h at 37°C with constant shaking at 900 rpm. The digested peptides were collected using a magnetic rack and washed with 25 µL 50 mM ammonium bicarbonate prior to transferring to a fresh eppendorf.

The samples were acidified by addition of 0.4% TFA prior to addition to C18 wash spin columns (Pierce, 89870). The samples were captured on the column by centrifugation at 2000 x g for 1 min. Samples were washed by sequential spins with 200 µL ACN, followed by 200 µL 50% ACN/ 0.1% TFA and finally 200 µL 0.1 % TFA at 2000 x g for 1 min. The acidified samples were loaded onto the C18 columns for three more spins at 2000 x g for 1 min to ensure all the peptides were captured. The peptides were washed with 100 µL 0.1% TFA and the columns transferred to a fresh Eppendorf. The peptides were eluted with 100 µL 50% ACN/ 0.1% TFA at 2000 x g for 1 min.

The eluted samples were dried for 1 ½ h at 45 °C in a Concentrator plus (Eppendorf). The dried samples were finally resuspended in 50 µL 0.5% formic acid and 30 µL loaded into mass spectrometry vials, for loading into the mass spectrometer. Remaining elutions were stored at -20°C.

2.8.3 Mass spectrometry

GST-VAPB peptides were analysed in an LTQ Orbitrap Elite hybrid ion trap-orbitrap mass spectrometer (Thermo Fisher Scientific) equipped with an EASY-Spray Ion Source hyphenated to a Dionex Ultimate 3000 uHPLC (Thermo Fisher Scientific). The peptides were trapped with an Acclaim™ PepMap™ 100 C18 trap column (3 µm particle size, 75 µm × 150 mm, Thermo Fisher Scientific, 164946) and separated on an EASY-Spray™ C18 column (2 µm particle size, 50 µm × 150 mm, Thermo Fisher Scientific, ES901) using a 2 min gradient with 0.1% formic acid in water (mobile phase A) and 0.1% formic acid in 80% acetonitrile (mobile phase B).

2.8.4 Analysis of mass spectrometry

Analysis of mass spectrometry was performed as previously described in (Woodley and Collins, 2019). Briefly, the raw MS/MS data files were used for protein identification using MaxQuant software (Cox and Mann, 2008) with default parameters using the E. coli proteome to check for bacterial contamination and referenced to a FASTA file containing the canonical human VAPB sequence. The protein group files generated by MaxQuant were then loaded into the Perseus platform (Tyanova *et al.*, 2016). The label-free quantification (LFQ) values were selected for calculation of variable modifications, oxidation (M) and phosphorylation (STY).

2.9 Electron microscopy

For visualisation with electron microscopy cells were washed with PBS to remove DMEM at room temperature. Cells were fixed in 3% glutaraldehyde in a buffer of 0.1M sodium phosphate/10% sucrose for 1 h prior to collection of cells by scraping. Cells were placed in a fresh Eppendorf and centrifuged at 6500 rpm for 2 min. The supernatant was removed and replaced with buffer (as above).

Cell pellets were then post-fixed using 2% aqueous osmium tetroxide for 2 h, washed briefly in distilled water and replaced with buffer for 10 min. The buffer wash step was repeated for a further 10 min. Subsequently, the cell pellet was dehydrated by treating for 1 h for each step, with increasing concentrations of aqueous solutions of ethanol (70%, 90%, 100%, 100% dried over copper sulphate). The samples were cleared of remaining ethanol in epoxypropane twice for 20 min.

Infiltration was in a 50/50 mix of epoxypropane (EPP) and araldite resin (a mix of CY212, DDSA, and BDMA) overnight on a rotor mixer. This mixture was evaporated free of EPP in a fume hood for 2 h before the mixture was replaced by 100% araldite resin. This mixture was replaced over an 8 h period before the samples were embedded in fresh resin mixture using a "coffin" style mould. These were polymerised in a 60 °C oven for between 48-72 h.

Sections were cut using a Reichart Jung Ultracut E ultramicrotome at ~85 nm and collected on nickel EM grids. These were air dried and then stained for 30 min in 2% uranyl acetate, washed in dH_2O for 30 min, and stained in Reynold's Lead citrate for 5 min, and then washed in dH_2O for 5 minutes.

Grids were examined using an FEI Tecnai Spirit at an operating voltage of 80kv. Images were recorded using a Gatan Orius 1000B camera and Gatan Digital Micrograph software.

2.10 Bioinformatics tools

2.10.1 Kinase prediction

To investigate the predicated kinase for identified phosphorylation sites, the online platform PhosphoSitePlus was utilised (Hornbeck *et al.*, 2015). The protein of interest was searched for on the platform and the queried phospho-site selected for analysis with the kinase prediction tool. This tool ranks the highest predicted kinase based on the kinase consensus phosphorylation sequence.

2.10.2 Protein sequence alignment

To investigate the sequence alignment of RMDN proteins, the software Jalview (version 2.11.3.3) was utilised. The FASTA format protein sequences for the alignment were obtained from UniProt (UniProt, 2021), and loaded into the Jalview software. The default parameters were used to perform alignments.

2.10.3 *In silico* protein modelling

To model protein structures and protein interactions *in silico*, the online platform AlphaFold3 (Abramson *et al.*, 2024) was utilised. Peptide sequences spanning the protein domains of interest were obtained from UniProt and loaded into the AlphaFold3 software using the default parameters. To model dimerisation the number of copies of the peptide of interest was changed to 2. The predicted protein structures and interactions were visualised and annotated with the software UCSF ChimeraX (version 1.8) (Meng *et al.*, 2023).

To visualise the confidence of the predicted protein interaction models as calculated by AlphaFold3, PAE viewer was utilised (Elfmann and Stulke, 2023). For each model the predicted local distance difference test (pLDDT) was reported as a measure of local confidence, where a higher score indicates higher confidence that the predicted model would agree with an experimental structure (Guo *et al.*, 2022). Additionally, the predicted alignment error (PAE) was reported as a measure of confidence in the relative position of two residues, with a lower score indicating low predicted error and high confidence (Guo *et al.*, 2022). Additionally, for models of protein interactions the predicted template modelling (pTM) score and interface predicted template modelling (ipTM) score were reported. The pTM measures how well the protein complex has been predicted, with scores over 0.5 suggesting the complex is similar to the true structure. The ipTM measures the accuracy of the predicted relative

positions of the subunits in the protein complex, with scores above 0.8 representing high confidence predictions (Magana and Kovalevskiy, 2024).

2.11 Statistical analysis

Statistical analysis was performed using the GraphPad Prism version 10.3.1 for windows (GraphPad Software, USA). All data is presented as mean ± SEM unless otherwise stated. For comparison between two samples, statistical analysis was performed by unpaired two-tailed t-test. For comparison between multiple samples, statistical analysis was performed by one-way ANOVA with Fisher's LSD test.

2.12 Figure creation

For creation of schematic figures, the online tool BioRender was utilised (https://www.biorender.com/). For experimental figures, the Adobe Illustrator (version 27.9.6) was utilised.

Chapter 3 Characterising the interaction between NEK1, C21orf2 and the VAPB/PTPIP51 ER-mitochondria tether

3.1 Introduction

The ER and mitochondria are physically tethered at specialised contact sites that are pivotal in the regulation of Ca^{2+} transfer between the organelles (De Vos *et al.*, 2012). One of the best characterised ER-mitochondria tethers is between VAPB on the ER membrane and its mitochondrial partner PTPIP51. This tether has particular significance in the regulation of Ca^{2+} dynamics, autophagy, lipid homeostasis and synaptic function (De Vos *et al.*, 2012; Gomez-Suaga *et al.*, 2017; Gómez-Suaga *et al.*, 2019). Dysregulation of ER-mitochondria contacts has been reported in multiple models of ALS, a progressive neurodegenerative disease, suggesting it may be an early event in disease aetiology (Lee *et al.*, 2024). Evidence of disrupted ER-mitochondria tethering in ALS is discussed in more detail in section 1.2.

Mutations in the gene *NEK1* are a cause of familial and sporadic ALS, and nonsynonymous mutations in the NEK1-interacting protein C21orf2 confer risk to developing the disease (Brenner *et al.*, 2016; van Rheenen *et al.*, 2016). The mechanisms by which NEK1 and C21orf2 mutations lead to ALS is not yet understood. Although as NEK1 LOF mutation iPSC-derived motor neurons exhibit DNA damage accumulation, it may involve the role of NEK1 in the DDR (Higelin *et al.*, 2018) (discussed in section 1.3.3.1). In response to DNA damage a portion of NEK1 is recruited to mitochondria where it phosphorylates the MAM protein VDAC1 to prevent cell death (Chen *et al.*, 2009; Chen *et al.*, 2010b). In addition to VDAC1, a proteomic study suggested that NEK1 may interact with the ER tethering protein VAPB (Cirulli *et al.*, 2015). Upon activation by DNA damage, NEK1 may be recruited to MAM to regulate signalling between the nucleus and mitochondria to promote cell survival (discussed in section 1.3.2.4).

The aim of this chapter was to validate and characterise the interaction of NEK1 and its interacting partner C21orf2 with the VAPB/PTPIP51 ER-mitochondria tether. As at the start of the project the NEK1/C21orf2 protein complex had not been well studied, we also characterised this interaction in parallel.

3.2 Development of a toolbox to investigate the NEK1/C21orf2 protein complex

In order to investigate the effect of loss of NEK1 function on ER-mitochondria contacts, NEK1 knock out (KO) HeLa cells were used as a model. Wild type parental and NEK1 knock KO HeLa cells, which have previously been characterised, were a gift from Dr Carl Laflamme (University of Montreal). As C21orf2 KO cells were not readily available, we utilised CRISPR/Cas9 genome editing to establish a HeLa C21orf2 KO cell line.

3.2.1 Creation and validation of C21orf2 knock out HeLa cells

Wild type HeLa cells were co-transfected with Edit-R trans-activating CRISPR RNA (tracrRNA), a puromycin resistant Edit-R Cas9 nuclease plasmid and Edit-R CRISPR RNA (crRNA) designed to target either exon 3 or 5 of the C21orf2 gene. The tracrRNA, crRNA and Cas9 nuclease form a complex which is targeted to the intended site of mutation. The Cas9 nuclease generates a site specific DSB, which is repaired through NHEJ (Ran *et al.*, 2013). NHEJ is an inefficient DNA repair method, which leads to small insertions and deletions (indels) that can cause nonsense mutations (Pannunzio *et al.*, 2018). This leads to nonsense-mediated decay and functional knock out of the gene. Successfully transfected cells were selected by growth in puromycin containing media. Single cell colonies were identified by seeding in a limiting dilution across 96 well plates. Cell cultures were scaled up from these colonies and screened for functional C21orf2 knock out by immunoblot and qPCR. To confirm functional knock out of C21orf2, the expanded colonies were first run on immunoblot and probed for endogenous C21orf2 and α-tubulin as a loading control. As C21orf2 is necessary for stabilisation of NEK1 protein (Watanabe *et al.*, 2020), the blots were also probed for endogenous NEK1 (Figure 3-1A). On immunoblot we observed three distinct phenotypes in the CRISPR edited cells: the addition of a C21orf2 positive band at a lower molecular weight (3D9, 3F10), loss of the full length C21orf2 band and addition of a smaller band (3F3, 3D10, 3C4) and loss of the full length C21orf2 band (5F3) (Figure 3-1B). The presence of an aspecific band below the full length C21orf2 has previously been reported with this antibody (Watanabe *et al.*, 2020).

As DNA repair by NHEJ leads to random insertion of indels, one possible explanation for the smaller band is due to the production of a truncated protein due to the insertion of a premature stop codon. If the indels within the coding exon are in multiples of three this would prevent a frameshift mutation. This would prevent induction of nonsense-mediated decay and thus cause translation of a truncated protein (Wang *et al.*, 2024b). As the 5F3 clone was the only line to exhibit both loss of full length C21orf2 and NEK1 protein, and did not exhibit a potentially truncated C21orf2 protein, this was chosen for further validation by quantification of C21orf2 mRNA levels.

RNA was extracted from the 5F3 HeLa cells and subjected to RT-qPCR, using primers specific to endogenous C21orf2 and GAPDH as a housekeeping control. The C21orf2 mRNA level was significantly decreased in the 5F3 clone by 75% (Figure 3-1C). As immunoblot and RT-qPCR analysis confirmed the functional knock out of C21orf2, the 5F3 clone was selected for experimental use as the C21orf2 KO HeLa cell line.

3.2.2 Validation of NEK1 and C21orf2 endogenous antibodies

In literature there is a lack of validated endogenous NEK1 and C21orf2 antibodies. Thus, we decided to test commercial antibodies for a range of biochemical techniques including immunoblot, immunoprecipitation and immunostaining. Wild type parental cell (PC) or wild type (WT) HeLa cells, or the corresponding NEK1 KO or C21orf2 KO HeLa cells as negative controls, were subjected to immunoprecipitation. For NEK1 we tested two endogenous NEK1 antibodies, whilst for C21orf2 we tested one endogenous C21orf2 antibody. The samples were immunoblotted with the corresponding endogenous anti-NEK1 and anti-C21orf2 antibodies, and an α-tubulin antibody as a loading control (Figure 3-2). Successful immunoblotting and immunoprecipitation of NEK1 and C21orf2 was observed with the Proteintech NEK1 antibody and the C21orf2 antibody (Figure 3-2B & C), which were used in future experiments. We were unable to validate the specificity of our endogenous antibodies for immunostaining (data not shown).

As we were unable to optimise endogenous antibodies to investigate the cellular localisation of NEK1 and C21orf2 using immunostaining, we decided to create tagged NEK1 and C21orf2 plasmid constructs. For these protein tags we have anti-tag antibodies that work reliably on immunoblot, co-immunoprecipitation and immunostaining.

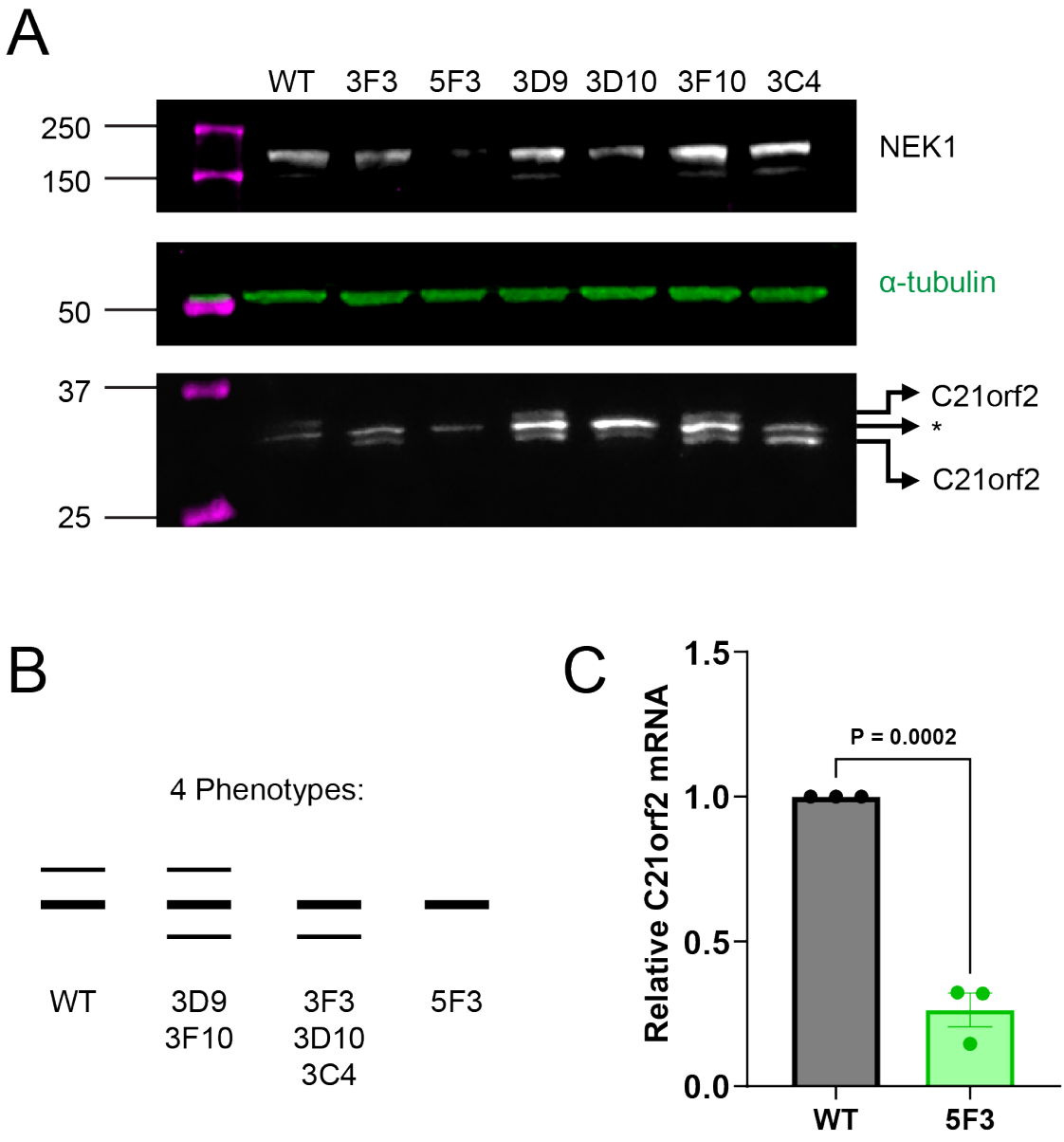

Figure 3-1 Validation of a C21orf2 knock out (KO) HeLa cell line by immunoblot and qPCR.

Wild type (WT) HeLa cells were subjected to CRISPR/Cas9 genome editing, targeting the *C21orf2* gene. Six CRISPR/Cas9 clones were isolated, expanded and validated for knock out of C21orf2 protein. Five clones targeting exon 5 (3F3, 3D9, 3D10, 3F10 and 3C4) and one clone targeting exon 3 (5F3) were selected.

A) The selected Cas9 edited clones were subjected to immunoblot with anti-NEK1, anti-C21orf2 and anti-α-tubulin antibodies. Per sample 45 µg protein was loaded. * denotes a non-specific band.

B) Four phenotypes were observed on immunoblot, with observed C21orf2 bands above and below a non-specific band. The 5F3 clone was chosen as it presented neither C21orf2 band.

C) RT-qPCR was used to quantify the relative C21orf2 mRNA levels of WT or 5F3 C21orf2 KO HeLa cells. Graph represents C21orf2 mRNA levels normalised to GAPDH as a housekeeping control. Data were analysed by two-tailed unpaired t-test, $N = 3$. Bars represent mean ± SEM.

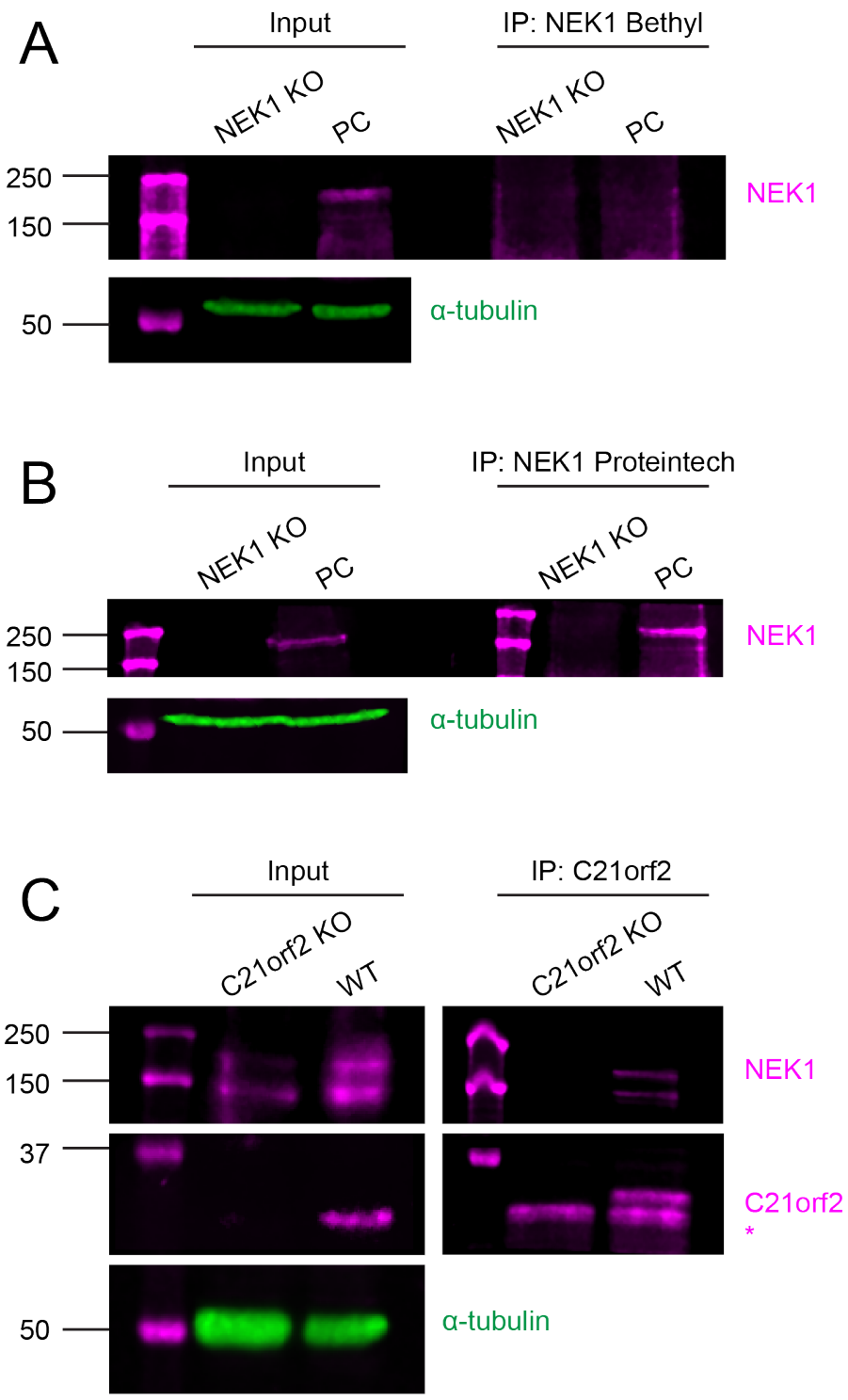

Figure 3-2 Validation of endogenous NEK1 and C21orf2 antibodies for immunoprecipitation.

A & B) Wild type parental (PC) or NEK1 knock out (KO) HeLa cells were subjected to immunoprecipitation with either one of two endogenous NEK1 antibodies and probed on immunoblot for endogenous NEK1 and α-tubulin as a loading control.

C) Wild type (WT) or C21orf2 KO HeLa cells were subjected to immunoprecipitation with an endogenous C21orf2 antibody and probed on immunoblot for endogenous NEK1, C21orf2 and α-tubulin as a loading control. Per sample 45 µg protein was loaded as input. * denotes a non-specific band.

3.2.3 Production of wild type and kinase dead V5-tagged NEK1 constructs

To detect specific colocalisation of NEK1 and C21orf2, we produced tagged constructs with different protein tags. For NEK1 we produced a N-terminal V5-tagged full length NEK1 construct. To allow for investigation of the role of NEK1 kinase activity in future experiments, site-directed mutagenesis was used to produce a kinase dead K33R mutation within the kinase domain of the V5-NEK1 (Spies *et al.*, 2016). Both constructs were validated by sequencing. The constructs were transfected into HEK293 cells and immunoblot was used to confirm expression of proteins at the correct molecular weight. As our V5 antibody produced a non-specific band at the same molecular weight as endogenous NEK1 (not shown), we instead used our endogenous NEK1 antibody (Proteintech) to confirm NEK1 overexpression. Samples were immunoblotted, probing for NEK1 and α-tubulin as a loading control. We observed a band for overexpressed V5-NEK1 at ~180 kDa, which coincides with published data (Figure 3-3A) (Feige *et al.*, 2006). To further confirm successful expression of V5-NEK1, we transfected WT HeLa cells with V5-NEK1 or V5-NEK1 K33R and immunostained the cells with an anti-V5 antibody. This confirmed diffuse cytoplasmic staining of the expressed proteins (Figure 3-3B), which is in line with data from the Human Protein Atlas and published literature (Chen *et al.*, 2008; Thul *et al.*, 2017).

3.2.4 Production of HA-tagged C21orf2 constructs

To investigate C21orf2 localisation and protein interactions, we used Gibson assembly to produce C-terminally HA-tagged C21orf2 protein constructs. As literature suggested the existence of a N-terminal mitochondrial localisation sequence in C21orf2, we wanted to investigate whether this may be involved in potential C21orf2 localisation and function at MAM (Krohn *et al.*, 1997). We produced a protein construct with disruption of this sequence (C21orf2 $\Delta 2 - 15$), without altering the leucine rich repeats, as the function of this domain has not been well characterised (Figure 3-4A).

HEK293 cells were transfected with empty vector pCI-neo, C21orf2-HA or C21orf2-HA $\Delta 2 - 15$ and immunoblotted with anti-HA and anti-α-tubulin antibodies. Both C21orf2 constructs expressed at the correct molecular weight (42 kDa and 40 kDa respectively) (Figure 3-4B). To further validate protein expression in cells, WT HeLa cells were transfected with the HA-tagged C21orf2 constructs and immunostained with an anti-HA antibody. This revealed cytoplasmic and punctate staining of both C21orf2 constructs (Figure 3-4C), which had not previously been reported and thus warranted further investigation.

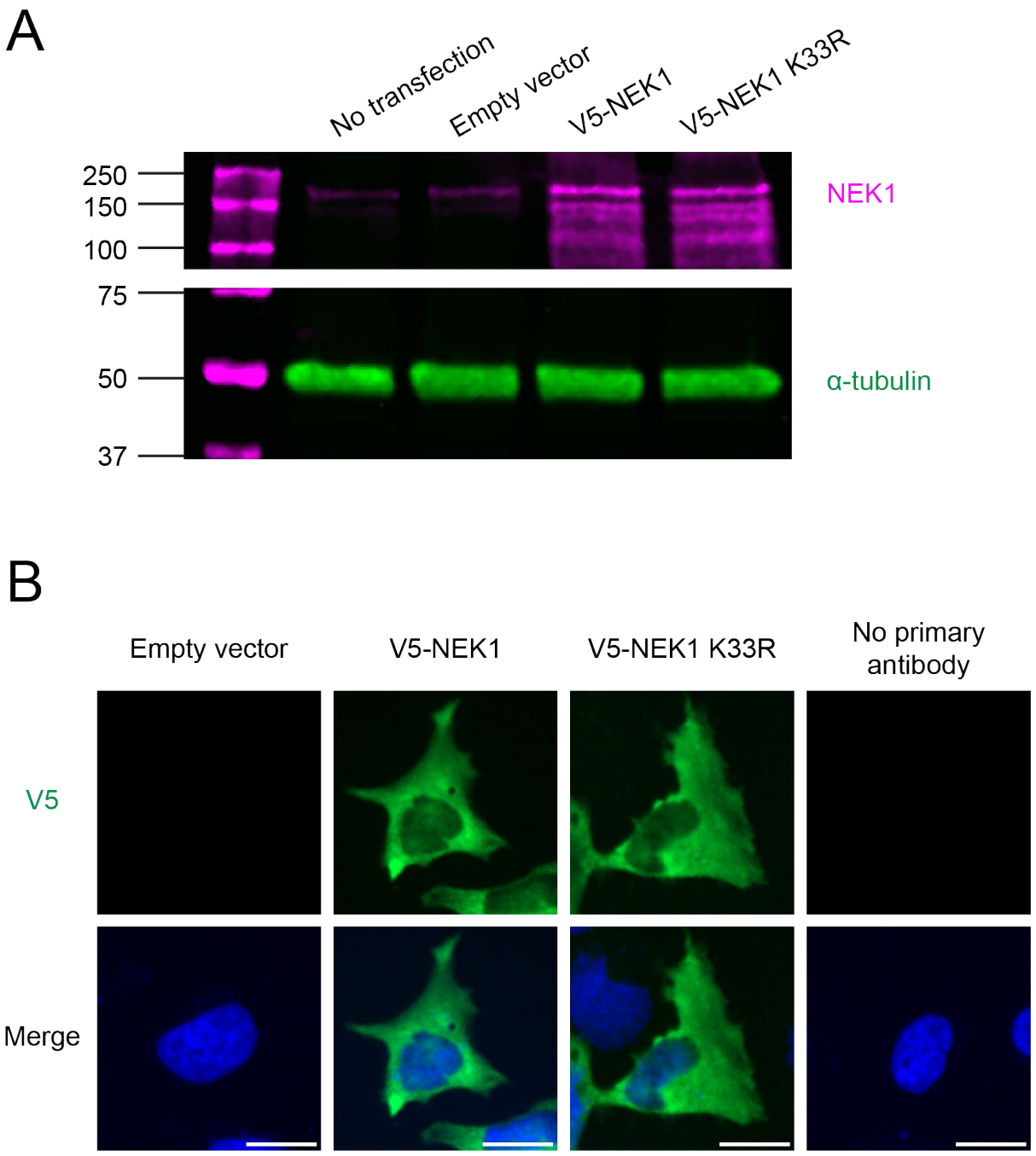

Figure 3-3 Characterisation of V5-tagged active and kinase dead NEK1.

A) HEK293 cells transfected with empty vector pCI-neo, wild type V5-NEK1 or kinase dead V5-NEK1 K33R were immunoblotted with anti-NEK1 and anti-α-tubulin antibodies. Per sample 45 µg protein was loaded. Both constructs expressed at the expected molecular weight at ~180 kDa.

B) Wild type HeLa cells were transfected with empty vector pCI-neo, wild type V5-NEK1 or kinase dead V5-NEK1 K33R and immunostained with a V5 antibody (green) and nuclear Hoechst stain (blue). Both constructs expressed diffusely throughout the cytoplasm. Scale bar = 20 µm.

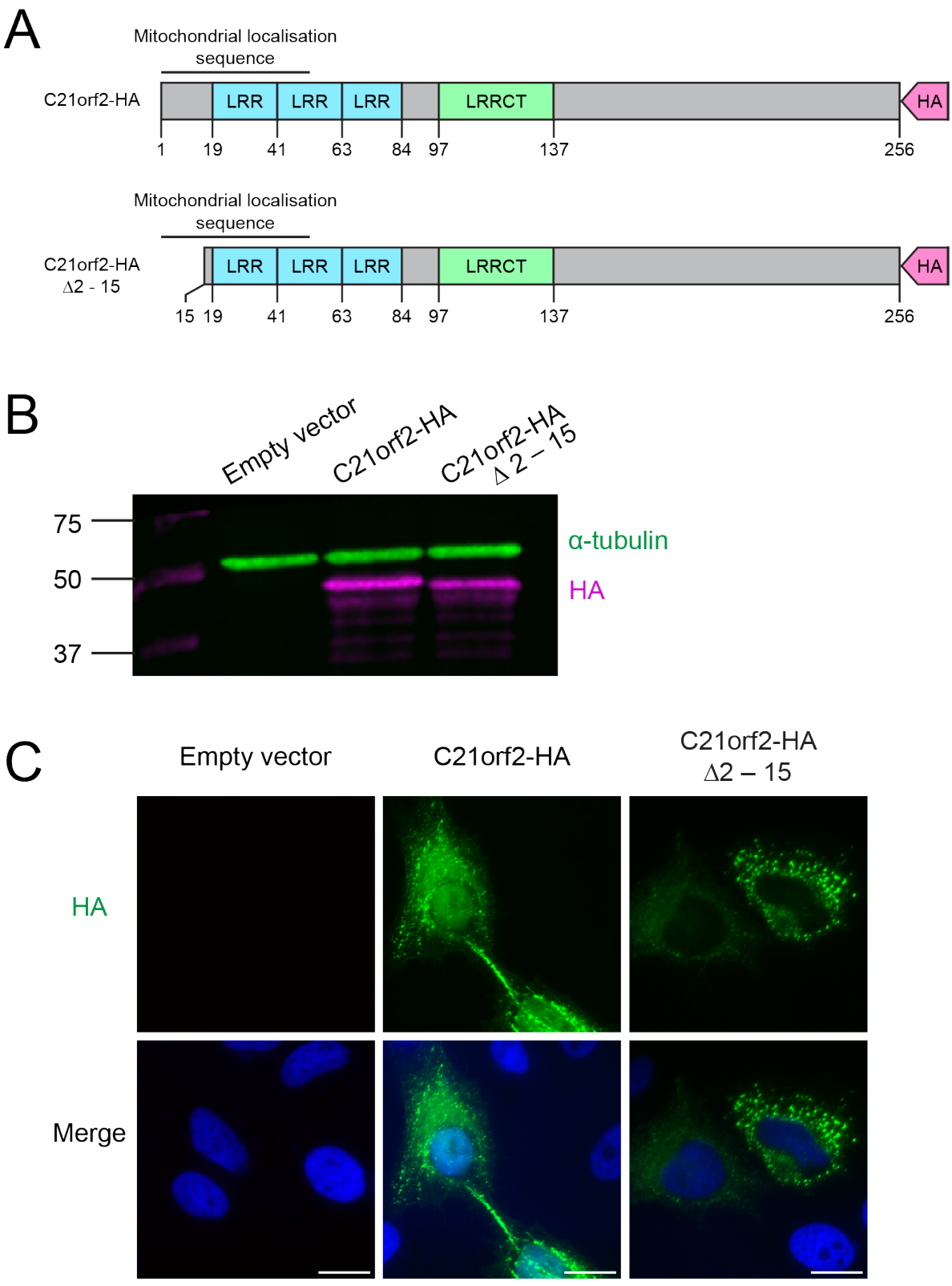

Figure 3-4 Characterisation of HA-tagged C21orf2 constructs.

Legend next page.

Figure 3-4 Characterisation of HA-tagged C21orf2 constructs.

A) Schematic of the C21orf2 protein structure, indicating the truncation of the putative mitochondrial localisation sequence. LRR = Leucine rich repeat, LRRCT = C-terminal LRR.

B) HEK293 cells transfected with empty vector pCI-neo, full length C21orf2-HA or truncated C21orf2-HA Δ2 – 15 were immunoblotted with anti-HA and anti-α-tubulin antibodies. Per sample 45 µg protein was loaded. Both constructs expressed at the expected molecular weight (42 kDa and 40 kDa respectively).

C) Wild type HeLa cells transfected with empty vector pCI-neo, C21orf2-HA or C21orf2-HA Δ2 – 15 were immunostained with an anti-HA antibody (green) and nuclear Hoechst stain (blue). Scale bar = 20 µm.

3.3 Characterisation of the NEK1/C21orf2 protein complex

3.3.1 NEK1 and C21orf2 do not localise to mitochondria

Currently there is conflicting evidence as to the cellular localisation of NEK1 and C21orf2. Literature suggests that both NEK1 and C21orf2 may exist diffuse throughout the cytoplasm (Chen *et al.*, 2008; Fang *et al.*, 2015), localised to mitochondria (Chen *et al.*, 2009; Krohn *et al.*, 1997), or localised to cilia and the centrosome (Gregorczyk *et al.*, 2023; Shalom *et al.*, 2008). During characterisation of our NEK1 and C21orf2 protein constructs, we observed punctate staining of C21orf2 that has not been reported in literature (Figure 3-4C). It was previously suggested that C21orf2 was a mitochondria protein (Krohn *et al.*, 1997), and it is well established that NEK1 is partially localised to the mitochondria in response to DNA damage (Chen *et al.*, 2009). Thus, we first investigated whether NEK1 and C21orf2 may be colocalising at mitochondria.

To investigate this WT HeLa cells were transfected with either empty vector pCI-neo, V5-NEK1, C21orf2-HA, or C21orf2-HA with a disrupted mitochondrial localisation sequence (C21orf2-HA Δ2 – 15). Cells were immunostained with either an anti-HA or anti-V5 antibody and co-stained with an antibody specific to the OMM protein TOM20 (Figure 3-5). Immunofluorescent staining revealed that C21orf2 positive puncta do not co-localise with mitochondrial marker TOM20 but appear to lie next to mitochondria. We also did not observe specific localisation of NEK1 to mitochondria. As only a small portion of NEK1 is proposed to localise to mitochondria, this could be masked by the large proportion of NEK1 diffuse in the cytosol.

3.3.2 Disruption of the C21orf2 N-terminal domain disrupts NEK1/C21orf2 interaction

It is well characterised that NEK1 and C21orf2 interact, but the details of their interaction are not yet clear (Fang *et al.*, 2015; Gregorczyk *et al.*, 2023; Watanabe *et al.*, 2020). We had previously confirmed that the N-terminal domain in C21orf2 did not function as a mitochondrial localisation sequence (Figure 3-5). Thus, we decided to investigate if this domain may have an alternative function in binding

to NEK1. To investigate this, HEK293 cells were co-transfected with either empty vector pCI-neo or V5-tagged NEK1 and either C21orf2-HA or C21orf2-HA $\Delta 2 - 15$. The samples were immunoprecipitated with an anti-V5 antibody to capture V5-NEK1. The samples were immunoblotted with anti-NEK1 and anti-HA antibodies, and an anti-GAPDH antibody as a loading control (Figure 3-6). Indeed, we observed that disruption of the C21orf2 N-terminal domain caused a significant reduction in C21orf2 binding to NEK1 (Figure 3-6).

As NEK1 and C21orf2 are considered to be functionally linked, we next determined to investigate if the proteins co-occur. WT HeLa cells were co-transfected with either empty vector pCI-neo or V5-tagged NEK1 and either C21orf2-HA or C21orf2-HA $\Delta 2 - 15$. The samples were immunostained with anti-V5 and anti-HA antibodies (Figure 3-7). When overexpressed on its own V5-NEK1 was diffuse throughout the cytoplasm, however when co-expressed with full length C21orf2-HA it was recruited to C21orf2-HA positive puncta. In line with our co-immunoprecipitation experiment, disruption of the C21orf2 N-terminal domain leads to loss of this NEK1 recruitment. Together this validates that the C21orf2 N-terminal domain is necessary for binding to and recruitment of NEK1.

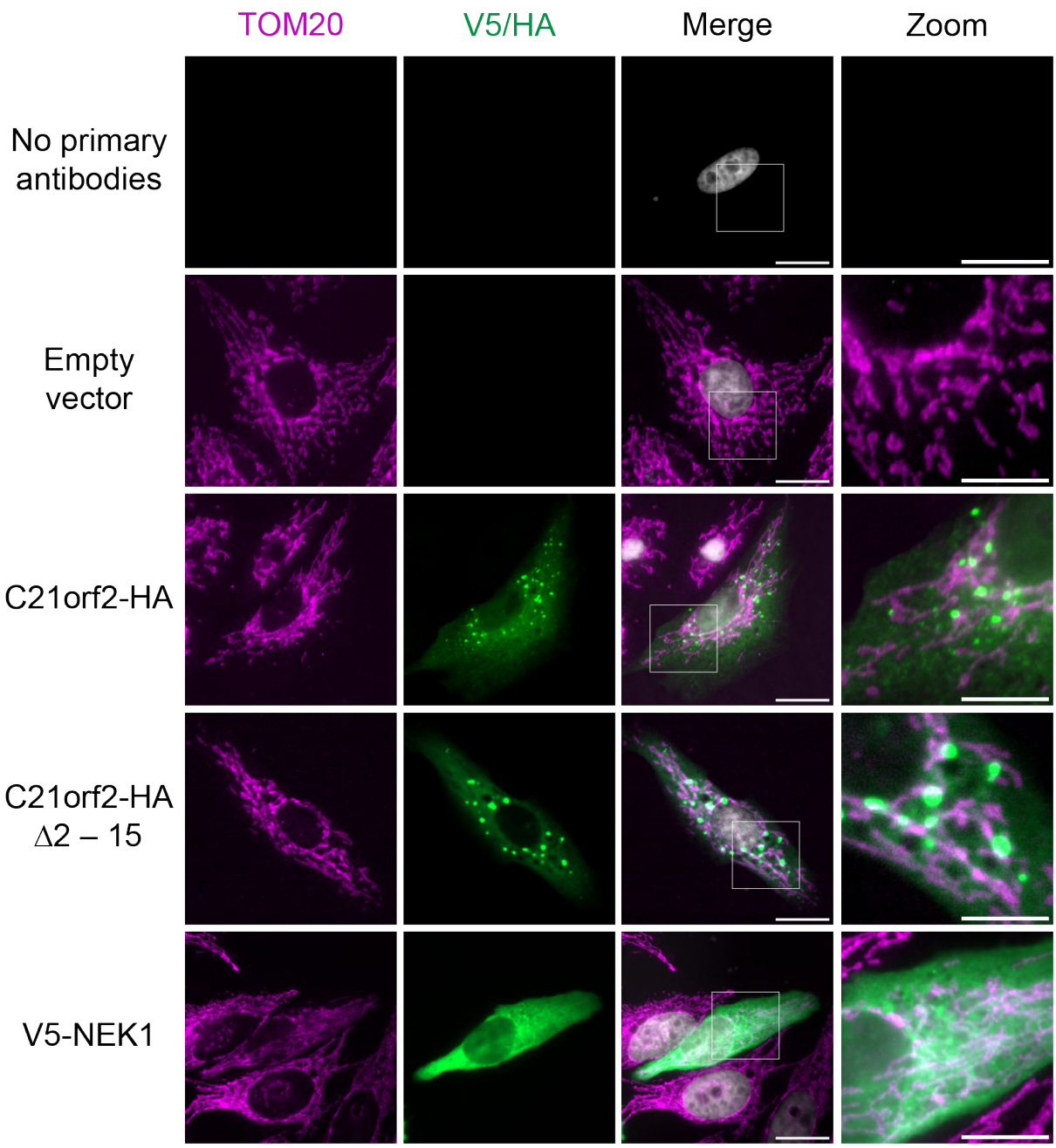

Figure 3-5 NEK1 and C21orf2 do not localise to mitochondria.

Wild type HeLa cells were transfected with empty vector pCI-neo, V5-NEK1, C21orf2-HA, or C21orf2-HA with a disrupted mitochondrial localisation sequence (C21orf2-HA Δ2 – 15). The samples were subjected to immunostaining with either an anti-HA or anti-V5 antibody (green), co-stained for the outer mitochondrial membrane protein TOM20 (magenta) and with nuclear Hoechst stain (grey). Scale bar = 20 µm, zoom = 10 µm. Figure represents *N* = 3.

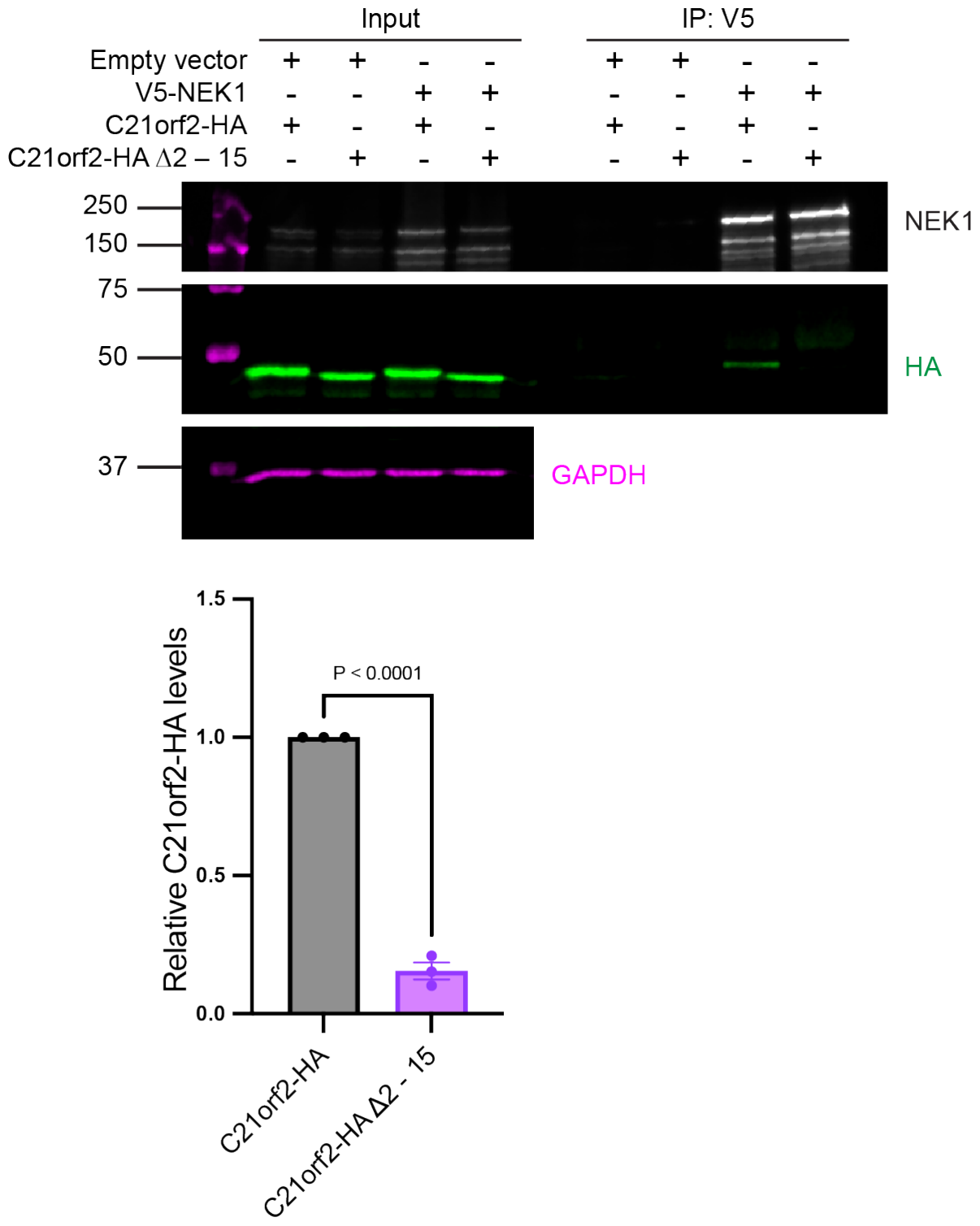

Figure 3-6 Disruption of the C21orf2 N-terminal domain prevents binding to NEK1.

HEK293 cells were co-transfected with either empty vector pCI-neo or V5-tagged NEK1 and either C21orf2-HA or N-terminally disrupted C21orf2-HA Δ2 – 15. The samples were immunoprecipitated with an anti-V5 antibody and immunoblotted, probing with anti-NEK1 and anti-HA antibodies, and an anti-GAPDH antibody as a loading control. Per sample 45 µg protein was loaded as input. Graph shows quantification of the level of overexpressed C21orf2 bound to V5-NEK1. Data were analysed by unpaired two-tailed t-test, *N* = 3. Bars represent mean ± SEM.

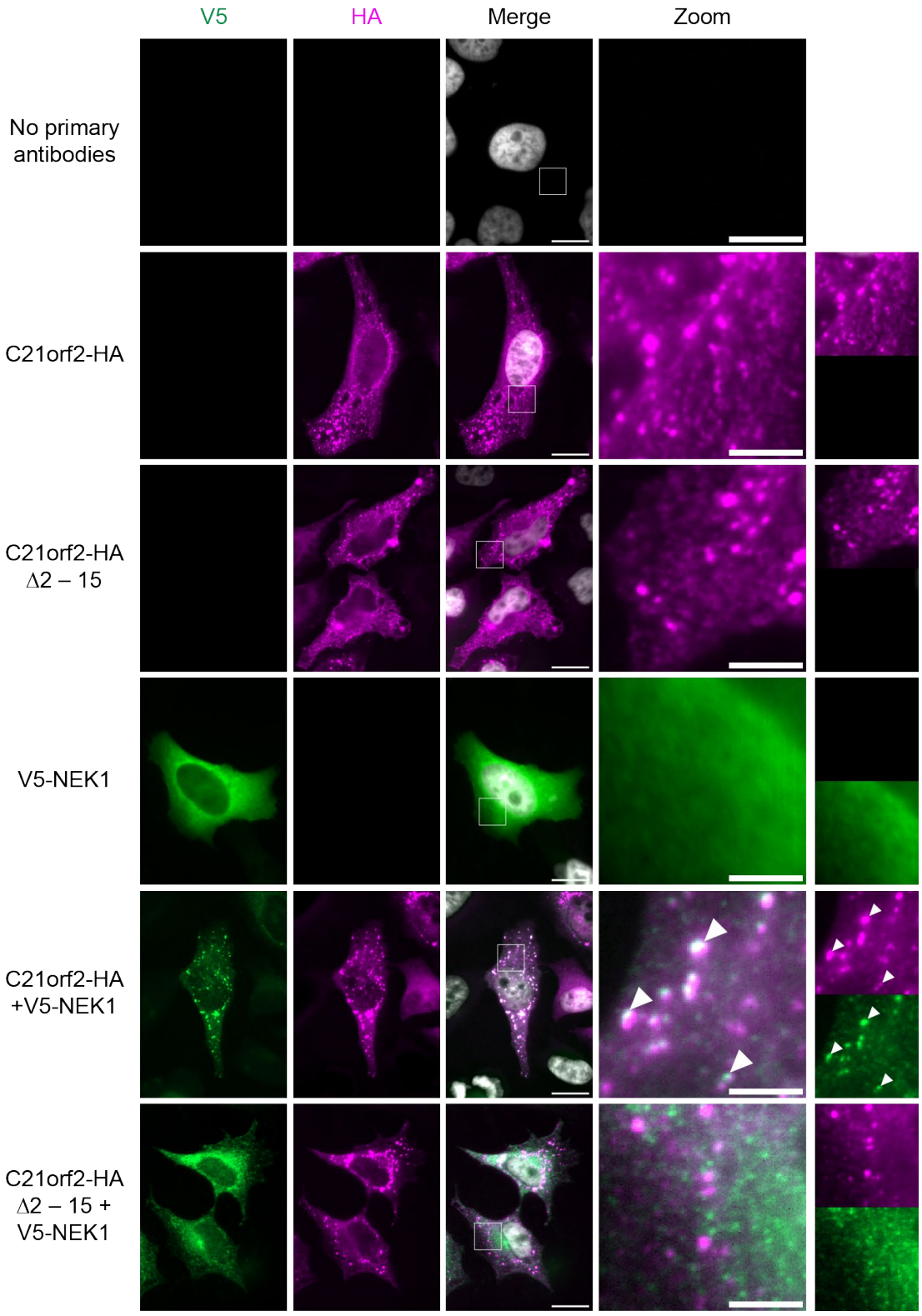

Figure 3-7 Disruption of the C21orf2 N-terminal domain prevents co-occurrence with NEK1.

Wild type HeLa cells were co-transfected with either empty vector pCI-neo or V5-tagged NEK1 and either full length C21orf2-HA or N-terminally disrupted C21orf2-HA Δ2 – 15. Samples were immunostained with anti-V5 (green) and anti-HA (magenta) antibodies and Hoechst nuclear stain (grey). Scale bar = 20 µm, zoom = 10 µm. White arrows indicate points of overlap between V5-NEK1 and C21orf2-HA. Figure represents *N* = 3.

3.3.3 C21orf2 localises to microtubules

In our previous experiments, immunofluorescent staining suggested that C21orf2 puncta lay next to mitochondria (Figure 3-5). One possible explanation could be that when overexpressed C21orf2 localises to an endosomal compartment. To investigate this, we used immunofluorescence to stain for a panel of endosomal-associated proteins. WT HeLa cells were transfected with pCI-neo empty vector or C21orf2-HA and immunostained with an anti-HA antibody and endogenous antibodies specific to either: PEX14 (peroxisomes), Rab5 (early endosomes), Rab7 (late endosomes), LAMP2 (lysosomes), PDI (ER) and LC3B (autophagosomes).

A more in-depth investigation of the localisation of C21orf2 revealed two distinct phenotypes: the punctate structures previously identified and filamentous structures (Figure 3-8). We observed that neither the C21orf2-positive puncta or filamentous staining specifically overlapped with any of the compartments tested (Figure 3-9). However, there was visible partial overlap between C21orf2 and each of the endosomal-associated proteins tested. As C21orf2 is essential for ciliogenesis, a process dependent on microtubule growth, we next investigated if the filamentous C21orf2 staining may be localised at microtubules.

To investigate this, WT HeLa cells were transfected with pCI-neo empty vector or C21orf2-HA and co-stained with an anti-HA antibody and an antibody specific to the microtubule protein α-tubulin. Immunofluorescent staining showed a partial overlap between C21orf2 positive filamentous structures and the α-tubulin positive microtubules (Figure 3-10). The C21orf2 positive punctate structures also decorated the microtubules, suggesting when overexpressed C21orf2 may be recruited to microtubules.

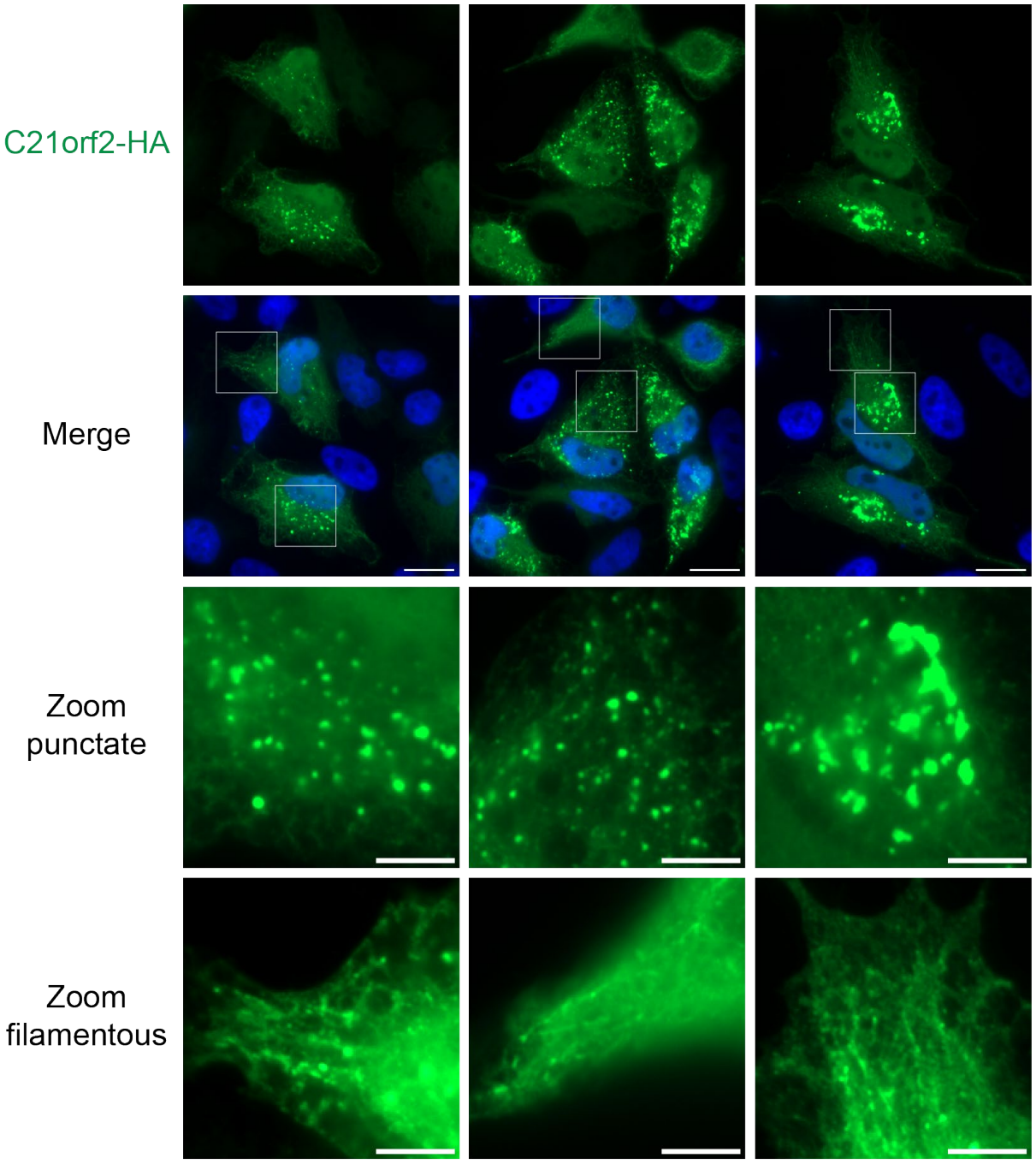

Figure 3-8 Overexpression of C21orf2 leads to two distinct phenotypes.

Wild type HeLa cells were transfected with full length C21orf2-HA and subjected to immunostaining with an anti-HA antibody (green) and nuclear Hoechst staining (blue). Example of punctate and filamentous C21orf2 staining are shown in the zoomed boxes. Scale bar = 20 µm, zoom = 5 µm. Figure represents *N* = 3.

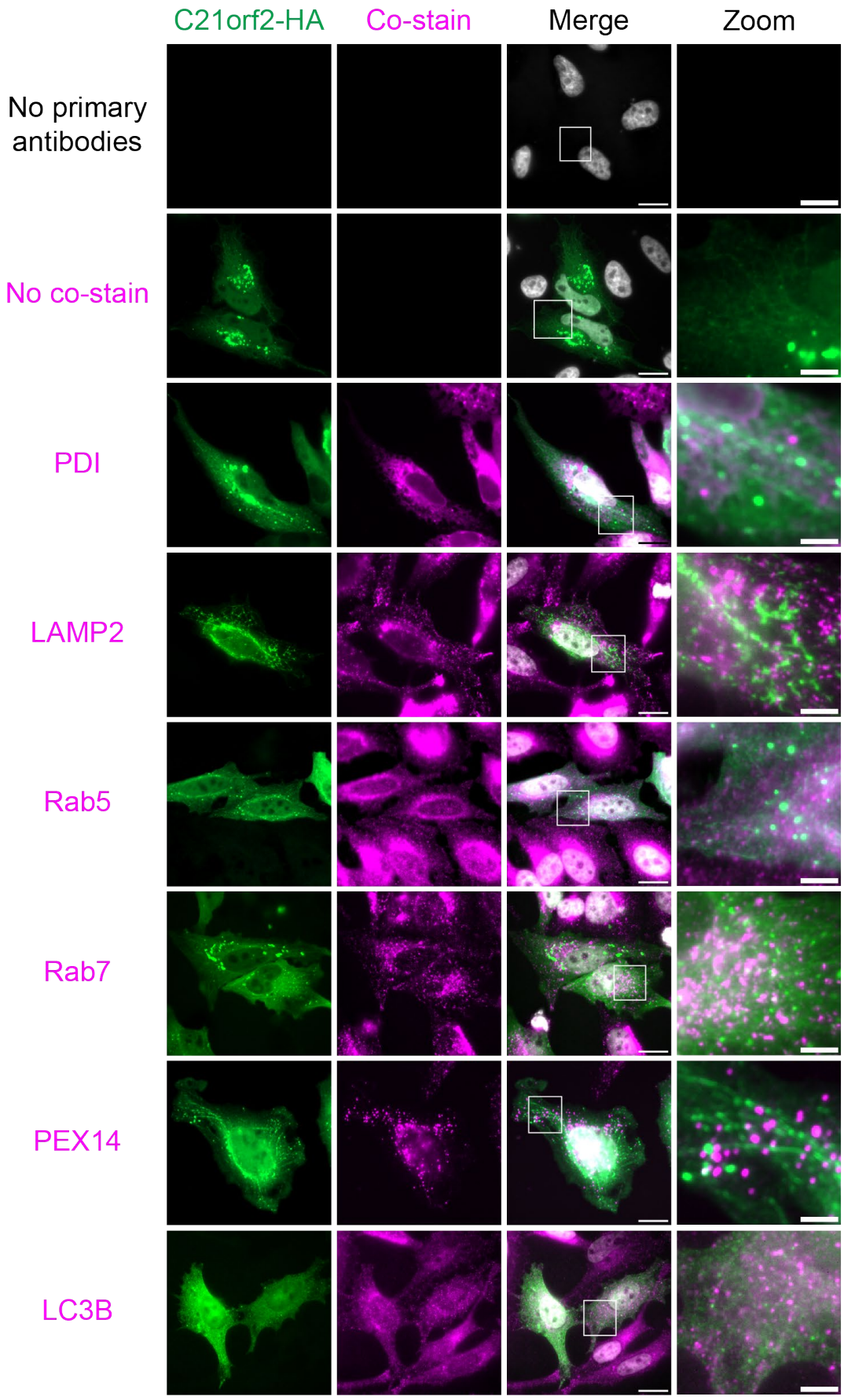

Figure 3-9 C21orf2 partially localises to endosomal compartments.
Legend on next page.

Figure 3-9 C21orf2 partially localises to endosomal compartments.

Wild type HeLa cells were transfected with pCI-neo empty vector or full length C21orf2-HA and subjected to immunostaining with an anti-HA antibody (green) and nuclear Hoechst staining (grey). The cells were co-stained with a panel of endogenous antibodies (magenta); PDI (ER), LAMP2 (lysosomes), Rab5 (early endosomes), Rab7 (late endosomes), PEX14 (peroxisomes), and LC3B (autophagosomes). Scale bar = 20 µm, zoom = 5 µm. Figure represents *N* = 3.

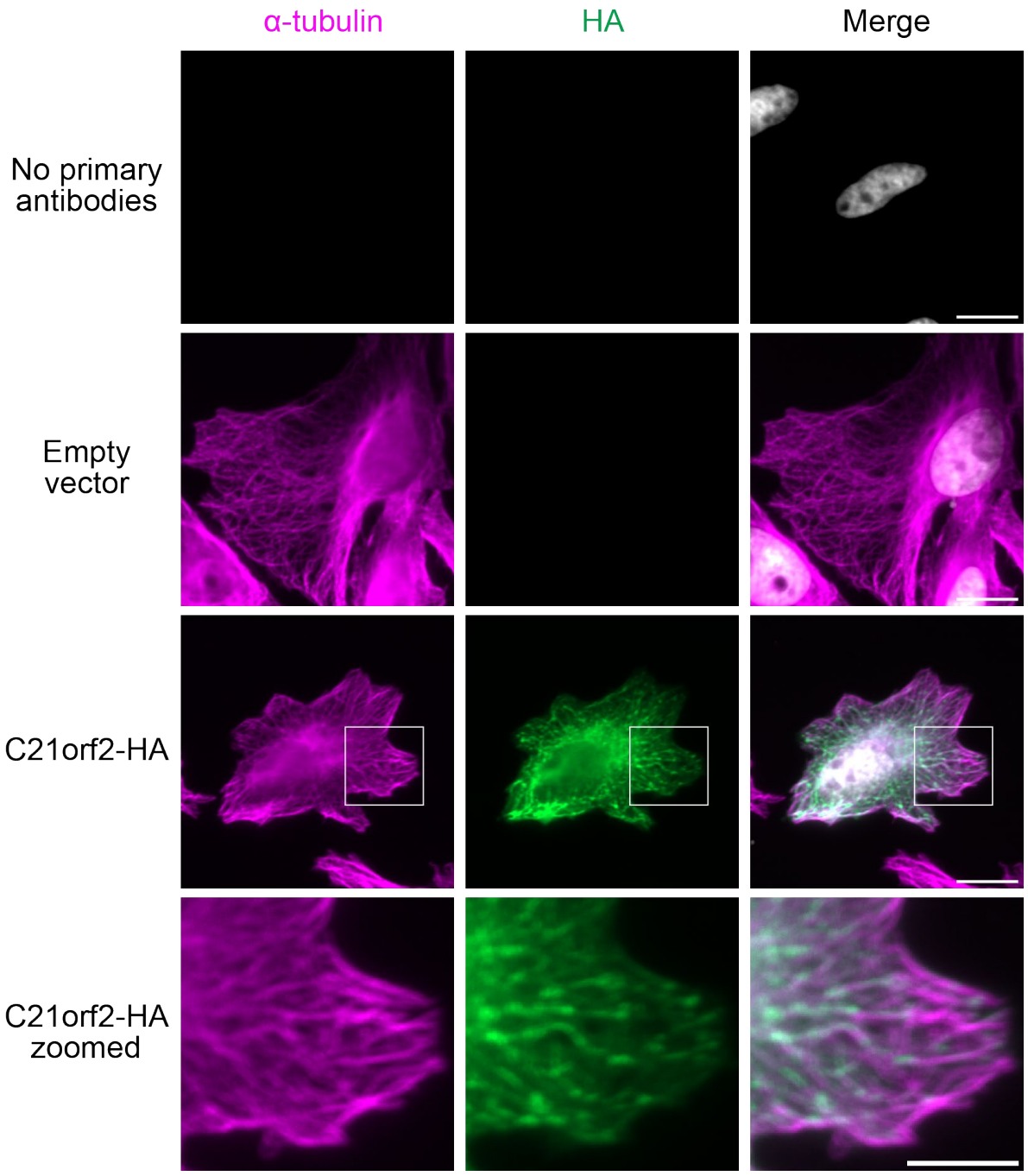

Figure 3-10 Overexpressed C21orf2 localises to microtubules.

Wild type HeLa cells were transfected with pCI-neo empty vector or full length C21orf2-HA and subjected to immunostaining with an anti-HA antibody (green), anti-α-tubulin (magenta) and nuclear Hoechst staining (grey). Scale bar 20 = µm, zoom = 10 µm. Figure represents *N* = 3.

3.4 NEK1 and C21orf2 interact with the VAPB/PTPIP51 tether

3.4.1 NEK1 interacts with PTPIP51

Proteomic and co-immunoprecipitation data have suggested an interaction between NEK1 and the MAM protein VAPB (Cirulli *et al.*, 2015). To investigate NEK1 interactions with the VAPB/PTPIP51 tether and maximise our chances of observing an interaction, HEK293 cells were co-transfected with pCI-neo or V5-NEK1 and either PTPIP51-HA (Figure 3-11A) or Myc-VAPB (Figure 3-11B). The samples were immunoprecipitated with an anti-V5 antibody to capture NEK1 and ran on immunoblot, probing with anti-NEK1 and either anti-Myc or anti-HA antibodies. When co-expressed we observed that NEK1 interacts with PTPIP51 but not VAPB. To determine if NEK1 interacts with endogenous PTPIP51, HEK293 cells lysed and immunoprecipitated with either an anti-NEK1 or anti-HA antibody as a non-specific control. The samples were probed for endogenous NEK1, PTPIP51 and actin as a loading control (Figure 3-12). We observed that endogenous NEK1 interacts with endogenous PTPIP51, but to a lower extent than when co-expressed with PTPIP51-HA (Figure 3-11A). This suggests that only a small portion of NEK1 may localise to MAM where it interacts with PTPIP51. One possible explanation for this effect, may be that PTPIP51 recruits NEK1 to these ER-mitochondria contact sites.

Overexpression of PTPIP51 recruits its ER binding partner VAPB to the mitochondria (De Vos *et al.*, 2012). As we had established that NEK1 can interact with PTPIP51, we wanted to test if overexpression of PTPIP51 would also recruit NEK1 to mitochondria. As we had previously observed that co-overexpression of C21orf2 recruits NEK1, we used this as a positive control (Figure 3-6). WT HeLa cells were co-transfected with either pCI-neo empty vector or V5-NEK1 with either C21orf2-HA or PTPIP51-HA, and the cells immunostained with anti-V5 and anti-HA tag antibodies. As observed in our previous experiments, when expressed alone NEK1 is diffuse throughout the cytoplasm, and is recruited to C21orf2 when co-expressed (Figure 3-13). However, when NEK1 was co-expressed with PTPIP51, we did not observe recruitment to mitochondria. This suggests that whilst NEK1 interacts with PTPIP51, the PTPIP51 protein does not influence localisation of NEK1.

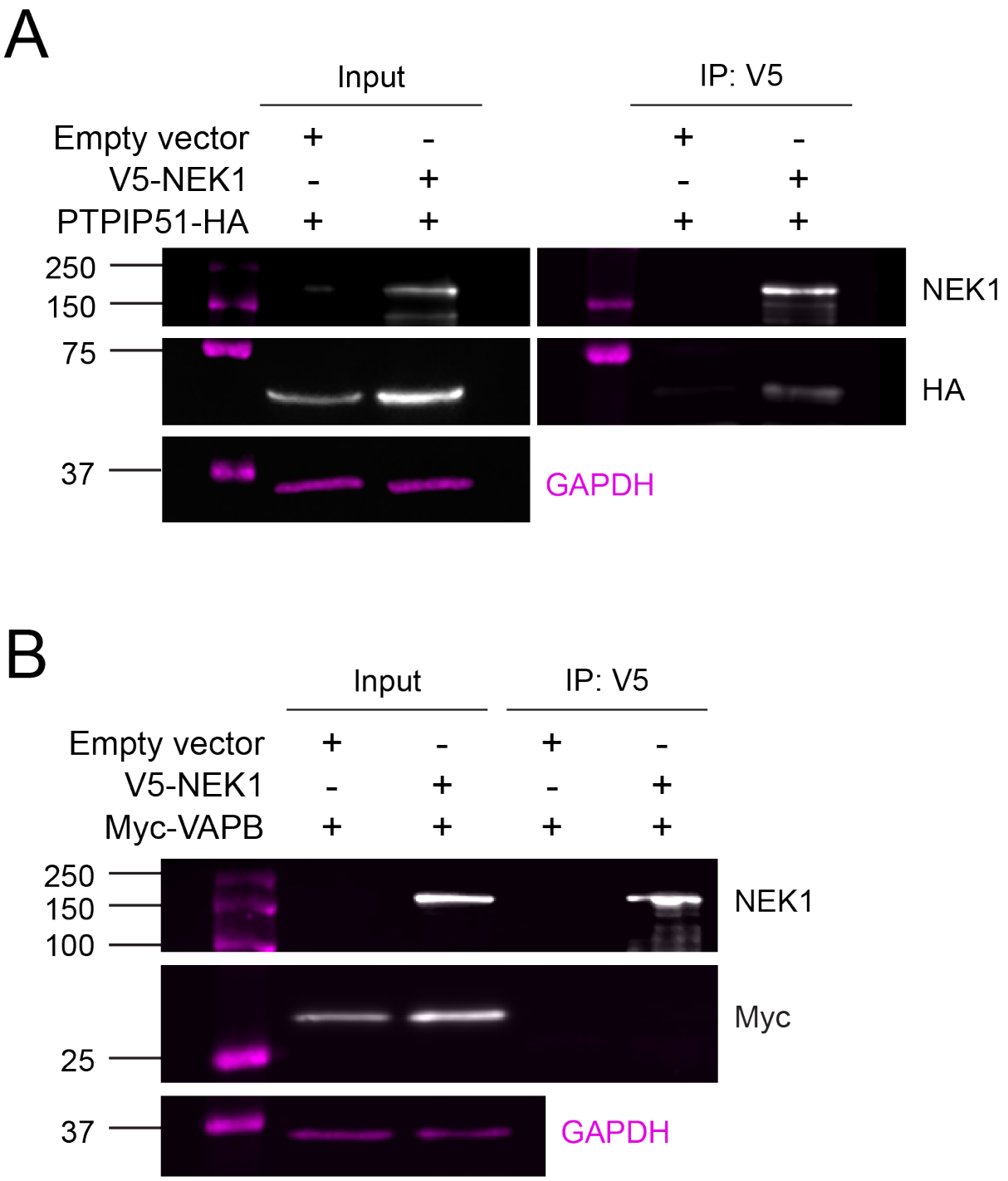

Figure 3-11 NEK1 interacts with exogenous PTPIP51.

HEK293 cells were co-transfected with pCI-neo empty vector or V5-NEK1 and either PTPIP51-HA **(A)** or Myc-VAPB **(B).** Samples were immunoprecipitated using an anti-V5 antibody and immunoblotted for endogenous NEK1, HA **(A)** or Myc **(B).** GAPDH was probed as a loading control. 45 µg protein per sample was loaded as input. Figures represent *N* = 3.

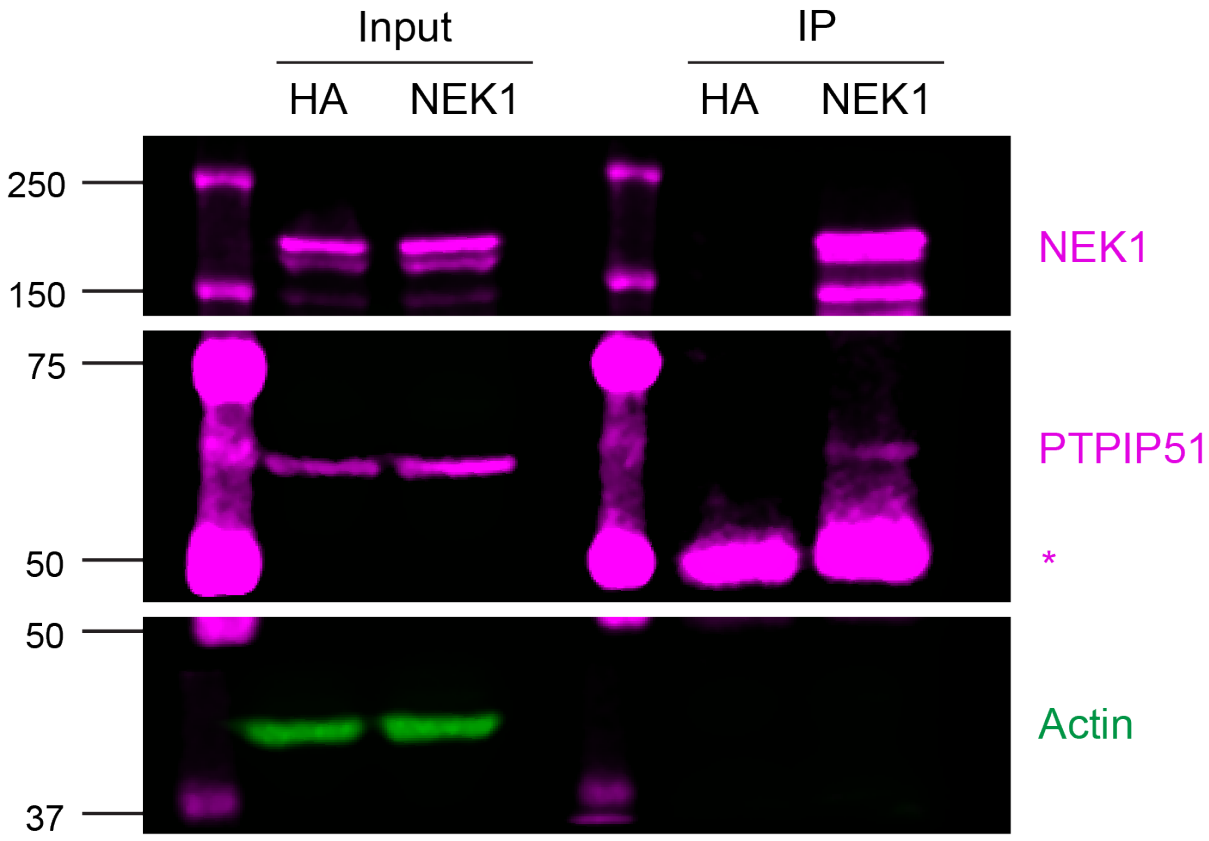

Figure 3-12 NEK1 interacts with endogenous PTPIP51.

HEK293 cells were lysed and NEK1 immunoprecipitated using an anti-NEK1 antibody. Immunoprecipitation with an anti-HA antibody was used as a negative control. Samples were immunoblotted for endogenous NEK1, PTPIP51 and actin as a loading control. * Denotes a non-specific antibody band. 45 µg protein per sample was loaded as input. Figure represents *N* = 3.

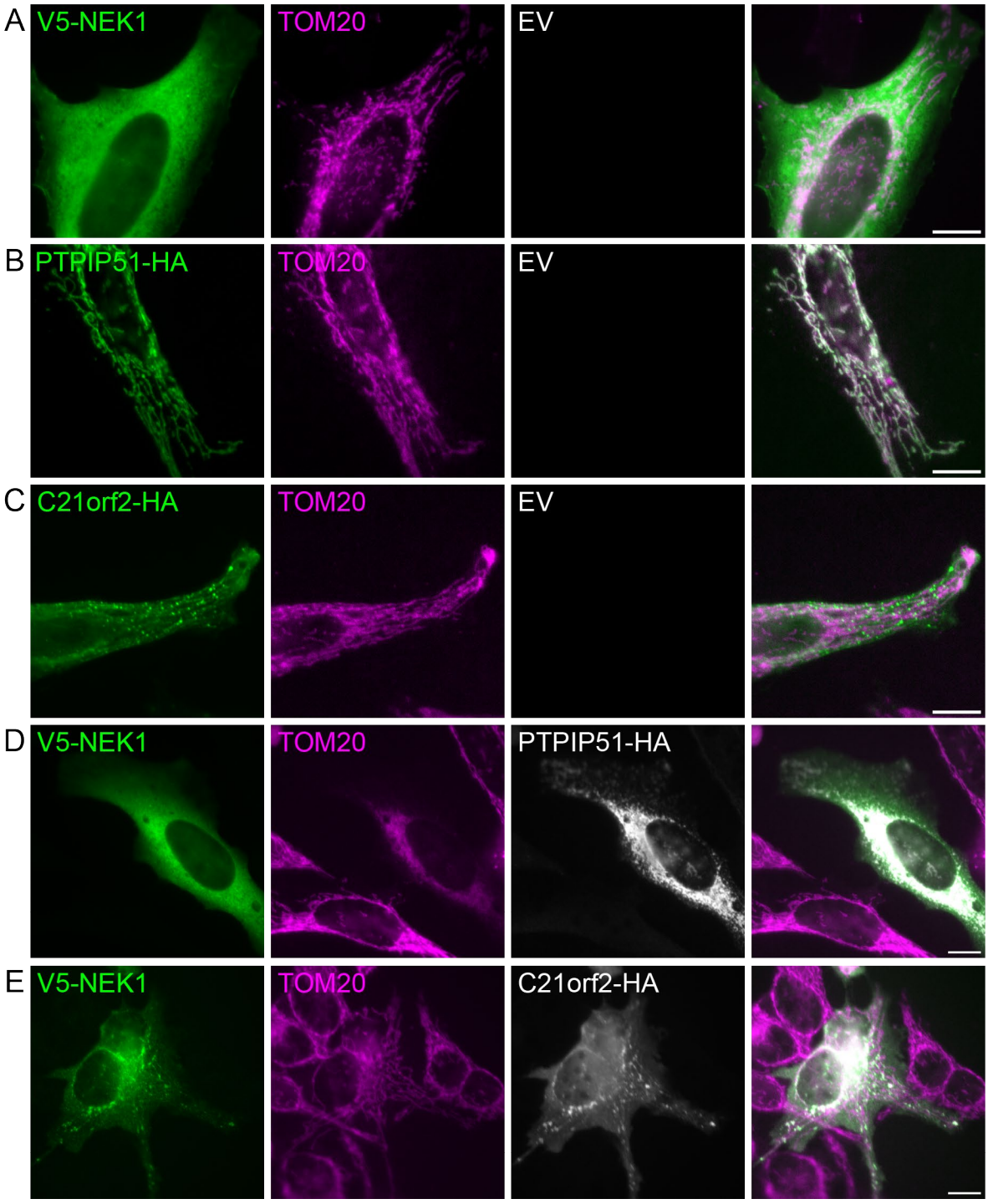

Figure 3-13 NEK1 is not recruited to mitochondria by PTPIP51.

Wild type HeLa cells were transfected with empty vector pCI-neo (EV) either V5-NEK1 **(A),** PTPIP51-HA **(B)** or C21orf2-HA **(C).** The cells were immunostained for outer mitochondrial membrane marker TOM20 (magenta) and the respective protein tag (green). HeLa cells co-transfected with V5-NEK1 and either PTPIP51-HA **(D)** or C21orf2-HA **(E)** were immunostained for TOM20 (magenta), V5 (green) and HA (grey). Scale bars = 20 µm. Figure represents *N* = 3.

3.4.2 C21orf2 interacts with PTPIP51

As we had confirmed that NEK1 binds to PTPIP51, we wanted to confirm whether the NEK1 interacting protein C21orf2 was involved in this interaction. To investigate C21orf2 protein interactions, pCI-neo empty vector or C21orf2-HA was co-expressed with Myc-VAPB. We were unable to co-express PTPIP51 as both protein constructs had a HA protein tag. The samples were immunoprecipitated with an anti-HA antibody to capture C21orf2 and ran on immunoblot, probing with anti-HA, anti-PTPIP51 and anti-Myc antibodies. In the same pattern as NEK1, we observed that when overexpressed C21orf2 interacted with endogenous PTPIP51, but we observed no interaction with VAPB (Figure 3-14). This further suggested that the NEK1/C21orf2 protein complex may bind to PTPIP51 at MAM.

3.4.3 C21orf2 may require NEK1 to bind to PTPIP51

We had now observed that both NEK1 and C21orf2 interact with PTPIP51 when overexpressed. As NEK1 is known to interact with the MAM protein VDAC1, we wanted to investigate whether NEK1 may recruit C21orf2 to these sites and be necessary for its interaction with PTPIP51. To test this, we utilised the C21orf2 $\Delta 2 - 15$ construct that exhibits reduced binding to NEK1 (Figure 3-6). HEK293 cells were transfected with pCI-neo empty vector, C21orf2-HA, or C21orf2-HA $\Delta 2 - 15$, and C21orf2 immunoprecipitated with an anti-HA antibody. The samples were run on immunoblot, probing with anti-HA and anti-NEK1 and anti-PTPIP51 antibodies. Samples were probed with an anti-GAPDH antibody as a loading control. We observed that the C21orf2-HA $\Delta 2 - 15$ construct bound less to PTPIP51 compared to full length C21orf2 (Figure 3-15). This confirms that the N-terminal domain of C21orf2 is necessary for its interaction with PTPIP51. This suggests that C21orf2 requires binding with NEK1 in order to interact with the VAPB/PTPIP51 tether.

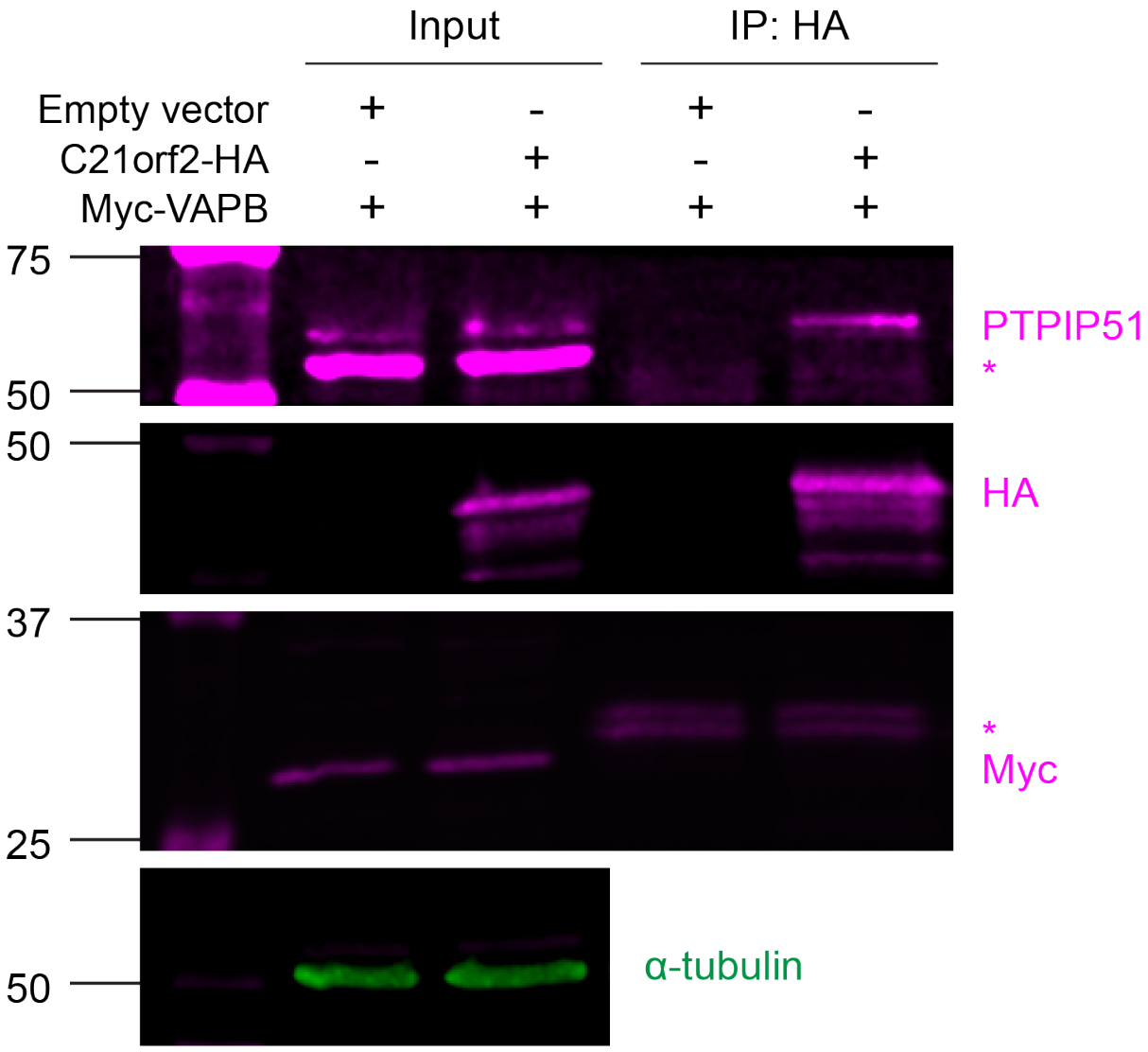

Figure 3-14 C21orf2 binds to PTPIP51.

HEK293 cells were co-transfected with either pCI-neo empty vector or C21orf2-HA, and Myc-VAPB. C21orf2 was immunoprecipitated using an anti-HA antibody. Samples were immunoblotted for HA, Myc, endogenous PTPIP51 and α-tubulin as a loading control. 45 µg protein per sample was loaded as input. * Denotes a non-specific antibody band. Figure represents *N* = 3.

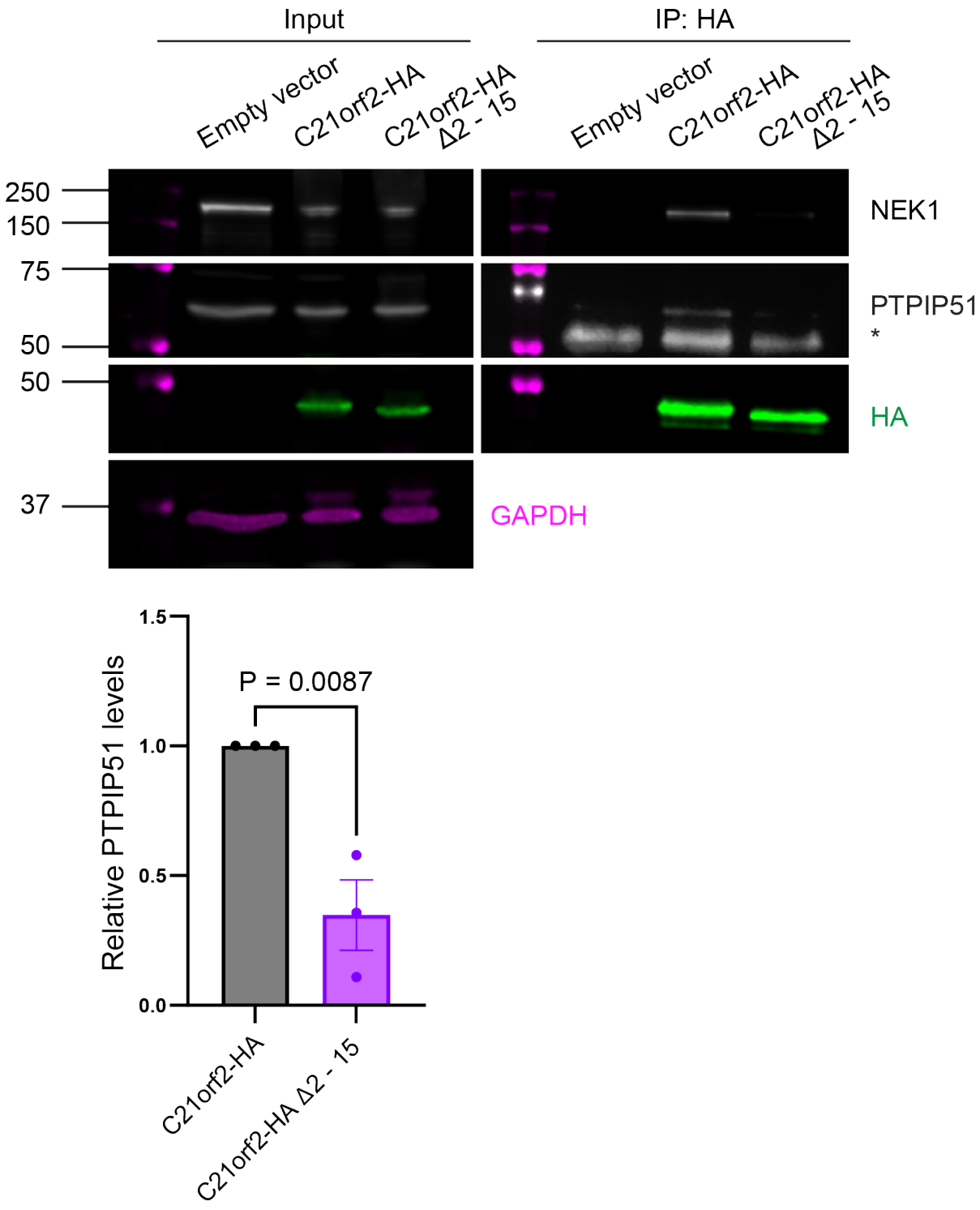

Figure 3-15 Disruption of the C21orf2 N-terminal domain prevents interaction with PTPIP51.

HEK293 cells were transfected with pCI-neo empty vector, C21orf2-HA or C21orf2-HA Δ2 – 15. The samples were immunoprecipitated with an anti-HA antibody and immunoblotted, staining with anti-HA, anti-NEK1 and anti-PTPIP51 antibodies. An anti-GAPDH antibody was used as a loading control. 45 µg protein per sample was loaded as input. Graph shows quantification of endogenous PTPIP51 normalised to the level of immunoprecipitated C21orf2-HA or C21orf2-HA Δ2 – 15. Data were analysed by unpaired two-tailed t-test, *N* = 3. Bars represent mean ± SEM.

3.4.4 NEK1 but not C21orf2 partially localises to MAM

As our data indicated an interaction between NEK1, C21orf2 and the VAPB/PTPIP51 ER-mitochondria tether (Figure 3-12, Figure 3-14), this indicated that NEK1 and C21orf2 may localise to MAM. To test this, HEK293 cells were fractionated by Percoll gradient centrifugation, as has previously been performed for VAPB and PTPIP51 (De Vos *et al.*, 2012). The protein fractions were immunoblotted, probing for endogenous NEK1 and C21orf2. To confirm specific isolation of cell fractions, the samples were probed for proteins known to localise to each fraction. PTPIP51 and VDAC1 were probed as markers of mitochondria and MAM. PDI and ACSL4 were probed as markers of ER and MAM.

As expected, each of the control proteins were enriched in their expected fractions (Figure 3-16). NEK1 was enriched in the small vesicle fraction, and a small portion was apparent in both the mitochondrial and MAM fractions. In line with our co-immunoprecipitation data, this suggests that only a small proportion of NEK1 protein localises to mitochondria/MAM. This may explain both the supposed cytoplasmic phenotype when overexpressed (Figure 3-5), and small proportion of NEK1 interacting with endogenous PTPIP51 (Figure 3-12). Whilst C21orf2 was not present in the mitochondrial or MAM fractions, C21orf2 was also enriched in the small vesicle fraction. This coincided with our immunostaining data that indicated C21orf2 partially localised to endosomal compartments but not mitochondria (Figure 3-5, Figure 3-9). Due to time limitations this experiment was only performed once, thus further experimentation will be necessary to confirm this result.

3.4.5 NEK1 binds directly to PTPIP51 *in vitro*

In our previous experiments, we had established using co-immunoprecipitation that NEK1 and C21orf2 interact with the VAPB/PTPIP51 tether by interaction with PTPIP51 (Figure 3-12, Figure 3-14). As we observed that NEK1 but not C21orf2 was enriched in the MAM cell fraction, it suggested that NEK1 and PTPIP51 interact may be the key binding proteins (Figure 3-16). To confirm the direct binding between NEK1 and PTPIP51, we used an *in vitro* GST-pull down assay. We firstly prepared and validated the recombinant cytosolic domains of PTPIP51 (AA 36-470; PTPIP51 ΔTM) and VAPB (AA 1-220; VAPB ΔTM) to be used in the assay. Empty vector GST and GST-tagged recombinant cytosolic domains of PTPIP51 and VAPB were produced and purified from E. coli and captured by incubation with gluathione sepharose beads. The samples were run on SDS-PAGE and the gel stained with Coomassie stain to view the purified proteins. Proteins of the correct molecular weight were observed for each of the GST-tagged proteins, GST (~28 kDa), GST-PTPIP51 (~77 kDa) and GST-VAPB (~54 kDa) (Figure 3-17).

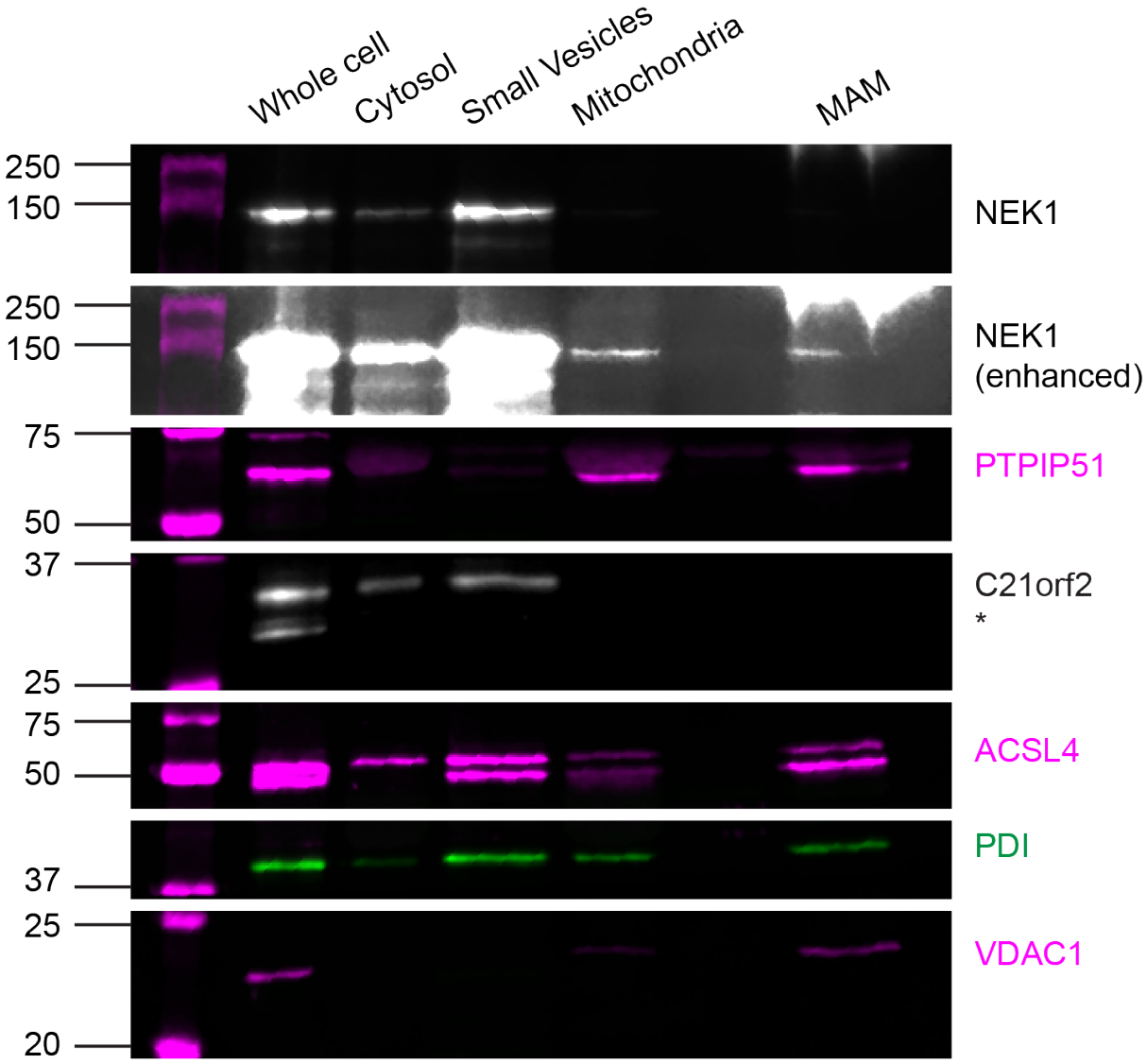

Figure 3-16 NEK1 but not C21orf2 partially localises to MAM.

Whole cell lysis and fractions of cytosol, small vesicles, mitochondria and mitochondria associated ER-membranes (MAM) were extracted from HEK293 cells by Percoll gradient centrifugation. Samples were immunoblotted, probing for endogenous NEK1 and C21orf2 and proteins known to localise to each of the fractions; PTPIP51 (Mitochondria/MAM), ACSL4 (ER/MAM), PDI (ER/MAM) and VDAC1 (Mitochondria/MAM). * Denotes a non-specific protein band. *N* = 1.

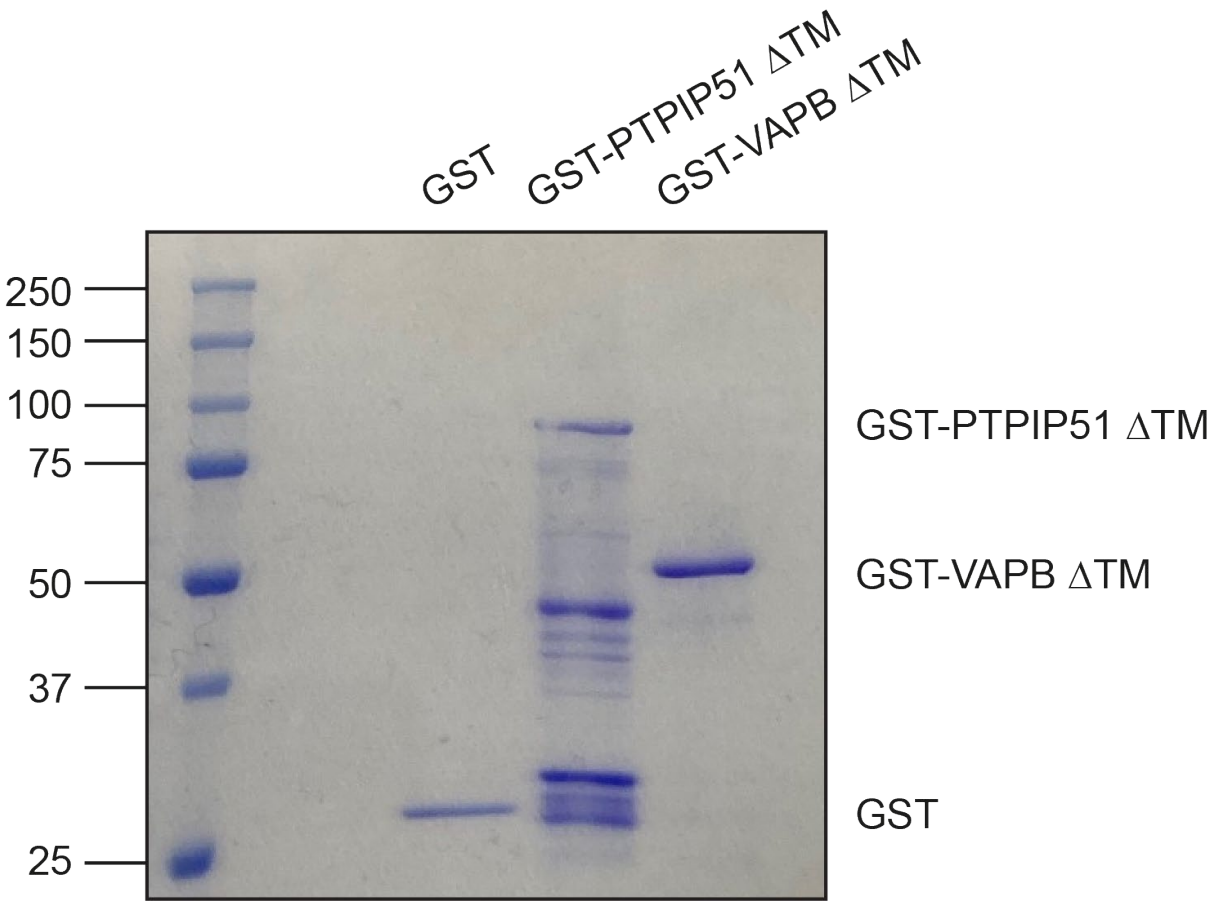

Figure 3-17 Purification of GST-tagged PTPIP51 and VAPB.

Empty vector GST and GST-tagged recombinant cytosolic domains of PTPIP51 (AA 36-470; PTPIP51 ΔTM) and VAPB (AA 1-220; VAPB ΔTM) were produced and purified from E. coli by incubation with gluathione sepharose beads. Eluted GST proteins were run on SDS-PAGE, stained with Coomassie stain, destained and imaged.

To determine the direct binding between NEK1, C21orf2 and the VAPB/PTPIP51 tether, NEK1 and C21orf2 were *in vitro* translated from the V5-NEK1 and C21orf2-HA template plasmid DNA constructs to produce 35S-methionine radiolabelled proteins. The radiolabelled *in vitro* translated NEK1 and C21orf2 were incubated with the GST-tagged PTPIP51 and VAPB captured on glutathione-coated beads and ran on SDS-PAGE before the gel was dried onto Whatmann paper and exposed to a phosphor-screen for imaging. We observed that in line with our co-immunoprecipitation experiment, NEK1 bound directly to PTPIP51 but not to VAPB (Figure 3-18A), whilst C21orf2 did not directly bind to PTPIP51 or VAPB (Figure 3-18B). This supports our co-immunoprecipitation data (Figure 3-15), suggesting that this interaction is mediated by direct binding between NEK1 and PTPIP51.

To determine which NEK1 domain may bind to PTPIP51, we created recombinant fragments of NEK1 protein domains. Site directed mutagenesis was used to insert premature stop codons in the V5-NEK1 at amino acids 258 (kinase domain), 378 (kinase & basic domains) or 732 (kinase, basic & coiled-coil domains) (Figure 3-19A). *In vitro* translation was used to radiolabel full length NEK1 or NEK1 protein fragments with 35S-methionine. SDS-PAGE of the *in vitro* translated NEK1 protein fragments confirmed translation of proteins of the correct size, 1-258 at ~30 kDa, 1-379 at ~43 kDa and 1-732 at ~76 kDa. We found that each of the protein fragments bound to PTPIP51 (Figure 3-19B). Considering that the NEK1 kinase domain alone was sufficient to bind to PTPIP51, and the fact that NEK1 is a kinase, this suggested that the interaction between NEK1 and the VAPB/PTPIP51 may be mediated by its kinase activity. Due to time limitations this experiment was only performed once, thus further experimentation will be necessary to confirm this result.

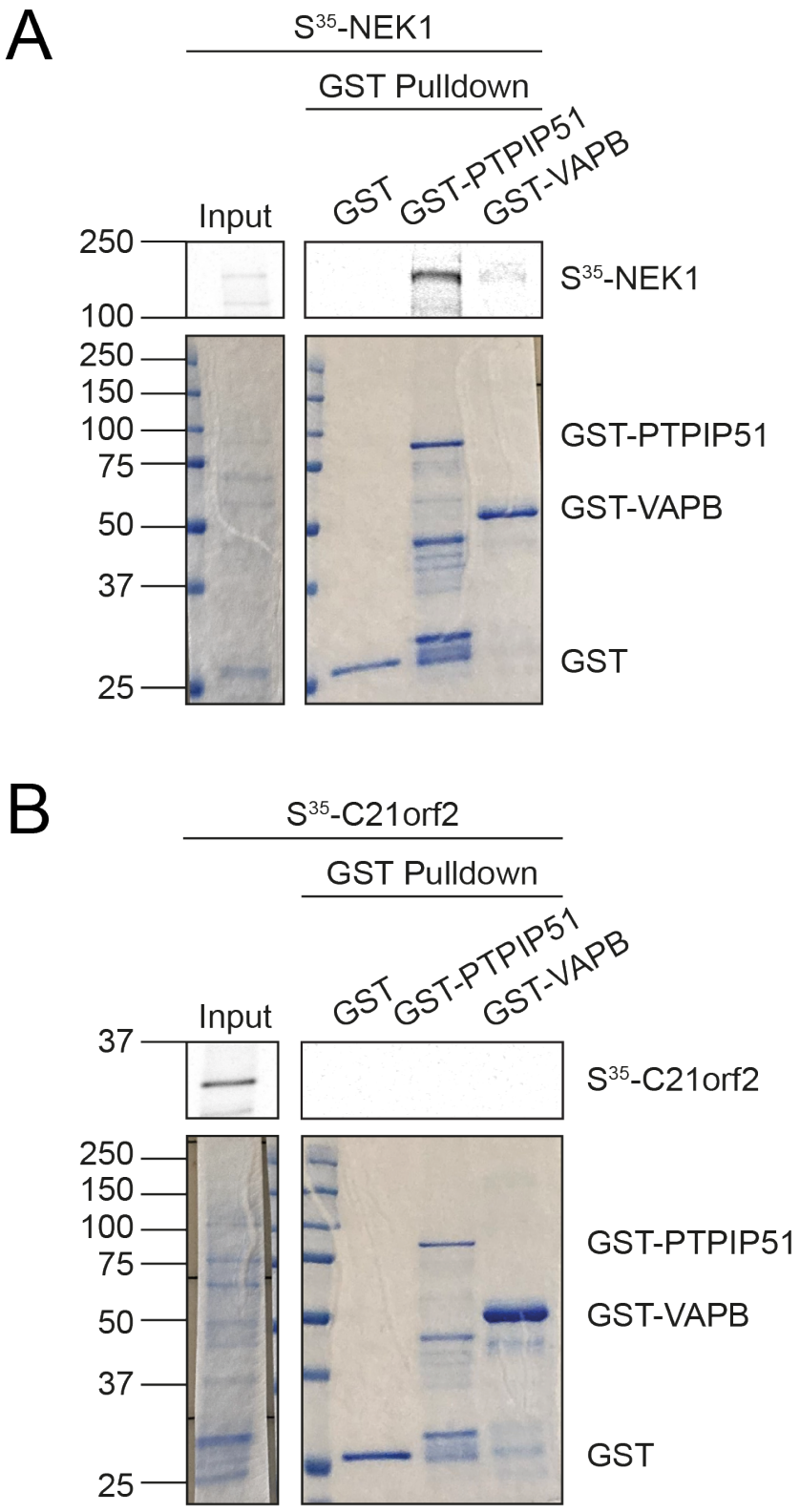

Figure 3-18 NEK1 binds directly to PTPIP51 *in vitro*.

In vitro translated 35S-radiolabeled NEK1 **(A)** or C21orf2 **(B)** were added to empty vector GST or GST-tagged recombinant cytosolic domains of PTPIP51 (AA 36-470) and VAPB (AA 1-220) immobilised on glutathione-coated beads and incubated for 1h at 4°C. 35S-radiolabeled proteins were visualized by phosphorimager (top panels). Coomassie-stained GST-tagged proteins in the pull-down samples are shown (bottom panels). Figures represent *N* = 3.

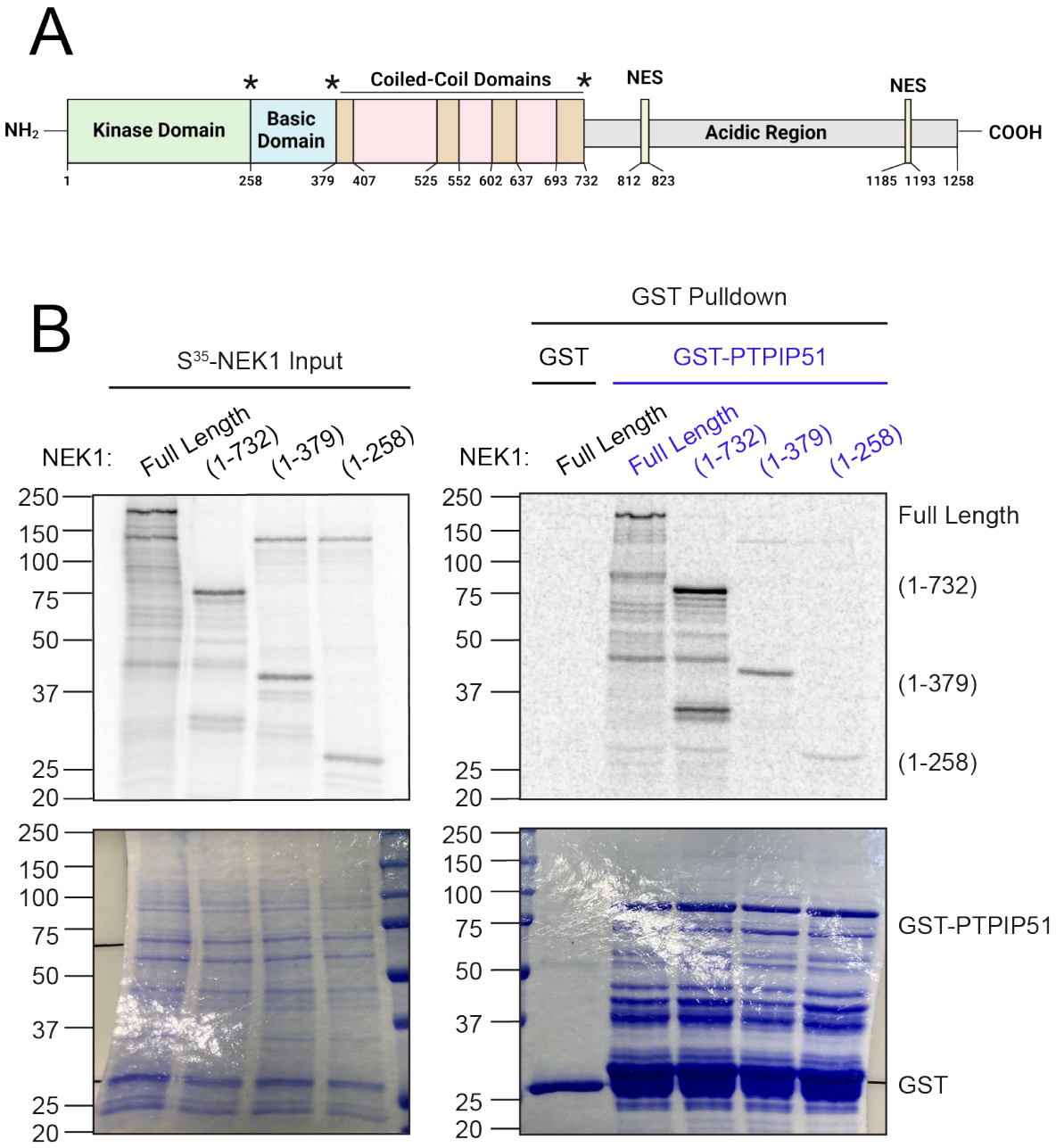

Figure 3-19 NEK1 protein fragments bind to PTPIP51 *in vitro*.

A) Schematic of NEK1 protein fragments produced with site-directed mutagenesis of premature stop codons (denoted by *), NES = nuclear export sequence.

B) 35S-radiolabelled fragments of NEK1 protein domains were incubated with GST or GST-PTPIP51 immobilised on glutathione-coated beads. 35S-radiolabelled NEK1 fragments were visualised by phosphorimager (top panels). Coomassie-stained GST and GST-PTPIP51 in the pull-down samples are shown (bottom panels). *N* = 1.

3.5 Discussion

3.5.1 Characterisation of the NEK1/C21orf2 protein complex

At the start of this project there was little known about the functional NEK1/C21orf2 protein complex, and conflicting information about the cellular localisation of either protein. It was initially established that C21orf2 was a mitochondrial protein (Krohn *et al.*, 1997). However, we found that C21orf2 when overexpressed did not localise to mitochondria (Figure 3-5), and endogenous C21orf2 is not enriched in mitochondrial or MAM cell fractions (Figure 3-16). Instead, we observed an enrichment of C21orf2 in the small vesicular cell fraction. Overexpression of C21orf2 led to two distinct phenotypes, globular punctate staining, and filamentous staining (Figure 3-8). We observed partial overlap of both phenotypes to multiple endosomal compartments (Figure 3-9), and partial overlap of C21orf2 staining to the microtubule marker α-tubulin (Figure 3-10). C21orf2 is known as a protein involved in regulation of primary cilia (Wheway *et al.*, 2015), thus its localisation to microtubules may be related to this function. In literature, it is reported that C21orf2 co-localised with the microtubule centrosomal marker γ-tubulin (De Decker *et al.*, 2022), although it is not clear if C21orf2 interacts with other microtubule components. One possible explanation for the microtubule localisation of C21orf2 could be due to its interaction with NEK1. A recent study reported that NEK1 is involved in microtubule homeostasis as loss of NEK1 destabilises microtubules and inhibits nuclear import (Mann *et al.*, 2023). Additionally, NEK1 was found to interact with multiple cytoskeletal proteins such as tubulin α-1B chain and elongation factor 1-α-1 (EF1A1) (Mann *et al.*, 2023). EF1A1 interacts with filamentous actin to regulate actin bundling (Vlasenko *et al.*, 2015). Interestingly, EF1A1 is a known interactor of PARP1, a protein pivotal in the mediation between autophagy and apoptosis in response to DNA damage (discussed in section 1.3.3) (Maruyama *et al.*, 2007). A proteomic study found that in response to genetic stress, PARP1 is in close proximity to proteins involved in microtubule polymerisation, such as the microtubule-associate protein targeting protein for Xklp2 (TPX2) which promotes microtubule assembly during (Mosler *et al.*, 2022; Moss *et al.*, 2009). Loss of NEK1 leads to increased PARP1 expression, possibly as a compensatory mechanism to promote NHEJ when HR is disrupted due to loss of functional NEK1 (Martins *et al.*, 2021). Thus, it is possible that NEK1 and C21orf2 located on the microtubules may be involved in microtubule stability in response to DNA damage, although this warrants further investigation.

3.5.2 NEK1 and C21orf2 interact with the VAPB/PTPIP51 tether.

Whilst we did not observe the enrichment of C21orf2 at mitochondria or MAM, we observed a small proportion of NEK1 enriched in these fractions (Figure 3-16). Literature states that in response to DNA damage a small portion of NEK1 is localised to mitochondria where it phosphorylates the MAM protein VDAC1 to prevent apoptosis (Chen *et al.*, 2009; Chen *et al.*, 2010b). Our data shows that

overexpression of NEK1 is diffuse throughout the cytoplasm and not localised to mitochondria with immunofluorescence (Figure 3-5). One possible explanation is that if only a fraction of NEK1 localises to mitochondria and the majority exists within the cytosol, we would not be able to observe a specific mitochondrial localisation with this technique. We were unable to optimise a proximity ligation assay to confirm interaction with mitochondrial or MAM proteins due to the cytoplasmic phenotype of overexpressed NEK1. However, one alterative could be to use CRISPR/Cas9 genome editing to endogenously tag NEK1. This would bypass our limitation of lack of suitable endogenous NEK1 antibodies for immunostaining and PLA.

In line with our observation that a portion of NEK1 is enriched at MAM, we observed that both exogenous and endogenous NEK1 interacts with the mitochondrial MAM tethering protein PTPIP51 (Figure 3-11, Figure 3-12). Contrary to published data (Cirulli *et al.*, 2015), we were unable to confirm an interaction between NEK1 and the PTPIP51 interacting partner VAPB (Figure 3-11). As multiple lines of evidence show that NEK1 is involved in mitochondrial homeostasis (discussed in section 1.3.4) (Basei *et al.*, 2024), it is possible that NEK1 interacts at MAM by directly interacting with PTPIP51 on the OMM. In line with this theory, we observed that NEK1 directly binds to PTPIP51 *in vitro,* which may be mediated by its kinase domain (Figure 3-18, Figure 3-19). Although the kinase domain of NEK1 alone was sufficient to bind PTPIP51 in vitro, we observed increased binding between the two proteins when the NEK1 coiled coil was present. Proteomic data suggests that the NEK1 coiled-coil domain is its main regulatory and binding domain (Surpili *et al.*, 2003). To confirm this, isolated NEK1 domain fragments should be produced to determine which domain is sufficient to bind to PTPIP51. Conversely, removal of individual domains could confirm their necessity for PTPIP51 binding. It is currently unclear how PTPIP51 mediates its protein interactions, as conflicting data suggests a role for the coiled-coil domain and FFAT motif (Mórotz *et al.*, 2022; Yeo *et al.*, 2021), thus creating PTPIP51 domain fragments in parallel would allow us to elucidate the protein binding mechanism.

In a similar fashion to NEK1, C21orf2 interacted with PTPIP51 when overexpressed, but not VAPB (Figure 3-14). We observed that when C21orf2 has reduced binding to NEK1, due to disruption of its N-terminal domain, it no longer binds to PTPIP51 (Figure 3-15). This suggests that NEK1 may be necessary for C21orf2 to interact with the VAPB/PTPIP51 tether. Additionally, as C21orf2 does not bind to PTPIP51 or VAPB *in vitro* (Figure 3-18), it is possible that NEK1 interaction with C21orf2 recruits the protein to MAM. In literature overexpression of PTPIP51 leads to recruitment of its binding partner VAPB to the mitochondria (De Vos *et al.*, 2012). When expressed alone NEK1 is diffuse throughout the cytoplasm but is recruited to C21orf2 positive tubules and puncta when co-expressed (Figure 3-13), further confirming the strong interaction between these proteins. We did not observe this effect with NEK1 co-expression with PTPIP51, suggesting that PTPIP51 does not recruit NEK1. One possible

explanation for this, is that NEK1 is recruited in response to cellular stimuli, such as DNA damage as is the case between NEK1 and VDAC1 (Chen *et al.*, 2009). It is currently not clear whether NEK1 is anchored to MAM by PTPIP51 once it is recruited, thus in future we could use cell fractionation with PTPIP51 knockdown to quantify the amount of NEK1 present at MAM and if this is affected by loss of PTPIP51.

3.5.3 Conclusion.

Together, we have identified a novel protein interaction between NEK1, C21orf2 and the VAPB/PTPIP51 ER-mitochondria tether, which we endeavoured to further elucidate within this study. A summary of the key findings of this chapter are shown in Figure 3-20.

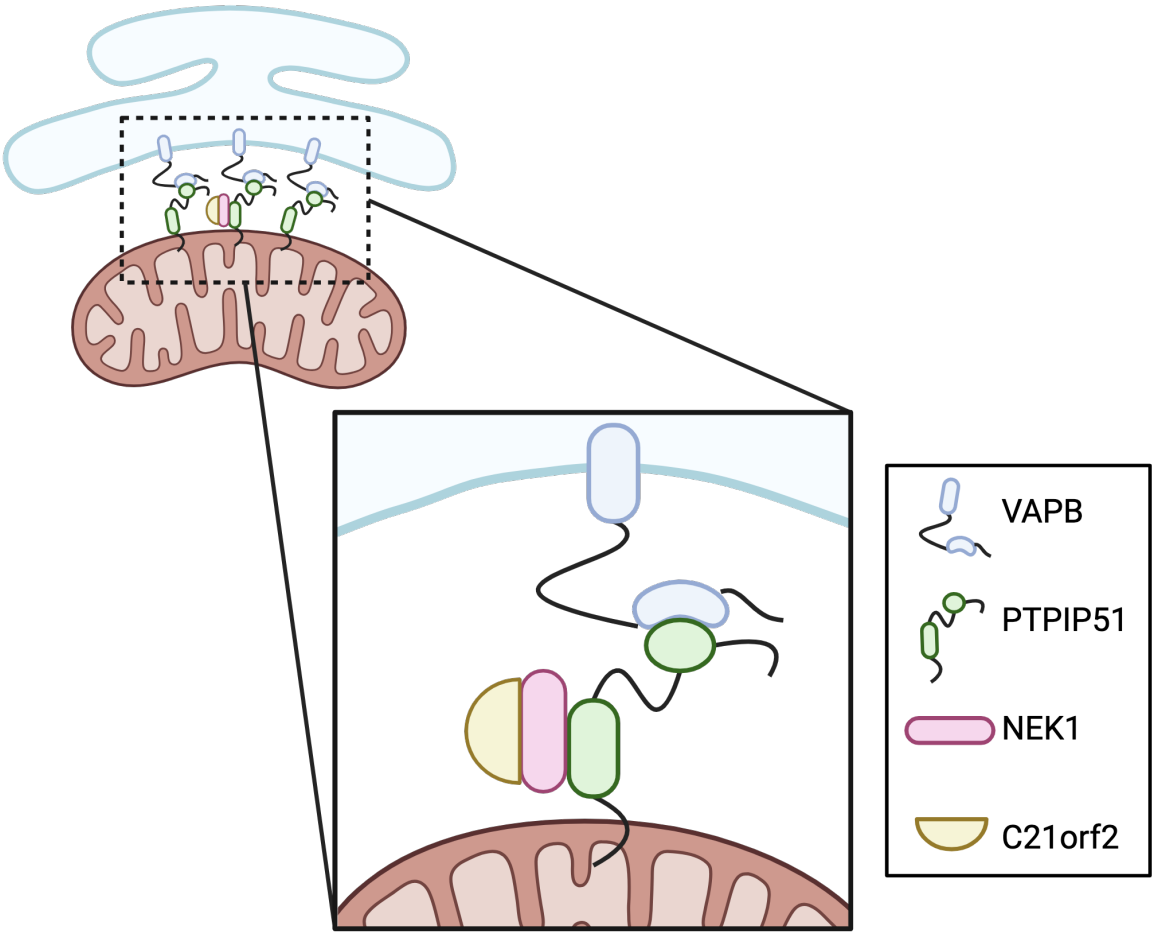

Figure 3-20 Summary of NEK1/C21orf2 interaction with the VAPB/PTPIP51 tether.

In this chapter we observed that NEK1 interacts with the VAPB/PTPIP51 tether by directly binding to PTPIP51 in co-immunoprecipitation and GST-pulldown assays. Whilst C21orf2 binds to PTPIP51 in co-immunoprecipitation assays, we did not observe a direct interaction with VAPB or PTPIP51 in the GST-pulldown. Reduced NEK1/C21orf2 interaction by disruption of the C21orf2 N-terminus ablates C21orf2/PTPIP51 binding, suggesting C21orf2 interacts with VAPB/PTPIP51 indirectly, through its binding to NEK1.

Chapter 4 NEK1 regulates the VAPB/PTPIP51 tether

4.1 Introduction

In chapter 3 we identified a novel interaction between the protein kinase NEK1, C21orf2 and the VAPB/PTPIP51 tether. We determined that NEK1 directly binds to PTPIP51 and found a portion of NEK1 protein enriched in mitochondrial and MAM cell fractions (Figure 3-12, Figure 3-16, Figure 3-18). Both PTPIP51 and its tethering partner VAPB contain NEK1 consensus phosphorylation motifs (VAPB: T143, T201 and T222, PTPIP51: T20 and T177) (Figure 4-15), so it is probable that NEK1 may regulate their binding by phosphorylation. In response to DNA damage, it is known that a portion of NEK1 is recruited to mitochondria to phosphorylate the MAM protein VDAC1 to prevent apoptosis (Chen *et al.*, 2009). Multiple lines of evidence suggest that there is signalling between the nucleus and mitochondria in response to DNA damage, in order to promote DNA repair and determine cell fate (Fang *et al.*, 2016) (discussed in section 1.3.2.3). Furthermore, it has been reported that in response to DNA damage there is increased formation of ER-mitochondria contacts, leading to increased mitochondrial Ca^{2+} uptake and induction of apoptosis (Zheng *et al.*, 2018). Therefore, we hypothesised that NEK1 may phosphorylate PTPIP51 and VAPB in order to regulate their interaction in response to DNA damage.

Disruption of MAM is a common pathomechanism in ALS (discussed in section 1.2.4) (Lee *et al.*, 2024). Loss of function mutations in *NEK1* are a cause of ALS, whilst missense mutations in the *C21orf2* confer susceptibility to developing the disease (Brenner *et al.*, 2016; van Rheenen *et al.*, 2016). Whether disruption of MAM is a feature of NEK1 and C21orf2-related ALS has not yet been investigated. In line with our hypothesis that NEK1 regulates VAPB/PTPIP51 tethering, we further hypothesised that loss of NEK1 function would disrupt this ER-mitochondria tether and the processes they regulate. In this chapter we aimed to elucidate the mechanism of NEK1-mediated regulation of VAPB/PTPIP51 tethering and determine if loss of NEK1 function would disruption of this tether.

4.2 Loss of NEK1 or C21orf2 function disrupts VAPB/PTPIP51 tethering

Our previous data evidenced that NEK1 and C21orf2 interact with the VAPB/PTPIP51 tether, mediated by direct binding between NEK1 and the mitochondrial protein PTPIP51 (Figure 3-12, Figure 3-14, Figure 3-18). To determine if NEK1 and C21orf2 may regulate the VAPB/PTPIP51 interaction, we used loss of function cell models to investigate whether functional knock out of NEK1 or C21orf2 would disrupt VAPB/PTPIP51 tethering. NEK1 KO, C21orf2 KO or their corresponding wild type parental HeLa cell lines (PC and WT HeLa respectively) were subjected to immunoprecipitation with an endogenous VAPB antibody. The samples were immunoblotted, probing for endogenous NEK1, C21orf2, PTPIP51, VAPB, and α-tubulin as a loading control (Figure 4-1). We observed that the NEK1 KO cells had significantly less PTPIP51 binding to VAPB, suggesting loss of NEK1 disrupts this ER-mitochondria tether (Figure 4-1A).

In the same fashion of loss of NEK1, we observed that there was significantly less VAPB/PTPIP51 interaction in the C21orf2 KO cells compared to WT cells (Figure 4-1D). To confirm specificity of this effect, we endeavoured to reintroduce NEK1 or C21orf2 into their respective KO cells to determine if we could rescue this effect. As NEK1 is a large protein, we had previously observed that expression of NEK1 by transfection of our V5-NEK1 plasmid construct was relatively inefficient (data not shown). As only a small portion of cells successfully express our NEK1 construct, a rescue effect may be masked using a technique such as co-immunoprecipitation. Thus, we opted to use a proximity ligation assay (PLA), where we could visualise NEK1 overexpression, and thus only quantify cells that had reintroduction of the NEK1 protein. We first validated the use of endogenous VAPB and PTPIP51 antibodies for PLA using the DuoLink PLA kit (Sigma). Incubation with either only VAPB, PTPIP51 or no antibodies results in no PLA signal being produced, confirming specificity of the technique (Figure 4-2).

To determine if loss of NEK1 leads to disrupted VAPB/PTPIP51 interaction, wild type parental cell (PC) HeLa cells were transfected with pCI-neo empty vector as a control. NEK1 KO HeLa cells were transfected with either pCI-neo empty vector or V5-NEK1 to determine if we could rescue loss of VAPB/PTPIP51 tethering by reintroducing NEK1 protein. In line with our co-immunoprecipitation data, we observed a significant decrease in VAPB/PTPIP51 tethering in the NEK1 KO cells compared to control cells (Figure 4-3). Reintroduction of NEK1 protein rescued VAPB/PTPIP51 tethering back to a similar level as wild type control cell line. This suggests the disruption of VAPB/PTPIP51 tethering is specifically due to loss of functional NEK1 protein.

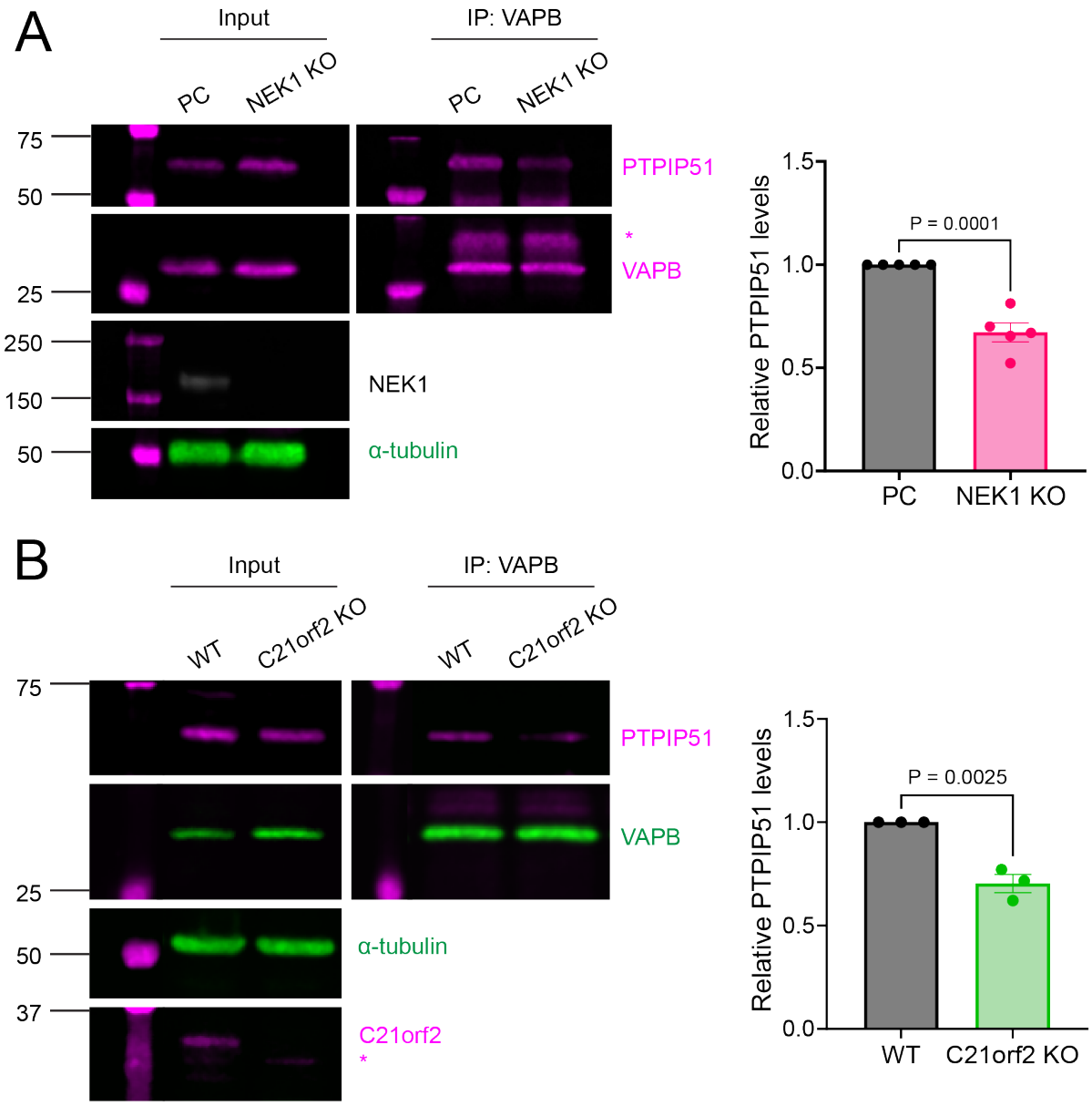

Figure 4-1 Loss of NEK1 or C21orf2 disrupts VAPB/PTPIP51 tethering.

Wild type parental (PC) and NEK1 knock out (KO) **(A)** or wild type (WT) and C21orf2 KO HeLa cells **(B)** were lysed and endogenous VAPB was immunoprecipitated using an anti-VAPB antibody. Inputs were probed for endogenous NEK1, C21orf2, PTPIP51, VAPB, and α-tubulin as a loading control on immunoblot. Immune pellets were probed for endogenous PTPIP51 and VAPB. For input 45 µg protein was loaded. * Denotes a non-specific antibody band. Graphs represent the quantification of PTPIP51 bound to VAPB on immunoblot normalised to the level of immunoprecipitated VAPB in the respective experiments. Bars represent mean ± SEM. Data were analysed by two-tailed unpaired t-test, NEK1 KO, *N* = 5, C21orf2 KO, *N* = 3.

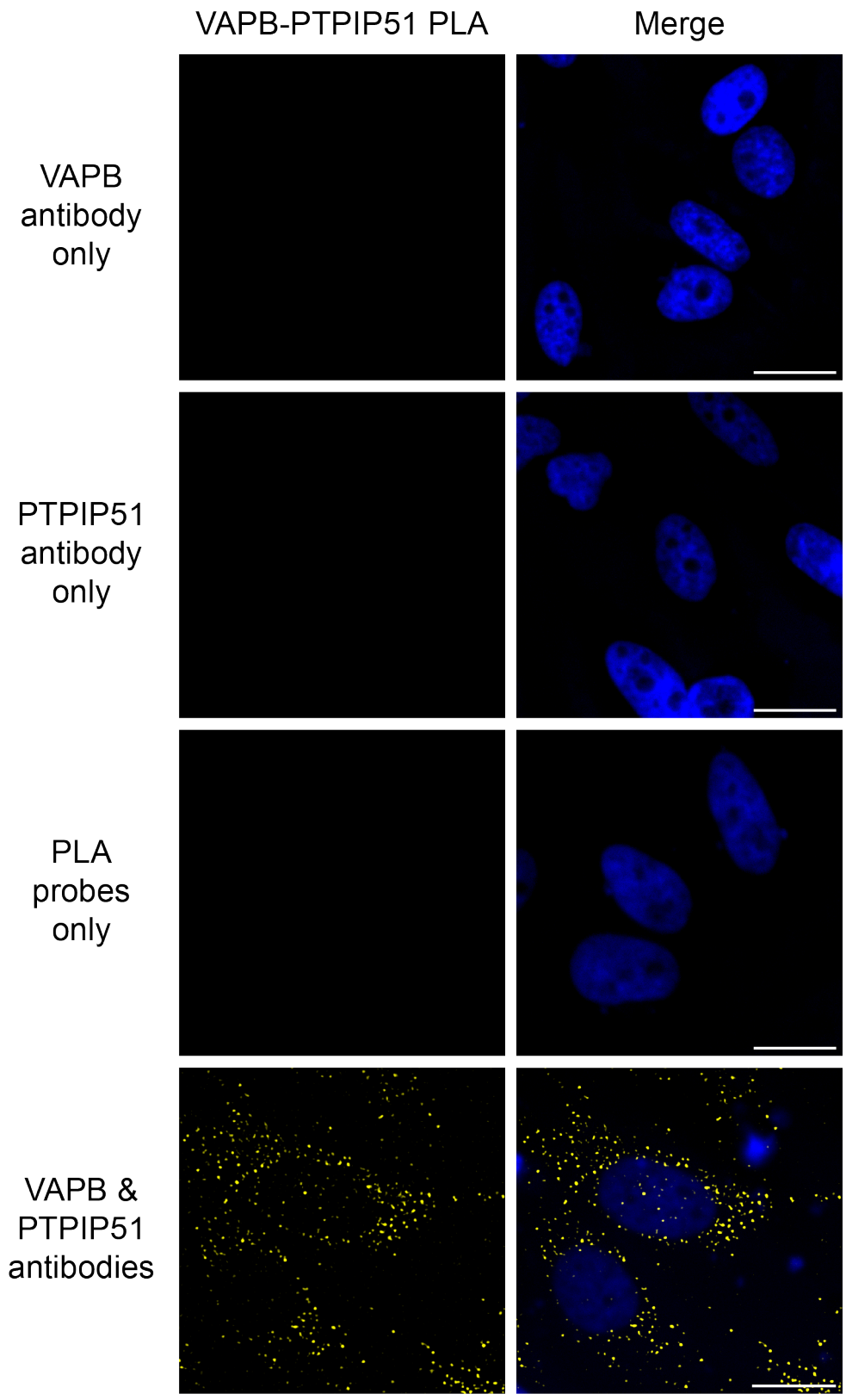

Figure 4-2 Validation of endogenous VAPB and PTPIP51 antibodies for PLA.

Wild type HeLa cells were subjected to proximity ligation assay (PLA) using endogenous anti-VAPB and anti-PTPIP51 antibodies (yellow). Samples were stained with nuclear Hoechst stain (blue). To confirm specificity, either only the anti-VAPB or anti-PTPIP51 antibody, or neither antibody was added. Scale bar = 20 µm.

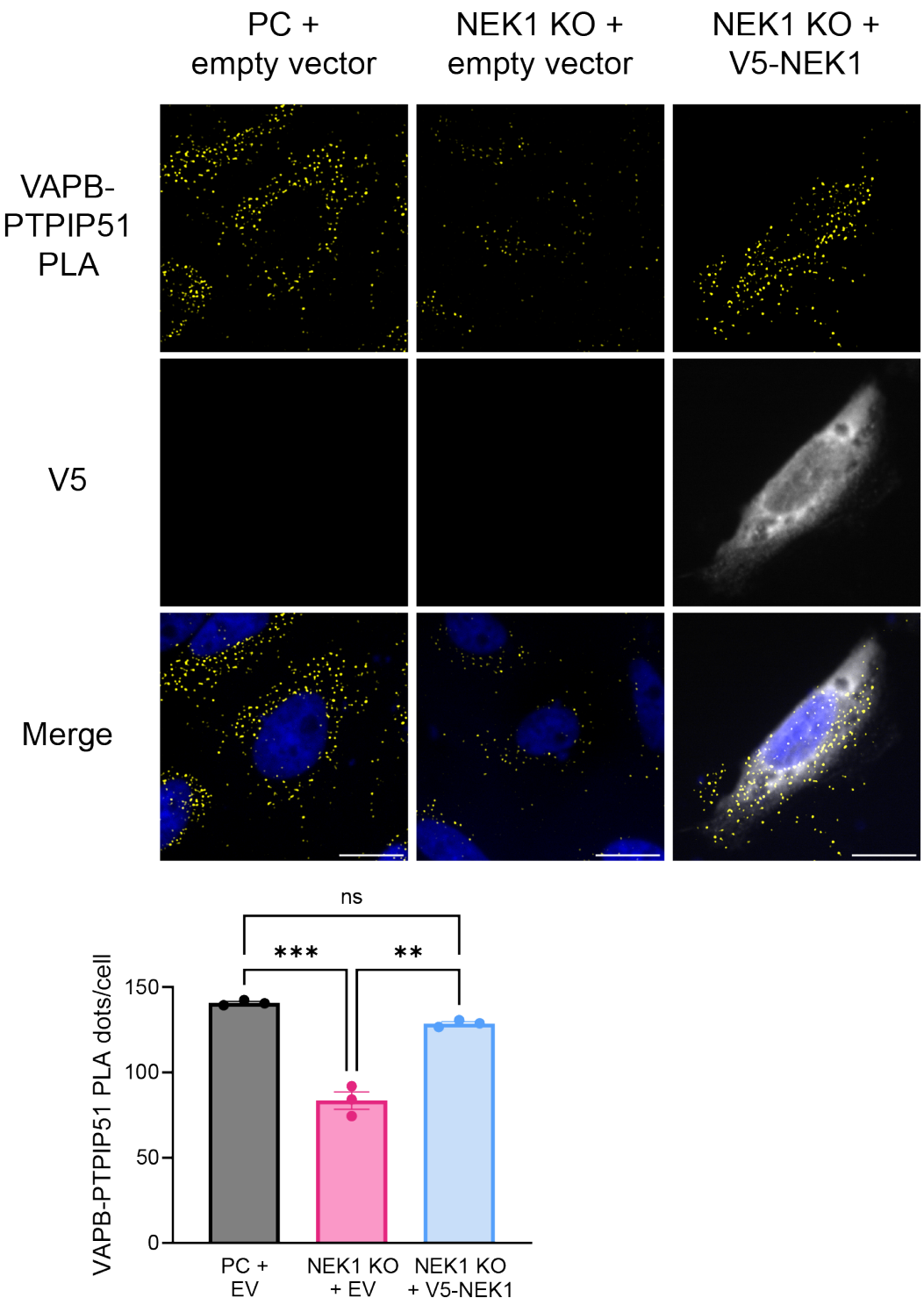

Figure 4-3 Reintroduction of NEK1 protein rescues disrupted VAPB/PTPIP51 tethering.

Wild type parental HeLa cells (PC) or NEK1 knock out (KO) HeLa cells were transfected with empty vector pCI-neo (EV) or V5-NEK1. Cells were subjected to proximity ligation assay (PLA) with endogenous anti-VAPB and anti-PTPIP51 antibodies (yellow) and co-stained with an anti-V5 antibody (grey) and Hoechst nuclear stain (blue). The number of PLA spots per cell was quantified. Bars display mean ± SEM, points display mean per independent repeat. Data were analysed by one-way ANOVA with Fisher's LSD; ** $P \leq 0.01$, *** $P \leq 0.001$, ns = non-significant. $N = 3$. $n > 165$ cells per sample, across three independent repeats. Scale bar = 20 µm.

Literature suggests that the VAPB/PTPIP51 interaction may be regulated by phosphorylation (Di Mattia *et al.*, 2020; Stoica *et al.*, 2016). Our previous data showed that the NEK1 kinase domain is sufficient to bind to PTPIP51 *in vitro* (Figure 3-19). Considering NEK1 is a kinase known to phosphorylate the MAM protein VDAC1 (Chen *et al.*, 2010b), we determined to elucidate whether NEK1 kinase activity may be responsible for regulation of VAPB/PTPIP51 tethering. To test this, we reintroduced either WT or kinase dead K33R V5-NEK1 into NEK1 KO HeLa cells by DNA transfection. The cells were subjected to PLA with endogenous VAPB and PTPIP51 antibodies. We observed that the kinase dead V5-NEK1 K33R was unable to rescue VAPB/PTPIP51 interaction (Figure 4-4). This suggests that NEK1 kinase activity is essential for regulating VAPB/PTPIP51 tethering.

As loss of NEK1 leads to loss of C21orf2 protein stabilisation (Watanabe *et al.*, 2020), our NEK1 KO HeLa cell lines also exhibit loss of C21orf2 protein. Due to this effect, we wanted to establish whether overexpressing C21orf2 alone was sufficient to rescue the defects with loss of NEK1. This would confirm whether the VAPB/PTPIP51 defects observed were due to specific loss of NEK1, or due to NEK1/C21orf2 complex deficiency. PC HeLa cells were transfected with pCI-neo empty vector and NEK1 KO HeLa cells were transfected with either pCI-neo empty vector, V5-NEK1, or C21orf2-HA. Reintroduction of C21orf2 did not rescue this tethering defect, suggesting that NEK1 specifically is necessary for regulation of VAPB/PTPIP51 interactions (Figure 4-5). Due to time limitations, this experiment was only performed once, thus replication is necessary to confirm this result.

To confirm this finding, we performed PLA on C21orf2 KO cells and reintroduced either wild type HA-tagged C21orf2 or our C21orf2-HA Δ2 – 15 construct which has diminished interaction with NEK1 (Figure 3-6). WT HeLa cells were transfected with pCI-neo empty vector and C21orf2 KO HeLa cells were transfected with either pCI-neo empty vector, C21orf2-HA or C21orf2-HA Δ2 – 15 (Figure 4-6A). In line with our co-immunoprecipitation data, we observed a significant loss of VAPB/PTPIP51 tethering in the C21orf2 KO cells compared to control cells (Figure 4-6B). Reintroduction of full length C21orf2-HA rescued this interaction. In line with our previous experiment (Figure 4-5), reintroduction of C21orf2 that has impaired NEK1 binding did not rescue this defect (Figure 4-6C). Together, this suggests that C21orf2 alone is not sufficient to rescue VAPB/PTPIP51 tethering and thus the ER-mitochondria tethering defects may be due to loss of NEK1 protein stabilisation. This further implicates a role for NEK1 in mediation of VAPB/PTPIP51 ER-mitochondria tethering.

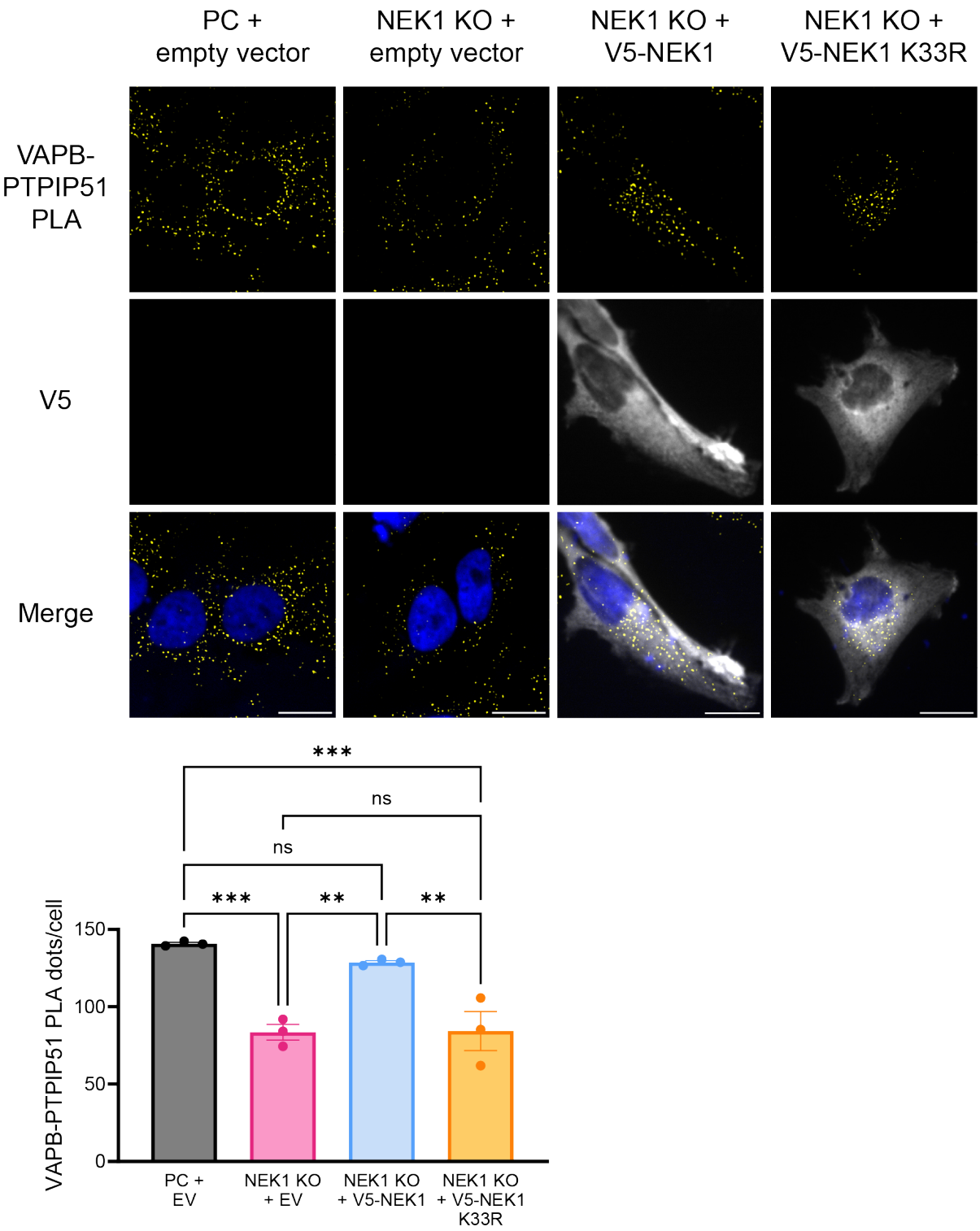

Figure 4-4 NEK1 kinase activity is necessary to regulate VAPB/PTPIP51 tethering.

Wild type parental HeLa cells (PC) or NEK1 knock out (KO) HeLa cells were transfected with empty vector pCI-neo (EV), V5-NEK1 or kinase dead V5-NEK1 K33R. Cells were subjected to PLA with endogenous anti-VAPB and anti-PTPIP51 antibodies (yellow) and co-stained with an anti-V5 antibody (grey) and Hoechst nuclear stain (blue). The number of PLA spots per cell was quantified. Bars display mean ± SEM, points display mean per independent repeat. Data were analysed by one-way ANOVA with Fisher's LSD; ** $P \leq 0.01$, *** $P \leq 0.001$, ns = non-significant. $N = 3$. $n > 165$ cells per sample, across three independent repeats. Scale bar = 20 µm.

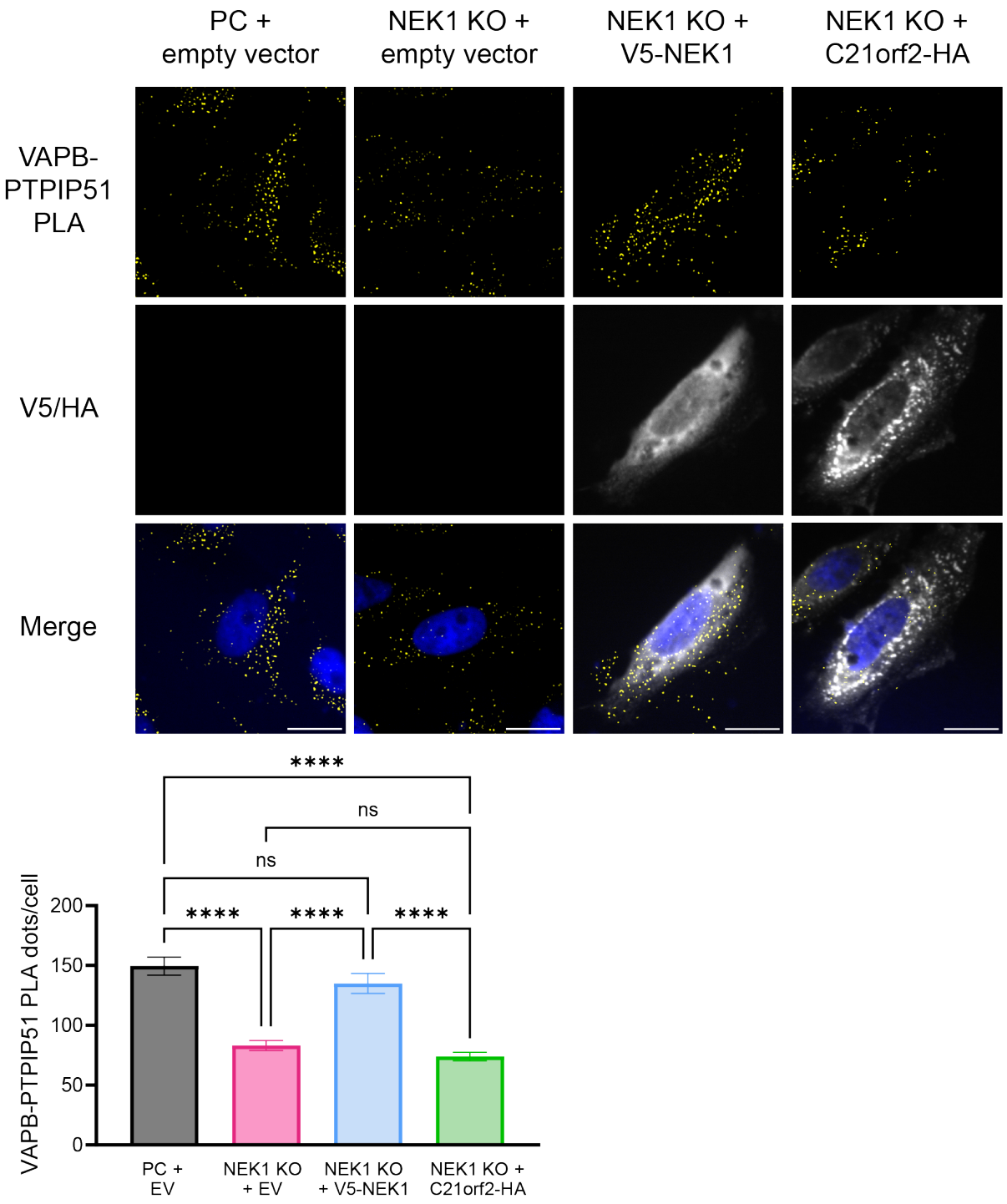

Figure 4-5 C21orf2 is unable to rescue NEK1-deficiency mediated VAPB/PTPIP51 tethering defects.

Wild type parental HeLa cells (PC) or NEK1 knock out (KO) HeLa cells were transfected with empty vector pCI-neo, V5-NEK1 or C21orf2-HA. Cells were subjected to PLA with endogenous anti-VAPB and anti-PTPIP51 antibodies (yellow) and co-stained with V5 or HA antibodies (grey) and Hoechst nuclear stain (blue). The number of PLA spots per cell was quantified. Bars display mean ± SEM, points display mean per independent repeat. Data were analysed by one-way ANOVA with Fisher's LSD; **** $P \leq 0.0001$, ns = non-significant. $N = 1$. $n > 97$ cells per sample from one independent repeat. Scale bar = 20 µm.

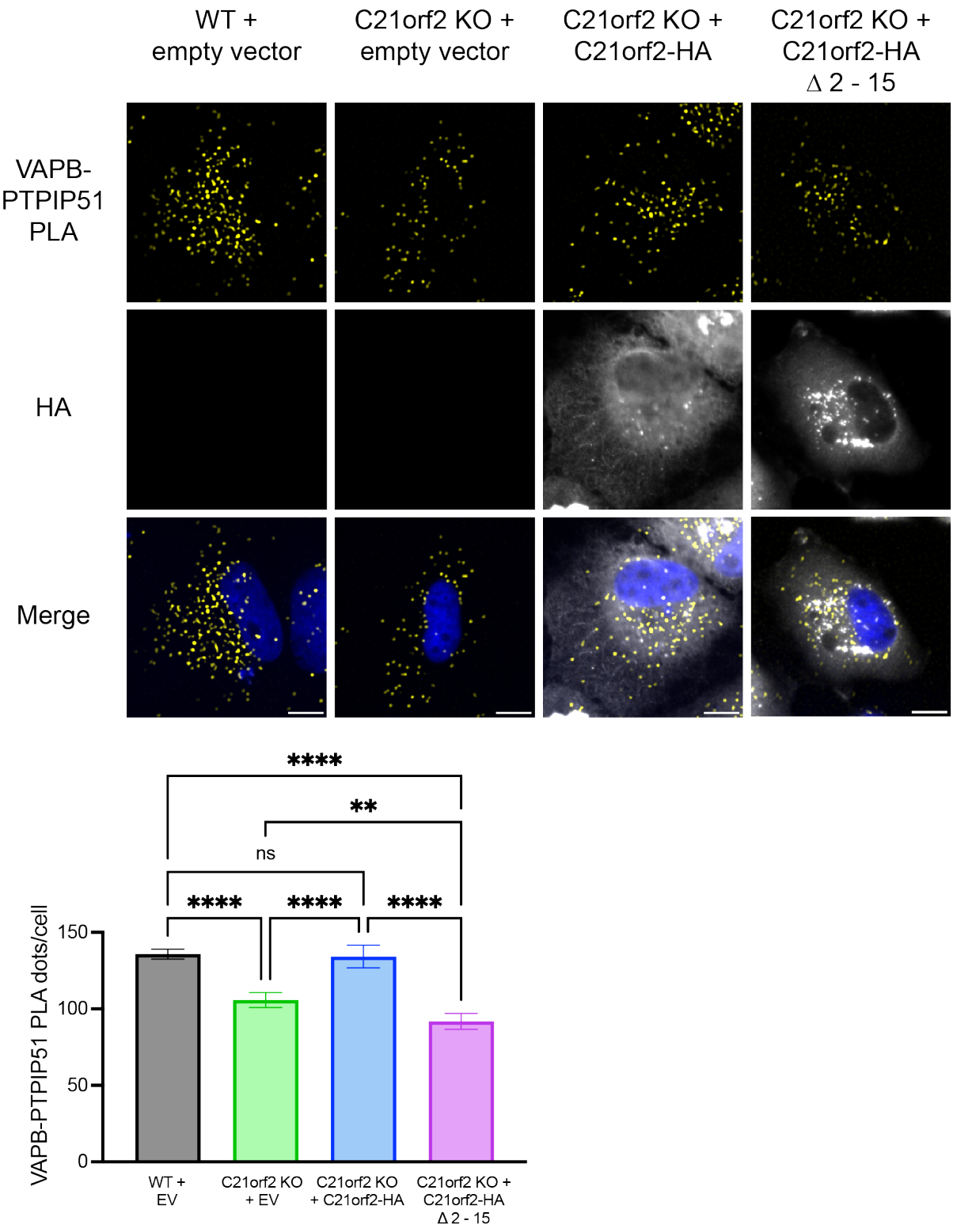

Figure 4-6 C21orf2 requires NEK1 to rescue VAPB/PTPIP51 tethering defects.

Wild type HeLa cells (WT) or C21orf2 knock out (KO) HeLa cells were transfected with empty vector pCI-neo, full length C21orf2-HA or C21orf2-HA Δ2 – 15. Cells were subjected to PLA with endogenous anti-VAPB and anti-PTPIP51 antibodies (yellow) and co-stained for HA (grey) and Hoechst for nuclear stain (blue). The number of PLA dots per cell was quantified. Graphs display mean ± SEM. Data were analysed by one-way ANOVA with Fisher's LSD; ** P ≤ 0.01, **** P ≤ 0.0001, ns = non-significant. *N* = 3, *n* > 450 cells per sample from three independent repeats. Scale bar = 10 µm.

4.3 Loss of NEK1 or C21orf2 decreases ER-mitochondria apposition

VAPB/PTPIP51 interaction correlates with apposition between the ER and mitochondria, as loss of either protein decreases contact between the organelles (Stoica *et al.*, 2014). During this study we had confirmed that NEK1 and C21orf2 deficient HeLa cells exhibit reduced VAPB/PTPIP51 tethering using PLA (Figure 4-3, Figure 4-6) and co-immunoprecipitation assays (Figure 4-1). To confirm a direct reduction in ER-mitochondria apposition, we utilised electron microscopy to image MAM. NEK1 and C21orf2 KO HeLa cells and their respective wild type control HeLa cells were subjected to electron microscopy (Figure 4-7, Figure 4-8). ER-mitochondria associations were quantified by determining the proportion of mitochondrial surface closely apposed to the ER (< 30 nm). As NEK1 has been implicated in regulation of mitochondrial homeostasis (discussed in 1.3.2.4), we also quantified mitochondrial size by measuring the area and perimeter of each mitochondrion.

In line with loss of VAPB/PTPIP51 tethering, we observed a significant decrease in ER-mitochondria apposition in our NEK1 KO HeLa cells (Figure 4-7). The percentage of mitochondrial surface in contact with the ER and the number of contact sites per mitochondrion was significantly reduced in NEK1-deficient cells compared to controls (Figure 4-7B & C). Compared to control cells, NEK1 KO cells had significantly smaller mitochondria, with reduced mitochondrion perimeter and area (Figure 4-7D & E). This suggests that NEK1 may regulate mitochondrial homeostasis, possibly by controlling levels of mitochondrial fission or fusion.

In line the loss of ER-mitochondria apposition found in our NEK1 KO cells, we observed loss of ER-mitochondria apposition with loss of C21orf2 compared to control cells (Figure 4-8). The percentage of mitochondrial surface in contact with the ER was significantly reduced in C21orf2-deficient cells compared to controls (Figure 4-8B). However, the number of contacts per mitochondrion was not significantly different between C21orf2 KO and WT cell lines (Figure 4-8C). We did not observe a change in mitochondrial morphology in the C21orf2 KO cells compared to wild type cells (Figure 4-8D & E). This suggests that only specific loss of NEK1 leads to disrupted mitochondrial morphology. This implicates that NEK1 may have a role in mitochondrial homeostasis independent of C21orf2. Due to time limitations, these experiments were only performed once, thus replication is necessary to confirm this result.

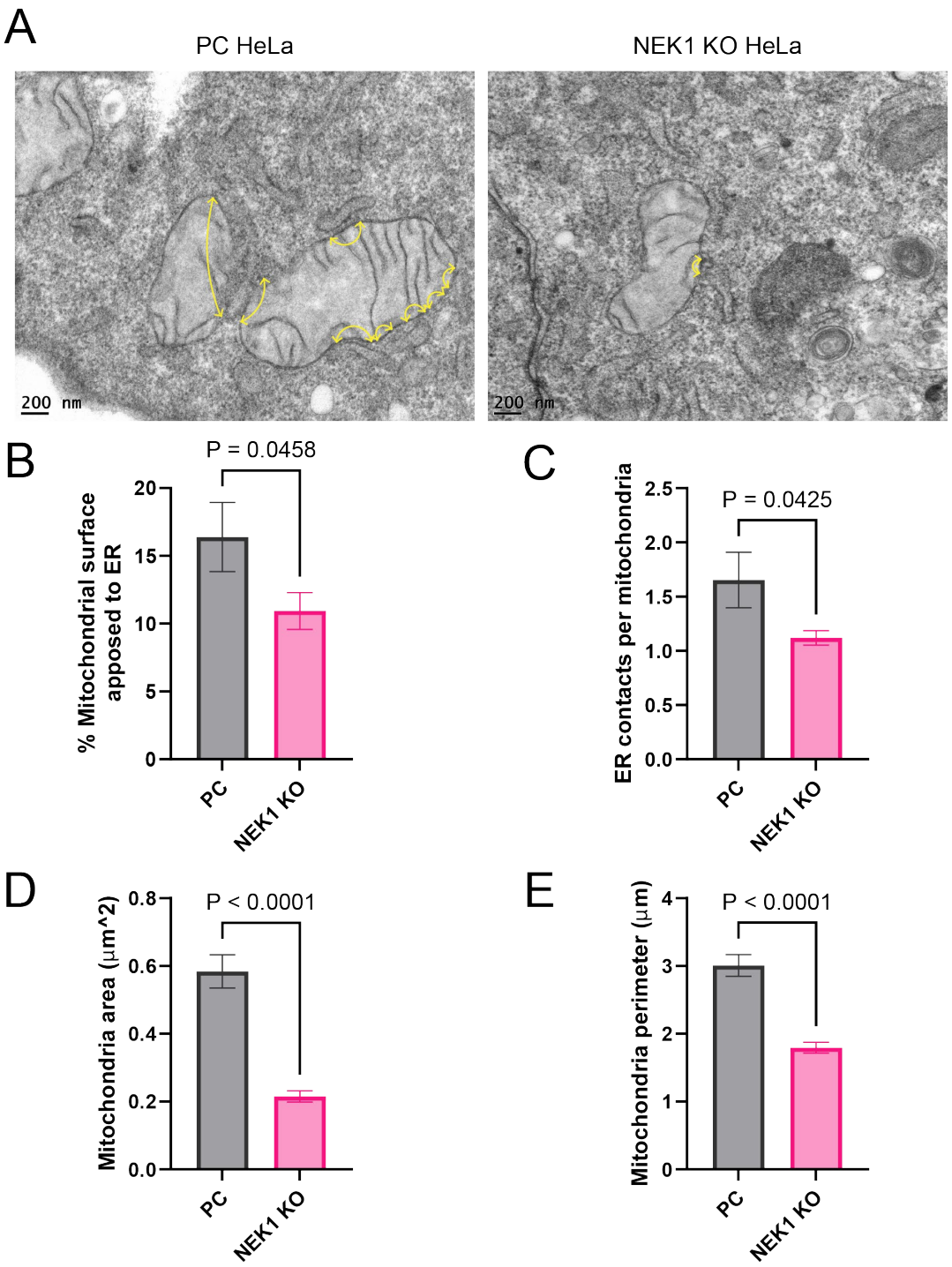

Figure 4-7 Loss of NEK1 leads to disrupted ER-mitochondria contact and mitochondrial size.

A) Electron micrographs of wild type parental cell (PC) or NEK1 knock out (KO) HeLa cells, yellow arrows indicate points of ER-mitochondria contact. Scale bar = 200 nm.

B) Quantification of the percentage of mitochondrial surfaced apposed to the ER (< 30 nm).

C) Quantification of the number of ER contacts per mitochondrion.

D) Quantification of mitochondrial perimeter.

E) Quantification of mitochondrial area. Graphs represent mean ± SEM. *N* = 1, *n* (mitochondria) PC = 43, NEK1 KO = 65. Electron microscopy was performed by Dr Chris Hill (University of Sheffield).

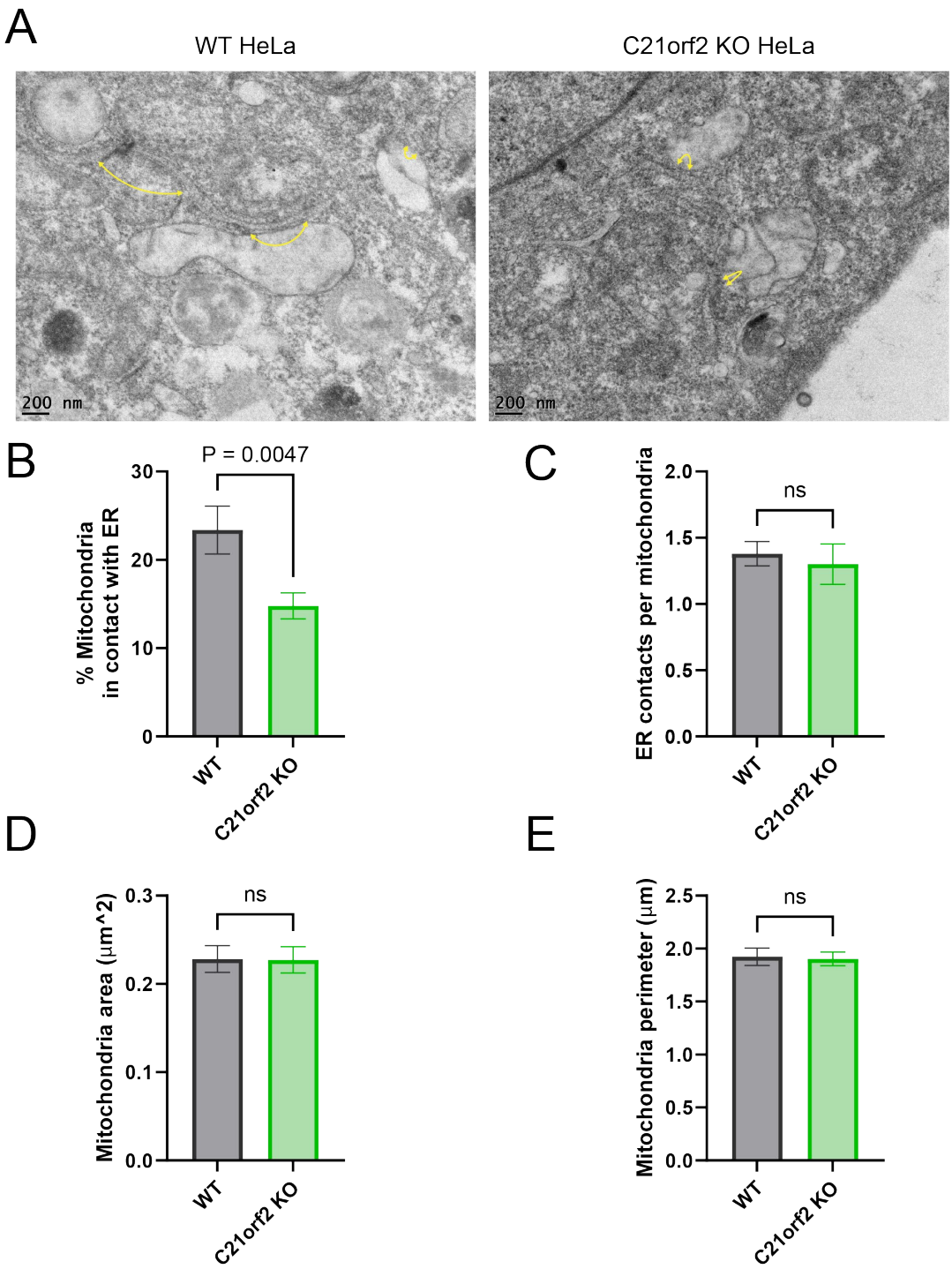

Figure 4-8 Loss of C21orf2 leads to disrupted ER-mitochondria contact.

A) Electron micrographs of wild type (WT) or C21orf2 knock out (KO) HeLa cells, yellow arrows indicate points of ER-mitochondria contacts. Scale bar = 200nm.

B) Quantification of the percentage of mitochondrial surfaced apposed to the ER (< 30 nm).

C) Quantification of the number of ER contacts per mitochondrion.

D) Quantification of mitochondrial area.

E) Quantification of mitochondrial perimeter. Graphs represent mean ± SEM. *N* = 1, *n* (mitochondria) WT = 47, C21orf2 KO = 81. Electron microscopy was performed by Dr Chris Hill (University of Sheffield).

Previous work has shown that loss of ER-mitochondria contacts leads to increased cytoplasmic Ca^{2+} levels due to reduced uptake into the mitochondria (De Vos *et al.*, 2012). Our previous data confirmed that loss of NEK1 and C21orf2 causes reduced ER-mitochondria apposition. To confirm that this correlated with disrupted ER-mitochondria Ca^{2+} transfer, we decided to measure cytoplasmic Ca^{2+} levels in response to release from ER stores. This technique has been well established in literature as a proxy measurement of mitochondrial Ca^{2+} uptake (De Vos *et al.*, 2012; Stoica *et al.*, 2014; Stoica *et al.*, 2016). To stimulate release of Ca^{2+} from the ER, the muscarinic acetylcholine receptor M3 (M3R) agonist Oxotremorine-M (Oxo-M) was used to initiate release through the IP3R (Figure 4-9). The cytoplasmic Ca^{2+} levels were measured using the radiometric Ca^{2+} indicator dye Fura-2-AM. In low cytoplasmic Ca^{2+} concentrations Fura-2 has an excitation maximum at 362 nm, whilst at high conditions it has an excitation maximum at 335 nm. Simultaneous measurement at 340 nm and 380 nm is used to calculate a Fura-2 ratio (340/380) that is directly proportional to the level of cytosolic Ca^{2+} (Oakes *et al.*, 1988).

To investigate Ca^{2+} transfer defects, NEK1 and C21orf2 KO HeLa cells and their corresponding wild type cell lines were incubated with Fura-2-AM dye. Despite attempting loading at multiple concentrations, temperatures and timescales, we experienced poor loading of Fura-2-AM dye into the HeLa cells (data not shown). Use of the surfactant polyol Pluronic F-127 (PF-127) that has previously been shown to increase Fura-2-AM loading (Maruyama *et al.*, 1989), caused intracellular compartmentalisation of the dye (Takeuchi *et al.*, 1989), which prevented measurement of cytoplasmic Ca^{2+} levels (data not shown).

Due to time limitations, we decided to use short interfering RNA (siRNA) to knock down the expression of NEK1 in HEK293 cells. We did not have a C21orf2 specific siRNA to use for these experiments. HEK293 cells were transfected with NEK1-targeting siRNA or non-targeting siRNA as a negative control. As loss of PTPIP51 has been shown to disrupt Ca^{2+} transfer, knock down of PTPIP51 was used as a positive control (De Vos *et al.*, 2012). To determine if any defect observed was due to loss of NEK1, cells were transfected with either empty vector mCherry or mCherry-tagged NEK1. The successful knockdown of NEK1 and PTPIP51 expression and transfection of mCherry-NEK1 was confirmed by immunoblot, probing for endogenous NEK1, PTPIP51 and α-tubulin as a loading control (Figure 4-10A).

In response to Oxo-M stimulated release of Ca^{2+} from ER stores, the peak cytoplasmic Ca^{2+} levels reached significantly higher levels in the NEK1 or PTPIP51 siRNA-treated cells compared to control cells (Figure 4-10B & C). This indicated decreased mitochondrial uptake of Ca^{2+}. Reintroduction of NEK1 protein by transfection of mCherry-NEK1 rescued this effect back to the level of the non-targeting siRNA control, confirming this effect was specifically due to loss of NEK1. Together this data

confirms that loss of NEK1 leads to disrupted ER-mitochondria tethering and disrupted Ca^{2+} transfer between the organelles.

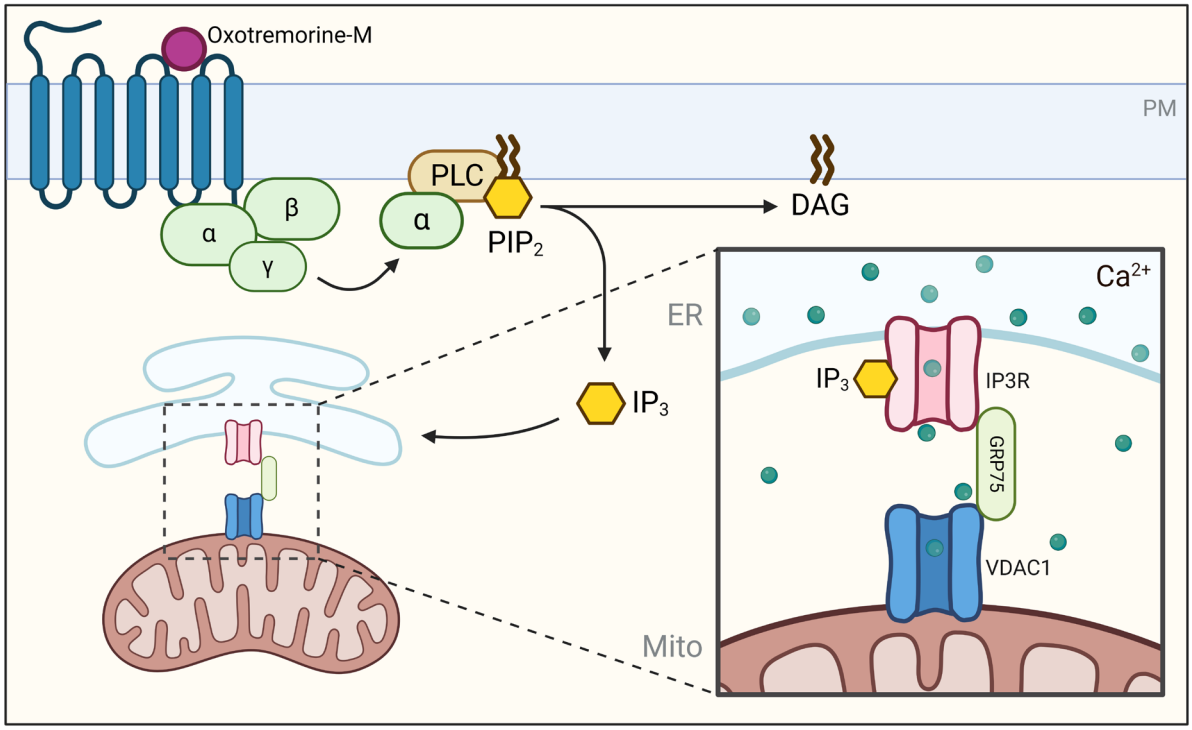

Figure 4-9 Summary of Oxotremorine-M stimulated Ca^{2+} release from ER stores.

To stimulate release of Ca^{2+} from ER stores, the muscarinic 3 receptor agonist Oxotremorine-M was used to stimulate IP3R channels. Oxotremorine-M stimulates muscarinic G-couple protein receptors which causes the activation of phospholipase C (PLC) enzymes to catalyse the phosphoinositide PIP_2 into diacylglycerol (DAG) and inositol-1,4,5-trisphosphate (IP_3). The substrate IP3 can then activate IP3R receptors on the ER-membrane to release Ca^{2+} into the cytoplasm. This can be taken up into mitochondria through the outer mitochondrial membrane by VDAC1 channels. PM = plasma membrane.

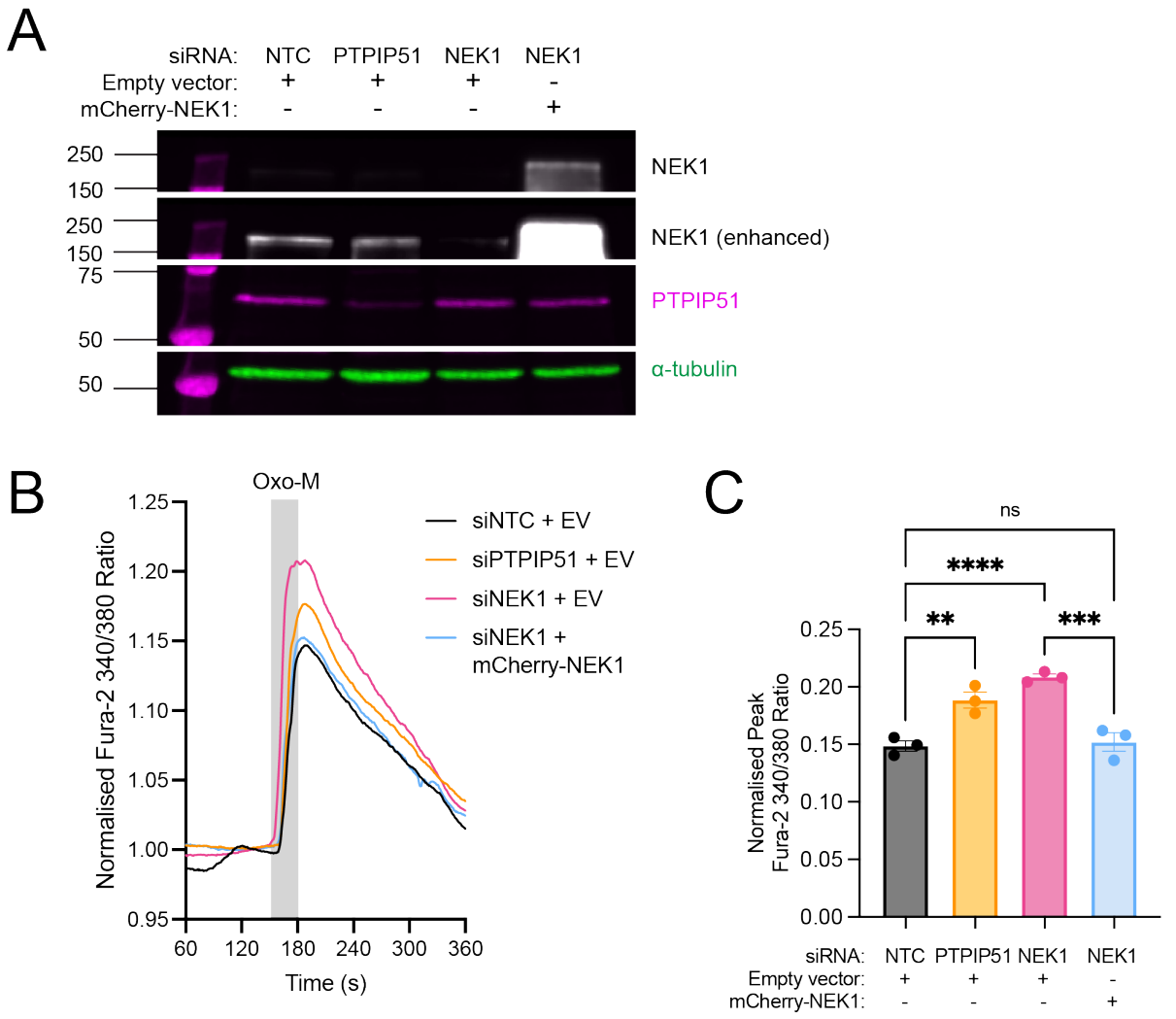

Figure 4-10 Loss of NEK1 disrupts transfer of calcium from ER stores to mitochondria.

HEK293 cells were treated with short interfering RNA (siRNA) targeting PTPIP51, NEK1 or a non-targeting control (NTC), and then transfected with empty vector mCherry (EV) or mCherry-tagged NEK1.

A) Samples were immunoblotted for endogenous NEK1, PTPIP51 and α-tubulin as a loading control to confirm successful knockdown. Per sample 45 µg protein was loaded.

B) Release of Ca^{2+} from ER stores was induced by treatment with 200µM Oxotremorine-M (Oxo-M). The trace shows cytoplasmic Ca^{2+} levels measured by the ratio of Fura-2 fluorescence at 340 nm and 380 nm.

C) Quantification of the peak response to Oxo-M. Graph represents mean ± SEM, points represent mean per biological repeat. Data were analysed by one-way ANOVA with Fisher's LSD; ns = non-significant, ** ≤ 0.01, *** P ≤ 0.001, **** P ≤ 0.0001. *N* = 3, *n* (cells) > 361 across 3 independent repeats.

4.4 Loss of NEK1 or C21orf2 disrupts the induction of autophagy

VAPB/PTPIP51 tethering is known to regulate autophagy, as silencing of either protein promotes autophagic flux (Gomez-Suaga *et al.*, 2017). Conversely, overexpression of VAPB or PTPIP51 inhibits autophagosome formation (Gomez-Suaga *et al.*, 2017). As we had observed that loss of NEK1 or C21orf2 reduces VAPB/PTPIP51 tethering, we postulated that cells lacking NEK1 or C21orf2 would exhibit increased autophagic flux. To investigate this, we monitored flux of the microtubule-associated protein 1A/1B light chain 3 (LC3) on immunoblot. The cytosolic LC3-I is lipidated to form LC3-II during the formation of autophagosomes (Mizushima and Yoshimori, 2007; Tanida *et al.*, 2008). Upon fusion with lysosomes LC3-II is degraded, and so the level of LC3-II can be measured as a proxy of autophagic flux (Klionsky *et al.*, 2021).

To initiate autophagy cells were treated with the mTOR inhibitor Torin1, as Torin1-induced autophagy has been shown to be affected by modulating VAPB/PTPIP51 levels (Gomez-Suaga *et al.*, 2017). As LC3-II is degraded upon fusion of autophagosomes with lysosomes, we inhibited the fusion of lysosomes with the V-ATPase inhibitor Bafilomycin A-1. NEK1 and C21orf2 KO HeLa cells and their respective control cell lines were treated with Bafilomycin A-1 and either DMSO control or Torin1. The samples were immunoblotted and the level of lipidated LC3-II quantified. In response to induction of autophagy with Torin1, both our control HeLa cell lines elicited a response as shown by increased LC3-II levels (Figure 4-11). At basal levels there was no significant difference between the levels of LC3-II in the NEK1 and C21orf2 KO cells and the control HeLa cells. In response to Torin1 stimualtion, both NEK1 and C21orf2 HeLa cell lines failed to induce autophagosome formation, evidenced by the lack of augmented LC3-II levels (Figure 4-11B &D). This suggested that NEK1 and C21orf2 may be necessary for the induction of autophagy by mediating ER-mitochondria contact sites, where autophagosome formation occurs (Hamasaki *et al.*, 2013).

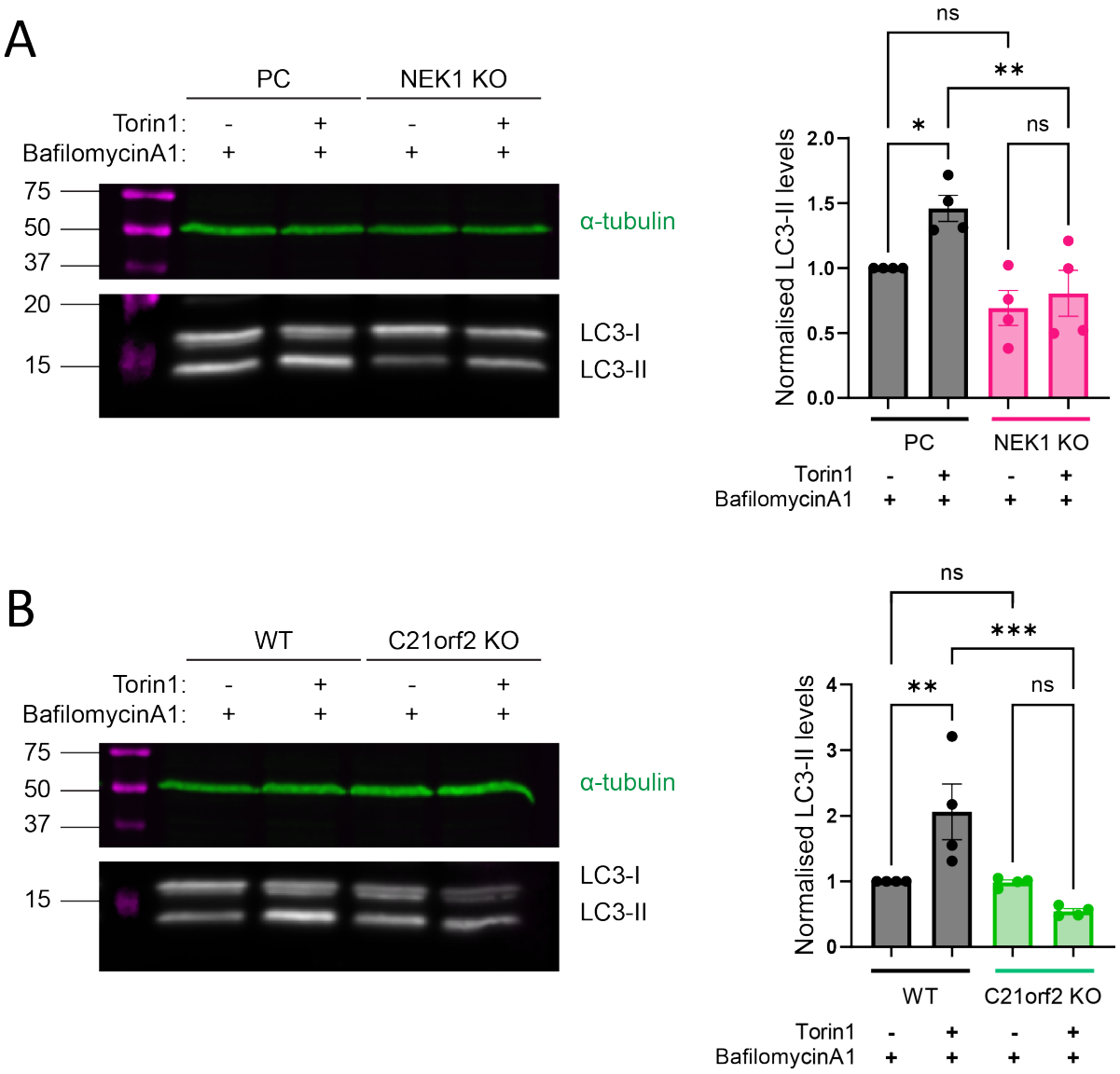

Figure 4-11 Loss of NEK1 or C21orf2 causes loss of induction of autophagy.

Wild type parental cell (PC) and NEK1 knock out (KO) **(A)** or wild type (WT) and C21orf2 KO HeLa cells **(B)** were incubated with BafilomycinA1 (100 nM, 6 h) to prevent autophagosome lysosome fusion, with or without Torin1 (250 nM, 3 h) to initiate autophagy. Samples were immunoblotted for LC3 and α-tubulin. The level of lipidated LC3-II was quantified and normalised against α-tubulin and are shown relative to the respective wild type BafA1-treated sample. Graphs represent mean ± SEM. Data were analysed by one-way ANOVA with Fisher's LSD, *N* = 4, ns = non-significant, * P ≤ 0.05, ** P ≤ 0.01, *** P ≤ 0.001.

4.5 NEK1 kinase activity regulates VAPB/PTPIP51 tethering

4.5.1 NEK1 activation by DNA damage promotes NEK1/PTPIP51 interaction

In response to DNA damage a portion of NEK1 is recruited to mitochondria where it phosphorylates the MAM protein VDAC1 to prevent apoptosis (Chen *et al.*, 2009). As our data indicated that a portion of NEK1 is localised to MAM and binds to PTPIP51 (3.4.1, 3.4.4), upon activation by DNA damage NEK1 may be recruited to MAM to regulate ER-mitochondria tethering. To determine if NEK1/PTPIP51 interaction is increased in response to DNA damage, HEK293 cells were co-transfected with pCI-neo empty vector or V5-NEK1 and PTPIP51-HA. To physiologically activate the NEK1 kinase, DNA damage in the form of DSBs was induced by the DNA topoisomerase inhibitor camptothecin (CPT) (Berniak *et al.*, 2013; Rodriguez-Hernandez *et al.*, 2006). Cells were treated with 10 µM CPT or with DMSO as a negative control for 1 h. Cells were immunoprecipitated with an anti-V5 antibody and immunoblotted, probing for endogenous NEK1, HA, and anti-α-tubulin as a loading control (Figure 4-12A). We observed a significant increase in the level of PTPIP51 binding to NEK1 with the induction of DNA damage, suggesting that when activated by DNA damage, NEK1 may be recruited to MAM as part of the DDR response (Figure 4-12B). To confirm successful induction of DNA damage, the samples were immunoblotted for the DNA damage induction markers γH2AX pS139 and Chk1 pS345 (Figure 4-12C). Phosphorylation of Chk1 at S345 is downstream of NEK1 in response to DNA damage induction, which confirms specific activation of NEK1 with CPT (Chen *et al.*, 2008).

4.5.2 NEK1 activation by DNA damage promotes VAPB/PTPIP51 tethering

As we had observed that upon activation by DNA damage NEK1 interaction with PTPIP51 was increased, we postulated that NEK1 may regulate VAPB/PTPIP51 tethering as part of a nucleus to mitochondria signalling pathway in the DDR (discussed in section 1.3.2.3). To investigate this, PC HeLa cells were treated with either 10 µM DMSO or CPT for 1 h and the cells subjected to PLA with endogenous VAPB and PTPIP51 antibodies to quantify VAPB/PTPIP51 interactions (Figure 4-13A). To determine that any effects are specifically due to activation of NEK1, we used NEK1 KO cells as a negative control. To confirm successful induction of DNA damage, the cells were co-stained for the DNA damage marker γH2AX pS139 (Figure 4-13B & D). As expected, activation of NEK1 by induction of DNA damage significantly increases VAPB/PTPIP51 tethering (Figure 4-13C). Loss of NEK1 ablated this effect, confirming that specific activation of NEK1 in response to DNA damage modulates the tethering between VAPB and PTPIP51.

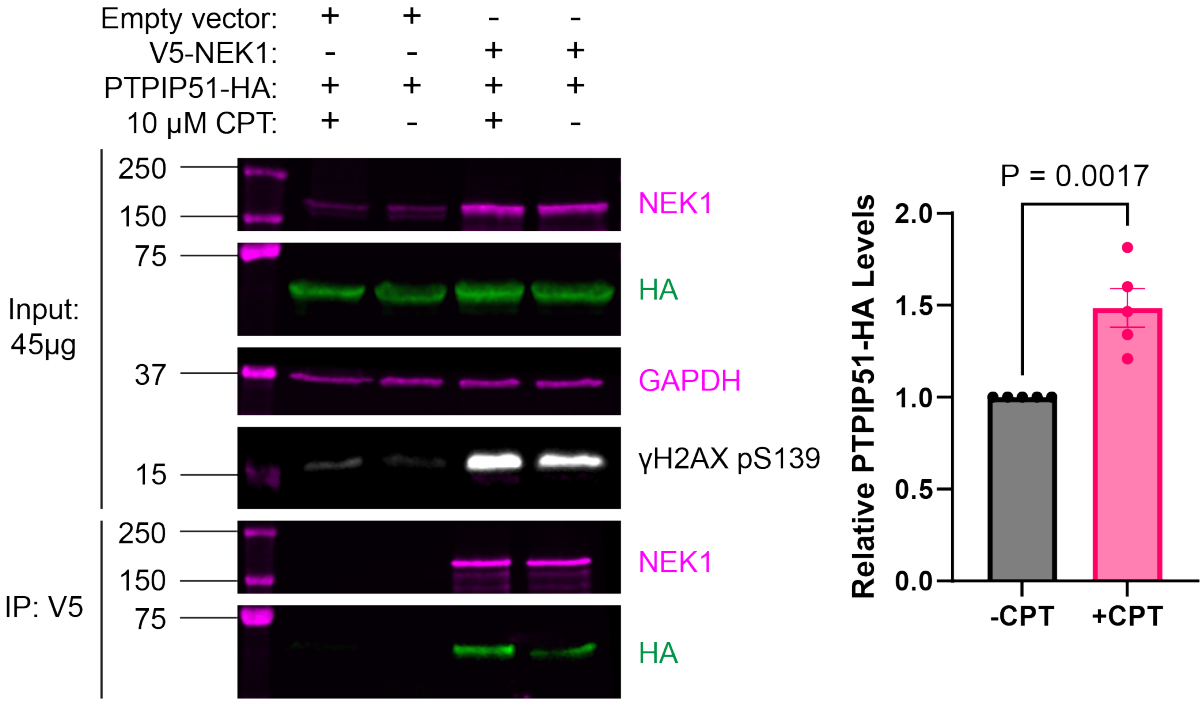

Figure 4-12 Induction of DNA damage promotes NEK1/PTPIP51 interaction.

HEK293 cells were co-transfected with pCI-neo empty vector or V5-NEK1 and PTPIP51-HA. The cells were incubated with 10 µM DMSO or camptothecin (CPT) for 1 h to induce DNA damage in the form of double strand breaks. Cells were immunoprecipitated with an anti-V5 antibody to capture NEK1 and immunoblotted with anti-NEK1 and anti-HA antibodies. GAPDH was probed as a loading control, whilst a phospho-γH2AX S139 antibody was used to confirm induction of DNA damage. Quantification of the relative amount of PTPIP51-HA normalised to the level of immunoprecipitated V5-NEK1. Data were analysed by two-tailed unpaired t-test, *N* = 5. Graph represents mean ± SEM.

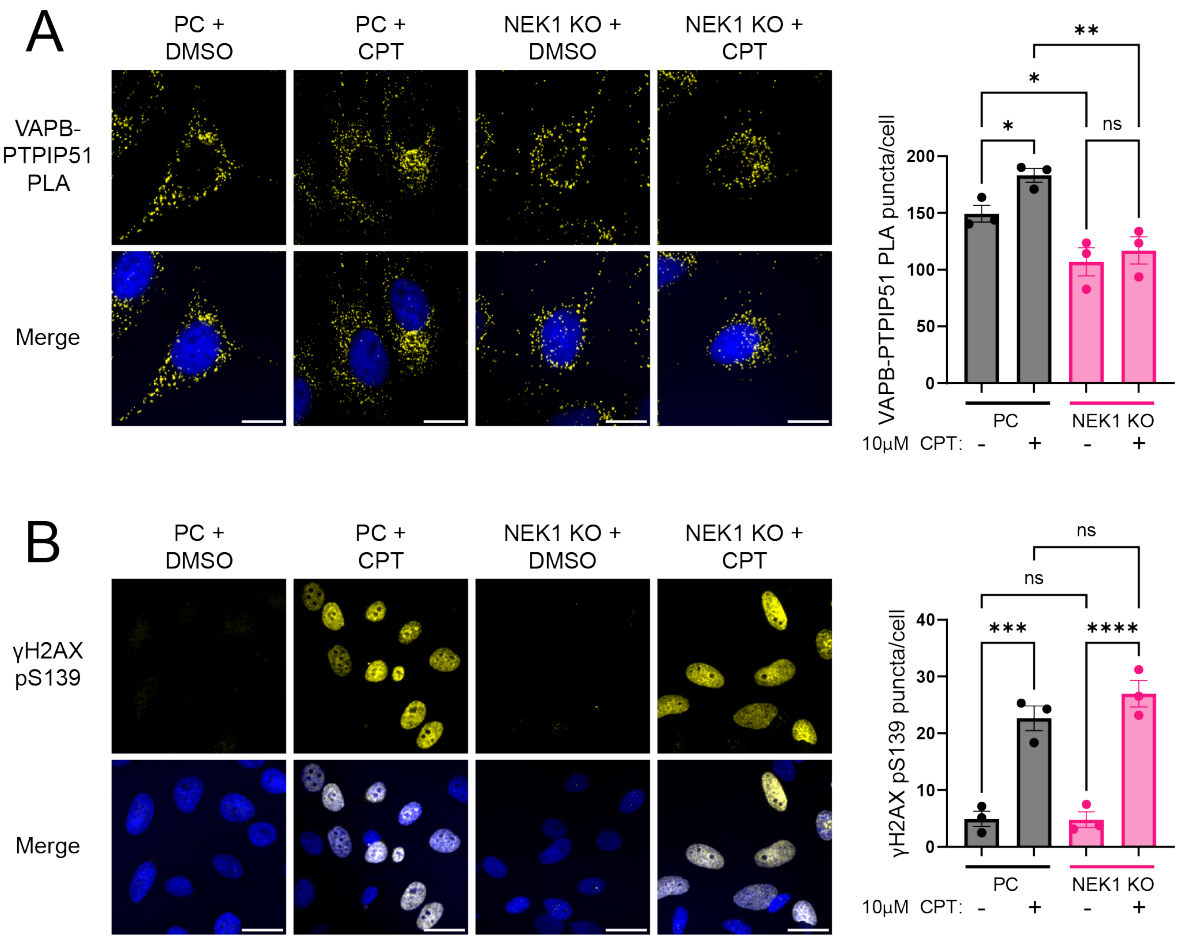

Figure 4-13 NEK1 regulates VAPB/PTPIP51 tethering in response to DNA damage.

A) Wild type parental cell (PC) or NEK1 knock out (KO) HeLa cells were treated with 10 μM DMSO or camptothecin (CPT) to induce DNA damage and subjected to proximity ligation assay (PLA) using anti-VAPB and anti-PTPIP51 antibodies (yellow) and co-stained with nuclear Hoechst stain (blue). Quantification of the number of PLA puncta per cell. Graph represents mean ± SEM, points show average per independent repeat. Data were analysed by one-way ANOVA with Fisher's LSD, *N* = 3, *n* (cells) > 765 across 3 independent repeats. ns = non-significant, * P ≤ 0.05, ** P ≤ 0.01. Scale bar = 20 μm.

B) To confirm successful induction of DNA damage, cells were stained for γH2AX pS139 (yellow) and co-stained with nuclear Hoechst stain (blue). Quantification of the nuclear H2AX pS139 intensity per cell. Graph represents mean ± SEM, points show average per independent repeat. Data were analysed by one-way ANOVA with Fisher's LSD, *N* = 3, *n* (cells) > 835 across 3 independent repeats. ns = non-significant, *** P ≤ 0.001, **** P ≤ 0.0001. Scale bar = 20 μm.

To determine if activation of NEK1 by DNA damage induction increases the transfer of Ca^{2+} from ER stores to mitochondria by increasing VAPB/PTPIP51 tetheirng, we utilised the Ca^{2+} indicator dye Fura-2 to measure the cytosolic Ca^{2+} concentration in response to IP3R-induced Ca^{2+} release from ER stores. HEK293 cells were treated with DMSO or CPT and immunoblotted for the DNA damage induction markers γH2AX pS139 and Chk1 pS345 to confirm treatment efficiency (Figure 4-14A). In response to Oxo-M induced Ca^{2+} release from ER stores, the cytoplasmic Ca^{2+} levels were significantly reduced in cells treated with camptothecin, suggesting an increased mitochondrial uptake of Ca^{2+} (Figure 4-14C). Together this confirms that activation of NEK1 in response to DNA damage leads to increased VAPB/PTPIP51 tethering and subsequent increase in Ca^{2+} transfer from the ER to mitochondria.

4.5.3 NEK1 phosphorylates VAPB *in vitro*

Our data so far showed that whilst loss of NEK1 disrupted VAPB/PTPIP51 binding (section 4.2), activation of NEK1 increased this interaction (section 4.5.2). As reintroduction of wild type V5-NEK1 but not kinase dead V5-NEK1 K33R was able to rescue the loss of VAPB/PTPIP51 binding in our NEK1 KO cells (Figure 4-3), it suggested that NEK1 kinase activity was responsible for this regulation. Both VAPB and PTPIP51 contain NEK1 consensus phosphorylation motifs (VAPB: T143, T201 and T222, PTPIP51: T20 and T177) (Figure 4-15). To investigate whether NEK1 phosphorylates VAPB or PTPIP51, we conducted an *in vitro* phosphorylation assay with the GST-tagged recombinant VAPB and PTPIP51 proteins used previously (Figure 3-15). As it has been well established that C21orf2 is a substrate of NEK1 (Watanabe *et al.*, 2020), we a GST-tagged C21orf2 plasmid as a positive control. Recombinant GST-tagged cytosolic domains of PTPIP51 and VAPB and full length C21orf2 were purified from E. coli and captured on glutathione-coated beads. The GST-proteins were incubated for 1 h at 37 °C with active recombinant NEK1 kinase (AA 1 – 477, Abcam, ab268812), supplemented with radiolabelled P32-ATP. The samples were run on SDS-PAGE before the gel was dried onto Whatmann paper and exposed to a phospho-screen for imaging. The GST-C21orf2 protein was expressed at the expected molecular weight (~55 kDa). In line with published data, we observed NEK1-phosphorylation of C21orf2, confirming the activity of the recombinant NEK1 kinase (Figure 4-16). We observed that *in vitro* NEK1 phosphorylates VAPB (Figure 4-16). Surprisingly, we did not observe NEK1 phosphorylation of PTPIP51 *in vitro* (Figure 4-16).

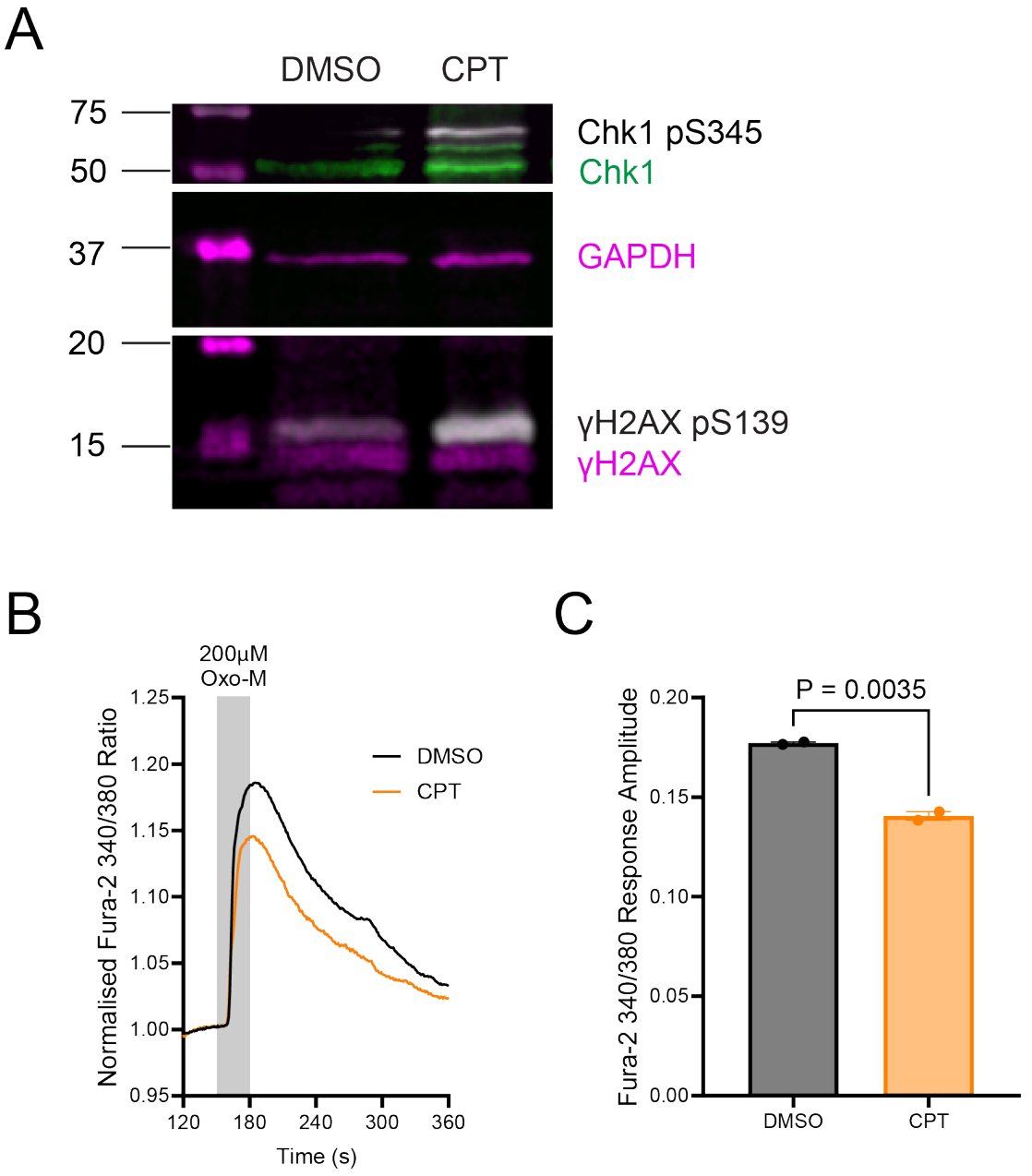

Figure 4-14 Induction of DNA damage promotes ER-mitochondria Ca^{2+} transfer.

A) HEK293 cells were treated with either 10 μM DMSO or camptothecin (CPT) to induce DNA damage. The samples were immunoblotted, probing for endogenous markers of DNA damage induction, Chk1 pS345 and γH2AX pS139. Total Chk1 and γH2AX protein and GAPDH were probed for as loading controls.

B) Release of Ca^{2+} from ER stores was induced by treatment of cells with 200 μM Oxotremorine-M (Oxo-M). The trace shows cytoplasmic Ca^{2+} levels measured by the ratio of Fura-2 fluorescence at 340 nm and 380 nm.

C) Quantification of the peak response amplitude to Oxo-M. Graph represents mean ± SEM, points show average per independent repeat. Data were analysed by two-tailed unpaired t-test, *N* = 2, n (cells) > 125.

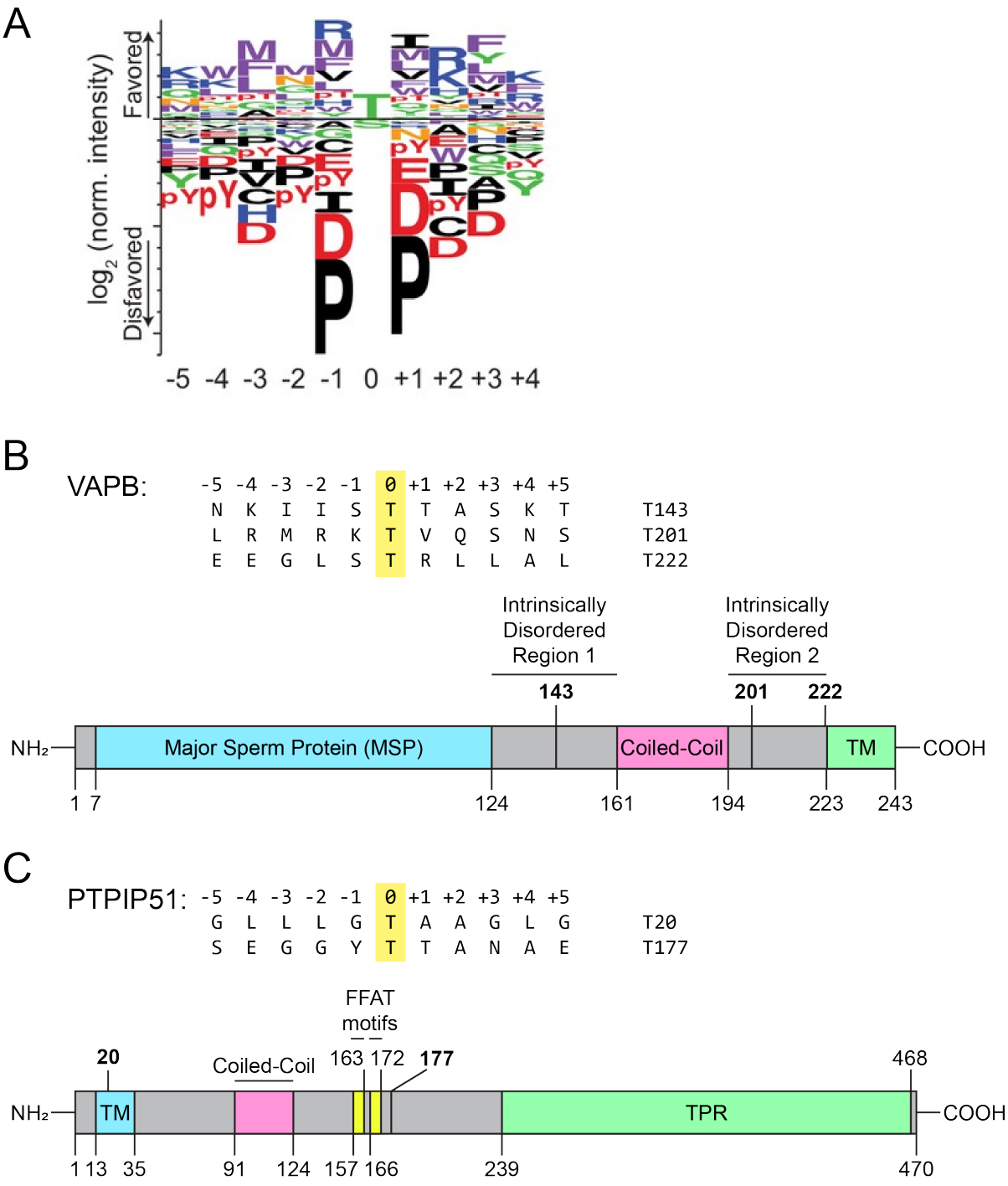

Figure 4-15 VAPB and PTPIP51 contain NEK1 consensus phosphorylation motifs.

A) Sequence logo of the NEK1 phosphorylation motif (van de Kooij *et al.*, 2019).

B) Schematic of the VAPB protein domains and potential NEK1 phosphorylation sites. TM = Transmembrane domain.

C) Schematic of the PTPIP51 protein domains and potential NEK1 phosphorylation sites, FFAT = two phenylalanines (FF) in an acidic tract (AT). TPR = tetratricopeptide repeat. Predicted NEK1 phosphorylation sites are in bold.

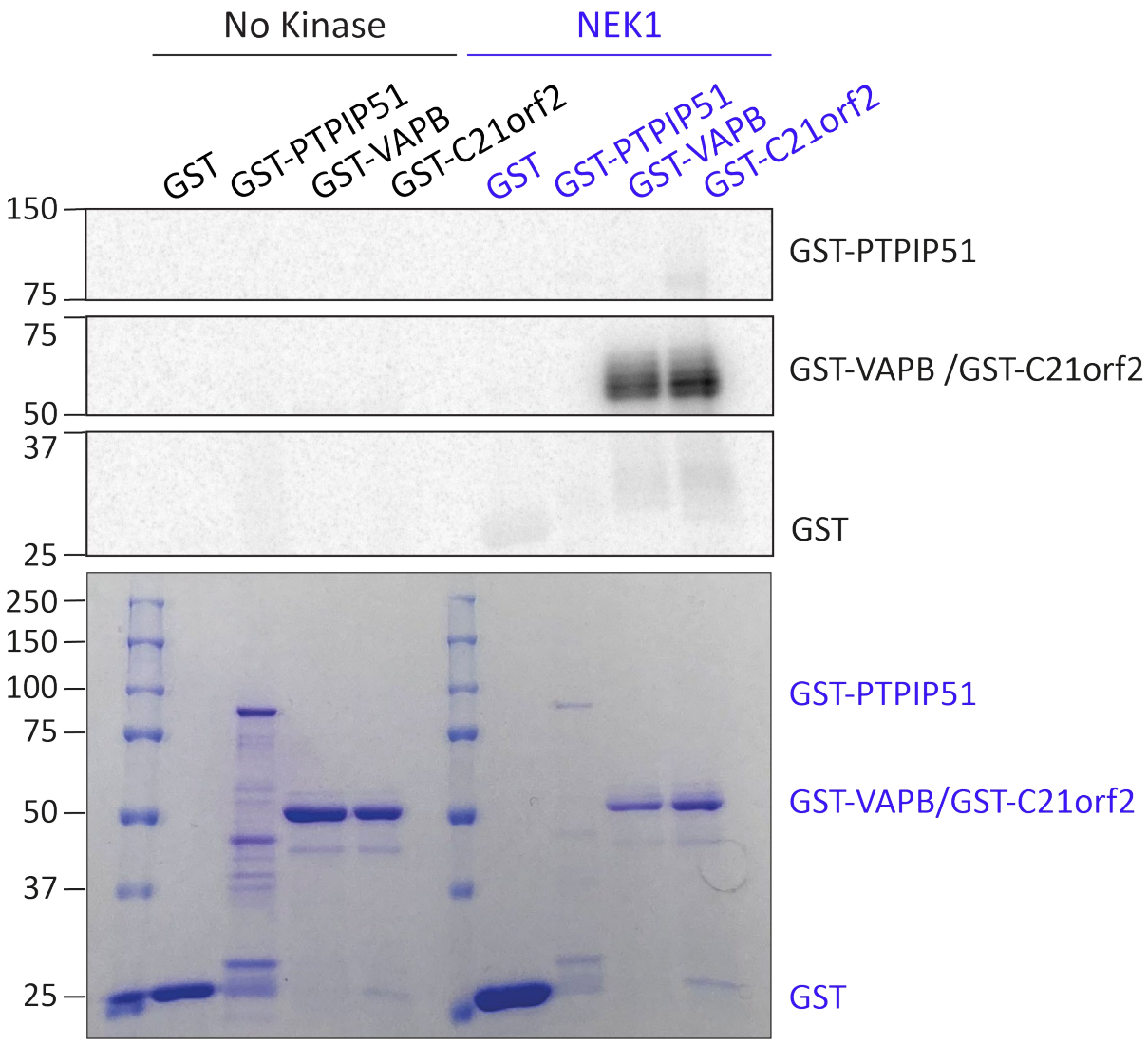

Figure 4-16 NEK1 phosphorylates VAPB *in vitro*.

Empty vector GST, GST-tagged recombinant cytosolic domains of PTPIP51 (AA 36-470), VAPB (AA 1-220) and full-length GST-tagged C21orf2 were immobilised on glutathione-coated beads and incubated with 32P-ATP for 1 hour at 37 °C with active recombinant NEK1 kinase. Coomassie-stained GST-tagged proteins in the pull-down samples are shown (bottom panel). 32P phosphorylated proteins were visualized by phosphorimager (top panels). *N* = 3.

To validate this phosphorylation and to determine the potential phospho-site in VAPB, we used mass spectrometry of the GST-tagged recombinant VAPB. The *in vitro* phosphorylation of GST-VAPB with or without recombinant active NEK1 was performed as in Figure 4-16. Briefly, the eluted GST-VAPB protein was reduced, alkylated and denatured by acidification prior to trypsin digestion using S-Trap digestion columns (Profiti) as detailed in section 2.8.1. The eluted peptides were then subjected to liquid chromatography tandem mass spectrometry (LC-MS/MS) analysis. Peptides corresponding to recombinant cytosolic VAPB were identified by LC-MS/MS, with 100% sequence coverage of the cytosolic VAPB (Figure 4-17A). We identified that VAPB was phosphorylated by NEK1 on Threonine 201 *in vitro* (Figure 4-17B).

4.5.4 Mutation of VAPB T201 may disrupt VAPB/PTPIP51 tethering

Evidence suggests that VAPB/PTPIP51 tethering is regulated by phosphorylation, although it is not clear if this is due to direct phosphorylation of either protein (Stoica *et al.*, 2014; Stoica *et al.*, 2016). As our data shows that activation of NEK1 promotes VAPB/PTPIP51 tethering (Figure 4-13) and NEK1 phosphorylates VAPB at T201 (Figure 4-16, Figure 4-17), we wanted to determine if phosphorylation of this phospho-site had a role in regulating VAPB/PTPIP51 interaction. To investigate this, site-directed mutagenesis was utilised to create Myc-tagged VAPB constructs with substitution of pT201 with an alanine (A) or glutamic acid (E), to act as phospho-deficient or phospho-mimetic proteins respectively. Prior to experimentation the mutant Myc-VAPB constructs were validated by sequencing (Figure 4-18B). Expression of proteins of the correct molecular weight was confirmed by immunoblotting HEK293 cells transfected with pCI-neo empty vector, Myc-VAPB, Myc-VAPB T201A or Myc-VAPB T201E, probing for Myc tag, endogenous PTPIP51 and α-tubulin as a loading control (Figure 4-18C).

A

MAKVEQVLSLEPQHELKFRGPFTDVVTTNLKLGNPTDRNVCFKVKTTAPRRYCVRPNSGII
DAGASINVSVMLQPFDYDPNEKSKHKFMVQSMFAPTDTSDMEAVWKEAKPEDLMDSKLRCV
FELPAENDKPHDVEINKIISTTASKTETPIVSKSLSSSLDDTEVKKVMEECKRLQGEVQRL
REENKQFKEEDGLRMRKTVQSNSPISALAPTGKEEGLSTRLLALVVLFFIVGVIIGKIAL

Peptide sequence	Peptide m/z	Modification
^{198}MRKpTVQSNSPISALAPTGKEEG^{219}	794.05	pT201

B

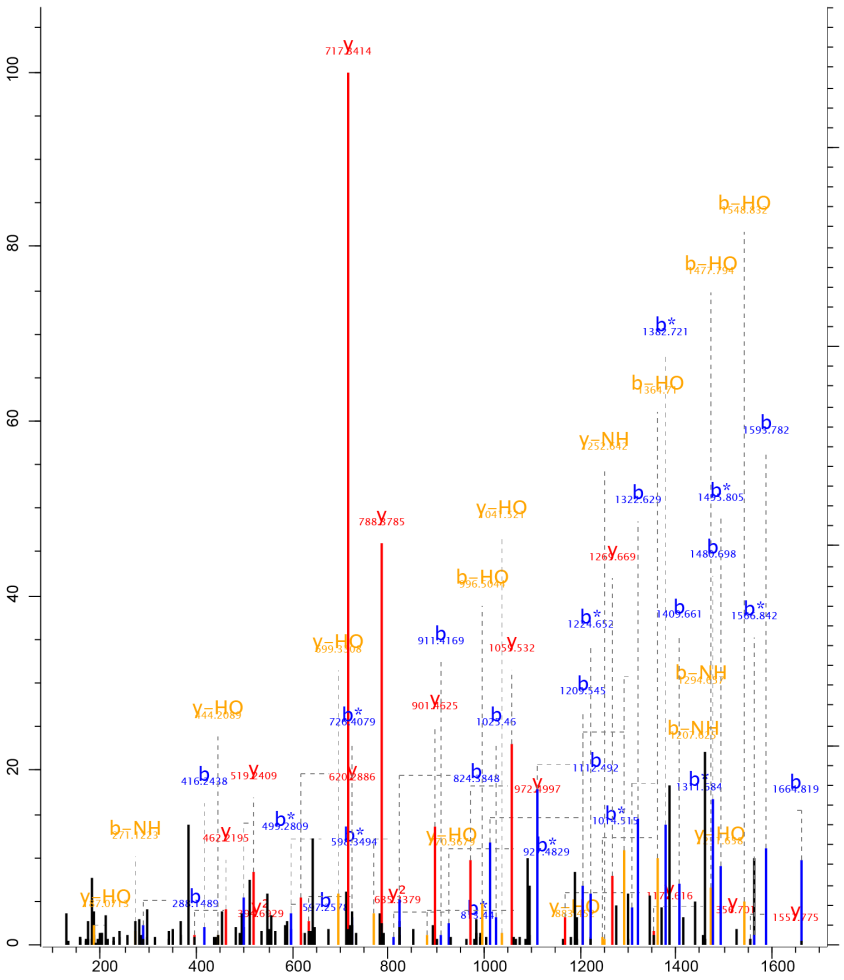

Figure 4-17 NEK1 phosphorylates VAPB *in vitro* at Threonine 201.

A) Sequence of full length human VAPB with the MS/MS sequence coverage of 90%, obtained after trypsin digestion of GST-VAPB, shown as underlined. One *in vitro* NEK1 phosphorylation site was identified (T201), highlighted in yellow. The VAPB phospho-peptide obtained by MS/MS sequencing with corresponding mass/charge (m/z) ratio is shown below, the phosphorylated residue is highlighted.

B) Tandem mass spectrometry spectrum of the VAPB phospho-peptide. The m/z of the ions is plotted against intensity and the detected ions of β and γ ion collisions annotated. Mass spectrometry was performed by Dr Rachel George and Dr Mark Collins (University of Sheffield, Faculty of Science, Mass Spectrometry Centre).

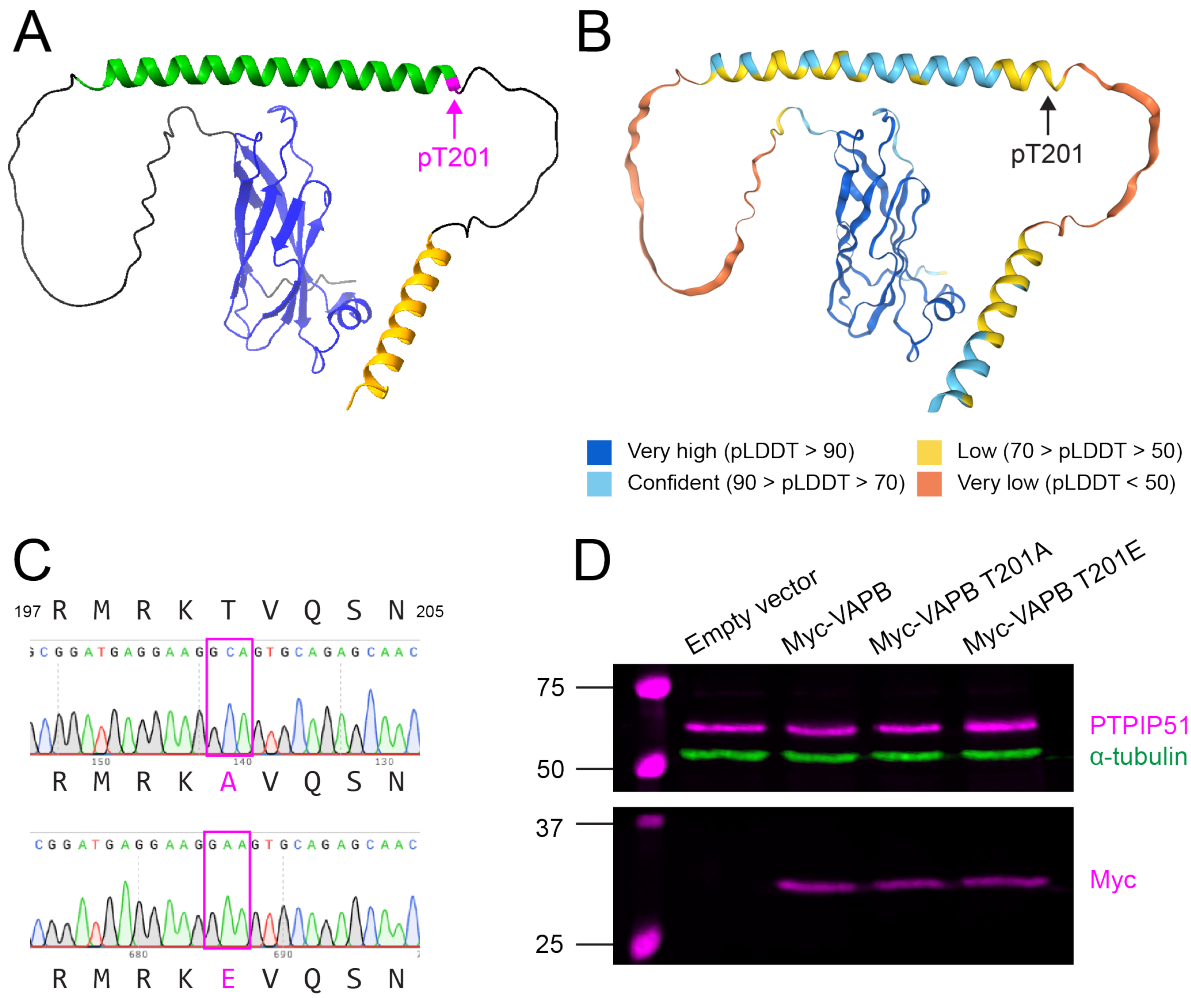

Figure 4-18 Production and validation of phospho-deficient and phospho-mimetic Myc-VAPB T201

A) Alpha-fold modelling of the human VAPB protein (Jumper *et al.*, 2021), the main protein domains are colour-coded as follows: orange = transmembrane, green = coiled-coil, blue = major-sperm (MSP). The potential NEK1 phosphorylation site pT201 is labelled in magenta. Visualised with ChimeraX (Meng *et al.*, 2023).

B) Visualisation of the predicted local distance difference test (pLDDT) scores, as a measure of confidence for the Alpha-fold prediction model of human VAPB. Visualised with PAE Viewer (Elfmann and Stulke, 2023).

C) DNA sequencing of the phospho-deficient T201A and phospho-mimetic T201E Myc-VAPB plasmic constructs.

D) HEK293 cells were transfected with pCI-neo empty vector, Myc-VAPB, Myc-VAPB T201A or Myc-VAPB T201E and immunoblotted, probing with anti-Myc and anti-PTPIP51 antibodies, and an anti-α-tubulin antibody as a loading control. Per sample 45 µg protein was loaded.

To determine if phosphorylation at VAPB T201 regulates VAPB/PTPIP51 binding, HEK293 cells were co-transfected with pCI-neo empty vector or V5-NEK1 and either wild type, T201A or T201E Myc-VAPB (Figure 4-19A). In the absence of NEK1 overexpression there was no significant difference in binding between PTPIP51 and the wild type, phospho-deficient and phospho-mimetic Myc-VAPB constructs (Figure 4-19B). Upon activation of NEK1 by overexpression, we observed an increase in PTPIP51 binding to wild type Myc-VAPB, but this effect was ablated with expression of the phospho-mimetic and phospho-deficient Myc-VAPB constructs (Figure 4-19B). Whilst it is definite that the T201A Myc-VAPB cannot be phosphorylated, we had anticipated that mutation with glutamic acid (E) would mimic the effect of phosphorylation due to the negatively charged amino acid. One explanation for these results is that glutamic acid mutation does not mimic phosphorylation but also shows a phospho-deficient phenotype, although this needs further investigation. Together, this suggests that upon activation, such as by DNA damage, phosphorylation of VAPB T201 by NEK1 may promote VAPB/PTPIP51 interaction.

4.5.5 Mutation of VAPB T201 may disrupt VAPB/VAPA dimerisation

The VAPB protein is known to form homodimers (VAPB/VAPB) or heterodimers with the VAP family protein VAPA (Nishimura *et al.*, 1999). VAPB dimerisation is suggested to be mediated by the coiled-coiled domain, as removal of this domain leads to significantly reduced dimerisation (Kim *et al.*, 2010a). Considering the VAPB phospho-site T201 resides at the end of the coiled-coil domain (Figure 4-18A), we postulated that mutation of this site may disrupt dimerization.

To quantify the VAPB/VAPA dimerisation, we measured the level of binding between overexpressed VAPB and VAPA by co-immunoprecipitation. HEK293 cells were co-transfected with either pCI-neo empty vector, FLAG-VAPA, and wild type, T201A or T201E Myc-VAPB (Figure 4-20A). Samples were immunoprecipitated with anti-FLAG antibody conjugated magnetic agarose beads and immunoblotted, probing with anti-FLAG and anti-Myc antibodies, and an anti-α-tubulin antibody as a loading control. We observed a significant decrease in binding between VAPB and VAPA with the phospho-deficient T201A mutation in VAPB (Figure 4-20B). In line with our previous result with PTPIP51 (Figure 4-19), we also observed reduced interaction between VAPB and Myc-VAPB T201E. This suggests that phosphorylation of VAPB T201 regulates VAPB/VAPA dimerisation.

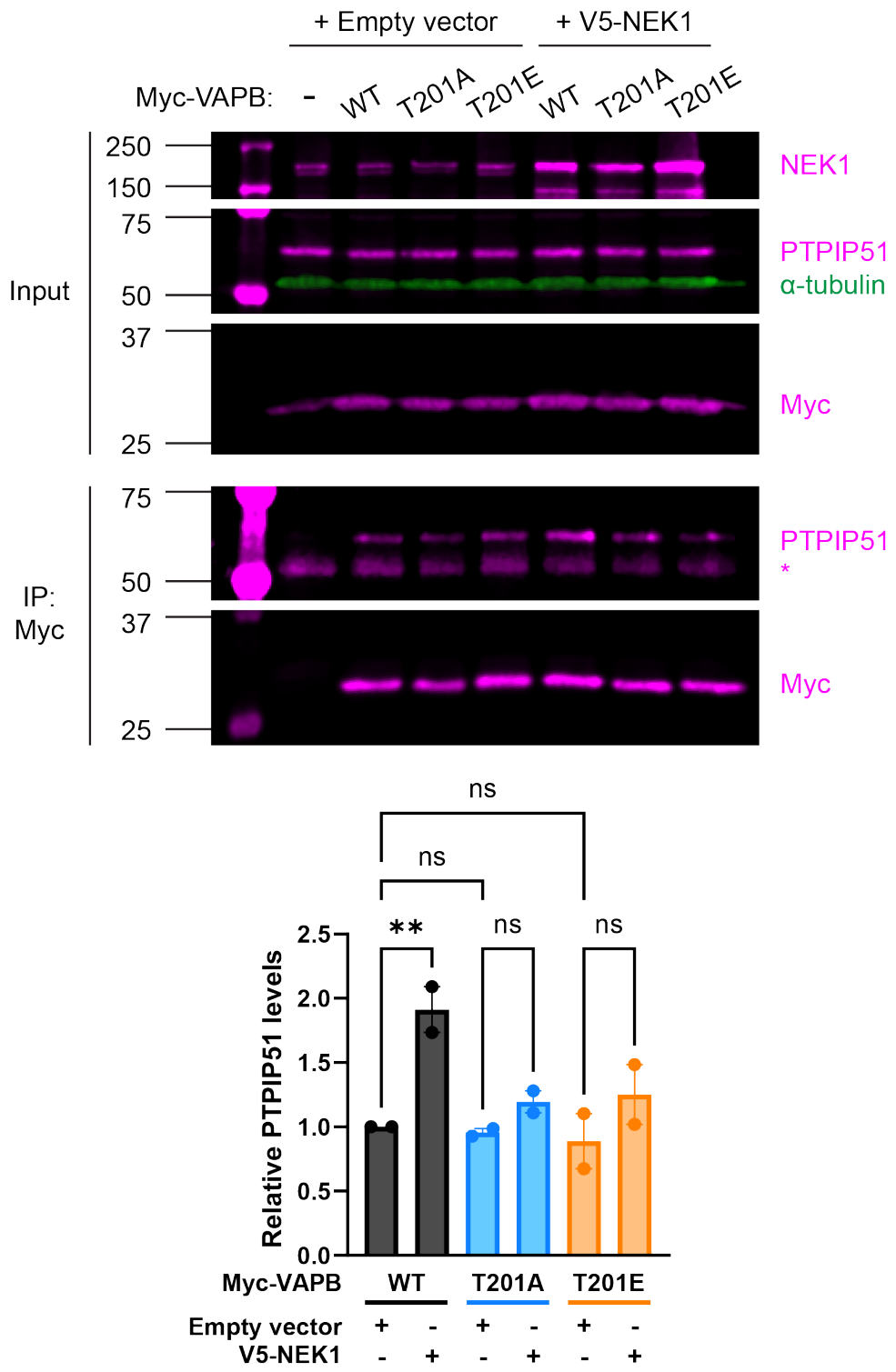

Figure 4-19 Mutation of VAPB T201 ablates NEK1 regulation of VAPB/PTPIP51 tethering.

HEK293 cells were co-transfected with pCI-neo empty vector or V5-NEK1 and either wild type (WT), phospho-deficient T201A or phospho-mimetic T201E Myc-VAPB. Samples were immunoprecipitated with an anti-Myc antibody and immunoblotted, probing with anti-NEK1, anti-Myc and anti-PTPIP51 antibodies, and an anti-α-tubulin antibody as a loading control. For input 45 µg protein was loaded. Graph represents quantification of the relative PTPIP51 protein levels normalised to the level of immunoprecipitated Myc-VAPB. Bars represent mean ± SEM. Data were analysed by one-way ANOVA with Fisher's LSD test, ns = non-significant, ** $P \leq 0.01$, $N = 2$.

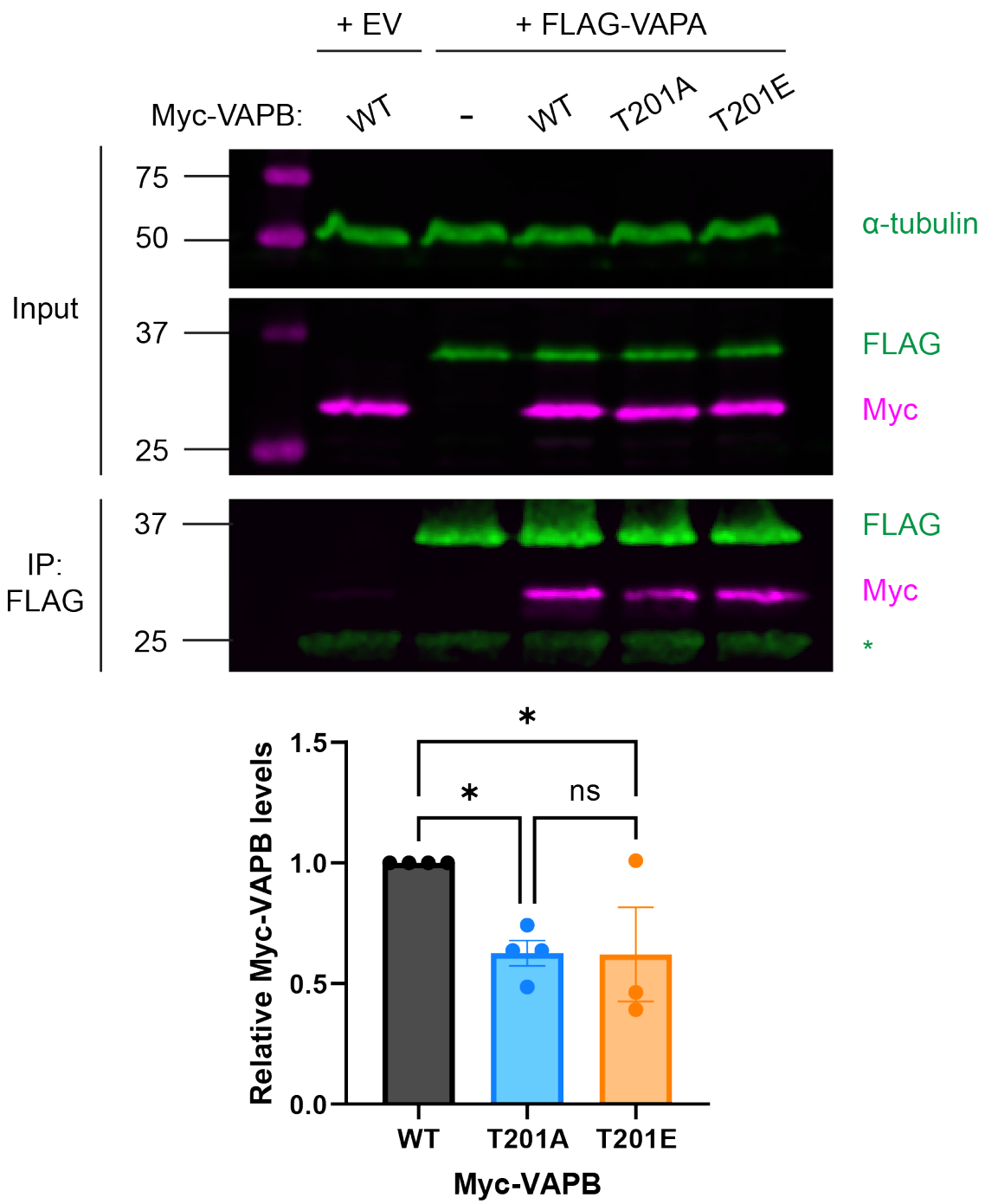

Figure 4-20 Mutation of VAPB T201 disrupts VAPB-VAPA interaction.

HEK293 cells were co-transfected with pCI-neo empty vector or FLAG-VAPA and either wild type (WT) Myc-VAPB, phospho-deficient Myc-VAPB T201A or phospho-mimetic Myc-VAPB T201E. Samples were immunoprecipitated with anti-FLAG conjugated beads and immunoblotted, probing with anti-FLAG and anti-Myc antibodies, and an anti-α-tubulin antibody as a loading control. For input 45 µg protein was loaded. Graph presents quantification of the relative Myc-VAPB protein levels normalised to the amount of immunoprecipitated FLAG-VAPA. Bars represent mean ± SEM. Data were analysed by one-way ANOVA with Fisher's LSD test, ns = non-significant, * $P \leq 0.05$, $N = 4$ (T201A), $N = 3$ (T201E). Immunoblots performed by Miss Eloise Brown.

4.5.6 Activation of NEK1 promotes VAPB and PTPIP51 phosphorylation in HeLa cells

Our experiments so far had determined that *in vitro* NEK1 phosphorylates VAPB at the phospho-site pT201 (Figure 4-16), and that inhibiting phosphorylation of this phospho-site leads to disruption of VAPB/PTPIP51 (Figure 4-19) and VAPB/VAPA interactions (Figure 4-20). To confirm NEK1 phosphorylation of VAPB at pT201 in cells, PC HeLa cells were co-transfected with a pEGFPc1-VAPB (eGFP-VAPB) (Mórotz et al., 2012) and either pCI-neo empty vector or V5-NEK1, to activate NEK1 by overexpression. NEK1 KO cells were also included to model loss of NEK1 function. VAPB was immunoprecipitated from cells using GFP-nanobody conjugated agarose beads and trypsin digested into peptides. The eluted peptides were desalted and then subjected to liquid chromatography tandem mass spectrometry (LC-MS/MS) analysis.

To confirm successful co-transfection of eGFP-VAPB and V5-NEK1, we took a portion of the lysate for mass spectrometry and subjected the samples to immunoblot, probing for GFP, endogenous NEK1 and GAPDH as a loading control (Figure 4-21). Peptides corresponding to VAPB were identified by LC-MS/MS, with 71% sequence coverage of full-length VAPB protein (Figure 4-22A). Surprisingly, we were unable to confirm the presence of phosphorylated VAPB T201 in cells. However, we found four sites that were significantly phosphorylated with overexpression of NEK1 (pT150, pS158, pS160 and pS206) (Figure 4-22B).

In addition to phosphorylation of VAPB, we observed phosphorylation of PTPIP51 at S46 upon overexpression of NEK1 (Table 4-1). In addition to phosphorylation of PTPIP51, we observed phosphorylation of a total of 31 proteins with activation of NEK1, including multiple known VAPB interactors such as OSBPL3, MAP6 and COPB2 (Table 4-1). This further implicates a role for NEK1 kinase activity in the regulation of VAPB/PTPIP51 tethering, although due to time limitations this experiment was only performed once, so further investigation and to fully understand the mechanisms of this interaction.

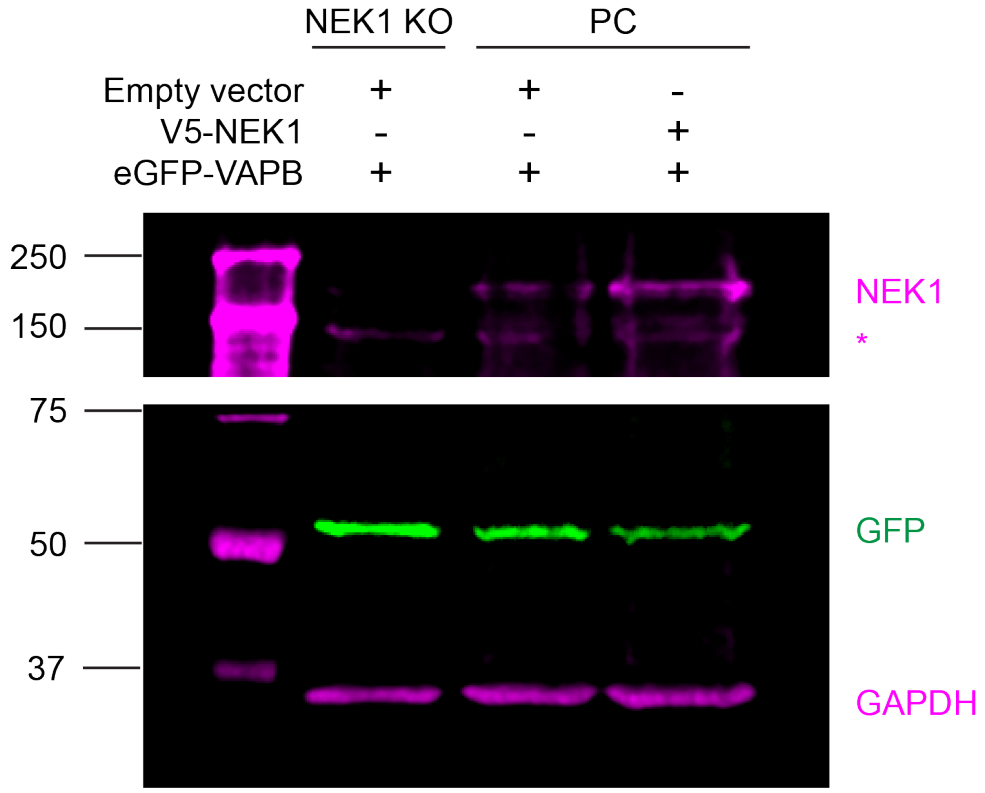

Figure 4-21 Confirmation of successful co-transfection of V5-NEK1 and eGFP-VAPB for mass spectrometry.

NEK1 knock out (KO) or wild type parental (PC) HeLa cells were co-transfected with eGFP-VAPB and either pCI-neo empty vector or V5-NEK1. Whole cell lysate was immunoblotted, probing with anti-NEK1 and anti-GFP antibodies, and an anti-GAPDH antibody as a loading control. For each sample 45 µg protein was loaded.

A

MAKVEQVLSLEPQHELKFRGPFTDVVTTNLKLGNPTDRNVCFKVKTTAPRRY
CVRPNSGIIDAGASINVSVMLQPFDYDPNEKSKHKFMVQSMFAPTDTSDMEA
VWKEAKPEDLMDSKLRCVFELPAENDKPHDVEINKIISTTASKTETPIVSKS
LSSSLDDTEVKKVMEECKRLQGEVQRLREENKQFKEEDGLRMRKTVQSNSPI
SALAPTGKEEGLSTRLLALVVLFFIVGVIIGKIAL

B

Peptide sequence	Modification
^{140}IISTTASKTEpTPIVSK^{155}	pT150
^{156}SLpSSSLDDTEVKK^{168}	pS158
^{156}SLSSpSLDDTEVKK^{168}	pS160
^{201}TVQSNpSPISALAPTGKEEGLSTR^{223}	pS206

C

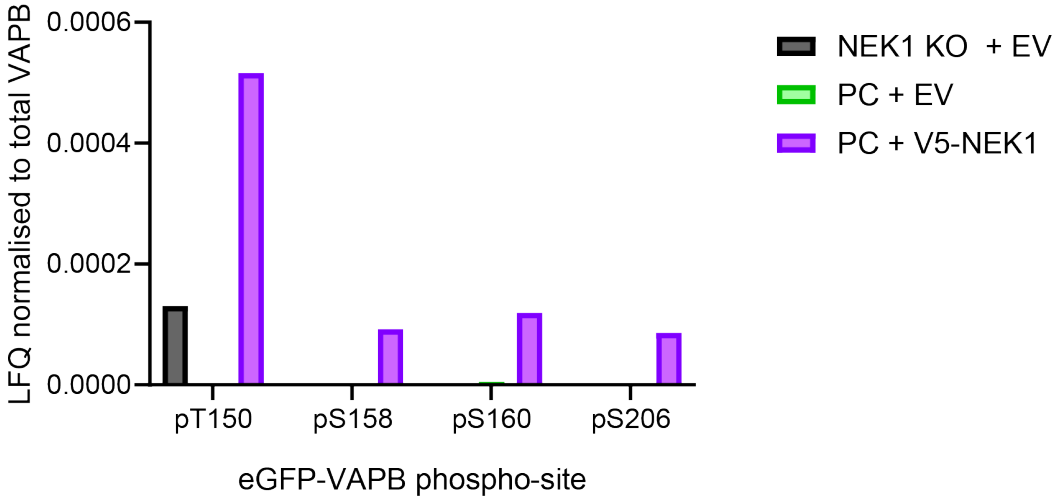

Figure 4-22 Identification of NEK1-induced VAPB phosphorylation sites in HeLa cells.

A) Sequence of full length human VAPB with the MS/MS sequence coverage of 71 %, obtained after trypsin digestion of eGFP-VAPB, shown as underlined. Four phosphorylation sites were identified, shown in magenta.

B) VAPB phospho-peptides obtained by MS/MS sequencing, the phosphorylated residues are highlighted.

C) Graph showing the label free quantification (LFQ) of phosphorylated VAPB peptides, normalised to total VAPB LFQ in NEK1 knock out (KO) cells with empty vector (EV) (grey), wild type parental (PC) cells (green) with EV and PC cells with NEK1 overexpression (purple). Bars represent the raw value *N* = 1. Mass spectrometry was performed by Dr Rachel George and Dr Mark Collins (University of Sheffield, Faculty of Science, Mass Spectrometry Centre).

Table 4-1 Phosphorylation sites in VAPB interactors identified with mass spectrometry.

Proteins that have been previously reported as VAPB interacting proteins are highlighted in blue.

Gene	Protein	Modification	Previously identified?
ABCD1	ATP-binding cassette sub-family D member 1	pS686	
BICD2	Protein bicaudal D homolog 2	pT408	Y
CACNA1A	Voltage-dependent P/Q-type calcium channel subunit alpha-1A	pY595	
CCDC188	Coiled-coil domain-containing protein 188	pS324	Y
CDK11A	Cyclin-dependent kinase 11A	pS200	
COPB2	Coatomer subunit beta	pS859	Y
FCRL2	Fc receptor-like protein 2	pS426	Y
GNS	N-acetylglucosamine-6-sulfatase	pS395	
ITIH6	Inter-alpha-trypsin inhibitor heavy chain H6	pT1166	
KITLG	Kit ligand	pT34 or pT41	
LRRC23	Leucine-rich repeat-containing protein 23	pT81	
LUZP1	Leucine zipper protein 1	pS482	
MAP6	Microtubule-associated protein 6	pS362	Y
MYO5C	Unconventional myosin-Vc	pT1646	
MYO7B	Unconventional myosin-VIIb	pS1503	
OSBPL3	Oxysterol-binding protein-related protein 3	pS265, pS303 & pS304	Y
PGM5	Phosphoglucomutase-like protein 5	pS511	Y
PLSCR3	Phospholipid scramblase 3	pT226	

Gene	Protein	Modification	Previously identified?
PTPIP51	Regulator of microtubule dynamics protein 3	pS46	Y
RASL12	Ras-like protein family member 12	pT80	
RINL	Ras and Rab interactor-like protein	pY278	
SELENOK	Selenoprotein K	pS5	Y
SHTN1	Shootin-1	pS512	Y
SYNE2	Nesprin-2	pT1053, pT1055 or pT1056	
TIPARP	Protein mono-ADP-ribosyltransferase	pS55	Y
TRPM2	Transient receptor potential cation channel subfamily M member 2	pS188	
TTN	Titin	pS21341	
UQCR11	Cytochrome b-c1 complex subunit 10	pY10	
USH1G	pre-mRNA splicing regulator USH1G	pS278	
ZFYVE26	Zinc finger FYVE domain-containing protein 26	pS293	
ZNF578	Zinc finger protein 578	pS357	

4.6 Discussion

4.6.1 Loss of NEK1 or C21orf2 disrupts VAPB/PTPIP51 tethering.

It is well established that regulation of the interaction between mitochondrial PTPIP51 and its MAM tethering partner VAPB is essential for multiple cell functions such as autophagy, Ca^{2+} homeostasis and lipid metabolism (De Vos *et al.*, 2012; Gomez-Suaga *et al.*, 2017; Yeo *et al.*, 2021). However, how VAPB/PTPIP51 tethering is regulated is not yet clear. In this chapter we show that loss of functional NEK1 protein reduced VAPB/PTPIP51 tethering (Figure 4-1), whilst activation of the NEK1 kinase by DNA damage promotes VAPB/PTPIP51 tethering (Figure 4-14), possibly due to phosphorylation of VAPB (Figure 4-19). Furthermore, we determine that activation of NEK1 by DNA damage induction promotes NEK1/PTPIP51 interaction (Figure 4-12), suggesting that NEK1 may be recruited to MAM to regulate VAPB/PTPIP51 tethering as a response to DNA damage (Figure 4-23).

In chapter 3 we reported that NEK1 and the NEK1-interacting protein C21orf2 can bind to the VAPB/PTPIP51 tether, via direct binding between NEK1 and PTPIP51. In line with this, we observed that disruption of VAPB/PTPIP51 tethering due to NEK1-deficiency can be rescued by reintroduction of NEK1, but not by overexpression of C21orf2 (Figure 4-3, Figure 4-5). This suggests that whilst C21orf2 is in close association with NEK1, with supposedly all C21orf2 protein binding to NEK1 protein (Gregorcykz et al. 2023), that NEK1 may act independently to regulate VAPB/PTPIP51 tethering. Indeed, loss of C21orf2 also leads to decreased VAPB/PTPIP51 binding which can be rescued by overexpression of wild type C21orf2 protein. However, if C21orf2 is unable to bind to NEK1 this rescue is ablated, suggesting NEK1 is the key protein for regulation of tethering (Figure 4-6). A potential explanation as to why we observe disrupted tethering in C21orf2 KO cells, is due to loss of NEK1 protein stabilisation (Watanabe et al., 2020). To further elucidate this mechanism, NEK1 should be reintroduced into C21orf2 KO cells. Additionally, Gregorcykz and colleagues (2023) found that mutation of NEK1 at D1277 prevents C21orf2 binding, which could be used as a control to confirm that NEK1 acts independent of C21orf2.

Using electron microscopy, we observed loss of mitochondrial apposition with loss of NEK1 or C21orf2 in HeLa cells. One difference noted between loss of NEK1 and C21orf2 was that loss of NEK1 leads to a significant decrease in mitochondrial size, but loss of C21orf2 does not (Figure 4-7, Figure 4-8). It was reported that cells from Kat2J NEK1-deficient mice exhibit abnormal fragmentation of mitochondria (Wang et al. 2021). This suggests that NEK1 but not C21orf2 may be involved in regulation of mitochondrial morphology. Considering we observe MAM defects in C21orf2 KO cells, it is unlikely that the mitochondrial fragmentation observed in NEK1 KO cells is the cause of MAM dysfunction.

In addition to loss of physical tethering between the ER and mitochondria, we report that loss of NEK1 leads to disrupted Ca^{2+} transfer between the organelles (Figure 4-10) and disrupted induction of autophagy (Figure 4-11). To measure Ca^{2+} transfer from the ER to mitochondria we utilised the cytoplasmic indicator dye Fura-2-AM. Whilst this technique allows reliable measurement of cytoplasmic Ca^{2+} that is not sensitive to differencing in dye loading, it does not measure the mitochondrial uptake. Thus, to further confirm that there is reduced uptake of Ca^{2+} from mitochondria, due to loss of MAM, rather than reduced release of ER, we should utilise a specific marker for mitochondrial Ca^{2+}. One possible method would be to use the Ca^{2+} sensitive fluorescent reporter Rhod-2. This has been used previously to measure changes in mitochondrial Ca^{2+} uptake in response to modulation of MAM (De Vos *et al.*, 2012; Stoica *et al.*, 2014; Stoica *et al.*, 2016). Although, as Rhod-2 is not a ratiometric indicator, it is sensitive to differences in loading into cells and has previously been reported to alter mitochondrial dynamics (Fonteriz *et al.*, 2010). An alternative to Rhod-2 could be to use genetically encoded Ca^{2+} indicators (GECI) that can specially target the ER and mitochondria (Suzuki *et al.*, 2014). This would allow for simultaneous quantification of Ca^{2+} release from the ER and uptake into the mitochondria. In our experiments we observed that knockdown of NEK1 caused a greater augmentation of Oxo-M induced cytoplasmic Ca^{2+} levels than with knockdown of PTPIP51 (Figure 4-10). As NEK1 phosphorylation closes the VDAC1 channel (Chen et al., 2008), it is unlikely that this effect is due to inhibition of VDAC1. However, to confirm that the effect of NEK1 depletion on Ca^{2+} transfer is independent of VDAC1, we could deplete cells of NEK1 and PTPIP51. As PTPIP51 depletion would disrupt MAM, we would expect therefore that loss of NEK1 should have no further effect.

We observed that physiological activation of NEK1 by induction of DNA damage promotes VAPB/PTPIP51 tethering (Figure 4-13), which correlates with increased Ca^{2+} transfer between the ER and mitochondria (Figure 4-14). It is well established transfer of Ca^{2+} between the ER and mitochondria is a mediator of cell death, as excessive uptake of Ca^{2+} by mitochondria promotes apoptosis (Pinton et al., 2008). Thus, it would have been interesting to test this with a functional study such as measuring apoptosis using well established lactate dehydrogenase (LDH) or cytochrome c release assays that are commercially available (Kari *et al.*, 2022).

Investigation with GST-pull down and mass spectrometry analysis confirmed the *in vitro* phosphorylation of VAPB by NEK1 kinase at pT201 (Figure 4-17). Phospho-mimetic or phospho-deficient mutation of this site ablates the ability of NEK1 to promote VAPB/PTPIP51 interaction when activated by overexpression (Figure 4-19). This phosphorylation site is positioned within the uncharacterised intrinsically disordered region of VAPB, which in VAPA has been shown to be essential for versatile tethering at membrane contact sites (Subra et al., 2023). One possible theory for these

results is that in response to activation such as by DNA damage, NEK1 is recruited to MAM where it phosphorylates VAPB to increase VAPB/PTPIP51 tethering, Ca^{2+} transfer and apoptosis. Whilst we would expect to see the phospho-mimicking VAPB pT201E construct to behave like the WT protein with activation of NEK1, it is possible the as glutamic acid is less negatively charged than phosphorylated threonine, it is not properly mimicking the effect. To validate this phosphorylation site, the production of a phospho-site specific antibody would be beneficial, as probing for pT201 in WT and NEK1 KO cells would determine if NEK1 phosphorylates this site.

In HeLa cells we were unable to validate the pT201 VAPB phosphorylation site, however due to time limitations this experiment was only repeated once, so there is a chance it was just not picked up in this repeat (Figure 4-22). One possible explanation for the NEK1-mediated phosphorylation of pT201 *in vitro* but not in cells, may be that due to removal of the VAPB transmembrane domain, there could be a confirmational change in the structure of the VAPB protein, leading to the exposure of phosphorylation sites that are inaccessible in full length VAPB. Trypsination in HeLa cells resulted in a lower VAPB sequence coverage than in vitro (71% vs 100%) and the pT201 site was only present on the end of peptides, so it is possible that digestion with another enzyme such as Asp-N Endopeptidase may produce peptides where phosphorylated pT201 is detectable (Gasteiger *et al.*, 2005).

Together, the data in this chapter suggest that in response to DNA damage, activated NEK1 is recruited to MAM where it binds to PTPIP51 and leads to downstream phosphorylation of VAPB and PTPIP51 to regulate VAPB/PTPIP51 tethering and Ca^{2+} transfer between the ER and mitochondria. Excessive NEK1 activation or prolonged exposure to DNA damage may in turn may lead to mitochondrial Ca^{2+} overload and initiation of apoptosis. Further experimentation should focus on elucidating the functional effects of NEK1 regulation of VAPB-PTPIP51 tethering, such as measuring apoptosis or DNA damage repair. Furthermore, it would be interesting to determine whether C21orf2 is involved in, or necessary for this response.

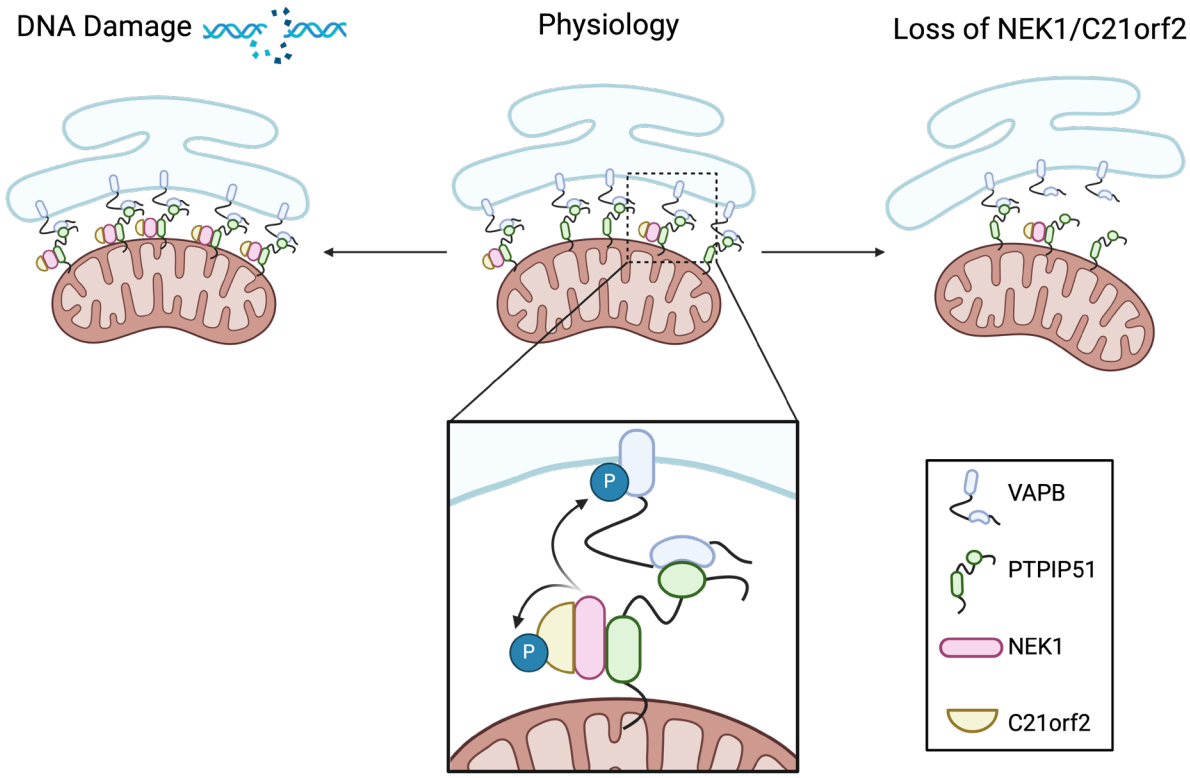

Figure 4-23 Summary of NEK1 regulation of VAPB/PTPIP51 tethering.

In response to activation of NEK1 by DNA damage, we observe increased VAPB/PTPIP51 tethering and Ca^{2+} transfer between the ER and mitochondria. Upon activation, NEK1 leads to downstream phosphorylation of VAPB, which may be necessary for regulating its interaction with PTPIP51. Loss of NEK1 or C21orf2 reduces VAPB/PTPIP51 tethering, ER-mitochondria apposition, Ca^{2+} transfer between the organelles and induction of autophagy.

Chapter 5 Characterisation of the VAPB/PTPIP51 tether

5.1 Introduction

Multiple labs have evidenced the interaction between VAPB and PTPIP51 following their discovery in 2012 however, it remains unclear how binding between the two proteins is mediated (Cabukusta *et al.*, 2020; De Vos *et al.*, 2012). In addition to VAPB, proteomic and co-immunoprecipitation data suggest that PTPIP51 binds to VAPA, although this interaction has not been well characterised (Cabukusta *et al.*, 2020). VAPB and VAPA both contain major sperm protein (MSP) domains, which are suggested to bind to proteins containing an FFAT (two phenylalanines [FF] in an acidic tract) motif, which has a consensus sequence of $E_1F_2F_3D_4A_5X_6E_7$, (Kaiser *et al.*, 2005; Loewen *et al.*, 2003). Binding between MSP domains and FFAT motif peptides has been extensively studied (Di Mattia *et al.*, 2020; Di Mattia *et al.*, 2018; Kaiser *et al.*, 2005; Loewen *et al.*, 2003). When in complex, the aromatic ring of the phenylalanine in position four and the side chain of the alanine in position 5 of the FFAT motif bind to a hydrophobic pocket at the surface of the MSP domain (Di Mattia *et al.*, 2020; Kaiser *et al.*, 2005). This hydrophobic pocket is formed by aliphatic portions of side chains of key residues within the domain, which are K87/F88/M89 in VAPB and K94/F95/M96 in VAPA (Cabukusta *et al.*, 2020; Di Mattia *et al.*, 2020). Indeed, mutation of these key binding residues reduces interaction between VAPB and FFAT-containing proteins (Cabukusta *et al.*, 2020; Kors *et al.*, 2022a).

PTPIP51 contains two FFAT-like motifs, one conventional FFAT-like motif ($_{166}$TFTDAES$_{172}$) and one phospho-FFAT motif ($_{157}$VYF**T**ASS$_{163}$) (Di Mattia *et al.*, 2020; Neefjes and Cabukusta, 2021) (Figure 5-1). Accordingly, multiple lines of evidence suggest that VAPB/PTPIP51 tethering is mediated by binding between the VAPB MSP domain and the PTPIP51 phospho-FFAT motif (Di Mattia *et al.*, 2018; Yeo *et al.*, 2021). Phosphorylation of the threonine in position four of the PTPIP51 phospho-FFAT motif has been suggested to act as a switch mechanism that regulates binding to the MSP domain of VAPB (Di Mattia *et al.*, 2020). Phospho-deficient mutation of the position four serine in the STARD3 phospho-FFAT prevents binding to VAPB, however this has not yet been proven for PTPIP51 (Di Mattia *et al.*, 2020). A recent study suggests that phosphorylation of the acidic tract flanking the FFAT motif is necessary to promote binding to the MSP domain (Kors *et al.*, 2022a). This is suggested to be due to the addition of negatively charged phosphate groups which bind to the basic electropositive surface of the MSP domain. Indeed, the PTPIP51 phospho-FFAT motif is preceded by a series of serine and threonine residues which may be phosphorylated (S149, S151, T152, S154) (Figure 5-1). Whether phosphorylation of these residues is necessary for binding is not yet understood.

Research so far has focussed on binding between VAPA/VAPB and the PTPIP51 phospho-FFAT. However, *in silico* modelling suggests that the phenylalanine and alanine in position two and five of the FFAT-like motif ($_{166}$TFTDAES$_{172}$) can bind to the hydrophobic pocket of the MSP domains of VAPA and VAPB which is discussed in more detail in section 5.2.2. Interestingly, we have also identified a third potential FFAT-like motif within PTPIP51 ($_{176}$YTTA$_{179}$), as AlphaFold3 *in silico* modelling suggests that this motif can bind to the MSP domain of VAPA and VAPB in the same fashion as previously identified PTPIP51 FFAT motifs (discussed in more detail in section 5.2.3).

Evidence for binding between PTPIP51 and the VAPA or VAPB has only been shown using short peptides spanning the FFAT motif (Di Mattia *et al.*, 2020; Yeo *et al.*, 2021). Thus, we decided to test whether disruption of key residues within the identified PTPIP51 FFAT-motifs would disrupt binding to VAPA and VAPB in cells using co-immunoprecipitation. Within this chapter we aimed to elucidate the binding mechanism between VAPA/VAPB and PTPIP51 and determine if phosphorylation regulates this interaction.

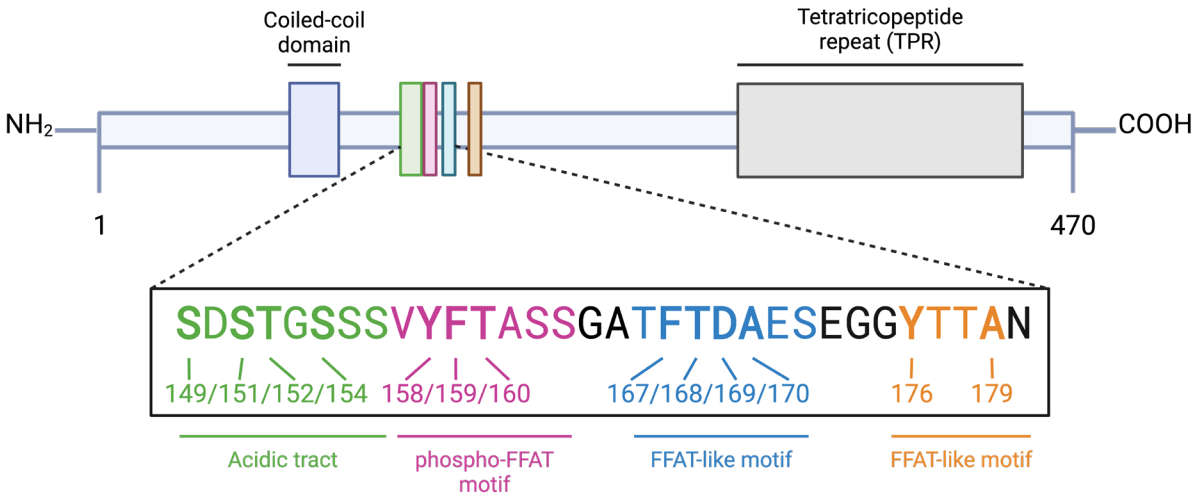

Figure 5-1 Summary of PTPIP51 mutations investigated within this study.

Schematic diagram of the PTPIP51 protein structure, with the protein motifs investigated in this study annotated. The acidic tract (green) of the phospho-FFAT motif (pink), the conventional FFAT-like motif (blue) and a new FFAT-like motif (orange) are labelled. Specific residues that were mutated to test their effect on binding to VAPA and VAPB are labelled and bolded.

5.2 *In silico* modelling of PTPIP51 binding to VAPA/VAPB using AlphaFold3

To first investigate the binding between VAPA/VAPB and PTPIP51, we used AlphaFold3 (Abramson *et al.*, 2024) to model the interaction between the MSP domain of VAPA and VAPB with peptides spanning the three identified PTPIP51 FFAT-like motifs. AlphaFold3 has recently been utilised to model protein-protein interactions and determine whether point mutations may change these protein-complexes (Wee and Wei, 2024). As this literature states that AlphaFold3 is limited in its capacity to accurately predict the interaction of small peptides, we ensured to scrutinise and report all confidence test scores for these models.

5.2.1 Modelling binding of the PTPIP51 phospho-FFAT motif with MSP domains

As literature suggests that the PTPIP51 phospho-FFAT motif ($_{157}$VYF**T**ASS$_{163}$) mediates binding to VAPB, we first modelled binding of this motif to the VAPB MSP domain (Figure 5-2A). Indeed, *in silico* modelling of the interaction between the VAPB MSP domain and a peptide of the PTPIP51 phospho-FFAT aligns with the proposal that the aromatic ring of the tyrosine and alanine in position two and five bind to the hydrophobic pocket of the MSP domain (Figure 5-2A). The modelling prediction by AlphaFold3 shows a very high degree of confidence in the accuracy of the local structure of the MSP domain and very high degree of confidence of the phospho-FFAT motif within the PTPIP51 peptide (Figure 5-2B) using the predicted local distance difference test (pLDDT). This suggests the predicted model of both structures accurately represents an experimental structure (Magana and Kovalevskiy, 2024). Additionally, the prediction presents low predicted aligned error (PAE) scores for the MSP domain and the key FFAT-like motif residues (Figure 5-2C), suggesting the model has confidently predicted the relative positioning of resides within the structures. Finally, the predicted template modelling (pTM) and interface predicted template modelling (ipTM) scores were both above 0.8 (0.87 and 0.81 respectively, Table 5-1), further suggesting a high accuracy model (Abramson *et al.*, 2024). Together this suggests that AlphaFold3 confidently predicts the binding of the PTPIP51 phospho-FFAT to the VAPB MSP domain.

In contrast, *in silico* modelling suggested that mutation of the phospho-FFAT by substitution with non-aromatic alanine residues (Y158A/F159A/T160A) would prevent binding to the MSP domain hydrophobic pocket (Figure 5-2D). Additionally, mutation of the phospho-FFAT spanning peptide reduced the confidence in the peptide structure (Figure 5-2E), increased the PAE score for the peptide (Figure 5-2F) and reduced both the pTM and ipTM scores (0.8 and 0.41 respectively, Table 5-1). This suggests low confidence in the predicted model of the peptide spanning the mutant phospho-FFAT motif interacting with the VAPB MSP domain. Together these predictions suggest that the phospho-FFAT may bind the VAPB MSP domain, and that mutation of key residues in the motif may preclude binding to VAPB.

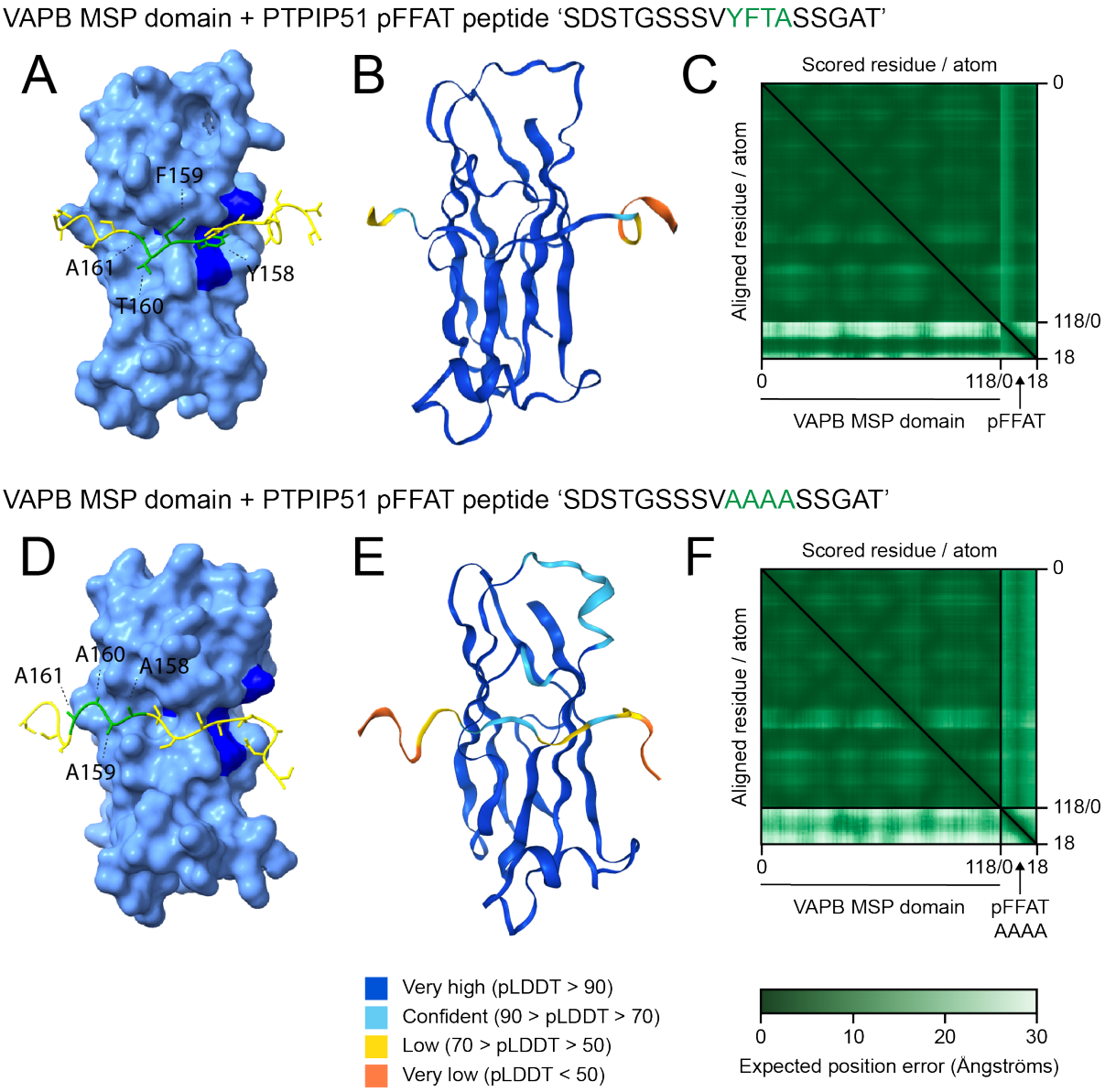

Figure 5-2 AlphaFold3 modelling of the PTPIP51 phospho-FFAT binding to the VAPB MSP domain.

A & D) AlphaFold3 modelling prediction of the interaction between the VAPB major sperm protein (MSP) domain (blue) and a PTPIP51 peptide spanning the phospho-FFAT motif (yellow) (**A**). Mutation of the Y158A/F159A/T160A residues in the PTPIP51 peptide is predicted to disrupt binding to the MSP domain (**D**). Key resides of the phospho-FFAT motif are highlighted in green and labelled. The key binding 'KFM' residues in the MSP domain are highlighted in dark blue.

B & E) predicted local distance difference test (pLDDT) scores of local confidences of the respective models. The wild type PTPIP51 peptide shows a high degree of local confidence (**B**), whilst mutation of the PTPIP51 peptide reduces local confidence of this model **(E).**

C & F) Predicted aligned error (PAE) scores of the respective models. Positioning between the key FFAT residues within the wild type PTPIP51 peptide and the MSP domain have low expected error **(C),** whilst mutation of the PTPIP51 peptide increases this error and reduces confidence of the model **(F).**

We next determined to investigate whether the PTPIP51 phospho-FFAT motif may mediate binding to VAPA. In line with the prediction for VAPB, *in silico* modelling of the interaction between the VAPA MSP domain and a peptide of the PTPIP51 phospho-FFAT showed that the tyrosine and alanine in position two and five bind to the hydrophobic pocket of the MSP domain (Figure 5-3A). The prediction showed a high degree of confidence in the accuracy of the local structure of the MSP domain and the phospho-FFAT motif within the PTPIP51 peptide (Figure 5-3B), albeit with lower confidence than predicted for VAPB. In line with this, the PAE scores for the MSP domain and the key FFAT-like motif residues were low (Figure 5-3C), the pTM and ipTM scores were 0.84 and 0.63 respectively (Table 5-1), further suggesting a moderately accurate prediction. Together this suggests that AlphaFold3 confidently predicts the binding of the PTPIP51 phospho-FFAT to the VAPA MSP domain, although with less confidence than for the binding between PTPIP51 and VAPB.

In agreement with the prediction of VAPB/PTPIP51 binding, *in silico* modelling suggested that mutation of the phospho-FFAT by substitution with non-aromatic alanine residues (Y158A/F159A/T160A) precludes binding to the MSP domain hydrophobic pocket (Figure 5-3D). This prediction showed reduced confidence in the PTPIP51 peptide structure (Figure 5-3E), increased the PAE score for the peptide (Figure 5-3F) and reduced both the pTM and ipTM scores (0.77 and 0.41 respectively, Table 5-1). Together these predictions suggest that the PTPIP51 phospho-FFAT motif may be necessary for binding to the VAPB and VAPA MSP domains, and that mutation of key residues within the motif may disrupt binding.

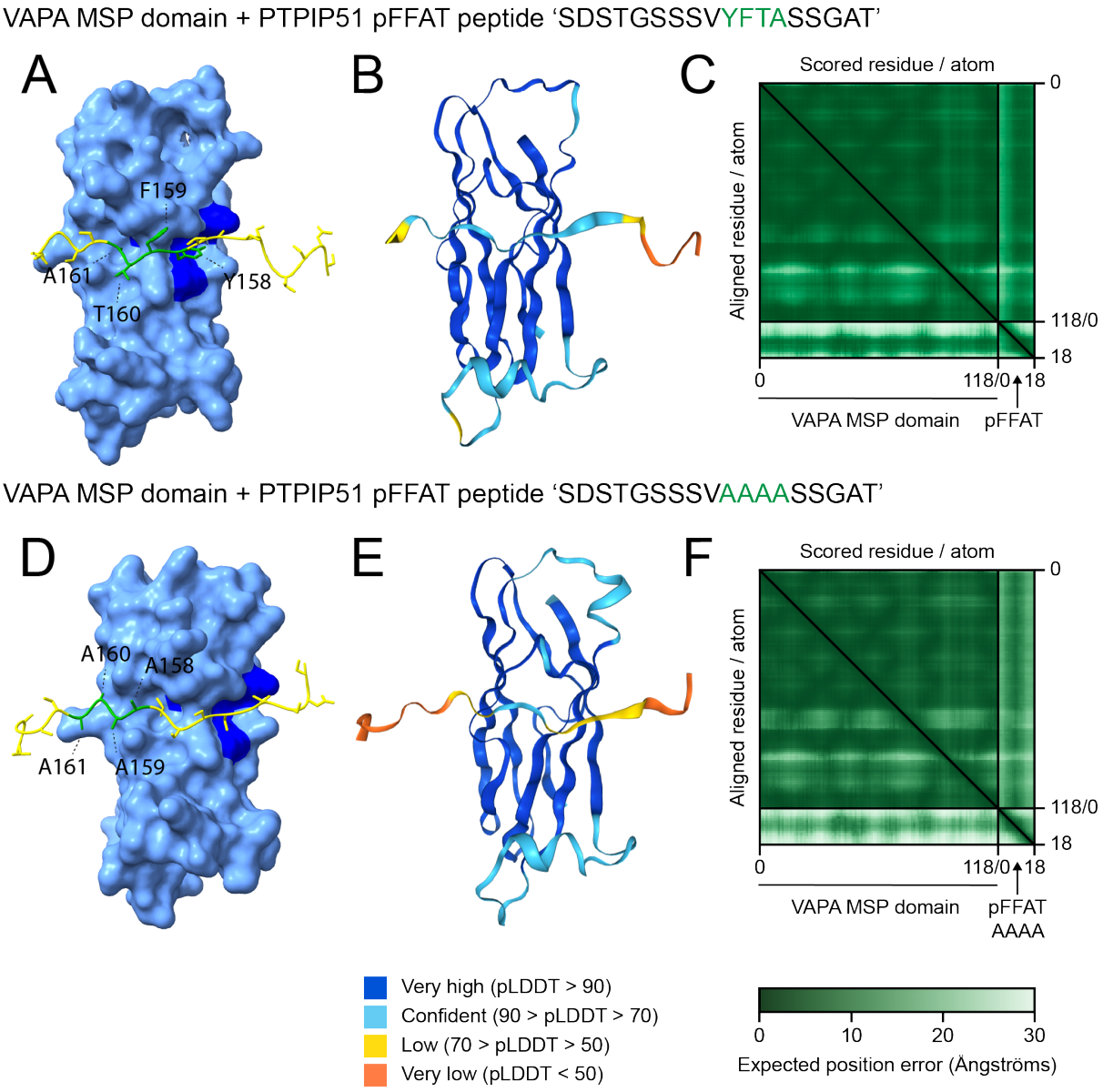

Figure 5-3 AlphaFold3 modelling of the PTPIP51 phospho-FFAT binding to the VAPA MSP domain.

A & D) AlphaFold3 modelling prediction of the interaction between the VAPA major sperm protein (MSP) MSP domain (blue) and a PTPIP51 peptide spanning the phospho-FFAT motif (yellow) (**A**). Mutation of the Y158A/F159A/T160A residues in the PTPIP51 peptide is predicted to disrupt binding to the MSP domain (**D**). Key resides of the phospho-FFAT motif are highlighted in green and labelled. The key binding 'KFM' residues in the MSP domain are highlighted in dark blue.

B & E) predicted local distance difference test (pLDDT) scores of local confidences of the respective models. The wild type PTPIP51 peptide shows a high degree of local confidence (**B**), whilst mutation of the PTPIP51 peptide reduces local confidence of this model **(E).**

C & F) Predicted aligned error (PAE) scores of the respective models. Positioning between the key FFAT residues within the wild type PTPIP51 peptide and the MSP domain have low expected error (**C**), whilst mutation of the PTPIP51 peptide increases this error and reduces confidence of the model (**F**).

5.2.2 Modelling binding of the PTPIP51 FFAT-like motif with MSP domains

As literature shows that PTPIP51 contains a second FFAT-like motif ($_{166}$TFTDAES$_{172}$), we next determined to investigate binding between this motif and the VAPA/VAPB MSP domains (Di Mattia *et al.*, 2020; Neefjes and Cabukusta, 2021). *In silico* modelling of the interaction between the VAPB and VAPA MSP domains and a peptide spanning the PTPIP51 FFAT-like motif suggested that the phenylalanine and alanine in position two and five bind to the hydrophobic pocket of the MSP domains (Figure 5-4A, Figure 5-5A). Analysis of the pLDDT scores showed a very high degree of confidence in the accuracy of the local structure of the MSP domains and the peptide spanning the FFAT-like motif for both predictions (Figure 5-4B, Figure 5-5B). Additionally, the prediction scored low PAE values for both MSP domains and the key FFAT-like motif residues within the peptide (Figure 5-4C, Figure 5-5C). The pTM and ipTM scores for both predictions were both above 0.8 (VAPB: pTM 0.91 and ipTM 0.85, VAPA: pTM 0.89 and ipTM 0.82, Table 5-1). Together this suggests high accuracy prediction of the binding of the PTPIP51 FFAT-like motif to the MSP domains, although with a higher confidence for the binding of the PTPIP51 peptide to the VAPB MSP domain.

In line with our prediction of the phospho-FFAT motif, *in silico* modelling suggests that mutation of the FFAT-like motif by substitution of the key phenylalanine residue with a non-aromatic alanine and substitution of the alanine with an acidic aspartic acid (F167A/A170D) would prevent binding to the MSP domains hydrophobic pocket (Figure 5-4D, Figure 5-5D). Mutation of the peptide spanning the FFAT-like motif reduced the confidence in the peptide structure (Figure 5-4E, Figure 5-5E), increased the PAE score for the peptide (Figure 5-4F, Figure 5-5F) and reduced both the pTM and ipTM scores (VAPB: pTM 0.87 and ipTM 0.57, VAPA: pTM 0.81 and ipTM 0.42, Table 5-1). This suggests low confidence in the prediction of the peptide spanning the mutant FFAT-like motif interacting with the VAPB and VAPA MSP domains. Together these predictions suggest that the FFAT-like motif may bind the VAPB and VAPA MSP domains, and that mutation of key residues in the motif may disrupt this binding.

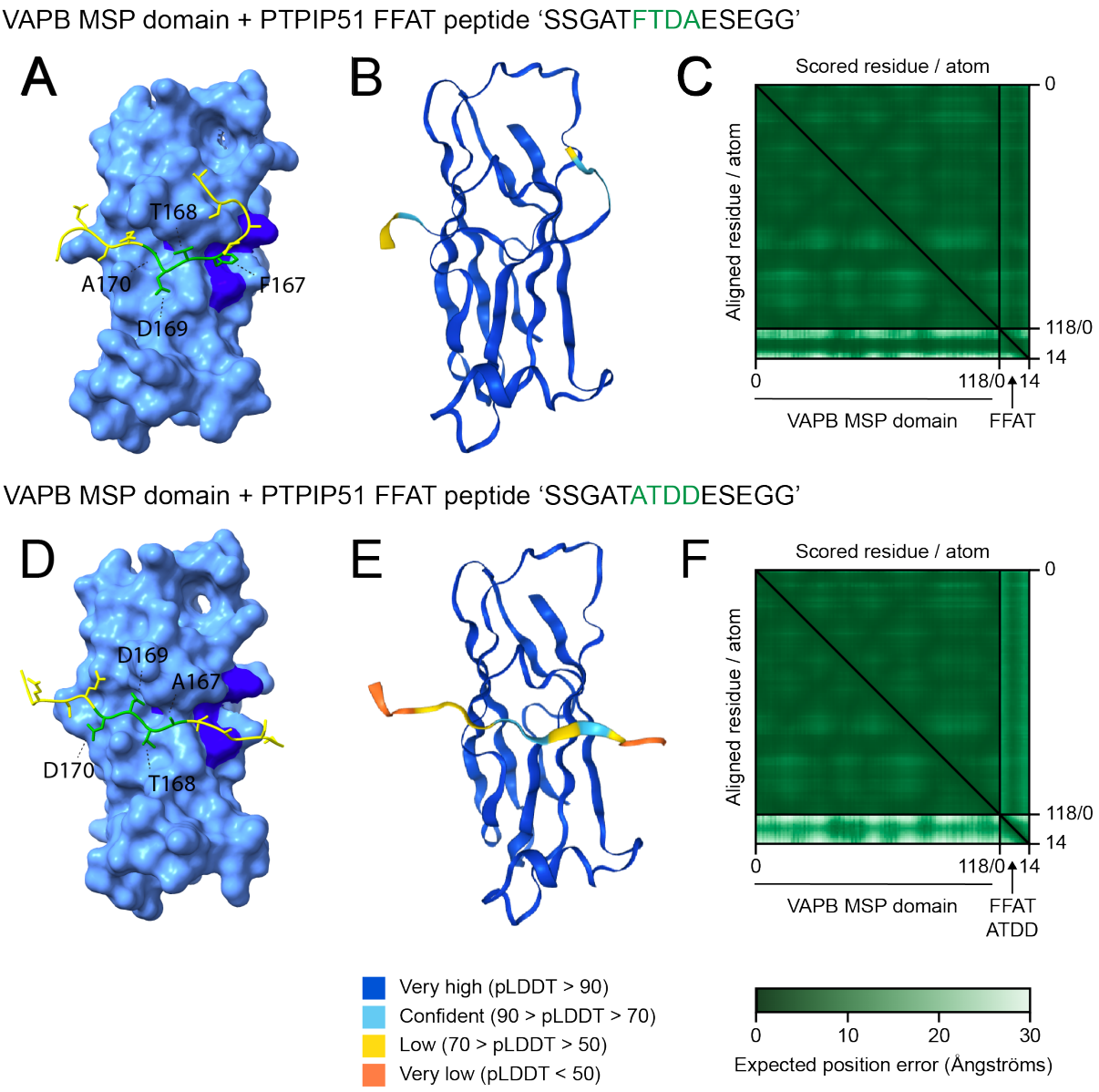

Figure 5-4 AlphaFold3 modelling of the PTPIP51 FFAT-like motif binding to the VAPB MSP domain.

A & D) AlphaFold3 modelling prediction of the interaction between the VAPB major sperm protein (MSP) MSP domain (blue) and a PTPIP51 peptide spanning the FFAT-like motif (yellow) **(A).** Mutation of the F167A/A170D residues in the PTPIP51 peptide is predicted to disrupt binding to the MSP domain **(D).** Key resides of the FFAT-like motif are highlighted in green and labelled. The key binding 'KFM' residues in the MSP domain are highlighted in dark blue.

B & E) predicted local distance difference test (pLDDT) scores of local confidences of the respective models. The wild type PTPIP51 peptide shows a high degree of local confidence **(B),** whilst mutation of the PTPIP51 peptide reduces local confidence of this model **(E).**

C & F) Predicted aligned error (PAE) scores of the respective models. Positioning between the key FFAT residues within the wild type PTPIP51 peptide and the MSP domain have low expected error **(C),** whilst mutation of the PTPIP51 peptide increases this error and reduces confidence of the model **(F).**

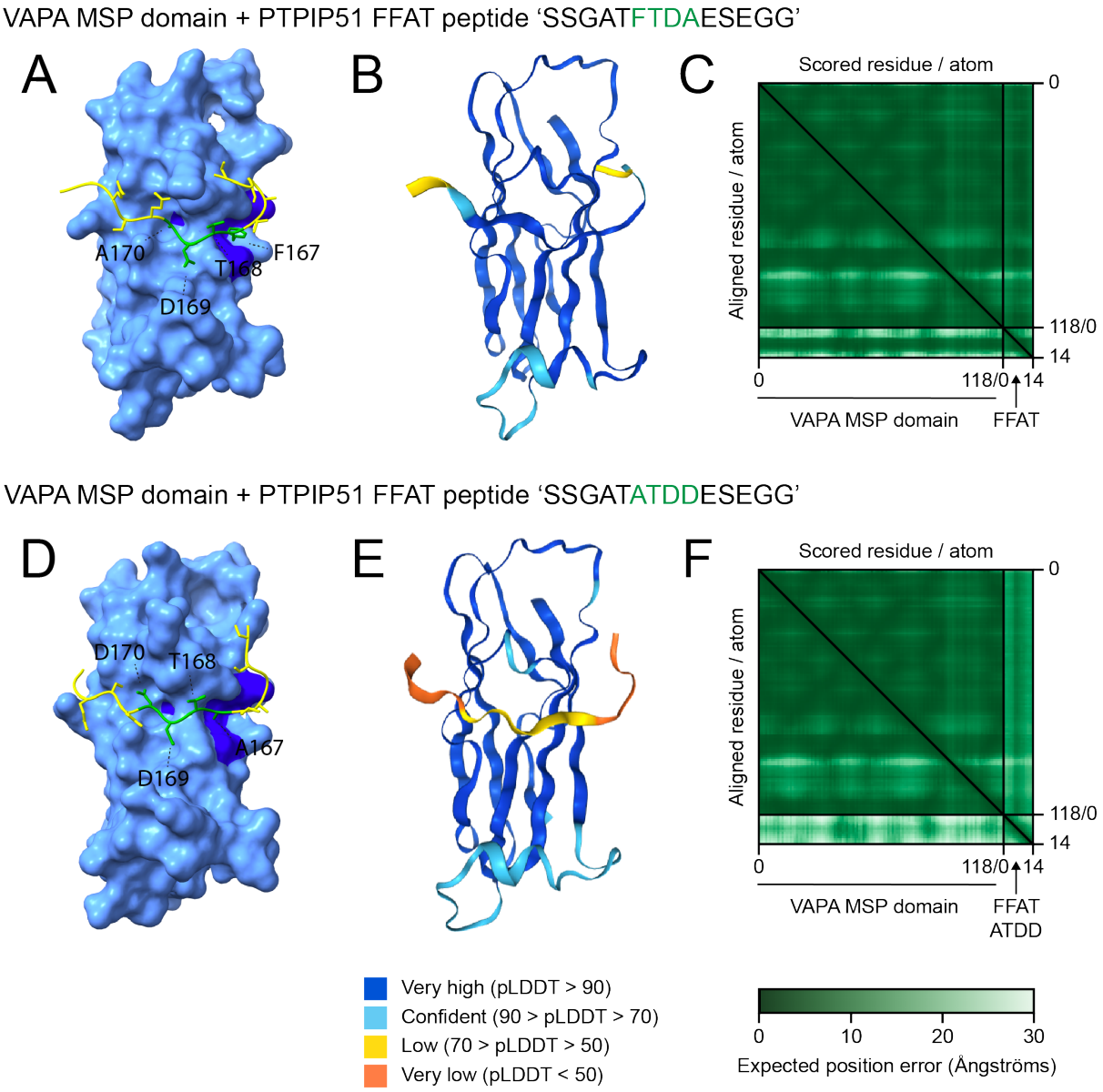

Figure 5-5 AlphaFold3 modelling of the PTPIP51 FFAT-like motif binding to the VAPA MSP domain.

A & D) AlphaFold3 modelling prediction of the interaction between the VAPA major sperm protein (MSP) MSP domain (blue) and a PTPIP51 peptide spanning the FFAT-like motif (yellow) **(A).** Mutation of the F167A/A170D residues in the PTPIP51 peptide is predicted to change binding to the MSP domain **(D).** Key resides of the FFAT-like motif are highlighted in green and labelled. The key binding 'KFM' residues in the MSP domain are highlighted in dark blue.

B & E) predicted local distance difference test (pLDDT) scores of local confidences of the respective models. The wild type PTPIP51 peptide shows a high degree of local confidence **(B),** whilst mutation of the PTPIP51 peptide reduces local confidence of this model **(E).**

C & F) Predicted aligned error (PAE) scores of the respective models. Positioning between the key FFAT residues within the wild type PTPIP51 peptide and the MSP domain have low expected error **(C),** whilst mutation of the PTPIP51 peptide increases this error and reduces confidence of the model **(F).**

5.2.3 Modelling binding of the PTPIP51 FFAT-like motif Y176 with MSP domains

During our investigation of the PTPIP51 phospho-FFAT and FFAT-like motifs, we identified a potential new FFAT-like motif within the protein ($_{176}$YTTA$_{179}$). Indeed, *in silico* modelling predicts that a peptide spanning this motif can bind to the MSP domain of VAPA and VAPB in the same fashion as previously identified PTPIP51 FFAT-like motifs (Figure 5-6A, Figure 5-7A). Analysis of the pLDDT scores showed a very high degree of confidence in the accuracy of the local structure of both VAPA and VAPB MSP domains (Figure 5-6B, Figure 5-7B). Key FFAT-like motif resides within the peptide were scored a very high degree of confidence, although the structure of resides surrounding the motif were not confidently predicted. In line with our previous predicted models, both the MSP domains and key FFAT-like motif residues within the peptide scored low PAE values (Figure 5-6C, Figure 5-7C). The pTM and ipTM scores for both predictions were lower for the predictions of the phospho-FFAT and FFAT-like motif (VAPB: pTM 0.81 and ipTM 0.74, VAPA: pTM 0.81 and ipTM 0.74, Table 5-1), possibly due to the low confidence in structure of the PTPIP51 peptide. These models suggest a moderately accurate prediction of the binding of the PTPIP51 Y176 FFAT-like motif to the MSP domains, although with a lower confidence compared to the previously identified phospho-FFAT and FFAT-like motifs.

Additionally, *in silico* modelling suggests that mutation of this FFAT-like motif by substitution of the key tyrosine residue with a non-aromatic alanine (Y176A) would change binding to the MSP domains hydrophobic pocket (Figure 5-6D, Figure 5-7D). Mutation of the peptide spanning the FFAT-like motif significantly reduced the confidence in the peptide structure (Figure 5-6E, Figure 5-7E), increased the PAE score for the peptide (Figure 5-6F, Figure 5-7F) and reduced both the pTM and ipTM scores (VAPB: pTM 0.78 and ipTM 0.32, VAPA: pTM 0.74 and ipTM 0.32, Table 5-1). Together, this suggests low confidence in the prediction of the peptide spanning the mutant FFAT-like Y176 motif interacting with the VAPB and VAPA MSP domains. This suggests that the FFAT-like Y176 motif may interact with the VAPB and VAPA MSP domains, and that mutation of key residues in the motif may prevent this interaction.

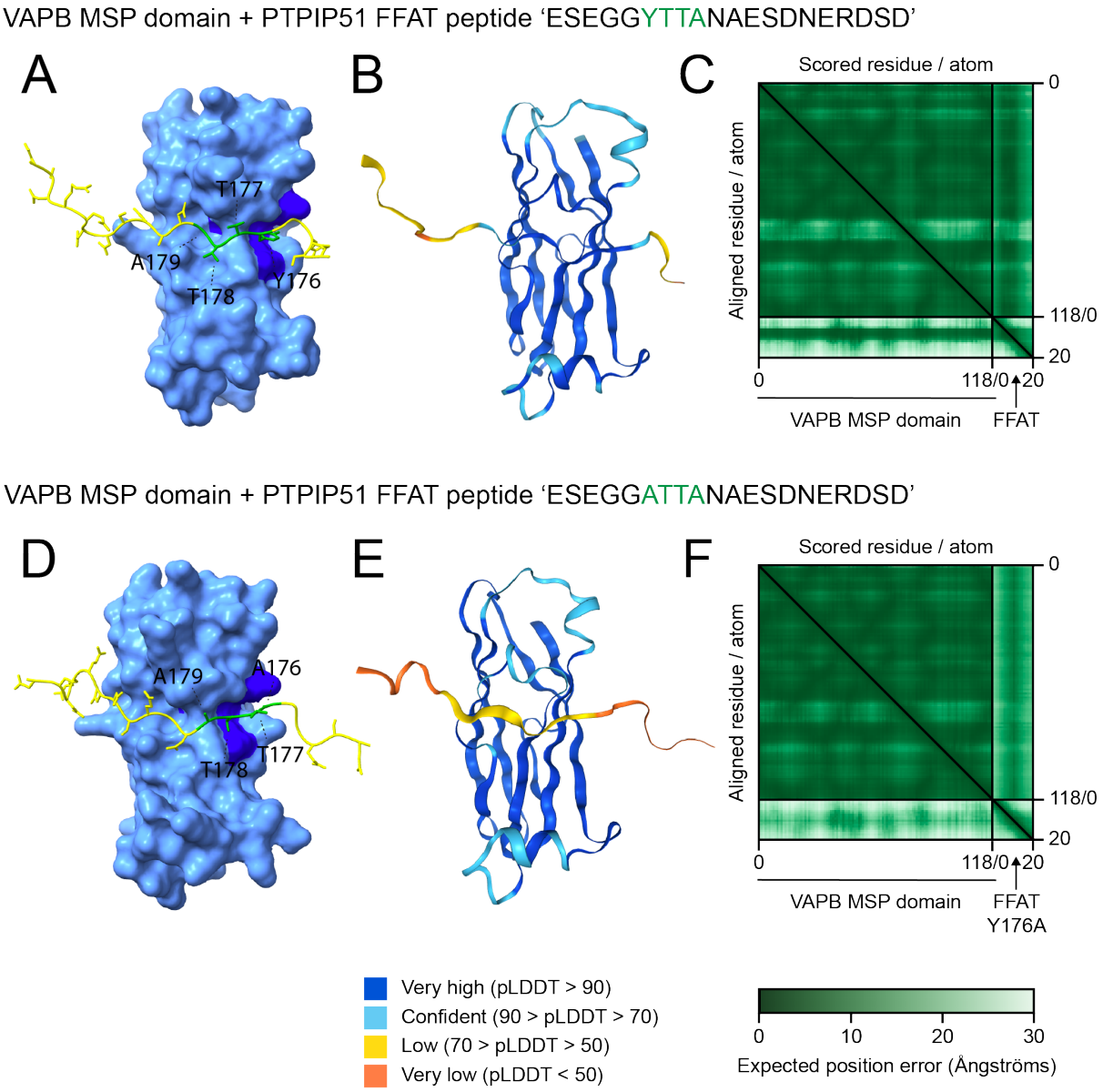

Figure 5-6 AlphaFold3 modelling of PTPIP51 Y176 binding to the VAPB MSP domains.

A & D) AlphaFold3 modelling prediction of the interaction between the VAPB major sperm protein (MSP) MSP domain (blue) and a PTPIP51 peptide spanning tyrosine 176 (yellow) **(A).** Mutation of the Y176A residue in the PTPIP51 peptide is predicted to disrupt binding to the MSP domain **(D).** The resides of a new potential FFAT-like motif are highlighted in green and labelled. The key binding 'KFM' residues in the MSP domain are highlighted in dark blue.

B & E) predicted local distance difference test (pLDDT) scores of local confidences of the respective models. The wild type PTPIP51 peptide shows a high degree of local confidence **(B),** whilst mutation of the PTPIP51 peptide reduces local confidence of this model **(E).**

C & F) Predicted aligned error (PAE) scores of the respective models. Positioning between the key FFAT residues within the wild type PTPIP51 peptide and the MSP domain have low expected error **(C),** whilst mutation of the PTPIP51 peptide increases this error and reduces confidence of the model **(F).**

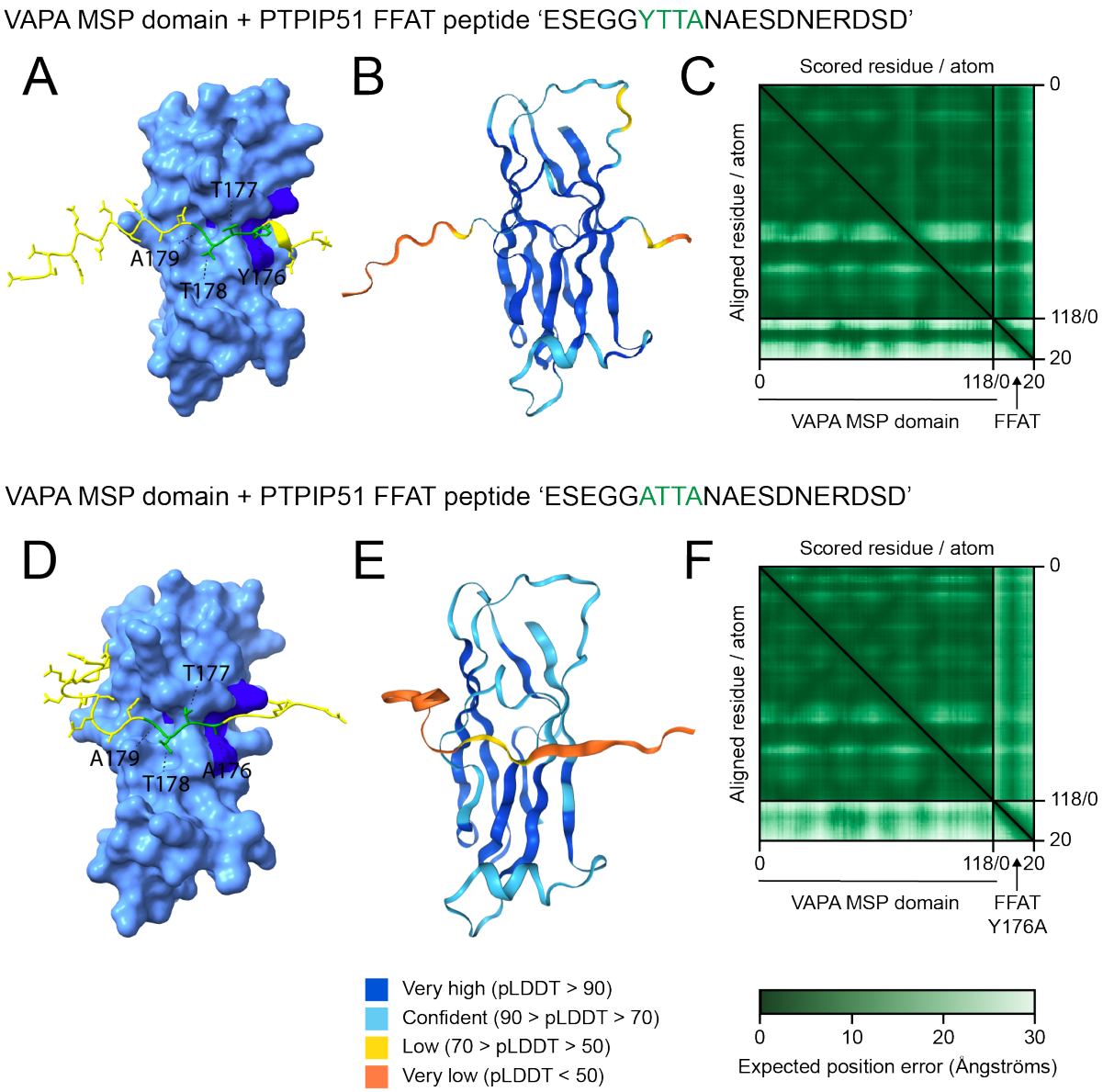

Figure 5-7 AlphaFold3 modelling of PTPIP51 Y176 binding to the VAPA MSP domains.

A & D) AlphaFold3 modelling prediction of the interaction between the VAPA major sperm protein (MSP) MSP domain (blue) and a PTPIP51 peptide spanning tyrosine 176 (yellow) **(A).** Mutation of the Y176A residue in the PTPIP51 peptide is predicted to disrupt binding to the MSP domain **(D).** The resides of a new potential FFAT-like motif are highlighted in green and labelled. The key binding 'KFM' residues in the MSP domain are highlighted in dark blue.

B & E) predicted local distance difference test (pLDDT) scores of local confidences of the respective models. The wild type PTPIP51 peptide shows a high degree of local confidence **(B),** whilst mutation of the PTPIP51 peptide reduces local confidence of this model **(E).**

C & F) Predicted aligned error (PAE) scores of the respective models. Positioning between the key FFAT residues within the wild type PTPIP51 peptide and the MSP domain have low expected error **(C),** whilst mutation of the PTPIP51 peptide increases this error and reduces confidence of the model **(F).**

5.3 Modelling PTPIP51 binding to VAPA/VAPB using co-immunoprecipitation

Previous research has confirmed that peptides spanning the PTPIP51 FFAT motifs bind to VAPA and VAPB (Di Mattia *et al.*, 2020; Yeo *et al.*, 2021). Thus, to confirm in cells that the FFAT motifs are necessary for binding to VAPA/VAPB, we utilised site-directed mutagenesis to disrupt key residues within the three identified FFAT-like motifs of a HA-tagged PTPIP51 protein construct. To disrupt the binding of aromatic amino acids in the FFAT motif, tyrosine or phenylalanine residues were substituted for alanine which lack a phenyl group. Conversely, to disrupt binding of an alanine, the residue was substituted for a phenylalanine for addition of an aromatic ring, or with a negatively charged aspartic acid.

To determine the effect of potential phospho-sites, threonine, serine, or tyrosine residues were substituted with an alanine which cannot be phosphorylated. Substitution of phospho-sites with a negatively charged aspartic or glutamic acid was used to mimic phosphorylation. These mutant PTPIP51-HA protein constructs were expressed in HEK293 cells and co-immunoprecipitated to capture PTPIP51. The immunoprecipitated were immunoblotted for HA, VAPA and VAPB, to quantify whether PTPIP51 interactions were disrupted upon mutation.

5.4 The PTPIP51 phospho-FFAT motif does not regulate binding to VAPA/VAPB

A recent study suggests that phosphorylation of the acidic tract flanking the FFAT motif is necessary to apply negative charge prior to binding to the basic electropositive surface of the MSP domain (Kors *et al.*, 2022a). The PTPIP51 phospho-FFAT motif is preceded by a series of serine and threonine residues which may be phosphorylated (S149, S151, T152, S154). To determine the contribution of phosphorylation the acidic tract on binding to VAPB, phospho-deficient alanine substitutions were inserted at possible phospho-sites within the acidic tract (S149, S151, T152, S154). HEK293 cells were transfected with empty vector pCI-neo, wild type or acidic tract mutant PTPIP51-HA (S149A/S151A/T152A/S154). PTPIP51-HA was immunoprecipitated with an anti-HA antibody and the immune pellet was probed for endogenous VAPB (Figure 5-8). Wild type PTPIP51 efficiently co-immunoprecipitated endogenous VAPB. Phospho-deficient mutation of the potential acidic tract phosphorylation sites did not preclude binding of VAPB to PTPIP51 (Figure 5-8). This suggests that phosphorylation of the PTPIP51 acidic tract flanking the phospho-FFAT is not necessary for binding to VAPB.

Phosphorylation of the serine in position four of the STARD3 phospho-FFAT has been shown to be necessary for binding to VAPB (Di Mattia *et al.*, 2020). It is suggested that the threonine in position four of the PTPIP51 phospho-FFAT may need to be phosphorylated to bind, however this has not been proven on protein level (Di Mattia *et al.*, 2020). *In silico* modelling predicts that disruption of the Y158/F159/T170 residues will prevent binding to the MSP domain (Figure 5-2, Figure 5-3). To

test the contribution of the phospho-FFAT motif to VAPA/VAPB binding, site-directed mutagenesis was used to key residues within the PTPIP51 phospho-FFAT motif (Y158 and F159) by substitution with an alanine that lacks an aromatic ring. To determine if phosphorylation of T160 may contribute to binding of PTPIP51 to VAPA/VAPA, a phospho-deficient substitution with an alanine was inserted.

HEK293 cells were transfected with empty vector pCI-neo, wild type, phospho-FFAT mutant PTPIP51-HA Y158A/F159A/T160A or acidic tract mutant PTPIP51-HA (S149A/S151A/T152A/S154). PTPIP51-HA was immunoprecipitated with an anti-HA antibody and the immune pellet was probed for endogenous VAPB and VAPA (Figure 5-9). Wild type PTPIP51 efficiently co-immunoprecipitated endogenous VAPB and VAPA. Mutation of neither the acidic tract nor the phospho-FFAT precluded binding of PTPIP51 to VAPA or VAPB. Together this shows that the PTPIP51 phospho-FFAT is not needed for binding. During our investigation of this, Mórotz and colleagues showed that deletion of this motif in PTPIP51 did not affect binding to VAPB, further confirming these results (Mórotz *et al.*, 2022).

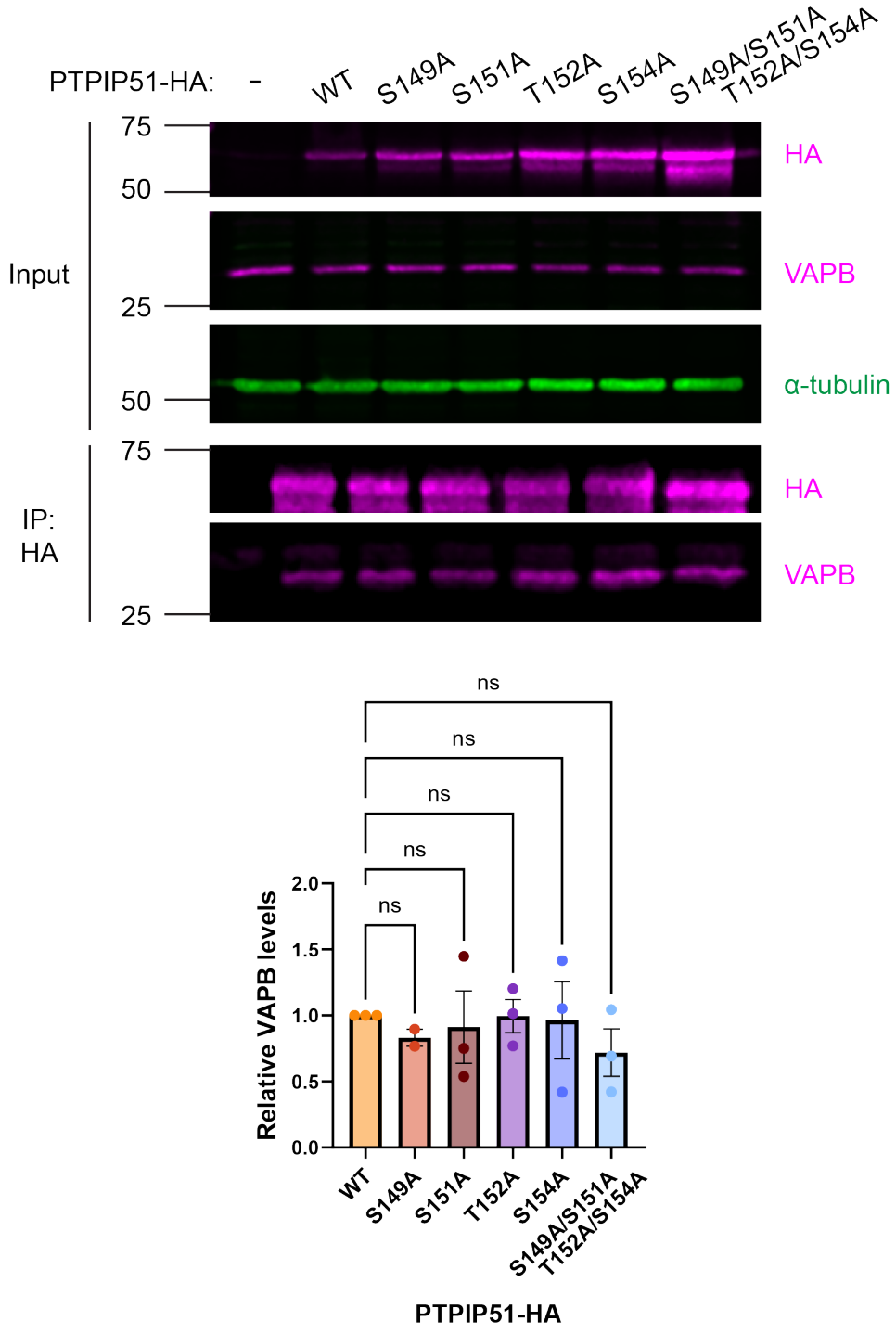

Figure 5-8 Phosphorylation of the PTPIP51 phospho-FFAT motif acidic tract is not necessary for VAPB binding.

HEK293 cells were transfected with empty vector pCI-neo, wild type (WT) PTPIP51-HA or phospho-deficient acidic tract PTPIP51-HA constructs (S149A/S151A/T152A/S154A). Cells were immunoprecipitated with an anti-HA antibody and immunoblotted, probing for HA, endogenous VAPB and α-tubulin antibody as a loading control. Graph shows the quantification of the level of endogenous VAPB normalised to the level of immunoprecipitated PTPIP51-HA. Bars represents mean ± SEM. Data were analysed by one-way ANOVA with Fisher's LSD, ns = non-significant, *N* = 3. For input 45 µg protein was loaded. Immunoblot performed by Miss Eloise Brown.

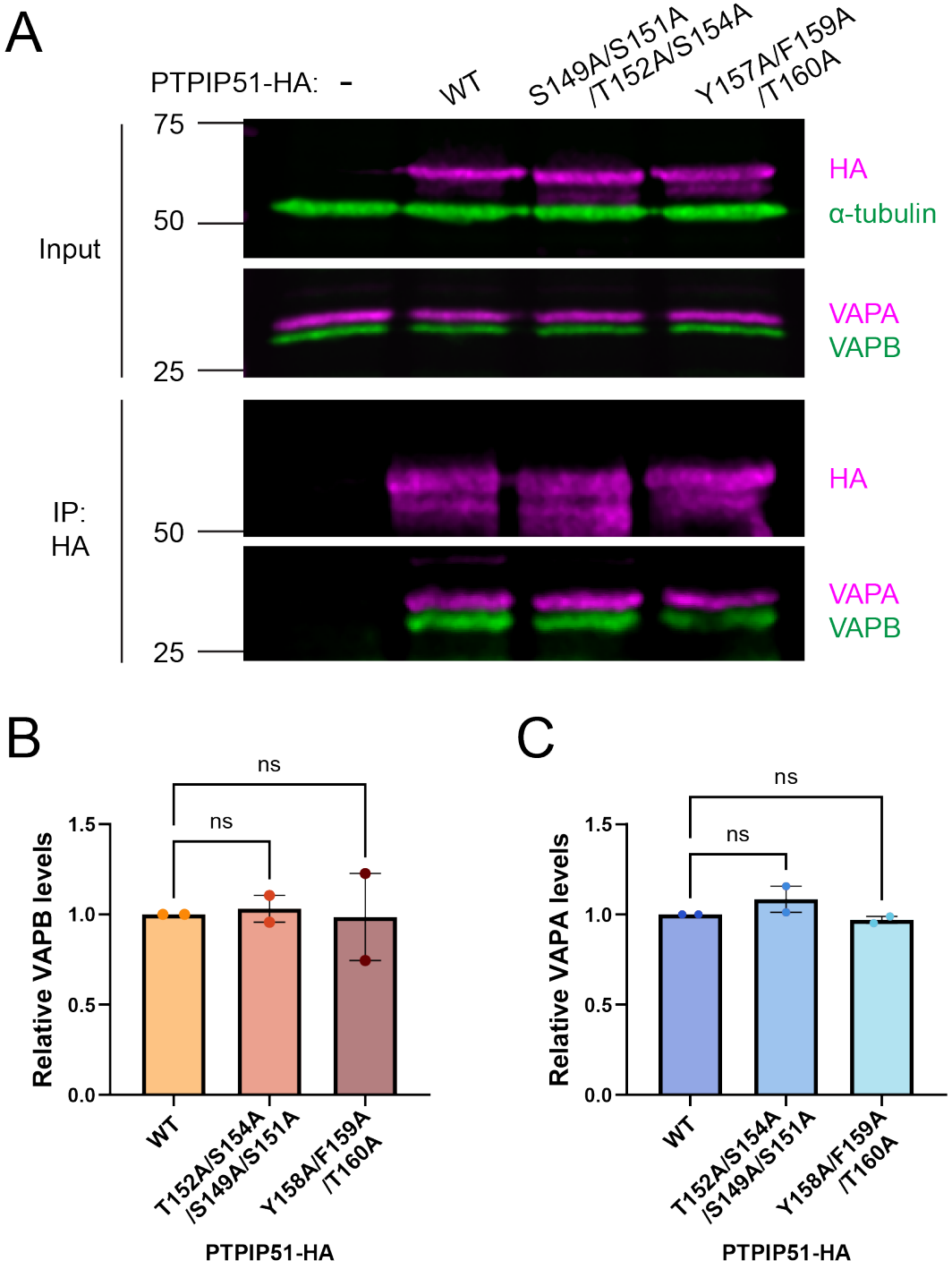

Figure 5-9 Disruption of the PTPIP51 phospho-FFAT motif does not disrupt binding to VAPA/VAPB.

A) HEK293 cells were transfected with empty vector pCI-neo, wild type (WT) PTPIP51-HA, phospho-FFAT mutant PTPIP51-HA Y158A/F159A/T160A, or phospho-deficient acidic tract mutant PTPIP51-HA S149A/S151/T152/S154A. Cells were immunoprecipitated with an anti-HA antibody and immunoblotted, probing for HA, endogenous VAPA, VAPB and α-tubulin antibody as a loading control.

B & C) Graphs show the quantification of the level of VAPB **(B)** or VAPA **(C)** normalised to the level of immunoprecipitated PTPIP51-HA. Bars represent mean ± SEM. Data were analysed by one-way ANOVA with Fisher's LSD, ns = non-significant, *N* = 2. For input 45 µg protein was loaded. Immunoblot performed by Miss Eloise Brown.

5.5 The PTPIP51 conventional FFAT-like motif does not regulate binding to VAPB/VAPA.

Whilst PTPIP51 contains two FFAT motifs, it is not well established whether the conventional FFAT-like motif ($_{166}$TFTDAES$_{172}$) may be involved in binding to VAPB or VAPA. Whilst literature has implicated the phospho-FFAT motif as the probable binding domain, our data shows this motif is not necessary for binding to VAPA or VAPB (section 5.4). *In silico* modelling using Alpha-fold suggests that the conventional FFAT-like motif can bind to the VAPA and VAPB MSP domains by binding to the hydrophobic pocket (Figure 5-4A, Figure 5-5A). In a similar fashion to the predicted modelling of the phospho-FFAT motif, the aromatic group of the phenylalanine 167 and the alanine 170 are predicted to bind to the key 'KFM' residues with the VAPA and VAPB MSP domains. Mutation of the F167 and A170 residues within this motif is predicted to disrupt binding to this MSP region (Figure 5-4D, Figure 5-5D). Following a similar approach to our investigation of the phospho-FFAT, we mutated these four key residues (F167/T168/D169/A170) within the motif (Figure 5-1). HEK293 cells were transfected with empty vector pCI-neo or wild type, F167A/A170D or F167A/T168A/D169A/A170D PTPIP51-HA Y158A/F159A/T160A. The samples were immunoprecipitated with an anti-HA antibody to capture PTPIP51 and immunoblotted for PTPIP51-HA, endogenous VAPA, VAPB and α-tubulin as a loading control (Figure 5-10). We observed that neither mutation of the FFAT-like motif residues disrupted the binding between PTPIP51 and VAPA or VAPB. This suggests that the PTPIP51 conventional FFAT-like motif is not necessary for binding to VAPA or VAPB (Figure 5-10).

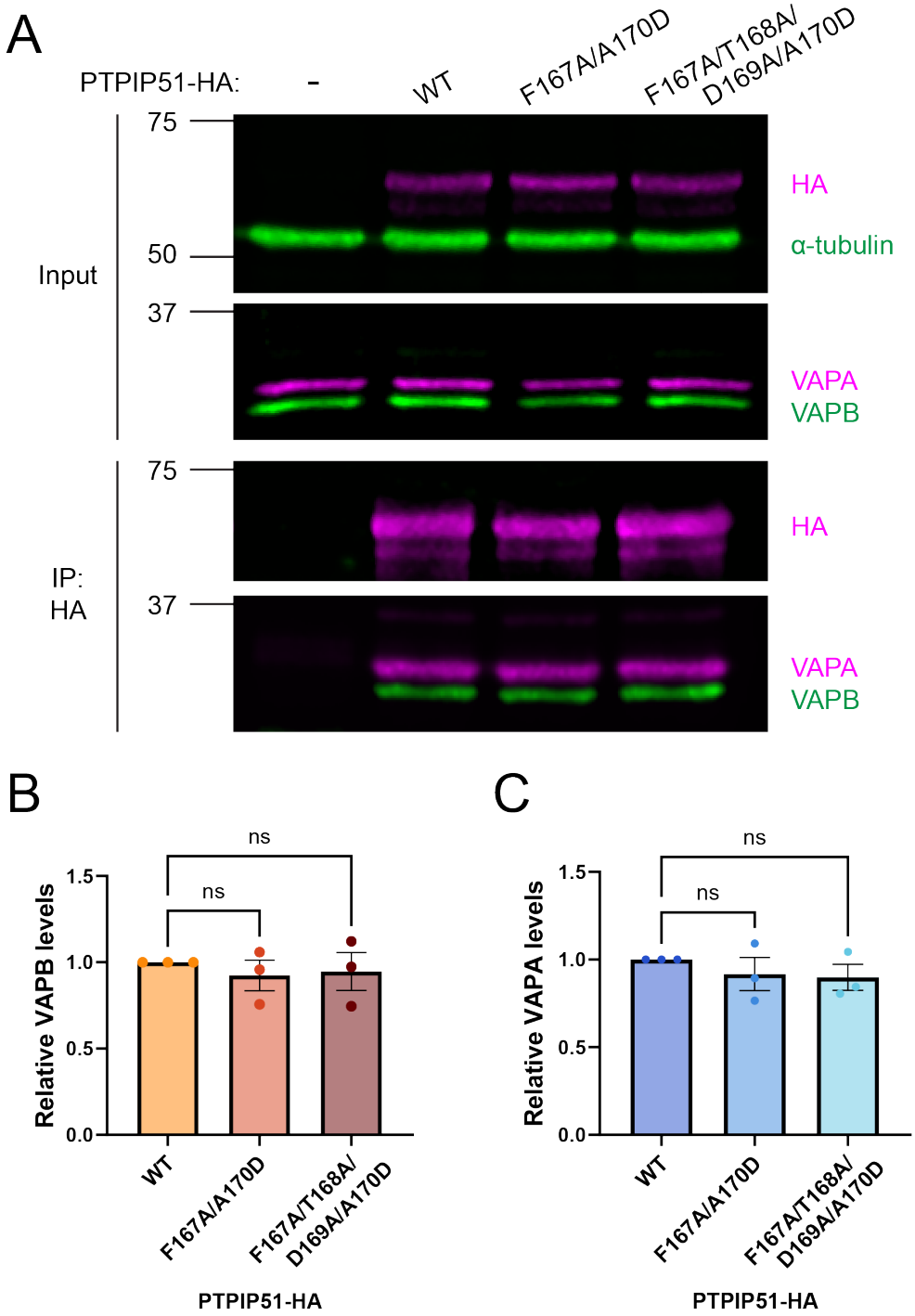

Figure 5-10 The PTPIP51 FFAT-like motif does not mediate binding to VAPA or VAPB.

A) HEK293 cells were transfected with empty vector pCI-neo, wild type (WT) PTPIP51-HA, PTPIP51-HA F167A/A170D or F167A/T168A/D167A/A170D. Cells were immunoprecipitated with an anti-HA antibody and immunoblotted, probing for HA, endogenous VAPA, VAPB and α-tubulin antibody as a loading control.

B & C) Graphs show the quantification of the level of VAPB **(B)** or VAPA **(C)** normalised to the level of immunoprecipitated PTPIP51-HA. Bars represent mean ± SEM. Data were analysed by one-way ANOVA with Fisher's LSD, ns = non-significant, *N* = 3. For input 45 µg protein was loaded. Immunoblot performed by Miss Eloise Brown.

5.6 The PTPIP51 tyrosine 176 is not necessary for binding to VAPB or VAPA.

In silico modelling indicated that a motif spanning PTPIP51 Y176 could act as a 3rd FFAT-like motif (Figure 5-1, Figure 5-6 & Figure 5-7). The phosphorylation status of this phospho-site by has previously been shown to regulate binding of PTPIP51 with RAF proto-oncogene serine/threonine-protein kinase 1 (Raf1), via binding to 14-3-3 (Brobeil *et al.*, 2011; Brobeil *et al.*, 2012). This site is suggested to be phosphorylated by the kinase Src family kinases Lyn and c-Src and dephosphorylated by protein tyrosine phosphatase 1B (PTP1B) (Brobeil *et al.*, 2011). To determine if phosphorylation of Y176 may also regulate binding to VAPA and VAPB, we used site directed mutagenesis to create phospho-deficient (alanine or phenylalanine) and phospho-mimetic (glutamic acid) mutants. In addition to Y176, modelling suggests that A179 may also be involved in binding to the MSP hydrophobic pocket, thus substation with a phenylalanine was used to disrupt binding of this residue.

HEK293 cells were transfected with empty vector pCI-neo or wild type or the panel of phospho-mutant PTPIP51-HA constructs. The samples were immunoprecipitated with an anti-HA antibody to capture PTPIP51 and immunoblotted for PTPIP51-HA, endogenous VAPA, VAPB and α-tubulin as a loading control (Figure 5-11). Phospho-deficient or phospho-mimetic mutation of PTPIP51 Y176 did not change binding to VAPB or VAPA. We observed that mutation of both Y176 and A179 did not disrupt the interaction between PTPIP51 with VAPA and VAPB. Together, this suggests that the PTPIP51 tyrosine 176 is not necessary for binding to VAPA or VAPB (Figure 5-11). However, due to time limitations this experiment was only repeat once, thus further experimental repeats are necessary to confirm this result.

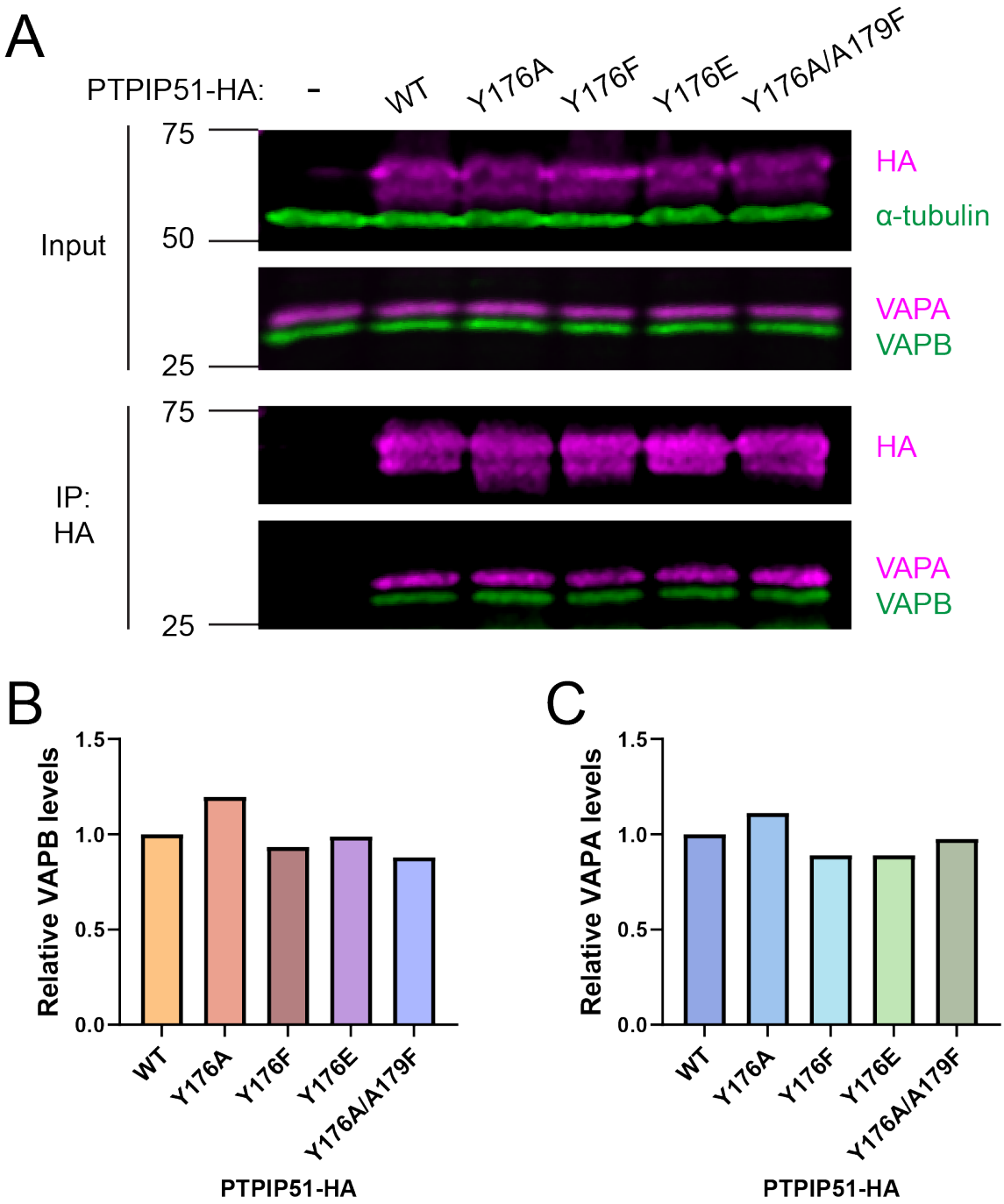

Figure 5-11 PTPIP51 tyrosine 176 is not necessary for binding to VAPA and VAPB.

A) HEK293 cells were transfected with empty vector pCI-neo, wild type (WT) PTPIP51-HA or PTPIP51-HA Y176 mutants (Y176A, Y176F, Y176E or Y176A/A179F). Cells were immunoprecipitated with an anti-HA antibody and immunoblotted, probing for HA, endogenous VAPA, VAPB and α-tubulin antibody as a loading control.

B & C) Graphs show the quantification of the level of VAPB **(B)** or VAPA **(C)** normalised to the level of immunoprecipitated PTPIP51-HA. *N* = 1. For input 45 µg protein was loaded. Immunoblot performed by Miss Eloise Brown.

5.7 Disruption of the MSP domain disrupts VAPB and VAPA binding to PTPIP51

Contrary to published data, within this study we found that disruption of PTPIP51 FFAT-like motifs does not change binding to VAPB or VAPA. Additionally, the phosphorylation site Y176 which is known to regulate PTPIP51 binding to Raf1 is not necessary for its interaction with VAPB or VAPA. One possibility for these results is that binding of PTPIP51 to VAP proteins is not mediated by their MSP domain. Data suggests that the MSP domain binds to FFAT motifs via a key hydrophobic pocket (Di Mattia *et al.*, 2020). Mutation of key residues within this groove have been shown to disrupt interaction of VAPA and VAPB with PTPIP51 (Cabukusta *et al.*, 2020). Thus, suggesting the MSP domain is necessary for interaction with PTPIP51.

To confirm this finding, we obtained DNA plasmid constructs of FLAG-VAPA and Myc-VAPB that had been mutated to disrupt the key MSP 'KFM' binding motif, K94D/M96D and K87D/M89D respectively (Figure 5-12) (Cabukusta *et al.*, 2020). HEK293 cells were transfected with empty vector pCI-neo, wild type FLAG-VAPA or Myc-VAPB, or their respective MSP mutant constructs. For immunoprecipitation of Myc-VAPB cells were immunoprecipitated with an anti-Myc antibody. Immunoprecipitation of FLAG-VAPA was completed using anti-FLAG antibody conjugated magnetic beads. The samples were immunoblotted for endogenous PTPIP51 and either Myc or FLAG (Figure 5-13, Figure 5-14). In line with published data, we observed that mutation of key residues within VAPA (Figure 5-14) and VAPB (Figure 5-13) depleted their interaction with PTPIP51. This confirms that the MSP domain is necessary for both VAPA and VAPB to bind to PTPIP51.

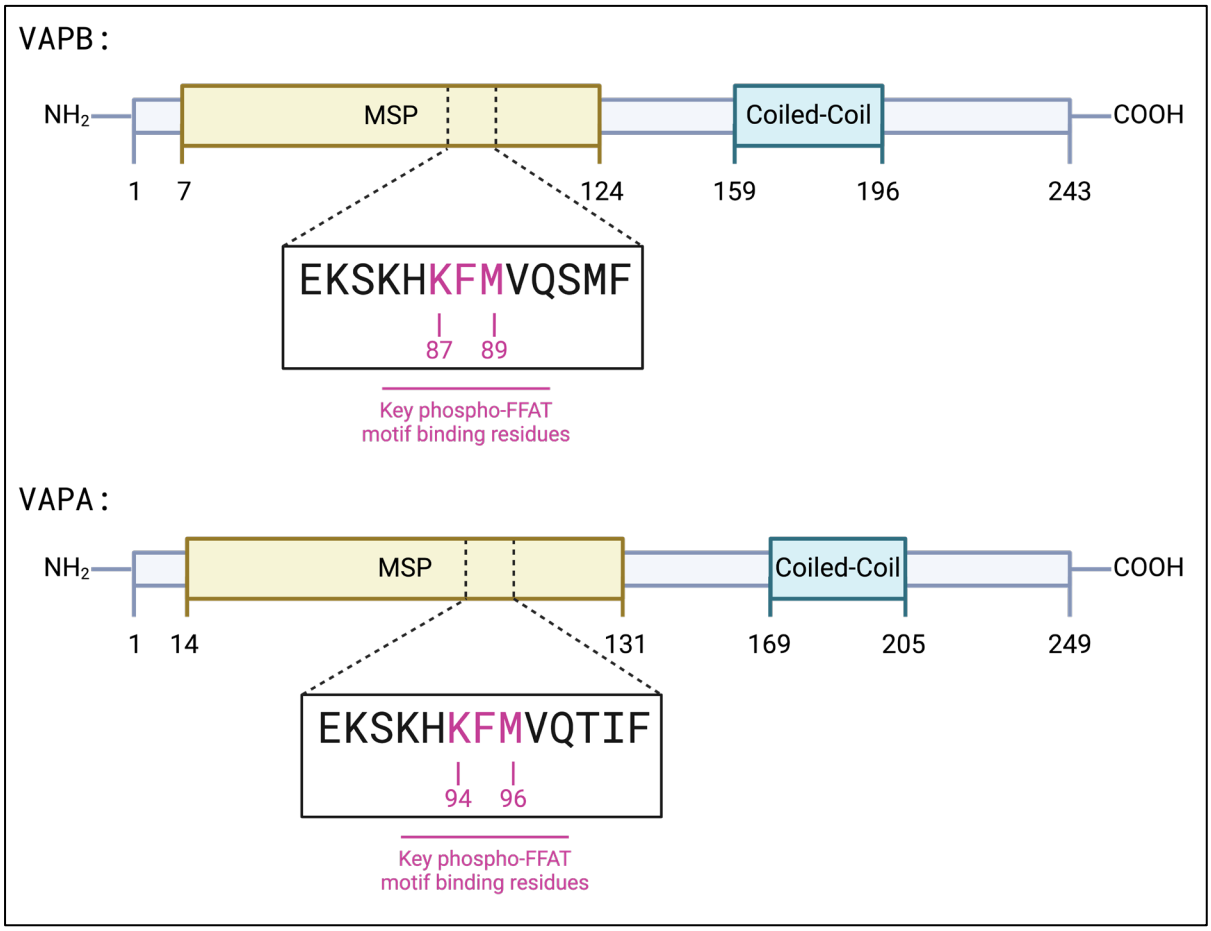

Figure 5-12 Summary of VAPB and VAPB MSP mutations investigated within this study.

Schematic diagram of the VAPB and VAPA protein structures. The key residues within the major sperm domain (MSP) of either protein that were mutated to determine their role in binding to PTPIP51 are highlighted in pink and labelled.

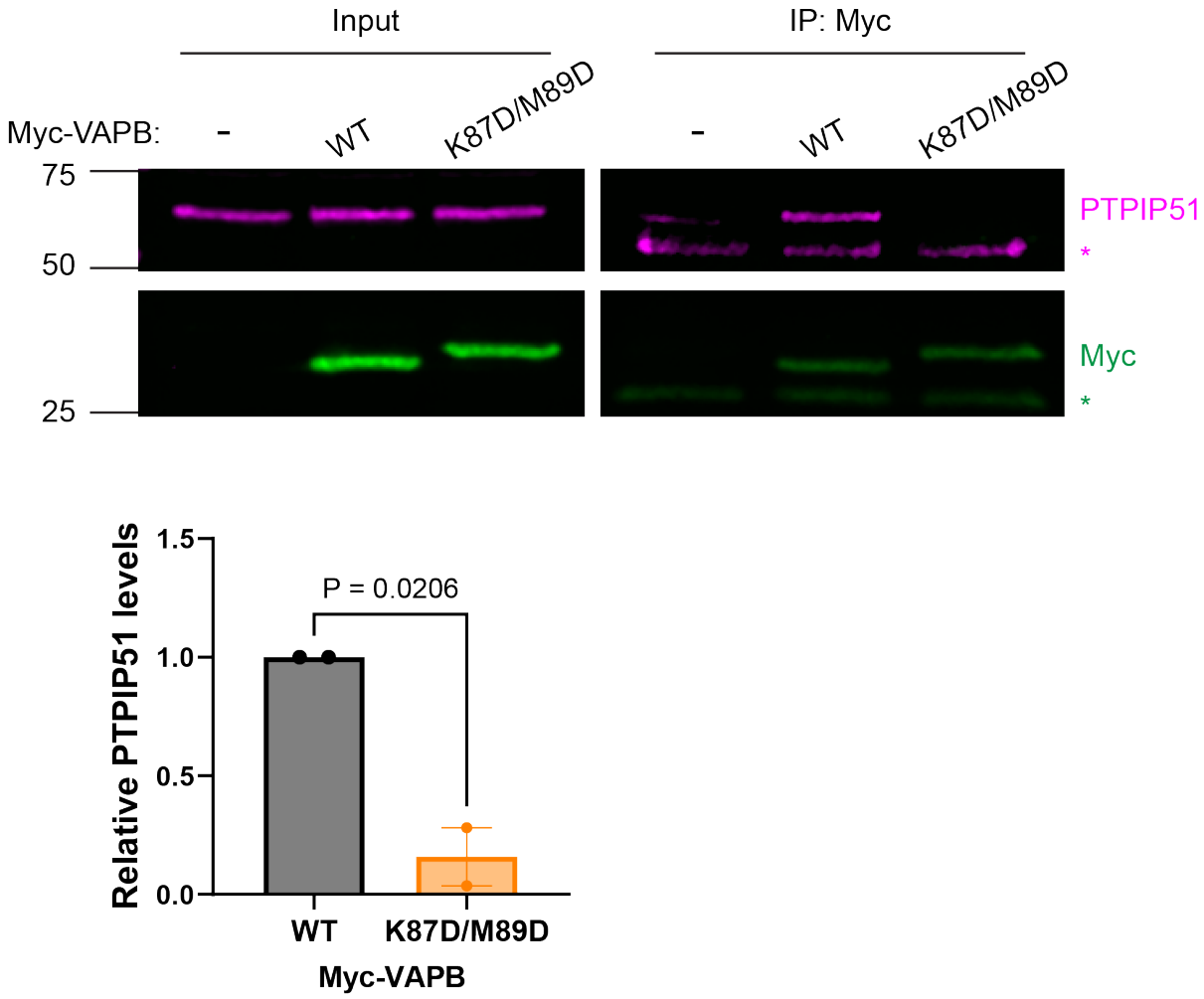

Figure 5-13 Mutation of key MSP domain residues disrupts VAPB binding to PTPIP51.

HEK293 cells were transfected with empty vector pCI-neo, wild type (WT) Myc-VAPB or major sperm protein (MSP) domain mutant Myc-VAPB K87D/M89D. Cells were immunoprecipitated with an anti-Myc antibody and immunoblotted, probing for Myc and endogenous PTPIP51. Graph shows the quantification of the level of PTPIP51 normalised to the level of immunoprecipitated Myc-VAPB. Bars represent mean ± SEM. Data were analysed by one-way ANOVA with Fisher's LSD, *N* = 2. For input 45 µg protein was loaded. Immunoblot performed by Miss Eloise Brown.

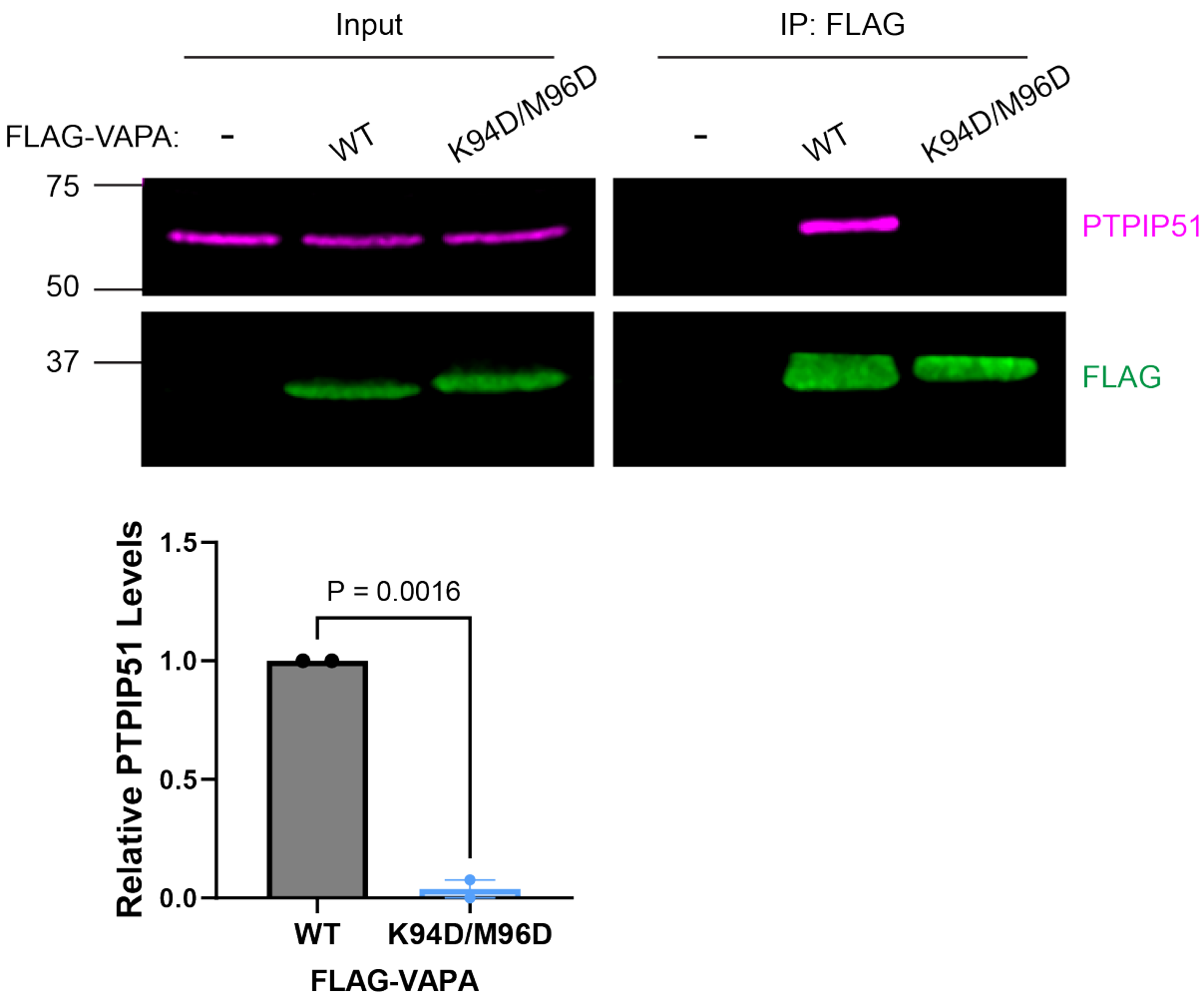

Figure 5-14 Mutation of key MSP domain residues disrupts VAPA binding to PTPIP51.

HEK293 cells were transfected with empty vector pCI-neo, wild type (WT) FLAG-VAPA or major sperm protein (MSP) domain mutant FLAG-VAPA K94D/M96D. Cells were immunoprecipitated with anti-FLAG conjugated beads and immunoblotted, probing for FLAG and endogenous PTPIP51. Graph shows the quantification of the level of PTPIP51 normalised to the level of immunoprecipitated FLAG-VAPA. Bars represent mean ± SEM. Data were analysed by one-way ANOVA with Fisher's LSD, *N* = 2. For input 45 µg protein was loaded. Immunoblot performed by Miss Eloise Brown.

5.8 Discussion

Multiple lines of evidence suggested that VAPB and VAPA interact with PTPIP51 by binding to an FFAT-like motif within PTPIP51 (Di Mattia *et al.*, 2020; Yeo *et al.*, 2021). PTPIP51 has been shown to contain two FFAT-like motifs, one conventional motif ($_{166}$TFTDAES$_{172}$) and one phospho-FFAT motif ($_{157}$VYF**T**ASS$_{163}$). It has not previously been established which of these FFAT motifs mediate binding to VAPA and VAPB. Studies previously suggested that the PTPIP51 FFAT-like motifs bind to the MSP domain of VAPA and VAPB (Di Mattia *et al.*, 2020; Kaiser *et al.*, 2005; Murphy and Levine, 2016). In these studies, they reported this interaction between the VAPB and VAPA MSP domains with peptides spanning the FFAT motif. However, whether disruption of these FFAT-like motifs in full length PTPIP51 protein prevents binding to VAPB or VAPA was not established.

In this chapter we show that the PTPIP51 FFAT-like motifs are not necessary for binding to VAPA and VAPB (sections 5.4 and 5.5). To investigate this, we used co-immunoprecipitation assays with overexpression of HA-tagged PTPIP51 with mutation of key residues within the motifs. Co-immunoprecipitation requires cell lysis, resulting in extraction of the proteins that are situated within membranes. This limits the technique, as we are unable to measure the level of protein-protein interactions within the context of the organelles that they localise, such as MAM. To overcome this limitation, we could utilise a technique such as proximity ligation assay , that allows quantification of protein interactions without disrupting cell morphology (Tubbs and Rieusset, 2016).

Studies investigating the interaction between VAPA and VAPB with FFAT motif containing proteins showed that phosphorylation of the phospho-FFAT may act as a switch to regulate binding (Di Mattia *et al.*, 2020; Kors *et al.*, 2022a; Kors *et al.*, 2022b). Our data shows that mutating the possible regulatory phospho-site within the PTPIP51 phospho-FFAT did not disrupt binding with VAPA or VAPB (Figure 5-8, Figure 5-9). In addition to this, whilst *in silico* modelling suggested the tyrosine 176 may mediate binding to the MSP domain (Figure 5-6, Figure 5-7), phospho-deficient mutation of this site had no effect (Figure 5-11). One possible explanation for this result is that phosphorylation of multiple phospho-sites within binding domains of PTPIP51 are necessary for its interaction with VAPA and VAPB. To determine this, we could test the endogenous binding between PTPIP51, VAPA and VAPB using co-immunoprecipitation, with the addition of phosphatase treatment. As the phosphatase PTP1B dephosphorylates PTPIP51 to regulate binding to Raf1, this could be used as a positive control (Brobeil *et al.*, 2011).

Within this study we only investigated the potential impact of disrupting individual FFAT-like motifs in PTPIP51. One possible mechanism for the interaction of PTPIP51 with VAPA or VAPB may involve the propensity of both identified FFAT-like motifs to bind. In line with our data, a recent study found that

removal of the phospho-FFAT motif does not disrupt binding to VAPB (Mórotz *et al.*, 2022). However, this study did not remove the second FFAT-like motif ($_{166}$TFTDAES$_{172}$). To confirm this theory, PTPIP51 binding to VAPA and VAPB could be tested with simultaneous mutation of both FFAT-like motifs. Another possible way to test the binding between VAPA, VAPB and PTPIP51 would be to investigate RMDN2. RMDN2 is a protein homologous to PTPIP51, although its protein function is not well characterised. Compared to PTPIP51, RMDN2 does not contain FFAT motifs, but there is conservation of amino acids spanning the tyrosine 176 in PTPIP51 (Figure 5-15A). *In silico* modelling suggests this conserved motif may bind to the VAPB MSP domain (Figure 5-15B). Analysis of the pLDDT scores of this predicted showed a very high degree of confidence in the accuracy of the local structure of the VAPB MSP domain and of key FFAT-like motif resides within the peptide (Figure 5-15C). In line with our previous predicted models, both the MSP domain and key FFAT-like motif residues within the RMDN2 peptide scored low PAE values (Figure 5-15D). The pTM and ipTM scores for the prediction were both above 0.8 (0.84 and 0.80 respectively, Table 5-1), suggesting a robust prediction of binding between the RMDN2 peptide and VAPB MSP domain. Indeed, proteomic studies suggest that VAPB binds to RMDN2 (Huttlin *et al.*, 2021; Huttlin *et al.*, 2017). Thus, investigating whether VAPB and RMDN2 bind in cells could confirm that VAPB is able to bind to PTPIP51 independent of any previously identified FFAT motifs.

Lastly, our finding confirms that mutation of key residues with the VAPB and VAPA MSP domains prevents binding to PTPIP51 (Figure 5-13, Figure 5-14). Considering we found no evidence of binding defects with disruption of PTPIP51 FFAT motifs, it is currently unclear whether MSP domains solely mediate binding to FFAT motifs as literature states (Kaiser *et al.*, 2005; Kim *et al.*, 2010a). A recent study found that removal of the PTPIP51 coiled-coil domain abolishes its interaction with VAPB (Mórotz *et al.*, 2022). Thus, one possible binding mechanism may be mediated by interaction between the PTPIP51 coiled-coil and the VAPB or VAPA MSP domain. However, *in silico* modelling does not predict binding between this coiled-coil domain and the VAPB MSP domain (Figure 5-16A & D). Indeed, AlphaFold3 prediction of the interaction between the VAPB MSP domain and a monomeric (Figure 5-16B) or dimeric (Figure 5-16E) form of the PTPIP51 coiled-coil domain showed a medium-to-low degree of confidence in the accuracy of the local structure with the pLDDT. Additionally, both predictions scored high PAE values (Figure 5-16C & F), and the pTM and ipTM scores for the prediction were both below 0.8 (Monomer: pTM 0.71, ipTM 0.20, Dimer: pTM 0.61, ipTM 0.20, Table 5-1). Together this suggests a low confidence prediction of binding between the PTPIP51 coiled-coil domain peptide and VAPB MSP domain.

To investigate this further, a protein fragment of the PTPIP51 coiled-coil domain should be produced. Co-immunoprecipitation of this protein fragment with VAPB or VAPA would determine if it is sufficient for interaction. Thus, further investigation is needed to elucidate the binding mechanism between PTPIP51, VAPA and VAPB.

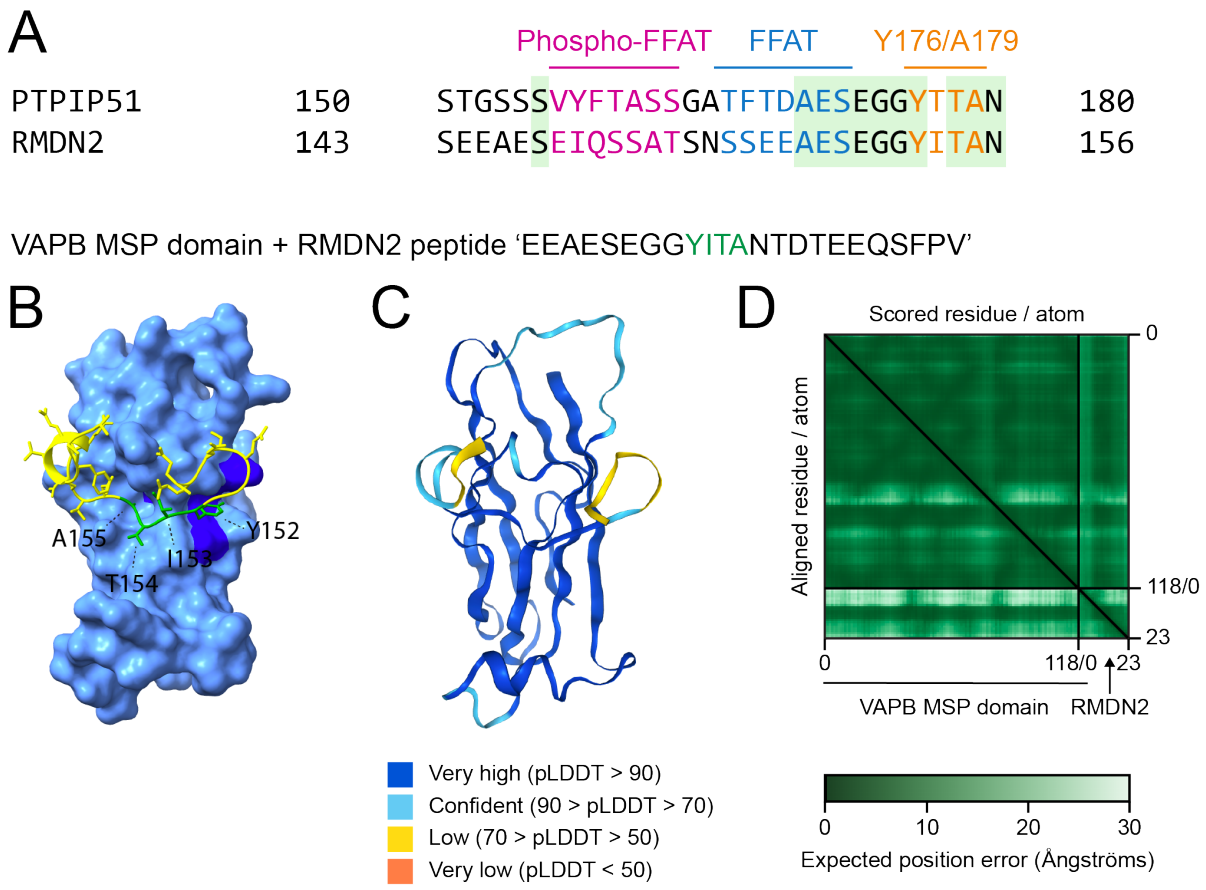

Figure 5-15 RMDN2 contains a conserved tyrosine residue that may regulate VAPB binding.

A) Partial sequence alignment between the PTPIP51 and RMDN2 proteins. Conserved residues are highlighted in green. RMDN2 does not contain a phospho-FFAT motif (pink) or FFAT motif (blue) but has conservation of an FFAT-like sequence Y152/A155 similar to PTPIP51 Y176/A179 (orange).

B) AlphaFold3 modelling prediction of the interaction between the VAPB major sperm protein (MSP) MSP domain (blue) and a RMDN2 peptide spanning the Y152/A155 residues (yellow). The resides of this new potential FFAT-like motif are highlighted in green and labelled. The key binding 'KFM' residues in the MSP domain are highlighted in dark blue.

C) predicted local distance difference test (pLDDT) scores of local confidences the predicted model.

D) Predicted aligned error (PAE) score of the model. Positioning between the key FFAT-like motif residues within the PTPIP51 peptide and the MSP domain have low expected error.

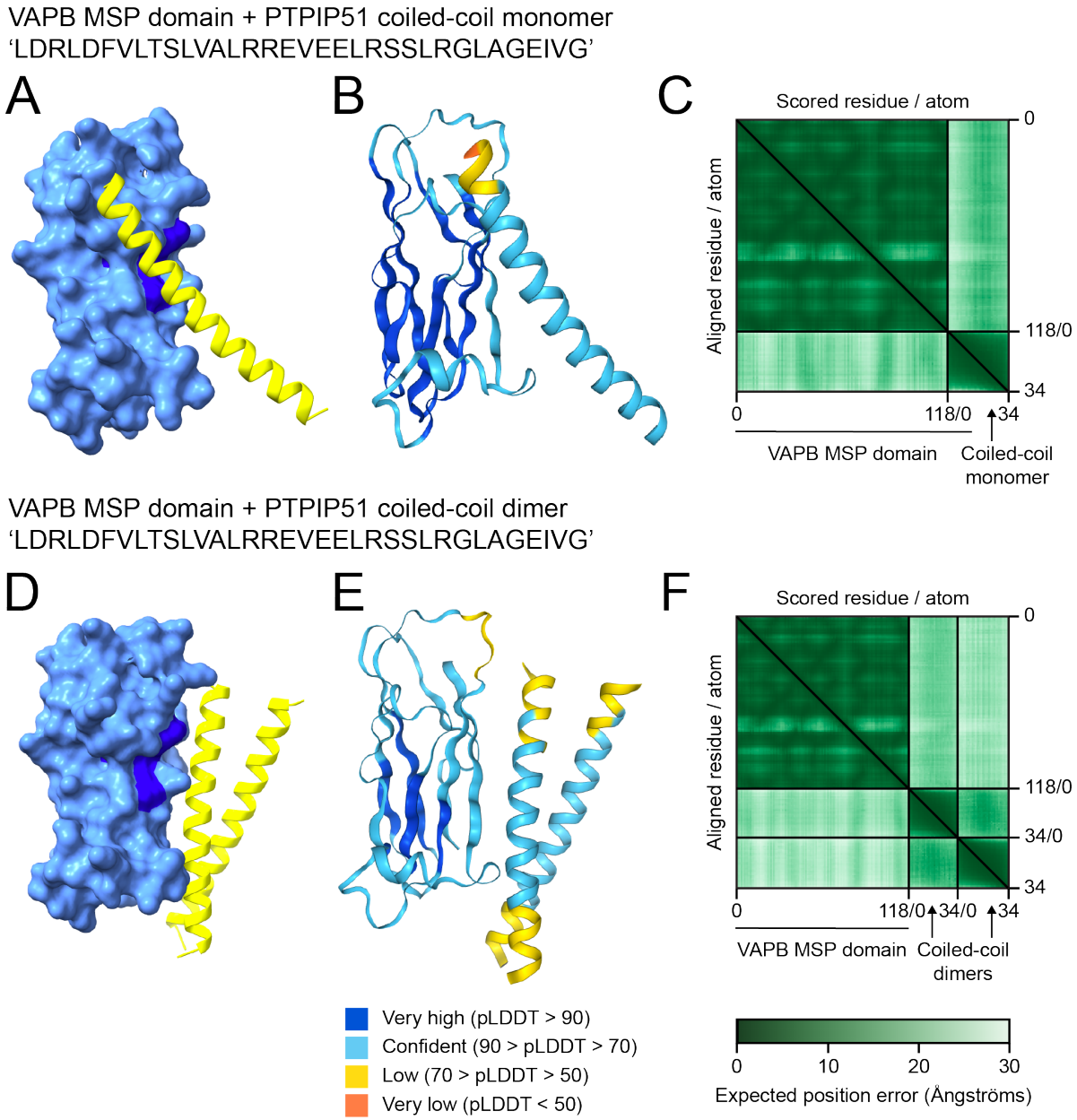

Figure 5-16 AlphaFold3 modelling does not predict PTPIP51 coiled coil binding to the VAPB MSP domain.

A & D) AlphaFold3 modelling predictions of the interaction between the VAPB major sperm protein (MSP) MSP domain (blue) and a monomeric **(A)** or dimeric **(D)** peptide of the PTPIP51 coiled-coil domain (yellow). The key binding 'KFM' residues in the MSP domain are highlighted in dark blue.

B & E) predicted local distance difference test (pLDDT) scores of local confidences for the respective predicted models. The structure of the VAPB MSP domain is confidently predicted in both models, although the PTPIP51 coiled-coil domain is less confidently predicted in both monomeric **(B)** and dimeric form **(E).**

C & F) Predicted aligned error (PAE) scores of the predicted models. The relative positioning of the VAPB MSP domain in respect to the PTPIP51 coiled-coil domain has a high expected position error in both monomeric **(C)** and dimeric form **(F).**

Table 5-1 Confidence values for predictions of protein interactions with AlphaFold3.

Figure	Model	ipTM	pTM
Figure 5-2	VAPB MSP domain & peptide spanning PTPIP51 phospho-FFAT motif 'SDSTGSSSVYFTASSGAT'	0.81	0.87
	VAPB MSP domain & peptide spanning mutant PTPIP51 phospho-FFAT motif 'SDSTGSSSVAAAASSGAT'	0.41	0.80
Figure 5-3	VAPA MSP domain & peptide spanning PTPIP51 phospho-FFAT motif 'SDSTGSSSVYFTASSGAT'	0.68	0.83
	VAPA MSP domain & peptide spanning mutant PTPIP51 phospho-FFAT motif 'SDSTGSSSVAAAASSGAT'	0.41	0.77
Figure 5-4	VAPB MSP domain & peptide spanning PTPIP51 FFAT-like motif 'SSGATFTDAESEGG'	0.85	0.91
	VAPB MSP domain & peptide spanning mutant PTPIP51 FFAT-like motif 'SSGATATDDESEGG'	0.57	0.87
Figure 5-5	VAPA MSP domain & peptide spanning PTPIP51 FFAT-like motif 'SSGATFTDAESEGG'	0.82	0.89
	VAPA MSP domain & peptide spanning mutant PTPIP51 FFAT-like motif 'SSGATATDDESEGG'	0.42	0.81
Figure 5-6	VAPB MSP domain & peptide spanning PTPIP51 FFAT-like Y176 motif 'ESEGGYTTANAESDNERDSD'	0.74	0.81
	VAPB MSP domain & peptide spanning mutant PTPIP51 FFAT-like Y176A motif 'ESEGGATTANAESDNERDSD'	0.32	0.78
Figure 5-7	VAPA MSP domain & peptide spanning PTPIP51 FFAT-like Y176 motif 'ESEGGYTTANAESDNERDSD'	0.74	0.81
	VAPA MSP domain & peptide spanning mutant PTPIP51 FFAT-like Y176A motif 'ESEGGATTANAESDNERDSD'	0.32	0.74
Figure 5-15	VAPB MSP domain & peptide spanning the RMDN2 conserved tyrosine residue 'EEAESEGGYITANTDTEEQSFPV'	0.80	0.84
Figure 5-16	VAPB MSP domain & monomeric peptide spanning the PTPIP51 coiled-coil domain	0.20	0.71
	VAPB MSP domain & dimeric peptide spanning the PTPIP51 coiled-coil domain	0.20	0.61

Chapter 6 Discussion

6.1 NEK1 may regulate nucleus to mitochondria signalling in the DDR

6.1.1 DNA damage repair

In response to genotoxic stress, a tightly regulated series of cell signalling pathways known as the DDR are triggered to promote DNA damage repair and cell survival (Giglia-Mari *et al.*, 2011). Upon activation by DNA damage, proteins localised in the nucleus such as PARP1 and SIRT1 consume NAD+ in order to promote DNA repair (Figure 1-11) (Cerutti *et al.*, 2014; Murata *et al.*, 2019). PARP1 condenses at sites of DNA breaks to mediate synapsis of broken DNA ends during DNA repair (Chappidi *et al.*, 2024). Whilst SIRT1 promotes the recruitment of DNA repair proteins such as Ku70 to the site of damage (Jeong *et al.*, 2007). In addition to NAD+, key DNA repair proteins such the DDR initiator protein ATM require ATP to initiate DNA repair (Kozlov *et al.*, 2003). The mitochondrial process OXPHOS synthesises ATP, and produces NAD+ as a byproduct of the electron transport chain due to oxidation of NADH by complex I (Chance and Williams, 1956). The electron transport chain also generates ROS as a byproduct of redox reactions by complexes I and III (Chance and Williams, 1956). Excessive levels of ROS can promote DNA damage (Mazat *et al.*, 2020). However, ROS can also promote DNA damage repair by activating ATM autophosphorylation and downstream stimulation of cell cycle arrest kinase Chk1 (Meng *et al.*, 2018; Xie *et al.*, 2021). As consumption by DDR proteins depletes cell levels of ATP and NAD+, this stimulates OXPHOS to meet cellular demands and promote DDR signalling. Thus, communication between the nucleus and mitochondria is necessary for this positive feedback cycle, to ensure sufficient NAD+ and ATP is available during the DDR process.

Influx of Ca^{2+} into the mitochondria promotes the synthesis of NAD+ and ATP by OXPHOS, as Ca^{2+} stimulates dehydrogenase enzymes with the TCA cycle to catalyse NADH and $FADH_2$, which are required for the electron transport chain (Figure 6-1) (Denton, 2009; Denton *et al.*, 1972). Indeed, transfer of Ca^{2+} between the ER and mitochondria is a key regulator of cell fate determination in response to cell stress, as prolonged mitochondrial Ca^{2+} influx promotes cell death (Shoshan-Barmatz *et al.*, 2010; Sukumaran *et al.*, 2021). ER to mitochondria transfer of Ca^{2+} is mediated by the IP3R-Grp75-VDAC1 protein complex (Atakpa-Adaji and Ivanova, 2023). It is well established that VAPB/PTPIP51 tethering mediates this Ca^{2+} transfer by promoting ER-mitochondria apposition and IP3R-VDAC1 association (Figure 6-1) (De Vos *et al.*, 2012; Gomez-Suaga *et al.*, 2017). In response to DNA damage a portion of NEK1 is recruited to mitochondria where it prevents apoptosis by phosphorylating VDAC1 (Chen *et al.*, 2009; Chen *et al.*, 2010b). Our data suggests that upon activation of NEK1 by DNA damage, it may also be recruited to MAM where VDAC1 localises to maintain Ca^{2+} homeostasis (Figure 3-16) (Ahumada-Castro *et al.*, 2021). Thus, one possible function of NEK1 at these contact sites may be to promote cell survival in response to DNA damage by regulation of

VAPB/PTPIP51 tethering and Ca^{2+} transfer. In agreement with this theory, we report that activation of NEK1 by camptothecin-induced DNA damage promotes NEK1 interaction with PTPIP51 and increases tethering between VAPB and PTPIP51 (Figure 4-12, Figure 4-13). This correlates with a decrease in the cytoplasmic Ca^{2+} levels upon IP3R-stimulated release from ER stores, which suggests an increase in mitochondrial Ca^{2+} uptake (Figure 4-14). Cells lacking NEK1 do not enhance VAPB/PTPIP51 tethering in response to DNA damage (Figure 4-13). Therefore, loss of NEK1-mediated regulation of VAPB/PTPIP51 tethering and Ca^{2+} transfer could prevent Ca^{2+} stimulated ATP and NAD+ production through the TCA cycle and OXPHOS. Insufficient production of ATP and NAD+ would prevent activation of DNA repair proteins such as PARP1 and ATM, leading to inefficient DNA repair and prolonged genotoxic damage. Thus, NEK1 may act as a key mediator of signalling between the nucleus and MAM in the DDR process.

It is well established that NEK1 and C21orf2 form a functional protein complex, and that C21orf2 is essential for efficient DNA damage repair (Fang *et al.*, 2015; Gregorczyk *et al.*, 2023; Watanabe *et al.*, 2020; Zelina *et al.*, 2024). Whilst literature has focussed on the mechanisms of NEK1 regulation of DNA damage repair, one possible role for C21orf2 in this pathway is to inhibit the degradation of NEK1 protein. Indeed, it has been reported that NEK1-mediated phosphorylation stabilises C21orf2 protein levels by inhibiting its interaction with the S phase kinase associated protein 1 (SKP1)–Cullin 1 (CUL1)-F box only protein 3 (SCF) complex, which in turn stabilises the NEK1 protein (Watanabe *et al.*, 2020). Multiple lines of evidence show that loss or mutation of C21orf2 lead to reduced levels of NEK1 protein in HeLa, HEK293 and iPSC-derived motor neurons (Fang *et al.*, 2015; Watanabe *et al.*, 2020; Zelina *et al.*, 2024), which coincides with a reduced NEK1 protein level in our C21orf2 knock out HeLa cells (Figure 3-1). Thus, C21orf2 may be necessary to stabilise NEK1 protein levels in order to facilitate the DDR (Figure 6-1).

In line with this mechanism, our data indicate that when exogenously expressed C21orf2 also interacts with the VAPB/PTPIP51 tether, via an indirect interaction with PTPIP51 (Figure 3-14, Figure 3-18). Furthermore, we observed that when C21orf2 has reduced binding to NEK1, due to disruption of its N-terminal domain, it no longer binds to PTPIP51 (Figure 3-15), suggesting that NEK1 is necessary for C21orf2 to interact with the VAPB/PTPIP51 tether. Whilst our data show that in physiological conditions endogenous C21orf2 is not present at MAM (Figure 3-16), it is suggested that in cells C21orf2 protein only exists when in complex with NEK1, but not vice versa, which would explain the C21orf2-independent roles of NEK1 such as mitosis regulation (Gregorczyk et al., 2023). Finally, C21orf2 was unable to correct VAPB/PTPIP51 tethering defects in cells lacking NEK1, confirming that NEK1 but not C21orf2 is necessary for regulation of this ER-mitochondria tether (Figure 4-5). Therefore, C21orf2 may be involved in the stabilisation of a population of NEK1 protein which is

recruited to MAM in response to DNA damage, however more research is necessary to confirm this theory.

6.1.2 Apoptosis

Activation of NEK1 kinase activity promotes phosphorylation of VAPB at multiple sites (Figure 4-22). In both our *in vitro* pulldown and in cell mass spectrometry experiments, we observed clustering of phosphorylated sites within the VAPB intrinsically disordered regions of VAPB (Figure 6-2). Recent evidence suggests that these disordered regions may act as flexible linkers that mediate protein interactions (Subra *et al.*, 2023). Truncation of the VAPA linker regions promotes localisation of VAPA to MAM and formation of tethers at these sites (Subra *et al.*, 2023). Whilst this has not been tested for VAPB, one possible explanation for phosphorylation of VAPB linker regions upon NEK1 activation may be to promote VAPB localisation and tethering to PTPIP51 at MAM.

Mass spectrometry of exogenously expressed VAPB revealed four phosphorylation sites (T150, S158, S160 and S206) with activation of NEK1 (Figure 4-22). The VAPB phosphorylation sites S158 and S160 have previously been identified in proteomic studies investigating DNA-damage induced phosphorylation (Beli *et al.*, 2012; Bennetzen *et al.*, 2010; Boeing *et al.*, 2016). Specifically, phosphorylation of S158 and S160 was found to be increased with induction of DNA damage by etoposide and irritating radiation (Beli *et al.*, 2012). The site S158 is predicted to be phosphorylated by the receptor-interacting serine/threonine-protein kinase 3 (RIPK3) (PhosphoSitePlus, Hornbeck *et al.*, 2015). RIPK3 forms a functional complex with the RIPK1, which it phosphorylates to regulate cell death by necroptosis and apoptosis (Ashida *et al.*, 2020; Cho *et al.*, 2009; He *et al.*, 2009). NEK1 has been shown to indirectly inhibit activation of RIPK1-mediated apoptosis (Amin *et al.*, 2018; Wang *et al.*, 2021a), suggesting NEK1 may act upstream of VAPB in order to mediate apoptosis (Figure 6-3).

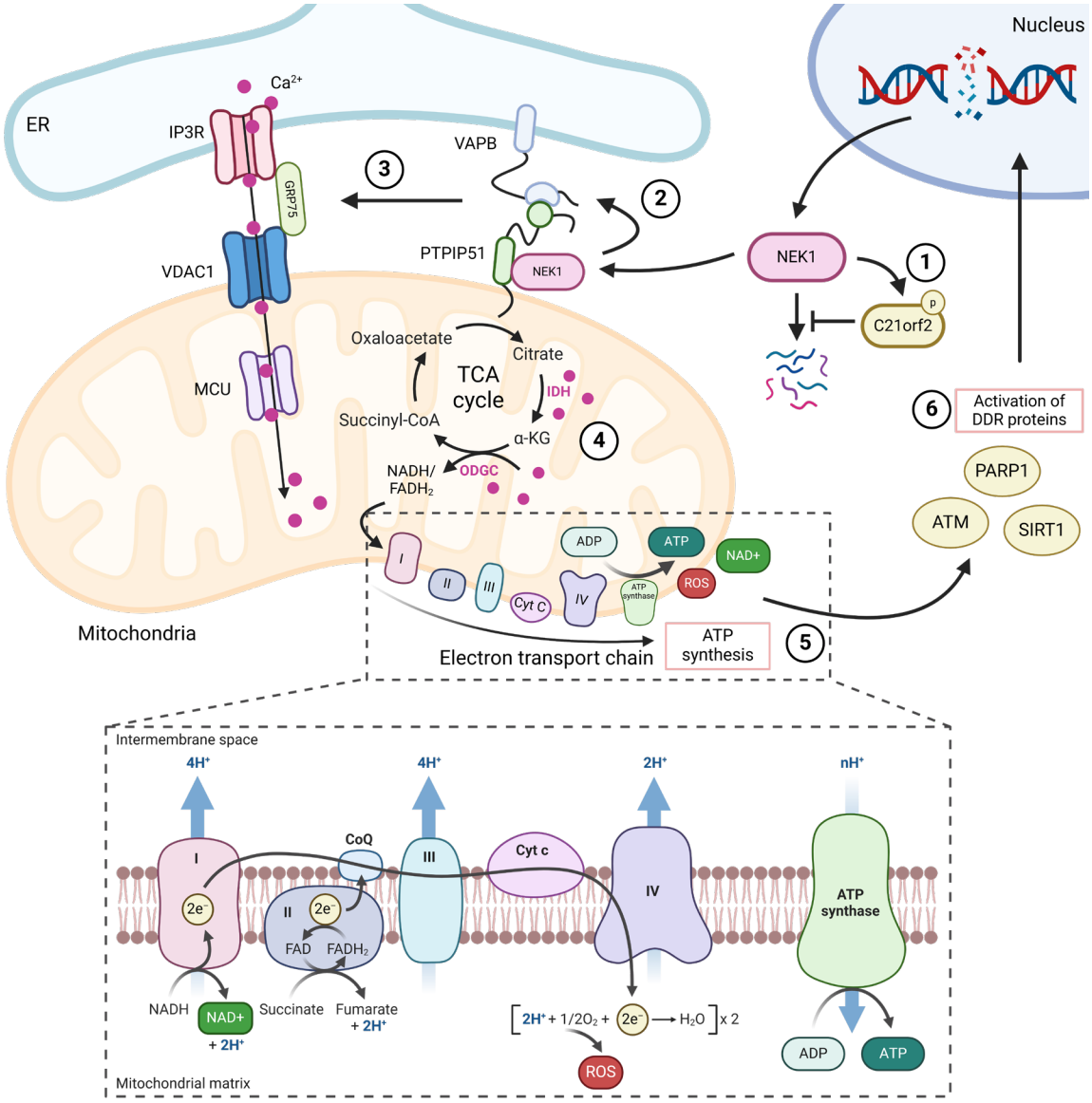

Figure 6-1 NEK1/C21orf2 regulation of VAPB/PTPIP51 tethering in response to DNA damage.

1) NEK1-mediated phosphorylation of C21orf2 stabilises protein levels by preventing C21orf2 interaction and ubiquitination by E3 ubiquitin ligases, which in turn stabilises the NEK1 protein.

2) In response to DNA damage, a portion of activated NEK1 interacts with PTPIP51 and promotes VAPB/PTPIP51 tethering.

3) This promotes IP3R/VDAC1 mediated transfer of Ca^{2+} from the ER to mitochondria.

4) Mitochondrial Ca2+ promotes the production of NADH and FADH2 by stimulating the dehydrogenases isocitrate dehydrogenase (IDH) and oxoglutarate dehydrogenase complex (ODGC) in the tricarboxylic acid (TCA) cycle.

5) NADH and FADH2 are utilised in the electron transport chain to produce ATP. This produces NAD+ and ROS as byproducts of redox reactions.

6) NAD+ can stimulate PARP1 and SIRT to promote DNA damage repair. ATP promotes DNA repair proteins such as ATM. ROS stimulates DNA repair proteins, but at excess levels can promote DNA damage.

The T160 phospho-site is suggested to be phosphorylated by the DNA-dependent protein kinase (DNA-PK) catalytic subunit (PRKDC), which acts as a sensor for DNA damage (Abe *et al.*, 2008). In response to DSBs, DNA-PK is recruited to the site of damage by the Ku70/Ku80 heterodimer (Spagnolo *et al.*, 2006). NEK1 is known to bind to Ku80, although it is not established whether NEK1 may phosphorylate Ku80 to regulate its function (Patil *et al.*, 2013). Upon activation of NEK1, we observed the presence of PRKDC peptides within our in cell VAPB mass spectrometry experiment, further implicating that DNA-PK may phosphorylate VAPB downstream of NEK1 activity (Figure 6-3). In response to prolonged DNA damage, excess levels of activated DNA-PK lead to activation of apoptosis (Hudson *et al.*, 2005). Together this suggests that NEK1 may lead to downstream phosphorylation of VAPB by DNA-PK to regulate apoptosis in response to DNA damage (Abe *et al.*, 2008).

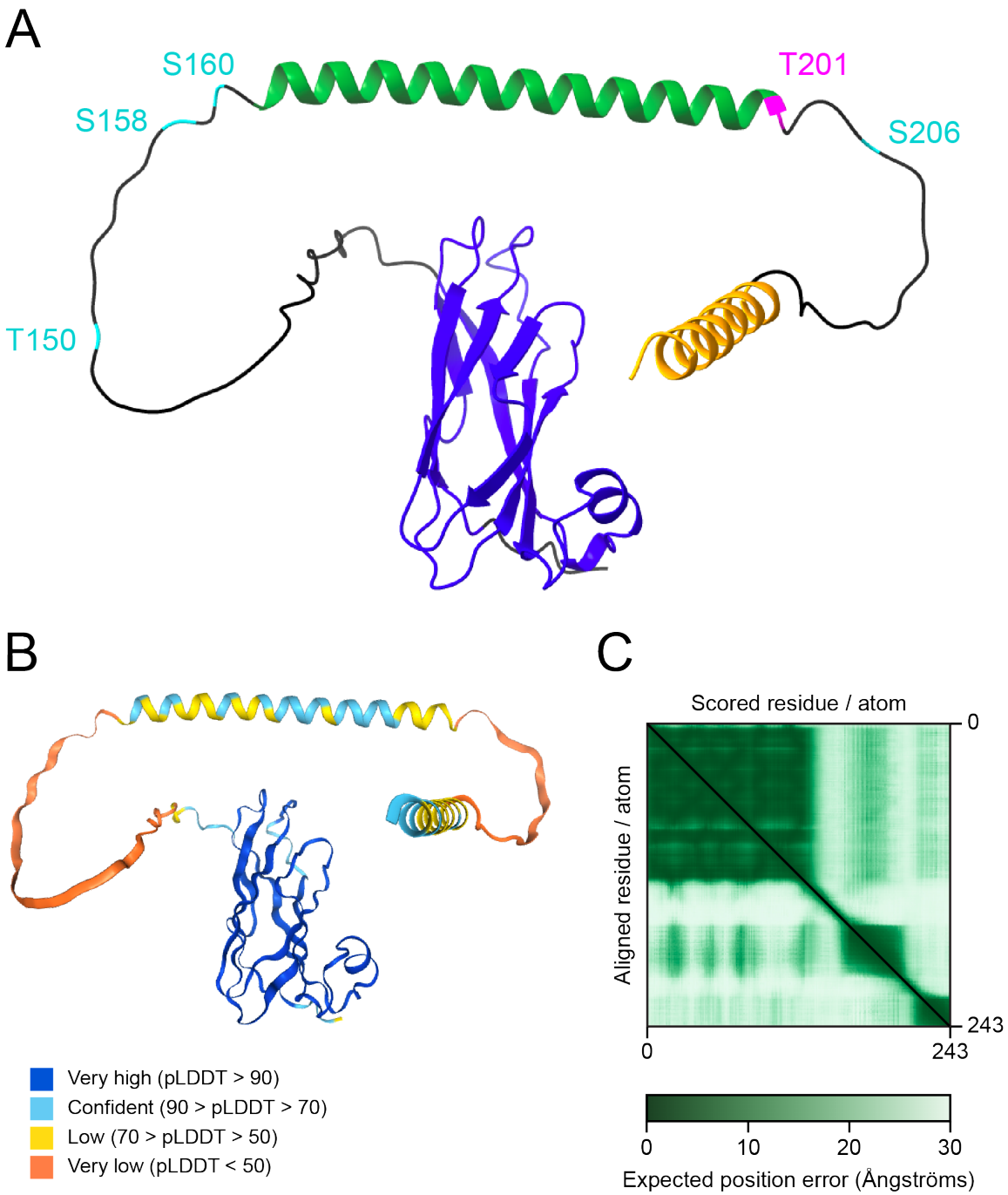

Figure 6-2 NEK1-induced VAPB phosphorylated sites cluster in disordered linker regions.

A) AlphaFold3 modelling prediction of the human VAPB protein, the main protein domains are colour-coded as follows: orange = transmembrane, green = coiled-coil, dark blue = major sperm protein (MSP). The potential NEK1 phosphorylation site pT201 identified *in vitro*, is labelled in magenta. The VAPB phosphorylation sites identified with activation of NEK1 in cells are labelled in cyan.

B) predicted local distance difference test (pLDDT) scores of local confidences for the predicted model.

C) Predicted aligned error (PAE) scores of the predicted model.

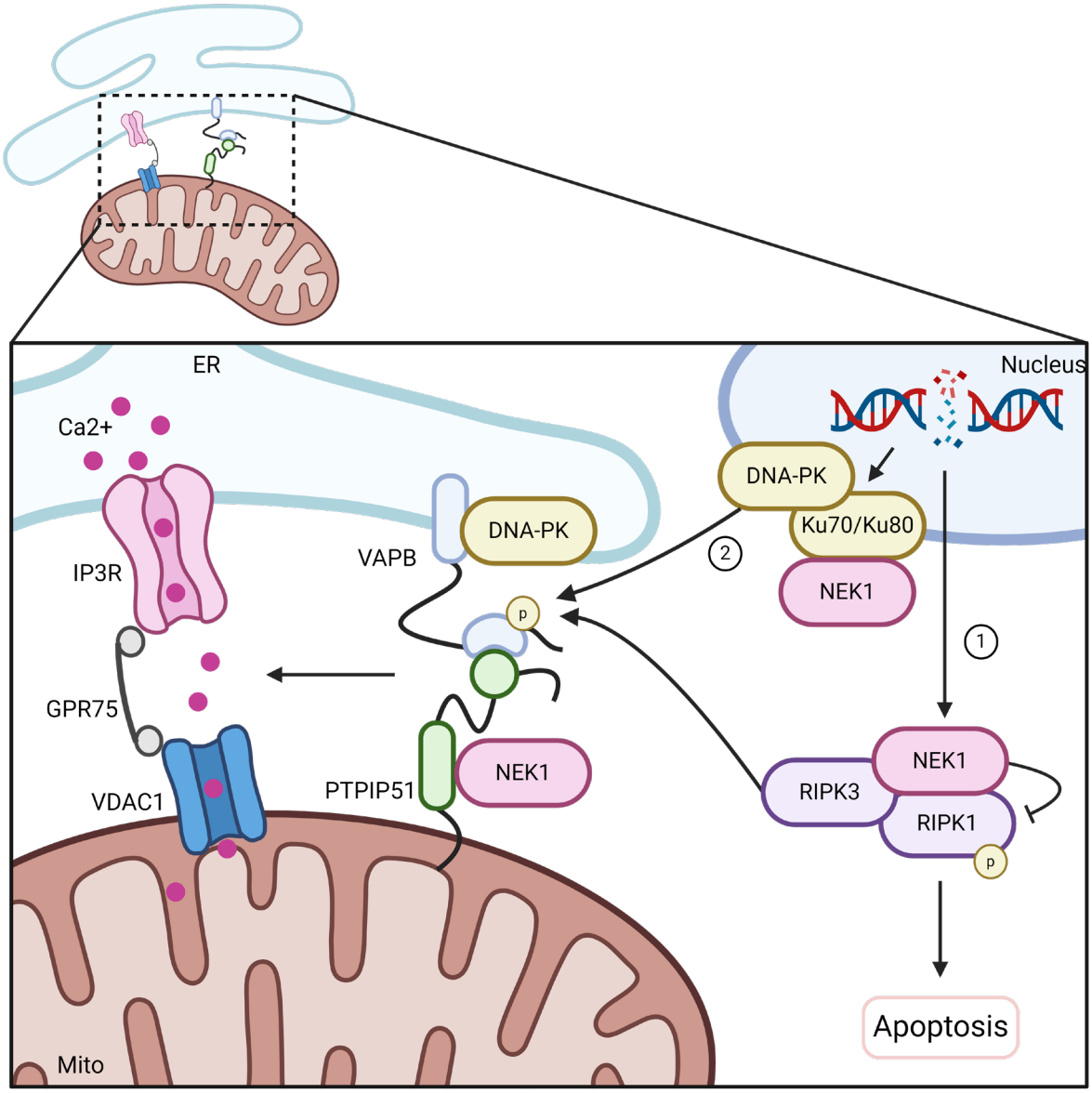

Figure 6-3 NEK1-induced phosphorylation of VAPB may regulate apoptosis.

1) In response to DNA damage NEK1 inhibits the activation of RIPK1 in order to prevent apoptosis. RIPK1 associates with RIPK3 in order to initiate RIPK1-dependent apoptosis. RIPK3 is predicted to phosphorylate VAPB at T158, although this needs further investigation.

2) In response to DNA damage activated DNA-PK recruits Ku70/Ku80 to promote DNA repair. NEK1 binds to Ku80, although the function of this interaction is unclear. We observed that DNA-PK binds to VAPB, and possibly phosphorylates VAPB at T160. Excess activation of DNA-PK leads to induction of apoptosis, possibly through excessive mitochondrial Ca^{2+} uptake.

In addition to phosphorylation of VAPB, we observed that activation of NEK1 by overexpression enhances the phosphorylation of PTPIP51 at S46 (**Error! Reference source not found.**). The PTPIP51 S46 phospho-site lies within a 14-3-3 binding domain (Yu *et al.*, 2008). Phosphorylation of this site negatively correlates with the level of apoptosis, as apoptotic cells exhibit reduced phosphorylation at PTPIP51 S46 (Brobeil *et al.*, 2012). This suggests that phosphorylation of PTPIP51 S46 may inhibit induction of apoptosis. It is not yet clear which kinase phosphorylates this site, although considering we do not observe phosphorylation of PTPIP51 by NEK1 *in vitro* (Figure 4-16), it is unlikely to be a direct NEK1 phosphorylation site. PhosphoSitePlus predicts this to be a large tumour suppressor kinase 2 (LATS2) phosphorylation site (Hornbeck *et al.*, 2015). LATS2 is well established as a negative regulator of Yes-associated protein 1 (YAP1), promoting YAP1/14-3-3 interaction and degradation (Figure 6-4) (Hao *et al.*, 2008; Zhao *et al.*, 2010). Regulation of YAP1 is mediated upstream by RASSF1 activation of STK3 and STK4 which phosphorylate LATS2 to promote YAP1 degradation (Guo *et al.*, 2011; Karchugina *et al.*, 2021). Disinhibition of YAP1 causes its nuclear translocation and transcription of both anti- and pro-apoptotic proteins, which is known at the Hippo pathway (Zhang *et al.*, 2018a). In response to DNA damage, LATS2 has been shown to prevent YAP1-mediated induction of apoptosis (Reuven *et al.*, 2013). Additionally, Chk1 phosphorylation of LATS2 at its kinase domain promotes LATS2 kinase activity to inhibit apoptosis by inhibition of CDK and phosphorylation of 14-3-3 (Okada *et al.*, 2011; Suzuki *et al.*, 2013a). Considering NEK is known to phosphorylate Chk1 during the DDR to promote DNA repair, one possible mechanism is through a NEK1 > Chk1 > LATS2 > PTPIP51 signalling cascade to inhibit apoptosis in response to DNA damage. Furthermore, NEK1 is known to directly phosphorylates YAP1 in order to stabilise the protein and promote cell survival by inhibiting apoptosis (Khalil and De Benedetti, 2022; Khalil *et al.*, 2020). This suggests that NEK1 may regulate YAP1 both directly and upstream, to promote cell survival upon genotoxic stress. Proteomic data suggests that VAPA and VAPB interact with STK3 and STK4 (Hauri *et al.*, 2013; Huttlin *et al.*, 2021). In our study we observed VAPB interaction with multiple proteins in this pathway including RASSF1, STK3 and STK4. In drosophila the STK3/3 orthologue Hpo and the VAPA/VAPA orthologue Vap33 were shown to interact in order to activate the YAP signalling pathway (Portela *et al.*, 2024). Thus VAPA, VAPB and PTPIP51 may be involved in this signalling cascade, which is regulated in part by NEK1. How NEK1 may act in this signalling cascade to regulate VAPB/PTPIP51 tethering is not yet clear, but regulation of apoptosis appears to be a possible function of this pathway.

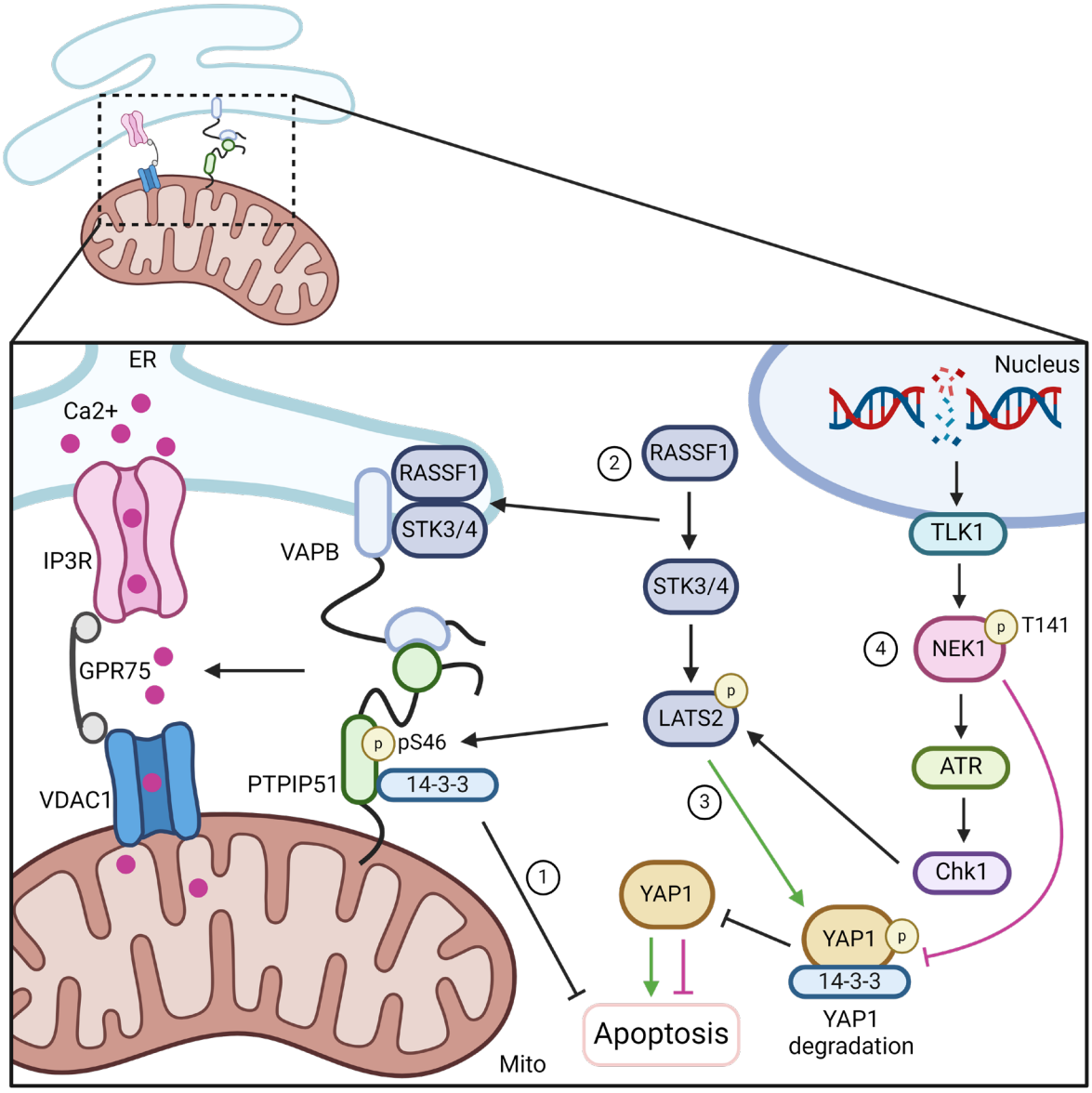

Figure 6-4 NEK1-induced phosphorylation of PTPIP51 may regulate apoptosis.

1) Phosphorylation of PTPIP51 S46 is upregulated with activation of NEK1. This site regulates binding to 14-3-3 as inhibits induction of apoptosis.

2) Phosphorylation of PTPIP51 S46 is predicted to be phosphorylated by LATS2. LATS2 is regulated upstream by RASSF1 and STK3/4 which are suggested to bind to VAPB.

3) LATS2 inhibits YAP2 mediated apoptosis by promoting YAP1/14-3-3 binding and degradation (green arrows).

4) In response to DNA damage the TLK1 > NEK1 > ATR > Chk1 pathway is activated to promote cell cycle arrest and DNA repair. NEK1 inhibits YAP1 by phosphorylation to stabilise the protein and inhibit apoptosis (pink arrows). Chk1 can phosphorylate LATS2 to promote its kinase activity.

In line with the theory that NEK1-induced phosphorylation of VAPB may promote apoptosis, MAM regulation of Ca^{2+} homeostasis had been linked to control of apoptosis (Bahar *et al.*, 2016). Elevated mitochondria Ca^{2+}, such as by prolonged influx through VDAC1 can promote mitochondrial depolarisation and opening of the mitochondrial permeability transition pore (mPTP) (Baumgartner *et al.*, 2009). Sustained opening of the mPTP leads to mitochondrial swelling and rupture, causing release of cytochrome c into the cytosol which promotes initiation of apoptosis (Bernardi *et al.*, 2023). In agreement with this, prolonged phosphorylation of VDAC1 by NEK1 leads to cell death (Chen *et al.*, 2009), suggesting NEK1 may have dual functions at MAM in the DDR. Upon activation by mild or transient genotoxic stress NEK1 may promote VAPB/PTPIP51 tethering to increase ER-mitochondria Ca^{2+} and DNA damage repair (section 1.3.2.4). However, upon excessive DNA damage NEK1 may promote apoptosis by indirect phosphorylation of VAPB and VDAC1-mediated opening of the mPTP. Due to time limitations, we were unable to investigate whether phosphorylation of the identified VAPB and PTPIP51 phospho-sites upregulated by NEK1 may regulate VAPB/PTPIP51 interaction. Therefore, further investigation into these phospho-sites may elucidate the mechanism of NEK1 regulation of MAM in response to DNA damage.

6.1.3 Cell cycle regulation

Of the four identified phosphorylation sites, T150 was found to be the most enriched phosphorylation site with NEK1 overexpression. This phosphorylation site has been identified 20 times in high throughput proteomic studies and has been shown to be phosphorylated in response to inhibition of mitosis (Dulla *et al.*, 2010; Kettenbach *et al.*, 2011; Santamaria *et al.*, 2011). In line with this, recent evidence suggests that like NEK1, VAPB is involved in regulation of cell cycle progression, as knock out of VAPB leads to cell cycle arrest and reduced proliferation in medulloblastoma cells (Faria Assoni *et al.*, 2023). Furthermore, VAPB has been shown to interact with the nucleoporin ELYS during anaphase by binding to the ELYS phospho-FFAT motif in a phosphorylation dependent manner (James *et al.*, 2024). Together this suggests that NEK1 may act upstream of VAPB, leading to phosphorylation of VAPB at T150 and progression of cell cycle. Thus, in line with the role of NEK1 in halting cell cycle progression during DNA repair, DNA damage induced NEK1 recruitment to MAM may promote cell cycle arrest via VAPB (Chen *et al.*, 2008; Pelegrini *et al.*, 2010). In future it would be interesting to determine whether NEK1 may regulate VAPB/ELYS interaction by direct phosphorylation of ELYS.

6.2 NEK1/AMPK signalling may regulate VAPB/PTPIP51 tethering

AMPK is a crucial cellular energy sensor that helps maintain energy balance and supports cell survival (Herzig and Shaw, 2018). Multiple lines of evidence suggest that AMPK is involved in the DDR by promoting ATP production to meet the metabolic needs of DNA repair proteins, and activating SOD proteins to cope with oxidative stress (Figure 1-6) (Gwinn *et al.*, 2008; Marino *et al.*, 2021). In response to metabolic stress, AMPK phosphorylates the NEK1-interacting kinase RIPK1 at S415 in order to inhibit stress-induced cell death (Figure 6-5) (Zhang *et al.*, 2023). In addition to regulation of apoptosis, RIPK1 has been shown to bind to AMPK to inhibit the induction of autophagy by inhibition of mTORC1 in response to energetic stress (Najafov *et al.*, 2021). This suggests that in response to DNA damage, AMPK may interact with RIPK1 in order to promote cell survival by limiting autophagy and apoptosis. In line with this potential role of AMPK, the activation of NEK1 inhibits RIPK1-dependent apoptosis (Amin *et al.*, 2018). NEK1-deficiency in mice leads to postnatal lethality and blood brain barrier damage (Wang *et al.*, 2021a). This is due to disinhibition of RIPK1 and thus sensitisation to RIPK1-dependent apoptosis. Interestingly, loss of NEK1 impairs the trafficking of glucose transporter GLUT1 to the plasma membrane, leading to metabolic defects (Wang *et al.*, 2021a). Considering AMPK promotes GLUT1 expression to increase glucose uptake in response to metabolic demands (Wu *et al.*, 2013), AMPK/NEK1 regulation of RIPK1 may act as an axis to regulate metabolism and cell death in response to genotoxic stress.

NEK1 is known bind to 14-3-3 (Sonntag *et al.*, 2017). Regulation of NEK1/14-3-3 binding is dependent on the phosphorylation of NEK1 T1052, which is a key residue within the 14-3-3 binding motif (Sonntag *et al.*, 2017). The NEK1 T1052 phospho-site has been reported to be phosphorylated by AMPK (Figure 6-5) (Jiang *et al.*, 2022; Sonntag *et al.*, 2017). AMPK-mediated phosphorylation of NEK1 T1052 has been reported in response to DNA damage induced by IR (Jiang *et al.*, 2022). This suggests that in response to DNA damage, AMPK may phosphorylate NEK1 in order to promote binding to 14-3-3. Currently the function of NEK1/14-3-3 binding is unclear. Studies have shown that 14-3-3 binding can modulate protein subcellular localisation by masking nuclear localisation or export sequences (Muslin and Xing, 2000). Our shows that NEK1 is partially localised to MAM and that NEK1/PTPIP51 interaction is increased upon DNA damage. Thus, one possible explanation is that AMPK-phosphorylation promotes 14-3-3 binding to NEK1 in order to promote NEK1 localisation at MAM, although further investigation is needed to confirm this.

GSK3β is a metabolic sensor involved in protein and lipid synthesis and glucose and mitochondrial metabolism pathways (Papadopoli *et al.*, 2021). The interaction between VAPB and PTPIP51 has been shown to be negatively regulated by the kinase GSK3β (Stoica *et al.*, 2014; Stoica *et al.*, 2016). Whilst the mechanisms of GSK3β regulation of VAPB/PTPIP51 tethering is not yet clear, one possible pathway

is through GSK3β/AMPK/NEK1 signalling (Figure 6-5). It is known that activated GSK3β binds to and phosphorylates AMPK in order to inhibit its kinase activity (Suzuki *et al.*, 2013b). Thus, GSK3β-mediated inhibition of AMPK may lead to reduced NEK1 recruitment to MAM, and reduced VAPB/PTPIP51 tethering. Multiple lines of evidence suggest that GSK3β is activated in response to genotoxic stress in order to activate DNA repair proteins such as p53-binding protein 1 (53BP1) and prevent activation of apoptosis by p53 (Ngok-Ngam *et al.*, 2013; Watcharasit *et al.*, 2002; Yang *et al.*, 2018). In response to DNA damage induction by cisplatin, GSK3β was found in the NEK1 protein interactome (Melo-Hanchuk *et al.*, 2017). One possible mechanism of GSK3β regulation of VAPB/PTPIP51 tethering is that under homeostatic conditions GSK3β inhibits AMPK, preventing NEK1 translocation and regulation at MAM. However, upon genotoxic stress, a portion of NEK1 binds to GSK3β in order to disinhibit AMPK. This could promote AMPK stimulated translocation of NEK1 to MAM to regulate VAPB/PTPIP51 binding. GSK3β has a predicted NEK1 phosphorylation site within its disordered region at T395, although whether this is a true phosphorylation site is not yet clear. Together this suggests, in response to DNA damage, NEK1, AMPK and GSK3β may form a signalling complex to regulate VAPB/PTPIP51 tethering. However, the specific mechanisms underlying this potential pathway is not yet clear.

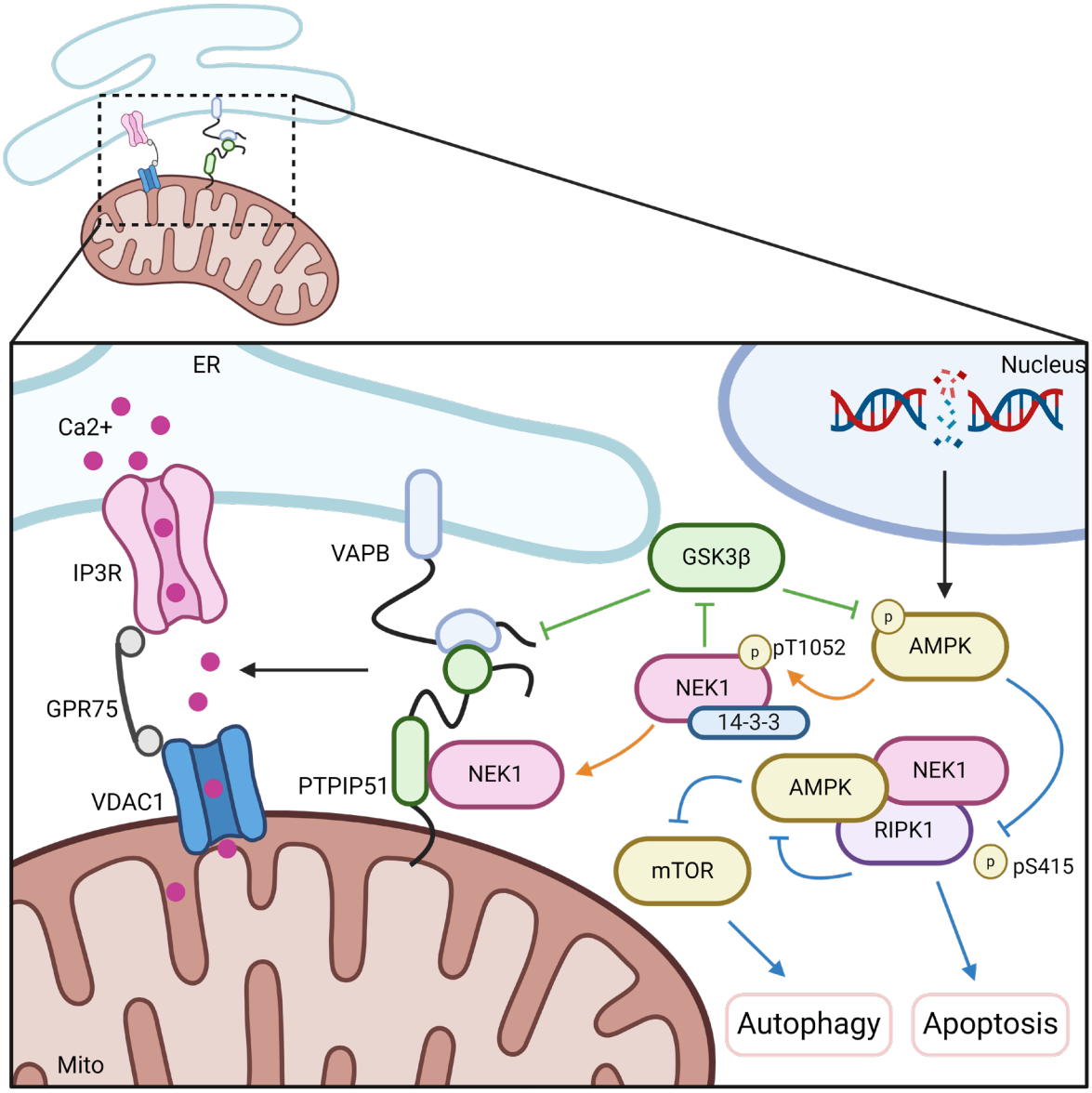

Figure 6-5 Potential NEK1/AMPK/GSK3β regulation of VAPB/PTPIP51 tethering.

Black arrow: In response to metabolic and genotoxic stress AMPK is activated to promote cell survival.
Blue arrows: AMPK phosphorylates RIPK1 to inhibit apoptosis. RIPK1 can bind to AMPK to inhibit induction of autophagy by mTOR disinhibition. NEK1 can also prevent apoptosis by inhibiting activation of RIPK1.
Orange arrows: AMPK phosphorylates NEK1 at T1052 to promote binding to 14-3-3. This interaction may promote NEK1 recruitment to MAM.
Green arrows: GSK3β inhibits VAPB/PTPIP51 tethering. This may be due to inhibition of AMPK as GSK3β binds to and phosphorylates AMPK to inhibit its kinase activity. NEK1 is suggested to interact with GSK3β. One possibility is upon DNA damage NEK1 binds to and inhibits GSK3β, leading to AMPK disinhibition and promotion of NEK1 recruitment to MAM.

6.3 Disruption of MAM disruption in NEK1/C21orf2 related ALS

6.3.1 NEK1 and C21orf2-deficiency disrupts VAPB/PTPIP51 tethering

Disruption of ER-mitochondria contacts has been well reported in multiple models of ALS (Lee *et al.*, 2024). In particular, there is increasing evidence that VAPB/PTPIP51 tethering is disrupted in sporadic (Hartopp *et al.*, 2022), FUS (Stoica *et al.*, 2016), TDP-43 (Stoica *et al.*, 2014) and C9orf72-related ALS (Gomez-Suaga *et al.*, 2022). Loss of function mutations in NEK1 cause familial and sporadic ALS (Brenner *et al.*, 2016; Kenna *et al.*, 2016). However, whether disruption of VAPB/PTPIP51 tethering is a characteristic of NEK1-ALS has not previously been investigated. Our data shows that NEK1 LOF in HeLa cells disrupts VAPB/PTPIP51 tethering and apposition between the ER and mitochondria (Figure 4-1, Figure 4-3, Figure 4-7). In line with loss of contact between the ER and mitochondria, NEK1 deficient cells exhibit disrupted Ca^{2+} transfer between the organelles (Figure 4-10). Dynamic changes in Ca^{2+} signalling is critical for synaptic transmission, as pre-synaptic Ca^{2+} levels mediate neurotransmitter release (Devine and Kittler, 2018). Whilst Ca^{2+} alterations regulate dendritic excitability and synaptic plasticity (Segal, 2005; Sjostrom *et al.*, 2008). VAPB/PTPIP51 tethers have been reported at synapses, where they regulate synaptic function and dendritic spine morphology (Gómez-Suaga *et al.*, 2019). Loss of synaptic function is well established to underlie motor neuron degeneration in ALS (Bae and Kim, 2017; Herms and Dorostkar, 2016). Thus, loss of VAPB/PTPIP51 tethering may contribute to ALS due to loss of Ca^{2+} regulation at synapses, leading to dendritic pathology.

As previously discussed, influx of Ca^{2+} into the mitochondria is essential for regulation of ATP (Figure 6-1) (Denton, 2009; Denton *et al.*, 1972). Reduced ER-mitochondria Ca^{2+} transfer and ATP production has been well reported in multiple models including SOD1 (Lautenschlager *et al.*, 2013; Scaricamazza *et al.*, 2020), TDP-43 (Stoica *et al.*, 2014; Wang *et al.*, 2019), FUS (Ghiasi *et al.*, 2012; Stoica *et al.*, 2016) related ALS. Motor neurons have high metabolic needs due to energetically demanding processes such as axonal transport (De Vos *et al.*, 2008). Thus, loss of ATP production due to reduced ER-mitochondria connection may prevent neurons from meeting cellular metabolic demands, leading to defective mitochondria function, axonal transport, and neurodegeneration (Cozzolino *et al.*, 2013; Millecamps and Julien, 2013). Production of ATP is also essential for the activation of key DNA damage repair proteins (Kozlov *et al.*, 2003). NEK1 LOF mutations in motor neurons causes accumulation of DNA damage, possibly due to reduced activation of ATM-mediated DNA repair (Higelin *et al.*, 2018). Thus, loss of NEK1-mediated VAPB/PTPIP51 tethering in response to DNA damage may prevent signalling between the nucleus and mitochondria in the DDR (Figure 6-1).

In line with the evidence that loss of NEK1 disrupts ER-mitochondria contacts, we observed that C21orf2 LOF in HeLa cells disrupts VAPB/PTPIP51 tethering (Figure 4-1, Figure 4-6) and apposition

between the ER and mitochondria (Figure 4-8). As previously discussed, C21orf2 is suggested to be necessary for the stabilisation of NEK1 protein levels by preventing its degradation by the UPS (Watanabe *et al*., 2020), thus loss of C21orf2 also leads to a loss of NEK1 phenotype (Figure 6-6). Furthermore, evidence suggests that the ALS-related V58L mutation in *C21orf2* leads to hyperphosphorylation of C21orf2 protein by NEK1. This leads to inhibition of C21orf2 association with the E3 ubiquitin ligase SCF complex and subsequent inhibition of C21orf2 and NEK1 protein degradation by the UPS, leading to co-aggregation of C21orf2 and NEK1 (Watanabe *et al*., 2020). Thus, aggregation of C21orf2 and NEK1 proteins lead to a NEK1 loss of function phenotype, similar to that seen in post-mortem tissue of patients with ALS-related *NEK1* mutations (Rifai *et al.,* 2024). In line with this, a recent study found that iPSC-derived motor neurones derived from *C21orf2* V58L ALS patients show post-transcriptional downregulation of NEK1, increased apoptosis, reduced mitochondrial activity and impaired DDR (Zelina *et al.,* 2024). Indeed, the NEK1 loss of function phenotype could be reverted by inhibition of the proteasome or by isogenic correction of the V58L mutations (Zelina *et al.,* 2024). Thus, ALS-related mutations in C21orf2 may lead to co-aggregation of NEK1 protein, preventing NEK1 to perform its critical functions in the DDR (Figure 6-6).

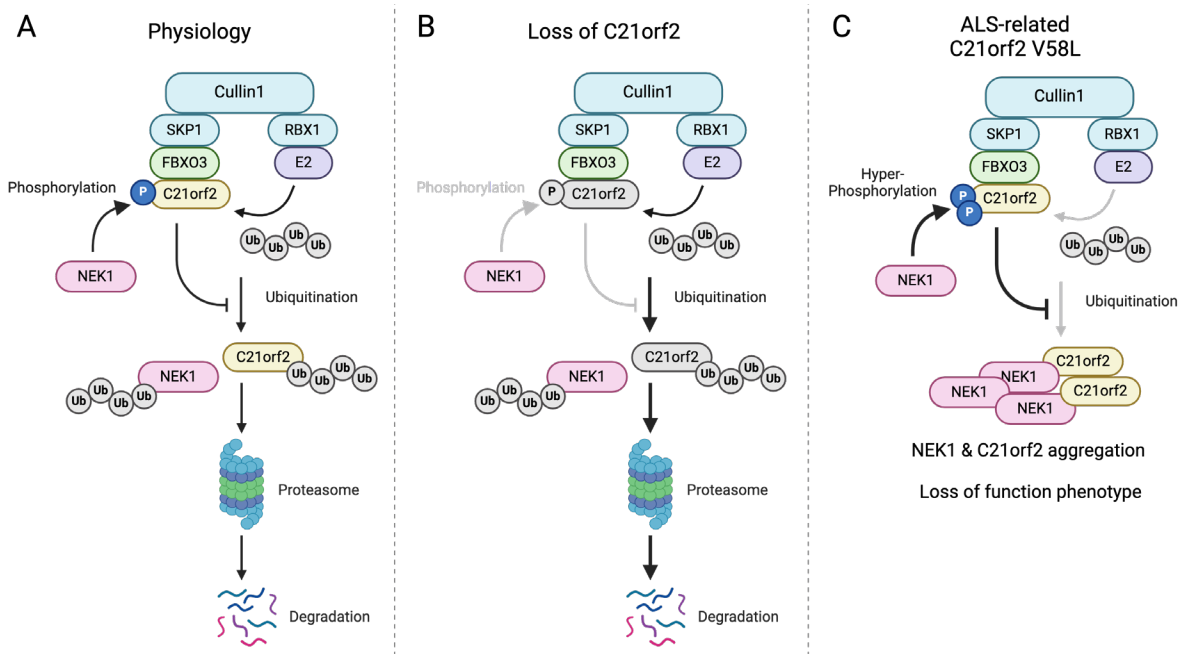

Figure 6-6 C21orf2-mediated disruption of NEK1 in ALS.

A) In physiological conditions, NEK1-mediated phosphorylation of C21orf2 prevents it's interaction with the F box only protein 3 (FBXO3), preventing its ubiquitination by the S phase kinase associated protein 1 (SKP1)-Cullin 1 E3 ubiquitin ligase complex. This in turn prevents degradation of both NEK1 and C21orf2 by attenuating degradation by the proteasome.

B) Loss of C21orf2 leads to destabilisation of NEK1 protein due to disinhibition of NEK1 degradation by the ubiquitin-proteasome system (UPS), and a NEK1 loss of function phenotype.

C) The ALS-related C21orf2 V58L mutation leads to hyperphosphorylation by NEK1, which in turn leads to excessive inhibition of the UPS and co-aggregation of NEK1 and C21orf2 protein. This results in a loss of function phenotype due to aggregation of NEK1 protein.

6.3.2 *NEK1* mutations as a 'second hit' in ALS aetiology

Accumulating evidence suggests that ALS is an oligogenic disease, with multiple genetic insults contributing to disease manifestation (Iacoangeli *et al.*, 2024). Approximately 1.8% of all cases, and 30 – 50% of NEK1 mutation carriers are oligogenic (Iacoangeli *et al.*, 2024; Lattante *et al.*, 2021; Nguyen *et al.*, 2018). It is well established that NEK1 LOF mutations lead to accumulation of DNA damage in ALS patient-derived motor neurons (Higelin *et al.*, 2018). Whilst to a lesser extent, patient derived C9orf72 mutant motor neurons also exhibit DNA damage accumulation (Higelin *et al.*, 2018). A recent study showed that motor neurons carrying both toxic C9orf72 repeat expansions and a NEK1 LOF mutation exhibit increased DNA damage levels compared to single mutant cells (Santangelo *et al.*, 2024). Interestingly, C9orf72 repeat expansions have been shown to inhibit VAPB/PTPIP51 tethering in iPSC-derived cortical neurons and mutant C9orf72 transgenic mice (Gomez-Suaga *et al.*, 2022). Toxic C9orf72 DPRs activate GSK3β which is known to inhibit VAPB/PTPIP51 tethering and AMPK activation (Gomez-Suaga *et al.*, 2022). One possibility is that NEK1 and C9orf72 may contribute to ALS pathology through GSK3β-mediated inhibition of VAPB/PTPIP51 tethering. As loss of VAPB/PTPIP51 interaction disrupts Ca^{2+} transfer between the ER and mitochondria, this may lead to decreased ATP production. As ATP is necessary for DNA damage repair, this could lead to insufficient DNA damage repair, DNA damage accumulation and neurodegeneration (Hargreaves and Crabtree, 2011).

Recent evidence shows that NEK1 expression is downregulated in the $TARDBP^{Q331K}$ transgenic mouse model (Jiang and Ngo, 2022; White *et al.*, 2018). In addition to downregulation, NEK was differentially spliced in post-mortem tissue from ALS cases exhibiting TDP-43 pathology (Ziff *et al.*, 2023). Considering TDP-43 pathology is observed in 97% of ALS cases, this suggests decreased NEK1 function may be a common characteristic of ALS (Mackenzie *et al.*, 2007). Indeed, TDP-43 has been reported in cases of ALS harbouring NEK1 LOF and missense mutations (Rifai *et al.*, 2024). Interestingly, the $NEK1^{R261H}$ missense mutation leads to NEK1-positive cytoplasmic aggregations that co-occur in cells with TDP-43 aggregates (Rifai *et al.*, 2024). Overexpression of wild type or mutant TDP-43 has been shown to inhibit VAPB/PTPIP51 tethering, possibly due to activation of GSK3β (Markovinovic *et al.*, 2024; Stoica *et al.*, 2014). Defective VAPB/PTPIP51 tethering and downstream synaptic function can be rescued by overexpression of VAPB or PTPIP51 (Markovinovic *et al.*, 2024). As our data shows that activation of NEK1 promotes VAPB/PTPIP51 tethering, stimulation of NEK1 may be a potential therapeutic target in TDP-43 associated ALS.

NEK1 is known to regulate the MAM protein VDAC1 in order to prevent cell death in response to genotoxic stress (Chen *et al.*, 2009). The Ca^{2+} transfer capacity of the IP3R-Grp75-VDAC1 channel is tightly regulated by apposition of the ER and mitochondria, which is controlled by VAPB/PTPIP51 tethering (De Vos *et al.*, 2012). Multiple lines of evidence suggest that VDAC1 activity is disrupted in

SOD1-related ALS. Transgenic $SOD1^{G93A}$ mice exhibit increased VDAC1 expression and increased protein oligomerisation which triggers apoptosis (Abu-Hamad *et al.*, 2008; Pittala *et al.*, 2020; Shteinfer-Kuzmine *et al.*, 2022). Wild type and mutant SOD1 has been shown to bind to VDAC1, leading to reduced channel activity (Shteinfer-Kuzmine *et al.*, 2022). Reduced VDAC1 activity would lead to decreased mitochondrial uptake of Ca^{2+}. A decrease in mitochondria Ca^{2+} could lead to decreased ATP production by OXPHOS, and thus inability to meet cellular energy demands which could contribute to motor neuron disease pathology (Cárdenas *et al.*, 2010). Interestingly, wild type SOD1 protein aggregations have been reported in cases of NEK1-related ALS, although it is not currently known if VDAC1 is defective in these cases (Forsberg *et al.*, 2019). Activating VDAC1 activity in $SOD1^{G93A}$ mice rescues mitochondrial defects (Magri *et al.*, 2024). Thus, investigating the NEK1/VDCA1/SOD1 axis could highlight a new therapeutic avenue to target mitochondrial disruption downstream of ER-mitochondrial defects in ALS.

Recent evidence suggests that the NEK1-interactor RIPK1 is also dysregulated in $SOD1^{G93A}$ mice (Ito *et al.*, 2016; Zelic *et al.*, 2024). In these mice RIPK1 expression is upregulated, leading to activation of RIPK1-dependent apoptosis and axonal pathology. Additionally, RIPK1 is inhibited by the ALS-associated protein OPTN (Ito *et al.*, 2016). ALS-associated loss of OPTN leads to disinhibition of RIPK1 and progressive axonal degeneration (Ito *et al.*, 2016). Whether NEK1 expression or function is changed in these models of ALS is not yet clear, but activation of NEK1 to promote RIPK1 inhibition may be a strategy for treatment of *SOD1* and *OPTN*-related ALS.

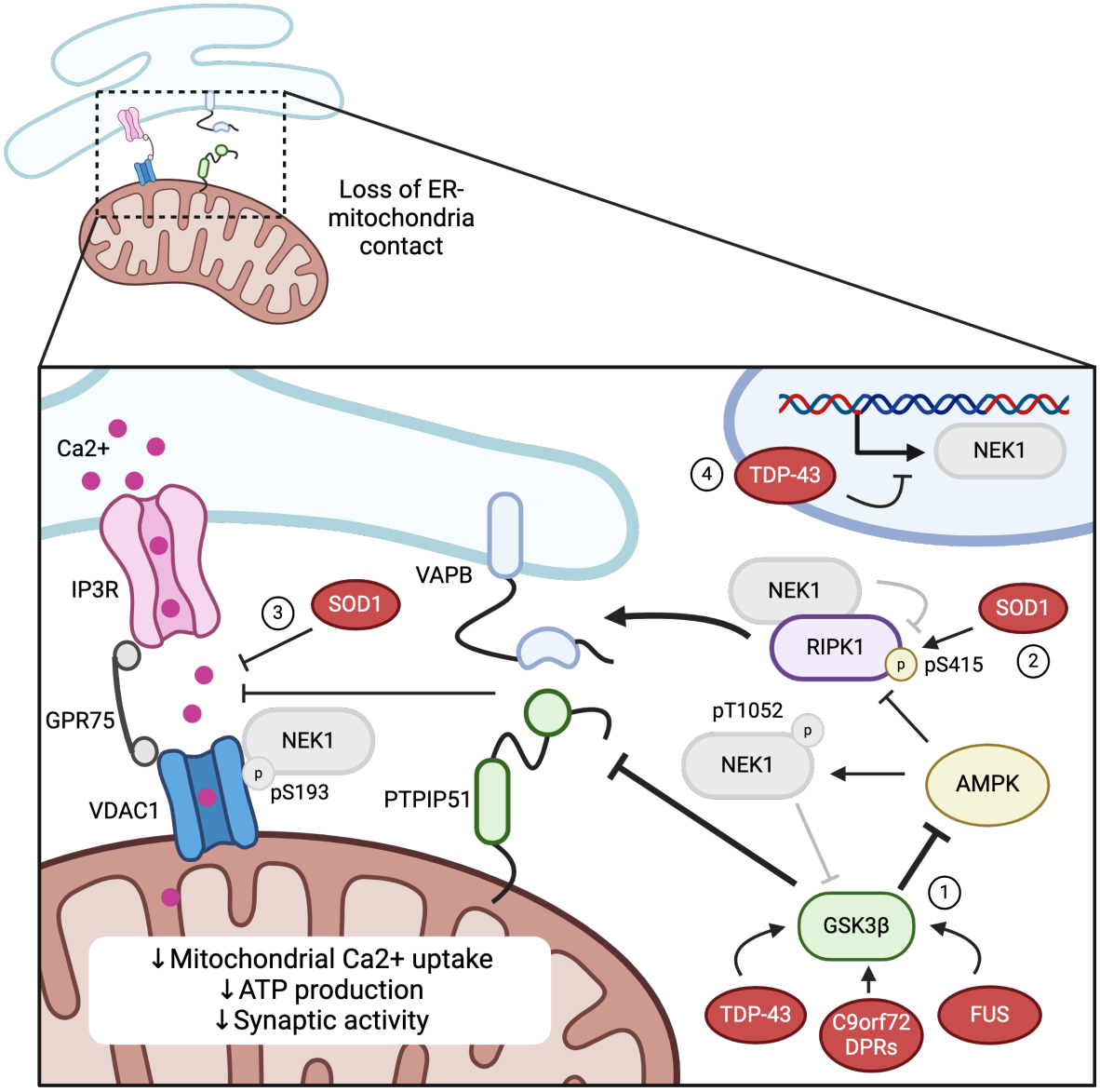

Figure 6-7 Potential mechanisms of MAM disruption in NEK1-related ALS.

Loss of NEK1 reduces VAPB/PTPIP51 tethering and Ca^{2+} transfer into mitochondria via IP3R/VDAC1. This may reduce ATP production and synaptic activity, leading to neurodegeneration.

1) C9orf72 toxic DPRs, TDP-43 and FUS activate GSK3β which inhibits AMPK and VAPB/PTPIP51 tethering. Loss of NEK1 may prevent disinhibition of AMPK and thus increased inhibition of VAPB/PTPIP51 tethering.

2) Mutant SOD1 activates RIPK1 leading to increased RIPK1-dependent apoptosis. This may promote RIPK1/RIPK3 phosphorylation of VAPB to disrupt VAPB/PTPIP51 tethering. This may be exacerbated by loss of NEK1-mediated RIPK1 inhibition.

3) SOD1 binds to VDAC1 to reduce the channel activity, preventing Ca^{2+} transfer, leading to mitochondrial dysfunction. Loss of NEK1 phosphorylation of VDAC1 may exacerbate this effect and promote apoptosis.

4) TDP-43 downregulates NEK1 expression, thus loss of NEK1 function may be a common pathogenic mechanism in 97% of ALS cases.

6.4 Future directions

6.4.1 How does NEK1-mediated phosphorylation regulate VAPB/PTPIP51 tethering?

In this study we investigated the role of NEK1-mediated regulation of VAPB/PTPIP51 tethering upon activation of NEK1 by DNA damage. We observed that upon activation by camptothecin, NEK1 interaction with the tethering protein PTPIP51 is increased. NEK1 interaction with PTPIP51 in this response promotes tethering between PTPIP51 and VAPB. Considering NEK1 can be activated by multiple genotoxic stressors, future experiments should confirm whether other NEK1-activating stressors such as cisplatin, H2O2 or IR would elicit the same response. Currently the binding mechanism between NEK1 and PTPIP51 is not yet established. To determine how NEK1 bind to PTPIP51, fragments of NEK1 and PTPIP51 protein domains should be created and tested for interactions in co-immunoprecipitation assays. To determine if NEK1 localisation at MAM is due to interaction with PTPIP51, cell fractionation should be performed in cells lacking PTPIP51 to determine if this disrupts NEK1 localisation to the sites.

Our data suggests that NEK1 regulates VAPB/PTPIP51 tethering by promoting phosphorylation of both proteins. It is currently unclear how phosphorylation of the proteins affects their binding. It is suggested that VAPB/PTPIP51 binding is mediated through the MSP and FFAT domains respectively (Di Mattia *et al.*, 2020; Yeo *et al.*, 2021). Our data suggests that disruption of PTPIP51 FFAT-like motifs does not disrupt binding to VAPB. However, disrupting the VAPB MSP domain ablates binding to PTPIP51. To confirm which domains, interact, protein fragments of the PTPIP51 domains and FFAT motifs should be produced and tested for interaction with VAPB on co-immunoprecipitation. Alternatively, simultaneous disruption of the three identified FFAT-like motifs in PTPIP51 should tested. This would determine whether VAPB/PTPIP51 binding can be mediated by more than one FFAT-like motif, which would explain why disruption of just one motif does not affect binding. Finally, to determine if VAPB/PTPIP51 interaction is mediated by direct phosphorylation cells should be treated phosphatases to cause dephosphorylation of the proteins.

Mass spectrometry data suggests that NEK1 activation causes of multiple VAPB and PTPIP51 phosphorylation sites. To determine the effect of these sites on VAPB/PTPIP51 phospho-deficient and phospho-mimicking mutation of the residues should be produced. These mutants should be tested for co-immunoprecipitation for the other protein to determine if phosphorylation of any of the sites directly mediates protein interactions. It is currently unclear which kinase directly phosphorylates these sites. To elucidate this, *in vitro* kinase assays can be utilised to test phosphorylation of recombinant wild type and phospho-deficient mutant proteins by predicted kinases such as GSK3β, AMPK and DNA-PK. If we establish which kinase directly phosphorylates VAPB and PTPIP51, we can next determine whether loss of NEK1 disrupts VAPB/PTPIP51 tethering by loss of kinase signalling. To

do this PLA of endogenous VAPB/PTPIP51 could be done in NEK1 KO with activation of the identified kinase. With the expectation that rescuing downstream kinase activity would restore VAPB/PTPIP51 tethering. Furthermore, this could be tested with physiological inhibition of the NEK1 kinase.

In this study we observe that loss of NEK1 leads to disruption of Ca^{2+} between the ER and mitochondria. Currently the effect of loss of NEK1-mediated Ca^{2+} homeostasis is not yet clear. Considering NEK1 is known to be involved in inhibition of apoptosis (Chen *et al.*, 2009), the level of apoptosis and cell viability should be measured in NEK1 KO cells using established assays, such as cytochrome c release or lactate dehydrogenase (LDH) (Crowley *et al.*, 2016; Kumar *et al.*, 2018). As NEK1 is established as protein involved in the DDR, the level of DNA damage should be determined by measurement of γH2AX foci or a comet assay (Mah *et al.*, 2010; Olive and Banáth, 2006). To determine these effects are due to NEK1-deficiency mediated loss of VAPB/PTPIP51 tethering, synthetic ER-mitochondria tethers should be used to reestablish if reconnecting the organelles corrects the defects (Csordas *et al.*, 2010).

6.4.2 How does loss of NEK1 regulation of VAPB/PTPIP51 tethering lead to ALS?

Our data suggests that loss of NEK1 leads to disrupted VAPB/PTPIP51, an effect that has been well reported in cell models of ALS. To determine if loss of NEK1-mediated MAM disruption is a contributor to ALS, this finding should be replicated in a more disease relevant model such as iPSC-derived motor neurons (Higelin *et al.*, 2018). As we have only investigated NEK1 LOF, expression of NEK1 missense mutation carrying plasmid constructs should be expressed in NEK1 KO cells to determine if these mutations lead to the same disruption. Additionally, the C21orf2^{V58L} missense mutation should be expressed in C21orf2 KO cells to determine if this mutation disrupts VAPB/PTPIP51 tethering.

In ALS synaptic impairment has been suggested to have an active role in pathogenesis due to its onset prior to axonal degeneration (Gómez-Suaga *et al.*, 2019). VAPB/PTPIP51 tethers have been identify at synapses and disruption of ER-mitochondria contacts has been shown to dysregulate synaptic activity (Gomez-Suaga et al., 2017). Thus, loss of NEK1/C21orf2 may affect synaptic function, particularly in response to DNA damage. To assess this, synaptic function at single synapse level can be measured in neurons with miRNA-induced NEK1/C21orf2 knockdown by FM dye and pHluorin assays (Gaffield and Betz, 2006; Royle *et al.*, 2008).

6.5 Conclusions

Within this study we have identified a novel signalling complex involving NEK1, C21orf2 and the VAPB/PTPIP51 tether that regulates ER-mitochondria interactions. We observe that NEK1 directly binds to PTPIP51, an interaction that is promoted by DNA damage. Induction of DNA damage promotes VAPB/PTPIP51 tethering which is NEK1-dependent, possibly by downstream phosphorylation of the proteins. Loss of NEK1 and C21orf2, causes reduced tethering between VAPB/PTPIP51 which correlates with loss of Ca^{2+} homeostasis and autophagic flux. This complex may provide a direct link between defective DNA damage repair and ER-mitochondria contacts in ALS and suggest a new axis for therapeutic intervention of ALS.

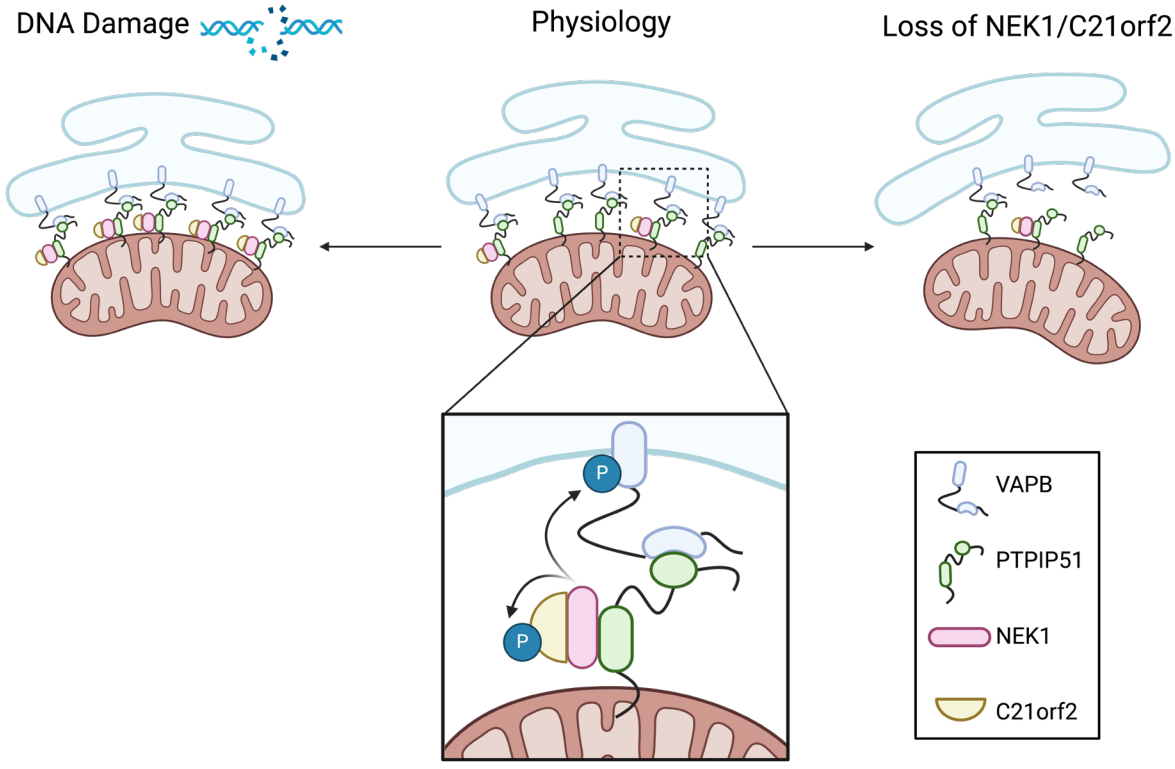

Figure 6-1 Conclusions of the thesis.

Within this study we have identified a novel signalling complex involving NEK1, C21orf2 and the VAPB/PTPIP51 tether that regulates ER-mitochondria interactions. In physiological conditions NEK1 directly binds to PTPIP51, an interaction that is promoted by DNA damage. Induction of DNA damage promotes VAPB/PTPIP51 tethering which is NEK1-dependent, possibly by downstream phosphorylation of the proteins. Loss of NEK1 and C21orf2, causes reduced tethering between VAPB/PTPIP51 which correlates with loss of Ca^{2+} homeostasis and autophagic flux. This complex may provide a direct link between defective DNA damage repair and ER-mitochondria contacts in ALS and suggest a new axis for therapeutic intervention of ALS.

References

Abe, T., Ishiai, M., Hosono, Y., Yoshimura, A., Tada, S., Adachi, N., Koyama, H., Takata, M., Takeda, S., Enomoto, T. and Seki, M. (2008) 'KU70/80, DNA-PKcs, and Artemis are essential for the rapid induction of apoptosis after massive DSB formation', *Cell Signal*, 20(11), pp. 1978-85.

Abel, O., Powell, J. F., Andersen, P. M. and Al-Chalabi, A. (2012) 'ALSoD: A user-friendly online bioinformatics tool for amyotrophic lateral sclerosis genetics', *Hum Mutat*, 33(9), pp. 1345-51.

Abramson, J., Adler, J., Dunger, J., Evans, R., Green, T., Pritzel, A., Ronneberger, O., Willmore, L., Ballard, A. J., Bambrick, J., Bodenstein, S. W., Evans, D. A., Hung, C. C., O'Neill, M., Reiman, D., Tunyasuvunakool, K., Wu, Z., Zemgulyte, A., Arvaniti, E., Beattie, C., Bertolli, O., Bridgland, A., Cherepanov, A., Congreve, M., Cowen-Rivers, A. I., Cowie, A., Figurnov, M., Fuchs, F. B., Gladman, H., Jain, R., Khan, Y. A., Low, C. M. R., Perlin, K., Potapenko, A., Savy, P., Singh, S., Stecula, A., Thillaisundaram, A., Tong, C., Yakneen, S., Zhong, E. D., Zielinski, M., Zidek, A., Bapst, V., Kohli, P., Jaderberg, M., Hassabis, D. and Jumper, J. M. (2024) 'Accurate structure prediction of biomolecular interactions with AlphaFold 3', *Nature*, 630(8016), pp. 493-500.

Abu-Hamad, S., Zaid, H., Israelson, A., Nahon, E. and Shoshan-Barmatz, V. (2008) 'Hexokinase-I protection against apoptotic cell death is mediated via interaction with the voltage-dependent anion channel-1: mapping the site of binding', *J Biol Chem*, 283(19), pp. 13482-90.

Ackerley, S., Thornhill, P., Grierson, A. J., Brownlees, J., Anderton, B. H., Leigh, P. N., Shaw, C. E. and Miller, C. C. (2003) 'Neurofilament heavy chain side arm phosphorylation regulates axonal transport of neurofilaments', *J Cell Biol*, 161(3), pp. 489-95.

Ahumada-Castro, U., Bustos, G., Silva-Pavez, E., Puebla-Huerta, A., Lovy, A. and Cárdenas, C. (2021) 'In the Right Place at the Right Time: Regulation of Cell Metabolism by IP3R-Mediated Inter-Organelle Ca^{2+} Fluxes', *Front Cell Dev Biol*, 9, p. 629522.

Ahumada-Castro, U., Silva-Pavez, E., Lovy, A., Pardo, E., Molgó, J. and Cárdenas, C. (2019) 'MTOR-independent autophagy induced by interrupted endoplasmic reticulum-mitochondrial Ca^{2+} communication: a dead end in cancer cells', *Autophagy*, 15(2), pp. 358-361.

Akçimen, F., Lopez, E. R., Landers, J. E., Nath, A., Chiò, A., Chia, R. and Traynor, B. J. (2023) 'Amyotrophic lateral sclerosis: translating genetic discoveries into therapies', *Nat Rev Genet*, 24(9), pp. 642-658.

Al-Jassar, C., Andreeva, A., Barnabas, D. D., McLaughlin, S. H., Johnson, C. M., Yu, M. and van Breugel, M. (2017) 'The Ciliopathy-Associated Cep104 Protein Interacts with Tubulin and Nek1 Kinase', *Structure*, 25(1), pp. 146-156.

Aliaga, L., Lai, C., Yu, J., Chub, N., Shim, H., Sun, L., Xie, C., Yang, W. J., Lin, X., O'Donovan, M. J. and Cai, H. (2013) 'Amyotrophic lateral sclerosis-related VAPB P56S mutation differentially affects the function and survival of corticospinal and spinal motor neurons', *Hum Mol Genet*, 22(21), pp. 4293-305.

Alpy, F., Rousseau, A., Schwab, Y., Legueux, F., Stoll, I., Wendling, C., Spiegelhalter, C., Kessler, P., Mathelin, C., Rio, M. C., Levine, T. P. and Tomasetto, C. (2013) 'STARD3 or STARD3NL and VAP form a novel molecular tether between late endosomes and the ER', *J Cell Sci*, 126(Pt 23), pp. 5500-12.

Amick, J., Tharkeshwar, A. K., Talaia, G. and Ferguson, S. M. (2020) 'PQLC2 recruits the C9orf72 complex to lysosomes in response to cationic amino acid starvation', *J Cell Biol*, 219(1).

Amin, P., Florez, M., Najafov, A., Pan, H., Geng, J., Ofengeim, D., Dziedzic, S. A., Wang, H., Barrett, V. J., Ito, Y., LaVoie, M. J. and Yuan, J. (2018) 'Regulation of a distinct activated RIPK1 intermediate bridging complex I and complex II in TNFalpha-mediated apoptosis', *Proc Natl Acad Sci U S A*, 115(26), pp. E5944-E5953.

Anagnostou, G., Akbar, M. T., Paul, P., Angelinetta, C., Steiner, T. J. and de Belleroche, J. (2010) 'Vesicle associated membrane protein B (VAPB) is decreased in ALS spinal cord', *Neurobiol Aging*, 31(6), pp. 969-85.

Anderson, E. M., Birmingham, A., Baskerville, S., Reynolds, A., Maksimova, E., Leake, D., Fedorov, Y., Karpilow, J. and Khvorova, A. (2008) 'Experimental validation of the importance of seed complement frequency to siRNA specificity', *RNA*, 14(5), pp. 853-61.

Anding, A. L., Wang, C., Chang, T. K., Sliter, D. A., Powers, C. M., Hofmann, K., Youle, R. J. and Baehrecke, E. H. (2018) 'Vps13D Encodes a Ubiquitin-Binding Protein that Is Required for the Regulation of Mitochondrial Size and Clearance', *Curr Biol*, 28(2), pp. 287-295.e6.

Arai, T., Hasegawa, M., Akiyama, H., Ikeda, K., Nonaka, T., Mori, H., Mann, D., Tsuchiya, K., Yoshida, M., Hashizume, Y. and Oda, T. (2006) 'TDP-43 is a component of ubiquitin-positive tau-negative inclusions in frontotemporal lobar degeneration and amyotrophic lateral sclerosis', *Biochem Biophys Res Commun*, 351(3), pp. 602-11.

Ash, P. E., Bieniek, K. F., Gendron, T. F., Caulfield, T., Lin, W. L., Dejesus-Hernandez, M., van Blitterswijk, M. M., Jansen-West, K., Paul, J. W., Rademakers, R., Boylan, K. B., Dickson, D. W. and Petrucelli, L. (2013) 'Unconventional translation of C9ORF72 GGGGCC expansion generates insoluble polypeptides specific to c9FTD/ALS', *Neuron*, 77(4), pp. 639-46.

Ashida, H., Sasakawa, C. and Suzuki, T. (2020) 'A unique bacterial tactic to circumvent the cell death crosstalk induced by blockade of caspase-8', *EMBO J*, 39(17), p. e104469.

Atakpa-Adaji, P. and Ivanova, A. (2023) 'IP(3)R at ER-Mitochondrial Contact Sites: Beyond the IP(3)R-GRP75-VDAC1 Ca(2+) Funnel', *Contact (Thousand Oaks)*, 6, p. 25152564231181020.

Bae, J. R. and Kim, S. H. (2017) 'Synapses in neurodegenerative diseases', *BMB Rep*, 50(5), pp. 237-246.

Bahar, E., Kim, H. and Yoon, H. (2016) 'ER Stress-Mediated Signaling: Action Potential and Ca(2+) as Key Players', *Int J Mol Sci*, 17(9).

Bang, J., Spina, S. and Miller, B. L. (2015) 'Frontotemporal dementia', *Lancet*, 386(10004), pp. 1672-82.

Bannwarth, S., Ait-El-Mkadem, S., Chaussenot, A., Genin, E. C., Lacas-Gervais, S., Fragaki, K., Berg-Alonso, L., Kageyama, Y., Serre, V., Moore, D. G., Verschueren, A., Rouzier, C., Le Ber, I., Augé, G., Cochaud, C., Lespinasse, F., N'Guyen, K., de Septenville, A., Brice, A., Yu-Wai-Man, P., Sesaki, H., Pouget, J. and Paquis-Flucklinger, V. (2014) 'A mitochondrial origin for frontotemporal dementia and amyotrophic lateral sclerosis through CHCHD10 involvement', *Brain*, 137(Pt 8), pp. 2329-45.

Barberio, J., Lally, C., Kupelian, V., Hardiman, O. and Flanders, W. D. (2023) 'Estimated Familial Amyotrophic Lateral Sclerosis Proportion: A Literature Review and Meta-analysis', *Neurol Genet*, 9(6), p. e200109.

Baron, D. M., Fenton, A. R., Saez-Atienzar, S., Giampetruzzi, A., Sreeram, A., Shankaracharya, Keagle, P. J., Doocy, V. R., Smith, N. J., Danielson, E. W., Andresano, M., McCormack, M. C., Garcia, J., Bercier, V., Van Den Bosch, L., Brent, J. R., Fallini, C., Traynor, B. J., Holzbaur, E. L. F. and Landers, J. E. (2022) 'ALS-associated KIF5A mutations abolish autoinhibition resulting in a toxic gain of function', *Cell Rep*, 39(1), p. 110598.

Bas, L., Papinski, D., Licheva, M., Torggler, R., Rohringer, S., Schuschnig, M. and Kraft, C. (2018) 'Reconstitution reveals Ykt6 as the autophagosomal SNARE in autophagosome-vacuole fusion', *J Cell Biol*, 217(10), pp. 3656-3669.

Basei, F. L., E Silva, I. R., Dias, P. R. F., Ferezin, C. C., Peres de Oliveira, A., Issayama, L. K., Moura, L. A. R., da Silva, F. R. and Kobarg, J. (2024) 'The Mitochondrial Connection: The Nek Kinases' New Functional Axis in Mitochondrial Homeostasis', *Cells*, 13(6).

Basso, M., Samengo, G., Nardo, G., Massignan, T., D'Alessandro, G., Tartari, S., Cantoni, L., Marino, M., Cheroni, C., De Biasi, S., Giordana, M. T., Strong, M. J., Estevez, A. G., Salmona, M., Bendotti, C. and Bonetto, V. (2009) 'Characterization of detergent-insoluble proteins in ALS indicates a causal link between nitrative stress and aggregation in pathogenesis', *PLoS One*, 4(12), p. e8130.

Basso, V., Marchesan, E., Peggion, C., Chakraborty, J., von Stockum, S., Giacomello, M., Ottolini, D., Debattisti, V., Caicci, F., Tasca, E., Pegoraro, V., Angelini, C., Antonini, A., Bertoli, A., Brini, M. and Ziviani, E. (2018) 'Regulation of ER-mitochondria contacts by Parkin via Mfn2', *Pharmacol Res*, 138, pp. 43-56.

Basten, S. G. and Giles, R. H. (2013) 'Functional aspects of primary cilia in signaling, cell cycle and tumorigenesis', *Cilia*, 2(1), p. 6.

Baumgartner, H. K., Gerasimenko, J. V., Thorne, C., Ferdek, P., Pozzan, T., Tepikin, A. V., Petersen, O. H., Sutton, R., Watson, A. J. and Gerasimenko, O. V. (2009) 'Calcium elevation in mitochondria is the main Ca2+ requirement for mitochondrial permeability transition pore (mPTP) opening', *J Biol Chem*, 284(31), pp. 20796-803.

Becker, T., Horvath, S. E., Bottinger, L., Gebert, N., Daum, G. and Pfanner, N. (2013) 'Role of phosphatidylethanolamine in the biogenesis of mitochondrial outer membrane proteins', *J Biol Chem*, 288(23), pp. 16451-16459.

Beghi, E., Mennini, T., Bendotti, C., Bigini, P., Logroscino, G., Chio, A., Hardiman, O., Mitchell, D., Swingler, R., Traynor, B. J. and Al-Chalabi, A. (2007) 'The heterogeneity of amyotrophic lateral sclerosis: a possible explanation of treatment failure', *Curr Med Chem*, 14(30), pp. 3185-200.

Behzadi, A., Pujol-Calderón, F., Tjust, A. E., Wuolikainen, A., Höglund, K., Forsberg, K., Portelius, E., Blennow, K., Zetterberg, H. and Andersen, P. M. (2021) 'Neurofilaments can differentiate ALS subgroups and ALS from common diagnostic mimics', *Sci Rep*, 11(1), p. 22128.

Beli, P., Lukashchuk, N., Wagner, S. A., Weinert, B. T., Olsen, J. V., Baskcomb, L., Mann, M., Jackson, S. P. and Choudhary, C. (2012) 'Proteomic investigations reveal a role for RNA processing factor THRAP3 in the DNA damage response', *Mol Cell*, 46(2), pp. 212-25.

Belikova, N. A., Vladimirov, Y. A., Osipov, A. N., Kapralov, A. A., Tyurin, V. A., Potapovich, M. V., Basova, L. V., Peterson, J., Kurnikov, I. V. and Kagan, V. E. (2006) 'Peroxidase activity and structural transitions of cytochrome c bound to cardiolipin-containing membranes', *Biochemistry*, 45(15), pp. 4998-5009.

Bennett, E. J., Bence, N. F., Jayakumar, R. and Kopito, R. R. (2005) 'Global impairment of the ubiquitin-proteasome system by nuclear or cytoplasmic protein aggregates precedes inclusion body formation', *Mol Cell*, 17(3), pp. 351-65.

Bennetzen, M. V., Larsen, D. H., Bunkenborg, J., Bartek, J., Lukas, J. and Andersen, J. S. (2010) 'Site-specific phosphorylation dynamics of the nuclear proteome during the DNA damage response', *Mol Cell Proteomics*, 9(6), pp. 1314-23.

Bernard-Marissal, N., Médard, J. J., Azzedine, H. and Chrast, R. (2015) 'Dysfunction in endoplasmic reticulum-mitochondria crosstalk underlies SIGMAR1 loss of function mediated motor neuron degeneration', *Brain*, 138(Pt 4), pp. 875-90.

Bernardi, P., Gerle, C., Halestrap, A. P., Jonas, E. A., Karch, J., Mnatsakanyan, N., Pavlov, E., Sheu, S. S. and Soukas, A. A. (2023) 'Identity, structure, and function of the mitochondrial permeability transition pore: controversies, consensus, recent advances, and future directions', *Cell Death Differ*, 30(8), pp. 1869-1885.

Berniak, K., Rybak, P., Bernas, T., Zarebski, M., Biela, E., Zhao, H., Darzynkiewicz, Z. and Dobrucki, J. W. (2013) 'Relationship between DNA damage response, initiated by camptothecin or oxidative stress, and DNA replication, analyzed by quantitative 3D image analysis', *Cytometry A*, 83(10), pp. 913-24.

Bhardwaj, A., Myers, M. P., Buratti, E. and Baralle, F. E. (2013) 'Characterizing TDP-43 interaction with its RNA targets', *Nucleic Acids Res*, 41(9), pp. 5062-74.

Bilsland, L. G., Sahai, E., Kelly, G., Golding, M., Greensmith, L. and Schiavo, G. (2010) 'Deficits in axonal transport precede ALS symptoms in vivo', *Proc Natl Acad Sci U S A*, 107(47), pp. 20523-8.

Biton, S. and Ashkenazi, A. (2011) 'NEMO and RIP1 control cell fate in response to extensive DNA damage via TNF-α feedforward signaling', *Cell*, 145(1), pp. 92-103.

Blair, H. A. (2023) 'Tofersen: First Approval', *Drugs*, 83(11), pp. 1039-1043.

Blauw, H. M., van Rheenen, W., Koppers, M., Van Damme, P., Waibel, S., Lemmens, R., van Vught, P. W., Meyer, T., Schulte, C., Gasser, T., Cuppen, E., Pasterkamp, R. J., Robberecht, W., Ludolph, A. C., Veldink, J. H. and van den Berg, L. H. (2012) 'NIPA1 polyalanine repeat expansions are associated with amyotrophic lateral sclerosis', *Hum Mol Genet*, 21(11), pp. 2497-502.

Bobrich, M., Brobeil, A., Mooren, F. C., Kruger, K., Steger, K., Tag, C. and Wimmer, M. (2011) 'PTPIP51 interaction with PTP1B and 14-3-3beta in adipose tissue of insulin-resistant mice', *Int J Obes (Lond)*, 35(11), pp. 1385-94.

Boehning, D., Patterson, R. L., Sedaghat, L., Glebova, N. O., Kurosaki, T. and Snyder, S. H. (2003) 'Cytochrome c binds to inositol (1,4,5) trisphosphate receptors, amplifying calcium-dependent apoptosis', *Nat Cell Biol*, 5(12), pp. 1051-61.

Boeing, S., Williamson, L., Encheva, V., Gori, I., Saunders, R. E., Instrell, R., Aygun, O., Rodriguez-Martinez, M., Weems, J. C., Kelly, G. P., Conaway, J. W., Conaway, R. C., Stewart, A., Howell, M., Snijders, A. P. and Svejstrup, J. Q. (2016) 'Multiomic Analysis of the UV-Induced DNA Damage Response', *Cell Rep*, 15(7), pp. 1597-1610.

Boice, A. G., Lopez, K. E., Pandita, R. K., Parsons, M. J., Charendoff, C. I., Charaka, V., Carisey, A. F., Pandita, T. K. and Bouchier-Hayes, L. (2022) 'Caspase-2 regulates S-phase cell cycle events to protect from DNA damage accumulation independent of apoptosis', *Oncogene*, 41(2), pp. 204-219.

Bosco, D. A., Morfini, G., Karabacak, N. M., Song, Y., Gros-Louis, F., Pasinelli, P., Goolsby, H., Fontaine, B. A., Lemay, N., McKenna-Yasek, D., Frosch, M. P., Agar, J. N., Julien, J. P., Brady, S. T. and Brown, R. H. (2010) 'Wild-type and mutant SOD1 share an aberrant conformation and a common pathogenic pathway in ALS', *Nat Neurosci*, 13(11), pp. 1396-403.

Boston-Howes, W., Gibb, S. L., Williams, E. O., Pasinelli, P., Brown, R. H. and Trotti, D. (2006) 'Caspase-3 cleaves and inactivates the glutamate transporter EAAT2', *J Biol Chem*, 281(20), pp. 14076-84.

Bottinger, L., Horvath, S. E., Kleinschroth, T., Hunte, C., Daum, G., Pfanner, N. and Becker, T. (2012) 'Phosphatidylethanolamine and cardiolipin differentially affect the stability of mitochondrial respiratory chain supercomplexes', *J Mol Biol*, 423(5), pp. 677-86.

Bowery, N. G., Bettler, B., Froestl, W., Gallagher, J. P., Marshall, F., Raiteri, M., Bonner, T. I. and Enna, S. J. (2002) 'International Union of Pharmacology. XXXIII. Mammalian gamma-aminobutyric acid(B) receptors: structure and function', *Pharmacol Rev*, 54(2), pp. 247-64.

Bozic, M., van den Bekerom, L., Milne, B. A., Goodman, N., Roberston, L., Prescott, A. R., Macartney, T. J., Dawe, N. and McEwan, D. G. (2020) 'A conserved ATG2-GABARAP family interaction is critical for phagophore formation', *EMBO Rep*, 21(3), p. e48412.

Bravo, R., Vicencio, J. M., Parra, V., Troncoso, R., Munoz, J. P., Bui, M., Quiroga, C., Rodriguez, A. E., Verdejo, H. E., Ferreira, J., Iglewski, M., Chiong, M., Simmen, T., Zorzano, A., Hill, J. A., Rothermel, B. A., Szabadkai, G. and Lavandero, S. (2011) 'Increased ER-mitochondrial coupling promotes

mitochondrial respiration and bioenergetics during early phases of ER stress', *J Cell Sci*, 124(Pt 13), pp. 2143-52.

Brenner, D., Müller, K., Wieland, T., Weydt, P., Böhm, S., Lulé, D., Hübers, A., Neuwirth, C., Weber, M., Borck, G., Wahlqvist, M., Danzer, K. M., Volk, A. E., Meitinger, T., Strom, T. M., Otto, M., Kassubek, J., Ludolph, A. C., Andersen, P. M. and Weishaupt, J. H. (2016) 'NEK1 mutations in familial amyotrophic lateral sclerosis', *Brain*, 139(Pt 5), p. e28.

Brobeil, A., Bobrich, M., Graf, M., Kruchten, A., Blau, W., Rummel, M., Oeschger, S., Steger, K. and Wimmer, M. (2011) 'PTPIP51 is phosphorylated by Lyn and c-Src kinases lacking dephosphorylation by PTP1B in acute myeloid leukemia', *Leuk Res*, 35(10), pp. 1367-75.

Brobeil, A., Bobrich, M., Tag, C. and Wimmer, M. (2012) 'PTPIP51 in protein interactions: regulation and in situ interacting partners', *Cell Biochem Biophys*, 63(3), pp. 211-22.

Brobeil, A., Graf, M., Oeschger, S., Steger, K. and Wimmer, M. (2010) 'PTPIP51-a myeloid lineage specific protein interacts with PTP1B in neutrophil granulocytes', *Blood Cells Mol Dis*, 45(2), pp. 159-68.

Brough, D., Schell, M. J. and Irvine, R. F. (2005) 'Agonist-induced regulation of mitochondrial and endoplasmic reticulum motility', *Biochem J*, 392(Pt 2), pp. 291-7.

Brown, E. J. and Baltimore, D. (2000) 'ATR disruption leads to chromosomal fragmentation and early embryonic lethality', *Genes Dev*, 14(4), pp. 397-402.

Budanov, A. V. and Karin, M. (2008) 'p53 target genes sestrin1 and sestrin2 connect genotoxic stress and mTOR signaling', *Cell*, 134(3), pp. 451-60.

Bunton-Stasyshyn, R. K., Saccon, R. A., Fratta, P. and Fisher, E. M. (2015) 'SOD1 Function and Its Implications for Amyotrophic Lateral Sclerosis Pathology: New and Renascent Themes', *Neuroscientist*, 21(5), pp. 519-29.

Burman, C. and Ktistakis, N. T. (2010) 'Regulation of autophagy by phosphatidylinositol 3-phosphate', *FEBS Lett*, 584(7), pp. 1302-12.

Butti, Z. and Patten, S. A. (2018) 'RNA Dysregulation in Amyotrophic Lateral Sclerosis', *Front Genet*, 9, p. 712.

Cabukusta, B., Berlin, I., van Elsland, D. M., Forkink, I., Spits, M., de Jong, A. W. M., Akkermans, J., Wijdeven, R. H. M., Janssen, G. M. C., van Veelen, P. A. and Neefjes, J. (2020) 'Human VAPome Analysis Reveals MOSPD1 and MOSPD3 as Membrane Contact Site Proteins Interacting with FFAT-Related FFNT Motifs', *Cell Rep*, 33(10), p. 108475.

Cady, J., Allred, P., Bali, T., Pestronk, A., Goate, A., Miller, T. M., Mitra, R. D., Ravits, J., Harms, M. B. and Baloh, R. H. (2015) 'Amyotrophic lateral sclerosis onset is influenced by the burden of rare variants in known amyotrophic lateral sclerosis genes', *Ann Neurol*, 77(1), pp. 100-13.

Caldecott, K. W. (2022) 'DNA single-strand break repair and human genetic disease', *Trends Cell Biol*, 32(9), pp. 733-745.

Campos, A. and Clemente-Blanco, A. (2020) 'Cell Cycle and DNA Repair Regulation in the Damage Response: Protein Phosphatases Take Over the Reins', *Int J Mol Sci*, 21(2).

Cao, S. S. and Kaufman, R. J. (2014) 'Endoplasmic reticulum stress and oxidative stress in cell fate decision and human disease', *Antioxid Redox Signal*, 21(3), pp. 396-413.

Cao, Y., Chen, Z., Hu, J., Feng, J., Zhu, Z., Fan, Y., Lin, Q. and Ding, G. (2021) 'Mfn2 Regulates High Glucose-Induced MAMs Dysfunction and Apoptosis in Podocytes via PERK Pathway', *Front Cell Dev Biol*, 9, p. 769213.

Cárdenas, C., Miller, R. A., Smith, I., Bui, T., Molgó, J., Müller, M., Vais, H., Cheung, K. H., Yang, J., Parker, I., Thompson, C. B., Birnbaum, M. J., Hallows, K. R. and Foskett, J. K. (2010) 'Essential regulation of cell bioenergetics by constitutive InsP3 receptor Ca2+ transfer to mitochondria', *Cell*, 142(2), pp. 270-83.

Carreras-Sureda, A., Pihán, P. and Hetz, C. (2018) 'Calcium signaling at the endoplasmic reticulum: fine-tuning stress responses', *Cell Calcium*, 70, pp. 24-31.

Carriedo, S. G., Yin, H. Z., Sensi, S. L. and Weiss, J. H. (1998) 'Rapid Ca2+ entry through Ca2+-permeable AMPA/Kainate channels triggers marked intracellular Ca2+ rises and consequent oxygen radical production', *J Neurosci*, 18(19), pp. 7727-38.

Cerutti, R., Pirinen, E., Lamperti, C., Marchet, S., Sauve, A. A., Li, W., Leoni, V., Schon, E. A., Dantzer, F., Auwerx, J., Viscomi, C. and Zeviani, M. (2014) 'NAD(+)-dependent activation of Sirt1 corrects the phenotype in a mouse model of mitochondrial disease', *Cell Metab*, 19(6), pp. 1042-9.

Cha, S. J., Choi, H. J., Kim, H. J., Choi, E. J., Song, K. H., Im, D. S. and Kim, K. (2020) 'Parkin expression reverses mitochondrial dysfunction in fused in sarcoma-induced amyotrophic lateral sclerosis', *Insect Mol Biol*, 29(1), pp. 56-65.

Chakrabarti, R., Ji, W. K., Stan, R. V., de Juan Sanz, J., Ryan, T. A. and Higgs, H. N. (2018) 'INF2-mediated actin polymerization at the ER stimulates mitochondrial calcium uptake, inner membrane constriction, and division', *J Cell Biol*, 217(1), pp. 251-268.

Chance, B. and Williams, G. R. (1956) 'The respiratory chain and oxidative phosphorylation', *Adv Enzymol Relat Subj Biochem*, 17, pp. 65-134.

Chang, L. and Monteiro, M. J. (2015) 'Defective Proteasome Delivery of Polyubiquitinated Proteins by Ubiquilin-2 Proteins Containing ALS Mutations', *PLoS One*, 10(6), p. e0130162.

Chang, Y., Kong, Q., Shan, X., Tian, G., Ilieva, H., Cleveland, D. W., Rothstein, J. D., Borchelt, D. R., Wong, P. C. and Lin, C. L. (2008) 'Messenger RNA oxidation occurs early in disease pathogenesis and promotes motor neuron degeneration in ALS', *PLoS One*, 3(8), p. e2849.

Chappidi, N., Quail, T., Doll, S., Vogel, L. T., Aleksandrov, R., Felekyan, S., Kuhnemuth, R., Stoynov, S., Seidel, C. A. M., Brugues, J., Jahnel, M., Franzmann, T. M. and Alberti, S. (2024) 'PARP1-DNA co-condensation drives DNA repair site assembly to prevent disjunction of broken DNA ends', *Cell*, 187(4), pp. 945-961 e18.

Chen, H. J., Anagnostou, G., Chai, A., Withers, J., Morris, A., Adhikaree, J., Pennetta, G. and de Belleroche, J. S. (2010a) 'Characterization of the properties of a novel mutation in VAPB in familial amyotrophic lateral sclerosis', *J Biol Chem*, 285(51), pp. 40266-81.

Chen, L. B. (1988) 'Mitochondrial membrane potential in living cells', *Annu Rev Cell Biol*, 4, pp. 155-81.

Chen, Y., Chen, C. F., Riley, D. J. and Chen, P. L. (2011) 'Nek1 kinase functions in DNA damage response and checkpoint control through a pathway independent of ATM and ATR', *Cell Cycle*, 10(4), pp. 655-63.

Chen, Y., Chen, P. L., Chen, C. F., Jiang, X. and Riley, D. J. (2008) 'Never-in-mitosis related kinase 1 functions in DNA damage response and checkpoint control', *Cell Cycle*, 7(20), pp. 3194-201.

Chen, Y., Craigen, W. J. and Riley, D. J. (2009) 'Nek1 regulates cell death and mitochondrial membrane permeability through phosphorylation of VDAC1', *Cell Cycle*, 8(2), pp. 257-67.

Chen, Y., Deng, J., Wang, P., Yang, M., Chen, X., Zhu, L., Liu, J., Lu, B., Shen, Y., Fushimi, K., Xu, Q. and Wu, J. Y. (2016) 'PINK1 and Parkin are genetic modifiers for FUS-induced neurodegeneration', *Hum Mol Genet*, 25(23), pp. 5059-5068.

Chen, Y., Gaczynska, M., Osmulski, P., Polci, R. and Riley, D. J. (2010b) 'Phosphorylation by Nek1 regulates opening and closing of voltage dependent anion channel 1', *Biochem Biophys Res Commun*, 394(3), pp. 798-803.

Cheroni, C., Peviani, M., Cascio, P., Debiasi, S., Monti, C. and Bendotti, C. (2005) 'Accumulation of human SOD1 and ubiquitinated deposits in the spinal cord of SOD1G93A mice during motor neuron disease progression correlates with a decrease of proteasome', *Neurobiol Dis*, 18(3), pp. 509-22.

Chiang, S. F., Huang, C. Y., Lin, T. Y., Chiou, S. H. and Chow, K. C. (2012) 'An alternative import pathway of AIF to the mitochondria', *Int J Mol Med*, 29(3), pp. 365-72.

Chio, A., Logroscino, G., Hardiman, O., Swingler, R., Mitchell, D., Beghi, E., Traynor, B. G. and Eurals, C. (2009) 'Prognostic factors in ALS: A critical review', *Amyotroph Lateral Scler*, 10(5-6), pp. 310-23.

Cho, Y. S., Challa, S., Moquin, D., Genga, R., Ray, T. D., Guildford, M. and Chan, F. K. (2009) 'Phosphorylation-driven assembly of the RIP1-RIP3 complex regulates programmed necrosis and virus-induced inflammation', *Cell*, 137(6), pp. 1112-23.

Choi, S. Y., Lee, J. H., Chung, A. Y., Jo, Y., Shin, J. H., Park, H. C., Kim, H., Lopez-Gonzalez, R., Ryu, J. R. and Sun, W. (2020) 'Prevention of mitochondrial impairment by inhibition of protein phosphatase 1 activity in amyotrophic lateral sclerosis', *Cell Death Dis*, 11(10), p. 888.

Chu, C. T., Ji, J., Dagda, R. K., Jiang, J. F., Tyurina, Y. Y., Kapralov, A. A., Tyurin, V. A., Yanamala, N., Shrivastava, I. H., Mohammadyani, D., Wang, K. Z. Q., Zhu, J., Klein-Seetharaman, J., Balasubramanian, K., Amoscato, A. A., Borisenko, G., Huang, Z., Gusdon, A. M., Cheikhi, A., Steer, E. K., Wang, R., Baty, C., Watkins, S., Bahar, I., Bayir, H. and Kagan, V. E. (2013) 'Cardiolipin externalization to the outer mitochondrial membrane acts as an elimination signal for mitophagy in neuronal cells', *Nat Cell Biol*, 15(10), pp. 1197-1205.

Chua, J. P., De Calbiac, H., Kabashi, E. and Barmada, S. J. (2022) 'Autophagy and ALS: mechanistic insights and therapeutic implications', *Autophagy*, 18(2), pp. 254-282.

Chung, J., Torta, F., Masai, K., Lucast, L., Czapla, H., Tanner, L. B., Narayanaswamy, P., Wenk, M. R., Nakatsu, F. and De Camilli, P. (2015) 'INTRACELLULAR TRANSPORT. PI4P/phosphatidylserine countertransport at ORP5- and ORP8-mediated ER-plasma membrane contacts', *Science*, 349(6246), pp. 428-32.

Cirulli, E. T., Lasseigne, B. N., Petrovski, S., Sapp, P. C., Dion, P. A., Leblond, C. S., Couthouis, J., Lu, Y. F., Wang, Q., Krueger, B. J., Ren, Z., Keebler, J., Han, Y., Levy, S. E., Boone, B. E., Wimbish, J. R., Waite, L. L., Jones, A. L., Carulli, J. P., Day-Williams, A. G., Staropoli, J. F., Xin, W. W., Chesi, A., Raphael, A. R., McKenna-Yasek, D., Cady, J., Vianney de Jong, J. M., Kenna, K. P., Smith, B. N., Topp, S., Miller, J., Gkazi, A., Al-Chalabi, A., van den Berg, L. H., Veldink, J., Silani, V., Ticozzi, N., Shaw, C. E., Baloh, R. H., Appel, S., Simpson, E., Lagier-Tourenne, C., Pulst, S. M., Gibson, S., Trojanowski, J. Q., Elman, L., McCluskey, L., Grossman, M., Shneider, N. A., Chung, W. K., Ravits, J. M., Glass, J. D., Sims, K. B., Van Deerlin, V. M., Maniatis, T., Hayes, S. D., Ordureau, A., Swarup, S., Landers, J., Baas, F., Allen, A. S., Bedlack, R. S., Harper, J. W., Gitler, A. D., Rouleau, G. A., Brown, R., Harms, M. B., Cooper, G. M., Harris, T., Myers, R. M., Goldstein, D. B. and Consortium, F. S. (2015) 'Exome sequencing in amyotrophic lateral sclerosis identifies risk genes and pathways', *Science*, 347(6229), pp. 1436-41.

Cohen, T. J., Hwang, A. W., Restrepo, C. R., Yuan, C. X., Trojanowski, J. Q. and Lee, V. M. (2015) 'An acetylation switch controls TDP-43 function and aggregation propensity', *Nat Commun*, 6, p. 5845.

Conforti, F. L., Spataro, R., Sproviero, W., Mazzei, R., Cavalcanti, F., Condino, F., Simone, I. L., Logroscino, G., Patitucci, A., Magariello, A., Muglia, M., Rodolico, C., Valentino, P., Bono, F., Colletti, T., Monsurrò, M. R., Gambardella, A. and La Bella, V. (2012) 'Ataxin-1 and ataxin-2 intermediate-length PolyQ expansions in amyotrophic lateral sclerosis', *Neurology*, 79(24), pp. 2315-20.

Contino, S., Porporato, P. E., Bird, M., Marinangeli, C., Opsomer, R., Sonveaux, P., Bontemps, F., Dewachter, I., Octave, J. N., Bertrand, L., Stanga, S. and Kienlen-Campard, P. (2017) 'Presenilin 2-Dependent Maintenance of Mitochondrial Oxidative Capacity and Morphology', *Front Physiol*, 8, p. 796.

Cortez, D., Guntuku, S., Qin, J. and Elledge, S. J. (2001) 'ATR and ATRIP: partners in checkpoint signaling', *Science*, 294(5547), pp. 1713-6.

Costa, R. M., Chigancas, V., Galhardo Rda, S., Carvalho, H. and Menck, C. F. (2003) 'The eukaryotic nucleotide excision repair pathway', *Biochimie*, 85(11), pp. 1083-99.

Costello, J. L., Castro, I. G., Hacker, C., Schrader, T. A., Metz, J., Zeuschner, D., Azadi, A. S., Godinho, L. F., Costina, V., Findeisen, P., Manner, A., Islinger, M. and Schrader, M. (2017a) 'ACBD5 and VAPB mediate membrane associations between peroxisomes and the ER', *J Cell Biol*, 216(2), pp. 331-342.

Costello, J. L., Castro, I. G., Schrader, T. A., Islinger, M. and Schrader, M. (2017b) 'Peroxisomal ACBD4 interacts with VAPB and promotes ER-peroxisome associations', *Cell Cycle*, 16(11), pp. 1039-1045.

Cox, J. and Mann, M. (2008) 'MaxQuant enables high peptide identification rates, individualized p.p.b.-range mass accuracies and proteome-wide protein quantification', *Nat Biotechnol*, 26(12), pp. 1367-72.

Coyne, A. N., Siddegowda, B. B., Estes, P. S., Johannesmeyer, J., Kovalik, T., Daniel, S. G., Pearson, A., Bowser, R. and Zarnescu, D. C. (2014) 'Futsch/MAP1B mRNA is a translational target of TDP-43 and is neuroprotective in a Drosophila model of amyotrophic lateral sclerosis', *J Neurosci*, 34(48), pp. 15962-74.

Cozzolino, M., Ferri, A., Valle, C. and Carrì, M. T. (2013) 'Mitochondria and ALS: implications from novel genes and pathways', *Mol Cell Neurosci*, 55, pp. 44-9.

Crighton, D., Wilkinson, S., O'Prey, J., Syed, N., Smith, P., Harrison, P. R., Gasco, M., Garrone, O., Crook, T. and Ryan, K. M. (2006) 'DRAM, a p53-induced modulator of autophagy, is critical for apoptosis', *Cell*, 126(1), pp. 121-34.

Crowley, L. C., Marfell, B. J., Scott, A. P. and Waterhouse, N. J. (2016) 'Analysis of Cytochrome c Release by Immunocytochemistry', *Cold Spring Harb Protoc*, 2016(12).

Csordás, G., Renken, C., Várnai, P., Walter, L., Weaver, D., Buttle, K. F., Balla, T., Mannella, C. A. and Hajnóczky, G. (2006) 'Structural and functional features and significance of the physical linkage between ER and mitochondria', *J Cell Biol*, 174(7), pp. 915-21.

Csordas, G., Varnai, P., Golenar, T., Roy, S., Purkins, G., Schneider, T. G., Balla, T. and Hajnoczky, G. (2010) 'Imaging interorganelle contacts and local calcium dynamics at the ER-mitochondrial interface', *Mol Cell*, 39(1), pp. 121-32.

Cucchi, D., Gibson, A. and Martin, S. A. (2021) 'The emerging relationship between metabolism and DNA repair', *Cell Cycle*, 20(10), pp. 943-959.

Dafinca, R., Scaber, J., Ababneh, N., Lalic, T., Weir, G., Christian, H., Vowles, J., Douglas, A. G., Fletcher-Jones, A., Browne, C., Nakanishi, M., Turner, M. R., Wade-Martins, R., Cowley, S. A. and Talbot, K. (2016) 'C9orf72 Hexanucleotide Expansions Are Associated with Altered Endoplasmic Reticulum Calcium Homeostasis and Stress Granule Formation in Induced Pluripotent Stem Cell-Derived Neurons from Patients with Amyotrophic Lateral Sclerosis and Frontotemporal Dementia', *Stem Cells*, 34(8), pp. 2063-78.

Daoud, H., Belzil, V., Martins, S., Sabbagh, M., Provencher, P., Lacomblez, L., Meininger, V., Camu, W., Dupré, N., Dion, P. A. and Rouleau, G. A. (2011) 'Association of long ATXN2 CAG repeat sizes with increased risk of amyotrophic lateral sclerosis', *Arch Neurol*, 68(6), pp. 739-42.

Darbyson, A. and Ngsee, J. K. (2016) 'Oxysterol-binding protein ORP3 rescues the Amyotrophic Lateral Sclerosis-linked mutant VAPB phenotype', *Exp Cell Res*, 341(1), pp. 18-31.

Datta, S. and Jaiswal, M. (2021) 'Mitochondrial calcium at the synapse', *Mitochondrion*, 59, pp. 135-153.

de Brito, O. M. and Scorrano, L. (2008) 'Mitofusin 2 tethers endoplasmic reticulum to mitochondria', *Nature*, 456(7222), pp. 605-10.

De Decker, M., Zelina, P., Moens, T. G., Eggermont, K., Moisse, M., Veldink, J. H., Van Den Bosch, L., Pasterkamp, J. R. and Van Damme, P. (2022) 'C21orf2 mutations found in ALS disrupt primary cilia function', *bioRxiv*, p. 2022.02.28.482239.

De Vos, K. J., Chapman, A. L., Tennant, M. E., Manser, C., Tudor, E. L., Lau, K. F., Brownlees, J., Ackerley, S., Shaw, P. J., McLoughlin, D. M., Shaw, C. E., Leigh, P. N., Miller, C. C. J. and Grierson, A. J. (2007) 'Familial amyotrophic lateral sclerosis-linked SOD1 mutants perturb fast axonal transport to reduce axonal mitochondria content', *Hum Mol Genet*, 16(22), pp. 2720-2728.

De Vos, K. J., Grierson, A. J., Ackerley, S. and Miller, C. C. (2008) 'Role of axonal transport in neurodegenerative diseases', *Annu Rev Neurosci*, 31, pp. 151-73.

De Vos, K. J., Morotz, G. M., Stoica, R., Tudor, E. L., Lau, K. F., Ackerley, S., Warley, A., Shaw, C. E. and Miller, C. C. (2012) 'VAPB interacts with the mitochondrial protein PTPIP51 to regulate calcium homeostasis', *Hum Mol Genet*, 21(6), pp. 1299-311.

DeJesus-Hernandez, M., Mackenzie, I. R., Boeve, B. F., Boxer, A. L., Baker, M., Rutherford, N. J., Nicholson, A. M., Finch, N. A., Flynn, H., Adamson, J., Kouri, N., Wojtas, A., Sengdy, P., Hsiung, G. Y., Karydas, A., Seeley, W. W., Josephs, K. A., Coppola, G., Geschwind, D. H., Wszolek, Z. K., Feldman, H., Knopman, D. S., Petersen, R. C., Miller, B. L., Dickson, D. W., Boylan, K. B., Graff-Radford, N. R. and Rademakers, R. (2011) 'Expanded GGGGCC hexanucleotide repeat in noncoding region of C9ORF72 causes chromosome 9p-linked FTD and ALS', *Neuron*, 72(2), pp. 245-56.

Delacote, F. and Lopez, B. S. (2008) 'Importance of the cell cycle phase for the choice of the appropriate DSB repair pathway, for genome stability maintenance: the trans-S double-strand break repair model', *Cell Cycle*, 7(1), pp. 33-8.

Deng, H. X., Chen, W., Hong, S. T., Boycott, K. M., Gorrie, G. H., Siddique, N., Yang, Y., Fecto, F., Shi, Y., Zhai, H., Jiang, H., Hirano, M., Rampersaud, E., Jansen, G. H., Donkervoort, S., Bigio, E. H., Brooks, B. R., Ajroud, K., Sufit, R. L., Haines, J. L., Mugnaini, E., Pericak-Vance, M. A. and Siddique, T. (2011) 'Mutations in UBQLN2 cause dominant X-linked juvenile and adult-onset ALS and ALS/dementia', *Nature*, 477(7363), pp. 211-5.

Denton, R. M. (2009) 'Regulation of mitochondrial dehydrogenases by calcium ions', *Biochim Biophys Acta*, 1787(11), pp. 1309-16.

Denton, R. M., Randle, P. J. and Martin, B. R. (1972) 'Stimulation by calcium ions of pyruvate dehydrogenase phosphate phosphatase', *Biochem J*, 128(1), pp. 161-3.

Deshimaru, M., Kinoshita-Kawada, M., Kubota, K., Watanabe, T., Tanaka, Y., Hirano, S., Ishidate, F., Hiramoto, M., Ishikawa, M., Uehara, Y., Okano, H., Hirose, S., Fujioka, S., Iwasaki, K., Yuasa-Kawada, J., Mishima, T. and Tsuboi, Y. (2021) 'DCTN1 Binds to TDP-43 and Regulates TDP-43 Aggregation', *Int J Mol Sci*, 22(8).

Devine, M. J. and Kittler, J. T. (2018) 'Mitochondria at the neuronal presynapse in health and disease', *Nat Rev Neurosci*, 19(2), pp. 63-80.

Di Mattia, T., Martinet, A., Ikhlef, S., McEwen, A. G., Nominé, Y., Wendling, C., Poussin-Courmontagne, P., Voilquin, L., Eberling, P., Ruffenach, F., Cavarelli, J., Slee, J., Levine, T. P., Drin, G., Tomasetto, C. and

Alpy, F. (2020) 'FFAT motif phosphorylation controls formation and lipid transfer function of inter-organelle contacts', *EMBO J*, 39(23), p. e104369.

Di Mattia, T., Wilhelm, L. P., Ikhlef, S., Wendling, C., Spehner, D., Nomine, Y., Giordano, F., Mathelin, C., Drin, G., Tomasetto, C. and Alpy, F. (2018) 'Identification of MOSPD2, a novel scaffold for endoplasmic reticulum membrane contact sites', *EMBO Rep*, 19(7).

Dong, R., Saheki, Y., Swarup, S., Lucast, L., Harper, J. W. and De Camilli, P. (2016) 'Endosome-ER Contacts Control Actin Nucleation and Retromer Function through VAP-Dependent Regulation of PI4P', *Cell*, 166(2), pp. 408-423.

Dooley, H. C., Razi, M., Polson, H. E., Girardin, S. E., Wilson, M. I. and Tooze, S. A. (2014) 'WIPI2 links LC3 conjugation with PI3P, autophagosome formation, and pathogen clearance by recruiting Atg12-5-16L1', *Mol Cell*, 55(2), pp. 238-52.

Du, Y., Wang, J., Xiong, J., Fang, N. and Ji, W. K. (2021) 'VPS13D interacts with VCP/p97 and negatively regulates endoplasmic reticulum-mitochondria interactions', *Mol Biol Cell*, 32(16), pp. 1474-1486.

Dulla, K., Daub, H., Hornberger, R., Nigg, E. A. and Körner, R. (2010) 'Quantitative site-specific phosphorylation dynamics of human protein kinases during mitotic progression', *Mol Cell Proteomics*, 9(6), pp. 1167-81.

Edelstein, A. D., Tsuchida, M. A., Amodaj, N., Pinkard, H., Vale, R. D. and Stuurman, N. (2014) 'Advanced methods of microscope control using μManager software', *J Biol Methods*, 1(2).

Egan, D. F., Shackelford, D. B., Mihaylova, M. M., Gelino, S., Kohnz, R. A., Mair, W., Vasquez, D. S., Joshi, A., Gwinn, D. M., Taylor, R., Asara, J. M., Fitzpatrick, J., Dillin, A., Viollet, B., Kundu, M., Hansen, M. and Shaw, R. J. (2011) 'Phosphorylation of ULK1 (hATG1) by AMP-activated protein kinase connects energy sensing to mitophagy', *Science*, 331(6016), pp. 456-61.

Elden, A. C., Kim, H. J., Hart, M. P., Chen-Plotkin, A. S., Johnson, B. S., Fang, X., Armakola, M., Geser, F., Greene, R., Lu, M. M., Padmanabhan, A., Clay-Falcone, D., McCluskey, L., Elman, L., Juhr, D., Gruber, P. J., Rüb, U., Auburger, G., Trojanowski, J. Q., Lee, V. M., Van Deerlin, V. M., Bonini, N. M. and Gitler, A. D. (2010) 'Ataxin-2 intermediate-length polyglutamine expansions are associated with increased risk for ALS', *Nature*, 466(7310), pp. 1069-75.

Elfmann, C. and Stulke, J. (2023) 'PAE viewer: a webserver for the interactive visualization of the predicted aligned error for multimer structure predictions and crosslinks', *Nucleic Acids Res*, 51(W1), pp. W404-W410.

Emde, A., Eitan, C., Liou, L. L., Libby, R. T., Rivkin, N., Magen, I., Reichenstein, I., Oppenheim, H., Eilam, R., Silvestroni, A., Alajajian, B., Ben-Dov, I. Z., Aebischer, J., Savidor, A., Levin, Y., Sons, R., Hammond, S. M., Ravits, J. M., Moller, T. and Hornstein, E. (2015) 'Dysregulated miRNA biogenesis downstream of cellular stress and ALS-causing mutations: a new mechanism for ALS', *EMBO J*, 34(21), pp. 2633-51.

Evangelista, M., Lim, T. Y., Lee, J., Parker, L., Ashique, A., Peterson, A. S., Ye, W., Davis, D. P. and de Sauvage, F. J. (2008) 'Kinome siRNA screen identifies regulators of ciliogenesis and hedgehog signal transduction', *Sci Signal*, 1(39), p. ra7.

Fang, E. F., Scheibye-Knudsen, M., Brace, L. E., Kassahun, H., SenGupta, T., Nilsen, H., Mitchell, J. R., Croteau, D. L. and Bohr, V. A. (2014) 'Defective mitophagy in XPA via PARP-1 hyperactivation and NAD(+)/SIRT1 reduction', *Cell*, 157(4), pp. 882-896.

Fang, E. F., Scheibye-Knudsen, M., Chua, K. F., Mattson, M. P., Croteau, D. L. and Bohr, V. A. (2016) 'Nuclear DNA damage signalling to mitochondria in ageing', *Nat Rev Mol Cell Biol*, 17(5), pp. 308-21.

Fang, X., Lin, H., Wang, X., Zuo, Q., Qin, J. and Zhang, P. (2015) 'The NEK1 interactor, C21ORF2, is required for efficient DNA damage repair', *Acta Biochim Biophys Sin (Shanghai)*, 47(10), pp. 834-41.

Faria Assoni, A., Giove Mitsugi, T., Wardenaar, R., Oliveira Ferreira, R., Farias Jandrey, E. H., Machado Novaes, G., Fonseca de Oliveira Granha, I., Bakker, P., Kaid, C., Zatz, M., Foijer, F. and Keith Okamoto, O. (2023) 'Neurodegeneration-associated protein VAPB regulates proliferation in medulloblastoma', *Sci Rep*, 13(1), p. 19481.

Farrawell, N. E., Bax, M., McAlary, L., McKenna, J., Maksour, S., Do-Ha, D., Rayner, S. L., Blair, I. P., Chung, R. S., Yerbury, J. J., Ooi, L. and Saunders, D. N. (2023) 'ALS-linked CCNF variant disrupts motor neuron ubiquitin homeostasis', *Hum Mol Genet*, 32(14), pp. 2386-2398.

Fazal, R., Boeynaems, S., Swijsen, A., De Decker, M., Fumagalli, L., Moisse, M., Vanneste, J., Guo, W., Boon, R., Vercruysse, T., Eggermont, K., Swinnen, B., Beckers, J., Pakravan, D., Vandoorne, T., Vanden Berghe, P., Verfaillie, C., Van Den Bosch, L. and Van Damme, P. (2021) 'HDAC6 inhibition restores TDP-43 pathology and axonal transport defects in human motor neurons with TARDBP mutations', *EMBO J*, 40(7), p. e106177.

Feige, E., Shalom, O., Tsuriel, S., Yissachar, N. and Motro, B. (2006) 'Nek1 shares structural and functional similarities with NIMA kinase', *Biochim Biophys Acta*, 1763(3), pp. 272-81.

Filadi, R., Greotti, E., Turacchio, G., Luini, A., Pozzan, T. and Pizzo, P. (2015) 'Mitofusin 2 ablation increases endoplasmic reticulum-mitochondria coupling', *Proc Natl Acad Sci U S A*, 112(17), pp. E2174-81.

Finelli, M. J., Liu, K. X., Wu, Y., Oliver, P. L. and Davies, K. E. (2015) 'Oxr1 improves pathogenic cellular features of ALS-associated FUS and TDP-43 mutations', *Hum Mol Genet*, 24(12), pp. 3529-44.

Foerster, B. R., Callaghan, B. C., Petrou, M., Edden, R. A., Chenevert, T. L. and Feldman, E. L. (2012) 'Decreased motor cortex γ-aminobutyric acid in amyotrophic lateral sclerosis', *Neurology*, 78(20), pp. 1596-600.

Fonteriz, R. I., de la Fuente, S., Moreno, A., Lobaton, C. D., Montero, M. and Alvarez, J. (2010) 'Monitoring mitochondrial [Ca(2+)] dynamics with rhod-2, ratiometric pericam and aequorin', *Cell Calcium*, 48(1), pp. 61-9.

Forsberg, K., Graffmo, K., Pakkenberg, B., Weber, M., Nielsen, M., Marklund, S., Brannstrom, T. and Andersen, P. M. (2019) 'Misfolded SOD1 inclusions in patients with mutations in C9orf72 and other ALS/FTD-associated genes', *J Neurol Neurosurg Psychiatry*, 90(8), pp. 861-869.

Frade, J. M. and Ovejero-Benito, M. C. (2015) 'Neuronal cell cycle: the neuron itself and its circumstances', *Cell Cycle*, 14(5), pp. 712-20.

Fray, A. E., Ince, P. G., Banner, S. J., Milton, I. D., Usher, P. A., Cookson, M. R. and Shaw, P. J. (1998) 'The expression of the glial glutamate transporter protein EAAT2 in motor neuron disease: an immunohistochemical study', *Eur J Neurosci*, 10(8), pp. 2481-9.

Freischmidt, A., Wieland, T., Richter, B., Ruf, W., Schaeffer, V., Müller, K., Marroquin, N., Nordin, F., Hübers, A., Weydt, P., Pinto, S., Press, R., Millecamps, S., Molko, N., Bernard, E., Desnuelle, C., Soriani, M. H., Dorst, J., Graf, E., Nordström, U., Feiler, M. S., Putz, S., Boeckers, T. M., Meyer, T., Winkler, A. S., Winkelman, J., de Carvalho, M., Thal, D. R., Otto, M., Brännström, T., Volk, A. E., Kursula, P., Danzer, K. M., Lichtner, P., Dikic, I., Meitinger, T., Ludolph, A. C., Strom, T. M., Andersen, P. M. and Weishaupt, J. H. (2015) 'Haploinsufficiency of TBK1 causes familial ALS and fronto-temporal dementia', *Nat Neurosci*, 18(5), pp. 631-6.

Freyre, C. A. C., Rauher, P. C., Ejsing, C. S. and Klemm, R. W. (2019) 'MIGA2 Links Mitochondria, the ER, and Lipid Droplets and Promotes De Novo Lipogenesis in Adipocytes', *Mol Cell*, 76(5), pp. 811-825 e14.

Friedman, J. R., Lackner, L. L., West, M., DiBenedetto, J. R., Nunnari, J. and Voeltz, G. K. (2011) 'ER tubules mark sites of mitochondrial division', *Science*, 334(6054), pp. 358-62.

Fry, A. M., Bayliss, R. and Roig, J. (2017) 'Mitotic Regulation by NEK Kinase Networks', *Front Cell Dev Biol*, 5, p. 102.

Fry, A. M., O'Regan, L., Sabir, S. R. and Bayliss, R. (2012) 'Cell cycle regulation by the NEK family of protein kinases', *J Cell Sci*, 125(Pt 19), pp. 4423-33.

Fumagalli, L., Young, F. L., Boeynaems, S., De Decker, M., Mehta, A. R., Swijsen, A., Fazal, R., Guo, W., Moisse, M., Beckers, J., Dedeene, L., Selvaraj, B. T., Vandoorne, T., Madan, V., van Blitterswijk, M., Raitcheva, D., McCampbell, A., Poesen, K., Gitler, A. D., Koch, P., Vanden Berghe, P., Thal, D. R., Verfaillie, C., Chandran, S., Van Den Bosch, L., Bullock, S. L. and Van Damme, P. (2021) 'C9orf72-derived arginine-containing dipeptide repeats associate with axonal transport machinery and impede microtubule-based motility', *Sci Adv*, 7(15).

Gaffield, M. A. and Betz, W. J. (2006) 'Imaging synaptic vesicle exocytosis and endocytosis with FM dyes', *Nat Protoc*, 1(6), pp. 2916-21.

Gal, J., Ström, A. L., Kilty, R., Zhang, F. and Zhu, H. (2007) 'p62 accumulates and enhances aggregate formation in model systems of familial amyotrophic lateral sclerosis', *J Biol Chem*, 282(15), pp. 11068-77.

Galmes, R., Houcine, A., van Vliet, A. R., Agostinis, P., Jackson, C. L. and Giordano, F. (2016) 'ORP5/ORP8 localize to endoplasmic reticulum-mitochondria contacts and are involved in mitochondrial function', *EMBO Rep*, 17(6), pp. 800-10.

Gandhi, S. and Abramov, A. Y. (2012) 'Mechanism of oxidative stress in neurodegeneration', *Oxid Med Cell Longev*, 2012, p. 428010.

Ganley, I. G., Lam, d. H., Wang, J., Ding, X., Chen, S. and Jiang, X. (2009) 'ULK1.ATG13.FIP200 complex mediates mTOR signaling and is essential for autophagy', *J Biol Chem*, 284(18), pp. 12297-305.

Ganne, A., Balasubramaniam, M., Ayyadevara, H., Kiaei, L., Shmookler Reis, R. J., Varughese, K. I. and Kiaei, M. (2023) 'In silico analysis of TUBA4A mutations in Amyotrophic Lateral Sclerosis to define mechanisms of microtubule disintegration', *Sci Rep*, 13(1), p. 2096.

Gao, W., Shen, Z., Shang, L. and Wang, X. (2011) 'Upregulation of human autophagy-initiation kinase ULK1 by tumor suppressor p53 contributes to DNA-damage-induced cell death', *Cell Death Differ*, 18(10), pp. 1598-607.

Garofalo, T., Matarrese, P., Manganelli, V., Marconi, M., Tinari, A., Gambardella, L., Faggioni, A., Misasi, R., Sorice, M. and Malorni, W. (2016) 'Evidence for the involvement of lipid rafts localized at the ER-mitochondria associated membranes in autophagosome formation', *Autophagy*, 12(6), pp. 917-35.

Gasteiger, E., Hoogland, C., Gattiker, A., Duvaud, S. e., Wilkins, M. R., Appel, R. D. and Bairoch, A. (2005) 'Protein Identification and Analysis Tools on the ExPASy Server', in Walker, J. M. (ed.) *The Proteomics Protocols Handbook*. Totowa, NJ: Humana Press, pp. 571-607.

Geisler, S., Holmström, K. M., Skujat, D., Fiesel, F. C., Rothfuss, O. C., Kahle, P. J. and Springer, W. (2010) 'PINK1/Parkin-mediated mitophagy is dependent on VDAC1 and p62/SQSTM1', *Nat Cell Biol*, 12(2), pp. 119-31.

Ghanbarpour, A., Valverde, D. P., Melia, T. J. and Reinisch, K. M. (2021) 'A model for a partnership of lipid transfer proteins and scramblases in membrane expansion and organelle biogenesis', *Proc Natl Acad Sci U S A*, 118(16).

Ghiasi, P., Hosseinkhani, S., Noori, A., Nafissi, S. and Khajeh, K. (2012) 'Mitochondrial complex I deficiency and ATP/ADP ratio in lymphocytes of amyotrophic lateral sclerosis patients', *Neurol Res*, 34(3), pp. 297-303.

Ghosh, I., Khalil, M. I. and De Benedetti, A. (2022) 'Preprint - Evidence that Nek1 does not phosphorylate Rad54-S572 during recovery from IR', *BioRxiv*.

Gibbs, K. L., Kalmar, B., Rhymes, E. R., Fellows, A. D., Ahmed, M., Whiting, P., Davies, C. H., Greensmith, L. and Schiavo, G. (2018) 'Inhibiting p38 MAPK alpha rescues axonal retrograde transport defects in a mouse model of ALS', *Cell Death Dis*, 9(6), p. 596.

Giglia-Mari, G., Zotter, A. and Vermeulen, W. (2011) 'DNA damage response', *Cold Spring Harb Perspect Biol*, 3(1), p. a000745.

Gilquin, B., Taillebourg, E., Cherradi, N., Hubstenberger, A., Gay, O., Merle, N., Assard, N., Fauvarque, M. O., Tomohiro, S., Kuge, O. and Baudier, J. (2010) 'The AAA+ ATPase ATAD3A controls mitochondrial dynamics at the interface of the inner and outer membranes', *Mol Cell Biol*, 30(8), pp. 1984-96.

Gittings, L. M., Alsop, E. B., Antone, J., Singer, M., Whitsett, T. G., Sattler, R. and Van Keuren-Jensen, K. (2023) 'Cryptic exon detection and transcriptomic changes revealed in single-nuclei RNA sequencing of C9ORF72 patients spanning the ALS-FTD spectrum', *Acta Neuropathol*, 146(3), pp. 433-450.

Glade, M. J. and Smith, K. (2015) 'Phosphatidylserine and the human brain', *Nutrition*, 31(6), pp. 781-6.

Gomez-Suaga, P., Morotz, G. M., Markovinovic, A., Martin-Guerrero, S. M., Preza, E., Arias, N., Mayl, K., Aabdien, A., Gesheva, V., Nishimura, A., Annibali, A., Lee, Y., Mitchell, J. C., Wray, S., Shaw, C., Noble, W. and Miller, C. C. J. (2022) 'Disruption of ER-mitochondria tethering and signalling in C9orf72-associated amyotrophic lateral sclerosis and frontotemporal dementia', *Aging Cell*, 21(2), p. e13549.

Gomez-Suaga, P., Paillusson, S., Stoica, R., Noble, W., Hanger, D. P. and Miller, C. C. J. (2017) 'The ER-Mitochondria Tethering Complex VAPB-PTPIP51 Regulates Autophagy', *Curr Biol*, 27(3), pp. 371-385.

Gómez-Suaga, P., Pérez-Nievas, B. G., Glennon, E. B., Lau, D. H. W., Paillusson, S., Mórotz, G. M., Calì, T., Pizzo, P., Noble, W. and Miller, C. C. J. (2019) 'The VAPB-PTPIP51 endoplasmic reticulum-mitochondria tethering proteins are present in neuronal synapses and regulate synaptic activity', *Acta Neuropathol Commun*, 7(1), p. 35.

Gong, B., Radulovic, M., Figueiredo-Pereira, M. E. and Cardozo, C. (2016) 'The Ubiquitin-Proteasome System: Potential Therapeutic Targets for Alzheimer's Disease and Spinal Cord Injury', *Front Mol Neurosci*, 9, p. 4.

Goode, A., Butler, K., Long, J., Cavey, J., Scott, D., Shaw, B., Sollenberger, J., Gell, C., Johansen, T., Oldham, N. J., Searle, M. S. and Layfield, R. (2016) 'Defective recognition of LC3B by mutant SQSTM1/p62 implicates impairment of autophagy as a pathogenic mechanism in ALS-FTLD', *Autophagy*, 12(7), pp. 1094-104.

Grabowska, W., Sikora, E. and Bielak-Zmijewska, A. (2017) 'Sirtuins, a promising target in slowing down the ageing process', *Biogerontology*, 18(4), pp. 447-476.

Green, J. R., Yunusova, Y., Kuruvilla, M. S., Wang, J., Pattee, G. L., Synhorst, L., Zinman, L. and Berry, J. D. (2013) 'Bulbar and speech motor assessment in ALS: challenges and future directions', *Amyotroph Lateral Scler Frontotemporal Degener*, 14(7-8), pp. 494-500.

Gregorczyk, M., Pastore, G., Munoz, I., Carroll, T., Streubel, J., Munro, M., Lis, P., Lange, S., Lamoliatte, F., Macartney, T., Toth, R., Brown, F., Hastie, J., Pereira, G., Durocher, D. and Rouse, J. (2023) 'Functional characterization of C21ORF2 association with the NEK1 kinase mutated in human in diseases', *Life Sci Alliance*, 6(7).

Guerrero, E. N., Mitra, J., Wang, H., Rangaswamy, S., Hegde, P. M., Basu, P., Rao, K. S. and Hegde, M. L. (2019) 'Amyotrophic lateral sclerosis-associated TDP-43 mutation Q331K prevents nuclear translocation of XRCC4-DNA ligase 4 complex and is linked to genome damage-mediated neuronal apoptosis', *Hum Mol Genet*, 28(18), pp. 3161-3162.

Gui, X., Luo, F., Li, Y., Zhou, H., Qin, Z., Liu, Z., Gu, J., Xie, M., Zhao, K., Dai, B., Shin, W. S., He, J., He, L., Jiang, L., Zhao, M., Sun, B., Li, X., Liu, C. and Li, D. (2019) 'Structural basis for reversible amyloids of hnRNPA1 elucidates their role in stress granule assembly', *Nat Commun*, 10(1), p. 2006.

Gulyas, G., Sohn, M., Kim, Y. J., Varnai, P. and Balla, T. (2020) 'ORP3 phosphorylation regulates phosphatidylinositol 4-phosphate and Ca(2+) dynamics at plasma membrane-ER contact sites', *J Cell Sci*, 133(6).

Guo, C., Zhang, X. and Pfeifer, G. P. (2011) 'The tumor suppressor RASSF1A prevents dephosphorylation of the mammalian STE20-like kinases MST1 and MST2', *J Biol Chem*, 286(8), pp. 6253-61.

Guo, F., Liu, X., Cai, H. and Le, W. (2018) 'Autophagy in neurodegenerative diseases: pathogenesis and therapy', *Brain Pathol*, 28(1), pp. 3-13.

Guo, H. B., Perminov, A., Bekele, S., Kedziora, G., Farajollahi, S., Varaljay, V., Hinkle, K., Molinero, V., Meister, K., Hung, C., Dennis, P., Kelley-Loughnane, N. and Berry, R. (2022) 'AlphaFold2 models indicate that protein sequence determines both structure and dynamics', *Sci Rep*, 12(1), p. 10696.

Gwinn, D. M., Shackelford, D. B., Egan, D. F., Mihaylova, M. M., Mery, A., Vasquez, D. S., Turk, B. E. and Shaw, R. J. (2008) 'AMPK phosphorylation of raptor mediates a metabolic checkpoint', *Mol Cell*, 30(2), pp. 214-26.

Hafner, A., Bulyk, M. L., Jambhekar, A. and Lahav, G. (2019) 'The multiple mechanisms that regulate p53 activity and cell fate', *Nat Rev Mol Cell Biol*, 20(4), pp. 199-210.

Haince, J. F., McDonald, D., Rodrigue, A., Dery, U., Masson, J. Y., Hendzel, M. J. and Poirier, G. G. (2008) 'PARP1-dependent kinetics of recruitment of MRE11 and NBS1 proteins to multiple DNA damage sites', *J Biol Chem*, 283(2), pp. 1197-208.

Hall, C. N., Klein-Flugge, M. C., Howarth, C. and Attwell, D. (2012) 'Oxidative phosphorylation, not glycolysis, powers presynaptic and postsynaptic mechanisms underlying brain information processing', *J Neurosci*, 32(26), pp. 8940-51.

Ham, S. J., Lee, D., Yoo, H., Jun, K., Shin, H. and Chung, J. (2020) 'Decision between mitophagy and apoptosis by Parkin via VDAC1 ubiquitination', *Proc Natl Acad Sci U S A*, 117(8), pp. 4281-4291.

Hamasaki, M., Furuta, N., Matsuda, A., Nezu, A., Yamamoto, A., Fujita, N., Oomori, H., Noda, T., Haraguchi, T., Hiraoka, Y., Amano, A. and Yoshimori, T. (2013) 'Autophagosomes form at ER-mitochondria contact sites', *Nature*, 495(7441), pp. 389-93.

Hammer, R. P., Tomiyasu, U. and Scheibel, A. B. (1979) 'Degeneration of the human Betz cell due to amyotrophic lateral sclerosis', *Exp Neurol*, 63(2), pp. 336-46.

Hammond, J. W., Huang, C. F., Kaech, S., Jacobson, C., Banker, G. and Verhey, K. J. (2010) 'Posttranslational modifications of tubulin and the polarized transport of kinesin-1 in neurons', *Mol Biol Cell*, 21(4), pp. 572-83.

Hao, Y., Chun, A., Cheung, K., Rashidi, B. and Yang, X. (2008) 'Tumor suppressor LATS1 is a negative regulator of oncogene YAP', *J Biol Chem*, 283(9), pp. 5496-509.

Hardiman, O., Al-Chalabi, A., Chio, A., Corr, E. M., Logroscino, G., Robberecht, W., Shaw, P. J., Simmons, Z. and van den Berg, L. H. (2017) 'Amyotrophic lateral sclerosis', *Nature Reviews Disease Primers*, 3(1), p. 17071.

Harding, O., Evans, C. S., Ye, J., Cheung, J., Maniatis, T. and Holzbaur, E. L. F. (2021) 'ALS- and FTD-associated missense mutations in TBK1 differentially disrupt mitophagy', *Proc Natl Acad Sci U S A*, 118(24).

Hargreaves, D. C. and Crabtree, G. R. (2011) 'ATP-dependent chromatin remodeling: genetics, genomics and mechanisms', *Cell Res*, 21(3), pp. 396-420.

Harper, J. W. and Elledge, S. J. (2007) 'The DNA damage response: ten years after', *Mol Cell*, 28(5), pp. 739-45.

Hartopp, N., Lau, D. H. W., Martin-Guerrero, S. M., Markovinovic, A., Morotz, G. M., Greig, J., Glennon, E. B., Troakes, C., Gomez-Suaga, P., Noble, W. and Miller, C. C. J. (2022) 'Disruption of the VAPB-PTPIP51 ER-mitochondria tethering proteins in post-mortem human amyotrophic lateral sclerosis', *Front Cell Dev Biol*, 10, p. 950767.

Hasegawa, M., Arai, T., Nonaka, T., Kametani, F., Yoshida, M., Hashizume, Y., Beach, T. G., Buratti, E., Baralle, F., Morita, M., Nakano, I., Oda, T., Tsuchiya, K. and Akiyama, H. (2008) 'Phosphorylated TDP-43 in frontotemporal lobar degeneration and amyotrophic lateral sclerosis', *Ann Neurol*, 64(1), pp. 60-70.

Hassan, R., Husin, A., Sulong, S., Yusoff, S., Johan, M. F., Yahaya, B. H., Ang, C. Y., Ghazali, S., Cheong, S. K. and Department of Standard Malaysia, M. (2015) 'Guidelines for nucleic acid detection and analysis in hematological disorders', *Malays J Pathol*, 37(2), pp. 165-73.

Hauri, S., Wepf, A., van Drogen, A., Varjosalo, M., Tapon, N., Aebersold, R. and Gstaiger, M. (2013) 'Interaction proteome of human Hippo signaling: modular control of the co-activator YAP1', *Mol Syst Biol*, 9, p. 713.

Hayashi, T. and Su, T. P. (2007) 'Sigma-1 receptor chaperones at the ER-mitochondrion interface regulate Ca(2+) signaling and cell survival', *Cell*, 131(3), pp. 596-610.

He, S., Wang, L., Miao, L., Wang, T., Du, F., Zhao, L. and Wang, X. (2009) 'Receptor interacting protein kinase-3 determines cellular necrotic response to TNF-alpha', *Cell*, 137(6), pp. 1100-11.

Hein, M. Y., Hubner, N. C., Poser, I., Cox, J., Nagaraj, N., Toyoda, Y., Gak, I. A., Weisswange, I., Mansfeld, J., Buchholz, F., Hyman, A. A. and Mann, M. (2015) 'A human interactome in three quantitative dimensions organized by stoichiometries and abundances', *Cell*, 163(3), pp. 712-23.

Herms, J. and Dorostkar, M. M. (2016) 'Dendritic Spine Pathology in Neurodegenerative Diseases', *Annu Rev Pathol*, 11, pp. 221-50.

Hernandez-Alvarez, M. I., Sebastian, D., Vives, S., Ivanova, S., Bartoccioni, P., Kakimoto, P., Plana, N., Veiga, S. R., Hernandez, V., Vasconcelos, N., Peddinti, G., Adrover, A., Jove, M., Pamplona, R., Gordaliza-Alaguero, I., Calvo, E., Cabre, N., Castro, R., Kuzmanic, A., Boutant, M., Sala, D., Hyotylainen, T., Oresic, M., Fort, J., Errasti-Murugarren, E., Rodrigues, C. M. P., Orozco, M., Joven, J., Canto, C., Palacin, M., Fernandez-Veledo, S., Vendrell, J. and Zorzano, A. (2019) 'Deficient Endoplasmic Reticulum-Mitochondrial Phosphatidylserine Transfer Causes Liver Disease', *Cell*, 177(4), pp. 881-895 e17.

Herzig, S. and Shaw, R. J. (2018) 'AMPK: guardian of metabolism and mitochondrial homeostasis', *Nat Rev Mol Cell Biol*, 19(2), pp. 121-135.

Hewitt, V. L., Miller-Fleming, L., Twyning, M. J., Andreazza, S., Mattedi, F., Prudent, J., Polleux, F., Vagnoni, A. and Whitworth, A. J. (2022) 'Decreasing pdzd8-mediated mito-ER contacts improves organismal fitness and mitigates Abeta(42) toxicity', *Life Sci Alliance*, 5(11).

Higelin, J., Catanese, A., Semelink-Sedlacek, L. L., Oeztuerk, S., Lutz, A. K., Bausinger, J., Barbi, G., Speit, G., Andersen, P. M., Ludolph, A. C., Demestre, M. and Boeckers, T. M. (2018) 'NEK1 loss-of-function mutation induces DNA damage accumulation in ALS patient-derived motoneurons', *Stem Cell Res*, 30, pp. 150-162.

Hirabayashi, Y., Kwon, S. K., Paek, H., Pernice, W. M., Paul, M. A., Lee, J., Erfani, P., Raczkowski, A., Petrey, D. S., Pon, L. A. and Polleux, F. (2017) 'ER-mitochondria tethering by PDZD8 regulates Ca(2+) dynamics in mammalian neurons', *Science*, 358(6363), pp. 623-630.

Hirokawa, N., Niwa, S. and Tanaka, Y. (2010) 'Molecular motors in neurons: transport mechanisms and roles in brain function, development, and disease', *Neuron*, 68(4), pp. 610-38.

Hoeijmakers, J. H. (2001) 'Genome maintenance mechanisms for preventing cancer', *Nature*, 411(6835), pp. 366-74.

Honrath, B., Metz, I., Bendridi, N., Rieusset, J., Culmsee, C. and Dolga, A. M. (2017) 'Glucose-regulated protein 75 determines ER-mitochondrial coupling and sensitivity to oxidative stress in neuronal cells', *Cell Death Discov*, 3, p. 17076.

Hornbeck, P. V., Zhang, B., Murray, B., Kornhauser, J. M., Latham, V. and Skrzypek, E. (2015) 'PhosphoSitePlus, 2014: mutations, PTMs and recalibrations', *Nucleic Acids Res*, 43(Database issue), pp. D512-20.

Hortobágyi, T., Troakes, C., Nishimura, A. L., Vance, C., van Swieten, J. C., Seelaar, H., King, A., Al-Sarraj, S., Rogelj, B. and Shaw, C. E. (2011) 'Optineurin inclusions occur in a minority of TDP-43 positive ALS and FTLD-TDP cases and are rarely observed in other neurodegenerative disorders', *Acta Neuropathol*, 121(4), pp. 519-27.

Hoshino, A., Mita, Y., Okawa, Y., Ariyoshi, M., Iwai-Kanai, E., Ueyama, T., Ikeda, K., Ogata, T. and Matoba, S. (2013) 'Cytosolic p53 inhibits Parkin-mediated mitophagy and promotes mitochondrial dysfunction in the mouse heart', *Nat Commun*, 4, p. 2308.

Hosokawa, N., Hara, T., Kaizuka, T., Kishi, C., Takamura, A., Miura, Y., Iemura, S., Natsume, T., Takehana, K., Yamada, N., Guan, J. L., Oshiro, N. and Mizushima, N. (2009) 'Nutrient-dependent mTORC1 association with the ULK1-Atg13-FIP200 complex required for autophagy', *Mol Biol Cell*, 20(7), pp. 1981-91.

Howland, D. S., Liu, J., She, Y., Goad, B., Maragakis, N. J., Kim, B., Erickson, J., Kulik, J., DeVito, L., Psaltis, G., DeGennaro, L. J., Cleveland, D. W. and Rothstein, J. D. (2002) 'Focal loss of the glutamate transporter EAAT2 in a transgenic rat model of SOD1 mutant-mediated amyotrophic lateral sclerosis (ALS)', *Proc Natl Acad Sci U S A*, 99(3), pp. 1604-9.

Huang, K. C., Chiang, S. F., Yang, P. C., Ke, T. W., Chen, T. W., Lin, C. Y., Chang, H. Y., Chen, W. T. and Chao, K. C. (2021) 'ATAD3A stabilizes GRP78 to suppress ER stress for acquired chemoresistance in colorectal cancer', *J Cell Physiol*, 236(9), pp. 6481-6495.

Huang, R., Xu, Y., Wan, W., Shou, X., Qian, J., You, Z., Liu, B., Chang, C., Zhou, T., Lippincott-Schwartz, J. and Liu, W. (2015) 'Deacetylation of nuclear LC3 drives autophagy initiation under starvation', *Mol Cell*, 57(3), pp. 456-66.

Huang, X., Oses-Prieto, J. A., Kawaguchi, R., Perrault, L., Frost, D., Chen, K., Guo, F., Zhang, B., Zhao, P., Ho, T. S.-Y., Pandey, R., Geschwind, D., Burlingame, A. L. and Woolf, C. J. (2024) 'NEK1 modulates neurite outgrowth in motor neurons through coordinating retromer formation', *bioRxiv*, p. 2024.05.06.592854.

Hübers, A., Just, W., Rosenbohm, A., Müller, K., Marroquin, N., Goebel, I., Högel, J., Thiele, H., Altmüller, J., Nürnberg, P., Weishaupt, J. H., Kubisch, C., Ludolph, A. C. and Volk, A. E. (2015) 'De novo FUS mutations are the most frequent genetic cause in early-onset German ALS patients', *Neurobiol Aging*, 36(11), pp. 3117.e1-3117.e6.

Hudson, J. J., Hsu, D. W., Guo, K., Zhukovskaya, N., Liu, P. H., Williams, J. G., Pears, C. J. and Lakin, N. D. (2005) 'DNA-PKcs-dependent signaling of DNA damage in Dictyostelium discoideum', *Curr Biol*, 15(20), pp. 1880-5.

Hung, V., Lam, S. S., Udeshi, N. D., Svinkina, T., Guzman, G., Mootha, V. K., Carr, S. A. and Ting, A. Y. (2017) 'Proteomic mapping of cytosol-facing outer mitochondrial and ER membranes in living human cells by proximity biotinylation', *Elife*, 6.

Huttlin, E. L., Bruckner, R. J., Navarrete-Perea, J., Cannon, J. R., Baltier, K., Gebreab, F., Gygi, M. P., Thornock, A., Zarraga, G., Tam, S., Szpyt, J., Gassaway, B. M., Panov, A., Parzen, H., Fu, S., Golbazi, A., Maenpaa, E., Stricker, K., Guha Thakurta, S., Zhang, T., Rad, R., Pan, J., Nusinow, D. P., Paulo, J. A., Schweppe, D. K., Vaites, L. P., Harper, J. W. and Gygi, S. P. (2021) 'Dual proteome-scale networks reveal cell-specific remodeling of the human interactome', *Cell*, 184(11), pp. 3022-3040 e28.

Huttlin, E. L., Bruckner, R. J., Paulo, J. A., Cannon, J. R., Ting, L., Baltier, K., Colby, G., Gebreab, F., Gygi, M. P., Parzen, H., Szpyt, J., Tam, S., Zarraga, G., Pontano-Vaites, L., Swarup, S., White, A. E., Schweppe, D. K., Rad, R., Erickson, B. K., Obar, R. A., Guruharsha, K. G., Li, K., Artavanis-Tsakonas, S., Gygi, S. P. and Harper, J. W. (2017) 'Architecture of the human interactome defines protein communities and disease networks', *Nature*, 545(7655), pp. 505-509.

Iacoangeli, A., Dilliott, A. A., Al Khleifat, A., Andersen, P. M., Başak, N. A., Cooper-Knock, J., Corcia, P., Couratier, P., de Carvalho, M., Drory, V., Glass, J. D., Gotkine, M., Lerner, Y., Hardiman, O., Landers, J. E., McLaughlin, R., Mora Pardina, J. S., Morrison, K. E., Pinto, S., Povedano, M., Shaw, C. E., Shaw, P. J., Silani, V., Ticozzi, N., Van Damme, P., van den Berg, L. H., Vourc'h, P., Weber, M., Veldink, J. H., Dobson, R. J., Rouleau, G. A., Chalabi, A. A. and Farhan, S. M. K. (2024) 'The oligogenic structure of amyotrophic lateral sclerosis has genetic testing, counselling, and therapeutic implications', *medRxiv*, p. 2024.03.21.24304693.

Insolera, R., Lőrincz, P., Wishnie, A. J., Juhász, G. and Collins, C. A. (2021) 'Mitochondrial fission, integrity and completion of mitophagy require separable functions of Vps13D in Drosophila neurons', *PLoS Genet*, 17(8), p. e1009731.

Itakura, E., Kishi-Itakura, C. and Mizushima, N. (2012) 'The hairpin-type tail-anchored SNARE syntaxin 17 targets to autophagosomes for fusion with endosomes/lysosomes', *Cell*, 151(6), pp. 1256-69.

Ito, Y., Ofengeim, D., Najafov, A., Das, S., Saberi, S., Li, Y., Hitomi, J., Zhu, H., Chen, H., Mayo, L., Geng, J., Amin, P., DeWitt, J. P., Mookhtiar, A. K., Florez, M., Ouchida, A. T., Fan, J. B., Pasparakis, M., Kelliher, M. A., Ravits, J. and Yuan, J. (2016) 'RIPK1 mediates axonal degeneration by promoting inflammation and necroptosis in ALS', *Science*, 353(6299), pp. 603-8.

Iwasawa, R., Mahul-Mellier, A. L., Datler, C., Pazarentzos, E. and Grimm, S. (2011) 'Fis1 and Bap31 bridge the mitochondria-ER interface to establish a platform for apoptosis induction', *EMBO J*, 30(3), pp. 556-68.

Iyama, T. and Wilson, D. M. (2013) 'DNA repair mechanisms in dividing and non-dividing cells', *DNA Repair (Amst)*, 12(8), pp. 620-36.

Jackson, S. P. and Bartek, J. (2009) 'The DNA-damage response in human biology and disease', *Nature*, 461(7267), pp. 1071-8.

James, C. and Kehlenbach, R. H. (2021) 'The Interactome of the VAP Family of Proteins: An Overview', *Cells*, 10(7).

James, C., Möller, U., Spillner, C., König, S., Dybkov, O., Urlaub, H., Lenz, C. and Kehlenbach, R. H. (2024) 'Phosphorylation of ELYS promotes its interaction with VAPB at decondensing chromosomes during mitosis', *EMBO Rep*, 25(5), pp. 2391-2417.

James, C., Müller, M., Goldberg, M. W., Lenz, C., Urlaub, H. and Kehlenbach, R. H. (2019) 'Proteomic mapping by rapamycin-dependent targeting of APEX2 identifies binding partners of VAPB at the inner nuclear membrane', *J Biol Chem*, 294(44), pp. 16241-16254.

Jeong, J., Juhn, K., Lee, H., Kim, S. H., Min, B. H., Lee, K. M., Cho, M. H., Park, G. H. and Lee, K. H. (2007) 'SIRT1 promotes DNA repair activity and deacetylation of Ku70', *Exp Mol Med*, 39(1), pp. 8-13.

Jiang, F., Ryan, M. T., Schlame, M., Zhao, M., Gu, Z., Klingenberg, M., Pfanner, N. and Greenberg, M. L. (2000) 'Absence of cardiolipin in the crd1 null mutant results in decreased mitochondrial membrane potential and reduced mitochondrial function', *J Biol Chem*, 275(29), pp. 22387-94.

Jiang, L. and Ngo, S. T. (2022) 'Altered TDP-43 Structure and Function: Key Insights into Aberrant RNA, Mitochondrial, and Cellular and Systemic Metabolism in Amyotrophic Lateral Sclerosis', *Metabolites*, 12(8).

Jiang, Q., Lin, J., Wei, Q., Li, C., Hou, Y., Zhang, L., Ou, R., Liu, K., Yang, T., Xiao, Y., Hadano, S. and Shang, H. (2023) 'Genetic and clinical characteristics of ALS patients with NEK1 gene variants', *Neurobiol Aging*, 123, pp. 191-199.

Jiang, Y., Cong, X., Jiang, S., Dong, Y., Zhao, L., Zang, Y., Tan, M. and Li, J. (2022) 'Phosphoproteomics Reveals the AMPK Substrate Network in Response to DNA Damage and Histone Acetylation', *Genomics Proteomics Bioinformatics*, 20(4), pp. 597-613.

Jimenez-Mateos, E. M., Gonzalez-Billault, C., Dawson, H. N., Vitek, M. P. and Avila, J. (2006) 'Role of MAP1B in axonal retrograde transport of mitochondria', *Biochem J*, 397(1), pp. 53-9.

Jiricny, J. (2006) 'The multifaceted mismatch-repair system', *Nat Rev Mol Cell Biol*, 7(5), pp. 335-46.

Johnson, B., Leek, A. N., Sole, L., Maverick, E. E., Levine, T. P. and Tamkun, M. M. (2018) 'Kv2 potassium channels form endoplasmic reticulum/plasma membrane junctions via interaction with VAPA and VAPB', *Proc Natl Acad Sci U S A*, 115(31), pp. E7331-E7340.

Johnson, J. O., Glynn, S. M., Gibbs, J. R., Nalls, M. A., Sabatelli, M., Restagno, G., Drory, V. E., Chiò, A., Rogaeva, E. and Traynor, B. J. (2014) 'Mutations in the CHCHD10 gene are a common cause of familial amyotrophic lateral sclerosis', *Brain*, 137(Pt 12), p. e311.

Johnson, J. O., Mandrioli, J., Benatar, M., Abramzon, Y., Van Deerlin, V. M., Trojanowski, J. Q., Gibbs, J. R., Brunetti, M., Gronka, S., Wuu, J., Ding, J., McCluskey, L., Martinez-Lage, M., Falcone, D., Hernandez, D. G., Arepalli, S., Chong, S., Schymick, J. C., Rothstein, J., Landi, F., Wang, Y. D., Calvo, A., Mora, G., Sabatelli, M., Monsurrò, M. R., Battistini, S., Salvi, F., Spataro, R., Sola, P., Borghero, G., Galassi, G., Scholz, S. W., Taylor, J. P., Restagno, G., Chiò, A., Traynor, B. J. and Consortium, I. (2010) 'Exome sequencing reveals VCP mutations as a cause of familial ALS', *Neuron*, 68(5), pp. 857-64.

Ju, J. S., Fuentealba, R. A., Miller, S. E., Jackson, E., Piwnica-Worms, D., Baloh, R. H. and Weihl, C. C. (2009) 'Valosin-containing protein (VCP) is required for autophagy and is disrupted in VCP disease', *J Cell Biol*, 187(6), pp. 875-88.

Julien, J. P., Côté, F. and Collard, J. F. (1995) 'Mice overexpressing the human neurofilament heavy gene as a model of ALS', *Neurobiol Aging*, 16(3), pp. 487-90; discussion 490-2.

Jumper, J., Evans, R., Pritzel, A., Green, T., Figurnov, M., Ronneberger, O., Tunyasuvunakool, K., Bates, R., Žídek, A., Potapenko, A., Bridgland, A., Meyer, C., Kohl, S. A. A., Ballard, A. J., Cowie, A., Romera-Paredes, B., Nikolov, S., Jain, R., Adler, J., Back, T., Petersen, S., Reiman, D., Clancy, E., Zielinski, M., Steinegger, M., Pacholska, M., Berghammer, T., Bodenstein, S., Silver, D., Vinyals, O., Senior, A. W., Kavukcuoglu, K., Kohli, P. and Hassabis, D. (2021) 'Highly accurate protein structure prediction with AlphaFold', *Nature*, 596(7873), pp. 583-589.

Jung, C. H., Jun, C. B., Ro, S. H., Kim, Y. M., Otto, N. M., Cao, J., Kundu, M. and Kim, D. H. (2009) 'ULK-Atg13-FIP200 complexes mediate mTOR signaling to the autophagy machinery', *Mol Biol Cell*, 20(7), pp. 1992-2003.

Kabashi, E., El Oussini, H., Bercier, V., Gros-Louis, F., Valdmanis, P. N., McDearmid, J., Mejier, I. A., Dion, P. A., Dupre, N., Hollinger, D., Sinniger, J., Dirrig-Grosch, S., Camu, W., Meininger, V., Loeffler, J. P., René, F., Drapeau, P., Rouleau, G. A. and Dupuis, L. (2013) 'Investigating the contribution of VAPB/ALS8 loss of function in amyotrophic lateral sclerosis', *Hum Mol Genet*, 22(12), pp. 2350-60.

Kaiser, S. E., Brickner, J. H., Reilein, A. R., Fenn, T. D., Walter, P. and Brunger, A. T. (2005) 'Structural basis of FFAT motif-mediated ER targeting', *Structure*, 13(7), pp. 1035-45.

Kannan, K. and Jain, S. K. (2000) 'Oxidative stress and apoptosis', *Pathophysiology*, 7(3), pp. 153-163.

Karchugina, S., Benton, D. and Chernoff, J. (2021) 'Regulation of MST complexes and activity via SARAH domain modifications', *Biochem Soc Trans*, 49(2), pp. 675-683.

Kari, S., Subramanian, K., Altomonte, I. A., Murugesan, A., Yli-Harja, O. and Kandhavelu, M. (2022) 'Programmed cell death detection methods: a systematic review and a categorical comparison', *Apoptosis*, 27(7-8), pp. 482-508.

Kawano, M., Kumagai, K., Nishijima, M. and Hanada, K. (2006) 'Efficient trafficking of ceramide from the endoplasmic reticulum to the Golgi apparatus requires a VAMP-associated protein-interacting FFAT motif of CERT', *J Biol Chem*, 281(40), pp. 30279-88.

Kenna, K. P., van Doormaal, P. T., Dekker, A. M., Ticozzi, N., Kenna, B. J., Diekstra, F. P., van Rheenen, W., van Eijk, K. R., Jones, A. R., Keagle, P., Shatunov, A., Sproviero, W., Smith, B. N., van Es, M. A., Topp, S. D., Kenna, A., Miller, J. W., Fallini, C., Tiloca, C., McLaughlin, R. L., Vance, C., Troakes, C., Colombrita, C., Mora, G., Calvo, A., Verde, F., Al-Sarraj, S., King, A., Calini, D., de Belleroche, J., Baas, F., van der Kooi, A. J., de Visser, M., Ten Asbroek, A. L., Sapp, P. C., McKenna-Yasek, D., Polak, M., Asress, S., Muñoz-Blanco, J. L., Strom, T. M., Meitinger, T., Morrison, K. E., Lauria, G., Williams, K. L., Leigh, P. N., Nicholson, G. A., Blair, I. P., Leblond, C. S., Dion, P. A., Rouleau, G. A., Pall, H., Shaw, P. J., Turner, M. R., Talbot, K., Taroni, F., Boylan, K. B., Van Blitterswijk, M., Rademakers, R., Esteban-Pérez, J., García-Redondo, A., Van Damme, P., Robberecht, W., Chio, A., Gellera, C., Drepper, C., Sendtner, M., Ratti, A., Glass, J. D., Mora, J. S., Basak, N. A., Hardiman, O., Ludolph, A. C., Andersen, P. M., Weishaupt, J. H., Brown, R. H., Al-Chalabi, A., Silani, V., Shaw, C. E., van den Berg, L. H., Veldink, J. H., Landers, J. E. and Consortium, S. (2016) 'NEK1 variants confer susceptibility to amyotrophic lateral sclerosis', *Nat Genet*, 48(9), pp. 1037-42.

Kettenbach, A. N., Schweppe, D. K., Faherty, B. K., Pechenick, D., Pletnev, A. A. and Gerber, S. A. (2011) 'Quantitative phosphoproteomics identifies substrates and functional modules of Aurora and Polo-like kinase activities in mitotic cells', *Sci Signal*, 4(179), p. rs5.

Khalfallah, Y., Kuta, R., Grasmuck, C., Prat, A., Durham, H. D. and Vande Velde, C. (2018) 'TDP-43 regulation of stress granule dynamics in neurodegenerative disease-relevant cell types', *Sci Rep*, 8(1), p. 7551.

Khalil, B., Cabirol-Pol, M. J., Miguel, L., Whitworth, A. J., Lecourtois, M. and Lievens, J. C. (2017) 'Enhancing Mitofusin/Marf ameliorates neuromuscular dysfunction in Drosophila models of TDP-43 proteinopathies', *Neurobiol Aging*, 54, pp. 71-83.

Khalil, M. I. and De Benedetti, A. (2022) 'Tousled-like kinase 1: a novel factor with multifaceted role in mCRPC progression and development of therapy resistance', *Cancer Drug Resist*, 5(1), pp. 93-101.

Khalil, M. I., Ghosh, I., Singh, V., Chen, J., Zhu, H. and De Benedetti, A. (2020) 'NEK1 Phosphorylation of YAP Promotes Its Stabilization and Transcriptional Output', *Cancers (Basel)*, 12(12).

Kim, B. W., Jeong, Y. E., Wong, M. and Martin, L. J. (2020) 'DNA damage accumulates and responses are engaged in human ALS brain and spinal motor neurons and DNA repair is activatable in iPSC-derived motor neurons with SOD1 mutations', *Acta Neuropathol Commun*, 8(1), p. 7.

Kim, H., Lee, S., Jun, Y. and Lee, C. (2022) 'Structural basis for mitoguardin-2 mediated lipid transport at ER-mitochondrial membrane contact sites', *Nat Commun*, 13(1), p. 3702.

Kim, H. J., Kim, N. C., Wang, Y. D., Scarborough, E. A., Moore, J., Diaz, Z., MacLea, K. S., Freibaum, B., Li, S., Molliex, A., Kanagaraj, A. P., Carter, R., Boylan, K. B., Wojtas, A. M., Rademakers, R., Pinkus, J. L., Greenberg, S. A., Trojanowski, J. Q., Traynor, B. J., Smith, B. N., Topp, S., Gkazi, A. S., Miller, J., Shaw, C. E., Kottlors, M., Kirschner, J., Pestronk, A., Li, Y. R., Ford, A. F., Gitler, A. D., Benatar, M., King, O. D.,

Kimonis, V. E., Ross, E. D., Weihl, C. C., Shorter, J. and Taylor, J. P. (2013) 'Mutations in prion-like domains in hnRNPA2B1 and hnRNPA1 cause multisystem proteinopathy and ALS', *Nature*, 495(7442), pp. 467-73.

Kim, J., Kundu, M., Viollet, B. and Guan, K. L. (2011) 'AMPK and mTOR regulate autophagy through direct phosphorylation of Ulk1', *Nat Cell Biol*, 13(2), pp. 132-41.

Kim, J., Lee, S., Kim, H., Lee, H., Seong, K. M., Youn, H. and Youn, B. (2021) 'Autophagic Organelles in DNA Damage Response', *Front Cell Dev Biol*, 9, p. 668735.

Kim, J. Y., Jang, A., Reddy, R., Yoon, W. H. and Jankowsky, J. L. (2016) 'Neuronal overexpression of human VAPB slows motor impairment and neuromuscular denervation in a mouse model of ALS', *Hum Mol Genet*, 25(21), pp. 4661-4673.

Kim, S., Leal, S. S., Ben Halevy, D., Gomes, C. M. and Lev, S. (2010a) 'Structural requirements for VAP-B oligomerization and their implication in amyotrophic lateral sclerosis-associated VAP-B(P56S) neurotoxicity', *J Biol Chem*, 285(18), pp. 13839-49.

Kim, S. H., Shanware, N. P., Bowler, M. J. and Tibbetts, R. S. (2010b) 'Amyotrophic lateral sclerosis-associated proteins TDP-43 and FUS/TLS function in a common biochemical complex to co-regulate HDAC6 mRNA', *J Biol Chem*, 285(44), pp. 34097-105.

Klionsky, D. J., Abdel-Aziz, A. K., Abdelfatah, S., Abdellatif, M., Abdoli, A., Abel, S., Abeliovich, H., Abildgaard, M. H., Abudu, Y. P., Acevedo-Arozena, A., Adamopoulos, I. E., Adeli, K., Adolph, T. E., Adornetto, A., Aflaki, E., Agam, G., Agarwal, A., Aggarwal, B. B., Agnello, M., Agostinis, P., Agrewala, J. N., Agrotis, A., Aguilar, P. V., Ahmad, S. T., Ahmed, Z. M., Ahumada-Castro, U., Aits, S., Aizawa, S., Akkoc, Y., Akoumianaki, T., Akpinar, H. A., Al-Abd, A. M., Al-Akra, L., Al-Gharaibeh, A., Alaoui-Jamali, M. A., Alberti, S., Alcocer-Gómez, E., Alessandri, C., Ali, M., Alim Al-Bari, M. A., Aliwaini, S., Alizadeh, J., Almacellas, E., Almasan, A., Alonso, A., Alonso, G. D., Altan-Bonnet, N., Altieri, D. C., Álvarez É, M. C., Alves, S., Alves da Costa, C., Alzaharna, M. M., Amadio, M., Amantini, C., Amaral, C., Ambrosio, S., Amer, A. O., Ammanathan, V., An, Z., Andersen, S. U., Andrabi, S. A., Andrade-Silva, M., Andres, A. M., Angelini, S., Ann, D., Anozie, U. C., Ansari, M. Y., Antas, P., Antebi, A., Antón, Z., Anwar, T., Apetoh, L., Apostolova, N., Araki, T., Araki, Y., Arasaki, K., Araújo, W. L., Araya, J., Arden, C., Arévalo, M. A., Arguelles, S., Arias, E., Arikkath, J., Arimoto, H., Ariosa, A. R., Armstrong-James, D., Arnauné-Pelloquin, L., Aroca, A., Arroyo, D. S., Arsov, I., Artero, R., Asaro, D. M. L., Aschner, M., Ashrafizadeh, M., Ashur-Fabian, O., Atanasov, A. G., Au, A. K., Auberger, P., Auner, H. W., Aurelian, L., et al. (2021) 'Guidelines for the use and interpretation of assays for monitoring autophagy (4th edition)(1)', *Autophagy*, 17(1), pp. 1-382.

Knoblochova, L., Duricek, T., Vaskovicova, M., Zorzompokou, C., Rayova, D., Ferencova, I., Baran, V., Schultz, R. M., Hoffmann, E. R. and Drutovic, D. (2023) 'CHK1-CDC25A-CDK1 regulate cell cycle progression and protect genome integrity in early mouse embryos', *EMBO Rep*, 24(10), p. e56530.

Komis, G., Illes, P., Beck, M. and Samaj, J. (2011) 'Microtubules and mitogen-activated protein kinase signalling', *Curr Opin Plant Biol*, 14(6), pp. 650-7.

Konopka, A., Whelan, D. R., Jamali, M. S., Perri, E., Shahheydari, H., Toth, R. P., Parakh, S., Robinson, T., Cheong, A., Mehta, P., Vidal, M., Ragagnin, A. M. G., Khizhnyak, I., Jagaraj, C. J., Galper, J., Grima, N., Deva, A., Shadfar, S., Nicholson, G. A., Yang, S., Cutts, S. M., Horejsi, Z., Bell, T. D. M., Walker, A. K., Blair, I. P. and Atkin, J. D. (2020) 'Impaired NHEJ repair in amyotrophic lateral sclerosis is associated with TDP-43 mutations', *Mol Neurodegener*, 15(1), p. 51.

Kors, S., Hacker, C., Bolton, C., Maier, R., Reimann, L., Kitchener, E. J. A., Warscheid, B., Costello, J. L. and Schrader, M. (2022a) 'Regulating peroxisome-ER contacts via the ACBD5-VAPB tether by FFAT motif phosphorylation and GSK3beta', *J Cell Biol*, 221(3).

Kors, S., Schrader, M. and Costello, J. L. (2022b) 'Multiple Ways to Keep FFAT Under Control!', *Contact (Thousand Oaks)*, 5, pp. 1-4.

Kozlov, S., Gueven, N., Keating, K., Ramsay, J. and Lavin, M. F. (2003) 'ATP activates ataxia-telangiectasia mutated (ATM) in vitro. Importance of autophosphorylation', *J Biol Chem*, 278(11), pp. 9309-17.

Kroemer, G., Galluzzi, L. and Brenner, C. (2007) 'Mitochondrial membrane permeabilization in cell death', *Physiol Rev*, 87(1), pp. 99-163.

Krohn, K., Ovod, V., Vilja, P., Heino, M., Scott, H., Kyriakou, D. S., Antonarakis, S., Jacobs, H. T., Isola, J. and Peterson, P. (1997) 'Immunochemical characterization of a novel mitochondrially located protein encoded by a nuclear gene within the DFNB8/10 critical region on 21q22.3', *Biochem Biophys Res Commun*, 238(3), pp. 806-10.

Krols, M., van Isterdael, G., Asselbergh, B., Kremer, A., Lippens, S., Timmerman, V. and Janssens, S. (2016) 'Mitochondria-associated membranes as hubs for neurodegeneration', *Acta Neuropathol*, 131(4), pp. 505-23.

Kuijpers, M., Yu, K. L., Teuling, E., Akhmanova, A., Jaarsma, D. and Hoogenraad, C. C. (2013) 'The ALS8 protein VAPB interacts with the ER-Golgi recycling protein YIF1A and regulates membrane delivery into dendrites', *EMBO J*, 32(14), pp. 2056-72.

Kulkarni, A., Chen, J. and Maday, S. (2018) 'Neuronal autophagy and intercellular regulation of homeostasis in the brain', *Curr Opin Neurobiol*, 51, pp. 29-36.

Kumar, P., Nagarajan, A. and Uchil, P. D. (2018) 'Analysis of Cell Viability by the Lactate Dehydrogenase Assay', *Cold Spring Harb Protoc*, 2018(6).

Kwiatkowski, T. J., Bosco, D. A., Leclerc, A. L., Tamrazian, E., Vanderburg, C. R., Russ, C., Davis, A., Gilchrist, J., Kasarskis, E. J., Munsat, T., Valdmanis, P., Rouleau, G. A., Hosler, B. A., Cortelli, P., de Jong, P. J., Yoshinaga, Y., Haines, J. L., Pericak-Vance, M. A., Yan, J., Ticozzi, N., Siddique, T., McKenna-Yasek, D., Sapp, P. C., Horvitz, H. R., Landers, J. E. and Brown, R. H. (2009) 'Mutations in the FUS/TLS gene on chromosome 16 cause familial amyotrophic lateral sclerosis', *Science*, 323(5918), pp. 1205-8.

Kwon, I., Xiang, S., Kato, M., Wu, L., Theodoropoulos, P., Wang, T., Kim, J., Yun, J., Xie, Y. and McKnight, S. L. (2014) 'Poly-dipeptides encoded by the C9orf72 repeats bind nucleoli, impede RNA biogenesis, and kill cells', *Science*, 345(6201), pp. 1139-45.

Lacomblez, L., Bensimon, G., Leigh, P. N., Guillet, P., Powe, L., Durrleman, S., Delumeau, J. C. and Meininger, V. (1996) 'A confirmatory dose-ranging study of riluzole in ALS. ALS/Riluzole Study Group-II', *Neurology*, 47(6 Suppl 4), pp. S242-50.

Lai, C., Lin, X., Chandran, J., Shim, H., Yang, W. J. and Cai, H. (2007) 'The G59S mutation in p150(glued) causes dysfunction of dynactin in mice', *J Neurosci*, 27(51), pp. 13982-90.

Lai, C. K., Gupta, N., Wen, X., Rangell, L., Chih, B., Peterson, A. S., Bazan, J. F., Li, L. and Scales, S. J. (2011) 'Functional characterization of putative cilia genes by high-content analysis', *Mol Biol Cell*, 22(7), pp. 1104-19.

Lattante, S., Doronzio, P. N., Conte, A., Marangi, G., Martello, F., Bisogni, G., Meleo, E., Colavito, D., Del Giudice, E., Patanella, A. K., Bernardo, D., Romano, A., Zollino, M. and Sabatelli, M. (2021) 'Novel variants and cellular studies on patients' primary fibroblasts support a role for NEK1 missense variants in ALS pathogenesis', *Human Molecular Genetics*, 30(1), pp. 65-71.

Lautenschlager, J., Prell, T., Ruhmer, J., Weidemann, L., Witte, O. W. and Grosskreutz, J. (2013) 'Overexpression of human mutated G93A SOD1 changes dynamics of the ER mitochondria calcium cycle specifically in mouse embryonic motor neurons', *Exp Neurol*, 247, pp. 91-100.

Lee, J., Pye, N., Ellis, L., Vos, K. and Mortiboys, H. (2024) 'Evidence of mitochondrial dysfunction in ALS and methods for measuring in model systems', *Int Rev Neurobiol*, 176, pp. 269-325.

Lee, J. H. and Paull, T. T. (2007) 'Activation and regulation of ATM kinase activity in response to DNA double-strand breaks', *Oncogene*, 26(56), pp. 7741-8.

Lee, Y. B., Chen, H. J., Peres, J. N., Gomez-Deza, J., Attig, J., Stalekar, M., Troakes, C., Nishimura, A. L., Scotter, E. L., Vance, C., Adachi, Y., Sardone, V., Miller, J. W., Smith, B. N., Gallo, J. M., Ule, J., Hirth, F., Rogelj, B., Houart, C. and Shaw, C. E. (2013) 'Hexanucleotide repeats in ALS/FTD form length-dependent RNA foci, sequester RNA binding proteins, and are neurotoxic', *Cell Rep*, 5(5), pp. 1178-86.

Lefebvre-Omar, C., Liu, E., Dalle, C., d'Incamps, B. L., Bigou, S., Daube, C., Karpf, L., Davenne, M., Robil, N., Jost Mousseau, C., Blanchard, S., Tournaire, G., Nicaise, C., Salachas, F., Lacomblez, L., Seilhean, D., Lobsiger, C. S., Millecamps, S., Boillée, S. and Bohl, D. (2023) 'Neurofilament accumulations in amyotrophic lateral sclerosis patients' motor neurons impair axonal initial segment integrity', *Cell Mol Life Sci*, 80(6), p. 150.

Levy, E., El Banna, N., Baille, D., Heneman-Masurel, A., Truchet, S., Rezaei, H., Huang, M. E., Beringue, V., Martin, D. and Vernis, L. (2019) 'Causative Links between Protein Aggregation and Oxidative Stress: A Review', *Int J Mol Sci*, 20(16).

Li, G., Li, J., Shao, R., Zhao, J. and Chen, M. (2021) 'FUNDC1: A Promising Mitophagy Regulator at the Mitochondria-Associated Membrane for Cardiovascular Diseases', *Front Cell Dev Biol*, 9, p. 788634.

Li, J., D'Angiolella, V., Seeley, E. S., Kim, S., Kobayashi, T., Fu, W., Campos, E. I., Pagano, M. and Dynlacht, B. D. (2013) 'USP33 regulates centrosome biogenesis via deubiquitination of the centriolar protein CP110', *Nature*, 495(7440), pp. 255-9.

Li, Y., Li, S. and Wu, H. (2022) 'Ubiquitination-Proteasome System (UPS) and Autophagy Two Main Protein Degradation Machineries in Response to Cell Stress', *Cells*, 11(5).

Liang, J., Xu, Z. X., Ding, Z., Lu, Y., Yu, Q., Werle, K. D., Zhou, G., Park, Y. Y., Peng, G., Gambello, M. J. and Mills, G. B. (2015) 'Myristoylation confers noncanonical AMPK functions in autophagy selectivity and mitochondrial surveillance', *Nat Commun*, 6, p. 7926.

Lieber, M. R. (2010) 'The mechanism of double-strand DNA break repair by the nonhomologous DNA end-joining pathway', *Annu Rev Biochem*, 79, pp. 181-211.

Lin, W. L. and Dickson, D. W. (2008) 'Ultrastructural localization of TDP-43 in filamentous neuronal inclusions in various neurodegenerative diseases', *Acta Neuropathol*, 116(2), pp. 205-13.

Liu, Q., Shu, S., Wang, R. R., Liu, F., Cui, B., Guo, X. N., Lu, C. X., Li, X. G., Liu, M. S., Peng, B., Cui, L. Y. and Zhang, X. (2016) 'Whole-exome sequencing identifies a missense mutation in hnRNPA1 in a family with flail arm ALS', *Neurology*, 87(17), pp. 1763-1769.

Liu, S., Ho, C. K., Ouyang, J. and Zou, L. (2013) 'Nek1 kinase associates with ATR-ATRIP and primes ATR for efficient DNA damage signaling', *Proc Natl Acad Sci U S A*, 110(6), pp. 2175-80.

Liu, T., Wang, L., Chen, G., Tong, L., Ye, X., Yang, H., Liu, H., Zhang, H., Lu, W., Zhang, S. and Du, D. (2023) 'PDZD8-mediated endoplasmic reticulum-mitochondria associations regulate sympathetic drive and blood pressure through the intervention of neuronal mitochondrial homeostasis in stress-induced hypertension', *Neurobiol Dis*, 183, p. 106173.

Liu, Y., Ma, X., Fujioka, H., Liu, J., Chen, S. and Zhu, X. (2019) 'DJ-1 regulates the integrity and function of ER-mitochondria association through interaction with IP3R3-Grp75-VDAC1', *Proc Natl Acad Sci U S A*, 116(50), pp. 25322-25328.

Livak, K. J. and Schmittgen, T. D. (2001) 'Analysis of relative gene expression data using real-time quantitative PCR and the 2(-Delta Delta C(T)) Method', *Methods*, 25(4), pp. 402-8.

Loewen, C. J., Roy, A. and Levine, T. P. (2003) 'A conserved ER targeting motif in three families of lipid binding proteins and in Opi1p binds VAP', *EMBO J*, 22(9), pp. 2025-35.

Logroscino, G., Traynor, B. J., Hardiman, O., Chio, A., Mitchell, D., Swingler, R. J., Millul, A., Benn, E., Beghi, E. and Eurals (2010) 'Incidence of amyotrophic lateral sclerosis in Europe', *J Neurol Neurosurg Psychiatry*, 81(4), pp. 385-90.

Lomen-Hoerth, C., Anderson, T. and Miller, B. (2002) 'The overlap of amyotrophic lateral sclerosis and frontotemporal dementia', *Neurology*, 59(7), pp. 1077-9.

Lomen-Hoerth, C., Murphy, J., Langmore, S., Kramer, J. H., Olney, R. K. and Miller, B. (2003) 'Are amyotrophic lateral sclerosis patients cognitively normal?', *Neurology*, 60(7), pp. 1094-7.

Lopez-Gonzalez, R., Lu, Y., Gendron, T. F., Karydas, A., Tran, H., Yang, D., Petrucelli, L., Miller, B. L., Almeida, S. and Gao, F. B. (2016) 'Poly(GR) in C9ORF72-Related ALS/FTD Compromises Mitochondrial Function and Increases Oxidative Stress and DNA Damage in iPSC-Derived Motor Neurons', *Neuron*, 92(2), pp. 383-391.

Losier, T. T., Rousseaux, M. W. C. and Russell, R. C. (2024) 'Identification of stress specific autophagy regulators from tandem CRISPR screens', *bioRxiv*, p. 2024.03.27.587008.

Lucena-Aguilar, G., Sanchez-Lopez, A. M., Barberan-Aceituno, C., Carrillo-Avila, J. A., Lopez-Guerrero, J. A. and Aguilar-Quesada, R. (2016) 'DNA Source Selection for Downstream Applications Based on DNA Quality Indicators Analysis', *Biopreserv Biobank*, 14(4), pp. 264-70.

Luo, J., Nikolaev, A. Y., Imai, S., Chen, D., Su, F., Shiloh, A., Guarente, L. and Gu, W. (2001) 'Negative control of p53 by Sir2alpha promotes cell survival under stress', *Cell*, 107(2), pp. 137-48.

Luty, A. A., Kwok, J. B., Dobson-Stone, C., Loy, C. T., Coupland, K. G., Karlstrom, H., Sobow, T., Tchorzewska, J., Maruszak, A., Barcikowska, M., Panegyres, P. K., Zekanowski, C., Brooks, W. S., Williams, K. L., Blair, I. P., Mather, K. A., Sachdev, P. S., Halliday, G. M. and Schofield, P. R. (2010) 'Sigma nonopioid intracellular receptor 1 mutations cause frontotemporal lobar degeneration-motor neuron disease', *Ann Neurol*, 68(5), pp. 639-49.

Lv, B. F., Yu, C. F., Chen, Y. Y., Lu, Y., Guo, J. H., Song, Q. S., Ma, D. L., Shi, T. P. and Wang, L. (2006) 'Protein tyrosine phosphatase interacting protein 51 (PTPIP51) is a novel mitochondria protein with an N-terminal mitochondrial targeting sequence and induces apoptosis', *Apoptosis*, 11(9), pp. 1489-501.

Mackenzie, I. R., Bigio, E. H., Ince, P. G., Geser, F., Neumann, M., Cairns, N. J., Kwong, L. K., Forman, M. S., Ravits, J., Stewart, H., Eisen, A., McClusky, L., Kretzschmar, H. A., Monoranu, C. M., Highley, J. R., Kirby, J., Siddique, T., Shaw, P. J., Lee, V. M. and Trojanowski, J. Q. (2007) 'Pathological TDP-43 distinguishes sporadic amyotrophic lateral sclerosis from amyotrophic lateral sclerosis with SOD1 mutations', *Ann Neurol*, 61(5), pp. 427-34.

Mackenzie, I. R., Frick, P., Grässer, F. A., Gendron, T. F., Petrucelli, L., Cashman, N. R., Edbauer, D., Kremmer, E., Prudlo, J., Troost, D. and Neumann, M. (2015) 'Quantitative analysis and clinico-pathological correlations of different dipeptide repeat protein pathologies in C9ORF72 mutation carriers', *Acta Neuropathol*, 130(6), pp. 845-61.

Maddison, D. C., Malik, B., Amadio, L., Bis-Brewer, D. M., Züchner, S., Peters, O. M. and Smith, G. A. (2023) 'COPI-regulated mitochondria-ER contact site formation maintains axonal integrity', *Cell Rep*, 42(8), p. 112883.

Maeda, S., Otomo, C. and Otomo, T. (2019) 'The autophagic membrane tether ATG2A transfers lipids between membranes', *Elife*, 8.

Magana, P. and Kovalevskiy, O. (2024) *AlphaFold, A practical guide*.

Magrane, J., Cortez, C., Gan, W. B. and Manfredi, G. (2014) 'Abnormal mitochondrial transport and morphology are common pathological denominators in SOD1 and TDP43 ALS mouse models', *Hum Mol Genet*, 23(6), pp. 1413-24.

Magrané, J., Sahawneh, M. A., Przedborski, S., Estévez, Á. and Manfredi, G. (2012) 'Mitochondrial dynamics and bioenergetic dysfunction is associated with synaptic alterations in mutant SOD1 motor neurons', *J Neurosci*, 32(1), pp. 229-42.

Magri, A., Lipari, C. L. R., Caccamo, A., Battiato, G., Conti Nibali, S., De Pinto, V., Guarino, F. and Messina, A. (2024) 'AAV-mediated upregulation of VDAC1 rescues the mitochondrial respiration and sirtuins expression in a SOD1 mouse model of inherited ALS', *Cell Death Discov*, 10(1), p. 178.

Mah, L. J., El-Osta, A. and Karagiannis, T. C. (2010) 'gammaH2AX: a sensitive molecular marker of DNA damage and repair', *Leukemia*, 24(4), pp. 679-86.

Mahjoub, M. R., Trapp, M. L. and Quarmby, L. M. (2005) 'NIMA-related kinases defective in murine models of polycystic kidney diseases localize to primary cilia and centrosomes', *J Am Soc Nephrol*, 16(12), pp. 3485-9.

Majounie, E., Renton, A. E., Mok, K., Dopper, E. G., Waite, A., Rollinson, S., Chiò, A., Restagno, G., Nicolaou, N., Simon-Sanchez, J., van Swieten, J. C., Abramzon, Y., Johnson, J. O., Sendtner, M., Pamphlett, R., Orrell, R. W., Mead, S., Sidle, K. C., Houlden, H., Rohrer, J. D., Morrison, K. E., Pall, H., Talbot, K., Ansorge, O., Hernandez, D. G., Arepalli, S., Sabatelli, M., Mora, G., Corbo, M., Giannini, F., Calvo, A., Englund, E., Borghero, G., Floris, G. L., Remes, A. M., Laaksovirta, H., McCluskey, L., Trojanowski, J. Q., Van Deerlin, V. M., Schellenberg, G. D., Nalls, M. A., Drory, V. E., Lu, C. S., Yeh, T. H., Ishiura, H., Takahashi, Y., Tsuji, S., Le Ber, I., Brice, A., Drepper, C., Williams, N., Kirby, J., Shaw, P., Hardy, J., Tienari, P. J., Heutink, P., Morris, H. R., Pickering-Brown, S., Traynor, B. J., Consortium, C.-A. F., FTLD/FTLD/ALS, F. r. n. o. and Consortium, I. (2012) 'Frequency of the C9orf72 hexanucleotide repeat expansion in patients with amyotrophic lateral sclerosis and frontotemporal dementia: a cross-sectional study', *Lancet Neurol*, 11(4), pp. 323-30.

Manganelli, V., Matarrese, P., Antonioli, M., Gambardella, L., Vescovo, T., Gretzmeier, C., Longo, A., Capozzi, A., Recalchi, S., Riitano, G., Misasi, R., Dengjel, J., Malorni, W., Fimia, G. M., Sorice, M. and Garofalo, T. (2021) 'Raft-like lipid microdomains drive autophagy initiation via AMBRA1-ERLIN1 molecular association within MAMs', *Autophagy*, 17(9), pp. 2528-2548.

Mann, J. R., McKenna, E. D., Mawrie, D., Papakis, V., Alessandrini, F., Anderson, E. N., Mayers, R., Ball, H. E., Kaspi, E., Lubinski, K., Baron, D. M., Tellez, L., Landers, J. E., Pandey, U. B. and Kiskinis, E. (2023) 'Loss of function of the ALS-associated NEK1 kinase disrupts microtubule homeostasis and nuclear import', *Sci Adv*, 9(33), p. eadi5548.

Manor, U., Bartholomew, S., Golani, G., Christenson, E., Kozlov, M., Higgs, H., Spudich, J. and Lippincott-Schwartz, J. (2015) 'A mitochondria-anchored isoform of the actin-nucleating spire protein regulates mitochondrial division', *Elife*, 4.

Marchi, S. and Pinton, P. (2014) 'The mitochondrial calcium uniporter complex: molecular components, structure and physiopathological implications', *J Physiol*, 592(5), pp. 829-39.

Marino, A., Hausenloy, D. J., Andreadou, I., Horman, S., Bertrand, L. and Beauloye, C. (2021) 'AMP-activated protein kinase: A remarkable contributor to preserve a healthy heart against ROS injury', *Free Radic Biol Med*, 166, pp. 238-254.

Marino, G., Niso-Santano, M., Baehrecke, E. H. and Kroemer, G. (2014) 'Self-consumption: the interplay of autophagy and apoptosis', *Nat Rev Mol Cell Biol*, 15(2), pp. 81-94.

Marino, M., Papa, S., Crippa, V., Nardo, G., Peviani, M., Cheroni, C., Trolese, M. C., Lauranzano, E., Bonetto, V., Poletti, A., DeBiasi, S., Ferraiuolo, L., Shaw, P. J. and Bendotti, C. (2015) 'Differences in protein quality control correlate with phenotype variability in 2 mouse models of familial amyotrophic lateral sclerosis', *Neurobiol Aging*, 36(1), pp. 492-504.

Markovinovic, A., Martín-Guerrero, S. M., Mórotz, G. M., Salam, S., Gomez-Suaga, P., Paillusson, S., Greig, J., Lee, Y., Mitchell, J. C., Noble, W. and Miller, C. C. J. (2024) 'Stimulating VAPB-PTPIP51 ER-

mitochondria tethering corrects FTD/ALS mutant TDP43 linked Ca', *Acta Neuropathol Commun*, 12(1), p. 32.

Martín-Guerrero, S. M., Markovinovic, A., Mórotz, G. M., Salam, S., Noble, W. and Miller, C. C. J. (2022) 'Targeting ER-Mitochondria Signaling as a Therapeutic Target for Frontotemporal Dementia and Related Amyotrophic Lateral Sclerosis', *Frontiers in Cell and Developmental Biology*, 10.

Martins, M. B., Perez, A. M., Bohr, V. A., Wilson Iii, D. M. and Kobarg, J. (2021) 'NEK1 deficiency affects mitochondrial functions and the transcriptome of key DNA repair pathways', *Mutagenesis*.

Maruyama, H., Morino, H., Ito, H., Izumi, Y., Kato, H., Watanabe, Y., Kinoshita, Y., Kamada, M., Nodera, H., Suzuki, H., Komure, O., Matsuura, S., Kobatake, K., Morimoto, N., Abe, K., Suzuki, N., Aoki, M., Kawata, A., Hirai, T., Kato, T., Ogasawara, K., Hirano, A., Takumi, T., Kusaka, H., Hagiwara, K., Kaji, R. and Kawakami, H. (2010) 'Mutations of optineurin in amyotrophic lateral sclerosis', *Nature*, 465(7295), pp. 223-6.

Maruyama, I., Hasegawa, T., Yamamoto, T. and Momose, K. (1989) 'Effects of pluronic F-127 on loading of fura 2/AM into single smooth muscle cells isolated from guinea pig taenia coli', *J Toxicol Sci*, 14(3), pp. 153-63.

Maruyama, T., Nara, K., Yoshikawa, H. and Suzuki, N. (2007) 'Txk, a member of the non-receptor tyrosine kinase of the Tec family, forms a complex with poly(ADP-ribose) polymerase 1 and elongation factor 1alpha and regulates interferon-gamma gene transcription in Th1 cells', *Clin Exp Immunol*, 147(1), pp. 164-75.

Maryanovich, M., Oberkovitz, G., Niv, H., Vorobiyov, L., Zaltsman, Y., Brenner, O., Lapidot, T., Jung, S. and Gross, A. (2012) 'The ATM-BID pathway regulates quiescence and survival of haematopoietic stem cells', *Nat Cell Biol*, 14(5), pp. 535-41.

Masuda, A., Takeda, J., Okuno, T., Okamoto, T., Ohkawara, B., Ito, M., Ishigaki, S., Sobue, G. and Ohno, K. (2015) 'Position-specific binding of FUS to nascent RNA regulates mRNA length', *Genes Dev*, 29(10), pp. 1045-57.

Matsumoto, G., Shimogori, T., Hattori, N. and Nukina, N. (2015) 'TBK1 controls autophagosomal engulfment of polyubiquitinated mitochondria through p62/SQSTM1 phosphorylation', *Hum Mol Genet*, 24(15), pp. 4429-42.

Mavlyutov, T. A., Epstein, M. L., Andersen, K. A., Ziskind-Conhaim, L. and Ruoho, A. E. (2010) 'The sigma-1 receptor is enriched in postsynaptic sites of C-terminals in mouse motoneurons. An anatomical and behavioral study', *Neuroscience*, 167(2), pp. 247-55.

Maynard, S., Fang, E. F., Scheibye-Knudsen, M., Croteau, D. L. and Bohr, V. A. (2015) 'DNA Damage, DNA Repair, Aging, and Neurodegeneration', *Cold Spring Harb Perspect Med*, 5(10).

Mazat, J. P., Devin, A. and Ransac, S. (2020) 'Modelling mitochondrial ROS production by the respiratory chain', *Cell Mol Life Sci*, 77(3), pp. 455-465.

McEwan, D. G., Popovic, D., Gubas, A., Terawaki, S., Suzuki, H., Stadel, D., Coxon, F. P., Miranda de Stegmann, D., Bhogaraju, S., Maddi, K., Kirchof, A., Gatti, E., Helfrich, M. H., Wakatsuki, S., Behrends, C., Pierre, P. and Dikic, I. (2015) 'PLEKHM1 regulates autophagosome-lysosome fusion through HOPS complex and LC3/GABARAP proteins', *Mol Cell*, 57(1), pp. 39-54.

McInerney-Leo, A. M., Harris, J. E., Leo, P. J., Marshall, M. S., Gardiner, B., Kinning, E., Leong, H. Y., McKenzie, F., Ong, W. P., Vodopiutz, J., Wicking, C., Brown, M. A., Zankl, A. and Duncan, E. L. (2015) 'Whole exome sequencing is an efficient, sensitive and specific method for determining the genetic cause of short-rib thoracic dystrophies', *Clin Genet*, 88(6), pp. 550-7.

McInerney-Leo, A. M., Wheeler, L., Marshall, M. S., Anderson, L. K., Zankl, A., Brown, M. A., Leo, P. J., Wicking, C. and Duncan, E. L. (2017) 'Homozygous variant in C21orf2 in a case of Jeune syndrome with

severe thoracic involvement: Extending the phenotypic spectrum', *Am J Med Genet A*, 173(6), pp. 1698-1704.

McLelland, G. L., Goiran, T., Yi, W., Dorval, G., Chen, C. X., Lauinger, N. D., Krahn, A. I., Valimehr, S., Rakovic, A., Rouiller, I., Durcan, T. M., Trempe, J. F. and Fon, E. A. (2018) 'Mfn2 ubiquitination by PINK1/parkin gates the p97-dependent release of ER from mitochondria to drive mitophagy', *Elife*, 7.

McMillin, J. B. and Dowhan, W. (2002) 'Cardiolipin and apoptosis', *Biochim Biophys Acta*, 1585(2-3), pp. 97-107.

Mead, R. J., Shan, N., Reiser, H. J., Marshall, F. and Shaw, P. J. (2023) 'Amyotrophic lateral sclerosis: a neurodegenerative disorder poised for successful therapeutic translation', *Nat Rev Drug Discov*, 22(3), pp. 185-212.

Mehta, A. R., Gregory, J. M., Dando, O., Carter, R. N., Burr, K., Nanda, J., Story, D., McDade, K., Smith, C., Morton, N. M., Mahad, D. J., Hardingham, G. E., Chandran, S. and Selvaraj, B. T. (2021) 'Mitochondrial bioenergetic deficits in C9orf72 amyotrophic lateral sclerosis motor neurons cause dysfunctional axonal homeostasis', *Acta Neuropathol*, 141(2), pp. 257-279.

Melino, G. (2005) 'Discovery of the ubiquitin proteasome system and its involvement in apoptosis', *Cell Death Differ*, 12(9), pp. 1155-7.

Melo-Hanchuk, T. D., Slepicka, P. F., Meirelles, G. V., Basei, F. L., Lovato, D. V., Granato, D. C., Pauletti, B. A., Domingues, R. R., Leme, A. F. P., Pelegrini, A. L., Lenz, G., Knapp, S., Elkins, J. M. and Kobarg, J. (2017) 'NEK1 kinase domain structure and its dynamic protein interactome after exposure to Cisplatin', *Sci Rep*, 7(1), p. 5445.

Meng, E. C., Goddard, T. D., Pettersen, E. F., Couch, G. S., Pearson, Z. J., Morris, J. H. and Ferrin, T. E. (2023) 'UCSF ChimeraX: Tools for structure building and analysis', *Protein Sci*, 32(11), p. e4792.

Meng, Y., Chen, C. W., Yung, M. M. H., Sun, W., Sun, J., Li, Z., Li, J., Li, Z., Zhou, W., Liu, S. S., Cheung, A. N. Y., Ngan, H. Y. S., Braisted, J. C., Kai, Y., Peng, W., Tzatsos, A., Li, Y., Dai, Z., Zheng, W., Chan, D. W. and Zhu, W. (2018) 'DUOXA1-mediated ROS production promotes cisplatin resistance by activating ATR-Chk1 pathway in ovarian cancer', *Cancer Lett*, 428, pp. 104-116.

Meyer, H. and Weihl, C. C. (2014) 'The VCP/p97 system at a glance: connecting cellular function to disease pathogenesis', *J Cell Sci*, 127(Pt 18), pp. 3877-83.

Millecamps, S. and Julien, J. P. (2013) 'Axonal transport deficits and neurodegenerative diseases', *Nat Rev Neurosci*, 14(3), pp. 161-76.

Mitne-Neto, M., Machado-Costa, M., Marchetto, M. C., Bengtson, M. H., Joazeiro, C. A., Tsuda, H., Bellen, H. J., Silva, H. C., Oliveira, A. S., Lazar, M., Muotri, A. R. and Zatz, M. (2011) 'Downregulation of VAPB expression in motor neurons derived from induced pluripotent stem cells of ALS8 patients', *Hum Mol Genet*, 20(18), pp. 3642-52.

Mitsumoto, H., Santella, R. M., Liu, X., Bogdanov, M., Zipprich, J., Wu, H. C., Mahata, J., Kilty, M., Bednarz, K., Bell, D., Gordon, P. H., Hornig, M., Mehrazin, M., Naini, A., Flint Beal, M. and Factor-Litvak, P. (2008) 'Oxidative stress biomarkers in sporadic ALS', *Amyotroph Lateral Scler*, 9(3), pp. 177-83.

Mizuno, Y., Amari, M., Takatama, M., Aizawa, H., Mihara, B. and Okamoto, K. (2006) 'Transferrin localizes in Bunina bodies in amyotrophic lateral sclerosis', *Acta Neuropathol*, 112(5), pp. 597-603.

Mizushima, N. and Yoshimori, T. (2007) 'How to interpret LC3 immunoblotting', *Autophagy*, 3(6), pp. 542-5.

Morfini, G. A., Bosco, D. A., Brown, H., Gatto, R., Kaminska, A., Song, Y., Molla, L., Baker, L., Marangoni, M. N., Berth, S., Tavassoli, E., Bagnato, C., Tiwari, A., Hayward, L. J., Pigino, G. F., Watterson, D. M., Huang, C. F., Banker, G., Brown, R. H. and Brady, S. T. (2013) 'Inhibition of fast axonal transport by pathogenic SOD1 involves activation of p38 MAP kinase', *PLoS One*, 8(6), p. e65235.

Mori, F., Kakita, A., Takahashi, H. and Wakabayashi, K. (2014) 'Co-localization of Bunina bodies and TDP-43 inclusions in lower motor neurons in amyotrophic lateral sclerosis', *Neuropathology*, 34(1), pp. 71-6.

Mori, F., Miki, Y., Kon, T., Tanji, K. and Wakabayashi, K. (2019) 'Autophagy Is a Common Degradation Pathway for Bunina Bodies and TDP-43 Inclusions in Amyotrophic Lateral Sclerosis', *J Neuropathol Exp Neurol*, 78(10), pp. 910-921.

Mori, F., Tanji, K., Miki, Y., Kakita, A., Takahashi, H. and Wakabayashi, K. (2010) 'Relationship between Bunina bodies and TDP-43 inclusions in spinal anterior horn in amyotrophic lateral sclerosis', *Neuropathol Appl Neurobiol*, 36(4), pp. 345-52.

Mórotz, G. M., De Vos, K. J., Vagnoni, A., Ackerley, S., Shaw, C. E. and Miller, C. C. (2012) 'Amyotrophic lateral sclerosis-associated mutant VAPBP56S perturbs calcium homeostasis to disrupt axonal transport of mitochondria', *Hum Mol Genet*, 21(9), pp. 1979-88.

Mórotz, G. M., Martín-Guerrero, S. M., Markovinovic, A., Paillusson, S., Russell, M. R. G., Machado, P. M. P., Fleck, R. A., Noble, W. and Miller, C. C. J. (2022) 'The PTPIP51 coiled-coil domain is important in VAPB binding, formation of ER-mitochondria contacts and IP3 receptor delivery of Ca', *Front Cell Dev Biol*, 10, p. 920947.

Mosler, T., Baymaz, H. I., Graf, J. F., Mikicic, I., Blattner, G., Bartlett, E., Ostermaier, M., Piccinno, R., Yang, J., Voigt, A., Gatti, M., Pellegrino, S., Altmeyer, M., Luck, K., Ahel, I., Roukos, V. and Beli, P. (2022) 'PARP1 proximity proteomics reveals interaction partners at stressed replication forks', *Nucleic Acids Res*, 50(20), pp. 11600-11618.

Moss, D. K., Wilde, A. and Lane, J. D. (2009) 'Dynamic release of nuclear RanGTP triggers TPX2-dependent microtubule assembly during the apoptotic execution phase', *J Cell Sci*, 122(Pt 5), pp. 644-55.

Mou, Y., Li, M., Liu, M., Wang, J., Zhu, G. and Zha, Y. (2022) 'OPTN variants in ALS cases: a case report of a novel mutation and literature review', *Neurol Sci*, 43(9), pp. 5391-5396.

Moulis, M., Grousset, E., Faccini, J., Richetin, K., Thomas, G. and Vindis, C. (2019) 'The Multifunctional Sorting Protein PACS-2 Controls Mitophagosome Formation in Human Vascular Smooth Muscle Cells through Mitochondria-ER Contact Sites', *Cells*, 8(6).

Moumen, A., Virard, I. and Raoul, C. (2011) 'Accumulation of wildtype and ALS-linked mutated VAPB impairs activity of the proteasome', *PLoS One*, 6(10), p. e26066.

Mullins, E. A., Rodriguez, A. A., Bradley, N. P. and Eichman, B. F. (2019) 'Emerging Roles of DNA Glycosylases and the Base Excision Repair Pathway', *Trends Biochem Sci*, 44(9), pp. 765-781.

Munoz, J. P., Ivanova, S., Sanchez-Wandelmer, J., Martinez-Cristobal, P., Noguera, E., Sancho, A., Diaz-Ramos, A., Hernandez-Alvarez, M. I., Sebastian, D., Mauvezin, C., Palacin, M. and Zorzano, A. (2013) 'Mfn2 modulates the UPR and mitochondrial function via repression of PERK', *EMBO J*, 32(17), pp. 2348-61.

Muraleedharan, R. and Dasgupta, B. (2022) 'AMPK in the brain: its roles in glucose and neural metabolism', *FEBS J*, 289(8), pp. 2247-2262.

Murata, M. M., Kong, X., Moncada, E., Chen, Y., Imamura, H., Wang, P., Berns, M. W., Yokomori, K. and Digman, M. A. (2019) 'NAD+ consumption by PARP1 in response to DNA damage triggers metabolic shift critical for damaged cell survival', *Mol Biol Cell*, 30(20), pp. 2584-2597.

Murphy, S. E. and Levine, T. P. (2016) 'VAP, a Versatile Access Point for the Endoplasmic Reticulum: Review and analysis of FFAT-like motifs in the VAPome', *Biochim Biophys Acta*, 1861(8 Pt B), pp. 952-961.

Muslin, A. J. and Xing, H. (2000) '14-3-3 proteins: regulation of subcellular localization by molecular interference', *Cell Signal*, 12(11-12), pp. 703-9.

Najafov, A., Luu, H. S., Mookhtiar, A. K., Mifflin, L., Xia, H. G., Amin, P. P., Ordureau, A., Wang, H. and Yuan, J. (2021) 'RIPK1 Promotes Energy Sensing by the mTORC1 Pathway', *Mol Cell*, 81(2), pp. 370-385 e7.

Nakamura, K., Aoyama-Ishiwatari, S., Nagao, T., Paaran, M., Obara, C. J., Sakurai-Saito, Y., Johnston, J., Du, Y., Suga, S., Tsuboi, M., Nakakido, M., Tsumoto, K., Kishi, Y., Gotoh, Y., Kwak, C., Rhee, H. W., Seo, J. K., Kosako, H., Potter, C., Carragher, B., Lippincott-Schwartz, J., Polleux, F. and Hirabayashi, Y. (2024) 'PDZD8-FKBP8 tethering complex at ER-mitochondria contact sites regulates mitochondrial complexity', *bioRxiv*.

Namba, T. (2019) 'BAP31 regulates mitochondrial function via interaction with Tom40 within ER-mitochondria contact sites', *Sci Adv*, 5(6), p. eaaw1386.

Naon, D., Zaninello, M., Giacomello, M., Varanita, T., Grespi, F., Lakshminaranayan, S., Serafini, A., Semenzato, M., Herkenne, S., Hernandez-Alvarez, M. I., Zorzano, A., De Stefani, D., Dorn, G. W., 2nd and Scorrano, L. (2016) 'Critical reappraisal confirms that Mitofusin 2 is an endoplasmic reticulum-mitochondria tether', *Proc Natl Acad Sci U S A*, 113(40), pp. 11249-11254.

Narendra, D., Tanaka, A., Suen, D. F. and Youle, R. J. (2008) 'Parkin is recruited selectively to impaired mitochondria and promotes their autophagy', *J Cell Biol*, 183(5), pp. 795-803.

Naruse, H., Ishiura, H., Mitsui, J., Takahashi, Y., Matsukawa, T., Yoshimura, J., Doi, K., Morishita, S., Goto, J., Toda, T. and Tsuji, S. (2021) 'Loss-of-function variants in NEK1 are associated with an increased risk of sporadic ALS in the Japanese population', *J Hum Genet*, 66(3), pp. 237-241.

Naumann, M., Pal, A., Goswami, A., Lojewski, X., Japtok, J., Vehlow, A., Naujock, M., Günther, R., Jin, M., Stanslowsky, N., Reinhardt, P., Sterneckert, J., Frickenhaus, M., Pan-Montojo, F., Storkebaum, E., Poser, I., Freischmidt, A., Weishaupt, J. H., Holzmann, K., Troost, D., Ludolph, A. C., Boeckers, T. M., Liebau, S., Petri, S., Cordes, N., Hyman, A. A., Wegner, F., Grill, S. W., Weis, J., Storch, A. and Hermann, A. (2018) 'Impaired DNA damage response signaling by FUS-NLS mutations leads to neurodegeneration and FUS aggregate formation', *Nat Commun*, 9(1), p. 335.

Neary, D., Snowden, J. S. and Mann, D. M. (2000) 'Cognitive change in motor neurone disease/amyotrophic lateral sclerosis (MND/ALS)', *J Neurol Sci*, 180(1-2), pp. 15-20.

Neefjes, J. and Cabukusta, B. (2021) 'What the VAP: The Expanded VAP Family of Proteins Interacting With FFAT and FFAT-Related Motifs for Interorganellar Contact', *Contact (Thousand Oaks)*, 4, p. 25152564211012246.

Ngok-Ngam, P., Watcharasit, P., Thiantanawat, A. and Satayavivad, J. (2013) 'Pharmacological inhibition of GSK3 attenuates DNA damage-induced apoptosis via reduction of p53 mitochondrial translocation and Bax oligomerization in neuroblastoma SH-SY5Y cells', *Cell Mol Biol Lett*, 18(1), pp. 58-74.

Nguyen, H. P., Van Mossevelde, S., Dillen, L., De Bleecker, J. L., Moisse, M., Van Damme, P., Van Broeckhoven, C., van der Zee, J. and Consortium, B. (2018) 'NEK1 genetic variability in a Belgian cohort of ALS and ALS-FTD patients', *Neurobiol Aging*, 61, pp. 255.e1-255.e7.

Nice, S. M., Sabrina, I., Valeria, C., Serena, S., Chiara, L., Paola, P., Alberto, B., Alessio, S., Silvia, P., Angelo, Q., Vincenzo, S., Patrizia, B. and Antonia, R. (2024) 'NEK1 haploinsufficiency impairs ciliogenesis in human iPSC-derived motoneurons and brain organoids', *bioRxiv*, p. 2024.02.29.582696.

Nicolas, A., Kenna, K. P., Renton, A. E., Ticozzi, N., Faghri, F., Chia, R., Dominov, J. A., Kenna, B. J., Nalls, M. A., Keagle, P., Rivera, A. M., van Rheenen, W., Murphy, N. A., van Vugt, J. J. F. A., Geiger, J. T., Van der Spek, R. A., Pliner, H. A., Shankaracharya, Smith, B. N., Marangi, G., Topp, S. D., Abramzon, Y., Gkazi, A. S., Eicher, J. D., Kenna, A., Mora, G., Calvo, A., Mazzini, L., Riva, N., Mandrioli, J., Caponnetto,

C., Battistini, S., Volanti, P., La Bella, V., Conforti, F. L., Borghero, G., Messina, S., Simone, I. L., Trojsi, F., Salvi, F., Logullo, F. O., D'Alfonso, S., Corrado, L., Capasso, M., Ferrucci, L., Moreno, C. A. M., Kamalakaran, S., Goldstein, D. B., Gitler, A. D., Harris, T., Myers, R. M., Phatnani, H., Musunuri, R. L., Evani, U. S., Abhyankar, A., Zody, M. C., Kaye, J., Finkbeiner, S., Wyman, S. K., LeNail, A., Lima, L., Fraenkel, E., Svendsen, C. N., Thompson, L. M., Van Eyk, J. E., Berry, J. D., Miller, T. M., Kolb, S. J., Cudkowicz, M., Baxi, E., Benatar, M., Taylor, J. P., Rampersaud, E., Wu, G., Wuu, J., Lauria, G., Verde, F., Fogh, I., Tiloca, C., Comi, G. P., Sorarù, G., Cereda, C., Corcia, P., Laaksovirta, H., Myllykangas, L., Jansson, L., Valori, M., Ealing, J., Hamdalla, H., Rollinson, S., Pickering-Brown, S., Orrell, R. W., Sidle, K. C., Malaspina, A., Hardy, J., Singleton, A. B., Johnson, J. O., Arepalli, S., Sapp, P. C., McKenna-Yasek, D., et al. (2018) 'Genome-wide Analyses Identify KIF5A as a Novel ALS Gene', *Neuron*, 97(6), pp. 1267-1288.

Niedermeyer, S., Murn, M. and Choi, P. J. (2019) 'Respiratory Failure in Amyotrophic Lateral Sclerosis', *Chest*, 155(2), pp. 401-408.

Nihei, K., McKee, A. C. and Kowall, N. W. (1993) 'Patterns of neuronal degeneration in the motor cortex of amyotrophic lateral sclerosis patients', *Acta Neuropathol*, 86(1), pp. 55-64.

Nihei, Y., Mori, K., Werner, G., Arzberger, T., Zhou, Q., Khosravi, B., Japtok, J., Hermann, A., Sommacal, A., Weber, M., Kamp, F., Nuscher, B., Edbauer, D., Haass, C., Degeneration, G. C. f. F. L. and Alliance, B. B. B. (2020) 'Poly-glycine-alanine exacerbates C9orf72 repeat expansion-mediated DNA damage via sequestration of phosphorylated ATM and loss of nuclear hnRNPA3', *Acta Neuropathol*, 139(1), pp. 99-118.

Nilaver, B. I. and Urbanski, H. F. (2023) 'Mechanisms underlying TDP-43 pathology and neurodegeneration: An updated Mini-Review', *Front Aging Neurosci*, 15, p. 1142617.

Nishimura, A. L., Al-Chalabi, A. and Zatz, M. (2005) 'A common founder for amyotrophic lateral sclerosis type 8 (ALS8) in the Brazilian population', *Hum Genet*, 118(3-4), pp. 499-500.

Nishimura, A. L., Mitne-Neto, M., Silva, H. C., Richieri-Costa, A., Middleton, S., Cascio, D., Kok, F., Oliveira, J. R., Gillingwater, T., Webb, J., Skehel, P. and Zatz, M. (2004) 'A mutation in the vesicle-trafficking protein VAPB causes late-onset spinal muscular atrophy and amyotrophic lateral sclerosis', *Am J Hum Genet*, 75(5), pp. 822-31.

Nishimura, Y., Hayashi, M., Inada, H. and Tanaka, T. (1999) 'Molecular cloning and characterization of mammalian homologues of vesicle-associated membrane protein-associated (VAMP-associated) proteins', *Biochem Biophys Res Commun*, 254(1), pp. 21-6.

O'Rourke, J. G., Bogdanik, L., Yáñez, A., Lall, D., Wolf, A. J., Muhammad, A. K., Ho, R., Carmona, S., Vit, J. P., Zarrow, J., Kim, K. J., Bell, S., Harms, M. B., Miller, T. M., Dangler, C. A., Underhill, D. M., Goodridge, H. S., Lutz, C. M. and Baloh, R. H. (2016) 'C9orf72 is required for proper macrophage and microglial function in mice', *Science*, 351(6279), pp. 1324-9.

Oakes, J. A., Davies, M. C. and Collins, M. O. (2017) 'TBK1: a new player in ALS linking autophagy and neuroinflammation', *Mol Brain*, 10(1), p. 5.

Oakes, S. G., Martin, W. J., Lisek, C. A. and Powis, G. (1988) 'Incomplete hydrolysis of the calcium indicator precursor fura-2 pentaacetoxymethyl ester (fura-2 AM) by cells', *Anal Biochem*, 169(1), pp. 159-66.

Oda, K., Arakawa, H., Tanaka, T., Matsuda, K., Tanikawa, C., Mori, T., Nishimori, H., Tamai, K., Tokino, T., Nakamura, Y. and Taya, Y. (2000) 'p53AIP1, a potential mediator of p53-dependent apoptosis, and its regulation by Ser-46-phosphorylated p53', *Cell*, 102(6), pp. 849-62.

Oishi, K., Okano, H. and Sawa, H. (2007) 'RMD-1, a novel microtubule-associated protein, functions in chromosome segregation in Caenorhabditis elegans', *J Cell Biol*, 179(6), pp. 1149-62.

Okada, N., Yabuta, N., Suzuki, H., Aylon, Y., Oren, M. and Nojima, H. (2011) 'A novel Chk1/2-Lats2-14-3-3 signaling pathway regulates P-body formation in response to UV damage', *J Cell Sci*, 124(Pt 1), pp. 57-67.

Okamoto, K., Hirai, S., Amari, M., Watanabe, M. and Sakurai, A. (1993) 'Bunina bodies in amyotrophic lateral sclerosis immunostained with rabbit anti-cystatin C serum', *Neurosci Lett*, 162(1-2), pp. 125-8.

Olive, P. L. and Banáth, J. P. (2006) 'The comet assay: a method to measure DNA damage in individual cells', *Nat Protoc*, 1(1), pp. 23-9.

Onesto, E., Colombrita, C., Gumina, V., Borghi, M. O., Dusi, S., Doretti, A., Fagiolari, G., Invernizzi, F., Moggio, M., Tiranti, V., Silani, V. and Ratti, A. (2016) 'Gene-specific mitochondria dysfunctions in human TARDBP and C9ORF72 fibroblasts', *Acta Neuropathol Commun*, 4(1), p. 47.

Osaka, M., Ito, D., Yagi, T., Nihei, Y. and Suzuki, N. (2015) 'Evidence of a link between ubiquilin 2 and optineurin in amyotrophic lateral sclerosis', *Hum Mol Genet*, 24(6), pp. 1617-29.

Osawa, T., Kotani, T., Kawaoka, T., Hirata, E., Suzuki, K., Nakatogawa, H., Ohsumi, Y. and Noda, N. N. (2019) 'Atg2 mediates direct lipid transfer between membranes for autophagosome formation', *Nat Struct Mol Biol*, 26(4), pp. 281-288.

Osman, C., Voelker, D. R. and Langer, T. (2011) 'Making heads or tails of phospholipids in mitochondria', *J Cell Biol*, 192(1), pp. 7-16.

Paillusson, S., Gomez-Suaga, P., Stoica, R., Little, D., Gissen, P., Devine, M. J., Noble, W., Hanger, D. P. and Miller, C. C. J. (2017) 'α-Synuclein binds to the ER–mitochondria tethering protein VAPB to disrupt Ca2+ homeostasis and mitochondrial ATP production', *Acta Neuropathologica*, 134(1), pp. 129-149.

Paillusson, S., Stoica, R., Gomez-Suaga, P., Lau, D. H. W., Mueller, S., Miller, T. and Miller, C. C. J. (2016) 'There's Something Wrong with my MAM; the ER-Mitochondria Axis and Neurodegenerative Diseases', *Trends Neurosci*, 39(3), pp. 146-157.

Pannunzio, N. R., Watanabe, G. and Lieber, M. R. (2018) 'Nonhomologous DNA end-joining for repair of DNA double-strand breaks', *J Biol Chem*, 293(27), pp. 10512-10523.

Papadopoli, D., Pollak, M. and Topisirovic, I. (2021) 'The role of GSK3 in metabolic pathway perturbations in cancer', *Biochim Biophys Acta Mol Cell Res*, 1868(8), p. 119059.

Papiani, G., Ruggiano, A., Fossati, M., Raimondi, A., Bertoni, G., Francolini, M., Benfante, R., Navone, F. and Borgese, N. (2012) 'Restructured endoplasmic reticulum generated by mutant amyotrophic lateral sclerosis-linked VAPB is cleared by the proteasome', *J Cell Sci*, 125(Pt 15), pp. 3601-11.

Park, J. M., Jung, C. H., Seo, M., Otto, N. M., Grunwald, D., Kim, K. H., Moriarity, B., Kim, Y. M., Starker, C., Nho, R. S., Voytas, D. and Kim, D. H. (2016) 'The ULK1 complex mediates MTORC1 signaling to the autophagy initiation machinery via binding and phosphorylating ATG14', *Autophagy*, 12(3), pp. 547-64.

Parobkova, E. and Matej, R. (2021) 'Amyotrophic Lateral Sclerosis and Frontotemporal Lobar Degenerations: Similarities in Genetic Background', *Diagnostics (Basel)*, 11(3).

Parzych, K. R. and Klionsky, D. J. (2014) 'An overview of autophagy: morphology, mechanism, and regulation', *Antioxid Redox Signal*, 20(3), pp. 460-73.

Patil, M., Pabla, N., Ding, H. F. and Dong, Z. (2013) 'Nek1 interacts with Ku80 to assist chromatin loading of replication factors and S-phase progression', *Cell Cycle*, 12(16), pp. 2608-16.

Pavan, I. C. B., Peres de Oliveira, A., Dias, P. R. F., Basei, F. L., Issayama, L. K., Ferezin, C. C., Silva, F. R., Rodrigues de Oliveira, A. L., Alves Dos Reis Moura, L., Martins, M. B., Simabuco, F. M. and Kobarg, J. (2021) 'On Broken Ne(c)ks and Broken DNA: The Role of Human NEKs in the DNA Damage Response', *Cells*, 10(3).

Peggion, C., Massimino, M. L., Bonadio, R. S., Lia, F., Lopreiato, R., Cagnin, S., Cali, T. and Bertoli, A. (2021) 'Regulation of Endoplasmic Reticulum-Mitochondria Tethering and Ca(2+) Fluxes by TDP-43 via GSK3beta', *Int J Mol Sci*, 22(21).

Pelegrini, A. L., Moura, D. J., Brenner, B. L., Ledur, P. F., Maques, G. P., Henriques, J. A., Saffi, J. and Lenz, G. (2010) 'Nek1 silencing slows down DNA repair and blocks DNA damage-induced cell cycle arrest', *Mutagenesis*, 25(5), pp. 447-54.

Peng, G., Gu, A., Niu, H., Chen, L., Chen, Y., Zhou, M., Zhang, Y., Liu, J., Cai, L., Liang, D., Liu, X. and Liu, M. (2022) 'Amyotrophic lateral sclerosis (ALS) linked mutation in Ubiquilin 2 affects stress granule assembly via TIA-1', *CNS Neurosci Ther*, 28(1), pp. 105-115.

Peretti, D., Dahan, N., Shimoni, E., Hirschberg, K. and Lev, S. (2008) 'Coordinated lipid transfer between the endoplasmic reticulum and the Golgi complex requires the VAP proteins and is essential for Golgi-mediated transport', *Mol Biol Cell*, 19(9), pp. 3871-84.

Perrone, F., Nguyen, H. P., Van Mossevelde, S., Moisse, M., Sieben, A., Santens, P., De Bleecker, J., Vandenbulcke, M., Engelborghs, S., Baets, J., Cras, P., Vandenberghe, R., De Jonghe, P., De Deyn, P. P., Martin, J. J., Van Damme, P., Van Broeckhoven, C., van der Zee, J. and consortium, B. N. (2017) 'Investigating the role of ALS genes CHCHD10 and TUBA4A in Belgian FTD-ALS spectrum patients', *Neurobiol Aging*, 51, pp. 177.e9-177.e16.

Petrungaro, C. and Kornmann, B. (2019) 'Lipid exchange at ER-mitochondria contact sites: a puzzle falling into place with quite a few pieces missing', *Curr Opin Cell Biol*, 57, pp. 71-76.

Piao, Y. S., Wakabayashi, K., Kakita, A., Yamada, M., Hayashi, S., Morita, T., Ikuta, F., Oyanagi, K. and Takahashi, H. (2003) 'Neuropathology with clinical correlations of sporadic amyotrophic lateral sclerosis: 102 autopsy cases examined between 1962 and 2000', *Brain Pathol*, 13(1), pp. 10-22.

Picco, V. and Pages, G. (2013) 'Linking JNK Activity to the DNA Damage Response', *Genes Cancer*, 4(9-10), pp. 360-8.

Pitaval, A., Senger, F., Letort, G., Gidrol, X., Guyon, L., Sillibourne, J. and Thery, M. (2017) 'Microtubule stabilization drives 3D centrosome migration to initiate primary ciliogenesis', *J Cell Biol*, 216(11), pp. 3713-3728.

Pittala, M. G. G., Reina, S., Cubisino, S. A. M., Cucina, A., Formicola, B., Cunsolo, V., Foti, S., Saletti, R. and Messina, A. (2020) 'Post-Translational Modification Analysis of VDAC1 in ALS-SOD1 Model Cells Reveals Specific Asparagine and Glutamine Deamidation', *Antioxidants (Basel)*, 9(12).

Polci, R., Peng, A., Chen, P. L., Riley, D. J. and Chen, Y. (2004) 'NIMA-related protein kinase 1 is involved early in the ionizing radiation-induced DNA damage response', *Cancer Res*, 64(24), pp. 8800-3.

Portela, M., Mukherjee, S., Paul, S., La Marca, J. E., Parsons, L. M., Veraksa, A. and Richardson, H. E. (2024) 'The Drosophila tumour suppressor Lgl and Vap33 activate the Hippo pathway through a dual mechanism', *J Cell Sci*, 137(4).

Portet, F., Cadilhac, C., Touchon, J. and Camu, W. (2001) 'Cognitive impairment in motor neuron disease with bulbar onset', *Amyotroph Lateral Scler Other Motor Neuron Disord*, 2(1), pp. 23-9.

Prado, F. (2018) 'Homologous Recombination: To Fork and Beyond', *Genes (Basel)*, 9(12).

Puls, I., Jonnakuty, C., LaMonte, B. H., Holzbaur, E. L., Tokito, M., Mann, E., Floeter, M. K., Bidus, K., Drayna, D., Oh, S. J., Brown, R. H., Ludlow, C. L. and Fischbeck, K. H. (2003) 'Mutant dynactin in motor neuron disease', *Nat Genet*, 33(4), pp. 455-6.

Quinet, G., Gonzalez-Santamarta, M., Louche, C. and Rodriguez, M. S. (2020) 'Mechanisms Regulating the UPS-ALS Crosstalk: The Role of Proteaphagy', *Molecules*, 25(10).

Rajpurohit, C. S., Kumar, V., Cheffer, A., Oliveira, D., Ulrich, H., Okamoto, O. K., Zatz, M., Ansari, U. A., Khanna, V. K. and Pant, A. B. (2020) 'Mechanistic Insights of Astrocyte-Mediated Hyperactive Autophagy and Loss of Motor Neuron Function in SOD1(L39R) Linked Amyotrophic Lateral Sclerosis', *Mol Neurobiol*, 57(10), pp. 4117-4133.

Ramesh, N. and Pandey, U. B. (2017) 'Autophagy Dysregulation in ALS: When Protein Aggregates Get Out of Hand', *Front Mol Neurosci*, 10, p. 263.

Ran, F. A., Hsu, P. D., Wright, J., Agarwala, V., Scott, D. A. and Zhang, F. (2013) 'Genome engineering using the CRISPR-Cas9 system', *Nat Protoc*, 8(11), pp. 2281-2308.

Rapizzi, E., Pinton, P., Szabadkai, G., Wieckowski, M. R., Vandecasteele, G., Baird, G., Tuft, R. A., Fogarty, K. E. and Rizzuto, R. (2002) 'Recombinant expression of the voltage-dependent anion channel enhances the transfer of Ca2+ microdomains to mitochondria', *J Cell Biol*, 159(4), pp. 613-24.

Rea, S. L., Majcher, V., Searle, M. S. and Layfield, R. (2014) 'SQSTM1 mutations--bridging Paget disease of bone and ALS/FTLD', *Exp Cell Res*, 325(1), pp. 27-37.

Reddy, P. H. (2009) 'Role of mitochondria in neurodegenerative diseases: mitochondria as a therapeutic target in Alzheimer's disease', *CNS Spectr*, 14(8 Suppl 7), pp. 8-13; discussion 16-8.

Ren, J., Liang, R., Wang, W., Zhang, D., Yu, L. and Feng, W. (2020) 'Multi-site-mediated entwining of the linear WIR-motif around WIPI β-propellers for autophagy', *Nat Commun*, 11(1), p. 2702.

Renton, A. E., Chio, A. and Traynor, B. J. (2014) 'State of play in amyotrophic lateral sclerosis genetics', *Nat Neurosci*, 17(1), pp. 17-23.

Renton, A. E., Majounie, E., Waite, A., Simón-Sánchez, J., Rollinson, S., Gibbs, J. R., Schymick, J. C., Laaksovirta, H., van Swieten, J. C., Myllykangas, L., Kalimo, H., Paetau, A., Abramzon, Y., Remes, A. M., Kaganovich, A., Scholz, S. W., Duckworth, J., Ding, J., Harmer, D. W., Hernandez, D. G., Johnson, J. O., Mok, K., Ryten, M., Trabzuni, D., Guerreiro, R. J., Orrell, R. W., Neal, J., Murray, A., Pearson, J., Jansen, I. E., Sondervan, D., Seelaar, H., Blake, D., Young, K., Halliwell, N., Callister, J. B., Toulson, G., Richardson, A., Gerhard, A., Snowden, J., Mann, D., Neary, D., Nalls, M. A., Peuralinna, T., Jansson, L., Isoviita, V. M., Kaivorinne, A. L., Hölttä-Vuori, M., Ikonen, E., Sulkava, R., Benatar, M., Wuu, J., Chiò, A., Restagno, G., Borghero, G., Sabatelli, M., Heckerman, D., Rogaeva, E., Zinman, L., Rothstein, J. D., Sendtner, M., Drepper, C., Eichler, E. E., Alkan, C., Abdullaev, Z., Pack, S. D., Dutra, A., Pak, E., Hardy, J., Singleton, A., Williams, N. M., Heutink, P., Pickering-Brown, S., Morris, H. R., Tienari, P. J., Traynor, B. J. and Consortium, I. (2011) 'A hexanucleotide repeat expansion in C9ORF72 is the cause of chromosome 9p21-linked ALS-FTD', *Neuron*, 72(2), pp. 257-68.

Reuven, N., Adler, J., Meltser, V. and Shaul, Y. (2013) 'The Hippo pathway kinase Lats2 prevents DNA damage-induced apoptosis through inhibition of the tyrosine kinase c-Abl', *Cell Death Differ*, 20(10), pp. 1330-40.

Richter, B., Sliter, D. A., Herhaus, L., Stolz, A., Wang, C., Beli, P., Zaffagnini, G., Wild, P., Martens, S., Wagner, S. A., Youle, R. J. and Dikic, I. (2016) 'Phosphorylation of OPTN by TBK1 enhances its binding to Ub chains and promotes selective autophagy of damaged mitochondria', *Proc Natl Acad Sci U S A*, 113(15), pp. 4039-44.

Rifai, O. M., Waldron, F. M., Sleibi, D., O'Shaughnessy, J., Leighton, D. J. and Gregory, J. M. (2024) 'Clinicopathological analysis of NEK1 variants in amyotrophic lateral sclerosis', *Brain Pathol*, p. e13287.

Ringholz, G. M., Appel, S. H., Bradshaw, M., Cooke, N. A., Mosnik, D. M. and Schulz, P. E. (2005) 'Prevalence and patterns of cognitive impairment in sporadic ALS', *Neurology*, 65(4), pp. 586-90.

Rocha, N., Kuijl, C., van der Kant, R., Janssen, L., Houben, D., Janssen, H., Zwart, W. and Neefjes, J. (2009) 'Cholesterol sensor ORP1L contacts the ER protein VAP to control Rab7-RILP-p150 Glued and late endosome positioning', *J Cell Biol*, 185(7), pp. 1209-25.

Rodriguez-Hernandez, A., Brea-Calvo, G., Fernandez-Ayala, D. J., Cordero, M., Navas, P. and Sanchez-Alcazar, J. A. (2006) 'Nuclear caspase-3 and caspase-7 activation, and poly(ADP-ribose) polymerase cleavage are early events in camptothecin-induced apoptosis', *Apoptosis*, 11(1), pp. 131-9.

Rodriguez-Vargas, J. M., Ruiz-Magana, M. J., Ruiz-Ruiz, C., Majuelos-Melguizo, J., Peralta-Leal, A., Rodriguez, M. I., Munoz-Gamez, J. A., de Almodovar, M. R., Siles, E., Rivas, A. L., Jaattela, M. and Oliver, F. J. (2012) 'ROS-induced DNA damage and PARP-1 are required for optimal induction of starvation-induced autophagy', *Cell Res*, 22(7), pp. 1181-98.

Rosen, D. R., Siddique, T., Patterson, D., Figlewicz, D. A., Sapp, P., Hentati, A., Donaldson, D., Goto, J., O'Regan, J. P., Deng, H., Rahmani, Z., Krizus, A., McKenna-Yasek, D., Cayabyab, A., Gaston, S. M., R., B., Tanzi, R. E., Halperin, J. J., Herzfeldt, B., Van den Bergh, R., Hung, W., Bird, T., Deng, G., Mulder, D. W., Symth, C., Laing, N. G., Soriano, E., Pericak-Vance, M. A., Haines, J., Rouleau, G. A., Gusella, J. S., Horvitz, H. R. and Brown Jr, R. H. (1993) 'Mutations in Cu/Zn superoxide dismutase gene are associated with familial amyotrophic lateral sclerosis', *Nature*, 364(6435), p. 362.

Rothstein, J. D., Van Kammen, M., Levey, A. I., Martin, L. J. and Kuncl, R. W. (1995) 'Selective loss of glial glutamate transporter GLT-1 in amyotrophic lateral sclerosis', *Ann Neurol*, 38(1), pp. 73-84.

Rouleau, G. A., Clark, A. W., Rooke, K., Pramatarova, A., Krizus, A., Suchowersky, O., Julien, J. P. and Figlewicz, D. (1996) 'SOD1 mutation is associated with accumulation of neurofilaments in amyotrophic lateral sclerosis', *Ann Neurol*, 39(1), pp. 128-31.

Rowland, A. A. and Voeltz, G. K. (2012) 'Endoplasmic reticulum-mitochondria contacts: function of the junction', *Nat Rev Mol Cell Biol*, 13(10), pp. 607-25.

Royle, S. J., Granseth, B., Odermatt, B., Derevier, A. and Lagnado, L. (2008) 'Imaging pHluorin-Based Probes at Hippocampal Synapses', in Vancura, A. (ed.) *Membrane Trafficking*. Totowa, NJ: Humana Press, pp. 293-303.

Russell, R. C., Tian, Y., Yuan, H., Park, H. W., Chang, Y. Y., Kim, J., Kim, H., Neufeld, T. P., Dillin, A. and Guan, K. L. (2013) 'ULK1 induces autophagy by phosphorylating Beclin-1 and activating VPS34 lipid kinase', *Nat Cell Biol*, 15(7), pp. 741-50.

Rutherford, N. J., Zhang, Y. J., Baker, M., Gass, J. M., Finch, N. A., Xu, Y. F., Stewart, H., Kelley, B. J., Kuntz, K., Crook, R. J., Sreedharan, J., Vance, C., Sorenson, E., Lippa, C., Bigio, E. H., Geschwind, D. H., Knopman, D. S., Mitsumoto, H., Petersen, R. C., Cashman, N. R., Hutton, M., Shaw, C. E., Boylan, K. B., Boeve, B., Graff-Radford, N. R., Wszolek, Z. K., Caselli, R. J., Dickson, D. W., Mackenzie, I. R., Petrucelli, L. and Rademakers, R. (2008) 'Novel mutations in TARDBP (TDP-43) in patients with familial amyotrophic lateral sclerosis', *PLoS Genet*, 4(9), p. e1000193.

Rutkowski, D. T. and Kaufman, R. J. (2004) 'A trip to the ER: coping with stress', *Trends Cell Biol*, 14(1), pp. 20-8.

Sakai, S., Watanabe, S., Komine, O., Sobue, A. and Yamanaka, K. (2021) 'Novel reporters of mitochondria-associated membranes (MAM), MAMtrackers, demonstrate MAM disruption as a common pathological feature in amyotrophic lateral sclerosis', *FASEB J*, 35(7), p. e21688.

Sakurikar, N., Eichhorn, J. M. and Chambers, T. C. (2012) 'Cyclin-dependent kinase-1 (Cdk1)/cyclin B1 dictates cell fate after mitotic arrest via phosphoregulation of antiapoptotic Bcl-2 proteins', *J Biol Chem*, 287(46), pp. 39193-204.

Salin Raj, P., Nair, A., Preetha Rani, M. R., Rajankutty, K., Ranjith, S. and Raghu, K. G. (2023) 'Ferulic acid attenuates high glucose-induced MAM alterations via PACS2/IP3R2/FUNDC1/VDAC1 pathway activating proapoptotic proteins and ameliorates cardiomyopathy in diabetic rats', *Int J Cardiol*, 372, pp. 101-109.

Sama, R. R., Ward, C. L., Kaushansky, L. J., Lemay, N., Ishigaki, S., Urano, F. and Bosco, D. A. (2013) 'FUS/TLS assembles into stress granules and is a prosurvival factor during hyperosmolar stress', *J Cell Physiol*, 228(11), pp. 2222-31.

Santamaria, A., Wang, B., Elowe, S., Malik, R., Zhang, F., Bauer, M., Schmidt, A., Silljé, H. H., Körner, R. and Nigg, E. A. (2011) 'The Plk1-dependent phosphoproteome of the early mitotic spindle', *Mol Cell Proteomics*, 10(1), p. M110.004457.

Santangelo, S., Invernizzi, S., Sorce, M. N., Casiraghi, V., Peverelli, S., Brusati, A., Colombrita, C., Ticozzi, N., Silani, V., Bossolasco, P. and Ratti, A. (2024) 'NEK1 haploinsufficiency worsens DNA damage but not defective ciliogenesis in C9ORF72 patient-derived iPSC-motoneurons', *bioRxiv*, p. 2024.03.07.582752.

Saotome, M., Safiulina, D., Szabadkai, G., Das, S., Fransson, A., Aspenstrom, P., Rizzuto, R. and Hajnoczky, G. (2008) 'Bidirectional Ca2+-dependent control of mitochondrial dynamics by the Miro GTPase', *Proc Natl Acad Sci U S A*, 105(52), pp. 20728-33.

Sassano, M. L., Derua, R., Waelkens, E., Agostinis, P. and van Vliet, A. R. (2021) 'Interactome Analysis of the ER Stress Sensor Perk Uncovers Key Components of ER-Mitochondria Contact Sites and Ca(2+) Signalling', *Contact (Thousand Oaks)*, 4, p. 25152564211052392.

Satish Tammana, T. V., Tammana, D., Diener, D. R. and Rosenbaum, J. (2013) 'Centrosomal protein CEP104 (Chlamydomonas FAP256) moves to the ciliary tip during ciliary assembly', *J Cell Sci*, 126(Pt 21), pp. 5018-29.

Sawa-Makarska, J., Baumann, V., Coudevylle, N., von Bülow, S., Nogellova, V., Abert, C., Schuschnig, M., Graef, M., Hummer, G. and Martens, S. (2020) 'Reconstitution of autophagosome nucleation defines Atg9 vesicles as seeds for membrane formation', *Science*, 369(6508).

Scarian, E., Fiamingo, G., Diamanti, L., Palmieri, I., Gagliardi, S. and Pansarasa, O. (2022) 'The Role of VCP Mutations in the Spectrum of Amyotrophic Lateral Sclerosis-Frontotemporal Dementia', *Front Neurol*, 13, p. 841394.

Scaricamazza, S., Salvatori, I., Giacovazzo, G., Loeffler, J. P., Rene, F., Rosina, M., Quessada, C., Proietti, D., Heil, C., Rossi, S., Battistini, S., Giannini, F., Volpi, N., Steyn, F. J., Ngo, S. T., Ferraro, E., Madaro, L., Coccurello, R., Valle, C. and Ferri, A. (2020) 'Skeletal-Muscle Metabolic Reprogramming in ALS-SOD1(G93A) Mice Predates Disease Onset and Is A Promising Therapeutic Target', *iScience*, 23(5), p. 101087.

Schludi, M. H., May, S., Grässer, F. A., Rentzsch, K., Kremmer, E., Küpper, C., Klopstock, T., Arzberger, T., Edbauer, D., Degeneration, G. C. f. F. L. and Alliance, B. B. B. (2015) 'Distribution of dipeptide repeat proteins in cellular models and C9orf72 mutation cases suggests link to transcriptional silencing', *Acta Neuropathol*, 130(4), pp. 537-55.

Schumacher, B., Pothof, J., Vijg, J. and Hoeijmakers, J. H. J. (2021) 'The central role of DNA damage in the ageing process', *Nature*, 592(7856), pp. 695-703.

Segal, M. (2005) 'Dendritic spines and long-term plasticity', *Nat Rev Neurosci*, 6(4), pp. 277-84.

Shalom, O., Shalva, N., Altschuler, Y. and Motro, B. (2008) 'The mammalian Nek1 kinase is involved in primary cilium formation', *FEBS Lett*, 582(10), pp. 1465-70.

Shao, Q., Yang, M., Liang, C., Ma, L., Zhang, W., Jiang, Z., Luo, J., Lee, J. K., Liang, C. and Chen, J. F. (2020) 'C9orf72 and smcr8 mutant mice reveal MTORC1 activation due to impaired lysosomal degradation and exocytosis', *Autophagy*, 16(9), pp. 1635-1650.

Shaw, P. J. and Ince, P. G. (1997) 'Glutamate, excitotoxicity and amyotrophic lateral sclerosis', *J Neurol*, 244 Suppl 2, pp. S3-14.

Shen, Y. and White, E. (2001) 'p53-dependent apoptosis pathways', *Adv Cancer Res*, 82, pp. 55-84.

Shepheard, S. R., Parker, M. D., Cooper-Knock, J., Verber, N. S., Tuddenham, L., Heath, P., Beauchamp, N., Place, E., Sollars, E. S. A., Turner, M. R., Malaspina, A., Fratta, P., Hewamadduma, C., Jenkins, T. M., McDermott, C. J., Wang, D., Kirby, J., Shaw, P. J., Project, M. C. and Project Min, E. (2021) 'Value of systematic genetic screening of patients with amyotrophic lateral sclerosis', *J Neurol Neurosurg Psychiatry*, 92(5), pp. 510-518.

Shi, Y., Lin, S., Staats, K. A., Li, Y., Chang, W. H., Hung, S. T., Hendricks, E., Linares, G. R., Wang, Y., Son, E. Y., Wen, X., Kisler, K., Wilkinson, B., Menendez, L., Sugawara, T., Woolwine, P., Huang, M., Cowan, M. J., Ge, B., Koutsodendris, N., Sandor, K. P., Komberg, J., Vangoor, V. R., Senthilkumar, K., Hennes, V., Seah, C., Nelson, A. R., Cheng, T. Y., Lee, S. J., August, P. R., Chen, J. A., Wisniewski, N., Hanson-Smith, V., Belgard, T. G., Zhang, A., Coba, M., Grunseich, C., Ward, M. E., van den Berg, L. H., Pasterkamp, R. J., Trotti, D., Zlokovic, B. V. and Ichida, J. K. (2018) 'Haploinsufficiency leads to neurodegeneration in C9ORF72 ALS/FTD human induced motor neurons', *Nat Med*, 24(3), pp. 313-325.

Shibata, N., Nagai, R., Uchida, K., Horiuchi, S., Yamada, S., Hirano, A., Kawaguchi, M., Yamamoto, T., Sasaki, S. and Kobayashi, M. (2001) 'Morphological evidence for lipid peroxidation and protein glycoxidation in spinal cords from sporadic amyotrophic lateral sclerosis patients', *Brain Res*, 917(1), pp. 97-104.

Shiloh, Y. and Ziv, Y. (2013) 'The ATM protein kinase: regulating the cellular response to genotoxic stress, and more', *Nat Rev Mol Cell Biol*, 14(4), pp. 197-210.

Shirane, M., Wada, M., Morita, K., Hayashi, N., Kunimatsu, R., Matsumoto, Y., Matsuzaki, F., Nakatsumi, H., Ohta, K., Tamura, Y. and Nakayama, K. I. (2020) 'Protrudin and PDZD8 contribute to neuronal integrity by promoting lipid extraction required for endosome maturation', *Nat Commun*, 11(1), p. 4576.

Shoshan-Barmatz, V., De Pinto, V., Zweckstetter, M., Raviv, Z., Keinan, N. and Arbel, N. (2010) 'VDAC, a multi-functional mitochondrial protein regulating cell life and death', *Mol Aspects Med*, 31(3), pp. 227-85.

Shteinfer-Kuzmine, A., Argueti-Ostrovsky, S., Leyton-Jaimes, M. F., Anand, U., Abu-Hamad, S., Zalk, R., Shoshan-Barmatz, V. and Israelson, A. (2022) 'Targeting the Mitochondrial Protein VDAC1 as a Potential Therapeutic Strategy in ALS', *Int J Mol Sci*, 23(17).

Sies, H. and Jones, D. P. (2020) 'Reactive oxygen species (ROS) as pleiotropic physiological signalling agents', *Nat Rev Mol Cell Biol*, 21(7), pp. 363-383.

Simabuco, F. M., Morale, M. G., Pavan, I. C. B., Morelli, A. P., Silva, F. R. and Tamura, R. E. (2018) 'p53 and metabolism: from mechanism to therapeutics', *Oncotarget*, 9(34), pp. 23780-23823.

Simmen, T., Aslan, J. E., Blagoveshchenskaya, A. D., Thomas, L., Wan, L., Xiang, Y., Feliciangeli, S. F., Hung, C. H., Crump, C. M. and Thomas, G. (2005) 'PACS-2 controls endoplasmic reticulum-mitochondria communication and Bid-mediated apoptosis', *EMBO J*, 24(4), pp. 717-29.

Singh, V., Connelly, Z. M., Shen, X. and De Benedetti, A. (2017) 'Identification of the proteome complement of humanTLK1 reveals it binds and phosphorylates NEK1 regulating its activity', *Cell Cycle*, 16(10), pp. 915-926.

Singh, V., Jaiswal, P. K., Ghosh, I., Koul, H. K., Yu, X. and De Benedetti, A. (2019) 'Targeting the TLK1/NEK1 DDR axis with Thioridazine suppresses outgrowth of androgen independent prostate tumors', *Int J Cancer*, 145(4), pp. 1055-1067.

Singh, V., Khalil, M. I. and De Benedetti, A. (2020) 'The TLK1/Nek1 axis contributes to mitochondrial integrity and apoptosis prevention via phosphorylation of VDAC1', *Cell Cycle*, 19(3), pp. 363-375.

Sjostrom, P. J., Rancz, E. A., Roth, A. and Hausser, M. (2008) 'Dendritic excitability and synaptic plasticity', *Physiol Rev*, 88(2), pp. 769-840.

Smith, B. N., Ticozzi, N., Fallini, C., Gkazi, A. S., Topp, S., Kenna, K. P., Scotter, E. L., Kost, J., Keagle, P., Miller, J. W., Calini, D., Vance, C., Danielson, E. W., Troakes, C., Tiloca, C., Al-Sarraj, S., Lewis, E. A., King, A., Colombrita, C., Pensato, V., Castellotti, B., de Belleroche, J., Baas, F., ten Asbroek, A. L., Sapp, P. C., McKenna-Yasek, D., McLaughlin, R. L., Polak, M., Asress, S., Esteban-Pérez, J., Muñoz-Blanco, J. L., Simpson, M., van Rheenen, W., Diekstra, F. P., Lauria, G., Duga, S., Corti, S., Cereda, C., Corrado, L., Sorarù, G., Morrison, K. E., Williams, K. L., Nicholson, G. A., Blair, I. P., Dion, P. A., Leblond, C. S., Rouleau, G. A., Hardiman, O., Veldink, J. H., van den Berg, L. H., Al-Chalabi, A., Pall, H., Shaw, P. J., Turner, M. R., Talbot, K., Taroni, F., García-Redondo, A., Wu, Z., Glass, J. D., Gellera, C., Ratti, A., Brown, R. H., Silani, V., Shaw, C. E., Landers, J. E. and Consortium, S. (2014) 'Exome-wide rare variant analysis identifies TUBA4A mutations associated with familial ALS', *Neuron*, 84(2), pp. 324-31.

Smith, B. N., Topp, S. D., Fallini, C., Shibata, H., Chen, H. J., Troakes, C., King, A., Ticozzi, N., Kenna, K. P., Soragia-Gkazi, A., Miller, J. W., Sato, A., Dias, D. M., Jeon, M., Vance, C., Wong, C. H., de Majo, M., Kattuah, W., Mitchell, J. C., Scotter, E. L., Parkin, N. W., Sapp, P. C., Nolan, M., Nestor, P. J., Simpson, M., Weale, M., Lek, M., Baas, F., Vianney de Jong, J. M., Ten Asbroek, A. L. M. A., Redondo, A. G., Esteban-Pérez, J., Tiloca, C., Verde, F., Duga, S., Leigh, N., Pall, H., Morrison, K. E., Al-Chalabi, A., Shaw, P. J., Kirby, J., Turner, M. R., Talbot, K., Hardiman, O., Glass, J. D., De Belleroche, J., Maki, M., Moss, S. E., Miller, C., Gellera, C., Ratti, A., Al-Sarraj, S., Brown, R. H., Silani, V., Landers, J. E. and Shaw, C. E. (2017) 'Mutations in the vesicular trafficking protein annexin A11 are associated with amyotrophic lateral sclerosis', *Sci Transl Med*, 9(388).

Smith, H. L., Southgate, H., Tweddle, D. A. and Curtin, N. J. (2020) 'DNA damage checkpoint kinases in cancer', *Expert Rev Mol Med*, 22, p. e2.

Sonntag, T., Moresco, J. J., Vaughan, J. M., Matsumura, S., Yates, J. R., 3rd and Montminy, M. (2017) 'Analysis of a cAMP regulated coactivator family reveals an alternative phosphorylation motif for AMPK family members', *PLoS One*, 12(2), p. e0173013.

Sorokin, S. P. (1968) 'Reconstructions of centriole formation and ciliogenesis in mammalian lungs', *J Cell Sci*, 3(2), pp. 207-30.

Spagnolo, L., Rivera-Calzada, A., Pearl, L. H. and Llorca, O. (2006) 'Three-dimensional structure of the human DNA-PKcs/Ku70/Ku80 complex assembled on DNA and its implications for DNA DSB repair', *Mol Cell*, 22(4), pp. 511-9.

Spektor, A., Tsang, W. Y., Khoo, D. and Dynlacht, B. D. (2007) 'Cep97 and CP110 suppress a cilia assembly program', *Cell*, 130(4), pp. 678-90.

Spies, J., Waizenegger, A., Barton, O., Sürder, M., Wright, W. D., Heyer, W. D. and Löbrich, M. (2016) 'Nek1 Regulates Rad54 to Orchestrate Homologous Recombination and Replication Fork Stability', *Mol Cell*, 62(6), pp. 903-917.

Sreedharan, J., Blair, I. P., Tripathi, V. B., Hu, X., Vance, C., Rogelj, B., Ackerley, S., Durnall, J. C., Williams, K. L., Buratti, E., Baralle, F., de Belleroche, J., Mitchell, J. D., Leigh, P. N., Al-Chalabi, A., Miller, C. C., Nicholson, G. and Shaw, C. E. (2008) 'TDP-43 mutations in familial and sporadic amyotrophic lateral sclerosis', *Science*, 319(5870), pp. 1668-72.

Stadler, A., Heloisa, B. G., Santiago, A., Deng, X., Crickley, R., Korbula, K., Mikolaskova, B., Huang, K., Zagrovic, B., Vaughan, S., Sunter, J. D. and Dong, G. (2022) 'Structural studies of cilia and flagella associated protein 410 (CFAP410) reveal its bimodular organization with an N-terminal LRR motif and a C-terminal tetrameric helical bundle', *bioRxiv*, p. 2022.09.21.508879.

Steenbergen, R., Nanowski, T. S., Beigneux, A., Kulinski, A., Young, S. G. and Vance, J. E. (2005) 'Disruption of the phosphatidylserine decarboxylase gene in mice causes embryonic lethality and mitochondrial defects', *J Biol Chem*, 280(48), pp. 40032-40.

Stenzinger, A., Marker, D., Koch, P., Hoffmann, J., Baal, N., Steger, K. and Wimmer, M. (2009) 'Protein tyrosine phosphatase interacting protein 51 (PTPIP51) mRNA expression and localization and its in

vitro interacting partner protein tyrosine phosphatase 1B (PTP1B) in human placenta of the first, second, and third trimester', *J Histochem Cytochem*, 57(2), pp. 143-53.

Stiff, T., O'Driscoll, M., Rief, N., Iwabuchi, K., Lobrich, M. and Jeggo, P. A. (2004) 'ATM and DNA-PK function redundantly to phosphorylate H2AX after exposure to ionizing radiation', *Cancer Res*, 64(7), pp. 2390-6.

Stoica, R., De Vos, K. J., Paillusson, S., Mueller, S., Sancho, R. M., Lau, K. F., Vizcay-Barrena, G., Lin, W. L., Xu, Y. F., Lewis, J., Dickson, D. W., Petrucelli, L., Mitchell, J. C., Shaw, C. E. and Miller, C. C. (2014) 'ER-mitochondria associations are regulated by the VAPB-PTPIP51 interaction and are disrupted by ALS/FTD-associated TDP-43', *Nat Commun*, 5, p. 3996.

Stoica, R., Paillusson, S., Gomez-Suaga, P., Mitchell, J. C., Lau, D. H., Gray, E. H., Sancho, R. M., Vizcay-Barrena, G., De Vos, K. J., Shaw, C. E., Hanger, D. P., Noble, W. and Miller, C. C. (2016) 'ALS/FTD-associated FUS activates GSK-3β to disrupt the VAPB-PTPIP51 interaction and ER-mitochondria associations', *EMBO Rep*, 17(9), pp. 1326-42.

Strong, M. J., Grace, G. M., Orange, J. B., Leeper, H. A., Menon, R. S. and Aere, C. (1999) 'A prospective study of cognitive impairment in ALS', *Neurology*, 53(8), pp. 1665-70.

Subra, M., Dezi, M., Bigay, J., Lacas-Gervais, S., Di Cicco, A., Araújo, A. R. D., Abélanet, S., Fleuriot, L., Debayle, D., Gautier, R., Patel, A., Roussi, F., Antonny, B., Lévy, D. and Mesmin, B. (2023) 'VAP-A intrinsically disordered regions enable versatile tethering at membrane contact sites', *Dev Cell*, 58(2), pp. 121-138.e9.

Sudria-Lopez, E., Koppers, M., de Wit, M., van der Meer, C., Westeneng, H. J., Zundel, C. A., Youssef, S. A., Harkema, L., de Bruin, A., Veldink, J. H., van den Berg, L. H. and Pasterkamp, R. J. (2016) 'Full ablation of C9orf72 in mice causes immune system-related pathology and neoplastic events but no motor neuron defects', *Acta Neuropathol*, 132(1), pp. 145-7.

Suk, T. R. and Rousseaux, M. W. C. (2020) 'The role of TDP-43 mislocalization in amyotrophic lateral sclerosis', *Mol Neurodegener*, 15(1), p. 45.

Sukumaran, P., Nascimento Da Conceicao, V., Sun, Y., Ahamad, N., Saraiva, L. R., Selvaraj, S. and Singh, B. B. (2021) 'Calcium Signaling Regulates Autophagy and Apoptosis', *Cells*, 10(8).

Sun, Y. M., Dong, Y., Wang, J., Lu, J. H., Chen, Y. and Wu, J. J. (2017) 'A novel mutation of VAPB in one Chinese familial amyotrophic lateral sclerosis pedigree and its clinical characteristics', *J Neurol*, 264(12), pp. 2387-2393.

Sung, W., Nahm, M., Lim, S. M., Noh, M. Y., Lee, S., Hwang, S. M., Kim, Y. H., Park, J., Oh, K. W., Ki, C. S., Kim, Y. E. and Kim, S. H. (2022) 'Clinical and genetic characteristics of amyotrophic lateral sclerosis patients with', *Brain Commun*, 4(6), p. fcac299.

Surpili, M. J., Delben, T. M. and Kobarg, J. (2003) 'Identification of proteins that interact with the central coiled-coil region of the human protein kinase NEK1', *Biochemistry*, 42(51), pp. 15369-76.

Suzuki, H., Yabuta, N., Okada, N., Torigata, K., Aylon, Y., Oren, M. and Nojima, H. (2013a) 'Lats2 phosphorylates p21/CDKN1A after UV irradiation and regulates apoptosis', *J Cell Sci*, 126(Pt 19), pp. 4358-68.

Suzuki, J., Kanemaru, K., Ishii, K., Ohkura, M., Okubo, Y. and Iino, M. (2014) 'Imaging intraorganellar Ca2+ at subcellular resolution using CEPIA', *Nat Commun*, 5, p. 4153.

Suzuki, N., Aoki, M., Warita, H., Kato, M., Mizuno, H., Shimakura, N., Akiyama, T., Furuya, H., Hokonohara, T., Iwaki, A., Togashi, S., Konno, H. and Itoyama, Y. (2010) 'FALS with FUS mutation in Japan, with early onset, rapid progress and basophilic inclusion', *J Hum Genet*, 55(4), pp. 252-4.

Suzuki, T., Bridges, D., Nakada, D., Skiniotis, G., Morrison, S. J., Lin, J. D., Saltiel, A. R. and Inoki, K. (2013b) 'Inhibition of AMPK catabolic action by GSK3', *Mol Cell*, 50(3), pp. 407-19.

Szabadkai, G., Bianchi, K., Varnai, P., De Stefani, D., Wieckowski, M. R., Cavagna, D., Nagy, A. I., Balla, T. and Rizzuto, R. (2006) 'Chaperone-mediated coupling of endoplasmic reticulum and mitochondrial Ca2+ channels', *J Cell Biol*, 175(6), pp. 901-11.

Takei, K., Watanabe, K., Yuki, S., Akimoto, M., Sakata, T. and Palumbo, J. (2017) 'Edaravone and its clinical development for amyotrophic lateral sclerosis', *Amyotroph Lateral Scler Frontotemporal Degener*, 18(sup1), pp. 5-10.

Takeuchi, K., Sato, S. I., Abe, K., Kimura, M., Abe, T. A., Yoshinaga, K. and Inaba, H. (1989) 'Intracellular compartmentalization of fura-2 dye demonstrated by laser-excitation fluorescence microscopy: a problem in measuring cytosolic free calcium concentration using fura-2 fluorescence in vascular smooth muscle cells', *Tohoku J Exp Med*, 159(1), pp. 23-35.

Tan, C. F., Eguchi, H., Tagawa, A., Onodera, O., Iwasaki, T., Tsujino, A., Nishizawa, M., Kakita, A. and Takahashi, H. (2007) 'TDP-43 immunoreactivity in neuronal inclusions in familial amyotrophic lateral sclerosis with or without SOD1 gene mutation', *Acta Neuropathol*, 113(5), pp. 535-42.

Tang, W. K. and Xia, D. (2016) 'Mutations in the Human AAA', *Front Mol Biosci*, 3, p. 79.

Tanida, I., Ueno, T. and Kominami, E. (2008) 'LC3 and Autophagy', *Methods Mol Biol*, 445, pp. 77-88.

Tao, Z., Wang, H., Xia, Q., Li, K., Jiang, X., Xu, G., Wang, G. and Ying, Z. (2015) 'Nucleolar stress and impaired stress granule formation contribute to C9orf72 RAN translation-induced cytotoxicity', *Hum Mol Genet*, 24(9), pp. 2426-41.

Tasseva, G., Bai, H. D., Davidescu, M., Haromy, A., Michelakis, E. and Vance, J. E. (2013) 'Phosphatidylethanolamine deficiency in Mammalian mitochondria impairs oxidative phosphorylation and alters mitochondrial morphology', *J Biol Chem*, 288(6), pp. 4158-73.

Tazelaar, G. H. P., Boeynaems, S., De Decker, M., van Vugt, J. J. F. A., Kool, L., Goedee, H. S., McLaughlin, R. L., Sproviero, W., Iacoangeli, A., Moisse, M., Jacquemyn, M., Daelemans, D., Dekker, A. M., van der Spek, R. A., Westeneng, H. J., Kenna, K. P., Assialioui, A., Da Silva, N., Povedano, M., Pardina, J. S. M., Hardiman, O., Salachas, F., Millecamps, S., Vourc'h, P., Corcia, P., Couratier, P., Morrison, K. E., Shaw, P. J., Shaw, C. E., Pasterkamp, R. J., Landers, J. E., Van Den Bosch, L., Robberecht, W., Al-Chalabi, A., van den Berg, L. H., Van Damme, P., Veldink, J. H., van Es, M. A. and Consortium, P. M. A. S. (2020) 'ATNX1 repeat expansions confer risk for amyotrophic lateral sclerosis and contribute to TDP-43 mislocalization', *Brain Commun*, 2(2), p. fcaa064.

Teng, Y., Ren, X., Li, H., Shull, A., Kim, J. and Cowell, J. K. (2016) 'Mitochondrial ATAD3A combines with GRP78 to regulate the WASF3 metastasis-promoting protein', *Oncogene*, 35(3), pp. 333-43.

Teuling, E., Ahmed, S., Haasdijk, E., Demmers, J., Steinmetz, M. O., Akhmanova, A., Jaarsma, D. and Hoogenraad, C. C. (2007) 'Motor neuron disease-associated mutant vesicle-associated membrane protein-associated protein (VAP) B recruits wild-type VAPs into endoplasmic reticulum-derived tubular aggregates', *J Neurosci*, 27(36), pp. 9801-15.

Thiel, C., Kessler, K., Giessl, A., Dimmler, A., Shalev, S. A., von der Haar, S., Zenker, M., Zahnleiter, D., Stöss, H., Beinder, E., Abou Jamra, R., Ekici, A. B., Schröder-Kress, N., Aigner, T., Kirchner, T., Reis, A., Brandstätter, J. H. and Rauch, A. (2011) 'NEK1 mutations cause short-rib polydactyly syndrome type majewski', *Am J Hum Genet*, 88(1), pp. 106-14.

Thul, P. J., Akesson, L., Wiking, M., Mahdessian, D., Geladaki, A., Ait Blal, H., Alm, T., Asplund, A., Bjork, L., Breckels, L. M., Backstrom, A., Danielsson, F., Fagerberg, L., Fall, J., Gatto, L., Gnann, C., Hober, S., Hjelmare, M., Johansson, F., Lee, S., Lindskog, C., Mulder, J., Mulvey, C. M., Nilsson, P., Oksvold, P., Rockberg, J., Schutten, R., Schwenk, J. M., Sivertsson, A., Sjostedt, E., Skogs, M., Stadler, C., Sullivan, D. P., Tegel, H., Winsnes, C., Zhang, C., Zwahlen, M., Mardinoglu, A., Ponten, F., von Feilitzen, K., Lilley, K. S., Uhlen, M. and Lundberg, E. (2017) 'A subcellular map of the human proteome', *Science*, 356(6340).

Tibshirani, M., Zhao, B., Gentil, B. J., Minotti, S., Marques, C., Keith, J., Rogaeva, E., Zinman, L., Rouaux, C., Robertson, J. and Durham, H. D. (2017) 'Dysregulation of chromatin remodelling complexes in amyotrophic lateral sclerosis', *Hum Mol Genet*, 26(21), pp. 4142-4152.

Traxinger, K., Kelly, C., Johnson, B. A., Lyles, R. H. and Glass, J. D. (2013) 'Prognosis and epidemiology of amyotrophic lateral sclerosis: Analysis of a clinic population, 1997-2011', *Neurol Clin Pract*, 3(4), pp. 313-320.

Tresse, E., Salomons, F. A., Vesa, J., Bott, L. C., Kimonis, V., Yao, T. P., Dantuma, N. P. and Taylor, J. P. (2010) 'VCP/p97 is essential for maturation of ubiquitin-containing autophagosomes and this function is impaired by mutations that cause IBMPFD', *Autophagy*, 6(2), pp. 217-27.

Tripathi, D. N., Chowdhury, R., Trudel, L. J., Tee, A. R., Slack, R. S., Walker, C. L. and Wogan, G. N. (2013) 'Reactive nitrogen species regulate autophagy through ATM-AMPK-TSC2-mediated suppression of mTORC1', *Proc Natl Acad Sci U S A*, 110(32), pp. E2950-7.

Tripathi, P., Guo, H., Dreser, A., Yamoah, A., Sechi, A., Jesse, C. M., Katona, I., Doukas, P., Nikolin, S., Ernst, S., Aronica, E., Glaß, H., Hermann, A., Steinbusch, H., Feller, A. C., Bergmann, M., Jaarsma, D., Weis, J. and Goswami, A. (2021) 'Pathomechanisms of ALS8: altered autophagy and defective RNA binding protein (RBP) homeostasis due to the VAPB P56S mutation', *Cell Death Dis*, 12(5), p. 466.

Troakes, C., Maekawa, S., Wijesekera, L., Rogelj, B., Siklós, L., Bell, C., Smith, B., Newhouse, S., Vance, C., Johnson, L., Hortobágyi, T., Shatunov, A., Al-Chalabi, A., Leigh, N., Shaw, C. E., King, A. and Al-Sarraj, S. (2012) 'An MND/ALS phenotype associated with C9orf72 repeat expansion: abundant p62-positive, TDP-43-negative inclusions in cerebral cortex, hippocampus and cerebellum but without associated cognitive decline', *Neuropathology*, 32(5), pp. 505-14.

Tsai, Y. S., Lin, K. P., Jih, K. Y., Tsai, P. C., Liao, Y. C. and Lee, Y. C. (2020) 'Hand-onset weakness is a common feature of ALS patients with a NEK1 loss-of-function variant', *Ann Clin Transl Neurol*, 7(6), pp. 965-971.

Tsuboi, M. and Hirabayashi, Y. (2021) 'New insights into the regulation of synaptic transmission and plasticity by the endoplasmic reticulum and its membrane contacts', *Proc Jpn Acad Ser B Phys Biol Sci*, 97(10), pp. 559-572.

Tubbs, E. and Rieusset, J. (2016) 'Study of Endoplasmic Reticulum and Mitochondria Interactions by In Situ Proximity Ligation Assay in Fixed Cells', *J Vis Exp*, (118).

Tudor, E. L., Galtrey, C. M., Perkinton, M. S., Lau, K. F., De Vos, K. J., Mitchell, J. C., Ackerley, S., Hortobagyi, T., Vamos, E., Leigh, P. N., Klasen, C., McLoughlin, D. M., Shaw, C. E. and Miller, C. C. (2010) 'Amyotrophic lateral sclerosis mutant vesicle-associated membrane protein-associated protein-B transgenic mice develop TAR-DNA-binding protein-43 pathology', *Neuroscience*, 167(3), pp. 774-85.

Turco, E., Witt, M., Abert, C., Bock-Bierbaum, T., Su, M. Y., Trapannone, R., Sztacho, M., Danieli, A., Shi, X., Zaffagnini, G., Gamper, A., Schuschnig, M., Fracchiolla, D., Bernklau, D., Romanov, J., Hartl, M., Hurley, J. H., Daumke, O. and Martens, S. (2019) 'FIP200 Claw Domain Binding to p62 Promotes Autophagosome Formation at Ubiquitin Condensates', *Mol Cell*, 74(2), pp. 330-346.e11.

Turkan, A., Hiromasa, Y. and Roche, T. E. (2004) 'Formation of a complex of the catalytic subunit of pyruvate dehydrogenase phosphatase isoform 1 (PDP1c) and the L2 domain forms a Ca2+ binding site and captures PDP1c as a monomer', *Biochemistry*, 43(47), pp. 15073-85.

Tyanova, S., Temu, T., Sinitcyn, P., Carlson, A., Hein, M. Y., Geiger, T., Mann, M. and Cox, J. (2016) 'The Perseus computational platform for comprehensive analysis of (prote)omics data', *Nat Methods*, 13(9), pp. 731-40.

UniProt, C. (2021) 'UniProt: the universal protein knowledgebase in 2021', *Nucleic Acids Res*, 49(D1), pp. D480-D489.

Upadhya, P., Birkenmeier, E. H., Birkenmeier, C. S. and Barker, J. E. (2000) 'Mutations in a NIMA-related kinase gene, Nek1, cause pleiotropic effects including a progressive polycystic kidney disease in mice', *Proc Natl Acad Sci U S A*, 97(1), pp. 217-21.

Urushihara, Y., Hashimoto, T., Fujishima, Y. and Hosoi, Y. (2023) 'AMPK/FOXO3a Pathway Increases Activity and/or Expression of ATM, DNA-PKcs, Src, EGFR, PDK1, and SOD2 and Induces Radioresistance under Nutrient Starvation', *Int J Mol Sci*, 24(16).

Urushitani, M., Kurisu, J., Tsukita, K. and Takahashi, R. (2002) 'Proteasomal inhibition by misfolded mutant superoxide dismutase 1 induces selective motor neuron death in familial amyotrophic lateral sclerosis', *J Neurochem*, 83(5), pp. 1030-42.

van Blitterswijk, M., van Es, M. A., Koppers, M., van Rheenen, W., Medic, J., Schelhaas, H. J., van der Kooi, A. J., de Visser, M., Veldink, J. H. and van den Berg, L. H. (2012) 'VAPB and C9orf72 mutations in 1 familial amyotrophic lateral sclerosis patient', *Neurobiol Aging*, 33(12), pp. 2950 e1-4.

Van Daele, S. H., Moisse, M., van Vugt, J. J. F. A., Zwamborn, R. A. J., van der Spek, R., van Rheenen, W., Van Eijk, K., Kenna, K., Corcia, P., Vourc'h, P., Couratier, P., Hardiman, O., McLaughin, R., Gotkine, M., Drory, V., Ticozzi, N., Silani, V., Ratti, A., de Carvalho, M., Mora Pardina, J. S., Povedano, M., Andersen, P. M., Weber, M., Başak, N. A., Shaw, C., Shaw, P. J., Morrison, K. E., Landers, J. E., Glass, J. D., van Es, M. A., van den Berg, L. H., Al-Chalabi, A., Veldink, J. and Van Damme, P. (2023) 'Genetic variability in sporadic amyotrophic lateral sclerosis', *Brain*, 146(9), pp. 3760-3769.

van de Kooij, B., Creixell, P., van Vlimmeren, A., Joughin, B. A., Miller, C. J., Haider, N., Simpson, C. D., Linding, R., Stambolic, V., Turk, B. E. and Yaffe, M. B. (2019) 'Comprehensive substrate specificity profiling of the human Nek kinome reveals unexpected signaling outputs', *Elife*, 8.

Van Den Bosch, L., Van Damme, P., Bogaert, E. and Robberecht, W. (2006) 'The role of excitotoxicity in the pathogenesis of amyotrophic lateral sclerosis', *Biochim Biophys Acta*, 1762(11-12), pp. 1068-82.

van Eersel, J., Ke, Y. D., Gladbach, A., Bi, M., Götz, J., Kril, J. J. and Ittner, L. M. (2011) 'Cytoplasmic accumulation and aggregation of TDP-43 upon proteasome inhibition in cultured neurons', *PLoS One*, 6(7), p. e22850.

van Es, M. A., Veldink, J. H., Saris, C. G., Blauw, H. M., van Vught, P. W., Birve, A., Lemmens, R., Schelhaas, H. J., Groen, E. J., Huisman, M. H., van der Kooi, A. J., de Visser, M., Dahlberg, C., Estrada, K., Rivadeneira, F., Hofman, A., Zwarts, M. J., van Doormaal, P. T., Rujescu, D., Strengman, E., Giegling, I., Muglia, P., Tomik, B., Slowik, A., Uitterlinden, A. G., Hendrich, C., Waibel, S., Meyer, T., Ludolph, A. C., Glass, J. D., Purcell, S., Cichon, S., Nöthen, M. M., Wichmann, H. E., Schreiber, S., Vermeulen, S. H., Kiemeney, L. A., Wokke, J. H., Cronin, S., McLaughlin, R. L., Hardiman, O., Fumoto, K., Pasterkamp, R. J., Meininger, V., Melki, J., Leigh, P. N., Shaw, C. E., Landers, J. E., Al-Chalabi, A., Brown, R. H., Robberecht, W., Andersen, P. M., Ophoff, R. A. and van den Berg, L. H. (2009) 'Genome-wide association study identifies 19p13.3 (UNC13A) and 9p21.2 as susceptibility loci for sporadic amyotrophic lateral sclerosis', *Nat Genet*, 41(10), pp. 1083-7.

van Rheenen, W., Shatunov, A., Dekker, A. M., McLaughlin, R. L., Diekstra, F. P., Pulit, S. L., van der Spek, R. A., Võsa, U., de Jong, S., Robinson, M. R., Yang, J., Fogh, I., van Doormaal, P. T., Tazelaar, G. H., Koppers, M., Blokhuis, A. M., Sproviero, W., Jones, A. R., Kenna, K. P., van Eijk, K. R., Harschnitz, O., Schellevis, R. D., Brands, W. J., Medic, J., Menelaou, A., Vajda, A., Ticozzi, N., Lin, K., Rogelj, B., Vrabec, K., Ravnik-Glavač, M., Koritnik, B., Zidar, J., Leonardis, L., Grošelj, L. D., Millecamps, S., Salachas, F., Meininger, V., de Carvalho, M., Pinto, S., Mora, J. S., Rojas-García, R., Polak, M., Chandran, S., Colville, S., Swingler, R., Morrison, K. E., Shaw, P. J., Hardy, J., Orrell, R. W., Pittman, A., Sidle, K., Fratta, P., Malaspina, A., Topp, S., Petri, S., Abdulla, S., Drepper, C., Sendtner, M., Meyer, T., Ophoff, R. A., Staats, K. A., Wiedau-Pazos, M., Lomen-Hoerth, C., Van Deerlin, V. M., Trojanowski, J. Q., Elman, L., McCluskey, L., Basak, A. N., Tunca, C., Hamzeiy, H., Parman, Y., Meitinger, T., Lichtner, P., Radivojkov-Blagojevic, M., Andres, C. R., Maurel, C., Bensimon, G., Landwehrmeyer, B., Brice, A., Payan, C. A.,

Saker-Delye, S., Dürr, A., Wood, N. W., Tittmann, L., Lieb, W., Franke, A., Rietschel, M., Cichon, S., Nöthen, M. M., Amouyel, P., Tzourio, C., Dartigues, J. F., Uitterlinden, A. G., Rivadeneira, F., Estrada, K., Hofman, A., Curtis, C., Blauw, H. M., van der Kooi, A. J., et al. (2016) 'Genome-wide association analyses identify new risk variants and the genetic architecture of amyotrophic lateral sclerosis', *Nat Genet*, 48(9), pp. 1043-8.

van Rheenen, W., van der Spek, R. A. A., Bakker, M. K., van Vugt, J. J. F. A., Hop, P. J., Zwamborn, R. A. J., de Klein, N., Westra, H. J., Bakker, O. B., Deelen, P., Shireby, G., Hannon, E., Moisse, M., Baird, D., Restuadi, R., Dolzhenko, E., Dekker, A. M., Gawor, K., Westeneng, H. J., Tazelaar, G. H. P., van Eijk, K. R., Kooyman, M., Byrne, R. P., Doherty, M., Heverin, M., Al Khleifat, A., Iacoangeli, A., Shatunov, A., Ticozzi, N., Cooper-Knock, J., Smith, B. N., Gromicho, M., Chandran, S., Pal, S., Morrison, K. E., Shaw, P. J., Hardy, J., Orrell, R. W., Sendtner, M., Meyer, T., Başak, N., van der Kooi, A. J., Ratti, A., Fogh, I., Gellera, C., Lauria, G., Corti, S., Cereda, C., Sproviero, D., D'Alfonso, S., Sorarù, G., Siciliano, G., Filosto, M., Padovani, A., Chiò, A., Calvo, A., Moglia, C., Brunetti, M., Canosa, A., Grassano, M., Beghi, E., Pupillo, E., Logroscino, G., Nefussy, B., Osmanovic, A., Nordin, A., Lerner, Y., Zabari, M., Gotkine, M., Baloh, R. H., Bell, S., Vourc'h, P., Corcia, P., Couratier, P., Millecamps, S., Meininger, V., Salachas, F., Mora Pardina, J. S., Assialioui, A., Rojas-García, R., Dion, P. A., Ross, J. P., Ludolph, A. C., Weishaupt, J. H., Brenner, D., Freischmidt, A., Bensimon, G., Brice, A., Durr, A., Payan, C. A. M., Saker-Delye, S., Wood, N. W., Topp, S., Rademakers, R., Tittmann, L., Lieb, W., Franke, A., Ripke, S., Braun, A., Kraft, J., et al. (2021) 'Common and rare variant association analyses in amyotrophic lateral sclerosis identify 15 risk loci with distinct genetic architectures and neuron-specific biology', *Nat Genet*, 53(12), pp. 1636-1648.

Vance, C., Rogelj, B., Hortobágyi, T., De Vos, K. J., Nishimura, A. L., Sreedharan, J., Hu, X., Smith, B., Ruddy, D., Wright, P., Ganesalingam, J., Williams, K. L., Tripathi, V., Al-Saraj, S., Al-Chalabi, A., Leigh, P. N., Blair, I. P., Nicholson, G., de Belleroche, J., Gallo, J. M., Miller, C. C. and Shaw, C. E. (2009) 'Mutations in FUS, an RNA processing protein, cause familial amyotrophic lateral sclerosis type 6', *Science*, 323(5918), pp. 1208-1211.

Vance, J. E. (1990) 'Phospholipid synthesis in a membrane fraction associated with mitochondria', *J Biol Chem*, 265(13), pp. 7248-56.

Vance, J. E. and Tasseva, G. (2013) 'Formation and function of phosphatidylserine and phosphatidylethanolamine in mammalian cells', *Biochim Biophys Acta*, 1831(3), pp. 543-54.

Vaziri, H., Dessain, S. K., Ng Eaton, E., Imai, S. I., Frye, R. A., Pandita, T. K., Guarente, L. and Weinberg, R. A. (2001) 'hSIR2(SIRT1) functions as an NAD-dependent p53 deacetylase', *Cell*, 107(2), pp. 149-59.

Venditti, R., Rega, L. R., Masone, M. C., Santoro, M., Polishchuk, E., Sarnataro, D., Paladino, S., D'Auria, S., Varriale, A., Olkkonen, V. M., Di Tullio, G., Polishchuk, R. and De Matteis, M. A. (2019) 'Molecular determinants of ER-Golgi contacts identified through a new FRET-FLIM system', *J Cell Biol*, 218(3), pp. 1055-1065.

Vera, J., Raatz, Y., Wolkenhauer, O., Kottek, T., Bhattacharya, A., Simon, J. C. and Kunz, M. (2015) 'Chk1 and Wee1 control genotoxic-stress induced G2-M arrest in melanoma cells', *Cell Signal*, 27(5), pp. 951-60.

Verde, F., Steinacker, P., Weishaupt, J. H., Kassubek, J., Oeckl, P., Halbgebauer, S., Tumani, H., von Arnim, C. A. F., Dorst, J., Feneberg, E., Mayer, B., Müller, H. P., Gorges, M., Rosenbohm, A., Volk, A. E., Silani, V., Ludolph, A. C. and Otto, M. (2019) 'Neurofilament light chain in serum for the diagnosis of amyotrophic lateral sclerosis', *J Neurol Neurosurg Psychiatry*, 90(2), pp. 157-164.

Verma, A. (2021) 'Clinical Manifestation and Management of Amyotrophic Lateral Sclerosis', in Araki, T. (ed.) *Amyotrophic Lateral Sclerosis*. Brisbane (AU).

Vicencio, J. M., Ortiz, C., Criollo, A., Jones, A. W., Kepp, O., Galluzzi, L., Joza, N., Vitale, I., Morselli, E., Tailler, M., Castedo, M., Maiuri, M. C., Molgó, J., Szabadkai, G., Lavandero, S. and Kroemer, G. (2009)

'The inositol 1,4,5-trisphosphate receptor regulates autophagy through its interaction with Beclin 1', *Cell Death Differ*, 16(7), pp. 1006-17.

Vinayagam, A., Stelzl, U., Foulle, R., Plassmann, S., Zenkner, M., Timm, J., Assmus, H. E., Andrade-Navarro, M. A. and Wanker, E. E. (2011) 'A directed protein interaction network for investigating intracellular signal transduction', *Sci Signal*, 4(189), p. rs8.

Vlasenko, D. O., Novosylna, O. V., Negrutskii, B. S. and El'skaya, A. V. (2015) 'Truncation of the A,A(*),A' helices segment impairs the actin bundling activity of mammalian eEF1A1', *FEBS Lett*, 589(11), pp. 1187-93.

Vucic, S., Lin, C. S., Cheah, B. C., Murray, J., Menon, P., Krishnan, A. V. and Kiernan, M. C. (2013) 'Riluzole exerts central and peripheral modulating effects in amyotrophic lateral sclerosis', *Brain*, 136(Pt 5), pp. 1361-70.

Wakana, Y., Kotake, R., Oyama, N., Murate, M., Kobayashi, T., Arasaki, K., Inoue, H. and Tagaya, M. (2015) 'CARTS biogenesis requires VAP-lipid transfer protein complexes functioning at the endoplasmic reticulum-Golgi interface', *Mol Biol Cell*, 26(25), pp. 4686-99.

Walczak, J., Dębska-Vielhaber, G., Vielhaber, S., Szymański, J., Charzyńska, A., Duszyński, J. and Szczepanowska, J. (2019) 'Distinction of sporadic and familial forms of ALS based on mitochondrial characteristics', *FASEB J*, 33(3), pp. 4388-4403.

Wang, B., Nguyen, M., Chang, N. C. and Shore, G. C. (2011) 'Fis1, Bap31 and the kiss of death between mitochondria and endoplasmic reticulum', *EMBO J*, 30(3), pp. 451-2.

Wang, H., Guo, W., Mitra, J., Hegde, P. M., Vandoorne, T., Eckelmann, B. J., Mitra, S., Tomkinson, A. E., Van Den Bosch, L. and Hegde, M. L. (2018) 'Mutant FUS causes DNA ligation defects to inhibit oxidative damage repair in Amyotrophic Lateral Sclerosis', *Nat Commun*, 9(1), p. 3683.

Wang, H., Qi, W., Zou, C., Xie, Z., Zhang, M., Naito, M. G., Mifflin, L., Liu, Z., Najafov, A., Pan, H., Shan, B., Li, Y., Zhu, Z.-J. and Yuan, J. (2021a) 'NEK1-mediated retromer trafficking promotes blood–brain barrier integrity by regulating glucose metabolism and RIPK1 activation', *Nature Communications*, 12(1), p. 4826.

Wang, P., Deng, J., Dong, J., Liu, J., Bigio, E. H., Mesulam, M., Wang, T., Sun, L., Wang, L., Lee, A. Y., McGee, W. A., Chen, X., Fushimi, K., Zhu, L. and Wu, J. Y. (2019) 'TDP-43 induces mitochondrial damage and activates the mitochondrial unfolded protein response', *PLoS Genet*, 15(5), p. e1007947.

Wang, P. Y., Ma, J., Kim, Y. C., Son, A. Y., Syed, A. M., Liu, C., Mori, M. P., Huffstutler, R. D., Stolinski, J. L., Talagala, S. L., Kang, J. G., Walitt, B. T., Nath, A. and Hwang, P. M. (2023) 'WASF3 disrupts mitochondrial respiration and may mediate exercise intolerance in myalgic encephalomyelitis/chronic fatigue syndrome', *Proc Natl Acad Sci U S A*, 120(34), p. e2302738120.

Wang, Q., Johnson, J. L., Agar, N. Y. and Agar, J. N. (2008) 'Protein aggregation and protein instability govern familial amyotrophic lateral sclerosis patient survival', *PLoS Biol*, 6(7), p. e170.

Wang, T., Liu, H., Itoh, K., Oh, S., Zhao, L., Murata, D., Sesaki, H., Hartung, T., Na, C. H. and Wang, J. (2021b) 'C9orf72 regulates energy homeostasis by stabilizing mitochondrial complex I assembly', *Cell Metab*, 33(3), pp. 531-546 e9.

Wang, W., Li, L., Lin, W. L., Dickson, D. W., Petrucelli, L., Zhang, T. and Wang, X. (2013) 'The ALS disease-associated mutant TDP-43 impairs mitochondrial dynamics and function in motor neurons', *Hum Mol Genet*, 22(23), pp. 4706-19.

Wang, W., Wu, T. and Kirschner, M. W. (2014) 'The master cell cycle regulator APC-Cdc20 regulates ciliary length and disassembly of the primary cilium', *Elife*, 3, p. e03083.

Wang, X. and Schwarz, T. L. (2009) 'The mechanism of Ca2+ -dependent regulation of kinesin-mediated mitochondrial motility', *Cell*, 136(1), pp. 163-74.

Wang, X. X., Chen, W. Z., Li, C. and Xu, R. S. (2024a) 'Current potential pathogenic mechanisms of copper-zinc superoxide dismutase 1 (SOD1) in amyotrophic lateral sclerosis', *Rev Neurosci*, 35(5), pp. 549-563.

Wang, Y., Duan, X., Zhou, X., Wang, R., Zhang, X., Cao, Z., Wang, X., Zhou, Z., Sun, Y. and Peng, D. (2022) 'ANXA11 mutations are associated with amyotrophic lateral sclerosis-frontotemporal dementia', *Front Neurol*, 13, p. 886887.

Wang, Y., Zhai, Y., Zhang, M., Song, C., Zhang, Y. and Zhang, G. (2024b) 'Escaping from CRISPR-Cas-mediated knockout: the facts, mechanisms, and applications', *Cell Mol Biol Lett*, 29(1), p. 48.

Wang, Z., Horemuzova, E., Iida, A., Guo, L., Liu, Y., Matsumoto, N., Nishimura, G., Nordgren, A., Miyake, N., Tham, E., Grigelioniene, G. and Ikegawa, S. (2017) 'Axial spondylometaphyseal dysplasia is also caused by NEK1 mutations', *J Hum Genet*, 62(4), pp. 503-506.

Wang, Z., Iida, A., Miyake, N., Nishiguchi, K. M., Fujita, K., Nakazawa, T., Alswaid, A., Albalwi, M. A., Kim, O. H., Cho, T. J., Lim, G. Y., Isidor, B., David, A., Rustad, C. F., Merckoll, E., Westvik, J., Stattin, E. L., Grigelioniene, G., Kou, I., Nakajima, M., Ohashi, H., Smithson, S., Matsumoto, N., Nishimura, G. and Ikegawa, S. (2016a) 'Axial Spondylometaphyseal Dysplasia Is Caused by C21orf2 Mutations', *PLoS One*, 11(3), p. e0150555.

Wang, Z., Miao, G., Xue, X., Guo, X., Yuan, C., Zhang, G., Chen, Y., Feng, D., Hu, J. and Zhang, H. (2016b) 'The Vici Syndrome Protein EPG5 Is a Rab7 Effector that Determines the Fusion Specificity of Autophagosomes with Late Endosomes/Lysosomes', *Mol Cell*, 63(5), pp. 781-95.

Watanabe, S., Horiuchi, M., Murata, Y., Komine, O., Kawade, N., Sobue, A. and Yamanaka, K. (2023) 'Sigma-1 receptor maintains ATAD3A as a monomer to inhibit mitochondrial fragmentation at the mitochondria-associated membrane in amyotrophic lateral sclerosis', *Neurobiol Dis*, 179, p. 106031.

Watanabe, S., Ilieva, H., Tamada, H., Nomura, H., Komine, O., Endo, F., Jin, S., Mancias, P., Kiyama, H. and Yamanaka, K. (2016) 'Mitochondria-associated membrane collapse is a common pathomechanism in SIGMAR1- and SOD1-linked ALS', *EMBO Mol Med*, 8(12), pp. 1421-1437.

Watanabe, Y., Nakagawa, T., Akiyama, T., Nakagawa, M., Suzuki, N., Warita, H., Aoki, M. and Nakayama, K. (2020) 'An Amyotrophic Lateral Sclerosis-Associated Mutant of C21ORF2 Is Stabilized by NEK1-Mediated Hyperphosphorylation and the Inability to Bind FBXO3', *iScience*, 23(9), p. 101491.

Watcharasit, P., Bijur, G. N., Zmijewski, J. W., Song, L., Zmijewska, A., Chen, X., Johnson, G. V. and Jope, R. S. (2002) 'Direct, activating interaction between glycogen synthase kinase-3beta and p53 after DNA damage', *Proc Natl Acad Sci U S A*, 99(12), pp. 7951-5.

Weber-Boyvat, M., Kentala, H., Peranen, J. and Olkkonen, V. M. (2015) 'Ligand-dependent localization and function of ORP-VAP complexes at membrane contact sites', *Cell Mol Life Sci*, 72(10), pp. 1967-87.

Webster, C. P., Smith, E. F., Bauer, C. S., Moller, A., Hautbergue, G. M., Ferraiuolo, L., Myszczynska, M. A., Higginbottom, A., Walsh, M. J., Whitworth, A. J., Kaspar, B. K., Meyer, K., Shaw, P. J., Grierson, A. J. and De Vos, K. J. (2016) 'The C9orf72 protein interacts with Rab1a and the ULK1 complex to regulate initiation of autophagy', *EMBO J*, 35(15), pp. 1656-76.

Wee, J. and Wei, G. W. (2024) 'Evaluation of AlphaFold 3's Protein-Protein Complexes for Predicting Binding Free Energy Changes upon Mutation', *J Chem Inf Model*, 64(16), pp. 6676-6683.

Welty, S., Teng, Y., Liang, Z., Zhao, W., Sanders, L. H., Greenamyre, J. T., Rubio, M. E., Thathiah, A., Kodali, R., Wetzel, R., Levine, A. S. and Lan, L. (2018) 'RAD52 is required for RNA-templated recombination repair in post-mitotic neurons', *J Biol Chem*, 293(4), pp. 1353-1362.

Wheway, G., Nazlamova, L. and Hancock, J. T. (2018) 'Signaling through the Primary Cilium', *Front Cell Dev Biol*, 6, p. 8.

Wheway, G., Schmidts, M., Mans, D. A., Szymanska, K., Nguyen, T. T., Racher, H., Phelps, I. G., Toedt, G., Kennedy, J., Wunderlich, K. A., Sorusch, N., Abdelhamed, Z. A., Natarajan, S., Herridge, W., van Reeuwijk, J., Horn, N., Boldt, K., Parry, D. A., Letteboer, S. J. F., Roosing, S., Adams, M., Bell, S. M., Bond, J., Higgins, J., Morrison, E. E., Tomlinson, D. C., Slaats, G. G., van Dam, T. J. P., Huang, L., Kessler, K., Giessl, A., Logan, C. V., Boyle, E. A., Shendure, J., Anazi, S., Aldahmesh, M., Al Hazzaa, S., Hegele, R. A., Ober, C., Frosk, P., Mhanni, A. A., Chodirker, B. N., Chudley, A. E., Lamont, R., Bernier, F. P., Beaulieu, C. L., Gordon, P., Pon, R. T., Donahue, C., Barkovich, A. J., Wolf, L., Toomes, C., Thiel, C. T., Boycott, K. M., McKibbin, M., Inglehearn, C. F., Stewart, F., Omran, H., Huynen, M. A., Sergouniotis, P. I., Alkuraya, F. S., Parboosingh, J. S., Innes, A. M., Willoughby, C. E., Giles, R. H., Webster, A. R., Ueffing, M., Blacque, O., Gleeson, J. G., Wolfrum, U., Beales, P. L., Gibson, T., Doherty, D., Mitchison, H. M., Roepman, R., Johnson, C. A., Consortium, U. K. and Genomics, U. o. W. C. f. M. (2015) 'An siRNA-based functional genomics screen for the identification of regulators of ciliogenesis and ciliopathy genes', *Nat Cell Biol*, 17(8), pp. 1074-1087.

White, M. A., Kim, E., Duffy, A., Adalbert, R., Phillips, B. U., Peters, O. M., Stephenson, J., Yang, S., Massenzio, F., Lin, Z., Andrews, S., Segonds-Pichon, A., Metterville, J., Saksida, L. M., Mead, R., Ribchester, R. R., Barhomi, Y., Serre, T., Coleman, M. P., Fallon, J. R., Bussey, T. J., Brown, R. H., Jr. and Sreedharan, J. (2018) 'TDP-43 gains function due to perturbed autoregulation in a Tardbp knock-in mouse model of ALS-FTD', *Nat Neurosci*, 21(4), pp. 552-563.

White, M. C. and Quarmby, L. M. (2008) 'The NIMA-family kinase, Nek1 affects the stability of centrosomes and ciliogenesis', *BMC Cell Biol*, 9, p. 29.

Willemse, S. W., Harley, P., van Eijk, R. P. A., Demaegd, K. C., Zelina, P., Pasterkamp, R. J., van Damme, P., Ingre, C., van Rheenen, W., Veldink, J. H., Kiernan, M. C., Al-Chalabi, A., van den Berg, L. H., Fratta, P. and van Es, M. A. (2023) 'UNC13A in amyotrophic lateral sclerosis: from genetic association to therapeutic target', *J Neurol Neurosurg Psychiatry*, 94(8), pp. 649-656.

Williams, K. L., Topp, S., Yang, S., Smith, B., Fifita, J. A., Warraich, S. T., Zhang, K. Y., Farrawell, N., Vance, C., Hu, X., Chesi, A., Leblond, C. S., Lee, A., Rayner, S. L., Sundaramoorthy, V., Dobson-Stone, C., Molloy, M. P., van Blitterswijk, M., Dickson, D. W., Petersen, R. C., Graff-Radford, N. R., Boeve, B. F., Murray, M. E., Pottier, C., Don, E., Winnick, C., McCann, E. P., Hogan, A., Daoud, H., Levert, A., Dion, P. A., Mitsui, J., Ishiura, H., Takahashi, Y., Goto, J., Kost, J., Gellera, C., Gkazi, A. S., Miller, J., Stockton, J., Brooks, W. S., Boundy, K., Polak, M., Muñoz-Blanco, J. L., Esteban-Pérez, J., Rábano, A., Hardiman, O., Morrison, K. E., Ticozzi, N., Silani, V., de Belleroche, J., Glass, J. D., Kwok, J. B., Guillemin, G. J., Chung, R. S., Tsuji, S., Brown, R. H., García-Redondo, A., Rademakers, R., Landers, J. E., Gitler, A. D., Rouleau, G. A., Cole, N. J., Yerbury, J. J., Atkin, J. D., Shaw, C. E., Nicholson, G. A. and Blair, I. P. (2016) 'CCNF mutations in amyotrophic lateral sclerosis and frontotemporal dementia', *Nat Commun*, 7, p. 11253.

Williams, K. L., Warraich, S. T., Yang, S., Solski, J. A., Fernando, R., Rouleau, G. A., Nicholson, G. A. and Blair, I. P. (2012) 'UBQLN2/ubiquilin 2 mutation and pathology in familial amyotrophic lateral sclerosis', *Neurobiol Aging*, 33(10), pp. 2527.e3-10.

Wong, Y. C. and Holzbaur, E. L. (2014) 'Optineurin is an autophagy receptor for damaged mitochondria in parkin-mediated mitophagy that is disrupted by an ALS-linked mutation', *Proc Natl Acad Sci U S A*, 111(42), pp. E4439-48.

Woo, J. A., Liu, T., Trotter, C., Fang, C. C., De Narvaez, E., LePochat, P., Maslar, D., Bukhari, A., Zhao, X., Deonarine, A., Westerheide, S. D. and Kang, D. E. (2017) 'Loss of function CHCHD10 mutations in cytoplasmic TDP-43 accumulation and synaptic integrity', *Nat Commun*, 8, p. 15558.

Woodley, K. T. and Collins, M. O. (2019) 'S-acylated Golga7b stabilises DHHC5 at the plasma membrane to regulate cell adhesion', *EMBO Rep*, 20(10), p. e47472.

Wu, C. H., Fallini, C., Ticozzi, N., Keagle, P. J., Sapp, P. C., Piotrowska, K., Lowe, P., Koppers, M., McKenna-Yasek, D., Baron, D. M., Kost, J. E., Gonzalez-Perez, P., Fox, A. D., Adams, J., Taroni, F., Tiloca, C., Leclerc, A. L., Chafe, S. C., Mangroo, D., Moore, M. J., Zitzewitz, J. A., Xu, Z. S., van den Berg, L. H., Glass, J. D., Siciliano, G., Cirulli, E. T., Goldstein, D. B., Salachas, F., Meininger, V., Rossoll, W., Ratti, A., Gellera, C., Bosco, D. A., Bassell, G. J., Silani, V., Drory, V. E., Brown, R. H. and Landers, J. E. (2012) 'Mutations in the profilin 1 gene cause familial amyotrophic lateral sclerosis', *Nature*, 488(7412), pp. 499-503.

Wu, N., Zheng, B., Shaywitz, A., Dagon, Y., Tower, C., Bellinger, G., Shen, C. H., Wen, J., Asara, J., McGraw, T. E., Kahn, B. B. and Cantley, L. C. (2013) 'AMPK-dependent degradation of TXNIP upon energy stress leads to enhanced glucose uptake via GLUT1', *Mol Cell*, 49(6), pp. 1167-75.

Wu, S., Lu, Q., Wang, Q., Ding, Y., Ma, Z., Mao, X., Huang, K., Xie, Z. and Zou, M. H. (2017) 'Binding of FUN14 Domain Containing 1 With Inositol 1,4,5-Trisphosphate Receptor in Mitochondria-Associated Endoplasmic Reticulum Membranes Maintains Mitochondrial Dynamics and Function in Hearts in Vivo', *Circulation*, 136(23), pp. 2248-2266.

Xia, C. H., Roberts, E. A., Her, L. S., Liu, X., Williams, D. S., Cleveland, D. W. and Goldstein, L. S. (2003) 'Abnormal neurofilament transport caused by targeted disruption of neuronal kinesin heavy chain KIF5A', *J Cell Biol*, 161(1), pp. 55-66.

Xie, X., Zhang, Y., Wang, Z., Wang, S., Jiang, X., Cui, H., Zhou, T., He, Z., Feng, H., Guo, Q., Song, X. and Cao, L. (2021) 'ATM at the crossroads of reactive oxygen species and autophagy', *Int J Biol Sci*, 17(12), pp. 3080-3090.

Xu, L., Wang, X., Zhou, J., Qiu, Y., Shang, W., Liu, J. P., Wang, L. and Tong, C. (2020) 'Miga-mediated endoplasmic reticulum-mitochondria contact sites regulate neuronal homeostasis', *Elife*, 9.

Xu, Y. F., Gendron, T. F., Zhang, Y. J., Lin, W. L., D'Alton, S., Sheng, H., Casey, M. C., Tong, J., Knight, J., Yu, X., Rademakers, R., Boylan, K., Hutton, M., McGowan, E., Dickson, D. W., Lewis, J. and Petrucelli, L. (2010) 'Wild-type human TDP-43 expression causes TDP-43 phosphorylation, mitochondrial aggregation, motor deficits, and early mortality in transgenic mice', *J Neurosci*, 30(32), pp. 10851-9.

Xu, Z., Poidevin, M., Li, X., Li, Y., Shu, L., Nelson, D. L., Li, H., Hales, C. M., Gearing, M., Wingo, T. S. and Jin, P. (2013) 'Expanded GGGGCC repeat RNA associated with amyotrophic lateral sclerosis and frontotemporal dementia causes neurodegeneration', *Proc Natl Acad Sci U S A*, 110(19), pp. 7778-83.

Yamanaka, T., Nishiyama, R., Shimogori, T. and Nukina, N. (2020) 'Proteomics-Based Approach Identifies Altered ER Domain Properties by ALS-Linked VAPB Mutation', *Sci Rep*, 10(1), p. 7610.

Yamano, K., Kikuchi, R., Kojima, W., Hayashida, R., Koyano, F., Kawawaki, J., Shoda, T., Demizu, Y., Naito, M., Tanaka, K. and Matsuda, N. (2020) 'Critical role of mitochondrial ubiquitination and the OPTN-ATG9A axis in mitophagy', *J Cell Biol*, 219(9).

Yang, S., Hwang, S., Kim, B., Shin, S., Kim, M. and Jeong, S. M. (2023) 'Fatty acid oxidation facilitates DNA double-strand break repair by promoting PARP1 acetylation', *Cell Death Dis*, 14(7), p. 435.

Yang, Y., Lei, T., Du, S., Tong, R., Wang, H., Yang, J., Huang, J., Sun, M., Wang, Y. and Dong, Z. (2018) 'Nuclear GSK3beta induces DNA double-strand break repair by phosphorylating 53BP1 in glioblastoma', *Int J Oncol*, 52(3), pp. 709-720.

Yasuda, K., Watanabe, T. M., Kang, M. G., Seo, J. K., Rhee, H. W. and Tate, S. I. (2022) 'Valosin-containing protein regulates the stability of fused in sarcoma granules in cells by changing ATP concentrations', *FEBS Lett*, 596(11), pp. 1412-1423.

Yeo, H. K., Park, T. H., Kim, H. Y., Jang, H., Lee, J., Hwang, G. S., Ryu, S. E., Park, S. H., Song, H. K., Ban, H. S., Yoon, H. J. and Lee, B. I. (2021) 'Phospholipid transfer function of PTPIP51 at mitochondria-associated ER membranes', *EMBO Rep*, 22(6), p. e51323.

Youle, R. J. and Narendra, D. P. (2011) 'Mechanisms of mitophagy', *Nat Rev Mol Cell Biol*, 12(1), pp. 9-14.

Yu, C., Han, W., Shi, T., Lv, B., He, Q., Zhang, Y., Li, T., Zhang, Y., Song, Q., Wang, L. and Ma, D. (2008) 'PTPIP51, a novel 14-3-3 binding protein, regulates cell morphology and motility via Raf-ERK pathway', *Cell Signal*, 20(12), pp. 2208-20.

Yu, W., Zhang, L., Wei, Q. and Shao, A. (2019) 'O(6)-Methylguanine-DNA Methyltransferase (MGMT): Challenges and New Opportunities in Glioma Chemotherapy', *Front Oncol*, 9, p. 1547.

Zeballos, C. M., Moore, H. J., Smith, T. J., Powell, J. E., Ahsan, N. S., Zhang, S. and Gaj, T. (2023) 'Mitigating a TDP-43 proteinopathy by targeting ataxin-2 using RNA-targeting CRISPR effector proteins', *Nat Commun*, 14(1), p. 6492.

Zelic, M., Blazier, A., Pontarelli, F., LaMorte, M., Huang, J., Tasdemir-Yilmaz, O. E., Ren, Y., Ryan, S. K., Krishnaswami, P., Levit, M., Sood, D., Chen, Y., Gans, J., Tang, X., Hsiao-Nakamoto, J., Huang, F., Zhang, B., Gaglia, G., Ofengeim, D. and Hammond, T. R. (2024) 'Glial state changes and neuroinflammatory RIPK1 signaling are a key feature of ALS pathogenesis', *bioRxiv*, p. 2024.04.12.589201.

Zelina, P., de Ruiter, A. A., Kolsteeg, C., van Ginneken, I., Vos, H. R., Supiot, L. F., Burgering, B. M. T., Meye, F. J., Veldink, J. H., van den Berg, L. H. and Pasterkamp, R. J. (2024) 'ALS-associated C21ORF2 variant disrupts DNA damage repair, mitochondrial metabolism, neuronal excitability and NEK1 levels in human motor neurons', *Acta Neuropathol Commun*, 12(1), p. 144.

Zhang, B., Tu, P., Abtahian, F., Trojanowski, J. Q. and Lee, V. M. (1997) 'Neurofilaments and orthograde transport are reduced in ventral root axons of transgenic mice that express human SOD1 with a G93A mutation', *J Cell Biol*, 139(5), pp. 1307-15.

Zhang, T., Xu, D., Trefts, E., Lv, M., Inuzuka, H., Song, G., Liu, M., Lu, J., Liu, J., Chu, C., Wang, M., Wang, H., Meng, H., Liu, H., Zhuang, Y., Xie, X., Dang, F., Guan, D., Men, Y., Jiang, S., Jiang, C., Dai, X., Liu, J., Wang, Z., Yan, P., Wang, J., Tu, Z., Babuta, M., Erickson, E., Hillis, A. L., Dibble, C. C., Asara, J. M., Szabo, G., Sicinski, P., Miao, J., Lee, Y. R., Pan, L., Shaw, R. J., Yuan, J. and Wei, W. (2023) 'Metabolic orchestration of cell death by AMPK-mediated phosphorylation of RIPK1', *Science*, 380(6652), pp. 1372-1380.

Zhang, X., Abdelrahman, A., Vollmar, B. and Zechner, D. (2018a) 'The Ambivalent Function of YAP in Apoptosis and Cancer', *Int J Mol Sci*, 19(12).

Zhang, Y. J., Gendron, T. F., Ebbert, M. T. W., O'Raw, A. D., Yue, M., Jansen-West, K., Zhang, X., Prudencio, M., Chew, J., Cook, C. N., Daughrity, L. M., Tong, J., Song, Y., Pickles, S. R., Castanedes-Casey, M., Kurti, A., Rademakers, R., Oskarsson, B., Dickson, D. W., Hu, W., Gitler, A. D., Fryer, J. D. and Petrucelli, L. (2018b) 'Poly(GR) impairs protein translation and stress granule dynamics in C9orf72-associated frontotemporal dementia and amyotrophic lateral sclerosis', *Nat Med*, 24(8), pp. 1136-1142.

Zhao, B., Li, L., Lei, Q. and Guan, K. L. (2010) 'The Hippo-YAP pathway in organ size control and tumorigenesis: an updated version', *Genes Dev*, 24(9), pp. 862-74.

Zhao, L., Lu, T., Gao, L., Fu, X., Zhu, S. and Hou, Y. (2017) 'Enriched endoplasmic reticulum-mitochondria interactions result in mitochondrial dysfunction and apoptosis in oocytes from obese mice', *J Anim Sci Biotechnol*, 8, p. 62.

Zhao, S., Chen, R., Gao, Y., Lu, Y., Bai, X. and Zhang, J. (2023) 'Fundamental roles of the Optineurin gene in the molecular pathology of Amyotrophic Lateral Sclerosis', *Front Neurosci*, 17, p. 1319706.

Zhao, Y. G., Liu, N., Miao, G., Chen, Y., Zhao, H. and Zhang, H. (2018) 'The ER Contact Proteins VAPA/B Interact with Multiple Autophagy Proteins to Modulate Autophagosome Biogenesis', *Curr Biol*, 28(8), pp. 1234-1245.e4.

Zhao, Y. G. and Zhang, H. (2019) 'Autophagosome maturation: An epic journey from the ER to lysosomes', *J Cell Biol*, 218(3), pp. 757-770.

Zhen, Y., Spangenberg, H., Munson, M. J., Brech, A., Schink, K. O., Tan, K. W., Sørensen, V., Wenzel, E. M., Radulovic, M., Engedal, N., Simonsen, A., Raiborg, C. and Stenmark, H. (2020) 'ESCRT-mediated phagophore sealing during mitophagy', *Autophagy*, 16(5), pp. 826-841.

Zheng, P., Chen, Q., Tian, X., Qian, N., Chai, P., Liu, B., Hu, J., Blackstone, C., Zhu, D., Teng, J. and Chen, J. (2018) 'DNA damage triggers tubular endoplasmic reticulum extension to promote apoptosis by facilitating ER-mitochondria signaling', *Cell Res*, 28(8), pp. 833-854.

Zhou, F., Wu, Z., Zhao, M., Murtazina, R., Cai, J., Zhang, A., Li, R., Sun, D., Li, W., Zhao, L., Li, Q., Zhu, J., Cong, X., Zhou, Y., Xie, Z., Gyurkovska, V., Li, L., Huang, X., Xue, Y., Chen, L., Xu, H., Liang, Y. and Segev, N. (2019) 'Rab5-dependent autophagosome closure by ESCRT', *J Cell Biol*, 218(6), pp. 1908-1927.

Zhou, Y. and Danbolt, N. C. (2014) 'Glutamate as a neurotransmitter in the healthy brain', *J Neural Transm (Vienna)*, 121(8), pp. 799-817.

Ziff, O. J., Neeves, J., Mitchell, J., Tyzack, G., Martinez-Ruiz, C., Luisier, R., Chakrabarti, A. M., McGranahan, N., Litchfield, K., Boulton, S. J., Al-Chalabi, A., Kelly, G., Humphrey, J. and Patani, R. (2023) 'Integrated transcriptome landscape of ALS identifies genome instability linked to TDP-43 pathology', *Nat Commun*, 14(1), p. 2176.